

THE UNIVERSITY *of* EDINBURGH

This thesis has been submitted in fulfilment of the requirements for a postgraduate degree (e. g. PhD, MPhil, DClinPsychol) at the University of Edinburgh. Please note the following terms and conditions of use:

- This work is protected by copyright and other intellectual property rights, which are retained by the thesis author, unless otherwise stated.
- A copy can be downloaded for personal non-commercial research or study, without prior permission or charge.
- This thesis cannot be reproduced or quoted extensively from without first obtaining permission in writing from the author.
- The content must not be changed in any way or sold commercially in any format or medium without the formal permission of the author.
- When referring to this work, full bibliographic details including the author, title, awarding institution and date of the thesis must be given.



The University of Edinburgh

Electrophysiological Functions of Microbes

Guillaume Terradot

A thesis submitted in fulfilment of the requirements for the degree of Doctor of Philosophy the

September 15, 2021

Abstract

Akin to neurons, all microbes maintain an electric potential (a.k.a. membrane voltage) across their membranes. The exact function and generation mechanism of microbial membrane voltage remains elusive. Microbes also maintain close to neutral intracellular pH and Ion Motive Forces, the most relevant of which is the Proton Motive Force (an electrochemical gradient of protons across the membrane). In this thesis, I propose a thermodynamically consistent framework for modelling cellular electrophysiology, and based on the models I propose that in bacteria *(i)* one important function of membrane voltage is to allow simultaneous maintenance of intracellular pH and PMF in environments bearing different extracellular pH and *(ii)* proton:ion antiporters are responsible for membrane voltage maintenance. Single-cell measurements of PMF and intracellular pH in *E. coli* support the main prediction of my model predictions, namely that the ability to maintain intracellular pH or membrane voltage is PMF dependent. I then evaluate in silico the energetic cost of maintaining intracellular pH and PMF in environments with different ionic composition and make predictions on how the growth-rate and growth-yield are expected to change upon ionic perturbations of the growth medium. I conclude by introducing an approach for the analysis of electrophysiological behaviors that I think is more intuitive and generic than the current teaching practices.

To some things that brought me here and now.

Acknowledgements

I thank all those that have been present, whether in my thoughts or whose I am lucky to share the company. To them: Maman, Papa, François, Louise, Gros-papa, Grand-maman, Mamie Co. Clément, Raphaël, Riyad, Ahmed, Anaïs, Bilal, Xavier, Joachim, Victor, Frédéric, Ihab, Ambroise, Jessica, James (×2), Vincent, Paul, Cristina, Sebastian and all the others who will recognize themselves, I renew my affection.

I also express my gratitude to all those I was able to share my work within the past years: Ilias Garnier, Sebastian Jaramillo-Riveri, Andreea Beica, Ricardo Honorato-Zimmer, Xavier Zaoui, Alan Munoz.

My appreciation goes to:

- Those who dedicated (a lot of) time to share their experience with me:
  - Vincent Danos, for all the discussions, his precious advices for the models I developed and his genuine interest in modeling anything I have been been interested in.
  - Andrea Weiße, who contributed to my initial understanding in on how to model biological systems.
  - My Ph.D. supervisors, Peter Swain and Teuta Pilizota, who allowed me to pursue the questions I was interested in, who taught me to be more rigorous and whom contribution to how this thesis unfolded is important.
- Other scientists I had the chance to collaborate with: Andreea Beica, Ekaterina Krasnopeeva and Leonardo Mancini.
- Colleagues who made daily Ph.D. work brighter than it would have been: Dario Miroli, James Freed, Jerko Rosko, Smitha Hedge, Alex McVey, Ekaterina Krasnopeeva, Leonardo Mancini.

Finally, a special thanks to the Darwin Trust who funded my Ph.D.

Contents

Introduction **15**

I Preamble 15

II Definitions and Functions of Electrophysiologically-related Variables 17

i Acidity of Aquaeous Solutions: pH 17

ii Osmotic Pressure 21

iii Membrane Potential 26

iv Electrochemical Gradient/Ionic Motive Forces 33

III Electrophysiological Mechanisms in Living Cells 35

i Transport Across Membranes 35

ii Maintenance of Electrophysiological Homeostases 41

iii Regulation and kinetics of transport across membranes. . . 45

IV Outline of this Thesis 50

1 Membrane Voltage Measurements with Nernstian Dyes in Bacteria: A Cautionary Tale **55**

I Preamble 55

II Introduction 59

III Methods 62

i Bacterial strains 62

ii Bacterial growth conditions 63

iii Fluorescence microscopy 64

iv Motor speed measurements 64

v Data analysis 65

IV Results 66

i Mathematical model of Nernstian dye's behavior defines its working parameter range 66

ii The working concentration of Nernstian dye Thioflavin T for *E. coli* is in μM range 71

iii Changing the membrane permeability during ThT loading can lead to loss of V_m . . . 73
V Discussion . . . 77

Appendices **83**
B Supplementary Material . . . 85
B.1 Supplementary Figures . . . 85
B.2 Supplementary Videos . . . 92
B.3 Supplementary Tables . . . 94
B.4 Intracellular pH estimation. . . . 95
B.5 Detailed description of the model . . . 95
B.6 Numerical simulations . . . 99
B.7 Distinguishing the inner from the outer membrane . . . 100

2 Mechanisms of Coordinated Electrophysiological Maintenance in Bacteria **103**
I Preamble . . . 103
II Introduction . . . 106
III Results . . . 108
i To generate electrochemical gradients of ions, and thus physiological membrane voltage, cells need to actively pump ions out . . . 109
ii The ability of the cell to maintain pH_i is directly related to the PMF it can generate . . . 112
iii At pH_e 5.5 *E. coli* exhibits pH_i homeostasis if the value of PMF is sufficiently high . . . 115
iv Model predicts the role of antiporters is to regulate $\Delta\psi$, and experimental evidence supports it: ΔpH is not maintained when PMF drops . . . 116
v Model predicts the role of antiporters is to regulate $\Delta\psi$, and experimental evidence supports it: expression of different antiporters depends on the pH of the external environment 119
vi Outer membrane voltage can offset effects of external environment on the cytoplasmic homeostases . . . 123
vii Additional Remark on Catalytic Efficiency . . . 125
IV Discussion . . . 126

V Methods . . . 129
i Strains and media . . . 129
ii Flagellar motor speed recording and analysis . . . 129
iii Intracellular pH measurements . . . 130
iv Obtaining computational results . . . 131

Appendices **133**
C SI Figures . . . 135
C Definitions and Derivations . . . 147
C.1 Cell shape . . . 147
C.2 Extracellular environment . . . 147
C.3 Full derivation of equations for $\Delta\psi$ . . . 149
C.4 Describing the movement of ions . . . 153
C.5 Energy budget of *E. coli* . . . 158
C.6 Periplasm . . . 158
D Model of E.coli Electrophysiology . . . 160
D.1 Model Reactions and Parameters . . . 160
D.2 Steady-State Characterization . . . 161
D.3 Boundaries on Electrochemical potentials . . . 162
D.4 Optimal Strategies for Chemiosmotic maintenance . . . 169
D.5 Solving Model of *E.coli*'s Electrophysiology . . . 177
E Generalization to other Models of Electrophysiology . . . 183
E.1 Thermodynamically Viable Steady-States for Arbitrary number and type of Transporters . . . 183
E.2 Thermodynamically Viable Steady-States for the Coupling ion (here Proton) . . . 187
E.3 Generalizing the Optimal Coordination of Cotransporters . 190
E Algorithms . . . 201

3 Interactions of Electrophysiological Maintenance with Growth Behaviors **203**
I Preamble . . . 203
II Introduction . . . 204
III Results . . . 210
i A Model for Studying Growth-Rate and Yield at Different Extracellular pH and Salinity. . . . 210

ii Relation of our Model to Pirt's Growth Law 214
iii Dependence of Growth-Rate on Electrophysiological Variables 215
iv Geometry-Dependent Cost of Maintenance Predicts Cell Cycle-Dependent Metabolic Oscillations and Environment-Dependent Distributions of Growth-Rates 221
v Growth-Rate and Yield Co-vary in a Stress-Specific Way . 225
vi Existence of a Trade-Off between Rate and Yield Depends on the Maintenance Cost 227
vii Yield Maximization Predicts Shift to Fermentative Catabolism upon Salinity or/and pH Challenges 231
IV Discussion 235

Appendices **251**
F Appendix 253
F.1 Description of the model 253
F.2 Chemio-osmotic-dependent Maintenance cost 257
F.3 Solving the model at balanced-growth 258
F.4 Model with two catabolic pathways 260
F.5 Parameter evaluation 263
G Supplementary Figures 267

4 Discussion **269**
I Preamble 269
II Summary of Previous Chapters 270
III Relevance to Additional Biological Topics 270
i Limitations of Electrophysiological Measurements in Bacteria 270
ii Extending the Model for more Ions 272
iii Heavy Metal Homeostasis and Electrophysiological Maintenance 276
iv Impact of Small Organic Ions on Membrane Voltage: Ammonium 281
v Intracellular sodium and potassium balance 283
vi Choice of Coupling Stoichiometries and Energetic Efficiency of IMF Maintenance 289
vii The Unreliability of the KO Experiment to Test Whether a pump Works as an Influx or Efflux Pump. 292

viii Relevance of Kinetic Asbtraction 295
IV Heuristics for Approaching Electrophysiological Processes 298
i Characterization of Active Transport Systems 299
ii Composability of Active Ionic Transporters 314
iii Specificities of the NaK-ATPase 321
iv Conclusion 329

Bibliography **331**

Introduction

I. Preamble

Common features to all what we refer to as life forms is that they are spatially confined. This reductionist axiom allows biologists to draw a line between what is and what is not *part of* a living organism. Having drawn this line, biologists will notice that the composition of what is *part of* a living organism (self) is not identical from its surroundings (a.k.a. environment). In particular, cells are the basic unit of living organisms and possess organic compounds in density and proportions that are very different from the environment they inhabit. These organic compounds are made of a handful of atomic species. These include Carbon, Oxygen, Hydrogen, Nitrogen, Phosphate, Sulphur; from which are built most molecules life forms are able to transform *via* biochemistry. Typically, cells assemble small organic compounds such as metabolites into macromolecules like lipids, mRNA, rRNA, proteins, DNA, *etc.* These serve as the functional basis of life: DNA for information storage, mRNA for mediating protein synthesis, proteins for transforming/assembling organic compounds, rRNA (as part of ribosomes) for protein assembly, lipids that serve as a barrier between the self and the environment. The ability of a bacterium to survive is conditioned by its ability to maintain some organic features, *e.g.* not too damaged membrane, DNA and proteins [1].

In spite of organic meaning *relating to or derived from living matter*, core properties that all living cells maintain relate to inorganic features. Indeed, cells maintain intracellular inorganic particles (Sodium, Potassium, Calcium, Iron, Chloride, Magnesium, *etc.*) in density and proportion different from that of the environment they inhabit. This distinct inorganic composition contributes to the cellular maintenance of physico-chemical properties: intracellular pH, osmotic pressure, membrane voltage, ionic electrochemical gradients across the membrane, all of which are important for survival.

Electrophysiology is, *stricto sensu*, the branch of physiology that is concerned

with electrical properties of living cells. Inorganic ions such as sodium Na^+, potassium K^+, chloride Cl^- contribute to electrostatic phenomena in cells. Electrostatic phenomena contribute to the build up of electrochemical gradients thereby impacting the intracellular composition in ions subsequently pH or osmotic pressure. We shall thus in this manuscript use *Electrophysiology* in a wider sense as it was initially intended: the branch of physiology that is concerned with *physico-chemical properties of cell inorganic ions contribute to, which are consequently interdependent with cellular electrostatic properties.* For the purpose of this discussion, we do not include in this broad definition the fact that some inorganic ions (in particular Potassium, Calcium, Magnesium, Iron) are used as cofactors for various biochemical processes. This brings us to the first question this thesis ambitions at partly elucidate:

How do cells, bacteria in particular, achieve maintenance of several electrophysiologically-related properties (intracellular pH, osmotic pressure, membrane voltage, electrochemical gradients for several ions) simultaneously ?

As opposed to mammalian cells, why do bacteria tune their membrane potential remains unclear, which brings us to the second question:

What is the function of tuning membrane voltage in bacteria ?

Time (or entropy) work to bring the composition of self to that of the environment, requiring living systems to spend energy to maintain their electrophysiological features, which brings us to the third question:

How much does it cost to maintain electrophysiological variables, how does it depend on the environmental composition, how does varying energy requirements relate to the reproduction rate and resource usage efficiency of a microbe ?

To that end we first give more context in what follows of the introduction. We first define pH, the values intracellular pH is maintained across organisms and why pH maintenance is important for biochemical processes. We then follow a similar plan for osmotic pressure: how we define it, to what values it is maintained, why is it important for survival. After this, we define membrane voltage. This part of the discussion is quite lengthy and is due to an extensive discussion on the assumptions underlying our definition of membrane voltage, as well as a comparison of (not exclusively) our approach with some existing popular model of membrane voltage. We then define electrochemical gradients as a property of

passive transport reactions before outlaying the diversity and unicity of active transport systems in living cells. We then briefly discuss their function which we use as a pivot to introduce what I think is a novelty of this work: the necessity of considering all electrophysiological-dependent variables at once, rather than disciplinary specific research on each of those variables, *e.g.* a scientific field for osmoregulation, one for pH, *etc.* We then briefly discuss the paradigmatic view on pH regulation in bacteria I hope to convince the reader of this thesis to reconsider. Finally, I use the plan of this thesis as an opportunity to describe how the work in this manuscript unfolded during my Ph.D.'s years and mention in short what I deem are the main contributions of this thesis.

II. Definitions and Functions of Electrophysiologically-related Variables

i. Acidity of Aquaeous Solutions: pH

Definition of pH. The pH of a solution is defined as the decimal logarithm of the hydrogen ion thermodynamic activity [2]:

$$\mathrm{pH} := -\log_{10}(a_{\mathrm{H}^+}) \tag{II.1}$$

In this thesis we will assume that all solutions are ideal such that Eq. (II.1) becomes [3]:

$$\mathrm{pH} = -\log_{10}(\underbrace{[\mathrm{H}^+]}_{molar}) \tag{II.2}$$

where the above equation for pH is standard in the relevant biological field [4]. Although $[\mathrm{H}^+]$ is, strictly speaking, the concentration of hydrogen ions in the solution, we shall assume that it is effectively the concentration of hydronium ions: $[\mathrm{H}^+] \equiv [\mathrm{H_3O}^+]$ which holds for sufficiently diluted solutions in which water is the solvent. *Although concentrations are often expressed in molar, as in Eq.* (II.2)*, we shall use SI units of moles per cubic meters (or equivalently milimolar) all along this thesis, which requires multiplying* $[H^+]$ *by* 10^3 *in Eq.* (II.2)*. From now on we will use milimolar units unless otherwise stated.*

Modulation of pH in aqueous solutions. Aqueous solutions can be acidified (equivalently increase in $[H_3O^+]$) by addition of a proton donor (a.k.a. acid) AH:

$$AH + H_2O \rightleftharpoons A^- + H_3O^+ \tag{II.3}$$

They can also be alkalinized (equivalently decrease in $[H_3O^+]$) by addition of a molecule that takes protons from water (a.k.a. base) B:

$$B + H_2O \rightleftharpoons BH^+ + OH^- \tag{II.4}$$

The decrease in hydronium ions is not directly visible from (II.4) but is mediated by self-ionization of water:

$$2H_2O \rightleftharpoons H_3O^+ + OH^- \tag{II.5}$$

i.e. the hydroxide ions OH^- released in the solution by addition of a base *via* reaction (II.4) reacts with hydronium ions to form water *via* reaction (II.5) thereby decreasing the concentration of hydronium ions and increasing pH of the solution.

Finally, another way to change the pH of a solution i is by transport of either a hydronium or hydroxide ion from/to a solution e:

$$H_3O^+_e \rightleftharpoons H_3O^+_i \tag{II.6}$$

$$OH^-_e \rightleftharpoons OH^-_i \tag{II.7}$$

Where the transport reactions above may be coupled to chemical reactions or other transport reactions as we shall see later. The main purpose of this thesis is to study how cells transport hydronium ions to maintain their intracellular pH across different extracellular pH. pH of a solution i may also be modulated by movement of a base B or an acid AH across from/to a solution e.
Importantly, we will assume in this thesis that the rate of reaction (II.5) is very fast in comparison to other reactions such that hydronium and hydroxide ions concentrations are related *via* the equilibrium constant K_w[1]:

$$[H_3O^+] \cdot [OH^-] = K_w \tag{II.8}$$

[1] An assumption that can be relaxed without affecting the qualitative conclusions of chapter 2.

and we will assume $K_w = 10^{-14}$, valid for an ideal solution with atmospheric pressure and temperature 298 Kelvins [5]. Similarly, the rates of acid/base reactions of the forms (II.3) and (II.4) will in this thesis assumed to be very fast in comparison to transport reactions such that the concentrations of the chemical species involved in these reactions will be constrained by the equilibrium constants of those reactions.

pH in living organisms. Cytoplasmic pH is a chemical property that is maintained relatively close to neutrality (pH 7) across all kingdoms of life. For instance [6] compiled data on 10 acidophilic bacteria (including archaea and eubacteria), that thrives in extracellular pH in the range 1–3, and found that all of them maintain a cytoplasmic pH between 4.6 and 7, with most of them maintaining ≈ 6.5 cytoplasmic pH (a.k.a. intracellular pH or pH_i). On the other hand of the spectrum, alkaliphilic bacteria, that thrives at extracellular pH (pH_e) in the range 9–13, maintain cytoplasmic pH lower than the extracellular one [7]. This suggests that proper functioning of cellular machinery is restricted to pH_i not too far from neutrality, as bacteria living in acid environments maintain pH_i greater than pH_e and bacteria living in alkaline environments maintain pH_i lower than pH_e. In humans, different types of cells also maintain not too far from 7 cytoplasmic pH, non exhaustively: Lymphocytes (involved in immune systems) have cytoplasmic pH around 7.0 [8], foreskin fibroblast (cells in skin) maintain cytoplasmic pH around 7.05 [9] while cardiac cells maintain cytoplasmic pH around 7.1 [10].

pH_i homeostasis. We shall now introduce the notion of *homeostasis*, taking the example of cytoplasmic pH. In the previous paragraph we described that across different organisms, across different types of cells in humans, pH_i was observed to be not too far from neutrality. pH homeostasis is quite a different notion and refers to the ability of a given organism (for unicellular organisms) or cell type (multicellular organisms) to keep its pH_i in a narrow range upon perturbations of its surrounding environment, for instance change in the pH of the medium it inhabits. For instance: *E. coli* maintains pH_i close to 7.5 in environments ranging from pH_e 5 to 9 [11], *S. cerevisae* maintains pH_i between 5 and 7 across pH_e ranging from 2 to 7 [12], neurons maintain cytoplasmic pH_i in the face of extracellular pH_e changes [13]. Note that, although we took as examples perturbations of the surrounding pH_e, the question of whether or not a cell is maintaining a homeostasis can pertain to any environmental perturbation.

For instance does a cell maintain approximately invariant pH_i across different salinity, sugar availability, *etc.* ? The notion of homeostasis we developed insofar is rather qualitative and its quantification is somewhat not necessary in this thesis. A seemingly appealing way to quantitatively describe the ability of a cell to maintain some quantity x in response to a perturbation ∂y would be the use of elasticity, as defined in the scope of economical sciences: $(\partial x/x)/(\partial y/y)$.

Of the importance of pH_i value. In the face of those observations one could naturally ask why is pH_i so thoroughly maintained not too far from neutrality across widely different organisms, cellular types and different environments. First, stability of macromolecules such as DNA [14] and proteins [15] are pH dependent. Meaning that if the intracellular space is too acidic (typically between 2 and 5) or too alkaline (typically above 10), DNA and proteins will start to denaturate [16], *i.e.* lose their geometrical structure that is crucial to their functions. Second, the reaction scheme of some enzymes may involve one or multiple protonotation steps where one intermediary conformation of the enzyme acts as an acid, *e.g.* below the enzyme E_1 can only turn the substrate S_1 into product P_1 if it is under protonated form E_1H^+:

$$E_1 + H_3O^+ \rightleftharpoons E_1H^+ + H_2O \qquad \text{(Step 1)}$$
$$E_1H^+ + S_1 \rightleftharpoons E_1H^+ + P_1 \qquad \text{(Step 2)}$$

On the other hand, the reaction scheme of some enzymes may involve one or multiple deprotonation steps, where one intermediary conformation of the enzymes acts as a base, *e.g.* below the enzyme E_2H^+ can only turn the substrate S_2 into product P_2 if it is under deprotonated form E_2:

$$E_2H^+ + OH^- \rightleftharpoons E_2 + H_2O \qquad \text{(Step 1)}$$
$$E_2 + S_2 \rightleftharpoons E_1H^+ + P_2 \qquad \text{(Step 2)}$$

In a simple scenario where activity of both E_1 and E_2 are crucial for cell survival, one understands why pH_i cannot be too acidic or too alkaline. If it is too acidic then the activity of E_2 will be severely impaired due to low $[OH^-]$, resulting in high fraction of E_2 under protonotated form in which it cannot turn S_2 into P_2. Similarly, if pH_i is too alkaline, the activity of E_1 will be severely impaired due to low $[H_3O^+]$, resulting in high fraction of E_1 under deprotonated form in which

it cannot turn S_1 into P_1. Within that scope, maintenance of near neutral pH_i enables H_2O to work both as a proton donor and a proton acceptor, enlarging the total number of viable (as in not too slow) biochemical reactions.

ii. Osmotic Pressure

Definition of Osmotic Pressure. The osmotic pressure of a cell can be seen as the "*Amount of physical pressure exerted on the membrane/cell wall for which there is no net movement of water across the membrane/cell wall*". This so far may seem a bit cryptic, so let us consider the movement of water from the extracellular space to the intracellular space:

$$H_2O_e \rightleftharpoons H_2O_i \tag{II.9}$$

The Gibbs free energy of the transport reaction above is [17]:

$$\Delta G_{H_2O} = \nu_s \cdot (p_i - p_e) + RT \cdot \ln\left(\frac{a_{w,i}}{a_{w,e}}\right) \overset{EQ.}{=} 0 \tag{II.10}$$

where ν_s is the molar volume of water, p_i, p_e are hydrostatic pressure in compartments i/e and $a_{w,i}/a_{w,e} := \phi_{w,i}/\phi_{w,e}$ where $\phi_{w,i}/\phi_{w,e}$ are the partial vapor pressures of water in compartment i and e:

$$\phi_{w,i/e} := \frac{[H_2O]_{i/e}}{\sum_x [x]_{i/e}} \tag{II.11}$$

which are effectively molar fraction, where we defined $[x]_i$, $[x]_e$ as the intracellular and extracellular concentrations of molecule x. If say both compartments i and e are composed of pure water, then $\phi_i = \phi_e = 1$ and the situation at equilibrium will be that depicted in figure 1 (Left) with equal total concentration of particles on both sides of the membrane and therefore null pressure exerted on the membrane.

The osmotic pressure $\Delta\Pi$ is defined as the difference in hydrostatic pressure $p_i - p_e$ that is required to achieve equilibrium for reaction (II.9) (or equivalently $\Delta G_{H_2O} = 0$) given fixed water molar fraction on both sides of the membrane (in each compartment i, e) such that after a few approximations (see [17] Eq. (2.136)

to (2.141)[2]):

$$\Delta\Pi = RT \sum_{x \backslash \mathrm{H_2O}} \phi_x \cdot ([x]_i - [x]_e) \tag{II.12}$$

in units Pascal or Joule/m^3 where R is the gas constant, T the temperature, $[x]_i$ and $[x]_e$ are respectively for intra/extracellular concentrations of x (in moles/m^3 of millimolar) and the sum is over all chemical compounds (with exception to water). ϕ_x normally depends on the concentration of x and is found experimentally. We will assume in this manuscript that $\forall x : \phi_x = 1$, such that Eq. (II.12) becomes Van't Hoff's law for osmotic pressure. As explained by [17], this approximation is only valid when $[x]_i$ and $[x]_e$ are sufficiently low thus may deviate significantly from the "*real*" osmotic pressure at physiological concentrations. This is the case in particular for proteins, for which ϕ_x is in general significantly different from 1. For instance, osmotic coefficients between 3 and 10 have been reported for some proteins in frogs [18]. In this work, osmotic coefficient is however measured one protein at a time and to my knowledge no such measurements have been performed for bacterial proteins. Osmotic coefficients of some solutes such as polyethylene glycol may also depend non linearly on their concentrations [19], complexifying even more the quantification of osmotic pressure in cells, which contains a mixture of proteins (each of which with a specific osmotic coefficient) and likely non ideal solutes. Because of the lack of reliable values for physiological ϕ_x we will however use the aforementioned approximation $\forall x : \phi_x = 1$. The reader shall therefore keep in mind that all along this thesis, the computed values of osmotic pressure are rather indicative than quantitative, refinement of which would require additional work that is beyond the scope of this manuscript. Be as it may, osmotic coefficient of small ions such as NaCl [20] are well approximated by 1. As such, the contribution of small ions to osmotic pressure in this thesis will be fairly reliable and everything else (than small ions) being the same, our definition of osmotic pressure is therefore expected to capture well how it covaries with membrane voltage upon changes in small ions content.

To give a more intuitive description of the phenomenon, when a solute S to which the membrane is not permeable is added on, *e.g.* the "In" side of the membrane, it decreases the partial vapor pressure of water $\phi_{w,i}$ in the "In" compartment, $\Delta G_{\mathrm{H_2O}}$ becomes negative and therefore spontaneous inward movement

[2] Assuming however that solutes can be present in either side of the membrane, *i.e.* in both compartments i and e, as opposed to [17].

of water occurs as depicted in figure 1 (Middle). This inward movement of water increases the pressure in the "In" compartment and deforms the membrane, that in turns apply at equilibrium a force of equal intensity of opposite direction due to its elastic properties such that the equilibrium state after addition of solute will look like that depicted in figure 1 (Right).

We thus far considered that the membrane was completely impermeable to else-than-water particles. Such will not be the case in this thesis. This apparent problem is however solved by assuming that water equilibrates across the membrane much faster than any other particles, such that the diffusion of water reaction (II.9) can be assumed to always be at equilibrium. This assumption is justified if the permeability of the membrane is orders of magnitude higher for water than for the solutes to which the membrane is permeable we will consider (small ions) as depicted in [21]. In other words, we assume in this thesis instantaneous equilibrium for passive transport of water across the membrane.

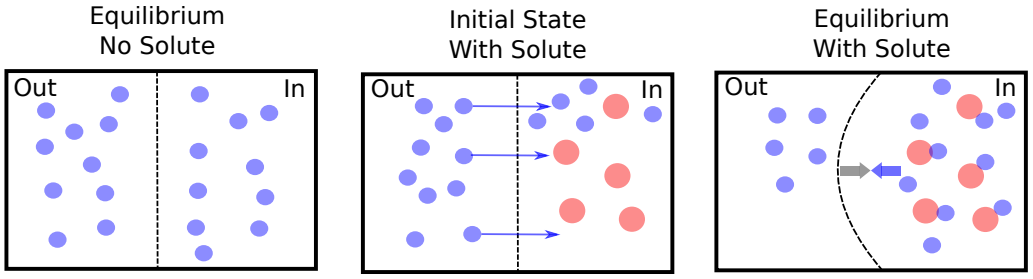


FIGURE 1: Scheme of osmosis across a semi-permeable membrane. The membrane (dotted line) is permeable to water (blue dots) and impermeable to a solute (red dots). (Left) When no solutes are present on either side of the membrane separating two compartments having identical volumes, the equilibrium state is characterized by the same amount of water molecules on both sides of the membrane, thus the pressure is identical on both sides of the membrane and the osmotic pressure is null. (Middle) We introduce solute on the "In" side of the membrane, the pressure is identical on both sides of the membrane (ten particles on each side), the state is however not at equilibrium. (Right) Equilibrium state towards which the initial state (Middle) converges in time; the water bound to solute molecules cannot move across the membrane thus equilibrium for the transport reaction (II.9) of free (or unbound) water imposes that there will be more total molecules of water (and total amount of molecules) on the right-hand side. The right-hand side has therefore higher pressure than the left-hand side, exerting a force on the membrane (Blue arrow) that is compensated at equilibrium by the elastic force of the membrane (grey arrow) that "fights" to return to its initial state.

Osmotic pressure in living organisms. The value osmotic pressure takes can

be quite different depending on the considered organism, or type of cells (for multicellular organisms). For instance, animal cells maintain near null osmotic pressure [22], while epidermal leaf plant cells can withstand osmotic pressure up to 20 atmospheres [23]. In bacteria, *E. coli* has osmotic pressure in the range 1–3 atmospheres [24, 25] while *B. subtilis* sometimes maintains osmotic pressure equal to 20 atmospheres [26]. Another model organism, *S. cerevisiae* maintains osmotic pressure around 6 atmospheres [27].

Importance of Osmotic pressure. One can at this stage wonder why maintaining osmotic pressure in a given range is important. This is perhaps best exemplified having a look at what happens to a cell during osmotic challenges as depicted in figure 2:

- When a healthy cell is put in a hypotonic solution (low osmolarity of the medium, decrease of $\sum_x [x]_e$ in Eq. (II.12)), water flows in the cell resulting in abrupt increase in osmotic pressure, potentially leading to cell lysis as shown on left panel of figure 2. Importantly, the ability of a cell to not explode upon such challenge is tight to the physical resistance of its membrane/cell wall. Indeed, as shown on the same panel, a plant cell possessing a cell wall with high resistance may not explode when subjected to a hypoosmotic challenge sufficient to lead to explosion of an animal cell, that does not possess a cell wall.
- The middle panel denotes the "normal" state of the cell, in an environment where it can maintain its homeostatic osmotic pressure. For some cells, *e.g.* blood cells depicted in the panel, homeostatic osmotic pressure maintenance is of particular importance as it relates to the cell having a healthy physiological shape[3].
- The right panel shows the scenario where a healthy cell is put in a hypertonic solution (high osmolarity of the medium (increase of $\sum_x [x]_e$ in Eq. (II.12)). In that case, water will flow out of the cell, leading to cells shrinking and losing shape consistency. Adaptation to hypertonic conditions usually involves accumulation of osmolytes in the intracellular space [28], leading to increase of $\sum_x [x]_i$ and recovery of healthy water content and shape.

[3]Here meant as an example that the proper physiological functioning of some cell types may depend more on their shapes than others.

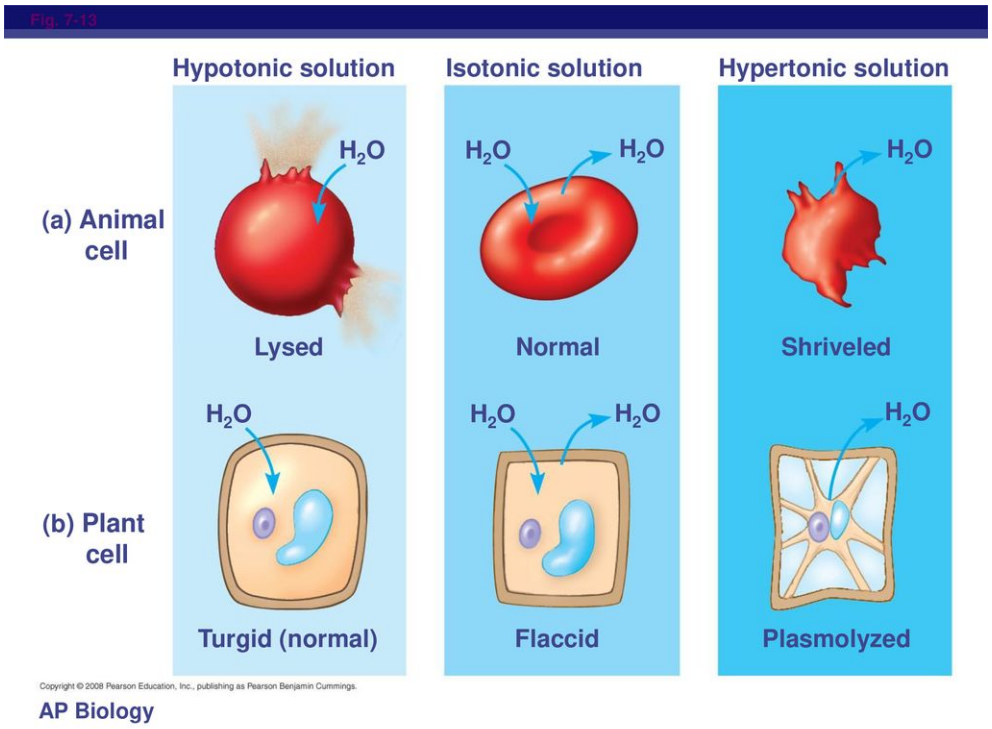


FIGURE 2: Responses of animal and plant cells to hypotonic (left panel) and hypertonic (right panel) challenges. Hypotonic challenges lead to high osmotic pressure and potentially cell lysis. Hypertonic challenges lead to transient negative osmotic pressures. In the process of restoring the osmotic pressure to positive values, the cell shrinks and loses water (right panel). Following a hypertonic challenge, cellular shape and water content may be restored by accumulation of osmolytes in the intracellular space [28].

To summarize, negative osmotic pressures are only observed transiently, however lead to unfit water content and cellular shape as osmotic pressure is restored to its equilibrium value. Accumulation of osmolytes can later restore physiological water content and shape. Upper bounds on osmotic pressures are somewhat more acute constraints, as a cell exceeding some osmotic pressure threshold (by *e.g.* a hypotonic challenge) will explode. What sets the maximal osmotic pressure a cell can withstand is related to the properties of its membrane/cell wall. Organisms possessing a cell wall can withstand an osmotic pressure of several atmosphere without exploding. For instance, osmotic pressure of *E. coli* and epidermal plant cells casually maintain 3 and 20 atmospheres respectively [29, 23]. Whereas human cells not possessing a cell wall maintain no higher than 0.2 atmosphere osmotic pressure [30].

iii. Membrane Potential

At the heart of cellular electrophysiology is the membrane voltage (also called membrane potential or transmembrane voltage/potential). We shall first discuss the mathematical definition we will use in this thesis and other common definitions used in the literature. Note that we will ignore in this thesis magnetic phenomena[4].

In this thesis, following others [31, 32, 17, 33, 34], we assume that the charge accumulated in close proximity to the membrane is equivalent to the surface charge on a parallel-plate capacitor which results in the following definition of membrane potential:

$$\Delta\psi = \frac{F}{S \cdot C_m} \underbrace{V \cdot \sum_x z_x \cdot [x]_i}_{Q_i} \tag{II.13}$$

Where F is Faraday constant, S is the cell's surface, V its volume and C_m the specific membrane capacitance. Q_i is referred to as the *total intracellular charge* and is effectively the net charge (in moles) contained in the intracellular space. Eq. (II.13) implicitly assumes that the electrostatic potential outside the cell is negligible. This assumption does not hold rigorously if some net charge exists in the intracellular space as the extracellular and the intracellular spaces are together

[4] Partly due to my lack of knowledge and the lack of discussion of these phenomena in the articles I came across.

electroneutral. It is however a good approximation if the extracellular space occupies much more volume than the intracellular space. Some authors do not make this assumption and therefore compute membrane potential as proportional to the the difference in intracellular and extracellular total charges [35, 17, 36]. Also, we will approximate the geometry of an *E. coli* cell by a spherocylinder as in [29]. This assumption is only expected to hold if the cell's surface is flat, meaning underestimates the surface of the cell if the membrane contains sufficiently high amount of invaginations (as mitochondria or chloroplast do). Thus, we assume all along this thesis flat cellular surfaces.

Comparison with dynamic equations for membrane voltage. The most popular way of theoretically deriving membrane voltage is not however given by Eq. (II.13), but rather by the Goldman-Hodkin-Katz (GHK) Voltage equation [37, 38]:

$$\Delta\psi = \frac{RT}{F} \ln\left(\frac{P_{\mathrm{K}^+} \cdot [\mathrm{K}^+]_e + P_{\mathrm{Na}^+} \cdot [\mathrm{Na}^+]_e + P_{\mathrm{Cl}^-} \cdot [\mathrm{Cl}^-]_i}{P_{\mathrm{K}^+} \cdot [\mathrm{K}^+]_i + P_{\mathrm{Na}^+} \cdot [\mathrm{Na}^+]_i + P_{\mathrm{Cl}^-} \cdot [\mathrm{Cl}^-]_e}\right) \tag{II.14}$$

Here shown for a simple system containing only three ionic species, where P_x holds for the permeability of the membrane to ion x, *i.e.* how fast x can cross the membrane. It is actually fairly straightforward to rederive it from our definition of voltage Eq. (II.13). Indeed, take first the time derivative of Eq. (II.13):

$$\frac{C_m \cdot S}{F \cdot V} \cdot \frac{d\Delta\psi}{dt} = \sum_x z_x \cdot \frac{d[x]_i}{dt} \tag{II.15}$$

where we assumed that $C_m \cdot S/F/V$ is time-invariant. GHK voltage equation (II.14) gives what is misleadingly often referred to as the *equilibrium potential*. This terminology does not reflect accuratly the state of the system, which does not need to be at equilibrium for GHK voltage equation to hold but rather in a state where the membrane voltage is time invariant, *i.e.* where the left-hand term of Eq. (II.15) is null:

$$0 = \sum_x z_x \cdot \frac{d[x]_i}{dt} \propto \sum_x I_x \tag{II.16}$$

The equation above is often written in terms of the current for each ion I_x, which is equivalent, up to a rescaling, to the molar flow of ionic charges $z_x d[x]_i/dt$. An additional, often underlooked, assumption required [39] to obtain GHK voltage equation (II.14) is that there are no electrogenic pumps[5]. In the case with no

[5]Equivalently, all pumps are electroneutral, *e.g.* *(i)* one K^+ out and one Na^+ in; *(ii)* one Cl^- in one K^+ in, *(iii)* one Na^+ in, one K^+ in, two Cl^- in, *etc.* Put differently, the action of an

electrogenic pumps, all transport terms vanishe in Eq. (II.16) and the only remaining terms are those for passive transport. Assuming passive diffusion across the membrane is given by GHK flux equation (see [37]), one then obtains Eq. (II.14) from (II.16). Versions of Eq. (II.14) exist in the presence of electrogenic pumps and require only rescaling of permeabilities by factors depending on the stoichiometries of electrogenic pump, see [39]. Another common mathematical definition of membrane voltage is the Millman's equation (a.k.a. Chord Condutance Equation). It is similar to GHK voltage equation in that it assumes no electrogenic transport and steady-state so Eq. (II.16) can be used to derive membrane voltage. The mathematical form of the voltage is however distinct from GHK voltage equation due to a different kinetic model for passive diffusion [40].

We are now set to discuss why we will use the *"static"* form of membrane voltage Eq. (II.13) rather than one of the more commonly used *"dynamic"* forms of membrane voltage, of which Eq. (II.14) is an example. Our argument can be broken down into four parts:

1. Static Voltage is Valid Dynamically. As opposed to GHK voltage equation (II.14) and alikes, the mathematical definition of membrane voltage we will use Eq. (II.13) is valid dynamically, *i.e.* out of steady-state. Although, we do not study time-varying behaviours in this thesis, this still supports the general use of the *"static"* rather than the *"dynamic"* definition of membrane voltage.

2. Static Voltage Requires knowledge of Less underdetermined parameters. When using *"dynamic"* definitions of membrane voltage, one requires for each considered ionic species setting one (often underdetermined) parameter, *e.g.* the permeability for GHK voltage equation, conductance for Millman's equation. As discussed in the final chapter, permeability of the membrane to each ion depends on many factors including the considered organism and the environmental condition. Such that besides neurons, electrophysiological behaviours of which have been extensively studied, the permeability of the membrane to each ion is in general not known with precision. This is in particular the case for *E. coli*, the model organism we will study in this

electroneutral pump does not *directly* change the charge of the cell. As we shall see later in this thesis, and quite counterintuitively, electroneutral pump can however contribute to make the cell electrically charged, in synergy with other electrogenic pumps.

thesis, for which, to our knowledge, no experimental measurements of ionic permeabilities are available. The *"static"* definition of membrane voltage requires only setting of one such (potentially depending on the organism and the environmental condition) parameter, a.k.a. the membrane capacitance, for which several experimental assessments are available, including for *E. coli* [41].

3. Static Voltage is invariant by the transport the cell has access to. As discussed before, there are as many *"dynamic"* forms of membrane voltage[6] than there are cells with different ionic transporters. Indeed, picking an appropriate *"dynamic"* form requires knowledge of which ionic transporters are available for the cell and what are their stoichiometries. Such is not the case for the *"static"* definition of membrane voltage, which is invariant by such considerations. This will reveal important in this thesis as we will be able to segregate the problem of voltage maintenance into two distinct steps: *(i)* how voltage depends on the intracellular composition and *(ii)* how availability of specific transport systems restricts which intracellular configurations are *achievable* by the cell.

4. Static Voltage is invariant by the choice of kinetics. As highlighted by the comparison between GHK voltage equation and Millman's, such *"dynamic"* definitions of membrane voltage require some assumptions to be made with respect to the kinetics of passive diffusion of ions across the membrane (*i.e.* how the rate of ion's passive diffusion depends on membrane voltage and concentrations). As discussed in [42] and chapter 1 and 2 of this thesis, there exists multiple kinetic models for the passive transport of ions across the membrane and it is not known with certainty which kinetic model best describes a given cell in a given environment. Once again, the *"static"* form we use is invariant by such considerations. Thus, we will be able in this thesis to analyze how the choice of passive diffusion's kinetics pertains to cellular behaviours after having set the voltage maintained by the cell.

It would be however unfair at this stage to call for *intrinsic* superiority of the *"static" versus* the *"dynamic"* definitions of membrane voltage. Indeed, they are rather fit to answer different types of questions in relations to the available experimental methods. For instance, GHK voltage equation can be seen as a rather

[6] Some of which may be equivalent, for instance when comparing two cells possessing only electroneutral transporters as discussed earlier.

simple model of how permeabilities contribute to setting the resting membrane potential[7]. As we showed, this model can be derived from the *"static"* definition of membrane voltage we defined in Eq. (II.13) that we will use in this thesis. The success of GHK's *model* for membrane voltage (rather than definition[8]) should not come as a surprise as it directly links permeabilities to membrane voltage. Indeed, tuning permeabilities is one of the core mechanism underlying action potential of mammalian cells, we should see in the next paragraph is the main phenomenon around which electrophysiology was initially built.

We thus far discussed *what is* membrane voltage (or how to compute it) and ignored the most interesting part of the discussion from a biological standpoint:

What are the physiological functions of membrane voltage ?

Historically, membrane voltage first was recognized as a variable which main function was to enable fast-paced communication between two cellular localization *via* action potentials. Key steps of a the action potential are *(i)* depolarization of a cellular location from a resting membrane voltage followed by *(ii)* repolarization and *(iii)* return to the resting membrane voltage [43]. The mechanism of action potential transmission was demonstrated by [44], wherein the membrane potential in Eq. (II.15) was shown to be controlled by voltage-gated channels (modulating the ionic current on the right-hand side *via* modifications of ionic permeabilities), enabling the mathematical reproduction of the experimentally observed time-dependent membrane potential during an action potential. In Mammals, the steady-in-time value that takes the membrane voltage takes outside these action potentials (termed *resting* membrane potential) has however been overlooked for a long time, considered to be merely a variable enabling action potential rather than having an importance of its own [45]. Many studies have since demonstrated the importance of regulating the resting membrane potential in diverse mammalian cells, as shown in figure 1.

[7]Note that the fact that the resting potential is usually much higher in mitochondria and bacteria than in neurones does not matter much with respect to the choice between the static and the dynamic models, both of which are *a priori* amenable to study the maintenance of an arbitrary value of the resting potential.

[8]I personally think the term "model" is preferable in most cases than "definition", as the latter may – in my understanding – induce the idea that the equation holds independently of the context it takes place. For instance, reading "GHK's definition for membrane voltage" or "GHK's voltage equation", I would be at first inclined to ignore that equation (II.14) does not necessarily hold for cells with non electroneutral transporters.

Function	Cell type	Reference
Circadian rhythm	Neurones	Belle et al., 2009
	Fibroblast	Noguchi et al., 2012
Biological sensing	Neurones	Feetham et al., 2015b
Contractility	Vascular smooth muscle cells	Nelson and Quayle, 1995
	Myofibroblasts	Chilton et al., 2005
Hearing	Cochlea outer hair cells	Ashmore, 2008
Volume control	Chondrocytes	Lewis et al., 2011a
	Retinal Muller cells	Netti et al., 2017
Secretion	Pancreatic β cells	Aguilar-Bryan and Bryan, 1999; Lin et al., 2005
Proliferation	Vascular smooth muscle cells	Nelson and Quayle, 1995
	Stem cells	Messenger and Warner, 1979
	Cancer cells	Wonderlin et al., 1995
Cell cycle	T-cells	Amigorena et al., 1990
	B-cells	Neher and Sakmann, 1976
Cancer progression	Melanocytes	Chernet and Levin, 2013a,b; Blackiston et al., 2011
Migration and wound healing	Corneal epithelial cells	Reid and Zhao, 2014; Chifflet et al., 2005
	Skin keratinocytes	Nuccitelli, 2003
Pigmentation	Skin melanocytes	Bellono et al., 2013
	Uveal melanocytes	Hodgkin and Huxley, 1952b
	Retinal pigment epithelium (RPE)	Cone and Tongier, 1973

TABLE 1: Figure taken from [45]. Non-exhaustive review of the functions of the resting membrane potential in different types of Mammalian Cells.

It now seems quite interesting to me to compare the historical developments of electrophysiology in animal tissues and in bacteria, organelles. The discovery that animal tissues respond to electrical impulse can be tracked back as far as the 18^{th} century and the first recording of membrane potential (during an action potential) were performed in the mid-1860s [46]. The basis of electrophysiology's modern theoretical framework only came in the 1940s-1950s and were mainly developed to explain the action potential in synergy with newly developed techniques allowing direct measurement of ionic currents across the membrane, a.k.a. voltage clamp [47]. This experimental technique not being available for small cells/organelles such as bacteria, mitochondria, chloroplasts, the existence of an electric potential across the membrane of bacteria and eukaryotic organelles such as mitochondria and chloroplasts was first theoretically postulated [48] years before it was measured, by means of intracellular concentration measurements of a charged particle not pumped by the cell *via* Nernst Equation, *e.g.* [49]. These days Nernst equation is the most common way of measuring membrane potential in bacteria, a matter we will discuss further in chapter 1. As opposed to animal cells, where the main topic of interest started of dynamical behaviours of membrane potential (with resting membrane potential being of little interest), in bacteria/mitonchondria/chloroplast the pioneer studies were with respect to the resting membrane potential with dynamical behaviours of membrane potential in bacteria found to have signalling functions only a few years ago [50]. In particular, resting membrane potential in bacteria, mitochondria and chloroplasts (we will refer to as simply membrane

voltage from now on) was postulated by Peter Mitchell [48] to be necessary to the energy transduction from products of substrate phosphorylation (NADH, FADH) to ATP. This hypothesis was contradicting the dominant view at the time: that transduction from NADH to ATP was chemical [51], *i.e.* not involving a physical force such as electrostatic [52]:

$$\mathrm{AH_2 + B + C \rightleftharpoons A\text{–}C + BH_2} \qquad \text{(Pre-Mitchell View, Step 1)}$$

$$\mathrm{A\text{–}C + ADP + P_{\mathit{i}} \rightleftharpoons A + C + ATP} \qquad \text{(Pre-Mitchell View, Step 2)}$$

Where here the half-reaction between B and $\mathrm{BH_2}$ is for cycling of the products of substrate phosphorylation and A–C is the hypothesized (at the time) energy-rich intermediate required for energy transduction between *e.g.* NADH and ATP. Mitchell hypothesized that this energy transduction was rather indirect, *i.e.* mediated by electro-chemical gradients of protons/hydroxide ions which is the cornerstone of the modern understanding of the coupling between respiratory chains and ATP synthesis[9]:

$$10 \cdot \mathrm{H_{\mathit{i}}^+ + NADH + H_{\mathit{e}}^+ + 1/2 \cdot O_2 \rightleftharpoons 10 \cdot H_{\mathit{e}}^+ + NAD^+ + H_2O} \qquad \text{(Modern View, Step 1)}$$

$$3.3 \cdot \mathrm{H_{\mathit{e}}^+ + ADP + P_{\mathit{i}} \rightleftharpoons 3.3 \cdot H_{\mathit{i}}^+ + ATP} \qquad \text{(Modern View, Step 2)}$$

Here shown with contemporary evaluation of the stoichiometries for the *oxidative* respiratory chain [10]. During the first step, chemical energy is provided by NADH reduction to build up an electrochemical gradient of protons directed inward (for bacteria) or outward (for mitochondria)[11]. This also result in global deacidification since a free proton is attached to water. During the second step, protons

[9] Although initial developments by Mitchell contained many flaws, as highlighted by [52]. Interestingly, a debate occured between Boyer and Mitchell. The former initially disagreed with the idea that the energy transduction from NADH to ATP was mediated by a proton gradient, based on its inability to foresee *how* (the catalytic mechanism by which) F1Fo was making use of the electrochemical gradient of protons to make ATP and his gradual acceptation of the chemiosmotic theory was conjoint with research on the catalytic mechanisms of F1Fo. Though the understanding on the F1Fo catalytic mechanism of Mitchell has been, to put it midly, incomplete, as has been examplified by his communication with Boyer, he did not think as understanding the catalytic mechanism of F1Fo to be a necessary condition for the main components of chemiosmotic theory to hold [53].

[10] Stoichiometries are discussed in chapter 2. Note that there are other types of respiratory chains than the *oxidative* one, *e.g.* nitrate respiration as shown in ending chapter of this thesis.

[11] Note that saying that the proton gradient is oriented inward/outward mean that protons spontaneously move inward/outward.

flowing along their electrochemical gradient (inward) provide an energy source that is used for ATP synthesis. Aside from the energy transduction we mentioned, membrane voltage is now recognized to be determinant in many bacterial functions as summarized in figure 3. In this thesis, as discussed later, we will focus on the interplay of membrane voltage, Proton Motive Force and extra/intracellular pHs.

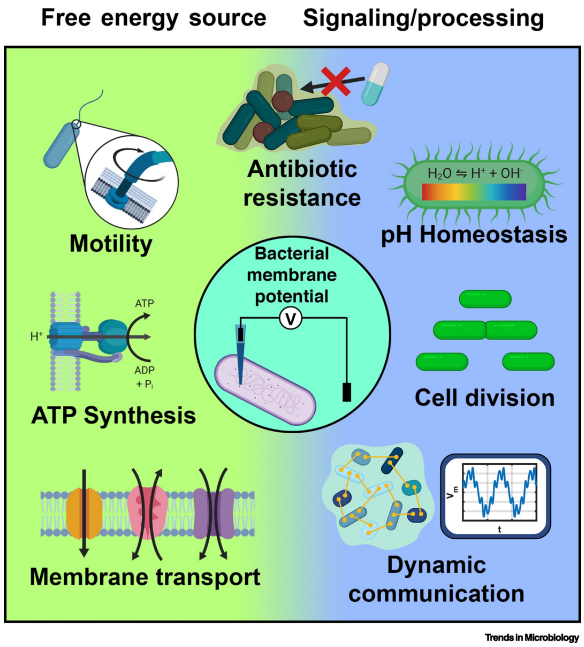


FIGURE 3: Figure taken from [54]. Scheme depicting the known functions of membrane voltage in bacteria. The main focus of this thesis is elucidating how membrane voltage play a key role in pH homeostasis and how it is maintained.

iv. Electrochemical Gradient/Ionic Motive Forces

This now seems a good place to introduce the fourth variable on which this thesis is built (along with pH, osmotic pressure and membrane voltage). The electrochemical gradient of an ion x across the membrane ΔG_x (also termed electrochemical potential difference, Ionic Motive Force or IMF) is defined as the free energy of the passive transport[12] of x across the membrane $x_e \to x_i$ (by

[12]Facilitators of passive transport across membranes includes fatty acid flip flop (for protons) [55] or integral proteins [42].

convention oriented inward) and follows:

$$\Delta G_x = \underbrace{z_x \cdot \Delta\psi}_{\text{Electrostatic}} + \underbrace{\frac{RT}{F} \cdot \ln\left(\frac{[x]_i}{[x]_e}\right)}_{\text{Diffusion}} \tag{II.17}$$

here expressed in volt units, where z_x, the electric charge carried by x may be negative (*e.g.* if $x \equiv$ Chloride then $z_x = -1$) or positive (*e.g.* if $x \equiv$ Sodium then $z_x = +1$). The IMF (II.17) can be understood as lumping the free energy variation seeding from two distinct forces: *(i)* Electrostatic and *(ii)* Entropic (or diffusion). I next try to provide the reader with an intuition of what that quantity pertains to in relations to some canonical properties of the potential of a reaction. For instance consider the PMF (or Proton Motive Force): the potential (or free energy variation) associated to the passive transport of protons inward $H_e^+ \rightarrow H_i^+$; we depict in figure 4 three scenarios of how protons may passively move across a membrane driven by electrostatic or/and entropic forces. In particular, the right panel denotes a state of the system where the *passive* transport of protons $H_e^+ \rightleftharpoons H_i^+$ is in "*local*" equilibrium[13]. To say that the last mentioned reaction is in equilibrium is equivalent to the flux of protons flowing inward being identical to the amount of protons flowing outward *via* this reaction. The electrochemical potential (II.17) has some interesting properties with respect to the behaviour of the reaction $x_e \rightleftharpoons x_i$. Indeed, when the latter reaction is at equilibrium then $\Delta G_x = 0$ and the distribution of x across the membrane follows Nernst's equation:

$$\Delta\psi = \frac{RT}{z_x F} \cdot \ln\left(\frac{[x]_e}{[x]_i}\right) \tag{II.18}$$

which is often used to experimentally evaluate the membrane potential, as briefly discussed before and extensively reviewed in chapter 1. The sign of the electrochemical potential also informs on the direction in which x spontaneously flows: if ΔG_x is negative, then ions will flow in the *forward* direction $x_e \rightarrow x_i$, if it is positive then ions will flow in the *reverse* direction $x_i \rightarrow x_e$. This property of ΔG_x (that the direction of the reaction is set by the sign of ΔG_x) is in fact not

[13]Equilibrium is in its most general sense a property of a set (or multiple) reactions. To say that a set of many reactions is in equilibrim is equivalent to say that each of the reactions of this set is at equilibrium. A set of reactions in non-equilibrium state is one where at least one reaction is not in equilibrium. For such a system (here meant as set of reactions), one may say that the sub-system consisting of the set of reactions that are in equilibrium is in "local" equilibrium.

specific to electrochemical potential but rather pertains to the direction of any reaction r in relation to its Gibbs free energy ΔG_r [56].

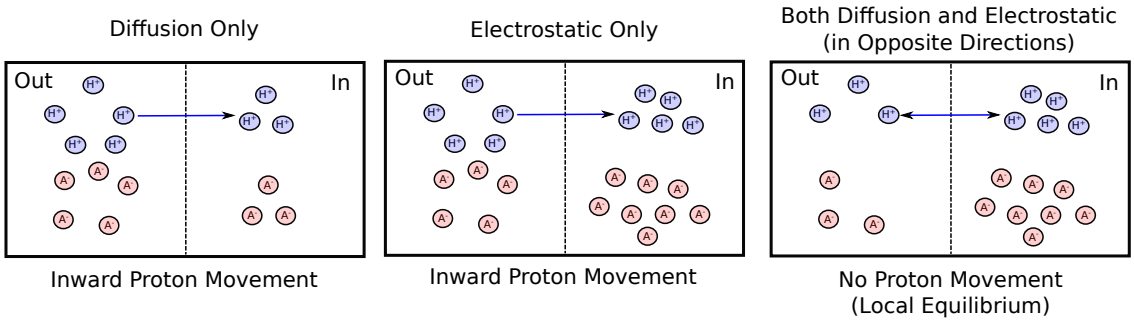


FIGURE 4: Qualitative illustration of electrochemical transport across a semi-membrane (permeable to protons, not permeable to anions A^-). (Left) No membrane voltage (null charge on both sides of the membrane), but more protons in than out, leading to entropic driven movement of protons inward (a.k.a. diffusion). (Middle) Negative membrane potential, no entropic gradient, protons move in as a result of electrotatic interactions alone. (Right) Negative membrane potential and presence of an entropic gradient in the opposite direction; *i.e.* some protons move inward due to electrostatic interactions and some move outward due to entropic force (Diffusion) leading to an equilibrium for proton transport where the state of the system is invariant by the passive transport of protons across the membrane.

III. Electrophysiological Mechanisms in Living Cells

i. Transport Across Membranes

An Overview of Passive and Active Transport Systems. Most cells maintain Ionic Motive Forces for different ions. For instance many bacteria maintain a Motive Force for Protons (PMF) [57], Sodium Motive Forces (SMF) are maintained in bacteria, mitochondria, chloroplasts [58], while Potassium Motive Force (KMF) are maintained in plant cells [59], bacteria [60] and likely in other organisms due to the presence of active transport systems for potassium. Besides their role as an energy intermediate, the function of why so many organisms maintain SMF remains unclear and is one of the thrust of this thesis. Biological membranes are leaky for ions, *i.e.* for any ion x there always exists a passive diffusion reaction $x_e \rightleftharpoons x_i$ that works in the direction that brings back the distribution of x on both side of the membrane to equilibrium, *i.e.* to $\Delta G_x = 0$ or Nernst equation (II.2). The latter property does not depend on the mechanism by which x passively diffuses across the membrane and holds independently of whether x moves across a channel, another integral membrane protein or directly through the lipid bilayer.

Indeed, the Gibbs free energy is a quantity that is *path-independent*. This can be understood as it does not depend on the specific mechanism by which the reaction is performed but only on the update on the state yielded by the said reaction. Consider for instance that proton can diffuse through the membrane *via* a channel A: $r_A := (\mathrm{A}) + x_e \rightleftharpoons (\mathrm{A}) + x_i$ or a channel B: $r_B := (\mathrm{B}) + x_e \rightleftharpoons (\mathrm{B}) + x_i$, the Gibbs free energy associated to channel A: ΔG_A and channel B: ΔG_B are such that $\Delta G_A = \Delta G_B = \Delta G_x$.
Since for any ion x there exists a passive diffusion reaction that works in the direction that brings ΔG_x to 0, maintaining a physiologically observed x motive force inevitably requires *at least* one *active* transport reaction that works in the direction that moves ΔG_x away from 0, *i.e.* that moves x in the opposite direction than does its passive diffusion reaction. The cell may "construct" (or evolve) an active transporter for x that couples passive diffusion of x: $x_e \rightleftharpoons x_i$ to one or many free energy providing reactions. We may write in general the coupling of $r_x : x_e \rightleftharpoons x_i$ with another reaction $r_y := y^\star \rightleftharpoons y$ as:

$$\sigma_y \cdot r_y \cap \sigma_x \cdot r_x := \sigma_y \cdot y^\star + \sigma_x \cdot x_e \rightleftharpoons \sigma_y \cdot y + \sigma_x \cdot x_i \tag{III.1}$$

where σ_x, σ_y are the stoichiometries, or define in which proportion r_y is coupled with r_x. The Gibbs free energy is a quantity that is additive upon lumping of reactions, such that:

$$\Delta G_{\sigma_y \cdot r_y \cap \sigma_x \cdot r_x} = \sigma_y \cdot \Delta G_y + \sigma_x \cdot \Delta G_x \tag{III.2}$$

where ΔG_y is the Gibbs free energy associated to $r_y := y^\star \rightleftharpoons y$. From the general reaction scheme (III.1) we may introduce the three most commonly found *functional* families of active ionic transport systems as depicted in figure 5:

1. Chemically Coupled/Chemically Driven Ionic Pumps. The first family of ionic active transporters couple a chemical reaction to the transport of ions. In *E.coli*, Examples of such reactions are those catalyzed by the respiratory chain (*e.g.* by the respiratory complex I), $\mathrm{F1F}_o$ and the potassium ATPase KdpFABC. Coupling stoichiometries are shown in table 2.
   Importantly, defining the coupling stoichiometries between two reactions composing an active transport reaction does not inform on the physiological direction in which it is performed. The direction in which those transport systems work (left to right or right to left in reaction (III.1)) in general

depends on the physiological condition. For instance, the direction in which F1F$_o$ works (whether it makes ATP from protons moving inward, or whether it uses ATP to move protons outward) depends on the PMF [61].

2. Electrochemically Coupled/Cotransporters. The second family of ionic active transport systems are those that draws their energy from the motive force of one particle to build motive force of another particles[14]. We show in table 2 examples of such cotransporters: ChaA, NhaB, NhaA and ClcA for *E.coli* and NHE1–10 in *Homo sapiens*. Those belong to a subtype of ionic exchangers so-called antiporters, which couple ionic movement in opposite directions. In particular, most bacteria possess many proton:cation antiporters. The reason why they are so diverse remains unclear [62]. Some cotransporters, couple movements of two particles in the same direction and are termed symporters. Although in *Homo sapiens* there are symporters coupling the movement of inorganic ions in the same direction (KCC, NCC, see table 2), symporters in bacteria, specifically *E. coli* are to my knowledge, restricted to coupling the movement of one inorganic ion and one organic substrate (glucose, lactose, proline)[15], see table 2.
   We enumerated here cotransporters than only coupled the movement of two ions. Some cotransporters couple the movement of three ions, see for instance the NKCC cotransporter in *Homo sapiens* [63].
   Also, some cotransporters have high affinity for several ions. For instance, ChaA from *E. coli* can exchange protons for *either* sodium or potassium ions, *i.e.* it catalyzes the reaction $H_e^+ + Na_i^+ \rightleftharpoons H_i^+ + Na_e^+$ in addition to the proton:potassium exchange shown in table 2.

3. Light Coupled/Light Driven Ionic Pumps. Last but not least, some transporters couple the movement of an ion or electron to de-energization of photons. Such transporters (*e.g.* Photosystem II, that couples light to the movement of electrons) are crucial to photosynthesis, where they partake in the energy transduction from light to ATP using PMF as an intermediary energy source [64]. Less known are proteorhodopsin, which also energizes the movement of protons by light. These are present in many bacteria [65].

[14] Those particles may be charged, in which case we are effectively talking of Ionic Motive Forces. When all particles involved in the cotransport are ions, then the cotransporter is termed an *ionic exchanger*.

[15] *E.coli* may possess such transporters but I never encountered anything in my readings mentioning the existence of these in *E.coli*.

4. Other types. Some active ionic transport systems do not fall in any of the most common categories mentioned above. One of such is the NaK-ATPase, arguably one of the most important ionic transport systems in mammals [66], that can be seen as a combination of two of the families of transporters introduced here, a.k.a. a *Chemically driven cotransporter*:

$$\mathrm{ATP} + 3 \cdot \mathrm{Na}_i^+ + 2 \cdot \mathrm{K}_e^+ \rightleftharpoons \mathrm{ADP} + \mathrm{Pi} + 3 \cdot \mathrm{Na}_e^+ + 2 \cdot \mathrm{K}_i^+ \qquad \text{(III.3)}$$

which use ATP hydrolysis to drive the antiport of sodium and potassium.

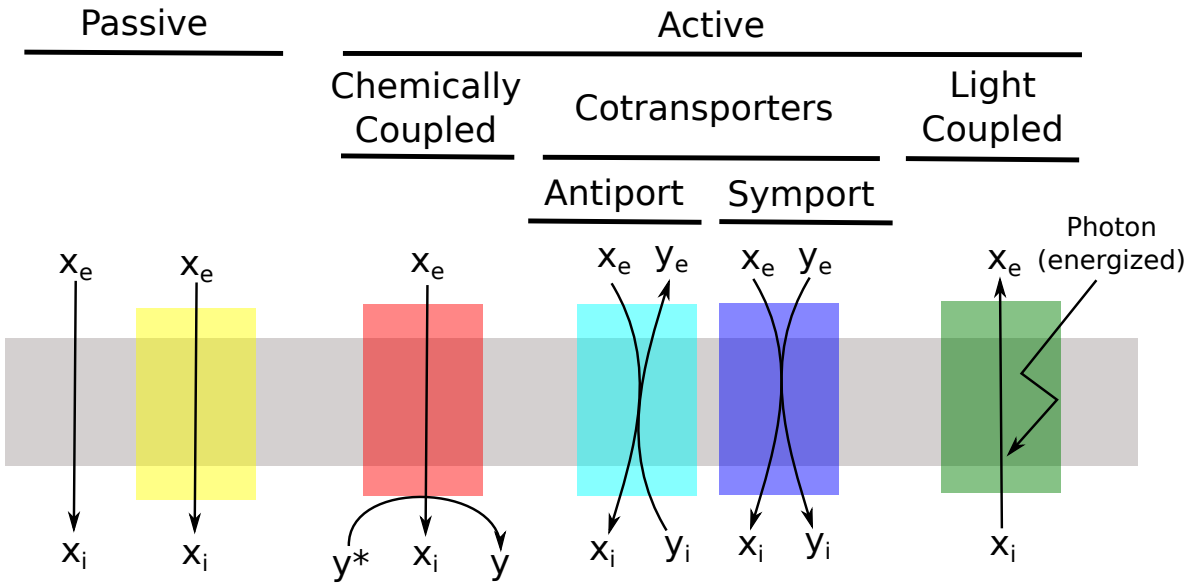


FIGURE 5: Scheme of the main families of transport systems. Some common transport systems do not fall in any of the families shown, for instance: *(i)* the NaK-ATPase is a chemically coupled antiporter, *(ii)* NKCC cotransporter moves three different types of ions simultaneously (Na^+, K^+ and Cl^-). The coupling direction shown for the light coupled transport system is indicative and could potentially be different, *i.e.* an energized photon allows inward movement of x and not outward as depicted. Direction of transport is indicative and can *a priori* be reversed, *e.g.* the antiport reaction shown in the direction $x_e + y_i \to x_i + y_e$ could work in the opposite direction: $x_i + y_e \to x_e + y_i$ depending on the electrochemical composition on both sides of the membrane.

Unicity and Diversity of Active Transport Systems. It is at this stage important to note that we presented in the previous paragraph a *partial* functional characterization of these transporters, as highlighted by the outsiders NKCC and NaK-ATPase that do not fall strictly in any of the functional categories we defined. In fact, functional classification of ionic transport systems does not relate to their phylogenetic classification, *e.g.* two distinct antiporters (falling in the same functional category) can be, evolutionarily speaking, further apart than two

Transporter	σ_x	x	σ_y	$y^\star$	y	Reference
F1F$_o$ (*E. coli*)	3.3	H^+	1	ADP + P_i	ATP	[67]
Respiratory Chain (*E. coli*)	10	H^+	1	$NAD^+ + H^+ + H_2O$	1/2 O_2 + NADH	[68]
KdpFABC (*E. coli*)	1	K^+	1	ADP + P_i	ATP	[69]
NHE1–10 (*H. sapiens*)	1	H^+	1	Na^+_i	Na^+_e	[70]
ChaA (*E. coli*)	1	H^+	1	K^+_i	K^+_e	[71]
NhaB (*E. coli*)	3	H^+	2	Na^+_i	Na^+_e	[72]
NhaA (*E. coli*)	2	H^+	1	Na^+_i	Na^+_e	[73]
ClcA (*E. coli*)	1	H^+	2	Cl^-_i	Cl^-_e	[74]
LacY (*E. coli*)	1	H^+	1	Lactose out	Lactose In	[75]
GlcP (*S. epidermis)*	1	H^+	1	Glucose out	Glucose In	[76]
PutP (*E. coli*)	1	Na^+	1	Proline Out	Proline In	[77]
NCC (*H. Sapiens*)	1	Na^+	1	K^+_e	K^+_i	[78]
KCC (*H. Sapiens*)	1	K^+	1	Cl^-_e	Cl^-_i	[79]
Proteorhodopsin	1	H^+	1	photon (de-energized)	photon (energized)	[80]
Photosynthesis	???	H^+	???	photon (de-energized)	photon (energized)	[64]

TABLE 2: List of various ionic active transport systems as parametrization of the reaction scheme (III.1).

transporters falling in distinct functional categories[16] as highlighted by [81]. Also, the quite lengthy enumeration of some ionic transport systems we made in the previous paragraph does not even come close to the diversity of such transport systems in living systems. Indeed, the most up to date comprehensive transporter database accounts for more than ten thousands distinct transport systems, although only a (significant) portion of which are ionic active transport systems [82]. As shown in the same paper, many phylogenetic families of ionic transport systems are virtually present in every kingdom of life, demonstrating that a lot of these systems were and still are a necessary component to the evolutionary success of many very different organisms. In particular, both archaea and eubacteria share strong structural homology for respiratory chain components and ATP synthase, suggesting that LUCA (Last Unknown Common Ancestor) harnessed energy *via* chemiosmotic coupling which may call for such cellular features being as essential as ribosomes for early life forms [83]. Strong homology of ionic transport systems in eubacteria, archae and eukaryotes is not restricted to those involved in energy transduction, see `http://www.tcdb.org/` [82], suggesting that LUCA possessed voltage-gating channels, proton:sodium/potassium antiporters, *etc.* This is consistent with the lack of closely related ionic pump from the IT superfamily among phylogenetically distant organisms (including archeas, bacteria), pointing out to the rarity of horizontal gene transfer events for these pumps [84]. One such family of ionic transporters is the CPA2 superfamily, that includes NhaA and a subset of

[16] Analogous to the canonical example that birds and bats evolved the ability to fly in phylogenetically unrelated ways.

the NHE1–10 (10 different antiporters) [85]. Consequently, electrophysiology, as the ability to control/generate electrochemical gradient *via* active ionic transport systems may be considered a common denominator of most life forms.

Physiological Functions of Active Transport Systems. The last statement should at this stage not come as a surprise. Indeed, not only electrochemical gradients are themselves important to power transport of various inorganic and organic molecules, but also intracellular pH, osmotic pressure, membrane voltage are important for macromolecule stability and intracellular biochemistry (pH_i), volume consistency and survival (osmotic pressure), energy transduction and signaling (membrane voltage). In fact, the three latter cellular variables and the electrochemical potential of any ionic species are interdependent, such that when the cell "choses" to maintain IMF for a specific ion it also impacts more or less directly pH_i, osmotic pressure and membrane voltage. For instance, consider that the cell maintains a given Sodium Motive Force (SMF) *via* active sodium transport systems. Given an extracellular sodium concentration, a choice of SMF will impact the intracellular sodium concentration and the membrane voltage *via* Eq. (II.17). The intracellular concentration of sodium and the membrane potential are related *via* Eq. (II.13), and intracellular sodium concentration impacts osmotic pressure Eq. (II.12). Membrane potential will then impact every IMF *via* Eq. (II.17) and in particular the PMF, thus the intracellular pH[17]. Also, different IMFs may depend on each other if, *e.g.* the SMF is maintained by a PMF driven ionic transporter. The network of how a choice of IMF (red) impacts the cellular physiology (green) in a given environment (blue) si shown in figure 7. Although any four variables in 7 can be chosen to solve the electrophysiological state, considering the two IMFs as control variables is practical because the interval of values an IMF must be in can be derived from thermodynamic considerations having specified which ionic transport systems are available and the chemical potential of the reactions that are coupled to the transport of these ions. We will discuss this topic in chapter 2 and more extensively talk about it in the discussion of the thesis.

[17]This provides an hypothesis other than the common one (use of SMF as an alternative to PMF in energy transduction processes) to the function of active sodium transport systems; which may potentially explain why active sodium transport systems are so widespread and diverses among every phyla.

ii. Maintenance of Electrophysiological Homeostases

Of the Intertwined Nature of Electrophysiology. We just saw that, conceptually, the activity of any ionic transporter can play a part in the maintenance of every electrophysiological variables that are deemed important to the cell. However[18], electrophysiology; we shall define here as *The coordinated maintenance of IMFs, membrane voltage, osmotic pressure, intracellular concentration – in particular pH_i – via active ionic transport systems and intracellular metabolism*[19] *in a given environment*; is far from being a *mechanistically* unified field. Such is especially the case in bacteria. Although PMF, membrane voltage, pH_i are known to covary across species and across pH_e for a given species (see figure 6 taken from [4]) thus are *phenomenologically* (or empirically) connected, a unified view on what are the underlying mechanisms to these correlations is lacking. Bacterial electrophysiology is in that sense a non-unified field from a *mechanistic* standpoint, meaning that a given ionic transport system is often seen as playing a part in the maintenance of one electrophysiological variable independently of the other. We may support our view with two examples. First, in recent reviews on osmo-regulation in bacteria, membrane voltage is never mentioned [86, 87, 28, 88] although many transporters involved in osmo-regulation actively move ions across the membrane, thus impact IMFs and membrane voltage. pH is in those reviews only mentioned once in [28, 88], far from presenting a comprehensive view on how they are interconnected. Finally, some authors mention that ionic transport systems shall make different contributions to osmotic and pH homeostasis, without however exploring in details those interactions [4]. Roughly, by these reviews, the field of osmotic pressure maintenance can be considered as the interplay between extra/intracellular monovalent ions (mainly sodium and potassium) and organic osmolytes (*e.g.* glutamate, sucrose) with osmotic pressure, as depicted in figure 7. Second, the field of pH homeostasis mostly focuses on the interplay between the PMF, the membrane potential, extra/intracellular pHs [89, 7, 4, 90]. While membrane potential is often measured in the study of pH_i homeostasis, it has been considered a phenomenological variable, one which value does not emerge from the conceptual models of pH_i homeostasis. This is examplified by most studies about pH_i homeostasis

[18] For reasons that, while certainly interesting to discuss, are beyond the scope of this thesis.

[19] Although not discussed in this introduction, the intracellular quantities of metabolites and their electric charge contribute to membrane voltage and osmotic pressure as suggested by how we have defined them. We will discuss the role of organic molecules in electrophysiological maintenance in chapter 1 and 2.

ignoring how membrane voltage depends – as outlined in figure 7 – on variables else than the PMF or the pH_i, *i.e.* other IMFs, intracellular composition in *e.g.*, sodium, potassium, chloride and intracellular content in charged osmolytes such as glutamate or arginine. Potential interplay of pH_i homeostasis with osmotic pressure has also been ignored.

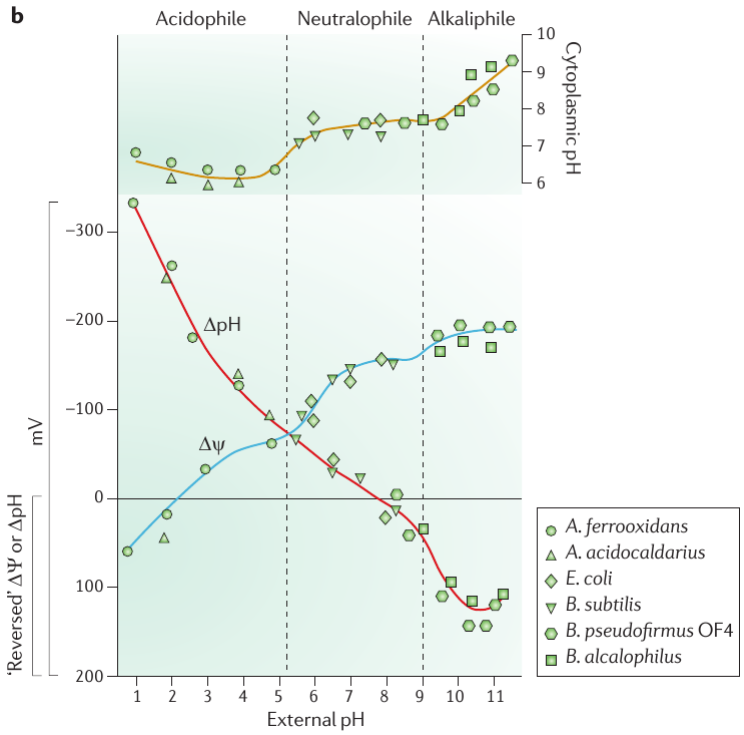


FIGURE 6: Figure taken from [4]. Phenomenology of the relationship between $\Delta pH = 60 \times (pH_e - pH_i)$ and membrane voltage $\Delta\psi$ (both in mV units) for different bacterial species across different extracellular pHs. PMF (in mV) can be computed as $\Delta\psi + \Delta pH$. While pH_i is maintained in a narrow range (relative to the range of pH_e), membrane voltage is positive at very acidic pH_e and becomes more and more negative as pH_e increases.

Current Paradigm for Mechanisms of pH_i homeostasis in bacteria. In the light of the contemporary view on the mechanisms of pH_i homeostasis, the last statement we made in the previous paragraph can seem quite surprising. Indeed, from the same reviews as before, the two main mechanisms of pH_i homeostasis involve: *(Mechanism I)* proton:ion antiporters (for potassium, sodium, chloride) and *(Mechanism II)* capture/release of protons by amino acids (such as glutamate) *via* decarboxylation reactions (that modulates the charge carried by intracellular organic osmolytes). We can already see at this stage from figure 7 that those

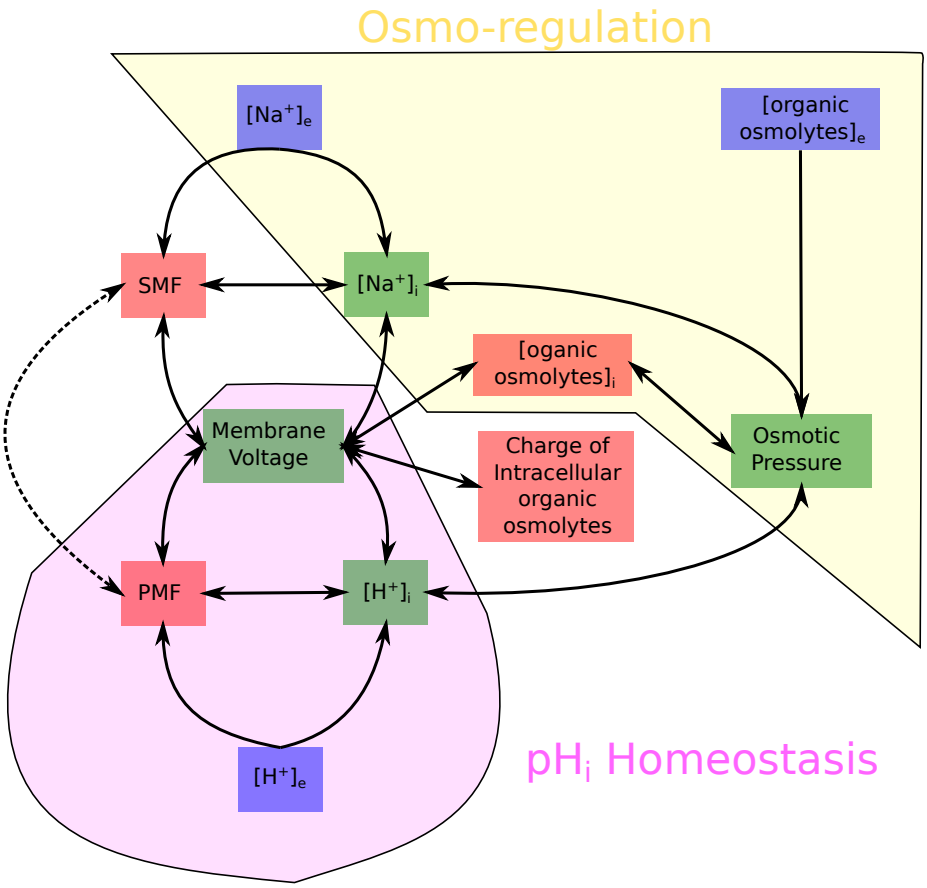


FIGURE 7: How electrophysiological variables depend on each other in a simple model with only two inorganic species (sodium and protons). Here the IMFs are considered as control variables and the extracellular concentrations as fixed constraints. In green are the cellular variables we can solve for. Note that for this model with two types of particles, there are four equations (electrochemical potential for SMF and PMF, osmotic pressure and membrane voltage) that link the eleven variables shown, such that fixing the three extracellular concentrations, the electrophysiological state can be solved by setting any of the 4 remaining 8 variables. The two shaded area denote the variables scientists in the osmoregulation (yellow) and in the pH_i homeostasis (magenta) fields study. We show here only Na^+ for space purposes, a more complete overview would require representation of chloride, potassium and potentially other ions. Each additional ion has three associated variables: IMF (red), intracellular concentration (green) and extracellular concentration (blue). The connections of each additional ion are identical to that of Na^+ with other state variables.

two mechanisms directly can tune state variables involved in membrane voltage maintenance (SMF, $[Na^+]_i$ for *(Mechanism I)*, charge of intracellular organic osmolytes for *(Mechanism II)*). In the field of pH_i homeostasis however, the impact of such mechanisms on membrane voltage is most often disregarded, which will prove inconsistent with the integrated electrophysiological model we define in chapter 2. The current view on pH_i homeostasis is that *(Mechanism I)* directly modulate pH_i *via* export/import of protons while *(Mechanism II)* directly modulate pH_i *via* capture/release of protons. Such that proteins involved in tolerance to acid challenges are hypothesized to function to *directly* deacidify the cytoplasm whereas proteins involved in tolerance to alkaline challenges are hypothesized to function to *directly* acidify the cytoplasm. The paradigmic view is shown in figure 8, where in response to acid challenge, *ClcA* works to deacidify the cytoplasm by moving protons out and chloride in, Acid Resistance Systems (ARS) deacidify the cytoplasm by attaching protons to amino acids *via* decarboxylation reactions. In response to alkaline challenge, *NhaA* moves protons in thereby directly acidifying the cytoplasm.

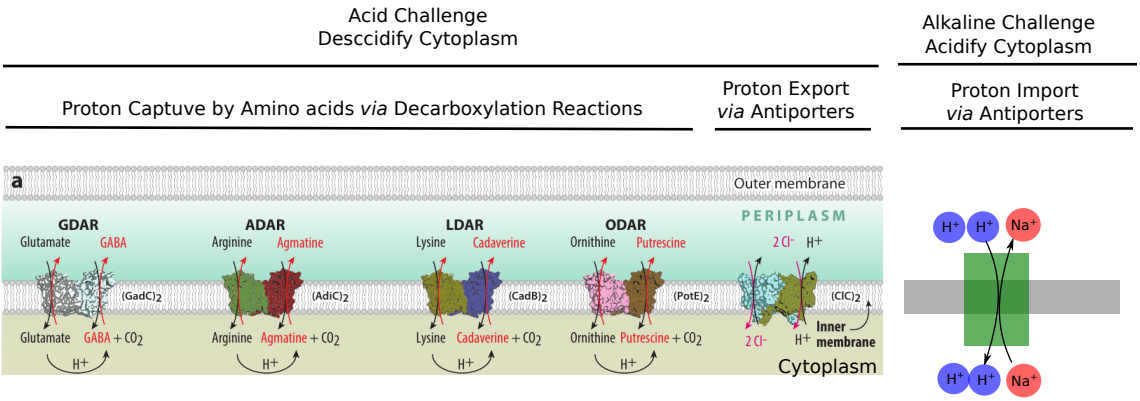


FIGURE 8: Paradigmic view of how pH_i is maintained in response to variations in extracellular pH. (Left) Bacterial response to acid challenge (pH_e is shifted to low values), taken from [90]; (Right) Bacterial response to alkaline challenge (pH_e is shifted to high values).

Mechanisms of Voltage Maintenance. In fact, rationalizing why most scientists have ignored how the mechanisms they identified as playing a role in pH_i homeostasis could impact voltage, the mechanisms by which bacteria maintain membrane voltage remains up to date an open question [54]. Such is not the case in mammals where the NaK-ATPase, reaction (III.3) is identified as the main component of resting membrane potential maintenance [17, 91], although the impact of other ionic exchangers on the value taken by the resting membrane

potential in such organisms is most of the time ignored, a topic we shall come back to only at the end of this thesis.

iii. Regulation and kinetics of transport across membranes.

The complexity of transporters' kinetics. What is likely considered a crucial component of most biological models (as in mathematical models) is defining how: *(i)* gene expression is regulated and *(ii)* how the rate at which enzymes (transporters in our case) catalyze reactions depends on the state of the system. In this thesis, we won't explicitly specify the kinetics of transporters, nor how their expression depends on the state of the system.

Indeed active ionic transporters have kinetic forms that are particularly complex, especially when comparing them to the classical kinetic form Michaelis-Menten shaped that is often assumed for modeling biochemical processes occurring within cells [92]. First of all, the activity of ionic transporters does not depend solely on concentrations (as it is expected for biochemical processes) but also on the membrane potential. The kinetics of any active ionic transporters can have complex dependency on membrane voltage beyond the general dependency of the rate of a reaction on its Gibbs free energy which we discuss specifically in the next subsection. In particular, alike to mammalian cells, bacteria possess voltage-gated ion channels and mechanosensitive channels [93] effectively making permeability of the membrane for ions voltage and pressure dependent. Active transporters' activities also are voltage dependent [89, 17]. Notably, some ionic transport systems exhibit strong pH-dependent activity as it is the case for some of the *E.coli*'s antiporters we modeled in this thesis. For instance, *NhaA* is active only at high pH, which involves a pH-sensor embedded in the protein [94]; *NhaA* can thus be seen as a *pH-gated* transporter. The state-dependent activity of such active ionic transporters can be very complex with for instance sodium concentrations impacting the sensitivity of the transporter's activity on membrane voltage [95, 96]. Outer membrane channels also integrate in a complex fashion an impressive amount of different signals: voltage, pH, ionic concentrations, *etc.* [97]. Our choice of not specifying the kinetics can thus be understood as an attempt of constructing electrophysiological models that do not lose generality by

specification of the antiporters' kinetics a cell possesses (beyond stoichiometric and thermodynamic consistency considerations). For instance, the kinetic models of active ionic transporters in [17] have more than ten underdetermined parameters.

The kinetic complexity of proteins involved in electrophysiological processes therefore seems far greater than that of proteins involved in biochemical processes. Here we mean by complexity, the variety of the signals these proteins integrate independently of gene regulation. Indeed, while regulation of gene expression can be seen as the dominant factor impacting the rate of biochemical reactions (*via* tuning the number catalysts), this regulation paradigm does not seem very effective at explaining how the rate of reactions involved in electrophysiological processes depends on the environmental and physiological states, in spite of (obviously) their expression being also transcriptionally regulated, for instance, the expression of *NhaA* increases with extracellular sodium concentration [89]. If the cell is seen as an automaton: a self-operating machine wherein gene expression is the control mechanism designed to automatically adjust its intracellular composition in response to environmental fluctuations, the electrophysiological component of a cell can almost be seen as an automaton within the automaton, by its ability to adjust the activities of the various ionic transporters independently of gene expression in response to environmental/physiological changes, therefore enabling adaptation of the electrophysiological variables on much shorter time scales than the coordination of its biochemistry. This motivates how we will model electrophysiology in chapter 3, *i.e.* as a set of cellular subprocesses behaving almost independently than the rest of cellular biochemical processes, the only interactions between the two being the energy demand of the electrophysiological submodel and the PMF-dependent ability to transduce energy from NADH to ATP. Also, the need for having such fast-paced control on electrophysiological variables suggests how crucial maintenance of such physico-chemical properties are important for cell survival. Osmotic pressure is a particularly good example, since increase of it beyond a certain threshold will simply result in cytolysis, therefore motivating the need for the ability to delegate to the physiological periphery (as in not directly under control of gene expression) some adaption responses.

Thermodynamically Consistent kinetics. Not specifying the kinetics of a transporter does not necessarily mean chosing its rate independently of the state

of the system. Rather, I mean that the functional form defining how its rate depends on the state must generic to all transporters involved in the model. One such general kinetic form accounts for "*thermodynamically consistent kinetics*", that must hold for any flux j_r of a reaction r (thus including transporters) in relation to its Gibbs free energy is [56]:

$$j_r = j_r^+ \cdot \left(1 - e^{\frac{F}{RT} \cdot \Delta G_r}\right) \tag{III.4}$$

Where j_r^+ is a variable that embeds the kinetic complexity of the reaction. The study of the kinetics of a reaction can thus be seen as the study on how j_r^+ depends on the state of the system, while the multiplication by $\left(1 - e^{\frac{F}{RT} \cdot \Delta G_r}\right)$ derives in part from thermodynamic considerations. Indeed, It seeds from a constraint which is often referred to as *local detailed balance*, *i.e.* that for an arbitrarily complex reaction scheme r *composed of elementary reactions* to have null rate $j_r = j_r^+ - j_r^- = 0$ is equivalent to its associated gibbs free energy being null too $\Delta G_r = 0$ (that is, assuming that $j_r^+ \neq 0$); equivalently:

$$\frac{F}{RT} \cdot \Delta G_r = \ln\left(\frac{j_r^-}{j_r^+}\right) \tag{III.5}$$

Meaning that one must be able to derive the thermodynamic quantity ΔG_r from kinetic considerations. In other words, *Thermodynamically consistent kinetics* are restricted to definitions of how j_r^+, j_r^- depend on the state that follow Eq. (III.5). For instance, it is straightforward to rewrite the steady-state kinetics for ionic transporters with quite complex mechanisms of reactions from [17] (*e.g.* Eqs. (2.79), (2.97), (2.100) as in Eq. (III.4) assuming standard definition for ΔG_r. To understand the assumptions underlying Eq. (III.4) we must first introduce the notion of *elementary reactions*.

Elementary Reactions. An *elementary* reaction is a reaction that follows mass-action kinetics, *i.e.* its rate is given as the product of its reactants scaled by a

constant k_e, for a (forward) elementary reaction e:

$$\sum_{x \in \text{Reactants}} \sigma_x \cdot x \rightarrow \sum_{x \in \text{Products}} \sigma_x \cdot x \tag{III.6}$$

The (forward) rate is given by:

$$j_e^+ = k_e^+ \cdot \prod_{x \in \text{Reactants}} [x]^{\sigma_x} \tag{III.7}$$

In fact, what defines an *elementary* reaction is the invariance of k_e^+ upon environmental fluctuations, and strictly speaking an elementary reaction is only elementary conditioned on a set of environments in between which k_e does not change. Indeed, how the rate scales with the reactants' concentrations can be seen as either a necessary condition so that ΔG_e indeed scales with the logarithms of concentrations (reverse direction) or a natural consequence of the rate scaling with the number of ways (a.k.a. number of symmetries N_e, a combinatorial number) a pool of reactant can react:

$$N_e = \prod_{x \in \text{Reactants}} \frac{x!}{(x - \sigma_x)!} \approx \prod_{x \in \text{Reactants}} x^{\sigma_x} \tag{III.8}$$

Where x denotes here counts (and not concentrations) and the approximation holds for sufficiently large counts of x. Importantly, one can always say that a reaction scales linearly with the above decomposing the rate as $j_e^+ = k_e \cdot N_e$ where N_e is the number of symmetries defined above and k_e^+ is in that case the average rate per unique symmetry, which highlights that what defines elementary reactions is not uniquely the scaling of the rate with the products of reactants' concentrations but also crucially the invariance of the variable k_e across environmental conditions.

Now, the definition of elementary reactions in relation to mass-action kinetics strictly holds for chemical reactions (that do not involve other forces than entropy). To include other forces, *i.e.* electrostatics, one must just recognize that, as any other reactions, elementary reactions need to be thermodynamically consistent, thus their rate must be such that Eq. (III.5) holds. For a reaction akin to Eq. (III.6) where going from the left-hand term to the right-hand term involves crossing an

electric field for some species $x \in y$:

$$j_e^+ = k_e^+ \cdot \prod_{x \in \text{Reactants}} [x]^{\sigma_x} \cdot \prod_{x \in y} e^{-(b+1)\cdot \frac{F}{RT} \cdot z_x \cdot \Delta\psi} \tag{III.9}$$

$$j_e^- = k_e^- \cdot \prod_{x \in \text{Products}} [x]^{\sigma_x} \cdot \prod_{x \in y} e^{-b\cdot \frac{F}{RT} \cdot z_x \cdot \Delta\psi} \tag{III.10}$$

and one can check that indeed Eq. (III.5) holds. We may remark at this stage that ohmic inspired kinetics, where the intensity (proportional to the flux of ions) scale linearly with the membrane potential, are inherently not thermodynamically consistent however hold approximately when $\frac{F}{RT} \cdot \Delta G_r$ is small enough so that $e^{\frac{F}{RT} \cdot \Delta G_r} \approx 1 + \frac{F}{RT} \cdot \Delta G_r$ (first term of Taylor expansion for exponential function).

Thermodynamic consistency for non elementary reactions (at steady state).

Assuming kinetics as in Eqs. (III.9), (III.10) for elementary reactions involving electrostatic forces, decomposing a reaction catalyzed by a protein (including transporters) as a sequence of elementary reactions, the kinetic of such a reaction can be written as Eq. (III.4) at steady-state, as can be seen in many examples from [56, 17]. In the case of chemical reactions (not involving electrostatic forces), it has been shown that catalytic reactions – that are characterized by the catalycist returning to its state prior the reaction once the reaction is terminated (a.k.a. a closed reaction loop) –, decomposed in many elementary reactions must follow Eq. (III.4) at steady-state [98, **?**]. While, it is likely possible to rigorously demonstrate that the functional form Eq. (III.4) must hold at steady-state for electrochemical, closed loop reactions, I did not do it and we will therefore assume that it holds on the basis that any electrochemical closed-loop reactions in [56, 17] can be written under the form Eq. (III.4) at steady-state. The kinetics for leakage across the membrane we use from [42] can also be written under the form of Eq. (III.4), as we will show in chapter 1 and 2. Therefore, all the electrophysiological reactions we use in this thesis have the characteristic form of Eq. (III.4) which holds independently of the specifics of the mechanisms of reactions of transporters. The models we introduce in this thesis thus can be considered an intermediary layer of description of electrophysiological processes, abstracting the mechanisms of reaction of transporter r in a single time-invariant

variable j_r^+, while taking into account the constraints imposed by detailed balance (hence they are more constrained than even more abstract flux based modeling, Flux Balance Analysis (FBA) is an example of, although some developements of FBA includes detailed balanced constraints).

IV. Outline of this Thesis

Aim of this Thesis. Succintly, this manuscript is an attempt to develop an integrated view of bacterial electrophysiology. We may decompose the latter as answering three questions: *(a)* How to develop, general, *thermodynamically consistent* models including active and passive transport systems, that are able to *recapitulate* major electrophysiological variables: IMFs, pH_i, voltage, osmotic pressure; *(b)* How active transport systems need to coordinate in order to preserve joint homeostasis of pH_i, PMF, osmotic pressure upon environmental fluctuations which we will show is expected to require proton:ion antiporters in *E. coli*; *(c)* How much energy does it cost to maintain these homeostases in different environments and how these varying energy requirements can impact the growth-rate and/or the growth-yield of a bacterium. While *(a)* allows derivations of relationships between different IMFs (dotted arrow in figure 7) and is a rather methodological problem: essentially to postulate kinetic models that preserve basic thermodynamic properties, *i.e.* the direction of a reaction in relation to its Gibbs free energy and the relationship between state variables at equilibrium, *(b)* is the core contribution of this thesis and leads to some biological "discoveries" with respect to bacterial electrophysiology. *(c)* is somewhat more loosely connected and aims at bridging recent models of cellular growth [99, 92, 100] with the models of bacterial electrophysiology developed in *(b) via* evaluation of energy expenditures required to maintain a certain electrophysiological state in a given environment.

Plan of this Thesis. The work embodied in chapter 1 and 2 was performed sequentially and it is interesting in that respect to contextualize what led to my contribution in [34][20] that constitutes the chapter 1 of this thesis.

[20]This paper is also part of the Ph.D. dissertation of Leonardo Mancini who performed the majority of the work and led the project with our common supervisor Teuta Pilizota. My contribution is the mathematical modeling part of the paper.

To that end, we first need to discuss some modeling assumptions made as well as some questions asked in chapter 2. The model of *E.coli*'s electrophysiology it describes ignores the contribution of extracellular organic osmolytes and is able to relate two types of environmental fluctuations –salinity (shown as $[Na^+]_e$ in figure 7) and pH_e – to the electrophysiological state of the cell (red and green in figure 7). To benchmark the models of *E.coli*'s electrophysiology developed in chapter 2 typically requires experimental measurements of the cellular response (green & red variables in figure 7; the more the better) upon perturbations of the environment (blue in figure 7). Due to time limitations and prioritization of our interests, salinity perturbations were experimentally ignored and we focused on expertimental perturbations of pH_e. Also, experimental measurements of osmotic pressure were deemed of low interests. This can be justified by the model having qualitatively very similar behaviour with respect to active transport of ions in the small interval of osmotic pressure *E.coli* maintains (1–3 atmosphere [24, 25]). I then came across that the most interesting piece of literature to compare our theoretical predictions and experimental results with was that concerned with pH_i homeostasis. Indeed, performing early *in silico* experiments with the model of *E.coli*'s electrophysiology in chapter 2, I noticed that the model maintained pH_i by a different mechanism than what the literature has been postulating while being consistent with the membrane voltage that had been measured across different pH_e (as depicted [4]). To compare my theoretical predictions with this literature we crucially needed the ability to measure any two of the three aforementioned variables, *i.e.* $\{pH_i, \text{PMF}\}$ or $\{pH_i, \text{Voltage}\}$ or $\{\text{PMF}, \text{Voltage}\}$; the third remaining variable being interpolatable by the definition of the PMF Eq. (II.17) since we know by construction of the medium the pH_e.

For independent reasons (than the models presented in this thesis) and during my Ph.D., Ekaterina Krasnopeeva mastered measurements of pH_i by fluorescence imaging[21] while Leonardo Mancini attempted to measure *physiological* membrane voltage using fluorescent Nerstian dyes, the most popular technique up to date to measure membrane voltage in bacteria. This technique, is in principle appealing, as it allows much like fluorescence imaging of pH_i, membrane voltage readouts of a large number of cells simultaneously, on a single cell level.

However, and this is the purpose of chapter 1, Leonardo Mancini demonstrated that some of these Nernstian dyes were, at most toxic for the cell, at least altering

[21] Technique by which pH_i can be measured simultaneously on a large number of cells, at the single cell level.

cellular physiology so that any membrane voltage readout thereby obtained would be that of a stressed cell, likely not reflecting its membrane voltage in the absence of the Nerstian dye. My contribution to this work is two folds: *(1)* I showed that from a modeling point of view, addition of an electrically charged particle that is "unknown" to the cell[22] would impair membrane voltage, potentially explaining the toxicity/unreliable readout after addition of a Nernstian dye; *(2)* that the dynamics of intracellular dye concentrations could be explained by a simple model of passive electrodiffusion of the dye across the membrane along with exponentially decaying membrane voltage. This paper/chapter also introduces some of the basic concepts underlying the modeling methodology we use in chapter 2 and 3.

We therefore turned in chapter 2 to the more tedious measurement of $\{\mathrm{pH}_i, \mathrm{PMF}\}$, that was performed entirely by Ekaterina Krasneepova. Indeed, the method employed to evaluate the PMF is *via* measurements of the rotational speed of the Bacterial Flagella Motor (See methods chapter 2), which can insofar be performed only one cell at a time and has significant failure rate. Nevertheless, it allowed validation of two of the most important predictions of our model: *(i)* the ability to maintain pH_i across different pH_e is PMF dependent, *(ii)* the ability to maintain voltage is PMF dependent. Those experiments support several important shifts in the understanding of both the function and underlying mechanisms of *E.coli*'s electrophysiology, that should in principle pertain to other bacterial species. First, an underlying assumption of the model that allows recovery of the experimental observations is that proton:ion antiporters are responsible for voltage maintenance in bacteria (the action of which depends on the PMF, connecting to previous point *ii*). More specifically, proton:anion antiporters allow maintenance of positive membrane voltage by depleting the intracellular environment of negative charges while proton:cation antiporters allow maintenance of negative membrane voltage by depleting the intracellular environment of positive charges. Interestingly, taking into account osmotic pressure allows us to make a simple prescription for bacteria: if a bacterium uses proton:ion symporters to generate voltage then it will burst (a.k.a cause cytolysis)[23], highlighting the non viability of such transport systems in membrane voltage maintenance as well as what one biologist can gain by acknowledging the need for the cell to maintain simultaneously several variables, studies of which may be considered to belong to distinct subdisciplines.

[22] Meaning for which a cell does not have an active transport system available. This could seed from the cell encountering this dye at very low frequency, and therefore it may not have the opportunity to evolve dedicated systems to rescue for the dye's toxicity.

[23] hence a possible reason to why they do not seem to possess any proton:ion symporters

The second main discovery is with respect to the mechanism of pH regulation. Contradicting the paradigmic view that *E.coli* uses proton:ion antiporters and decarboxylation systems to *directly* deacidify or acidify the cytoplasm, our model supports that the value of pH_i is rather a consequence of the global coordination of transport systems, where proton:ion antiporters and decarboxylation systems are *directly* responsible for tuning the voltage and only *indirectly* responsible for pH_i maintenance in response to pH_e perturbations[24]. This highlights what is likely the main function of the ability to tune membrane voltage and perhaps explains the necessity for LUCA to possess a diversity of active ionic transport systems: the ability to perform simultaneous maintenance of PMF (required for chemiosmotic coupling, that enables higher energetic efficiency catabolisms) and pH_i (for stability of macromolecules and properly functioning biochemistry) across different pH_e.

Now maintaining time-invariant electrochemical gradients, subsequently time-invariant pH_i and osmotic pressure in a given environment requires continuous energy spending. This is what we study in chapter 3: how perturbations of the ionic composition of growth media is predicted to impact the energy requirement for the cell to remain in a "healthy, out of equilibrium, state". We then make predicates on how this relates to major determinants of the evolutionary success of a species (a.k.a. fitness): its growth yield and growth-rate. In fact, the question asked in this chapter is what initially spurred my interest in ionic transport in bacteria, the content of chapter 2, ending up becoming the core of this thesis, being an incidental discovery. I chose, to avoid redundancy and because it may seem quite far apart to the content of this introduction, to not discuss in details those problematics herein. The reader will find in chapter 3, a preliminary discussion that specifically introduces bacterial electrophysiology in relation with growth behaviours. Importantly, I do not explore in chapters 1 and 2 the effect of substrate deficiency[25], *i.e.* I assume in these chapters that the only constraints the modeled cell (that includes a choice of available reactions) is facing are thermodynamic and energetics constraints. These constraints are stringent enough to support the main conclusions of chapter 2, demonstrating that higher (than what has been most common in computational biology) level of

[24]Importantly, our hypothesis is consistent with the range of pHe where decarboxylation systems and various antiporters have been shown to be active

[25]The phenomenon by which pumping rates may become too low to support some states of the model due to insufficient quantities of substrates.

coarse graining for the kinetics of biological reactions[26] can be a more amenable approach for the modeling and understanding of electrophysiological processes.

Main Contributions of this Thesis. I show here what I deem the main contributions of this manuscript to the topic of biology:

1. *Proton:ion antiporters can be responsible for voltage maintenance.*

2. *Ability to tune membrane voltage is a necessary condition for maintaining simultaneously PMF and pHi at different pH_e, and may have originated from this necessity.*

3. *Different energy requirements to maintain a given electrophysiological state (PMF, pH_i and osmotic pressure) at different pH_e and salinity may underly the changes in growth-rate/yield that have been observed when changing the pH_e or/and salinity of a growth-culture.*

[26] I mean here by higher level of coarse graining, *kinetic* models requiring less dependent variables that given an identical state of the system are sufficient to generate any steady-state achievable by any of their less coarse-grained, thermodynamically consistent, versions.

Chapter 1

Membrane Voltage Measurements with Nernstian Dyes in Bacteria: A Cautionary Tale

I. Preamble

My Contributions to this Chapter. The content of this chapter is strictly a copy/paste of an article published under the name "A general work-flow for characterization of Nernstian dyes and their effects on bacterial physiology" in *biophysical journal* [34]. The only change I made in this thesis is the numeration of the various sections/subsections. This article seeds from the Ph.D.'s project of Leonardo Mancini (the lead author), who performed the vast majority of the *in vivo* experimental work as well as led the project with our common Ph.D. supervisor Teuta Pilizota. My contribution to this chapter consists in the entirety of the computational work. As such, I wrote the subsections i, B.5, B.6, B.7 as well as designed the mathematical models, the numerical experiments and the corresponding figures.

How this Chapter Articulates with the rest of this Thesis. Briefly, this chapter demonstrates that the most popular technique to measure membrane potential in bacteria is, well, potentially unreliable. This technique relies on the use of so-called "Nernstian Dyes" that have known valency and are assumed to equilibrate across the membrane, meaning that after some time, the voltage can be evaluated by

measuring the intracellular concentration of the said dye x *via* Nernst equation:

$$\Delta\psi = \frac{RT}{z_x \cdot F} \cdot \ln\left(\frac{[x]_e}{[x]_i}\right)$$

Note that here, $[x]_e$, $[x]_i$ denote concentrations in the extracellular and cytoplasmic space respectively, such that the membrane potential is the voltage difference between the extracellular and cytoplasmic space, thus includes the voltage difference across the periplasm[1], a topic we should discuss further in chapter 2. As a side note, if such dyes were used to measure the membrane potential across the membrane of an organelle of an eukaryotic cell, for instance mitochondria, the experiment shall consist in measuring the concentrations of the dye in the cytoplasmic space and inside the mitochondria. In particular, Leonardo Mancini shows that:

1. Wild type *E.coli* reacts very differently to addition of the lipophilic cation Thioflavine T (ThT) to the medium than a strain which does not possess the TolC active transporter, suggesting that ThT may be a substrate for TolC. If such is the case, then ThT is actively pumped and is not expected to equilibrate across the membrane and follow Nernst Equation above. Thus any membrane potential assessment relying on Nernst equation in the Wild Type is likely to deviate from the "real" membrane potential.

2. ThT is toxic for *E.coli*, thus the voltage readout obtained are that of a non-healthy cell, thus probably not accounting for the physiological membrane potential prior addition of the dye (measurement of which shall be the main purpose of any experimental method aiming at measuring membrane potential).

These two observations can be seen as first hints to one of the main message of this thesis: *Electrophysiological behaviours are strongly context-dependent, i.e. strongly depend on the environmental composition and the transport machinery a cell has access to* [2].

[1] which is not negligible, at least in *E.coli*.

[2] Although interesting, note that in this work no other Nernstian dyes were used in an attempt to measure the membrane potential of *E.coli*. These conclusions are thus hypothetical, as it is plausible that observed toxicity of ThT is specific, *i.e.* the mechanism mediating the toxicity is not reproducible with a different dye

Accordingly, the mathematical models in this chapter demonstrate that addition of charged particles that equilibrate across the membrane (as are Nernstian dyes) tends to make membrane potential closer to 0. This phenomenon qualitatively holds independently of how the model generates the physiological membrane voltage prior addition of the dye. The models introduced in this chapter are minimal and introduce basic concepts that will pertain to the following chapters as well as the discussion. In spite of their simplicity, they demonstrate however that the extent to which addition of a Nernstian dye will mitigate membrane voltage depends on the precise mechanisms by which the cell maintains its physiological membrane potential. This supports once more the context-dependence of electrophysiological perturbations. In addition, we show in this chapter that the simple kinetic forms that we will use for leakage along this thesis (passive diffusion of ions across the membrane) can explain the dynamics of dye entry into *E.coli* assuming exponential decay of membrane potential following addition of the dye to the growth-medium (which is supported by Bacterial Flagella Motors measurements). This demonstrates once more, in a different scenario (see [42] for other scenarii), how well these kinetic descriptions can account for electrodiffusive transport across biological membranes.

Remarks on the models in this chapter. I would like to first highlight one apparent limitation of the model: if the model predicts qualitatively that addition of a charged particle equilibrating across the membrane will depolarize the cell, it predicts that it shall happen at a large extent only for extracellular ThT concentrations much higher than what is used experimentally by Leonardo Mancini. This suggests that ThT may impair electrophysiological capabilities of *E.coli* by mechanisms the model does not account for or/and that ThT can bond to intracellular particles as discussed at the end of this thesis. The second remark is with respect to the last appendix of this chapter, which may lead to some confusions. Indeed, I write that the membrane potential is the sum of the voltage across the outer membrane and that across the inner membrane. Later in this thesis, we shall specifically talk of membrane potential as the voltage across the inner membrane, that is the only potential relevant to most ionic pumps, which are located within the inner membrane. Finally, the choice of symbol for some variables is not the same in this chapter than the rest of this thesis. Notably we use in this chapter V_m for membrane potential whereas $\Delta\psi$ is used in other chapters of this thesis. To avoid confusion about symbols, the reader may refer to

appendix ??? (**TODO**), showing the symbol conversion table. Finally, footnotes are specifically used in this chapter to elaborate on questions asked by my thesis's examinors.

A general work-flow for characterization of Nernstian dyes and their effects on bacterial physiology

Leonardo Mancini[1], Guillaume Terradot[1,*], Tian Tian[2,*], YingYing Pu[2], Y Li[2], Chien-Jung Lo[3], Fan Bai[2] and Teuta Pilizota[1,+].

[1]Centre for Synthetic and Systems Biology University of Edinburgh, Edinburgh, UK
[2]Biomedical Pioneering Innovation Center (BIOPIC), School of Life Sciences, Peking University, Beijing 100871, China
[3]Department of Physics and Graduate Institute of Biophysics, National Central University, Jhongli, Taiwan 32001, ROC
[*]these authors contributed equally to this work
[+]Corresponding author:teuta.pilizota@ed.ac.uk

Abstract

The electrical membrane potential (V_m) is one of the components of the electrochemical potential of protons across the biological membrane (proton motive force), which powers many vital cellular processes. As V_m also plays a role in signal transduction, measuring it is of great interest. Over the years a variety of techniques has been developed for the purpose. In bacteria, given their small size, Nernstian membrane voltage probes are arguably the favourite strategy, and their cytoplasmic accumulation depends on V_m according to the Nernst equation. However, a careful calibration of Nernstian probes that takes into account the trade-offs between the ease with which the signal from the dye is observed, and the dyes' interactions with cellular physiology, is rarely performed. Here we use a mathematical model to understand such trade-offs, and apply the results to asses the applicability of the Thioflavin T dye as V_m sensor in *Escherichia coli*. We

identify the conditions in which the dye turns from a V_m probe into an actuator, and, based on the model and experimental results, propose a general work-flow for the characterization of Nernstian dye candidates.

Keywords: Nernstian probes, single-cell microscopy, *Escherichia coli*

Significance Statement

The phospholipid bilayer of a biological membrane is virtually impermeable to charged molecules. Much like in a rechargeable battery, cells harness this property to store an electrical potential that fuels life reactions but also transduces signals. For the case of bacteria, which are small in size and possess a stiff cell wall, arguably the most popular approach to measuring membrane voltage are Nernstian probes that accumulate across the bacterial membrane according to the Nernst equation. The present study characterizes the undesired effects Nernstian probes can have on cell physiology, which can be crucial for the accurate interpretation of experimental results. Using mathematical modelling and experiments, the study provides a general, simple work-flow to characterize and minimize these effects.

II. Introduction

Living cells maintain an electric potential difference (V_m) across the plasma membrane that acts like a capacitor. This is achieved by active transport of ions:

$$V_m = F \cdot \frac{Q_{in}}{C} \tag{II.1}$$

where Q_{in} is the intracellular charge (in moles), C the membrane capacitance and F the Faraday constant. Membrane potential stands at the basis of fundamental biological processes, such as signal transduction and energy production [101, 48]. For the latter, V_m adds up to the chemical potential of protons, arising from their concentration difference across the membrane, to result in the proton electrochemical gradient, so called proton motive force (PMF). The PMF drives numerous cellular processes, most notably the production of ATP [48], import of nutrients or osmolites [102, 103, 104, 105] rotation of the bacterial flagellar motor [106], and it is necessary for cell division [107].

The notion that V_m lies at the very basis of life motivated decades long efforts to measure it [108]. The first direct technique dates to 1939 and relies on the mechanical insertion of microelectrodes into squid giant axons [109]. The method led to the development of the patch-clamp technique, which advanced the understanding of neuron signal transduction [110, 111, 112]. However, applicability of microelectrodes for the measurement of bacterial V_m is limited, owing to the small size of the organisms and the presence of the cell wall [113, 114]. Some of the subsequently developed methods overcome such limits with the use of molecular sensors [115], grouped in two categories: conformational-change-based sensors and Nernstian sensors. The former are static molecules or proteins that sit inside the membrane, or in its close proximity, and change conformation or electron distribution in response to changes in V_m, which in turn affect the optical properties of the chromophores [116, 117, 118][3]. Here we focus on the latter, the Nernstian sensors, and on the parameter range in which they serve as V_m indicators, using *Escherichia coli* as the model organism.

Nernstian sensors are charged molecules that can diffuse across the biological membranes and distribute according to the Nernst equation:

$$V_m = \frac{RT}{zF} \ln\left(\frac{c_{out}}{c_{in}}\right) \tag{II.2}$$

where R, T, z, F, c_{out}, c_{in} denote respectively gas constant, temperature, valence of the charged molecule, Faraday's constant, external and internal concentration of the charged molecule. For a measurement to be attained, these molecules need to emit a signal that is a proxy for their number. Therefore, Nernstian V_m dyes are usually radio-labeled or fluorescent molecules [115, 119], and V_m is calculated from equation (II.2) by measuring the cytoplasmic (c_{in}) and the external dye concentration (c_{out}) [120].

However, Nernstian dyes are used in complex biological systems and a number of factors can be responsible for an incomplete adherence to a fully Nernstian behavior. In Fig.1.1 we give a cartoon representation of the trade-offs imposed on a Nernstian dye by plotting the dye intensity inside *E. coli's* cytoplasm against the time. The chosen dye concentration should be such that the signal is sufficiently above the background (ΔI is sufficiently large). Yet, with increasing dye concentration, cell's V_m is more likely to be affected by the dye. This caveat is

[3] An example of which is the "Mermaid" system developed in [116], that consists in proteins having different fluorescence for different values of the membrane potential.

inherent to positively charged dyes as these directly lower V_m and more so at higher concentrations [57]. The first requirement for a Nernstian dye is, thus, existence of a range of concentrations that give sufficient signal without extensively affecting the V_m. Likewise, cellular processes should not interfere with the Nernstian behavior of the dye, for example by actively importing or exporting it. Instead, the dye should be able to diffuse across the membrane and its diffusion constant will determine the time it takes for the dye to equilibrate across the membrane in agreement with equation (II.2) (τ_{eq} in Fig. 1.1). All phenomena that occur quicker than τ_{eq} are beyond the dye's temporal resolution, and all the measurements taken before τ_{eq} do not faithfully report V_m. Lastly, different dyes bind to the membrane or form aggregates to a different extent [120, 121]). However, as long as the dyes do not self-quench at any point [122], or undergo signal enhancements, a constant and well defined correlation function between the free dye concentration and the signal can be obtained, thus enabling quantitative V_m measurements (most commonly this is done by separating the signal from the free and bound dye with careful calibration [120, 121]).

To summarize, to be used as an ideal Nernstian sensor, a cationic dye should: (i) give a sufficiently high signal without affecting cell's V_m; (ii) diffuse through the membrane with τ_{eq} on the order of minutes; (iii) stay inert, despite being charged, and not form bonds or in any way interact with cell; (iv) have constant signal per molecule. Yet, when using such dyes these requirements are rarely assessed in a systematic manner before measurements commence. In this work we identify a work-flow that should be adopted, for a given choice of the dye, organism and external environment, in order to identify the parameter range in which Nernstian dyes act as sensors, rather than actuators, i.e. molecules that actively decrease or increase the V_m. We start with a mathematical model that helps us understand relationships and define trade-offs between dye working concentration and signal intensity, equilibration time and V_m perturbation. We then show how the identified work-flow can be used to benchmark new Nernstian dyes by characterizing the recently reported dye Thioflavin T (ThT) used in *Bacillus subtilis* [50], for use in *E. coli*. We describe the physiological range in which ThT enables V_m sensing in *E. coli*, and, in the range where we find it turns into an actuator, we investigate the mechanistic reasons. Our work-flow can be applied to the characterization of

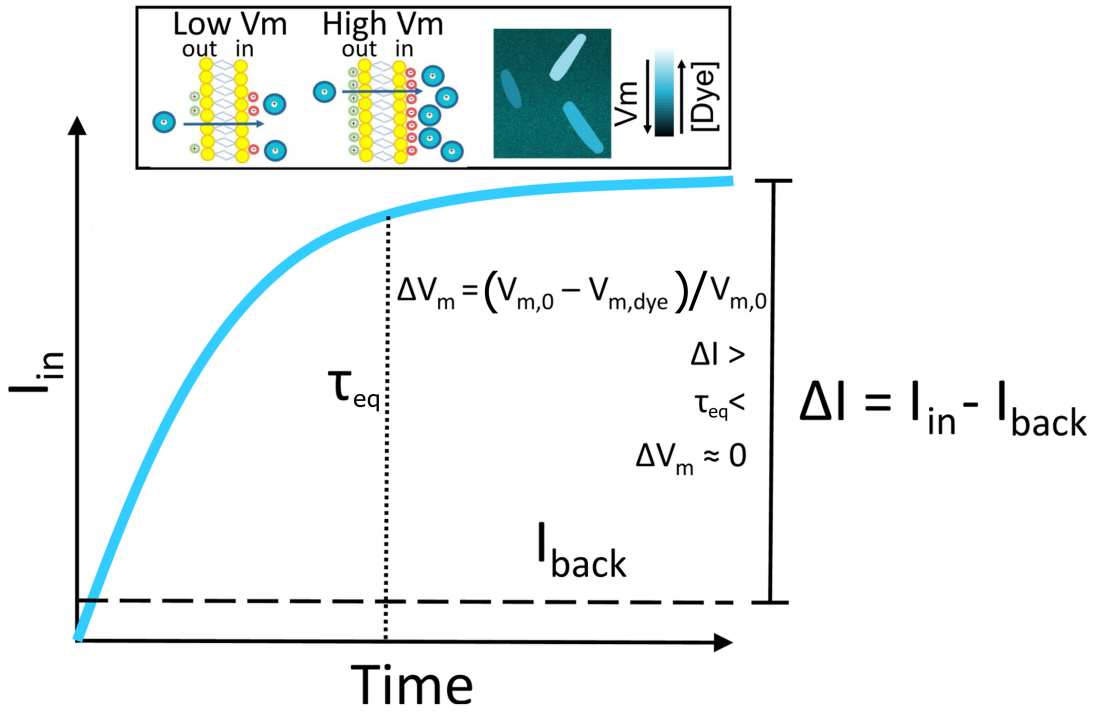


FIGURE 1.1: A schematic plot of a Nernstian dye equilibration curve. Equilibration time, τ_{eq}, is defined as the time at which the dye internalized by the cell, dye I_{in}, reaches the 90% of its final value. $V_{m,0}$ and $V_{m,dye}$ indicate the membrane potential before and after the addition of the dye, respectively. I_{back} is the fluorescence intensity of the background. Inset: cartoon showing the mechanism of accumulation of cationic dyes, which accumulate more in cells with a more negative V_m.

other Nernstian dyes and provide novel insights for the established ones[4].

III. Methods

i. Bacterial strains

All experiments where no mutation is explicitly indicated were carried out in the MG1655 strain. For the BFM speed assay we used MG1655 carrying the FliC-sticky mutation from [123]. Δ*tolC* mutants were obtained from the Keio collection [124]. Kanamycin resistance of the Keio deletion strain was removed via one-step inactivation with the plasmid pCP20 [125]. Kanamycin resistance inactivation and elimination of the pCP20 plasmid were confirmed via Kanamycin (50 μg/ml), Chloramphenicol (31 μg/ml) and Ampicillin (100 μg/ml) sensitivity tests. Both

[4]Note that if the workflow is *a priori* applicable to a large variety of dyes and organisms, the conclusions with respect to the impact of ThT on *E.coli* physiology are *a priori* both ThT and E.coli specific.

the strain carrying the $\Delta tolC$ mutation and MG1655 wild-type were transformed with plasmid pTP20-mKate2 (Fig. SI1) for cytoplasmic volume measurements. pTP20-mKate2 contains the red fluorescent protein mKate2 and the ribosomal binding site (RBS) of mCherry. The plasmid was constructed as follows: the backbone from pWR20 [126] and the sequence containing the RBS of mCherry and mKate2 were PCR amplified. The products were purified, cleaved with the restriction enzymes AvrII and NotI (NEB, UK) and ligated using T4 DNA ligase (Promega, UK). Chemically competent cells were transformed with the ligation mixes and transformants were confirmed by colony PCR and subsequently sequenced. A map of the plasmid and the primers are given in SI (Fig. SI1 and Table SI1). All the strains used in the study are summarized in the Table SI2.

ii. Bacterial growth conditions

Cells for fluorescence microscopy were grown from an overnight culture by diluting it 1:80 times in LB (0.5% Yeast Extract, 1% Bacto tryptone, 1% NaCl). The culture was shaken at 220 rpm at 37°C and harvested at OD_{600}=0.3-0.5. Cells were then washed into fresh LB or MM9 + glucose medium (50mM Na_2HPO_4, 25mM NaH_2PO_4, 8.5mM NaCl, 18.7mM NH4Cl, 0.1mM $CaCl_2$, 1mM KCl, 2mM $MgSO_4$, 1x MEM essential amino acids (Gibco, UK) and 0.3% glucose). For the simultaneous BFM speed and ThT fluorescence measurements cells were grown from an overnight culture by diluting it 1:80 times in TB (1% Bacto tryptone, 0.5% NaCl) at 200 rpm and 30°C. Cells were harvested at OD_{600}=0.8 as before [127] and washed to fresh MM9 via centrifugation. Growth curves in the presence of ThT were obtained in a Spectrostar Omega microplate reader (BMG, Germany) using a flat-bottom 96-well plate that was covered with a lid during the experiments (Costar, UK). Each well contained 200μl of growth media, either MM9 + glucose or MM9 + glycerol (50mM Na_2HPO_4, 25mM NaH_2PO_4, 8.5mM NaCl, 18.7mM NH4Cl, 0.1mM $CaCl_2$, 1mM KCl, 2mM $MgSO_4$, 1x MEM essential amino acids (Gibco, UK) and 0.3% glycerol), and was inoculated with 2μl (1:100 dilution) of an overnight culture and a given concentration of ThT. Plates were grown at 37°C with 300 rpm shaking (double orbital mode). ThT (Acros organics, USA) solutions were prepared from a 10 mM stock of ThT in water made at least monthly and stored at 4°C in the dark.

iii. Fluorescence microscopy

Imaging was carried out in a custom-built microscope with a 100x oil immersion objective lens (Nikon, Japan), Neutral White LED as a source of illumination (Cairn Research Ltd, UK) and images were taken with an iXon Ultra 897 EMCCD camera (Andor, UK) [128, 129]. ThT fluorescence was measured with ZET436/20x and ET525/40m, and mKate2 and PI fluorescence with ET577/25x and ET632/60m (Chroma Technology, USA) excitation and emission filters, respectively. Images were taken at 1 min intervals, exposure time was 50 ms and Andor camera gain 25. We note that ThT undergoes a spectral shift and intensity increase when highly concentrated or when spatially constricted, either by binding to amyloid fibrils or by viscosity [130, 131, 132]. Our choice of filters aims at minimizing these effects and the damage that shorter wavelengths cause to *E. coli* [133]. Cells were imaged in a custom-built flow-cell (Fig. SI2, [123]), and attached to the coverslip surface as before [127, 123]. Briefly, 1% Poly-L-Lysine (Sigma, UK) is flushed through the flow cell and washed with 3-5 ml of growth media after 10 s. Polystyrene particles (beads) with a diameter of 1 μm (Bangs Laboratories, USA), were delivered into the flow-cell and allowed to attach to the coverslip surface. After 10 min unattached beads were flushed away with 1-2 ml of growth media. Next, 200 μl of cells were delivered to the flow-cell and allowed to attach for 10-30 min, after which the unattached cells were removed with 1 ml of growth medium. 10 μM ThT in growth media was delivered with a peristaltic pump (Fusion 400, Chemyx, USA) using 50 μl/min flow rate while imaging. We deliver 5 μM of PI stain (MP Biomedicals, USA) in the same way. 5mM PI stock solution (in water) was stored at 4°C in the dark. Images were stabilized in x, y and z position using a bead attached to the cover-slip and back-focal-plane interferometry [126, 134]. Cells grow attached to the Poly-L-Lysine surface with expected growth rates (given the medium), as previously reported [135] and seen in SI Video 1 and 2.

iv. Motor speed measurements

Single motor speeds were measured as before [127, 123]. Briefly, we sheared flagellar filaments by passing them through two syringes with narrow-gauge needles (26 gauge) connected by plastic tubing. The cell attachment protocol was as above, except 0.5 μm beads (Polysciences, USA) were delivered after cell attachment allowing them to attach to filament stubs. Motor speed was measured during continuous flow that delivered MM9 + glucose medium supplemented with 10

μM ThT. Back-focal-plane interferometry setup and recording conditions are as before [127].

v. Data analysis

Motor speed traces

Raw traces of the position of the bead attached to the filament stub were analyzed by a moving-window discrete Fourier transform as in [127]. From the obtained motor speed traces DC frequency (50 Hz) was removed, speeds lower then 5 Hz ignored, and subsequently a median filter (window size 11) was applied [123]. We note that we use a wild type strain for which the BFM can change rotational direction, which appears as a negative speed after application of the moving-window Fourier transform. However, for the purpose of the PMF measurements, these short intervals can be disregarded, and we only show the speed values above 0 Hz.

Fluorescence images

The image analysis was carried out with a custom written software. From fluorescence images, rectangles containing 'flat' cells, i.e. cells that are uniformly attached to the coverslip surface, as well as background rectangles within each cell-containing rectangle, were manually selected [134, 126]. The edge of the cell was identified within the cell-containing rectangle by applying a global threshold via the Otsu's method [136]. Total cells' intensity values were obtained by summing up and averaging pixel belonging to the cells. Values obtained from the background rectangles at the time points when ThT was loaded in the channel but cells had not taken it up yet, were subtracted from the cell intensity values. The beads used for image stabilization stain easily with ThT, and were used as a point of reference for dye entry (which in our case occurred 7 to 10 min from the start of imaging). We show fluorescence intensity traces that start at the point of ThT entry, but note that cells were exposed to fluorescence illumination in the 7-10 min interval before. For the low fluorescence values characteristic of the early stages of dye equilibration, our script fails to identify cells, in which case we linearly interpolate values between two closest events of successful cell identification. Cell area was measured from intensity profiles, by normalizing them and counting the pixels above 30% of maximum intensity as described previously [126, 134]

Plate reader data

Individual growth curves were analyzed with the software deODorizer from [137]. To extract the maximum growth rate, 3 or more repeats in the same condition were aligned by the chosen OD value (usually OD∼0.4) using the growth curve that reached it first (in the given condition). The maximum growth rates given in Fig. 1.3C were normalized by the maximum growth rate in $[\text{Dye}]_{out}$=0 condition.

IV. Results

i. Mathematical model of Nernstian dye's behavior defines its working parameter range

To predict and understand the mutual effects of dye concentration and cell physiology we turn to a mathematical model. We assume that the cytoplasmic and extracellular liquids are electrical conductors separated by a membrane, which we treat as a parallel-plate capacitor (equation B.1) [31, 32]. We model the membrane as a single lipid barrier and do not distinguish between the inner and outer membrane of *E. coli*. In the SI we discuss a more detailed model that includes both membranes and allows for the existence of a small V_p across the outer membrane, in addition to the V_m across the inner membrane. We account for four types of charge carriers and assume that all are monovalent to simplify the model without altering the results with respect to V_m dye behavior: *(i)* negatively charged molecules to which the membrane is close to non-permeable denoted Y (this includes surface charges on the inside of the membrane), *(ii)* cationic species actively pumped outward denoted C^+, *(iii)* anionic species, which equilibrates across the membrane A^- and *(iv)* cationic species that equilibrate across the membrane (playing the part of a cationic dye). Thus Q_{in} is:

$$Q_{in} = V_{cell} \cdot \underbrace{\sum_x z_x [x]_i}_{\text{General Form}} = V_{Cell} \cdot \underbrace{\left([Dye]_{in} + [C^+]_{in} - [A^-]_{in} - [Y]_{in}\right)}_{\text{This manuscript}} \qquad \text{(IV.1)}$$

where V_{cell} is the intracellular volume, z_x valency of species x and $[x]_i$ its intracellular concentration (we only consider $z_x = \pm 1$). The extracellular concentrations and $[Y]_{in}$ are constants set by the initial conditions (we assume that the cell does not affect the ionic composition of its environment and we treat $[Y]_{in}$ as unable to

cross the membrane). We also assume that the cell uses only one type of pumps for cations, and note that $[Dye]_{in}$ and $[Dye]_{out}$ are experimentally determined from fluorescence intensity signal (see Fig. 1.6 later in the text).

The charge separation, and thus V_m, is achieved in the close proximity of the bilayer, so that the rest of the cell's cytoplasm stays electroneutral [32, 138], and in two ways. First, by pumping C^+_{in} outwards and thus creating a negatively charged intracellular environment, and second by maintaining $[Y]_{in}$. Pumping C^+ outwards against its electrochemical gradient requires free energy, which we consider a constant and label ΔG_E (where $\Delta G_E < 0$). For example, in the case of a proton:ion antiporter with 1:1 exchange stoichiometry the free energy is the PMF itself, for a similar antiporter with 2:1 proton:ion stoichiometry it is $2 \times$ PMF, and for ATP hydrolysis, ΔG_E is the amount of work given by hydrolyzing one ATP.

The rate at which C^+ is pumped out of the whole cell, given in mol/m^3/s, is:

$$j_P = k_P \cdot \left(1 - e^{\Delta G_P/(RT)}\right) \tag{IV.2}$$

where k_P is a function that describes the specifics of the transport mechanism by a given pump, here, we keep it a constant. ΔG_P depends on the electrochemical potential of the pumped cation (ΔG_{C^+}) and ΔG_E. Therefore, the rate of pumping (positive flux means C^+ is extruded) depends on the intracellular ionic composition via V_m and $[C^+]_{in}$:

$$\Delta G_P = \Delta G_E - \Delta G_{C^+} \tag{IV.3}$$

$$\Delta G_{C^+} = F \cdot V_m + RT \cdot \ln\left(\frac{[C^+]_{in}}{[C^+]_{out}}\right) \tag{IV.4}$$

Note that in order for the pump to move C^+ outward $j_P > 0$, and consequently $\Delta G_E < \Delta G_{C^+}$, i.e. the free-energy providing reaction has to be able to overcome the electrochemical gradient of the C^+. The chosen functional dependency of j_P gives the simplest pump kinetics, sufficient for our purpose, which can be expanded to include more complex pumping scenarios [17].

Finally, the dye, the anion and the cation leak through the membrane (positive flux means x is moved inward) at the rate:

$$j_{L,x} = k_{L,x} \cdot \left(1 - e^{\Delta G_x/(RT)}\right),\ x \in \{Dye, C^+, A^-\} \tag{IV.5}$$

$$\Delta G_x = F \cdot V_m + RT \cdot \ln\left(\frac{[x]_{in}}{[x]_{out}}\right) \tag{IV.6}$$

Similarly to k_P, $k_{L,x}$ is a function whose shape depends on the mechanisms by which an ion leaks across the *E. coli* membrane, which in turn depends on the electrostatic potential at a position z within the membrane, $V(z)$. To the best of our knowledge, $V(z)$, and consequently $dV(z)/dz$, are not known for *E. coli*. Therefore, we chose Eyring's model that has been verified for cationic leakage across the mitochondrial membrane [139], and which assumes $V(z)$ abruptly changes in the middle of the lipid bilayer, such that $dV(z)/dz = 0$ everywhere but at the geometrical middle of the membrane where $dV(z)/dz = V_m$ [42][5]. We then have:

$$k_{L,x} = \frac{S_{cell}}{V_{cell}} \cdot P_x \cdot [x]_{out} \cdot e^{-\frac{F \cdot V_m}{2 \cdot RT}},\ \text{with } x \in \{Dye, C^+, A^-\} \tag{IV.7}$$

where S_{cell} denotes the cell's surface area and P_x the permeability of the membrane for $x \in \{Dye, C^+, A^-\}$ (obtained by assuming the solubility-diffusion model [140]).
At steady-state Dye and A^- equilibrate across the membrane according to Nernst equation ($d[Dye]_{in}/dt = j_{L,Dye} = 0 \Leftrightarrow \Delta G_{Dye} = 0$, leading to (II.2)), whereas for the monovalent cation $d[C^+]_i/dt = 0 \Leftrightarrow j_{L,C^+} = j_P$. Next we introduce a new variable ("*pump-leak ratio*") defined as:

$$\rho = k_P/k_{L,C^+} = k_P \cdot \frac{V_{cell}}{S_{cell} \cdot P_{C^+} \cdot [C^+]_{out}} \cdot e^{\frac{F \cdot V_m}{2 \cdot RT}} \tag{IV.8}$$

and re-write the steady-state condition for C^+ as:

$$\left(1 - e^{\Delta G_{C^+}/(RT)}\right) = \rho \cdot \left(1 - e^{(\Delta G_E - \Delta G_{C^+})/(RT)}\right) \tag{IV.9}$$

[5] Although We kept $dV(z)/dz = V_m$ as in [42], this equation is missing a dirac delta function of the left-hand side in order to be dimensionally consistent.

Given a certain extracellular composition ($[Dye]_{out}$, $[C^+]_{out}$ and $[A^-]_{out}$), and taking into account that $[Dye]_{in}$ and $[A^-]_{in}$ are defined by the Nernst equation at steady-state, equation (IV.9) gives us a unique solution for steady-state V_m for a set of $\{[Y]_{in}, \rho, \Delta G_E\}$ values, while reducing the number of computational steps needed to reach it (see also the later paragraph describing computational steps of the model further).

We note from Eq. (IV.9) that changing the functional dependency of k_{L,C^+} or k_P does not affect how the steady-state $V_{m,0}$ depends on ρ. However, the dynamics of dye equilibration and the steady-state potential after addition of the dye, relative to the steady-state potential in absence of the dye, ($\Delta V_m = (V_{m,0} - V_{m,Dye})/V_{m,0}$) do. For example, had we assumed that the mechanism by which the ions leak across the *E. coli* membrane is better described by the Goldman–Hodgkin–Katz flux equation for $k_{L,x}$ [37], we would have obtained a slightly different dye equilibration profile (Fig. SI3). However, the conclusions we reach based on our model predictions will not change, because we are interested in the changes of the intracellular dye concentration dynamics at different extracellular dye concentrations, $V_{m,0}$ or P_{Dye}. These partial derivatives of the intracellular dye concentration are invariant to the choice of $k_{L,x}$ and k_P.

Having constructed the model, we obtain the computational data in Fig. 1.2 in two steps. In the first step we allow the ODE system described by Eqs. SI 20, 21 to reach the steady-state ($V_{m,0}$) for a 3-D grid of $\{[Y]_{in}, \rho, \Delta G_E\}$. We note that in this step we do not need to specify cation permeability nor the rate function for leakage k_{L,C^+}, because we define the values of ρ, which is the ratio of the two (ρ=0 for the anion and the dye). We then use the obtained $V_{m,0}$ as the initial condition for the second step of the numerical experiment, which requires us to specify: *(i)* the rate function for leakage (Eq. (IV.7)), *(ii)* the permeability of the membrane to the dye P_{Dye} and *(iii)* the concentration of the dye in the extracellular space $[Dye]_{out}$, which does not affect the cation pumping rate in our model.

To explore the trade-offs imposed on a Nernstian dye (Fig. 1.1), we first look at the choice of the working concentration. Increasing the $[Dye]$ gives better signal-to-noise ratio, but can affect $V_{m,0}$, as depicted in Fig. 1.2A. For a fixed $V_{m,0}$, $[Y]_i$ and ΔG_E, changing the external dye concentrations ($[Dye]_{out}$) improves the signal-to-noise ratio and shortens τ_{eq}, but at the same time increasingly depolarizes the membrane. The extent by which ΔV_m drops does not solely depend on the $[Dye]_{out}$, but also on the initial $V_{m,0}$. Fig. 1.2B shows dye equilibration profile for a fixed $[Dye]_{out}$, but for different $V_{m,0}$ indicating that highly polarized cells

are more susceptible to V_m loss. Apart from the value of $V_{m,0}$, ΔV_m will also depend on the charged permeable and non-permeable species that are generating it, as shown in Fig. SI4. If a given $V_{m,0}$ value is generated in the presence of a higher concentration of charged, impermeable intracellular species or at a higher energetic cost, ΔV_m will increase for the same $[Dye]_{out}$. Thus, the extent to which a given $[Dye]$ becomes an actuator[6] and affects the ΔV_m is context dependent and the dye working concentration should be determined for each specific physiological condition. Additionally, Fig. 1.2A shows that increasing $[Dye]_{out}$ shortens τ_{eq}, but only when $V_{m,0}$ is affected, as seen in Fig. SI5.

Lastly, we look at the dye equilibration profile for different permeabilities of the membrane to the dye (P_{Dye}) in Fig. 1.2C, and show that for higher P_{Dye} same concentration of the dye lowers $V_{m,0}$ more. Fig. SI4 shows τ_{eq} as a function of P_{Dye} for different $V_{m,0}$.

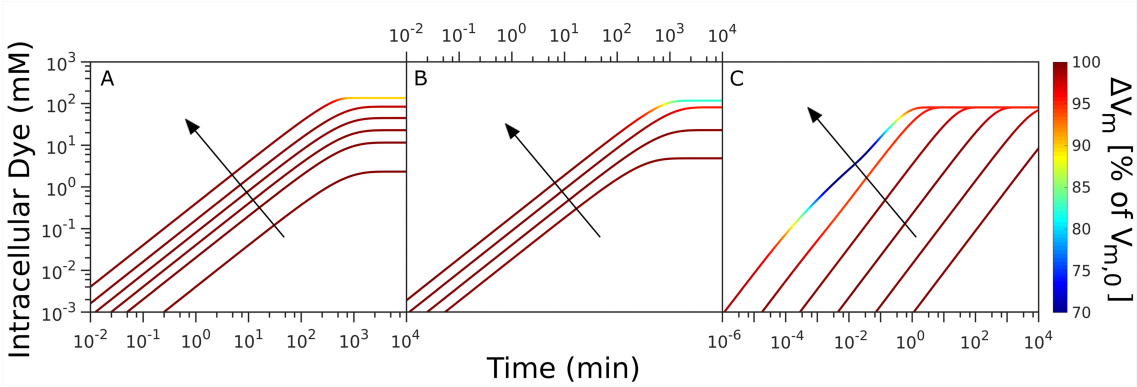


FIGURE 1.2: Computational data describing the parameter landscape associated with cationic dye usage as Nernstian sensors. (A) $V_{m,0} = -140$ mV, $Y_i = 150$ mM, $I_{Na} = 210$ mV. Intracellular Dye concentration as a function of time, for extracellular dye concentrations 10, 50, 100, 200, 400 and 1000 μM. The arrow indicated increasing $[Dye]_{out}$. (B) Extracellular dye concentration of 100 μM, $Y_i = 150$ mM, $\Delta G_E = -210$ mV. Intracellular dye concentration as a function of time, for different $V_{m,0}$: -220, -180, -140 and -100 mV. The arrow indicates increasing absolute value of the $V_{m,0}$. (C) Extracellular dye at 100 μM, $V_{m,0} = -180$ mV, $Y_i = 150$ mM, $\Delta G_E = -210$ mV. Intracellular dye concentration as a function of time, for different apparent permeabilities of the membrane to the dye: 10^{-12}, $10^{-10.8}$, $10^{-9.6}$, $10^{-8.4}$, $10^{-7.2}$, 10^{-6} m/s. The arrow indicates increasing permeability.

[6]meaning, becomes a component of the cell system that starts affecting how the cell works.

ii. The working concentration of Nernstian dye Thioflavin T for *E. coli* is in μM range

Guided by the model predictions we devise an experimental work-flow for assessing the parametric range in which a candidate cationic dye behaves like an ideal Nernstian sensor. We choose Thioflavin T (ThT) for the purpose, it has recently been used as a V_m dye in *B. subtilis* [50], but it has not been characterized for use in *E. coli*. We start by identifying the working concentration that gives sufficiently large signal, yet minimizes the membrane voltage perturbation, ΔV_m. Because we do not have access to ΔV_m directly we grow the cells in the presence of ThT and use the growth rate as a proxy for affected ΔV_m. We also know from our model predictions that ΔV_m is context dependant, so we perform the experiment in two different media. Fig. 1.3A and B show *E. coli* growth curves in MM9 media supplemented with glucose or glycerol respectively (see *Materials and Methods* for detailed media composition), and in the presence of a range of ThT concentrations. To asses the effect of different ThT concentrations in these two media, we plot growth rates, obtained from growth curves in Fig. 1.3A and B, against the ThT concentration. Fig. 1.3C demonstrates that 10 μM ThT or less does not significantly affect the growth rate in either media, and we call this concentration MNC (Maximum Non-Inhibitory Concentration). The growth rate reduction we observe for higher ThT concentrations is media dependent (Fig. 1.3C). The result is consistent with the finding of our model that the effect of the dye on cell's physiology is environment dependent. It could be caused by a different $V_{m,0}$, difference in charged permeable and non-permeable species that achieve the $V_{m,0}$, difference in the initial membrane permeability or any combination of these factors.

We next check that the highest ThT concentration, which does not affect the growth rate (MNC), 10 μM, gives sufficiently high signal-to-noise ratio by observing the dye equilibration in different media. For this purpose we no longer grow the cells in the presence of ThT (see also *Materials and Methods*). We note that if sufficient ΔI is achieved with 10 μM ThT we would further check that $\Delta V_m < 1\%$ by measuring the τ_{eq} with both 10 μM and a lower dye concentration. If $\Delta V_m < 1\%$, we expect τ_{eq} not to change based on the results of our model (Fig. 1.2A). Fig. 1.3D shows I_{in} in time in LB and Fig. 1.3E the same in MM9 media supplemented with glucose. In both cases fresh media with ThT is continuously supplied using a customized flow-cell (see *Materials and Methods*), and in both

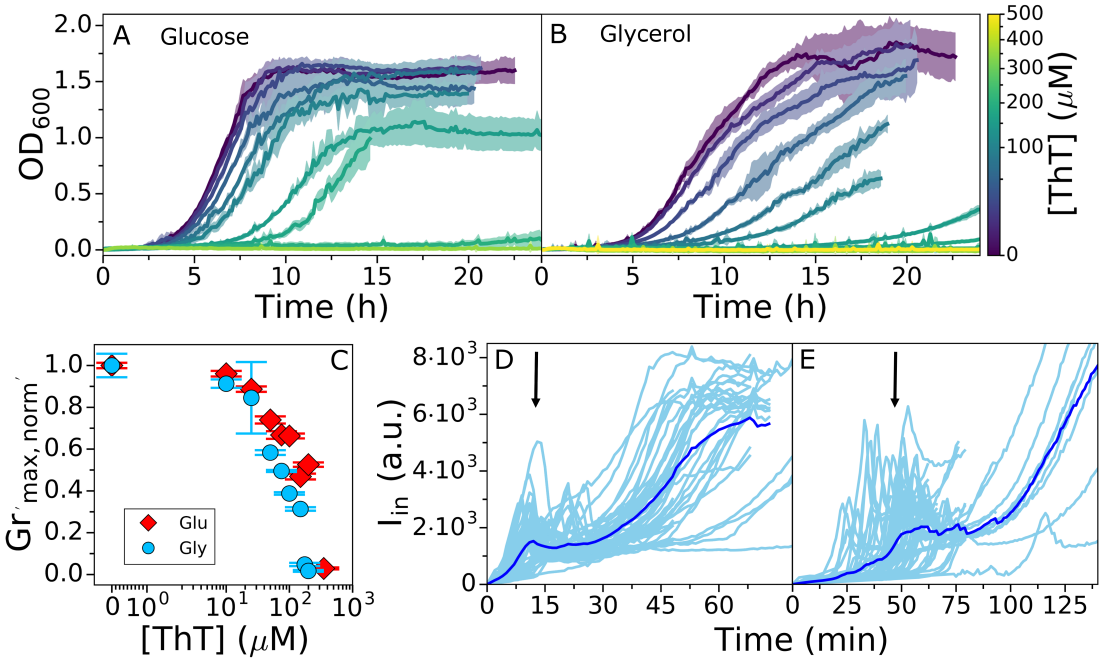


FIGURE 1.3: *E. coli* growth in the presence of ThT. *E. coli* growing in MM9 media supplemented with (A) glucose or (B) glycerol at increasing ThT concentration (colour-map). ThT concentrations in (A) are 10, 25, 50, 75, 100, 200, 350 μM and in (B) 10, 25, 50, 75, 100, 150, 175, 200 μM. The error bars are standard deviations. (C) Maximum growth rates from (A) and (B) for each ThT concentration are given in red and blue respectively. Each condition was done at least in triplicate and error bars are the standard deviation. (D) I_{in} against time in LB and in (E) MM9 + glucose media. Individual cells are shown in cyan (45 in (D) and 52 in (E) from at least 9 independent experiments), and the average trace is shown in blue. The imaging conditions and $I_{ex} = 10\mu M$ are the same for (E) and (D). The black arrows indicate the intensity peaks.

cases ΔI is sufficiently high. However, observed profiles are different from expected (Fig. 1.1), and show a characteristic initial peak and a subsequent large increase that plateaus (SI Video 3). We reasoned that the peak could either be a real fluctuation in V_m or it could indicate an unknown dye export mechanism.

Deletion of the multi-drug efflux pumps component TolC influences ThT dynamics in *E. coli*

To determine whether the observed peak in I_{in} is due to active export of the dye we first check that in *E. coli* ThT is not a multi-drug-efflux pump substrate. We are motivated by previous reports that show dyes, such as ethidium bromide and Nile red, are substrates of pumps belonging to the five bacterial structural families: ABC (ATP-binding cassette), RND (resistance/nodulation/division),

MATE (multidrug and toxic compound extrusion), MFS (major facilitator superfamily) and SMR (small multidrug resistance) [141, 142, 143, 144, 145]. Fig. 1.4A shows dye equilibration curves in a wild type (WT) strain compared to the strain bearing a deletion of TolC, which is a gene encoding for an outer membrane protein (OMP) that is a ubiquitous component of multi-drug efflux pumps [146]. The I_{in} peak in the deletion mutant did not disappear, instead the intensity level of the peak was even higher, suggesting that the qualitative difference between the expected (Fig. 1) and the observed equilibration curve (Fig. 4A) is not due to ThT export by TolC. Interestingly, in the mutant, the peak also occurred earlier in time during the loading and with less cell-to-cell variability. We next tested the effect of the ThT dye on the $\Delta\,TolC$ mutant growth rates, and for this purpose we again grew the two strains in the presence of ThT, Fig. 1.4B. We found that at the MNC for the WT, the mutants' growth was inhibited over the course of our experiment. Two different mechanisms could explain the results in Fig. 1.4: (i) ThT is a substrate of the multi-drug efflux pumps or (ii) membrane permeability of the TolC mutant is higher [147]. In the first scenario, the strain lacking TolC accumulates more ThT than the WT (Fig. 4A), and is therefore more affected by it (Fig. 4B). In the second scenario, based on our model, we expect the intensity peak to appear earlier and at a higher $[Dye_{in}]$ (Fig. SI12 C and D), which is what we observe in Fig. 1.4A. We currently cannot distinguish between the two hypothesis, which could be contributing to the observed equilibration profiles at the same time.

iii. Changing the membrane permeability during ThT loading can lead to loss of V_m

We next tested our second hypothesis that the I_{in} peak is due to a decrease in V_m. To this end, we performed measurements of bacterial flagellar motor (BFM) speed [123] during ThT loading. BFM is a rotary molecular motor roughly 50 nm in size that enables bacterial swimming [106] via PMF driven rotation [148, 149, 150, 151]. The motor speed (ω) varies linearly with PMF [151, 152], which enables its use as a PMF indicator, and when $pH_{in} = pH_{out}$, as a V_m indicator as well [123]. In our conditions, pH_{out} is 7 and pH_{in} is 7.86 (Fig. SI7) making the contribution to the PMF from ΔpH $\sim$50 mV. Thus, even if during our experiment ΔpH goes to 0, we can learn about the V_m behaviour from the PMF measurements via the motor speed. We measure ω as before, using back-focal-plane interferometry [153] and a

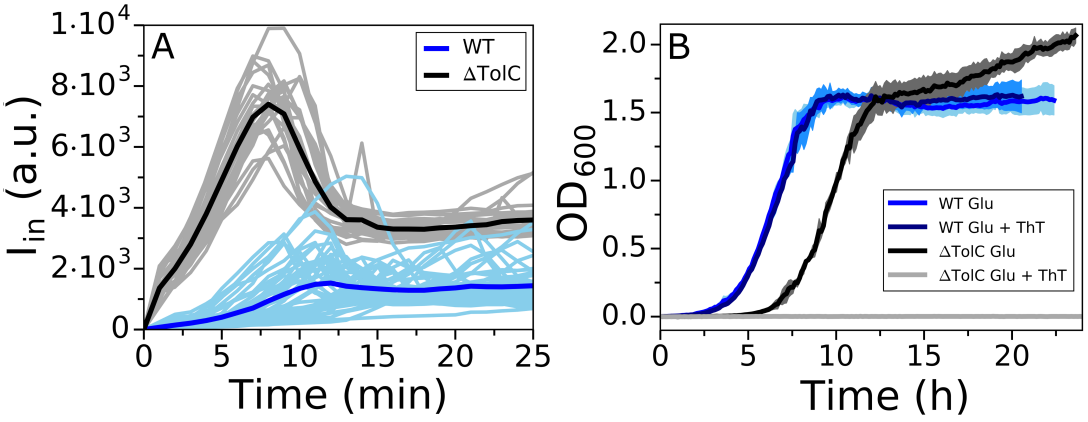


FIGURE 1.4: Comparison of WT and ΔTolC mutant response to ThT. (A) I_{in} versus time for the WT (cyan) and ΔTolC (gray) loaded in LB. WT traces are reproduced from Fig. 3D and ΔTolC traces were obtained from 5 independent experiments to give 23 single cell traces. Averaged traces for the WT and ΔTolC are given in blue and black respectively. (B) Growth curves of WT and ΔTolC in MM9 + glucose media are given in blue (reproduced from Fig. 1.3A) and black, respectively. Growth curves in the same media, but in the presence of 10 μM ThT, are given in cyan (WT) and gray (ΔTolC). The shaded areas show standard deviation and cyan and blue growth curves for the WT overlap.

polystyrene bead attached to a short filament stub (see *Materials and Methods*) [123, 127, 154, 155].

Fig. 1.5A and Fig. SI8 show simultaneous measurements of ThT intensity and normalized motor speed during dye equilibration in MM9 + glucose. The motor speed decreases during ThT equilibration and BFM stops at the point of I_{in} peak. Furthermore, BFM does not resume spinning even as I_{in} further increases, suggesting that the second ThT intensity increase that culminates in a plateau, is not driven by V_m. To confirm the result, during ThT equilibration, we supplemented the medium with propidium iodide (PI). PI permeates bacterial membrane that lost its integrity and significantly enhances its quantum yield upon binding to DNA, which is commonly interpreted as an indication of cell death [156, 157]. We found that the cells stained with PI although ThT intracellular concentration remained high, Fig. 1.5B and Fig. SI9. In addition, at the time point of I_{in} decrease cellular volume suddenly increases, and cytoplasmically expressed fluorescent protein mCherry-mKate2 hybrid (referred to as mKate2 for brevity) [158] starts leaking out of the cell, Fig. 1.5C, SI Video 4.

These results are in contradiction with our estimate of dye working concentration, and we wondered, based on Fig. 1.2C, if the changes in P_{Dye} could be the explanation. The cell culture in Fig. 1.3 was briefly exposed to light at 600 nm every 7.5 min, whereas cells in our flow-cell were exposed to light of 435 nm every

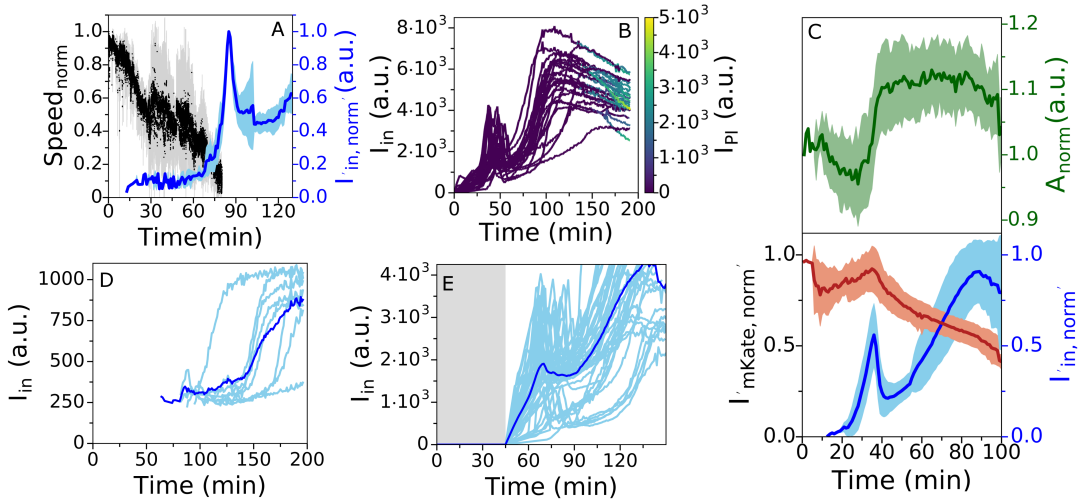


FIGURE 1.5: (A) Average traces of ThT fluorescence (in blue) and motor speed (in black) simultaneously measured in 5 individual cells (individual cell traces are given in Fig. SI6). The shaded areas show the standard deviation and the motor speed has been normalized to the initial value as described in *Materials and Methods*. (B) ThT (y axes) and PI (colour-map) equilibration profile in LB. 25 individual traces are given. (C) Average of ThT (in blue), mKate2 (in red) fluorescence and cell area (in green) simultaneously measured in 12 individual cells from 3 independent experiments. The shaded areas show the standard deviation. (D) Equilibration profile of 1 μM ThT in LB. 8 single cell traces and average trace are given in cyan and blue, respectively. (E) Equilibration profile of 10 μM ThT in LB in the absence (gray shaded area) and presence of epifluorescent illumination (light area). The dye was flown in the flow cell for the whole length of the experiment, imaging conditions in the light area were the same as in Figure 3 and 5D. 44 cells from 8 independent experiments are given.

minute for the purpose of imaging the ThT dye. We have previously reported loss of V_m and PMF due to light-induced decrease of *E. coli* membrane's resistance at effective powers higher than $\sim$ 17 mW/cm^2, and for a combination of 395 and 475 nm wavelengths [123]. Light damage is wavelength dependent [133], and we therefore characterized the light damage caused by our imaging conditions, i.e. 435 nm wavelength and effective power of $P_{eff} \sim 11$ mW/cm^2. Fig. SI10 shows a decrease in BFM motors' speed, and thus cell's PMF. However, the PMF is not fully lost, indicating that the loss of PMF observed in Fig. 1.5A is likely caused by the combination of light induced increase in P_{Dye} and exposure to 10 μM ThT.

To prove it, we exposed the bacteria to 10 μM ThT in LB as before, but this time we observe the cells under bright-field illumination for 45 min, at which point we turn on the 435 nm light used for epifluorescence imaging of ThT. Fig. 1.5E shows that after 45 min, cells not exposed to 435 nm light did not take up ThT. This is in contrast to Fig.1.3D where cells exposed to 435 nm light from the start, took up ThT in the first 30 min.

Actively changing membrane permeability has been used to facilitate loading of Nernstian sensors [120], and Fig. 1.5E shows that this can change the dye into an actuator because it can influence V_m. Our mathematical model predicts that if a given concentration of the dye is lowering V_m, an even lower concentration of the dye will result in a change of τ_{eq} (Fig. SI5). Because the dye equilibration profiles in Fig. 1.3D do not follow the theoretically expected curve (Fig. 1.1) we cannot calculate τ_{eq}. However, from Fig. 1.5A we know that initial rise in the dye intensity is still driven by V_m, therefore we can qualitatively compare the timing of the initial rise at different $[Dye]_{out}$. Fig. 1.5D shows that for 1 μM concentration of ThT the rise in I_{in} happens later in time than at $[Dye]_{out} = 10\mu$M (Fig. 1.3D). Thus, 10 μM ThT in LB, under 435 nm light, affects V_m. Assessing the suitability of the dye working concentration by confirming that a lower dye concentration does not alter τ_{eq} is a suitable additional control we propose, especially if P_{Dye} is being altered as part of the experiments.

We note that in our plate reader experiments (Fig. 1.2) we observed the effect of the dye (above 10μM) on cell growth, while in our microscopy experiments, in the absence of light damage, ThT does not permeate WT cells. We thus wanted to confirm that at higher concentrations ThT permeates the cells on a longer time scale, and for the purpose we imaged the cells from the wells at representative ThT concentrations in MM9+glucose (10, 50 and 100 μM) and MM9+glycerol (10 μM). As expected, we found that on a longer time scale in MM9 glucose cell brightness increases with the extracellular dye concentration and that in MM9+glycerol, at 10μM, ThT signal from the cells is overall greater than in glucose (Fig. SI11).

Having identified the mechanisms behind the shape of the ThT loading curve we observed in Fig. 1.3 we should now be able to reproduce it with our mathematical model. We focus only on the part of the equilibration curve that is V_m driven, i.e. up to the point V_m drops to zero (as indicated in Fig. Fig 1.5A). Beyond, the increase in I_{in} is not driven by Nernstian equation, and thus not accounted for in our model. Based on Fig 1.5A we assume that V_m decays exponentially immediately after addition of the dye [123]: $V_m(t) = V_{m,0} \cdot 2^{t/t_{1/2}}$ where $t_{1/2}$ is the time at which voltage is half that of $V_{m,0}$. The dynamics of dye entry are then modelled by Eyring's rate law Eq. (IV.7) taking into account $V_{m,0}$, $t_{1/2}$ and P_{Dye} (see *Supplementary Information* for further details on the model). Fig. SI12 shows that the model reproduces the peak in $[Dye]_{in}$ observed in Fig. 1.3. Immediately upon addition, the positively charged dye moves inwards because its extracellular concentration is higher than the intracellular and the cell is

negatively polarized. Thus, $[Dye]_{in}$ increases and becomes greater than $[Dye]_{out}$ until the electrochemical potential reaches $\Delta G_{Dye} = 0$ (at the peak). As the V_m decays and since $[Dye]_{in} > [Dye]_{out}$, the dye now starts moving outwards and its intracellular concentration decreases. In Fig. SI12B $[Dye_{in}]$ decreases to zero, while experimental I_{in} starts increasing after the peak and never reaches zero. The difference is explained by the fact that cells with high I_{in} after the peak are no longer viable (Fig. 1.5A and Fig. 1.5B) and thus the behaviour of the dye is no longer governed with Nernstian equation. In Fig. SI12E and F we indicate the part of the experimental equilibration curve to which our model is applicable.

The time at which the peak occurs as well as its intensity depend on P_{Dye} as follows: *(i)* the time of the peak decreases with increasing P_{Dye} and increases with increasing $t_{1/2}$, and *(ii)* the intensity of the peak increases with increasing P_{Dye} and $t_{1/2}$, Fig SI9 C and D. The dye still equilibrates according to equation (II.2), however, this is achieved transiently at the time of the peak, which is the time point at which V_m can be calculated from equation (II.2). Since the V_m varies during the course of the experiment, the V_m measured at the peak is not equal to the $V_{m,0}$. Nonetheless, if we measure $V_m(t)/V_{m,0}$ as well as calculate the V_m at the time of the peak using eq. (II.2), in principle we can estimate $V_{m,0}$ as well. Therefore, charged dyes can be used to estimate initial V_m even in conditions where they act as actuators and collapse V_m, if the dynamical shape of the V_m loss is known.

V. Discussion

Nernstian probes are a popular choice for estimating bacterial V_m, because the concentration of the free dye directly depends on V_m according to the Nernst equation. Despite the wide usage, the probes are often not sufficiently calibrated before use in different conditions. Here we present a mathematical model that shows trade-offs between requirements imposed on the dye: sufficient signal-to-noise ratio, sufficiently short dye equilibration time and minimum effect on the cells' physiology. Based on the model results we characterize in *E. coli* the fluorescent dye Thioflavin T, recently used in *B. Subtilis* [50]. Finally, we propose a general work-flow for the characterization of Nernstian dye candidates (Fig. 1.6).

Results of our model show that the dye working concentration which does not affect V_m is context dependant, e.g. it can be different for different external media.

The model also predicts that if $\Delta V_m = 0$ at a chosen dye working concentration, lower dye concentration should leave τ_{eq} unchanged. The finding offers a simple test to confirm the suitability of the chosen dye working concentration.

For the case of *E. coli* and ThT as the candidate Nernstian dye, we experimentally find that the dye equilibration profile does not follow the theoretical expectation (Fig. 1.1). We test two possible explanations for the shape of the equilibration profile we observe in Fig. 1.2: (a) involvement of active efflux pumps and (b) significant V_m decrease during ThT equilibration. While we find that the strain lacking one of the efflux pumps shows a different equilibration profile when compared to the wild type, it still does not behave as theoretically expected. Instead, we find that the permeability of *E. coli's* membrane to ThT is low. Permeabilizing the membrane by light of relatively short wavelengths to facilitate sufficient ThT entrance into the cell causes significant V_m reduction, which subsequently results in cell death. The finding is consistent with previous results that show that *E. coli*'s membrane needs to be permeabilized with EDTA to achieve experimentally reasonable loading times of TMRM dye [120]. EDTA is thought to increase the permeability of *E. coli* by chelating the metal ions that cross-link the LPS [159]. Some evidence also suggests that it might interact directly with lipids destabilizing the membrane [160]. The equilibration profiles we observe for the efflux pump mutant strain can be explained either by the change in membrane permeability between the two strains or by active efflux.

We summarize the results from our model and experiments, as well as previous work on Nernstian V_m dye usage, in a work-flow (Fig. 1.6). We believe it is sufficiently simple and general to provide a common standard for bench-marking the cationic dye behavior and thus improve the robustness of V_m measurements. It starts with a protocol to identify the dye working concentration (Fig. 1.6, steps 1-4). This is first carried out by assaying the effect of the dye on bacterial growth, as we did in Fig. 1.3A-C, because it is a physiological variable that is easy to measure and it will likely be affected by changes in V_m (step 1). In step 1 we identify the Maximum Non-inhibitory Concentration (MNC), as the maximum dye concentration that does not affect growth. We use it to measure the dye equilibration profile in step 2. This allows us not only to make sure that with the MNC we are obtaining the expected shape of the equilibration profile, but also that the MNC gives sufficiently high intracellular signal. Next, we further test, as we did by comparing Fig. 1.3D and 1.5D, whether the MNC is affecting V_m by checking that τ_{eq} for the MNC and a chosen concentration below

it, stay the same (step 3). If the below-MNC concentration and the MNC do not show the same τ_{eq}, steps 1 to 3 need to be repeated for progressively lower dye concentrations until either the signal from the intracellular dye becomes too low, or τ_{eq} do not differ between the two tested concentrations. In the second case, the higher concentration can be considered suitable. The next step in the work-flow is more commonly performed when assaying V_m dyes [115, 120], where cells' V_m is changed in a known way, e.g. by exposing the cells to ionophores and observing V_m collapse (step 5). Finally, quantifying V_m requires estimation of $[Dye]_{in}$ from I_{in} measurements, which can be done by distinguishing the free from the bound dye and by taking into account that the obtained I_{in} is a convolution of $[Dye]_{in}$ and the microscope point spread function [121, 120] (step 6). As the dye's behaviour is context dependent, steps 1-6 should be repeated for each new experimental condition. Furthermore, if the dye fails any of the steps in the proposed work-flow, it is not suitable for use as a Nernstian sensor. For example, ThT for the case of *E. coli* failed in steps 2 and 3, which is why we did not need to perform subsequent steps of the work-flow.

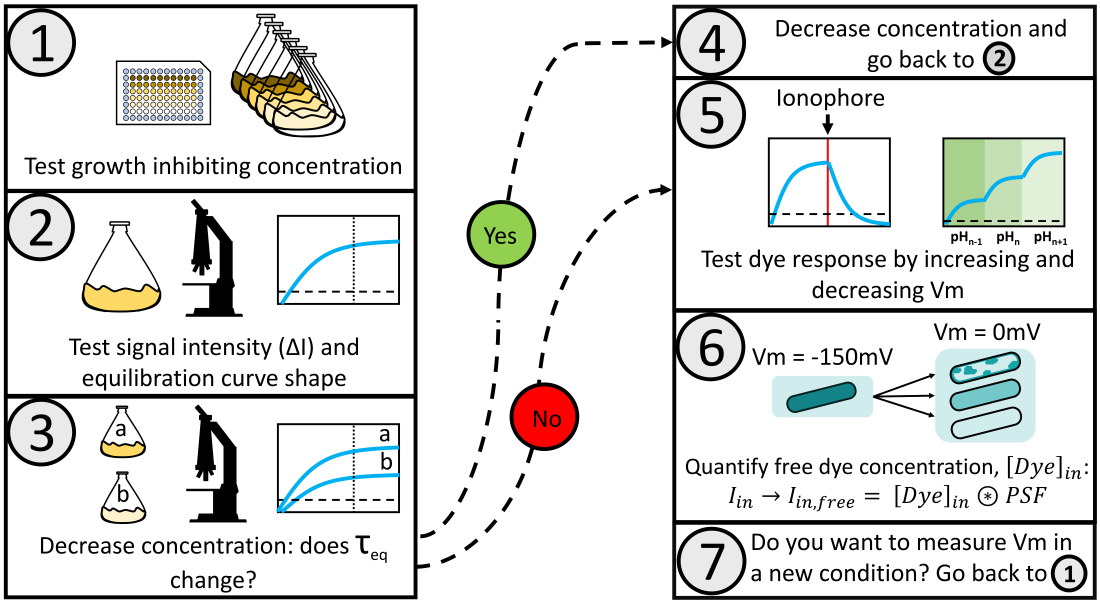


FIGURE 1.6: Proposed work-flow for characterizing the Nernstian behavior of a candidate cationic membrane voltage dye. The working concentration is estimated in steps 1 to 4, we define it as the maximum dye concentration that does not affect membrane voltage and that yields sufficient amount of signal. (1) The MNC is estimated. (2) The MNC is tested for sufficient signal intensity and the shape of the equilibration profile is inspected. (3) The effect of the dye on V_m is determined by measuring τ_{eq} at different below-MNC concentrations. (4) Different τ_{eq} for different dye concentrations indicate that the probe is altering V_m and the working concentration should be reduced and the protocol resumed from (2). Equal τ_{eq} indicates that the probe is not altering V_m. (5) Common procedures to test the expected Nernstian dye responses can then be applied, such as the introduction of a ionophore that neutralizes V_m, or changes in external pH that induce changes in V_m [120]. (6) I_{in} from the free dye should be separated from the I_{in} from the bound dye, and $[Dye]_{in}$ should be calculated from I_{in} by taking into account the microscope's points spread function. (7) Because the effects depend on the physiological state of the cell, the procedure should be repeated for every experimental condition.

Author Contributions

LM, GT, CJL, BF and TP conceived the experiments and the computational work. LM, TT, YP and YL performed experiments. GT performed computational work. LM analyzed experimental data, and LM, GT, CJL, BF and TP interpreted the results and wrote the manuscript.

Acknowledgements

We thank Dario Miroli for help with image analysis, Nathan Lord and Sebastian Jaramillo-Riveri for donating us the construct containing the hybrid mCherry-mKate2 sequence and Angela Dawson for retrieving the ΔTolC mutant from the

Keio collection. This work was financially supported by the Cunningham Trust scholarship ACC/KWF/PhD1 to TP and LM, the National Natural Science Foundation of China under grants No. 31722003 and No. 31770925 to FB, the Ministry of Science and Technology, Republic of China, under contract No. MOST-107-2112-M-008-025-MY3 to CJL and Human Frontiers Program grant RGP0041/2015 to TP, FB and CJL. TP acknowledges the support of UK Research Councils Synthetic Biology for Growth programme and is a member of the BBSRC/EPSRC/MRC funded Synthetic Biology Research Centre (BB/M018040/1).

Appendices

B. Supplementary Material

B.1. Supplementary Figures

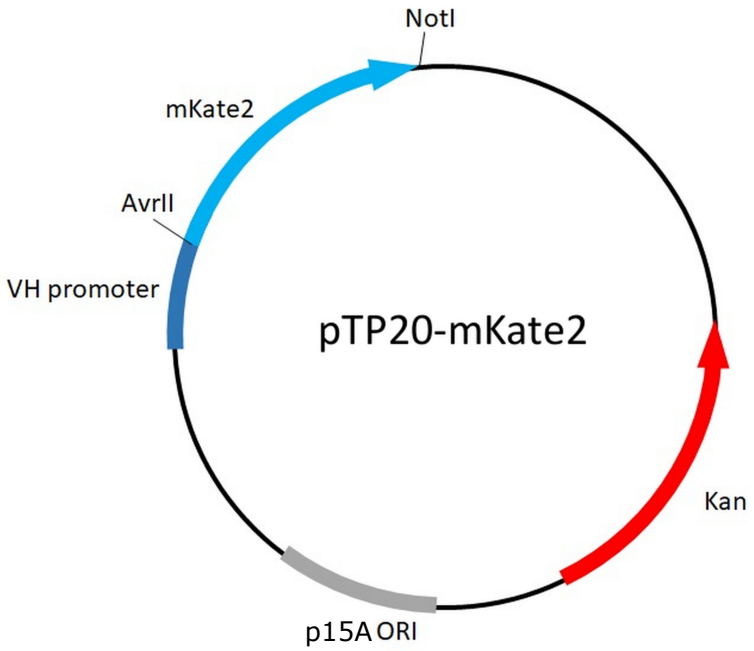


Figure 7: Plasmid map of pTP20-mKate2 showing the insertion site of mCherry-mKate2 hybrid (mKate2 for brevity) [158]. The constitutive cytochrome oxidase promoter from *Vibrio Harveyi* [126], the origin of replication and the Kanamycin resistance cassette are indicated.

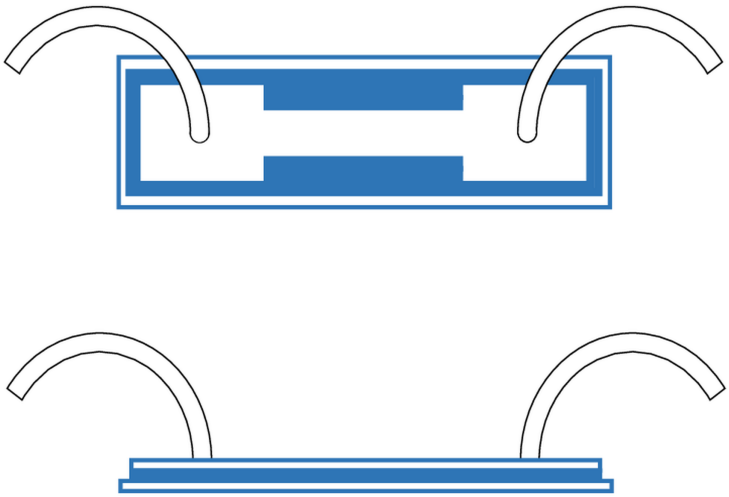


FIGURE 8: Schematic of our flow-cell. Microscope slide and coverslip are held together by custom cut Gene Frames (Thermo Fisher Scientific, UK). To exchange liquids, we drill two holes on the microscope slide and attach tubing using epoxy glue on the outside of the slide [123].

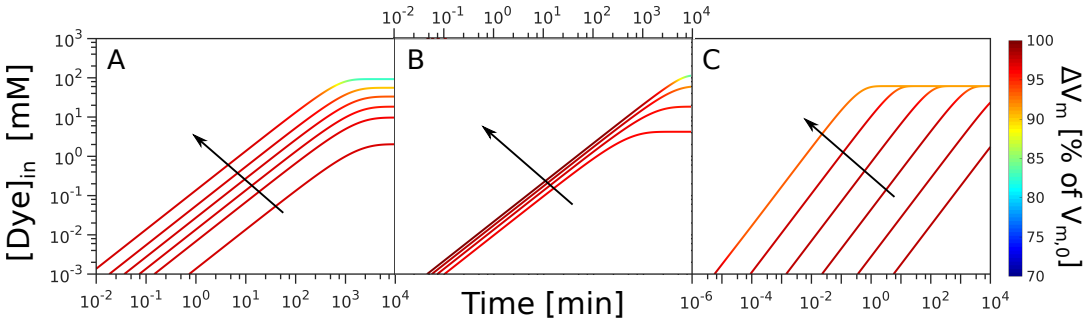


FIGURE 9: Dynamics of the dye loading assuming GHK rate law for leakage (Eq. (B.14)), where we assumed Eyring rate (law Eq. (B.13)) in Fig. 2 of the main text. (A) Intracellular Dye concentration as a function of time, for extracellular dye concentrations 10, 50, 100, 200, 400 and 1000 μM. The arrow indicated increasing $[Dye]_{out}$, and $V_{m,0} = -140$ mV, $Y_i = 150$ mM, $\Delta G_E = -210$ mV. (B) Intracellular dye concentration as a function of time for different $V_{m,0}$: -220, -180, -140 and -100 mV. The arrow indicates increasing absolute value of the $V_{m,0}$, and $[Dye]_{out} = 100$ μM, $Y_i = 150$ mM and $\Delta G_E = -210$ mV. (C) Intracellular dye concentration as a function of time for different apparent permeabilities of the membrane (with respect to the dye): 10^{-12}, $10^{-10.8}$, $10^{-9.6}$, $10^{-8.4}$, $10^{-7.2}$, 10^{-6} m/s. The arrow indicates increasing permeability, and $V_{m,0} = -180$ mV, $Y_i = 150$ mM, $\Delta G_E = -210$ mV and $[Dye]_{out} = 100$ μM.

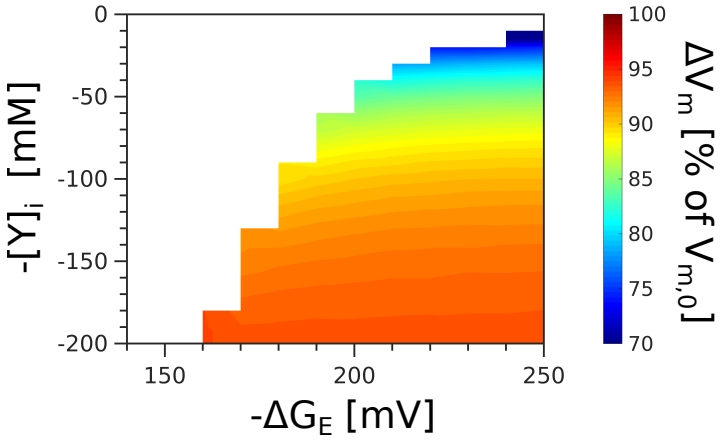


FIGURE 10: ΔV_m depends on the free energy available for transport of $[C^+]$ as well as on the contribution of charged impermeable species ($[Y_i]$), even for the same value of $V_{m,0}$. $[Dye]_{out} = 100$ μM. $V_{m,0} = -180$ mV. Colour scale on the right gives ΔV_m values.

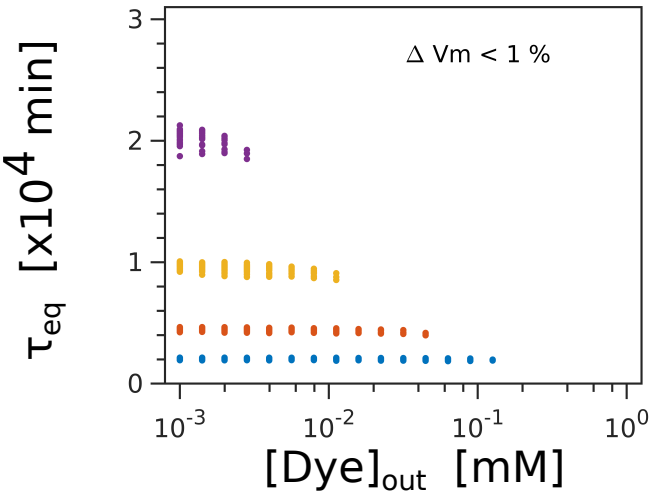


FIGURE 11: Equilibration time, τ_{eq}, as a function of $[Dye]_{out}$ for different $V_{m,0}$ values. The permeability of the dye was set to $P_{Dye} = 10^{-10}$ m/s. Purple, yellow, red and blue are $V_{m,0}$ of -220, -180, -140 and -100 mV (± 5 mV), respectively. For each value of $[Dye]_{out}$ we plot all the values of τ_{eq} that yield the desired $V_{m,0} \pm 5$ mV, where $\{[Y]_{in}, \rho, \Delta G_E\}$ were varied in the range specified in Table 4. The simulations that change $V_{m,0}$ by less than 1% mV are plotted, showing that when $\Delta V_m \sim 0$, τ_{eq} is a function of $V_{m,0}$ only.

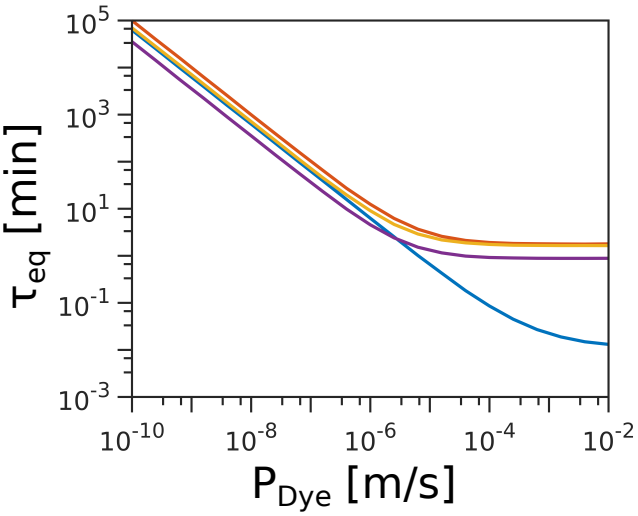


FIGURE 12: Equilibration time, τ_{eq}, as a function of the dye permeability. The following were set: $[Y]_i = 150$ mM, $\Delta G_E = -210$ mV, $[Dye]_{in} = 100$ μM. The blue, red, yellow and purple lines are for $V_{m,0}$ of -220, -180, -140 and -100 mV, respectively. For each of them, ΔV_m is permeability invariant and takes the respective values of 83%, 93%, 96% and 97%.

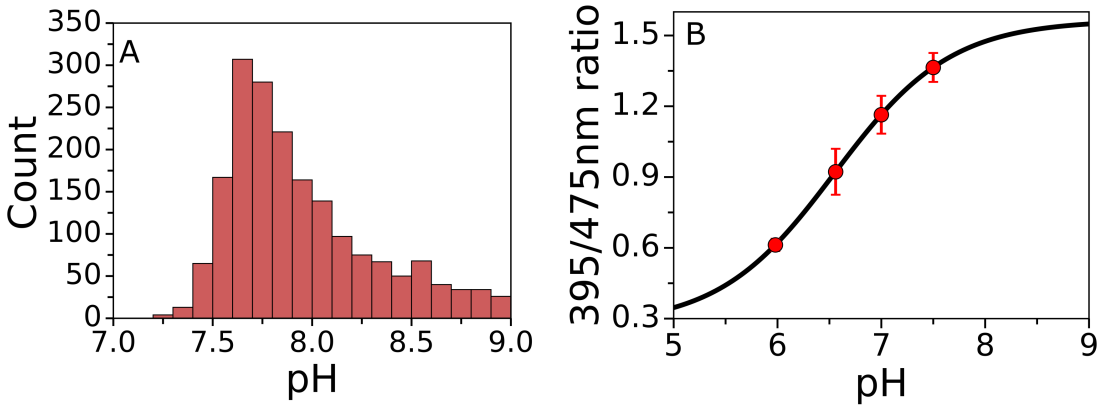


FIGURE 13: Intracellular pH measurements. (A) Using chromosomally expressed pHluorin [123, 161] we measure intracellular pH in 2346 individual cells. The median value of the distribution is 7.86. (B) *In vivo* pHluorin calibration curve where the cells were exposed to 40 mM potassium benzoate and 40mM methylamine hydrochloride in order to collapse internal pH [161]. Data points are an average of ∼400 cells and error bars give the standard deviation.

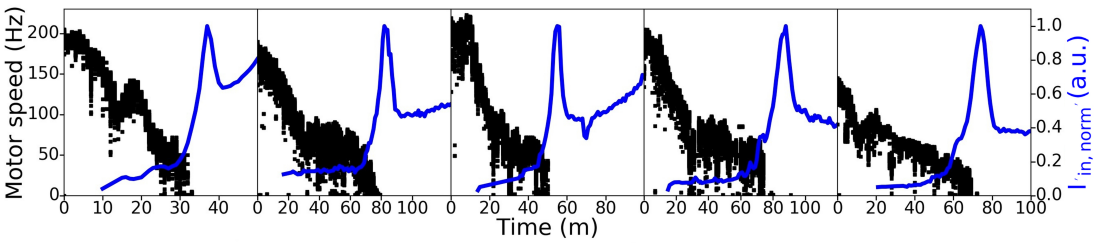


FIGURE 14: Individual motor traces (black) that were averaged in Fig. 5A. ThT intensity traces are given in blue, and imaging and exposure setting are as specified in *Material and Methods*.

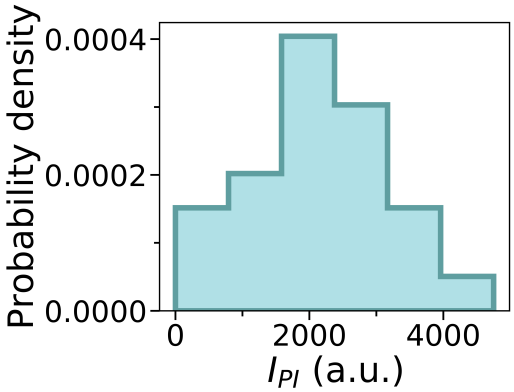


FIGURE 15: Probability density function of the final intensity values of propidium iodide from Fig. 5B ($I(t_f)$ with $t_f = 185$ min). Cell count is 25 from 3 different experiments.

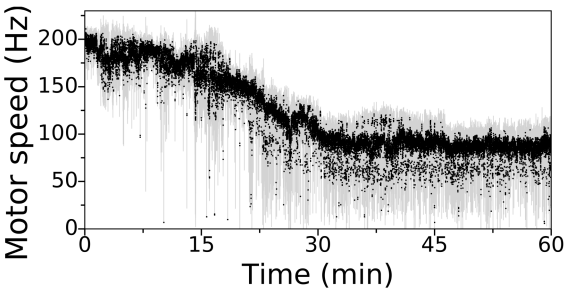


FIGURE 16: Light-induced damage quantified by measuring PMF loss via bacterial flagellar motor speed, over the length of an hour. The experiment was carried out as in Fig. 5A, but ThT was not added to the MM9 + glucose media, which was continuously supplied through out the experiment with a flow rate of 50 μl/min. Black shows the average of three individual motor speed recordings, each on a different cell, and grey area shows the standard deviation.

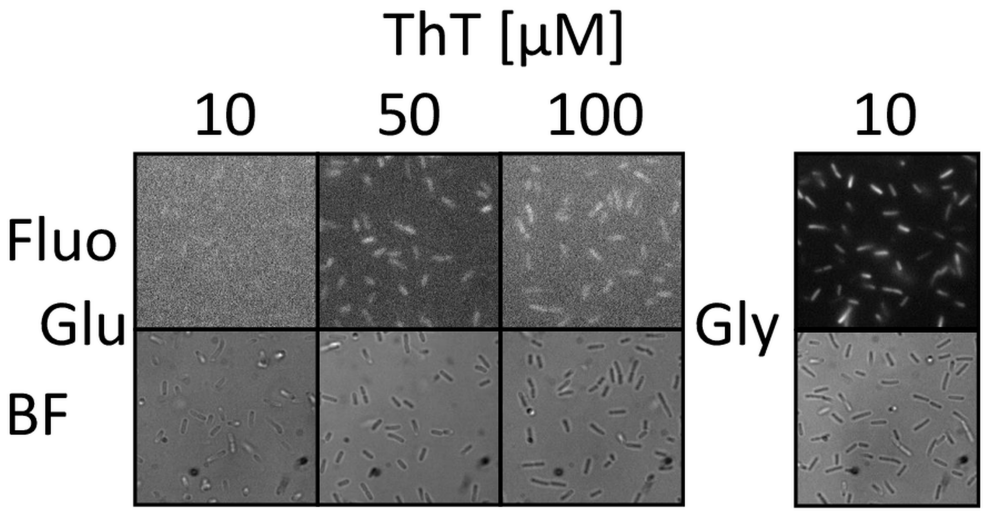


FIGURE 17: Cells grown in the plate reader (Fig 3A, B and C) in the presence of ThT were imaged, in order to estimate the extent of dye equilibration. "Fluo" abbreviation indicates fluorescence intensity and "BF", the brightfield image. Imaging conditions for ThT are the same as those used throughout the paper (Fig.3D & E, 4A, 5A, B, C & D). Cells were imaged after 7 h of growth in the plate reader (OD= 0.5- 0.6 when grown on glucose and 0.4 on glycerol) when 10 and 50 μM ThT was present, and after 8.5 h (OD 0.7 when grown on glucose) for the 100 μM ThT case.

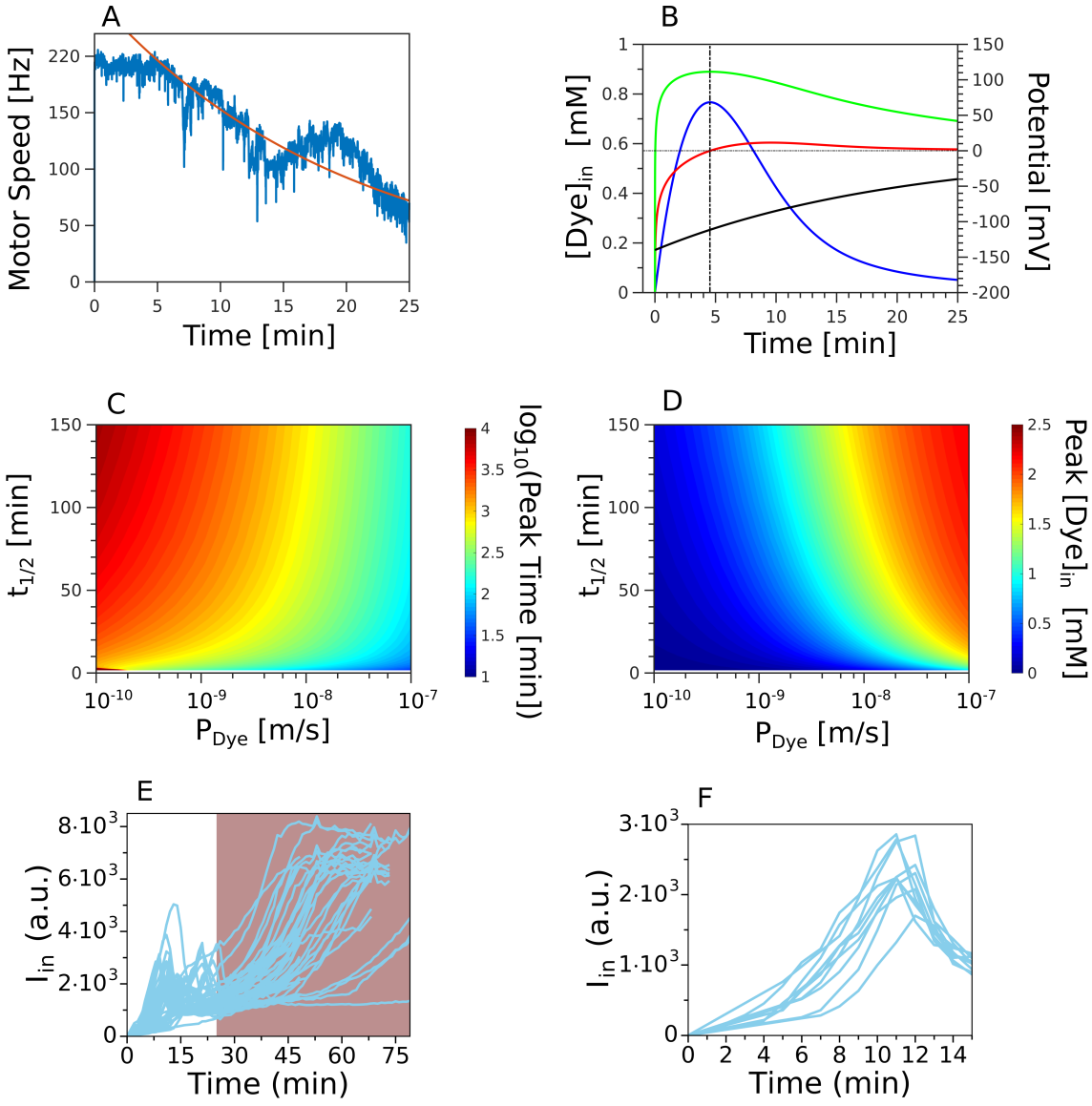
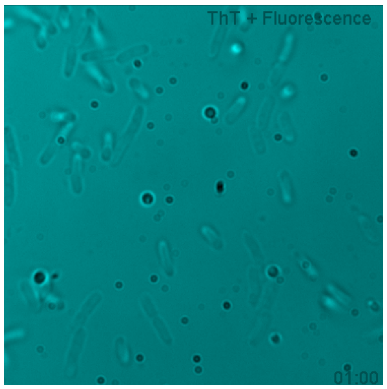
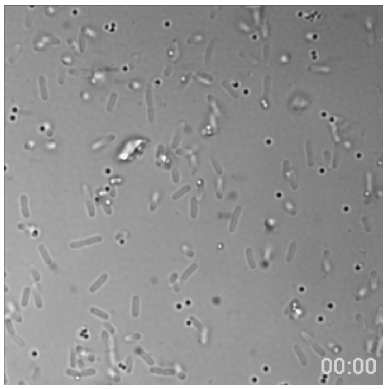


FIGURE 18: (A) Exponential decay of V_m during ThT loading leads to an intensity peak. Exponential fit (in red and starting from the time we observe the decay) to the first motor speed trace shown in Fig. SI5. The half-time of the decay is $t_{1/2} = 16.4$ min, which we use as the decay time of V_m. (B) Dye equilibration profile for the case of exponentially decaying V_m (black) is plotted in blue. The permeability of the dye was set to $P_{Dye} = 10^{-8}$ m/s, $[Dye]_{out} = 10^{-2}$ mM, and $V_{m,0} = -140$ mV. Green line depicts the contribution of the concentration gradient to the dye electrochemical potential $\ln([Dye]_{in}/[Dye]_{out})$ and red line the electrochemical potential of the dye. (C) Peak time (in log scale) and (D) peak intracellular dye concentration as a function of $t_{1/2}$ and the dye permeability. For both (C) and (D) we assumed $V_{m,0} = -140$ mV. (E) The model is relevant for the part of the equilibration profile that is driven by V_m. Subsequent increase in ThT intensity (shaded in red) does not obey Nernstian equation, because V_m is zero (Fig. 5A) and cell membrane is compromised (Fig. 5B). The traces are reproduced from Fig. 3D. (F) 10 example traces from Fig. 3D showing the portion of the equilibration curve described by our model.

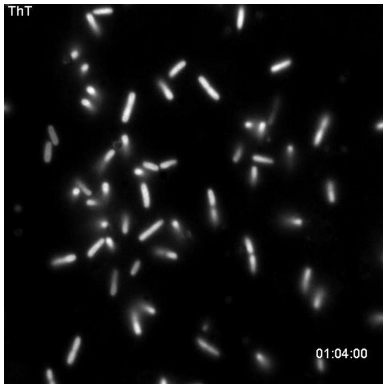
B.2. Supplementary Videos



VIDEO 1: *E. coli* growing in LB medium in our flow cell before addition of the ThT dye (images shown in gray-scale). In yellow we colour the frames that correspond to addition of the dye but without epifluorescence imaging. While the dye is present in the medium, it does not enter the cytoplasm, and thus the cells continue to grow. We colour in cyan the frames where both the ThT and epifluorescence imaging is happening at the same time. ThT now enters the cytoplasm and cells stop growing. The brightfield images correspond to one of the experiments presented in Fig. 5E.



VIDEO 2: Growth of *E. coli* in our flow cell, in MM9 + glucose medium, in the presence of epifluorescence illumination. The brightfield images are from one of the experiments in Fig. SI10. Cells grow in our flow cell when epifluorescence imaging is turned on.



VIDEO 3: Equilibration of ThT in LB. Dynamics of ThT equilibration in a flow slide in LB medium from the experiments in Fig. 3D. Images are taken every minute.



VIDEO 4: Characteristic single cell volume change and cytoplasmic marker loss during ThT equilibration. Dynamics of cytoplasmic mKate2 fluorescent signal (right) during ThT equilibration (left) from the experiment in Fig. 5 C. Images are taken every minute.

B.3. Supplementary Tables

Plasmid	Fragment	Primers
pTP20-mKate2	pWR20 backbone [126]	5' AAAGCGGCCGCGGTGATTGATTGAGCAAG 3' 5' AAACCTAGGATGTATATCTCCTTAACTAGGT 3'
pTP20-mKate2	mCherry-mKate2 hybrid [158]	5' AATGCGGCCGCTTATCTGTGCCCCAGTTT 3' 5' ATACCTAGGATGGTTAGTAAAGGAGAAGAA 3'

TABLE 1: Plasmids and primers used in this work.

Strain	Origin	Figure
MG1655		3, 4A, 5B, 5E, 5D and SI 2, 9
MG1655-*pTP20-mKate2*	This work	5C
EK01	[123]	5A and SI 4,5,7
EK07	[123]	SI 10
BW25113 Δ*tolC* pTP20-mKate2	This work	4A, 4B

TABLE 2: List of *E. coli* strains used in this work.

Name	Symbol	Value	Units	Reference
Faraday constant	F	96485	C/mol	
Gas constant	R	8.31	J/mol/K	
Temperature	T	298	K	
Avogadro Number	N_A	6.02×10^{23}	mol^{-1}	
Cell length	l_{cell}	2.95×10^{-6}	m	[162]
Cell width	w_{cell}	1.07×10^{-6}	m	[162]
Cell surface	S_{cell}	9.91×10^{-12}	m^2	Eq. SI(B.3)
Cell volume	V_{cell}	2.33×10^{-18}	m^3	Eq. SI(B.4)
Membrane Specific Capacitance	C_m	6.5×10^{-3}	F/m^2	[41]
Total Membrane Capacitance	C	6.45×10^{-14}	F	Eq. SI(B.2)
Total Extracellular ionic concentration	Π_e	200	mol/m^3	
Membrane Permeability to C^+	P_{C^+}	1.8×10^{-9}	m/s	[163] (K^+)
Membrane Permeability to A^-	P_{A^-}	1.4×10^{-10}	m/s	[163] (Cl^-)

TABLE 3: Parameters used for the simulations. The cell length and width in MM9+glucose were obtained from our fluorescence microscopy measurements and are consistent with [162].

Sampled parameters	Range of values	Spacing	Number of values
ΔG_E	$-250\text{mV} \leq \Delta G_E/F \times 10^{-3} \leq -50\text{mV}$	Linear	21
$[Y]_{in}$	$0 \leq [Y]_{in} \leq 200$ Moles/meter^3	Linear	21
ρ	$10^{-4} \leq \rho \leq 10^5$	$\log_{10}$	1000

TABLE 4: Value of parameters used when solving Eqs. SI 20 and 21 to obtain $V_{m,0}$.

B.4. Intracellular pH estimation.

To estimate the intracellular pH we used *EK07* cells grown to OD 0.8 in TB at 30°C and transferred to MM9 + glucose media, as for the experiments in Fig. 5A and as in [127]. Imaging was carried out in a flow-cell with a 50 ms exposure time and gain set to 300. Illumination at 395 nm and 470 nm was provided by a narrow spectrum UV LED and a Neutral White LED (Cairn Research Ltd, UK), respectively [123]. The filters used were ET470/40x and ET525/40m (Chroma Technology, USA) for the excitation at 470 nm and the emission of both [123]. The *in vivo* calibration curve of *EK07* cells expressing pHluorin was obtained by collapsing cytoplasmic pH using 40 mM potassium benzoate and 40 mM methylamine hydrochloride [164]. The mixture was added to MM9 + glucose media and the pH of the solution was adjusted to 5.98, 6.56, 7 or 7.5, respectively. The media at different pH were introduced into the flow-cell and imaging was carried out 5 min after [129]. Data was fitted to a sigmoid: $R395/475 = \frac{a_1 e^{k(pH \breve{} pH_0)} + a_2}{e^{k(pH \breve{} pH_0)} + 1}$ where a_1, a_2, k and pH_0 are fitting parameters as in [123] ($a_1 = 1.56449665$, $a_2 = 0.27090295$, k = 1.79203546 and $pH_0 = 6.55202883$).

B.5. Detailed description of the model

As mentioned in the main text we treat the *E. coli's* membrane as a parallel-plate capacitor and write the V_m as [32]:

$$V_m = F \cdot \frac{Q_{in}}{C} \tag{B.1}$$

where Q_{in} is the intracellular total charge (in mole) and C the membrane capacitance that depends on the membrane specific capacitance and the cell's surface area:

$$C = S_{cell} \cdot C_m \tag{B.2}$$

To calculate S_{cell} we assume the cell is a spherocylinder with 3:1 length to width ratio (determined from our microscopy images and consistent with [162]) and write as in [134]:

$$S_{cell} = \pi w_{cell} \cdot l_{cell} \tag{B.3}$$

$$V_{cell} = \pi \left(\frac{w_{cell}}{2}\right)^2 \left(l_{cell} - \frac{w_{cell}}{3}\right) \tag{B.4}$$

where l_{cell}, w_{cell} and V_{cell} are cell length, width and volume respectively.

Equation (3) in the main text lists the ionic species that contribute to Q_{in} and we assume electroneutrality in the extracellular space such that:

$$[C^+]_{out} - [A^-]_{out} + [Dye]_{out} = 0 \tag{B.5}$$

We keep the total ionic concentration in the extracellular medium, Π_e, fixed in the simulations:

$$[C^+]_{out} + [A^-]_{out} + [Dye]_{out} = \Pi_e \tag{B.6}$$

Consequently from SI Eqs. (B.5) and (B.6), the ionic composition of the medium only depends on the choice of $[Dye]_{out}$ and follows:

$$[C^+]_{out} = \frac{\Pi_e}{2} - [Dye]_{out} \tag{B.7}$$

$$[A^-]_{out} = \frac{\Pi_e}{2} \tag{B.8}$$

Separation of charges, and thus V_m, is governed by two type of reactions: leakage and active pumping, which means that the intracellular concentration of charged species we consider, changes in time as follows:

$$\frac{d[A^-]_{in}}{dt} = j_{L,A^-} \tag{B.9}$$

$$\frac{d[Dye]_{in}}{dt} = j_{L,Dye} \tag{B.10}$$

$$\frac{d[C^+]_{in}}{dt} = j_{L,C^+} - j_P \tag{B.11}$$

where equations (4) and (7) in the main text give reaction rates $j_{L,x}$, j_P, respectively. Given that chemical species Y cannot cross the membrane, Y contributes to Q_{in} in time invariant manner determined by the initial conditions only. $k_{L,x}$, k_P in the equations (4) and (7) in the main text describe the detailed mechanism by

which ions leak or are pumped across the biological membrane. In the main text we mentioned we chose k_P to be a constant and $k_{L,x}$ we base on Eyring's model [42] (equation (9) of the main text).

Choosing the forward rate of pumping k_P to be a constant implies the choice of a reversible rate function that describes at least a 2-step reaction operating always in the saturating regime for all its input variables (substrate/product concentrations and voltage), *i.e.* we assume $k_P \approx N_{Pump} \cdot v_{max}$ where N_{Pump} is the number of pumps and v_{max} the maximum rate per pump. In general, k_P is expected to depend on the input variables, and one can derive the specific functional dependency if one assumes a particular mechanism of action for the pump. To do so, we would also need to specify additional parameters characteristic for a given pump, such as affinities for its substrate, dependency on V_m, etc. This is out of the scope of this work, where we model a generic pump, and we refer the reader to [17] to find some examples of other rate laws for electrogenic pumps.

Eyring's model for $k_{L,x}$ is a special case of the so-called trapezoidal energy barrier model, which is a general model for describing the dynamics of ionic leakage across the membrane and is given as

$$j_{L,x} = \frac{S_{cell}}{V_{cell}} P_x \cdot b \cdot u \frac{[x]_{out} \cdot e^{u/2} - [x]_{in} \cdot e^{-u/2}}{e^{bu/2} - e^{-bu/2}} \tag{B.12}$$

where $u = -\dfrac{F}{RT} \cdot V_m$, P_x the so-called apparent permeability of the membrane for species x, and b is the so-called fractional width of the trapezoid. The SI Eq. (B.12) is the Eq. 7 in [42], which we multiply by $\dfrac{S_{cell}}{V_{cell}}$ to have the flux in units mole/volume/time rather than mole/surface/time, and which was first derived in [165, 166].

The apparent permeability is defined as: $P_x = \overline{P}_x \cdot \dfrac{[x]_{out}^{(interface)}}{[x]_{out}^{(bulk)}}$ where $\overline{P}_x$ is the specific permeability of the membrane for x and $[x]_{out}^{(interface)}$, $[x]_{out}^{(bulk)}$ are respectively the concentrations of x at the interface of the membrane and in the bulk (far away from the membrane). When $V_m = 0$ we expect $[x]_{out}^{(interface)} = [x]_{out}^{(bulk)}$ and the apparent and specific permeabilities to be identical. When $V_m \neq 0$ the ionic concentrations at the membrane is different compared to the bulk, ordinarily positive at the extracellular and negative at the intracellular interface, which can influence the *apparent* membrane permeability (see section 4 of [167] for more details).

In Eq. (B.12) b is parameter that characterizes the shape of the voltage drop

across the membrane ($0 \leq b \leq 1$). More specifically, b characterizes $\frac{dV(z)}{dz}$ where z denote the position within the membrane. If $b = 0$, $V(z)$ abruptly changes in the middle of the lipid bilayer such that $\frac{dV(z)}{dz} = 0$ everywhere but at the geometrical middle of the membrane. This is known as the single Eyring barrier assumption and taking into the account the equation for the electrochemical potential (8) given in the main text, it reduces the SI Eq. (B.12) to:

$$j_{L,x} = \frac{S_{cell}}{V_{cell}} P_x \cdot [x]_{out} \cdot e^{-\frac{F}{2RT} \cdot z_x \cdot V_m} \cdot \left(1 - e^{\frac{\Delta G_x}{RT}}\right) \tag{B.13}$$

which is equivalent to the equations (7) and (9) in the main text. If $b = 1$, $\frac{dV(z)}{dz} =$ constant across the membrane. This was assumed by Goldman to derive the Goldman–Hodgkin–Katz (GHK) flux equation, and it it reduces the SI Eq. (B.12) to:

$$j_{L,x} = -\frac{S_{cell}}{V_{cell}} P_x \frac{z_x F}{RT} \cdot V_m \frac{[x]_{out}}{1 - e^{\frac{z_x F}{RT} V_m}} \cdot \left(1 - e^{\frac{\Delta G_x}{RT}}\right) \tag{B.14}$$

If $V_m < 0$, $\Delta G_x < 0$, $j_{L,x} > 0$ species x moves from the outside to the intracellular environment, as expected. As mentioned before, we use Eyring's assumption for our simulations and, for simplicity, we also assume that the surface partition coefficient $\frac{[x]_{out}^{(interface)}}{[x]_{out}^{(bulk)}}$ is constant, thus P_x is a constant as well.

Detailed derivation of SI equations (13) and (14) To obtain Eqs. (B.13) and (B.14) from Eq. (B.12) we first notice that $\Delta G_x / RT = -u + \ln([x]_{in}/[x]_{out})$ so that Eq. (B.12) becomes:

$$
\begin{aligned}
j_{L,x} &= \frac{S_{cell}}{V_{cell}} P_x \cdot b \cdot u \frac{[x]_{out} e^{u/2}}{e^{bu/2} - e^{-bu/2}} \left(1 - \frac{[x]_{in}}{[x]_{out}} e^{-u}\right) \\
&= \frac{S_{cell}}{V_{cell}} P_x \cdot b \cdot u \frac{[x]_{out} e^{u/2}}{e^{bu/2} - e^{-bu/2}} \left(1 - e^{\frac{\Delta G_x}{RT}}\right) \\
&= \frac{S_{cell}}{V_{cell}} P_x \cdot b \cdot u \frac{[x]_{out}}{e^{(b-1)u/2} - e^{-(b+1)u/2}} \left(1 - e^{\frac{\Delta G_x}{RT}}\right)
\end{aligned}
\tag{B.15}
$$

When $b = 1$, Eq. (B.15) is equivalent to:

$$
j_{L,x} = \frac{S_{cell}}{V_{cell}} P_x \cdot u \frac{[x]_{out}}{1 - e^{-u}} \left(1 - e^{\frac{\Delta G_x}{RT}}\right) \tag{B.16}
$$

Which is equivalent to Eq. (8) in [42].

In order to show how to obtain Eq. (B.13) from Eq. (B.12) we first introduce the hyperbolic sinus: $2 \cdot \sinh(bu/2) = e^{bu/2} - e^{-bu/2}$ such that Eq. (B.15) is written:

$$
j_{L,x} = \frac{S_{cell}}{V_{cell}} P_x \cdot b \cdot u \frac{[x]_{out} e^{u/2}}{2 \sinh(bu/2)} \left(1 - e^{\frac{\Delta G_x}{RT}}\right) \tag{B.17}
$$

We then use the fact that $\lim_{b \to 0} \left(\frac{2 \sinh(bu/2)}{b}\right) = u$ and consequently when $b \to 0$ Eq. (B.17) reduces to Erying's rate equation (B.13).

B.6. Numerical simulations

The first step of our numerical experiment consists in finding parameter sets consistent with establishing a particular value of $V_{m,0}$, that is the membrane voltage in the absence of the dye. We assume that before the addition of the dye, the cell is in steady-state $\forall x : dx/dt = 0$ and consequently:

$$
\frac{d[A^-]_{in}}{dt} = 0 \Leftrightarrow \Delta G_{L,A^-} = 0 \tag{B.18}
$$

$$
\frac{d[C^+]_{in}}{dt} = 0 \Leftrightarrow j_P = j_{L,C^+} \tag{B.19}
$$

Thus, at steady-state, A^- equilibrates according to Nernst Eq. (2) in the main text and C^+ according to Eq. (11) in the main text. Consequently, to obtain the $V_{m,0}$ we solve the following ordinary differential equation system in a 3-dimensional grid $\{\Delta G_E, [Y]_{in}, \rho\}$ (see SI Table 4):

$$\frac{d[A^-]_{in}}{dt} = 1 - e^{\frac{\Delta G_{A^-}}{RT}} \tag{B.20}$$

$$\frac{d[C^+]_{in}}{dt} = 1 - e^{\frac{\Delta G_{C^+}}{RT}} - \rho \cdot \left(1 - e^{\frac{\Delta G_P}{RT}}\right) \tag{B.21}$$

As shown in Fig. SI1, the influence of the dye on ΔV_m depends on how $V_{m,0}$ was generated, and we can achieve the same value of $V_{m,0}$ by different parametrizations of $\{\rho, \Delta G_E, [Y]_{in}\}$.

The second part of the numerical experiment consists of choosing a starting steady-state set of values for $\{V_{m,0}, \Delta G_E, [Y]_{in}\}$ and a given $[Dye]_{out}$. We also select the values for the permeability of the membrane to cations, anions and the dye (P_{C^+}, P_{A^-} and P_{Dye}, respectively) and keep them fixed through out the experiment (values are given in SI Table 3). Lastly, to obtain the dye equilibration profile we need to implement the rate-laws for pumping and leakage we discussed above, and then solve the ODE system of SI equations (B.9) to (B.11) using the stiff solver "ode15s" from MATLAB R2018b. The initial *intracellular* concentration of the dye we chose is $[Dye]_{in} = 10^{-10} mM$, and the k_P value is chosen based on the steady-state solution for $V_{m,0}$ and using Eq. (10) in the main text. Specifically, for a chosen set of $\{V_{m,0}, \Delta G_E, [Y]_{in}\}$ we find ρ that gives $V'_{m,0} \approx V_{m,0}$ and use it to set k_P from the definition of ρ in Eq. (10) in the main text:

$$k_P = \frac{S_{cell}}{V_{cell}} \cdot P_{C^+} \cdot [C^+]_{out} \cdot \rho(V'_{m,0}) \cdot e^{-\frac{FV'_{m,0}}{2RT}}. \tag{B.22}$$

B.7. Distinguishing the inner from the outer membrane

In the main text we assumed cell's cytoplasm is separated from the environment by one membrane, effectively ignoring any potential charge separation across the outer membrane of *E. coli*. While active transport of cations proceeds across the inner membrane for the case of *E. coli*, e.g. NhaA [168] or KefB/C [169], surface charge on the outer membrane can lead to Donnan potential [138, 170], and we call

this trans-outer-membrane voltage V_p. In the absence of pumps moving cations between the periplasmic and extracellular space, the ions equilibrate across the outer membrane according to Nernst equation. Therefore, for the periplasmic concentrations we can write:

$$[C^+]_p = [C^+]_{out} \cdot e^{-\frac{F}{RT}V_p} \tag{B.23}$$

$$[Dye^+]_p = [Dye^+]_{out} \cdot e^{-\frac{F}{RT}V_p} \tag{B.24}$$

$$[A^-]_p = [A^-]_{out} \cdot e^{+\frac{F}{RT}V_p} \tag{B.25}$$

We used the measured value for $V_p \sim -30$ mV (negative in the periplasm) [170] to estimate $[Dye^+]_p \approx 3.2 \times [Dye^+]_{out}$. Thus, in the presence of such a V_p, the overall membrane voltage $V_m^\star$ would become $V_m^\star = V_m + V_p$ [32] and the impact of the dye on V_m is as if there was no V_p but the $[Dye_{out}]$ was ~ 3.2 times greater. Similarly, to account for the effect of the trans-outer-membrane voltage, all the concentrations $[x]_{out}$ refered to in the main text should be corrected by a factor $e^{-z_x \frac{F}{RT}V_p}$.

Chapter 2

Mechanisms of Coordinated Electrophysiological Maintenance in Bacteria

I. Preamble

My Contributions to this Chapter. This chapter is the result of the dominant project of my Ph.D. I designed the models and the underlying analysis framework developed in the appendix. Vizualizations of the results as well as the underlying computational experiments are the results of numerous iterations where most feedback came from my Ph.D.'s supervisors Peter Swain and Teuta Pilizota. I would like also to thanks Sebastian Jaramillo-Riveri and Vincent Danos, discussions with whom enabled the idea of vizualizing the reachable state space I develop thoroughly in the discussion and which served as a reasoning basis for the computational analyses performed in this chapter. Choice of the *in vivo* experiments that could best corroborate the models are the results of several iterations between Teuta Pilizota, Ekaterina Krasneepova and me. Ekaterina Krasneepova performed the entirety of the experimental work presented in this chapter.

How this Chapter Articulates with the rest of this Thesis. At this point, the reader should be already familiar with most of the modeling assumptions we are making in this chapter. Indeed, the definition of membrane potential was extensively discussed in the introduction and we will not use more elaborated kinetic models that those introduced in chapter 1 for passive transport across the membrane. Similarly, the kinetics for active transports are similar to those introduced in chapter 1, which functional forms only retains the generic dependency

on the state that seeds from detailed balanced constraints:

$$j_r = j_r^+ \cdot \left(1 - e^{\frac{F}{RT} \cdot \Delta G_r}\right)$$

where $j_r \in \mathbb{R}$ is the net flux of reaction r, $j_r^+ \in \mathbb{R}^+$ its forward flux and $\Delta G_r \in \mathbb{R}$ is the Gibbs free energy associated to reaction r. However, as opposed to chapter 1 wherein we characterized the model by it would do in response to underlying control variables, in this chapter we characterize *what the models cannot do*, which I think is an interesting approach in that it is unusual in computational biology. To that end, we introduce two categories of constraints: *(i)* thermodynamic constraints, that only allow some states to be possibly achieved[1] at steady-state with access to given transporters and *(ii)* Constraints based on prior biological knowledge, *i.e.* Stoichiometries for the transport systems, Gibbs free energy associated to ATP hydrolysis or NADH reduction, osmotic pressure cannot be too high, range of pH_i maintained, valency of macromolecules are restriced to some range.

Analyzing the coordination of several electrophysiological variables simultaneously (osmotic pressure, PMF, membrane potential and pH_i), along with studying what the models cannot do allows us to draw generalizable conclusions from the study of our models. For instance: For instance *(i)* a cell generating membrane potential with symporters would need to possess a cell wall able to withstand high osmotic pressure, *(ii)* in spite of PMF being necessary to generate membrane potential, intracellular charges carried by protons do not directly contribute to the build up of membrane potential[2]. Also, the coupling stoichiometry of an antiporter and its type (whether it is a proton:anion or proton:cation antiporter) is what determines its prevalence at different extracellular pH, *etc.* The reasoning of this chapter, that consists in incrementally eliminating non-achievable configurations of the system, presents a theoretical argument that the paradigmatic view on the mechanisms by which pH_i is maintained is not correct. In particular, we argue that the main functions of proton:ion antiporters, decarboxylating enzymes is to

[1] Without violating second law of thermodynamics

[2] This is a subtle difference. Indeed this is the gradient of protons across the membrane that allows movement of relevant charges to generate the gradient of charge (membrane potential) across the membrane and protons are present only at low concentrations such that for an identical proton gradient, two different intracellular concentrations of protons and everything else being the same, would yield a nearly identical membrane potential

modulate the membrane potential and that the ability to modulate the membrane potential in different environments seeds from the need to simultaneously maintain pH_i that is necessary for survival and to enable respiration, which requires sufficiently high PMF. Based on our model of electrophysiological maintenance, we validate experimentally two predictions that have not been made before in the literature: *(a)* that low PMF entails loss of pH_i homeostasis at pH_e sufficiently far from 7[3], *(b)* that dissipation of the PMF entails loss of the ability to maintain membrane potential. In addition, we report a decrease in PMF as well as an increase of the membrane potential to PMF ratio in alkaline pH_e[4]. The latter support our prediction that antiporters with higher proton to cation stoichiometric ratio must be used in alkaline environments, as has been observed for *E.coli*.

We also introduce the notion of *optimal strategy for electrophysiological maintenance*, that sets non-ambiguously how a particular cell must coordinate the activity of its various ionic pumps in order to save as much energy as possible for non-maintenance related functions. Although not developed extensively in this chapter, we see the optimal cost of electrophysiological maintenance as an additional physical constraint that restricts the possible electrophysiological behaviours of bacteria. Accordingly, we will make use of our ability to theoretically evaluate the cost of electrophysiological maintenance in chapter 3, in order to study how the ionic composition of the environment and the values to which the cell maintains its osmotic pressure, PMF, pH_i, impact high level behaviors of bacteria, such as their growth-rate and growth-yield.

Additional Remark. We generalize in the appendix some results that we obtained for the model of *E.coli*'s electrophysiology. In particular, we demonstrate how to enumerate thermodynamically viable steady-states for models containing arbitrary number of ionic pumps of arbitrary types. We then derive a formula for the minimal cost of maintaining a set of electrochemical potentials for models where PMF is fixed and all other ions have access to an arbitrary number of proton:ion antiporters of any stoichiometries. Thus, most of the computational analysis we perform to analyze *E.coli*'s model are in principle applicable to a important variety of electrophysiological models.

[3]For reasons distinct than accrued cost of pH_i maintenance when pH_e deviates too much from neutrality, a topic we should discuss at the end of this chapter and in the following one.

[4]Which as we will see later, is enabled by accrued activity of proton:cation antiporters with high proton to cation stoichiometric ratio.

Abstract

Maintenance of both intracellular pH (pH_i) and Proton Motive Force (PMF) is crucial for cell survival. Indeed, while near neutral pH_i is important for stability of macromolecules, sufficiently high PMF enables energy transduction *via* the respiratory chain, a very efficient way of making ATP from various substrates, including glucose[5]. In Bacteria, proton:ion antiporters as well as decarboxylases are currently seen as mechanisms allowing pH_i maintenance *via* direct control over the entry or exit of protons from the cytoplasm. Contrary to this view, we hypothesize that such mechanisms are used for controlling membrane potential, modulation of which enables sufficiently high PMF across a wide range of pH_e, *e.g.* decarboxylation (in isolation) acidifies the pH_i but allows modulation of membrane potential *via* modulation of the charge carried by amino-acids, which in turns allows overall desacidification of the intracellular space[6]. A consequence of our model of simultaneous pH_i, PMF, membrane potential and osmotic pressure maintenance crucially predicts that lower PMF restricts the pH_e range wherein a cell is able to maintain its pH_i as well as the extent to which the cell can polarize. Consistent with our postulate, we find that *(i)* lowering PMF by depriving *E.coli* Cells of oxygen results in loss of pH_i homeostasis at less acidic pH_e than *E.coli* high PMF cells in aerobic conditions, *(ii)* lowering PMF by addition of a protonophore CCCP results in complete depolarization of the cells. Finally, our model predicts pH-dependent activity of several antiporters *ClcA*, *NhaB*, *NhaA* qualitatively similar to what has been reported in the literature and provides a framework for evaluating the energetic cost of maintaining electrophysiological homeostases.

Keywords: pH hoemostasis | single-cell electrophysiology | mathematical modeling of bacterial cells | Mechanisms of Voltage generation | proton:ion antiporters

II. Introduction

Living cells maintain intracellular composition different from the external environment, and often, properties of the inside are kept within a certain range, so called homeostasis. For example, and perhaps unsurprisingly given the effect

[5] we will focus on this substrate for reference cellular parameters (shape, growth-rate, energy requirement for growth) in this and the following chapters

[6] One of the aim of this chapter is to explain that counter-intuitive statement

of pH on protein stability [171], intracellular pH (pH_i) is maintained close to neutral in organisms across all kingdoms of life, from archaea and eubacteria [4] to mammalian cells [172]. Neutralophilic bacteria, such as *Escherichia coli*, have been reported to maintain cytoplasmic pH close to 7.5 in a range of external pH values (pH_e) [173]. Several reports show that upon a sudden shift in pH_e from neutral ($\sim$ 7.5) to acidic ($\sim$ 5.5), *E. coli's* cytoplasm initially changes with the pH_e shift, but then quickly recovers to be maintained within a narrow range ($\sim$7.5), Fig. 2.1A [173, 174, 175]. More recently, this view has been challenged with reports on permanent changes in internal pH upon the environmental pH change, Fig. 2.1A [176, 177, 178].

Explanations offered for the discrepancy in the measurements include inaccuracies in the pH sensor calibration and usage, and strain to strain differences [176]. However, pH homeostasis has thus far not been looked at in the context of all the cellular physiological variables that are influenced by it. For example, osmotic pressure of the cell (Π) depends on the difference between the total concentration of all of the available solutes across the membrane [28], thus protons are included. The electrical potential across the membrane (so called membrane voltage or membrane potential, $\Delta\psi$, which we use interchangeably hence forth) corresponds to the total difference in charges accumulated close to the membrane, again protons are included. Proton Motive Force (PMF), the electrochemical gradient of protons, is influenced both by $\Delta\psi$ and the difference between the inside and the outside pH (ΔpH), whereas the electrochemical gradients of all the other ions present in the cell (Ion Motive Forces (IMFs)), are influenced by the $\Delta\psi$ and thus indirectly protons. The intertwined nature of these physiological variables, suggest that we need to look at their maintenance in a coordinated fashion, in order to understand the homeostasis of even just one of them, for instance internal pH.

To do so, we build a simplified mathematical model of cellular electrophysiology. We find that the cell's ability to maintain pH_i is set by the maximum achievable PMF, which is determined by the composition of the environment, cellular ion pumps as well as charged intracellular molecules that cannot easily cross the biological membrane. We employ assays for time-course, single-cell, concurrent measurements of PMF and pH_i that we recently developed [179, 180], to measure *E. coli's* internal pH during external pH shifts at two different PMF values. In agreement with the model prediction, we find that at a given pH_e *E. coli* maintains pH_i if the PMF is sufficiently high, and does not, if the PMF falls below a critical

value. Our results can reconcile all previous observations [173, 174, 175, 176, 177], as they suggest these were made on cells with different values of PMF (e.g. anaerobic versus aerobic environment)[7]. Lastly, our model suggests, in agreement with experiments, that pH_i is not maintained directly, instead the homeostasis is a consequence of membrane voltage maintenance.

III. Results

Mathematical model of cellular electrophysiology enables synergistic view of intracellular homeostasis

In order to take into account the intertwined nature of pH_i maintenance, and without losing in generality we build a mathematical model of cells' electrophysiology by including only the following species: protons (H^+), hydroxide ions (OH^-), one small monovalent cation (C^+)[8], one small monovalent anion (A^-) and molecules that cannot cross the biological membrane (captive molecules), Fig. 2.1B. All ions in the model can leak across the biological membrane [17], but H^+, C^+ and A^- can also be pumped across the membrane with a set of pumps, each of which is characterized with a specific stoichiometric ratio and an electrochemical potential. For example, a pump can be an antiporter moving one H^+ into the cell and C^+ out (stoichiometric ratio of 1), or an antiporter moving two H^+ into the cell and one C^+ out (stoichiometric ratio of 2). Captive molecules, their average amount and valency, is maintained by cellular processes which we do not consider in the model (e.g. glutamate).

The specific electrochemical gradient is defined as:

$$\Delta G_x = z_x \Delta\psi + \frac{RT}{F} \cdot \ln \frac{[x]_i}{[x]_e} \tag{III.1}$$

where x is the small ion (internal or external to the cell denoted by subscripts i and e), z_x its valency (here ± 1 only), R, T and F the gas constant, temperature and

[7] Indeed, [176, 177] find that *E. coli* does not maintain pHi as well as the observations from [173, 174, 175], in media containing similar substrate. One (very hypothetical without actually doing the experiments) way to reconcile these observations in that in [176, 177] cells run out of oxygen in the course of the experiment.

[8] We thus in this chapter (and the following one) ignore the case where the cell has to manage several gradients of small cations – for instance potassium and sodium –. We will discuss in the closing chapter of this thesis some constraints for cells being in environments bearing different types of small cations and the mathematical relationships between the model with only one small cation and models with arbitrary numbers of types of small cations.

Faraday constant respectively, and $\Delta\psi$ the membrane voltage. ΔG_x, expressed in Volts, effectively gives information on the minimal amount of energy (or work) needed to move a mole of ion x against its electrochemical gradient. While ΔG_x is linear in $\Delta\psi$, it is logarithmic in the concentration ratio of the small ion x.

Build up of membrane voltage, i.e. separation of charge across the biological membrane is enabled by its hydrophobic properties, so that it effectively acts as a capacitor. Therefore, $\Delta\psi$ is proportional to the amount of intracellular charge Q_i, scaled by the specific membrane capacitance C_m [31, 32, 33, 34]:

$$\Delta\psi = \frac{F}{S \cdot C_m} \underbrace{V \cdot \sum_x z_x [x]_i}_{Q_i} \tag{III.2}$$

where $[x]_i$ denotes intracellular concentration of molecule x and V, S are cellular volume and surface (we assume a cell is a spherocylinder with 3:1 length to width ratio, see also *Supplementary Information* and [29]). In (III.2) x now includes captive molecules, which may or may not be charged, as well as ions. We allow molecules x to have $z_x = 0$, in which case they do not contribute to $\Delta\psi$, because all cytoplasmic species in our model contribute to the osmotic pressure of the cell:

$$\Delta\Pi = RT \sum_x \left([x]_i - [x]_e\right) \tag{III.3}$$

To change the extracellular environment we proceed as follows. We start with a solution of water at pH 7, to which we add either an acid ($[\mathrm{AH}]_0$ is mole of AH per mole of water) or a base ($[\mathrm{COH}]_0$) in order to change pH_e. To change the external salt concentration we add $[\mathrm{CA}]_0$ (in a range 0.5 to 500 mM). We assume that upon addition external environment equilibrates and stays constant (i.e. the cell's activity does not change it), which allows us to utilize the known dissociation and association constants (pK_a and pK_b), mass conservation and the charge neutrality of the solution to fully define the external environment (see also *Supplementary Information* for further details).

i. To generate electrochemical gradients of ions, and thus physiological membrane voltage, cells need to actively pump ions out

Having defined the model and accounted for all the physiological variables linked to pH_i homeostasis, we first solve it for the simplest case, i.e. we do not account

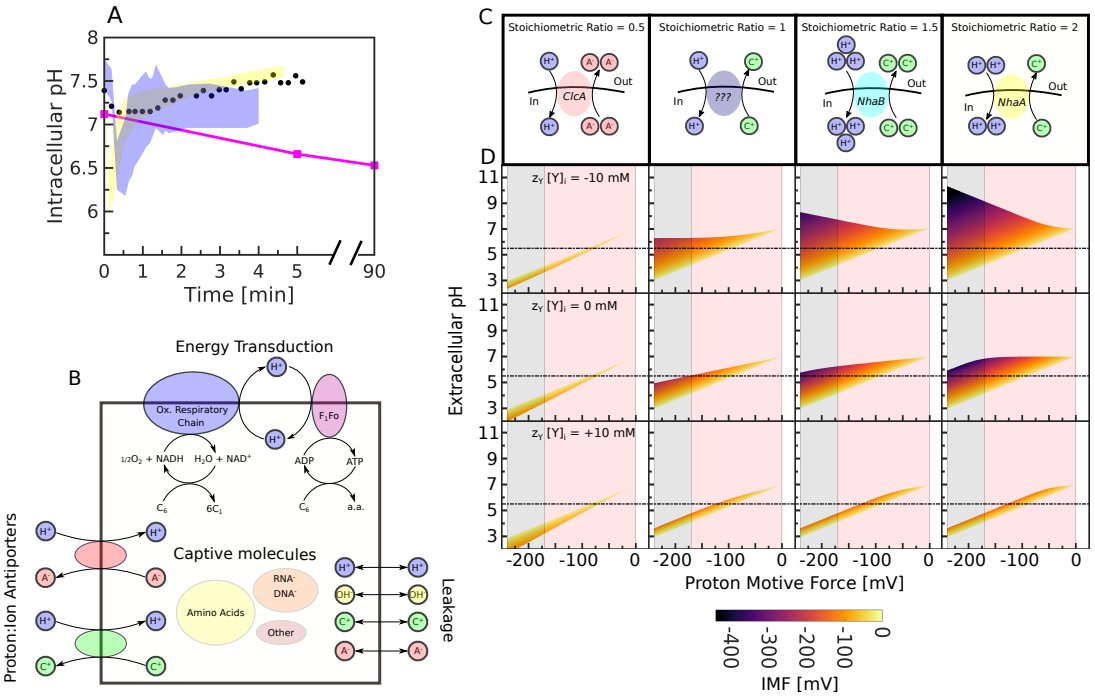


FIGURE 2.1: The ability of the cell to maintain pH_i is directly related to the PMF it can generate. (A) We plot previously reported experimental results on pH_i homeostasis. Pink squares shows data from [176] where cells were transitioned from pH_e 7.2 to 5.6. Black dots are population data from [173] where cells were transition from pH_e 7.5 to 5.5, yellow shaded area is the pH_i range measured in individual cells upon pH_e transition from 7.5 to 5.5 [174], and blue shaded area is pH_i range obtained from single cell data upon pH_e shift from 7.5 to 5.5 [175]. (B) Simplified model of *E. coli*'s electrophysiology. We distinguish between small ions which both leak and are pumped across the membrane, and captive molecules which the cells maintains by process we do not consider in the model. The two classes of species contribute to membrane voltage and osmotic pressure. For simplicity, only two small cations (protons and another representative small cation C^+) and two small anions (hydroxide ions and another representative small anion A^-) are accounted for. The energy transduction components generate PMF by either the respiratory chain (aerobic mode) or F_1F_o (anaerobic mode). We keep NADH, NAD^+, ATP, ADP, and external environment concentrations fixed in the model. Proton:ion antiporters can further exchange protons for the small cation C^+ or anion A^- thereby generating the corresponding Ionic Motive Forces (IMF). (C) Cartoons of antiporters we include in our model. The stoichiometric ratio of an antiporter is the ratio of characteristic stoichiometric coefficients, i.e. the number of protons divided by the number of ions that it exchanges. Of the four stoichiometries we chose to include, three have known equivalents in *E. coli*: ClcA [74], NhaB [72] and NhaA [73]. (D) Allowed solutions for each antiporter are plotted for a given PMF and pH_e value ($pHe \in [2, 12]$, $\Delta G_H \in [-240, 0]$ mV) and while keeping $[CA]_0 = 100$ mM, $z_Y \cdot [Y]_i \in \{-10, 0, +10\}$ mM and pH_i=7. Colour scale given on the right indicates allowed IMF (ΔG_x) values. The horizontal black line indicates pH_e=5.5 and shaded gray and red areas indicate PMF values characteristic for respiration and fermentation, respectively. The predicted values were obtained assuming a fixed free energy of ATP hydrolysis across conditions.

for active ion pumping and set $\Delta G_{A^-} = \Delta G_{C^+} = \Delta G_{H^+} = 0$. In such a scenario ions leak across the membrane, eventually equilibrate (with $\Delta G_x = 0$ (III.1) becomes Nernst equation) and generate $\Delta\psi$ that is referred to as Donnan potential[9]. Because we are interested in Donnan potential at different extracellular ion concentrations, and at different captive molecule concentrations, we rewrite (III.2) by splitting the contributions of individual charged molecules and expressing internal ion concentrations as a function of externals using (III.1) (see *Supplementary Information* for full derivation):

$$\Delta\psi = \frac{F}{S \cdot C_m} V \cdot \left(z_Y \cdot [\mathrm{Y}]_i + [\mathrm{H}^+]_i - [\mathrm{OH}^-]_i + [\mathrm{C}^+]_e \cdot e^{\frac{F}{RT}(-\Delta\psi)} - [\mathrm{A}^-]_e \cdot e^{\frac{F}{RT}(\Delta\psi)} \right) \tag{III.4}$$

where we denote the captive molecules with $[Y]_i$ (valency z_Y).

To solve equation (III.4) for $\Delta\psi$ at different total external ion concentrations and for different values of $\mathrm{z}_Y[\mathrm{Y}]_i$ we include following additional considerations and assumptions. For most microbes, including acidophiles and *E. coli* even when reported to not show pH_i homeostasis, cytoplasmic pH stays within 6 to 8 range [4, 176]. Thus, the contribution from $[\mathrm{H}^+]_i$ and $[\mathrm{OH}^-]_i$ to $\Delta\psi$ is up to ± 3.5 mV, which is two orders of magnitude smaller than experimentally measured $\Delta\psi$ (~ -140 mV [181]), so we neglect it[10]. Given our assumption on *E. coli*'s shape and length to width ratio, the surface to volume ratio is $\sim 4.25 \times 10^6$ m^{-1} and we use previously reported $C_m \sim 6.5 \times 10^{-3}$ F/m [41], so that $\frac{F}{S \cdot C_m} V \sim 3.5$ $\mathrm{Vmol}^{-1}\mathrm{m}^{-3}$. With the above assumptions included, we solve (III.4) for $\Delta\psi$ and in Fig. 5 show obtained Donnan potential ($\Delta\psi$) at different external ion concentrations and for different values of $\mathrm{z}_Y[\mathrm{Y}]_i$. Captive molecules (at up to experimentally reported concentrations 300 mM [182]) can enable generation of physiological $\Delta\psi$, but only in low salinity environments (1-10 mM). In environments of higher external salinity, the captive molecule concentrations (and at a physiological average valency) needed to achieve physiological $\Delta\psi$ raises cellular osmotic pressure above experimentally observed values that range between 0.3 and 3 atm [183, 24][11],

[9] A state that does not depend on the permeability of the membrane for different ions

[10] A perhaps clearer rephrasing of this statement is that pumps that only move protons across the membrane locally do not contribute to a build-up of membrane potential; where locally means in a system where these pumps work in isolation, *i.e.* the proton gradient thereby generated is not coupled to the transport of different ionic species.

[11] For *E. coli* cells, possessing a cell wall.

Fig. 6. Thus, our model predicts that to achieve $\Delta\psi$ above Donnan potential, in medium of standard external salinity and while maintaining physiological osmotic pressure, *E. coli* needs to actively pump small ions and equation for $\Delta\psi$ becomes:

$$\Delta\psi = 3.5 \cdot \left(z_Y \cdot [\mathrm{Y}]_i + [\mathrm{C}^+]_e \cdot e^{\frac{F}{RT}(\Delta G_{C^+} - \Delta\psi)} - [\mathrm{A}^-]_e \cdot e^{\frac{F}{RT}(\Delta G_{A^-} + \Delta\psi)} \right) \tag{III.5}$$

Fig. 7A shows 4 possible scenarios a cell could adopt when pumping ions: it could pump anions only ($\Delta G_{C^+} = 0$), either in (top left in Fig. 7 A) or out (bottom right), or it could pump cations only ($\Delta G_{A^-} = 0$), again in both directions (top right and bottom left in Fig. 7 A). Pumping anions or cations in to generate physiological $\Delta\psi$, results in very large osmotic pressures, and only pumping cations out, generates Π and negative $\Delta\psi$ in the experimentally observed range (this conclusion does not change even if we allow both anions and cations to be pumped simultaneously, Fig. 8). Fig. 7B to D show the influence of captive charges in different extracellular ion concentrations on the values of $\Delta\psi$ the cell can obtain, as well as decomposition of $\Delta\psi$ according to intracellular anions, cations or captive molecule concentrations.

ii. The ability of the cell to maintain pH_i is directly related to the PMF it can generate

Having learned that pumping cations (that are not protons) out of the cell results in physiological $\Delta\psi$ and Π values, we next wish to explore the influence of changes in pH_e on pH_i, $\Delta\psi$ and PMF. To do so, instead of setting the values of IMFs, as we did in the previous chapter, we model their generation. We use the following equation to describe the movement of an ion across the membrane:

$$\frac{dx_i}{dt} = -\frac{dx_e}{dt} = j_x + \sum_n \sigma_{x,n} \cdot j_n \tag{III.6}$$

where j_x is the flux of ions due to leakage, j_n flux of ions due to a specific pumping reaction n and $\sigma_{x,n}$ the stoichiometric coefficient of that reaction. For energy transduction we consider, and denote with ΔG_n, two specific ion pumping reactions: respiration and fermentation. For example, we define the respiration

reaction as the coupling of the redox reaction $R^\star \rightleftharpoons R$ to the export of protons $H_i \rightleftharpoons H_e$:

$$R^\star + \sigma_{H,R} \cdot H_i \rightleftharpoons R + \sigma_{H,R} \cdot H_e \tag{III.7}$$

where $\sigma_{H,R}$ is a stoichiometric coefficient that determines the number of protons moved across the membrane per turnover of a respiratory reaction, and we define ΔG_R as the potential of the redox reaction $R^\star \rightleftharpoons R$. For the overall rate of the respiratory reaction to be positive so that protons are moved out of the cell:

$$j_{H,R} > 0 \Leftrightarrow \Delta G_{H,R} = \Delta G_R - \sigma_{H,R} \cdot \Delta G_H < 0 \tag{III.8}$$

Note that the minus sign in front of the PMF is in line with its definition: positive for protons moving into the cell and negative vice versa. We make similar considerations for ATP production by F_1F_o ATP-synthase that couples ATP production to transport of protons (PMF) [48]:

$$ADP + \sigma_{H,F1Fo} \cdot H_e \rightleftharpoons ATP + \sigma_{H,F1Fo} \cdot H_i \tag{III.9}$$

where $\sigma_{H,F1Fo}$ is the characteristics ATP-synthase stoichiometric coefficient (the number of protons moved across the membrane per hydrolyzed ATP), $ATP \equiv ATP^{4-} + H_2O$ and $ADP \equiv ADP^{3-} + HPO_4^{2-} + H_i^+$. For the flux of ATP to be positive the total ΔG of the reaction needs to be negative and we have:

$$j_{F1Fo} > 0 \Leftrightarrow \Delta G_{F1Fo} = \sigma_{H,F1Fo} \cdot \Delta G_H - \Delta G_{ATP} < 0 \tag{III.10}$$

Thus, (III.8) and (III.10) set the boundaries on PMF in respiratory regime:

$$\frac{\Delta G_R}{\sigma_{H,R}} < \Delta G_H < \frac{\Delta G_{ATP}}{\sigma_{H,F1Fo}} \tag{III.11}$$

To estimate the values of PMF within these boundaries we use previously reported ΔG_{ATP} for exponentially growing cells that respire on glucose $\sim$ -560 mV [182], with $\sigma_{H,F1Fo} = 3.3$ [67] (see also *Supplementary Information*). For ΔG_R we use -2290 mV (based on Gibbs free energy of the half-reactions from [184]), with 10 protons moved per reduced NADH [68], and obtain -229 mV $< \Delta G_H < -170$ mV . When $\Delta G_H > \frac{\Delta G_{ATP}}{\sigma_{H,F1Fo}}$, ATP is hydrolyzed by F_1F_o and protons are extruded (thus making ATP *via* oxidative phosphorylation is not possible).

Next we assume that antiporters are responsible for the membrane voltage maintenance in the cell, because ATP driven ion efflux pumps have not been reported in *E. coli* (appart from F1Fo). We treat the action of a given antiporter in a similar fashion to energy transduction (and summarize all the reactions we consider in the model in Table SI2):

$$\sigma_{\mathrm{H},a} \cdot \mathrm{H}_e + \sigma_{x,a} \cdot x_i \rightleftharpoons \sigma_{\mathrm{H},a} \cdot \mathrm{H}_i + \sigma_{x,a} \cdot x_e \tag{III.12}$$

where subscript a denotes the specific antiporter. For the rate $j_{x,a}$ of such an antiporter to be positive, the overall ΔG needs to be negative and we have:

$$j_{x,a} > 0 \Rightarrow \Delta G_{x,a} = \sigma_{\mathrm{H},a} \cdot \Delta G_H - \sigma_{x,a} \cdot \Delta G_x < 0 \tag{III.13}$$

(III.13) sets the boundaries of allowed IMFs for a given antiporter, and for the PMF values in either respiratory (-229 mV to -170 mV) or fermentative regime (-170mV to 0 mV). With the obtained allowed IMF values we can now solve (III.5) for $\Delta\psi$, providing we chose the extracellular environment. In Fig. 2.1C and D we choose $[\mathrm{CA}]_0$=100 mM, vary $\mathrm{pH}_e \in [2, 7]$ while keeping pH_i=7, take into account discussed constraints ((III.8), (III.10) and (III.13)), and solve (III.5) for a given antirporter and for three different values of $z_Y[Y]_i$. For a proton:anion antiporter $\Delta G_{C^+} = 0$, and for a proton:cation antiporter $\Delta G_{A^-} = 0$. Fig. 2.1C shows cartoons of chosen antiporters, all but one of which have analogues in *E. coli*[12] [74, 72, 73], and Fig. 2.1D shows allowed values of IMFs for a given PMF and pH_e. Also, contrary to what is sometimes assumed [185], we show that electroneutral antiporters can generate membrane potential, here shown as a range of ΔpH. The range of external pH values for which the cell maintains pH_i=7 varies for different antiporters and with different values of PMF, because each antiporter generates $\Delta\psi$ in a different range, Fig. 13. For example, for pH_e=5.5 and using NhaA, the cell can maintain pH_i=7 only if PMF < -100 mV. Using ClcA with reported stoichiometry and assumed direction of pumping (1 proton out and 2 anions in [74, 186] gave no allowed solution. To achieve physiological PMF in such a scenario we would need to introduce an additional chloride pump that maintains chloride motive force. However, our model predicts physiological PMF if we assume ClcA works in the opposite direction with the reported stoichiometry. The finding is

[12] analogue with known stoichiometries. Indeed a large amount of antiporters in *E.coli* have unknown stoichiometries and it may be the case that they possess an electroneutral antiporter as depicted on the scheme.

not contradictory with the experimental results, e.g. ClcA reconstituted in the artificial vesicles can pump in both directions depending on the imposed chloride motive force [74, 186]. The direction of pumping of ClcA was instead assumed upon the expectation that it removes protons from the cytoplasm in acidic pH_e, we discuss this further in the *Discussion*.

In Fig. 2.1D we indicate the values of PMF the cells generate when working in either respiratory or fermentative regime, calculated based on the assumption of constant free energy for ATP hydrolysis. We note, however, that free energy of ATP hydrolysis could change in different external environments, which would change the specified PMF transition value (from respiratory/ to fermentative condition).

The range of pH_e for which the cell maintains pH_i depends also on the captive molecules, which we illustrate by selecting three different values of $z_Y \cdot [Y]_i$ in Fig. 2.1D and Fig. 10. Finally, in Fig. 2.1D we set the $[CA]_0$ and now wondered how our results and conclusions would change if we chose different values. For the purpose, we rewrite (III.5) (see *Supplementary Information*) to easily ask what is the difference in $\Delta\psi$ we obtain if we assume that $[CA]_0 \to +\infty$ and pH_e=7, versus if we assume any other values. Fig. 11 shows that this difference does not change significantly with $[CA]_0$ and pH_i for a given $z_Y \cdot [Y]_i$ range, but the value of the error does change with $z_Y \cdot [Y]_i$ (for realistic $z_Y \cdot [Y]_i$ the error is between 0.1-1 mV).

iii. At pH_e 5.5 *E. coli* exhibits pH_i homeostasis if the value of PMF is sufficiently high

In order to experimentally confirm our theoretical prediction on the role of PMF and $\Delta\psi$ maintenance for pH_i homeostasis, we need to be able to concurrently measure PMF and pH_i in individual bacteria, as well as control the value of PMF. For the purpose, we employ our previously developed assays, which rely on the measurements of bacterial flagellar motor speed as a PMF indicator, and use a ratiometric pH sensor (pHluorin) as an indicator of pH_i [179, 187]. Briefly, the bacterial flagellar motor is a rotary nanomachine roughly 50 nm in size whose rotation is powered by the PMF [106]. The relationship between the PMF and the motor speed is linearly proportional, irrespective of the load on the motor [151, 152]. Thus, measuring motor speed changes is equivalent to measuring the relative change in PMF. We measure the motor speed by attaching the cells

to the cover slip surface [180], and attaching a plastic bead to the genetically modified flagellar filament [188, 154, 189, 179, 190]. The rotation of the motor, now rotating the plastic bead, is measured by placing the bead in a heavily attenuated optical trap and performing back-focal-plane interferometry [153, 191]. The strains used for the experiments carry a gene encoding pHluorin enabling readout of pH_i. Fig. 2.2A gives a cartoon representation of our experimental setup. To change the value of PMF we perform the experiment in a sealed tunnel-slide configuration, see also *Materials and Methods* [29, 189, 179], where cells eventually run out of oxygen and the PMF value becomes less negative (i.e. drops in absolute terms) [192], Fig. 2.2B. The timing of the PMF change slightly varies with the concentrations of cells on the tunnel-slide surface, as seen in Fig. 12 and similarly to previously observed for a population of swimming cells [192]. We can now change the external pH from 7.0 to 5.5 and observe pH_i, first at a higher absolute PMF that is maintained in the presence of oxygen, followed by lower absolute PMF when the oxygen in the tunnel-slide is deprived (arrows in Fig. 2.2B). Fig. 2.2C shows the motor speed values (reflecting the relative difference in PMF values) in anaerobic and aerobic conditions (measured at the time point indicated by arrows in Fig. 2.2B), and Fig. 2.2D the corresponding pH_i values for a given pH_e. For the higher absolute PMF value in the aerobic environment pH_i is maintained (gray shaded area) over a wider pH_e range in agreement with our model predictions. Fig. 2.2E and F show dynamics of absolute PMF and pH_i changes upon transition to pH_e=5.5 (in *Supplementary Information* we give single-cell examples across the all tested pH_e values, Fig. 13). Upon transition to pH_e cytoplasm temporarily acidifies and begins recovery to initial value while PMF is kept higher (i.e. while oxygen is present). Upon deprivation of oxygen and lowering of the absolute value of the PMF, pH_i drops back to the level seen immediately upon pH_e transition. For external pH_e below 5 no dynamic recovery is observed and both the absolute PMF value and internal pH_i drop immediately with the internal pH_e change.

iv. Model predicts the role of antiporters is to regulate $\Delta\psi$, and experimental evidence supports it: ΔpH is not maintained when PMF drops

As no ATP-driven ion efflux pumps have been reported in *E. coli* we assumed in our model that antiporters are solely responsible for ion efflux. Consequently, the model predicts that antiporters are not maintaining specific inside ion concentrations,

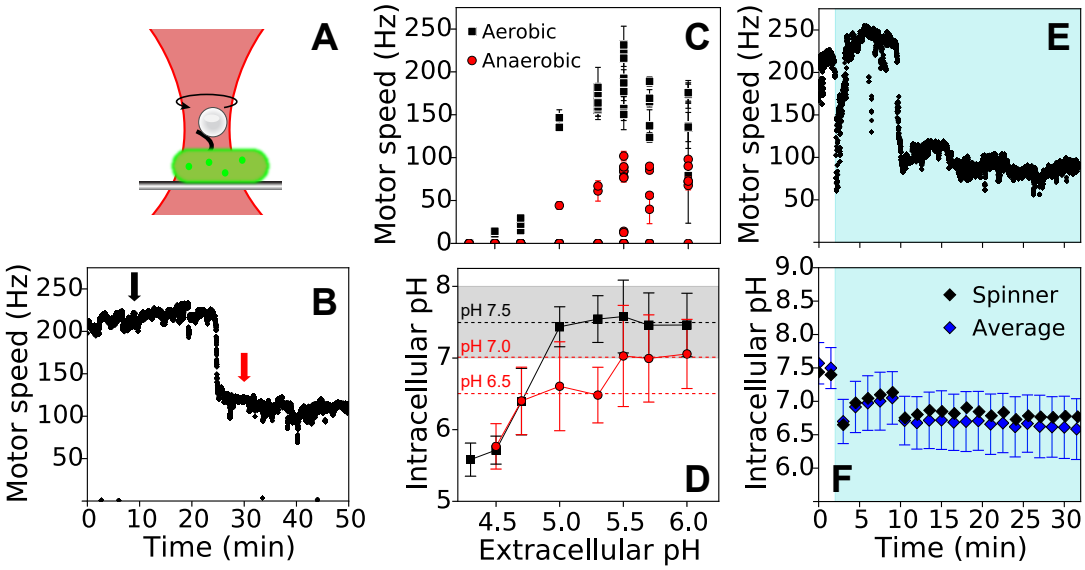


FIGURE 2.2: At pH_e 5.5 *E. coli* exhibits pH_i homeostasis if the value of PMF is sufficiently high. (A) Schematics of the experiment in which we immobilize *E. coli* on a glass coverslip via poly-L-lysin (*Materials and Methods* [180, 189, 179]). A polystyrene bead is attached to a "sticky" flagella stub and placed in the focus of a heavily attenuated laser for high speed position detection (*Materials and Methods*). Cell cytoplasm is shown in green to illustrate that the readings from the genetically encoded fluorescent pH sensor are taken simultaneously with the speed measurements. (B) An example of single cell motor speed trace in a sealed tunnel-slide at the pH_e=7.0 and in the presence of 20 mM glucose. Sharp speed drop at $\sim$ 25 min indicates the point of oxygen depletion. Arrows denote time points where "aerobic" (black) and "anaerobic" (red) speeds are taken for analysis. (C) Single cell motor speeds dependency on the pH_e is shown. "Aerobic" and "anaerobic" speeds are calculated as the mean of $\pm$ 45 s interval around the time points indicated in (B), error bars are standard deviation. (D) pH_i is plotted against the pH_e. Intracellular pH is calculated as the mean of population of 90 to 316 cells for the time points indicated in (B). Error bars represent standard deviation. Grey shading shows the region of internal pH homeostasis (7.0-8.0). (E) An example of single cell motor speed trace upon transition to pH_e=5.5. For the first 2 min cells are at pH_e=7 and at t=2 min pH_e is changed to 5.5 (indicated by the blue shade) and the tunnel-slide is sealed (*Materials and Methods*). At the point of pH_e transition, and due to flow, the bead rotated by the motor moves out of the laser detection region resulting in the loss of signal (sharp speed drop visible at the point of transition). (F) pH_i dynamics at low extracellular pH. The cell with the bead attached to the motor whose speed is monitored and plotted in (E), is shown with black diamonds. Blue diamonds show the mean and the standard deviation for all the cells in the field of view ($\sim$ 30). As in (E), blue shaded region indicates the period where pH_e is 5.5.

instead they regulate $\Delta\psi$, and internal ion concentrations, given the external environment, are a consequence. For example, antiporters will not move a proton outside of the cell to maintain pH_i while keeping $\Delta\psi$ the same [89, 62, 4], instead they will adjust $\Delta\psi$ in order to keep PMF fixed. Their stoichiometry and ΔG_x then insure that doing so results in pH_i within a neutral range. Our assumption that PMF is maintained is inline with our experimental observations in Fig. 2.2, but also in line with recent observations that PMF is kept fixed across a range of growth rates [193, 194]. Given the prediction, we now look for experimental evidence that can support this subtle but important difference. Deleting or over-expressing individual antiporters will affect the pH_i homeostasis upon a pH_e change under both scenarios, potentially making the difference difficult to distinguish experimentally. Aided by the model we therefore look for scenarios that can separate possible roles of antiporters. We select antiporters from Fig. 2.1C with stoichiometric ratio 0.5, 1.5 and 2 (as these have equivalents in *E. coli*) and include an ion efflux pump that is powered by ATP with stoichiometric ratio 0.5, Fig. 2.3A. In Fig. 2.3B we show ΔpH and $\Delta\psi$ against PMF, where similar to Fig. 2.1D, we explore the allowed IMF range that each transporter can maintain. We then show the resulting allowed membrane voltage range and ΔpH as a function of PMF for $z_Y \cdot [Y]_i/[\mathrm{CA}]_0$ of +0.1 for the anionic pump and -0.1 for the cationic pumps. The notable difference between the two scenarios: (a) ion efflux powered by PMF or (b) ion efflux powered by ATP, is in the alkaline range and especially as absolute value of PMF drops. When $\Delta\psi$ is maintained by proton:ion antiporters, when PMF is 0 so is the ΔpH, because $\Delta\psi$ is set by captive molecules alone (see Fig. 5). When $\Delta\psi$ is maintained by an ATP driven cationic pump, the ability to maintain membrane potential is independent of the PMF, and thus ΔpH can be maintained without the PMF. To test the model prediction, in alkaline regime we treat the cells with 100 μM carbonyl cyanide m-chlorophenylhydrazone (CCCP), which is a known protonophore [195] and therefore collapses PMF. Fig. 2.3C shows PMF measurements upon two alkaline shifts (to pH_e 8.15 and 8.45) and subsequent CCCP addition. In both cases the absolute value of PMF drops to a lower value upon the alkaline shift and to 0 with addition of CCCP. Intracellular pH rises immediately upon the alkaline shift. Upon CCCP addition, i.e. collapse of PMF, ΔpH is zero. In Fig. 2.3D we superimpose the experimental points over the theoretical prediction for the NhaA antiporter to emphasize that we do not

observe ΔpH in absence of PMF and in agreement with our model assumption[13]. The finding is also in agreement with usage of CCCP in mammalian cells, where the main pump responsible for membrane voltage maintenance is the ATP driven NaK-ATPase [196]. Consequently, CCCP is used to determine the value of $\Delta\psi$ from the measured ΔpH upon CCCP treatment [197, 198]. Interestingly, all of the experimental points in Fig. 2.3C (superimposed to Fig. 2.3D) were obtained in the presence of oxygen, yet these fall in the PMF range attributed to fermentative regime. As mentioned, the values were calculated assuming a fixed free energy of ATP hydrolysis, which could change at high pH_e. Alternatively, cells could switch to fermentative regime even in the presence of oxygen.
In Fig. 2.3C and Fig. 14 it is also visible that PMF becomes less negative upon alkaline shift and pH_i homeostasis proceeds at this new value and in agreement with previous measurements [199]. We use the known range of PMF values during respiration on glucose (see *Supplementary Information*) to calculate $\Delta\psi$ in Fig. 14, showing that it stays roughly constant. Previous measurements of $\Delta\psi$ upon an alkaline shift observed a $\sim$ 10 mV change (upon an alkaline shift a slight increase followed by a slight decrease, but all within 10 mV), which is consistent with our results as it is within our error bars [199]. As the absolute value of PMF drops upon an alkaline shift, roughly constant membrane potential means that it contributes more to the PMF (Fig. 14).

v. Model predicts the role of antiporters is to regulate $\Delta\psi$, and experimental evidence supports it: expression of different antiporters depends on the pH of the external environment

An additional way of confirming our predicted role of antiporters is to look at their activity when present simultaneously. We start by noting that in Fig. 2.1D we treated all the allowed solutions for a given antiporter as equally likely. However, this is not the case because different allowed solutions cost the cells differently. In order to take the cost into account we define it as a number of protons pumped out of the cell for other reasons than ATP production. Thus, the cost is the

[13] I agree that this supporting evidence is relatively weak. Indeed, we observe that loss of PMF is correlated with loss of voltage which if it *must* occur within our model assumption is still a possible behaviour with *e.g.* the cation-ATPase. The value of the supporting evidence is then in my opinion: our assumption has one possible behaviour (when PMF reaches 0) while other models have distinct possible behaviours, thus the experimental realisation that this behaviour is observed still strengthened our hypothesis relative to other hypothesis, while I agree not demonstrating it rigoroulsy.

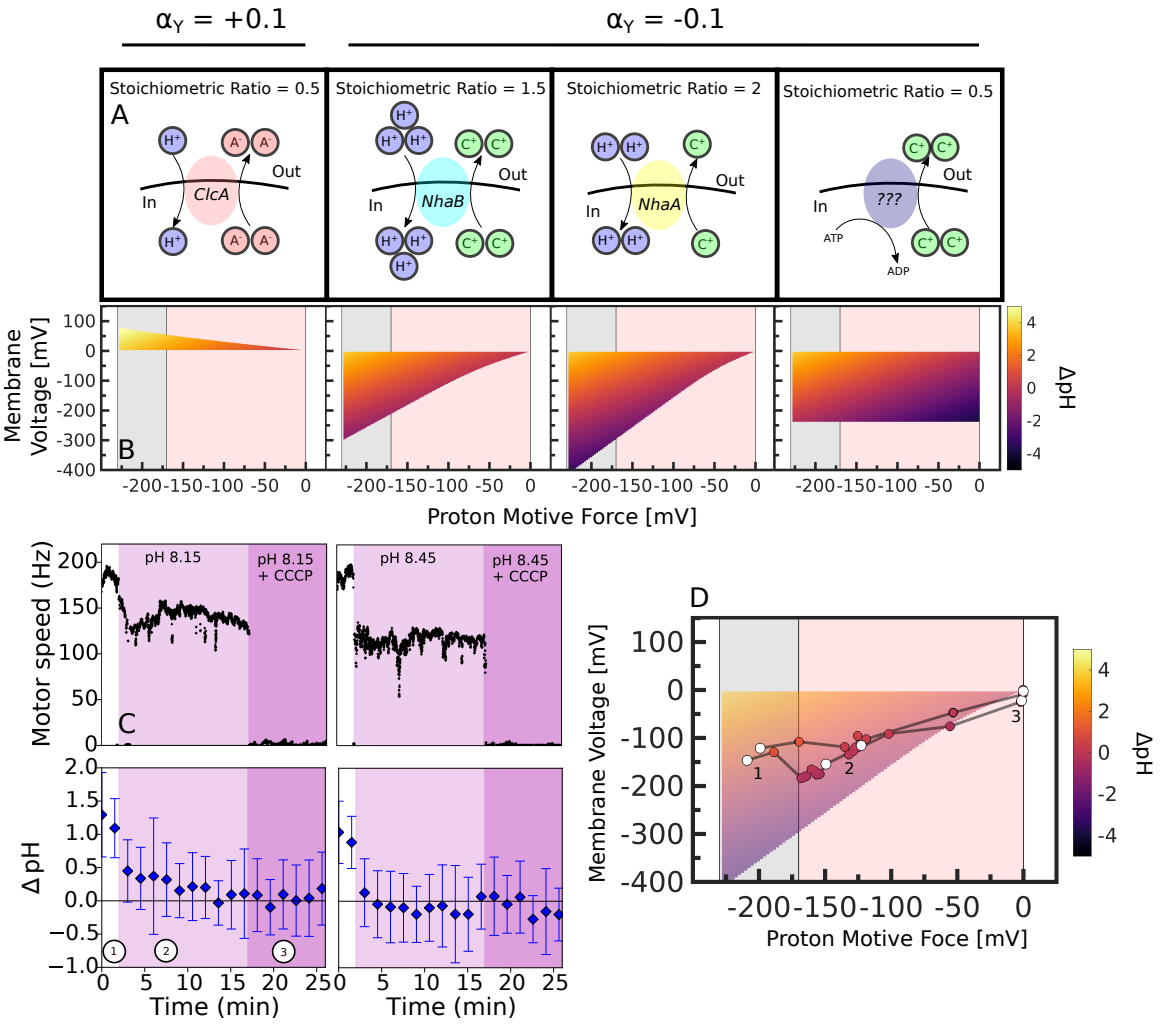


FIGURE 2.3: Proton:ions antiporters are responsible for voltage generation in *E. coli*. (A) Cartoons of ionic pumps we include in our model. We compare three antiporters of *E. coli* with known stoichiometries and an hypothetical ATP driven cationic pump with stoichiometry 1 ATP per two cations. (B) Allowed membrane voltage as a function of the PMF with the colour scale denoting $\Delta\text{pH} = \text{pH}_i - \text{pH}_e$. To gain computational speed membrane voltage is here computed using SI Eq. 23 where we set the left hand side to 0 and α_x=1/2. We know from Fig. 11 that the error yielded by the approximation compared to using (III.5) is less than 10 mV when $[\text{CA}]_0 \in [10, 1000]$ mM, $\text{pH}_e \in [3, 11]$, $\text{pH}_i \in [4, 10]$ and $\text{Abs}(z_Y \cdot [Y]_i) \geq 1$. We set $\alpha_Y = z_Y \cdot [Y]_i \ / \ [\text{CA}]_0 = +0.1$ for anionic pumps and α_Y = -0.1 for cationic. The anionic pump allows maintenance of positive voltage while cationic pumps allow maintenance of negative voltage. (C) Single cell motor speed (top panels) reflecting PMF dynamics and the average ΔpH (bottom panels) upon alkaline shift (from pH 7 to 8.15 or 8.45), followed by addition of protonophore CCCP. White region (annotated 1) shows motor speed and ΔpH at external pH 7.0; shift to alkaline pH_e is indicated with pink shading and annotated 2; and to CCCP with purple shading and 3. ΔpH is plotted as the mean of ≥30 cells with standard deviation.(D) Experimental points from (C) are plotted in membrane voltage vs PMF space obtained for NhaA (in B) and for both pH 8.15 and 8.45. ΔpH is color coded according to the scale on the right. PMF is calculated from the motor speed using conversion factor 1.13 mV/Hz (Fig. 14). Membrane voltage is calculated according to the (III.1) for protons, where ΔG_{H^+} is the PMF and the logarithms of the ratio of intracellular to extracellular proton concentrations is ΔpH. White dots annotated by numbers illustrate specific time points of the experiments as defined in (C). The gray and red shadings were kept as in (B), these indicated respiratory and fermentative PMF regimes, calculated assuming a fixed free energy of ATP hydrolysis.

difference between the flux of protons due to the respiratory chain and the action of F_1F_o-ATP synthase, and that difference is the sum of proton leakage (j_{H^+}) and flux of protons due to the action of antirporters (j_n):

$$\text{Cost} = j_{H^+} + \sum_n \sigma_{H^+,n} \cdot j_n \tag{III.14}$$

where fluxed are defined as before [187, 200] and we write the dependency of a reaction rate on the reaction potential ΔG as:

$$j = j^+ \cdot \left(1 - e^{\frac{F}{RT} \cdot \Delta G}\right) \tag{III.15}$$

j^+ is a function that describes the specifics of the transport mechanism [187]. For ion leakage we have:

$$j_x = j_x^+ \cdot \left(1 - e^{\frac{F}{RT} \cdot \Delta G_x}\right) \tag{III.16}$$

with j_x^+

$$j_x^+ = \frac{S}{V} \cdot P_x \cdot [x]_e \cdot f_b(\Delta\psi) \tag{III.17}$$

where P_x the permeability of the membrane to a specific ion and $f_b(\Delta\psi)$ a function of membrane potential that can takes different functional dependencies given the value of $b \in [0, 1]$ (for $b = 0$ the model for leakage is the Goldman–Hodgkin–Katz (GHK) flux equation and when $b = 1$ it is the Erying's model [42, 187], see also *Supplementary Information*).

For the antiporters the rate reaction is:

$$j_n = j_n^+ \cdot \left(1 - e^{\frac{F}{RT} \cdot \Delta G_n}\right) \tag{III.18}$$

where j_n^+ is a function that describes the specifics of the transport mechanism by a given antiporter [187].

We now allow the three antiporters present in *E. coli* (Fig. 2.1B) to operate simultaneously, and we calculate the cost of obtaining a given PMF for any of the allowed IMFs (for details on the calculation see *Supplementary Information*). In Fig. 2.4A we give the value of j_n^+ that minimizes the cost of maintaining the PMF at two representative values (one for fermentative and one for the oxidative condition), while keeping pH_i at 7 and in a range of different pH_e. For both values of the PMF the minimum cost solutions utilize only one of the transporters in

a specific pH_e range: ClcA between 2 and 5, NhaB between 5 and 9 and NhaA between 9 and 12. The prediction is in agreement with previous work that reported NhaA is important for survival at alkaline pH [201, 89, 73], with an increase in activity from pH_e 6.5 [202], while ClcA has been reported as important for cell survival at acidic pH [203].

In Fig. 2.4B we show that amount of captive charge the cell needs to keep to minimize the cost changes with pH_e, and the valency of the captive molecules changes with external pH (where the value of PMF the cell keeps offsets the transition). Changes in the overall charge of the species we consider captive molecules, in response to acid stress, have been reported. For example, acid resistance systems convert negatively charged glutamate into neutral γ-aminobutyric acid (GABA). They also convert arginine, lysine and ornithine into agmatine, cadaverine and putrescine respectively, each carrying one more positive charge [90, 204, 205]. Thus, at low pH_e the amount of positively and negatively charged captive molecules increases and decrease, respectively, shifting the average valency of captive molecules from negative to positive.

Fig. 2.4C decomposes the cost into contributions from proton leakage as opposed to the action of the antiporters. At acid pH_e the total cost is mostly due to the action of antiporters, whereas at alkaline pH_e the leakage of protons and hydroxide ions costs the cell more. The leakage of H^+ and OH^- is concavely shaped with respect to the pH_e, because it scales linearly with the concentration (and pH is defined as the log of the concentration). In Fig. 16 we characterize exhaustively how the optimal cost of maintaining electrochemical gradients depends on *(i)* the homeostases sought to be maintained (PMF and pH_i) and *(ii)* the composition of the environment (its salinity and pH_e). First, we observe that low PMF is cheaper to maintain however restrict the range of pH_i that can be maintained at a given pH_e (the white area denotes non-achievable states). Second, the cost generally increases with the salinity. Interestingly, the increase in cost with salinity is more pronounced in the neutral-alkaline range ($pH_e > 6$) and in the very acidic range ($pH_e < 4$) where the cell is sufficiently polarized. This is because the cost of maintaining the action of antiporters increases with salinity while the cost of compensating for proton and hydroxide leakage remains invariant by change in salinity. Perhaps the most interesting behaviour is the observation that at low PMF, high salinity (*e.g.* fermenters in the sea), the cost is minimized by maintaining lower pH_i in acidic environments and higher pH_i in alkaline environment. Such

is not the case in environments where the salinity is low and the PMF is high (respirers in lakes), wherein minimizing the cost entails increasing pH_i when pH_e decreases and decreasing pH_i when pH_e increases. Should the permeabilities for different ions of *E.coli*'s membrane indeed results in minimization of the cost by alkalinization of cytoplasm in response to extracellular acidification this raises the question of whether *E.coli* can implement it. Indeed, tuning pH_i in response to pH_e in order to minimize the costs in both setups {low salinity, high PMF } and {high salinity, low PMF } would require a regulatory system that is able to shift the monotonicity of pH_i with respect to fluctuations in pH_e, conditionally on the salinity and the PMF maintained. This certainly seems harder to implement than a monotonic regulatory system that always increases/decreases pH_i in response to increase/decrease in pH_e. Be as it may, if *E.coli* were able to perform such non-monotonic regulations this would enrich the regulation paradigms currently in place. Finally, figure SI (12) can in principle be used to determine which electrophysiological configurations of *E. coli* are achievable. Indeed, consider that *E.coli* has a maximal energy budget it can generate, then this figure forbids all the behaviors that yield energetic requirements above this maximal budget. Precisely evaluating this would require reliable assessment of the permeabilities as well as the parameter b in the equation defining the rate of leakage.

vi. Outer membrane voltage can offset effects of external environment on the cytoplasmic homeostases

Thus far our model considered a single barrier separating the cells' inside from the environment. However, the envelope of Gram-negative bacteria, such as *E. coli*, consist of an inner and an outer membrane, with the space in-between termed periplasm [206]. Energy transducing pumps, such as the respiratory chain components [207], F_1F_o ATP synthase and proton:ion antiporters [208] ($F1F_o$, *NhaA* and *NhaB*) [209] (*ClcA*, curated) are localized in the inner membrane, while the outer-membrane contains many porins that allow fast movement of ions between the periplasm and the extracellular space [97, 210]. Therefore, we assume that the periplasm and the extracellular space are at ionic equilibrium and follow Nernst Equation, i.e. we set (III.1) to zero and obtain:

$$[x]_e = [x]_p \cdot e^{-\frac{Fz_x}{RT}\cdot\Delta\psi_p} \tag{III.19}$$

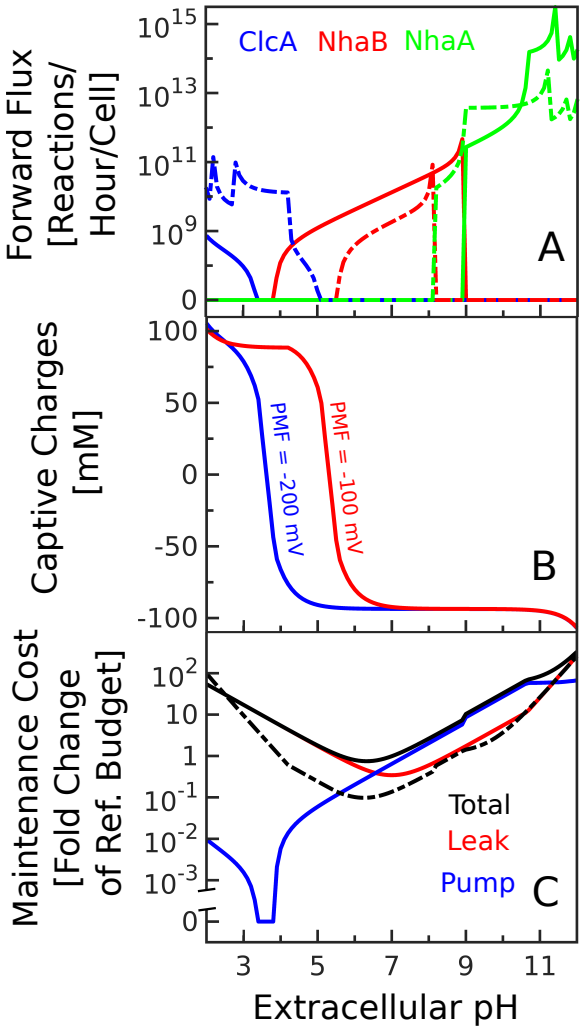


FIGURE 2.4: Maintaining pH_i, PMF and osmotic pressure at minimal cost predicts *E. coli*'s optimal homeostatic strategy across different pH_e. In (A), (B) and (C) we maintain pH_i close to 7, keep z_Y in the [-2,2] range, set osmotic pressure to 1 atm, PMF to either -200 or -100 mV and $[CA]_0$ to 50 mM. The membrane is characterized by its ionic permeabilities: $P_{H^+} = P_{OH^-} = 10^{-4}$ m/s, $P_{A^-} = 1.5 \times 10^{-10}$ m/s and $P_{C^+} = 5 \times 10^{-10}$ m/s. Finally, We set b in (III.17) to 1 (Erying's model). (A) Forward flux (j_n^+) that minimizes the energetic cost of maintaining electrophysiological homeostasis for different pH_e uses only one specific antiporter depending on the pH_e: ClcA in blue, NhaB in red and NhaA in green. The full and dashed lines denote PMF of -200 and -100 mV, respectively. (B) $z_Y \cdot [Y]_i$ values that minimizes the energetic cost of maintaining electrophysiological homeostasis for different pH_e. Blue and red denote PMF of -200 and -100 mV. (C) The minimal cost of maintaining electrophysiological homeostasis at different pH_e calculated relative to a reference budget, which we estimate for *E. coli* growing in minimal media with glucose and doubling every 60 min (see also *Supplementary Information*). The full and dashed black line denotes the total maintenance cost for -200 and -100 mV PMF, respectively. The maintenance of PMF = -200 mV is broken down in two contributions: the cost of powering the ionic antiporters (blue) and the cost of compensating proton and hydroxide ions leakage (red).

where $[x]_p$, $\Delta\psi_p$ are the periplasmic concentration of ions and the Donnan potential across the outer membrane. (III.5) now becomes

$$\Delta\psi = 3.5\cdot\left(z_Y\cdot[\mathrm{Y}]_i + [\mathrm{C}^+]_p\cdot e^{\frac{F}{RT}\left(\Delta G_{C^+}-\Delta\psi-\Delta\psi_p\right)} - [\mathrm{A}^-]_p\cdot e^{\frac{F}{RT}\left(\Delta G_{A^-}+\Delta\psi+\Delta\psi_p\right)}\right) \tag{III.20}$$

From (III.19) and (III.20) it is visible that $\Delta\psi_p$ either increases or decreases the environmental ionic concentrations "felt" by the inner membrane, e.g. a Donnan outer membrane potential of -30 mV (as reported in [170]) increases the cation concentration ~ 3.3 times, and decreases the anion concentration by the same amount. Therefore, the pH difference across the inner membrane will be different to the pH difference between the cytoplasm and the external environment. In alkaline pH_e perisplasmic pH will be lower than pH_e, and in the acid pH_e range periplasmic pH will be higher. If we assume that periplasm can hold a certain amount of captive charges[14], the $[\mathrm{CA}]_0$ will influence the difference between pH_e and periplsamic pH as well, as shown in Fig. 16.

vii. Additional Remark on Catalytic Efficiency

Although we did not make much use of it (besides figure 4), the kinetic form we use Eq. (C.35) depends on the Gibbs free energy associated with the reaction. Such that when ΔG_n of the reaction n goes close to 0 it slows down the reaction rate. Some of the reachable states we assumed the pumps can achieve in figures 2.1 and 2.3 would therefore result in poor catalytic efficiency of the said antiporters. We show in figure SI (13) the catalytic efficiency regimes on the reachability diagram from figure 2.3. Near the maximal IMF that each antiporter *NhaB* and *NhaA* can maintain, the antiporter loses in catalytic efficiency. This is a possible reason as to why in spite of *NhaB* being sufficient to maintain the state experimentally observed, it is better to maintain these states with *NhaA*. Indeed, as shown in figure SI (13), although the experimental points are achievable for *NhaB* it corresponds to states in which NhaB has significantly lower catalytic efficiency than *NhaB*. Thus these regions, in spite of being accessible by *NhaB* require pumps with higher catalytic efficiency to be maintained such as with NhaA.

[14]Cell wall possesses some charges under the form of teichoic acids.

IV. Discussion

Maintenance of bacterial homeostasis has been of interest to researchers for decades. However, homeostasis of internal pH, osmotic pressure or membrane voltage are often looked at in isolation, despite the fact these variables are intrinsically linked. Here, we present a model that allows us to look at all the relevant homeostatic variables simultaneously and by doing so offer experimentally confirmed predictions. Specifically, we demonstrate that to maintain physiological $\Delta\psi$ while keeping osmotic pressure in a reasonable range, neutralophiles need to pump cations out. We also show that a decrease in the absolute value of the PMF impairs the ability of *E. coli* to maintain its pH_i close to the homeostatic target of ~ 7.5. This leads us to hypothesize that the contradictory observations from [173, 174, 175] and [176, 177] can be reconciled if the latter were performed on cells in the less negative PMF regime, which may have been caused by anoxic conditions.

The main assumption of our model is that proton:cation antiporters regulate $\Delta\psi$, rather than the internal pH itself. For example, previous work interprets decarboxylation of amino acids as deacidification of the cytoplasm by directly consuming cytoplasmic protons [90][15]. Similarly, because NhaA pumps protons in, its role in alkaline resistance is interpreted as directly acidifying the cytoplasm [89, 4]. Our assumption on the role of antiporters in $\Delta\psi$ maintenance fundamentally changes the view on pH maintenance. That is, decarboxylation of amino acids reduces/increases the amount of negative/positive captive molecules, allowing to shift the membrane voltage from negative to even positive values. And, because NhaA has a higher proton to cation stoichiometric ratio than NhaB, it allows maintenance of more negative $\Delta\psi$, which is required for simultaneous maintenance of PMF and pH_i at alkaline pH_e. Finally, rather than moving protons out to lower pH_i (and thus chloride in) ClcA works to move chloride out and proton in, thereby allowing generation of positive voltage necessary for simultaneous maintenance

[15] A good way to explain it is the following. Picture two systems, a system (i) that can move protons out thus desacidifying the cytoplasm but that does not shift the valency of captive charges from negative to positive. That system is unable to maintain PMF and phi homeostasis in very aicidc conditions. Now picture another system (ii) that does not move protons out but that is able to shift the valency of captive molecules from negative to positive; this system, in interaction with other pumps is able to maintain pHi and PMF homeostasis in very acidic pHe. Now decarboxylation can be understood as a reaction system performing (i) and (ii) simultaneously. People have previously understood the function (i) as being the relevant one in maintaining pHi at very acidic pHe, we have shown however that (ii) was necessary, and decarboxylation systems can perform this necessary function. Thus I think that decarboxylation systems are important not because of (i) but because of (ii).

of PMF and pH_i at very low pH_e. We have already mentioned that to the best of our knowledge the direction of ClcA was inferred from the assumption that it serves to deacidify the cytoplasm, rather than experimental results, but we also note that the interpretation by which ClcA lowers pH_i leads to the prediction that $\Delta\psi$ becomes more negative at acidic pH_e, which is opposite from what was previously observed experimentally [211]. These experimental observations are, however, in line with our model predictions.

Our interpretation thus agrees with all previous observations, but highlights the importance of the stoichiometric ratio rather than the electrogenicity (the net amount of charge transferred per catalyzed reaction) when evaluating the capability of an antiporter to generate $\Delta\psi$[16]. The model we introduced could also serve as a backbone to study how an antiporter with defined mechanism of action (such as in [95, 96]) plays out in maintaining pH_i, PMF, voltage, osmotic pressure upon specific environmental changes, for instance changes in pH_e or Na^+ concentration.

Moving away from bacteria, proton:cation antiporters are widespread in nearly all living species, and defects in such antiporters in mammalian cells are associated with diseases (e.g. cancer [212], autism [213] or hypertension [214]). In mammals, the members of the NHE (to which *NhaA* belongs) and the CLC (to which *ClcA* belongs) gene families are also thought to play a role in pH_i maintenance [70, 215]. However, in mammalian cells the main ionic transporter responsible for maintainance of $\Delta\psi$ (between the extracellular space and the cytoplasm) is the chemically driven electrogenic antiporter Na/K ATPase [91], and mitochondria are responsible for respiratory activity. Thus, maintaining the PMF across other compartments (e.g. between cytoplasm and extracellular space) may not be as crucial as in eubacteria and archaea, and consequently, activity of proton:ion antiporters (in eukaryotes located in the plasma membrane) may not be as strongly constrained, and may have evolved annex functions or specialize in pH_i maintenance by other mechanisms than modulating membrane potential.[17]

[16] The electrogenicity is the net amount of charge transferred by a reaction, for instance picking a compartment of reference in, a 2:1 proton:cation antiporter has an electrogenicity of +1 (its action changes the internal charge by +1), a 1:2 proton:anion antiporter has an electrogenicity of -1. As for the stoichiometric ratio we already discussed it, and talk about it extensively in the appendix of this chapter.

[17] More generally, maintenance of electrochemical gradients across different pairs of compartments shall in principle be subjected to different constraints, and a similar reaction system (for instance a proton:cation antiporter), may have evolved a distinct function depending on how important it is to maintain some homeostaeses across a pair of compartment.

When it comes to the energetic cost of maintaining chemiosmotic homeostasis in bacteria, our model predicts that the permeability of the membrane to small ions plays a crucial role and that it is energetically cheaper to generate intermediary $\Delta\psi$ values with antiporters of lower stoichiometric ratios. We propose that most bacteria have a diversity of antiporters catalyzing the same type of ionic exchange, but with distinct stoichiometric ratios, precisely to tune the energetic cost. Taking into account some published estimates of the membrane permeability we were able to calculate that the cost of chemiosmotic maintenance can account for a significant portion of *E. coli*'s energy budget, even in neutral environments. More importantly, the chemiosmotic maintenance cost is a convex function of pH_e minimal for extracellular pH around 6.5 and increasing exponentially for pH_e outside this value. We hypothesize that the increase in chemiosmotic maintenance cost explains impairments of *E.coli*'s growth rate in acidic or alkaline environments [216, 217], via the previously observed reduction of growth yield [218]. The hypothesis is inline with predictions that the maintenance of chemiosmotic homeostasis is one the main components of the so-called maintenance expenditures [60]. Distinguishing between maintenance and growth expenditures can be traced back as far as [219]. Succinctly, to make energy available for the cell requires turning environmental substrate into waste through catabolism. The more energy is required by maintenance processes, the less is available for growth related processes, thereby impairing the growth yield [220]. Along the similar lines, we also demonstrated that increased salinity leads to increased energetic cost of maintaining membrane potential. Consequently, this could explain the observed decrease in growth-rate of *E. coli* in high NaCl environments [221], and predicts that reduced growth-rate should be associated with a reduced growth yield. There are some experimental indications that the latter is the case [222][18].

Interestingly, some alkalinophiles actively tune their surrounding pH [223], which could be in part to maximize its carrying capacity. Alkalinophiles also maintain more negative $\Delta\psi$ compared to neutralophiles [4], and one of the key features of their ability to cope with high pH_e are proton:sodium antiporters [224]. If those antiporters are responsible for voltage maintenance in alkalinophiles as we suggest they are in neutralophiles, their distinctive characteristic will be high proton to sodium stoichiometric ratio. On the other hand, acidophiles possess membranes that bear unusually low permeabilities to protons [225], which could

[18] We will discuss later the implications of the cost of electrophysiological maintenance on growth properties in chapter 3, which is dedicated to the matter.

be explained by the requirement to keep the energetic cost of maintaining the PMF at low pH_e at minimum. Furthermore, and as does *E. coli* under severe acid stress [211], acidophiles maintain a positive membrane voltage [4], which is necessary to maintain both near neutral pH_i and negative PMF at low pH_e. Active pumping of cation inwards, by *e.g.* by potassium ATPases, has been hypothesized as needed for maintenance of positive membrane voltage [6]. We, however, showed that in order to keep osmotic pressure in check, the only viable strategy for generating positive membrane voltage is to pump anions out. In agreement with this, active transport of chloride out has been demonstrated in the acidophile *Bacillus coagulans* [226]. Based on our model we hypothesize that active anion transporters might be widespread among acidophiles and required for adaptation to low pH_e.

V. Methods

i. Strains and media

For simultaneous measurements of pH_i and the single-cell motor speed we use two strains of *E. coli*. The first is a derivative of MG1655 derivative (EK07 [179]) with sticky filaments and chromosomal expression of pHluorin. The second is the AB1157 strain [192] modified to carry the sticky flagellin encoding gene $fliC^{sticky}$ [188, 179] and transformed with pkk223-3-pHluorin(M153R) plasmid [227]. $FliC^{sticky}$ makes filaments hydrophobic so that they readily stick to polystyrene spheres (beads) [188]. With the two strains, we confirmed that there are no significant strain to strain differences in the behaviour we observe. We used strain EK07 for pH_e=5.5 experiments; strains EK07 and AB1157 for a pH_e of 5.7 and 6.0; strain AB1157 for a pH_e of 4, 4.3, 4.5, 4.7, 5, and 5.3; and strain EK07 for a pH_e of 8.15 and 8.45. Bacteria were diluted (x 10^{-3}) from the frozen overnight culture (OD≈3) and grown in lysogeny broth (LB: 10 g tryptone, 5 g yeast extract, 10 g NaCl per 1 l) in conical flask at 37 with shaking (220 rpm).

ii. Flagellar motor speed recording and analysis

Cells were harvested at the OD=2.0 to maximize the fraction with expressed bacterial flagellar motor (Spectronic 200E Spectrophotometer, Thermo Scientific, UK). Cells were prepared for microscopy according to the protocol published in

Speed recording protocol: https://www.protocols.io/view/bfm-speed-recording-with-back-focal-plane-interfer-bch2it8e. Tunnel-slides were made as described in Tunnel slide protocol: https://www.protocols.io/view/tunnel-slide-preparation-for-motor-speed-recording-bcjdiui6. Experiments were performed in the motility buffer (BMB: aqueous solution of 6.2 mM K_2HPO_4, 3.8 mM KH_2PO_4, 67 mM NaCl, and 0.1 mM EDTA, pH 7.02) supplemented with 20 mM glucose.

For aerobic-anaerobic shifts shown in Fig. 2.2B and 12, cells were kept in glucose supplemented BMB in the tunnel slide, where fresh BMB was flushed in just prior to the recording and the slide was sealed with CoverGrip™ Coverslip Sealant (Biotium, USA) to prevent oxygen diffusion. For experiments presented in Fig. 2.2 C-F and 13, bead rotation was recorded for 2 min in BMB+glucose in aerobic conditions, at which point the buffer was replaced with the pH-adjusted BMB. The slide was immediately sealed and recording continued for another 30 min. pH 5.5 buffer was adjusted with the mixture of organic acids (0.9 mM acetate, 3.8 mM lactate, 1.4 mM formate and 0.45 mM succinate), whereas the rest of the buffers were pH adjusted using lactic acid only. The motor speed recording was uninterrupted for the duration of the experiment (total of 32 min). For alkaline shifts in Fig. 2.3 we recorded bead rotation for 2 minutes before flushing BMB adjusted with NaOH to pH 8.15 or 8.45. Slide was not sealed to allow another flush of BMB supplemented with 100 μM CCCP at 17 minutes and recording was continued for another 10 minutes.

Relative (x,y) bead coordinates recorded with position sensitive detector were converted to the flagellar motor rotational frequencies by applying a flat top discrete Fourier transform with 1.6384 s window and 0.1 s step size [179, 189]. Resulting time series was median-filtered with additional removal of 50 Hz AC frequency values and values below 10 Hz [179, 189].

iii. Intracellular pH measurements

Internal pH of the bacteria was measured with ratiometric pHluorin [228, 180]. The imaging protocol and sensor calibration is described in https://www.protocols.io/view/cytoplasmic-ph-measurements-with-phluorin-bhi7j4hn. Images were taken every 90 s with 50 ms exposure time.

Fluorescence images of pHluorin were analysed as before [179, 180]. Otsu threshold followed by binary erosion and binary dilation was applied to both

475 nm and 395 nm excitation images and mean intensity was calculated for each cell in both channels. The ratio of these values with the background subtracted was later converted to the pH units using the calibration curve generated as described in [180].

iv. Obtaining computational results

To obtain the optimal behaviour of *E.coli*'s model shown in figure 2.4 we first set the values for the PMF and osmotic pressure we wish the model to maintain as well as the salinity of the environment $[\mathrm{CA}]_0$. Then for each pair of $\{\mathrm{pH}_e, \mathrm{pH}_i\}$ in a grid we proceed as follows. We first compute the composition of the environment in small ions from $\{[\mathrm{CA}]_0, \mathrm{pH}_e\}$. We then compute the value of the membrane voltage required to maintain the given PMF and pH_i at the given pH_e. Assuming the model must minimize energy expenditures, if the membrane voltage is positive, then cations are not pumped, if the membrane voltage is negative, then anions are not pumped. This allows us to directly compute the intracellular concentrations in cations/anions from the composition of the extracellular environment and the value of positive/negative membrane voltage. From the stoichiometries of the ionic transporters and the PMF, we then compute the boundaries on electrochemical potential of anions (if membrane voltage is positive) and of cations (if membrane voltage is negative) which we map to a range of allowed intracellular concentrations for A^- and C^+ respectively. Together with the required osmotic pressure and the boundaries on the average valency of captive charges, this range of allowed intracellular concentrations maps to a range of allowed captive charge concentration $[Y]_i$. At this stage, there might simply not be any allowed $[Y]_i$, reflecting that there exists no parametrization of the model permitting to achieve the required pH_i, PMF and osmotic pressure at the given extracellular pH. If some range of $[Y]_i$ is allowed, then we derive that in order to minimize the cost we must jointly minimize $[Y]_i$ and maximize z_Y, we thus select the minimal $[Y]_i$ allowed. Finally, the state minimizing the cost and maintaining intracellular pH, PMF and osmotic pressure is fully defined by computing the intracellular concentration of cations (if membrane voltage is negative) or anions (if membrane voltage is positive) *via* previous computations of the extracellular composition, $[Y]_i$, $[\mathrm{A}^-]_i$ (if voltage is negative), $[\mathrm{C}^+]_i$ (if voltage is positive) and the required osmotic pressure. When the voltage is negative, depending on the value of ΔG_{C^+} required to maintain membrane voltage, we derive in SI whether the cell must pump cations *via NhaB*

or *NhaA*, which completes the derivation of the optimal behaviour of the model. Importantly, when a desired pH_i is not achievable (that is given values of PMF, osmotic pressure and extracellular pH), we show the model's behaviour for the closest pH_i value the model is able to maintain to the initially required pH_i.

ACKNOWLEDGEMENTS

We would like to thank all members of Pilizota and Swain labs as well as Sebastian Jaramillo-Riveri, Xavier Zaoui, Vincent Danos, Joshua Shaevitz and Peter Lund for support and useful discussions. We would like to thank Joanne Slonezewski and Linda Kenny for providing and helping us with reproducing their previously published data in Fig. 2.1A. TP, GT and EK were supported by the Human Frontier Science Program grant (RGP0041/2015), GT is supported by The Darwin Trust, University of Edinburgh.

Appendices

C. SI Figures

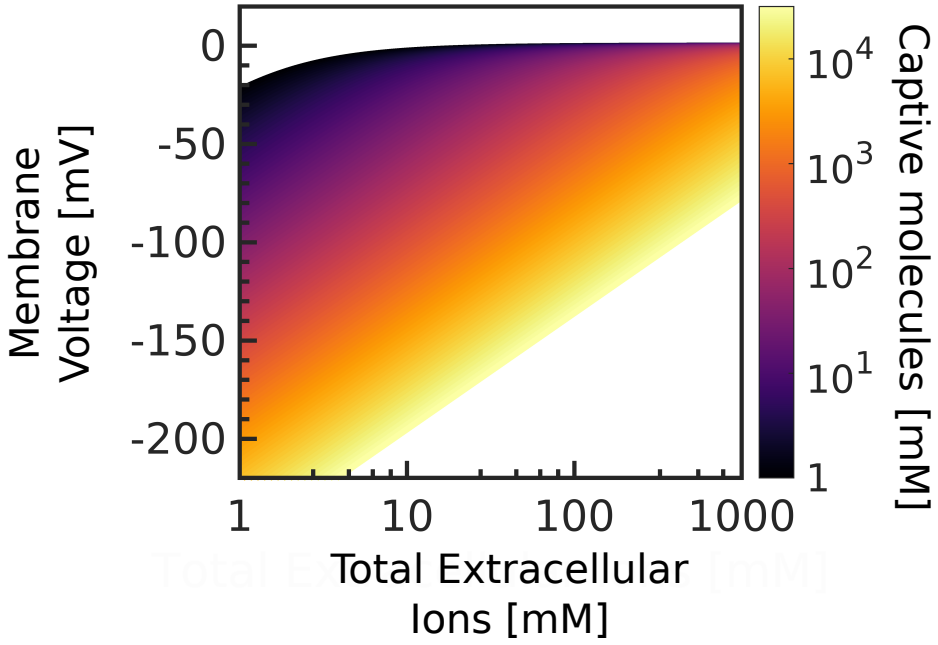


FIGURE 5: Membrane voltage values in the absence of ion pumping (Donnan potential) obtained for different total external ion concentrations and different amounts of captive molecules. We fix $pH_i = 7$, and note that the $\Delta\psi$ values would change by ± 3.5 mV for pH_i between 6 and 8, and ± 35 mV for pH_i between 5 and 9. Color scale given on the right depicts different amounts of (negative) net captive molecules $z_Y \cdot [Y]_i$.

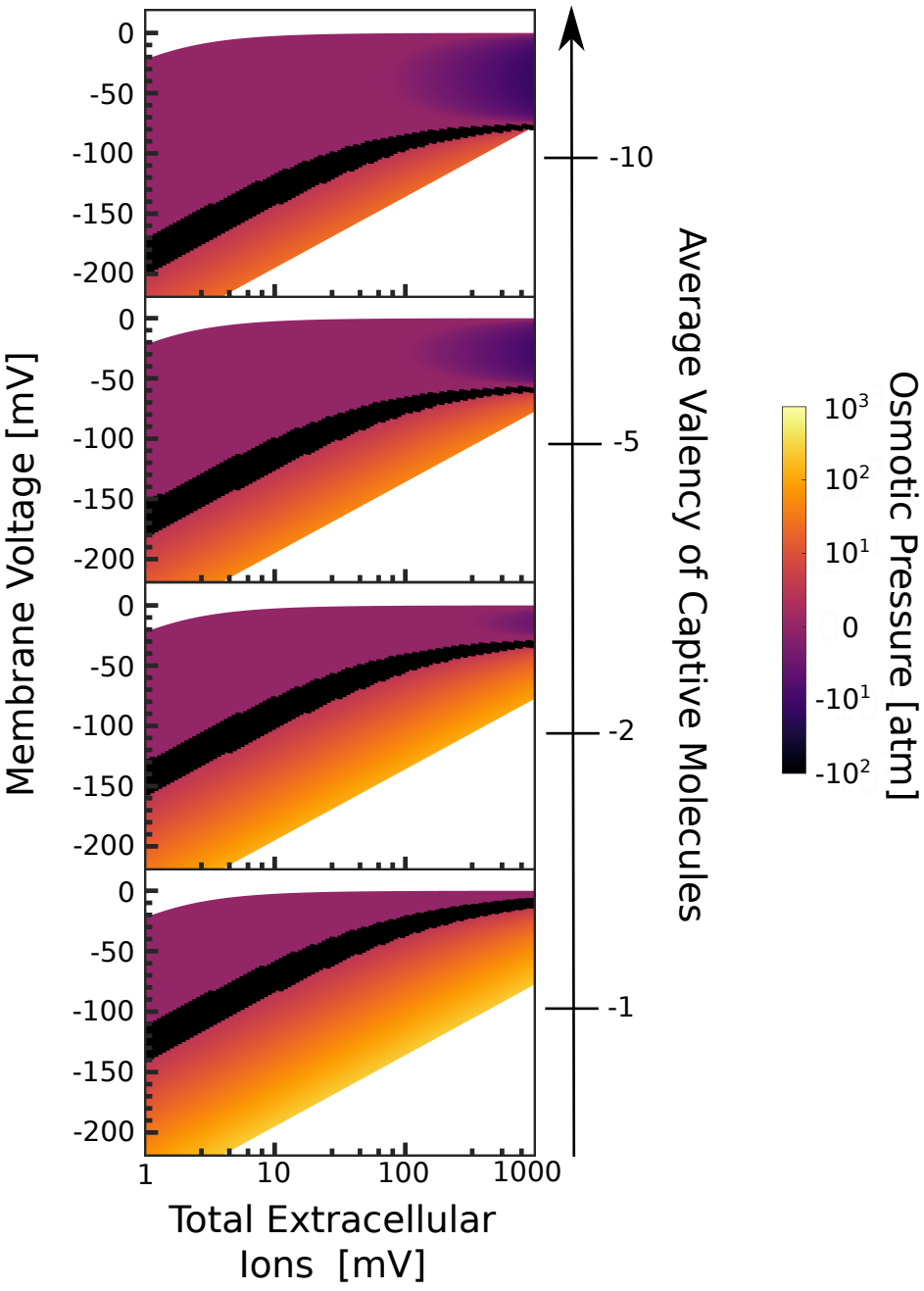


FIGURE 6: Membrane voltage values in the absence of ion pumping (Donnan potential) at different external ion concentrations and with corresponding osmotic pressure (colour scale). As in Fig. 5 we fix $\mathrm{pH}_i = 7$ and $\Delta\psi$ values plotted would deviate from these values as discussed in the caption of Fig. 5 for pH_i between 5 to 9. To calculate osmotic pressure we fix the average valency of captive molecules to $z_Y = -1, -2, -5$ and -10 (indicated on the right of the figure). The black area denotes the experimentally observed range of osmotic pressure for *E. coli* ($1 \leq \Pi \leq 3$ atm [24, 229]). For a reference total extracellular concentration of ions (~ 100 mM) it is impossible to generate physiological voltage of ~ -140 mV with captive molecules alone, without building excessive osmotic pressure or requiring non-physiological average valencies of captive molecules.

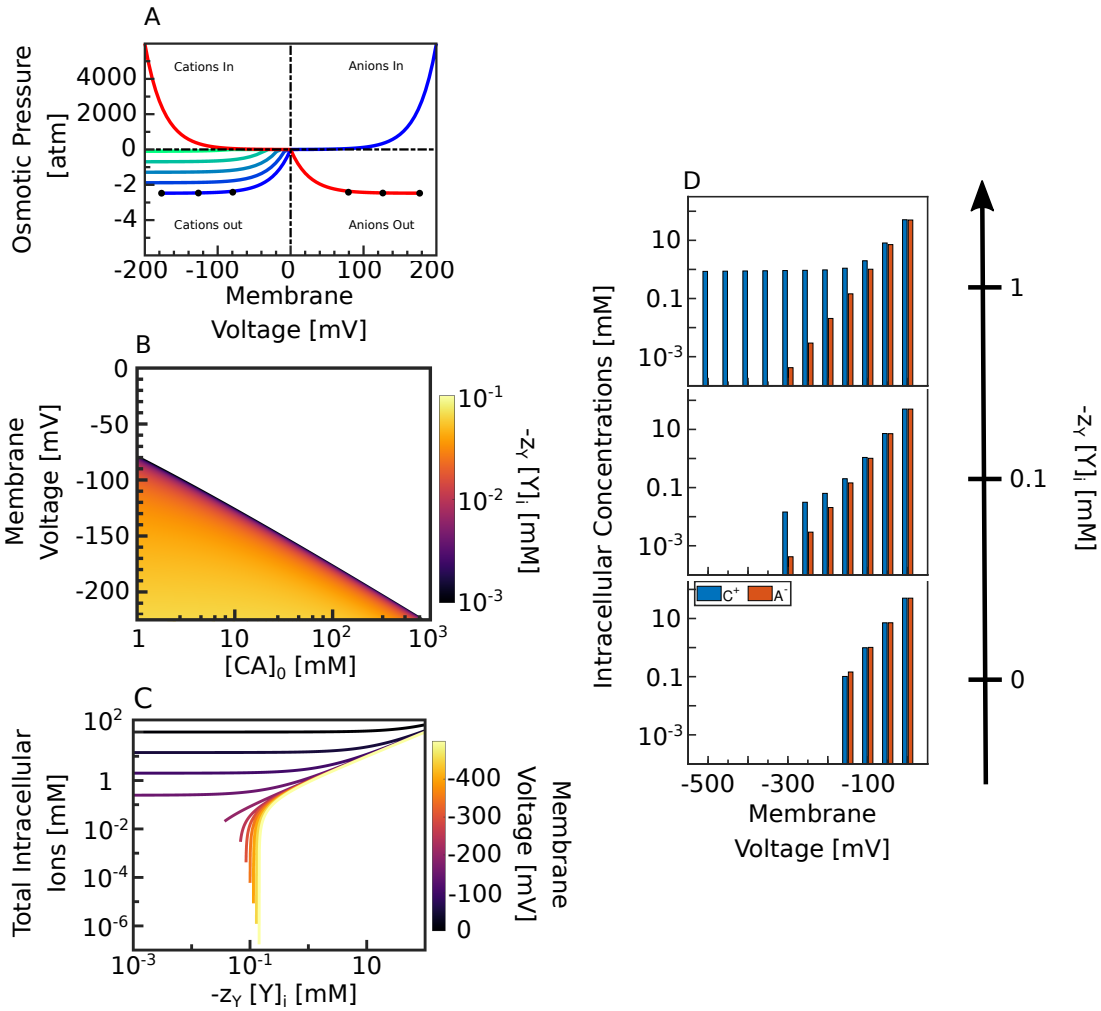


FIGURE 7: (A) Osmotic pressure values plotted against membrane voltage when one cation (blue), or one anion (red), are pumped either in or out of the cell. To obtain the plotted $\Delta\psi$ values we set $\mathrm{pH}_i = 7$ (as in Fig. 5 and 6 these values would deviate by ± 35 mV for pH_i between 5 and 9). When only anions are pumped we set $\Delta G_{C^+} = 0$ and vary ΔG_{A^-} between $\pm$ 500 mV, and similarly, when cations only are pumped we set $\Delta G_{A^-} = 0$ and vary ΔG_{C^+} between $\pm$ 500 mV. $[\mathrm{Y}]_i = 0$ in all but bottom left, where darkest blue indicates $[\mathrm{Y}]_i$ =0 and lines from dark blue to light blue $[\mathrm{Y}]_i$= 0, 12, 24, 36 and 48 % of the total extracellular ionic concentration $(2 \cdot [CA]_0)$. Black dots on the dark blue line in the bottom left, and on the red line in the bottom right indicate the minimum/maximum $\Delta\psi$ that can be reached for total extracellular ion concentrations of 1, 10 and 100 mM (the dot for 1 mM is the one closest to $\Delta\psi = 0$). For all the other lines in the figure, $[\mathrm{CA}]_0$=50 mM (close to common extracellular media salt concentrations). Apart from the minimum/maximum value of $\Delta\psi$ that can be reached, changing the total extracellular ion concentration will not change the $\Delta\psi$ behaviour. (B) Maximum achievable $\Delta\psi$ when cations are pumped out as a function of captive molecules (colour scale) and $[\mathrm{CA}]_0$ at pH_i = 7. (C) $\Delta\psi$ (for cations pumped out) is composed of the contribution from the charged molecules (x axis, only negative $z_Y[Y]_i$ are considered and the absolute value is plotted) and intracellular ions contribution (y axis). We set $\mathrm{pH}_e = \mathrm{pH}_i = 7$; $[\mathrm{CA}]_0 = 50$ mM. Cells that harbour small amounts of $z_Y[Y]_i$ become increasingly depleted of small ions as the absolute value of $\Delta\psi$ increases. Since membrane voltage is maintained by pumping cations out, it becomes impossible to increase the absolute value of $|Deltaψ$ when $[\mathrm{C}]_i \to 0$. (D) Intracellular ionic composition at different membrane voltage values and for three values of $z_Y[Y]_i$. Pumping cations out results in $[\mathrm{A}]_i > [\mathrm{C}]_i$ when $z_Y \cdot [Y]_i = 0$ and $[\mathrm{C}]_i > [\mathrm{A}]_i$ when $z_Y \cdot [Y]_i < -0.1$ mM.

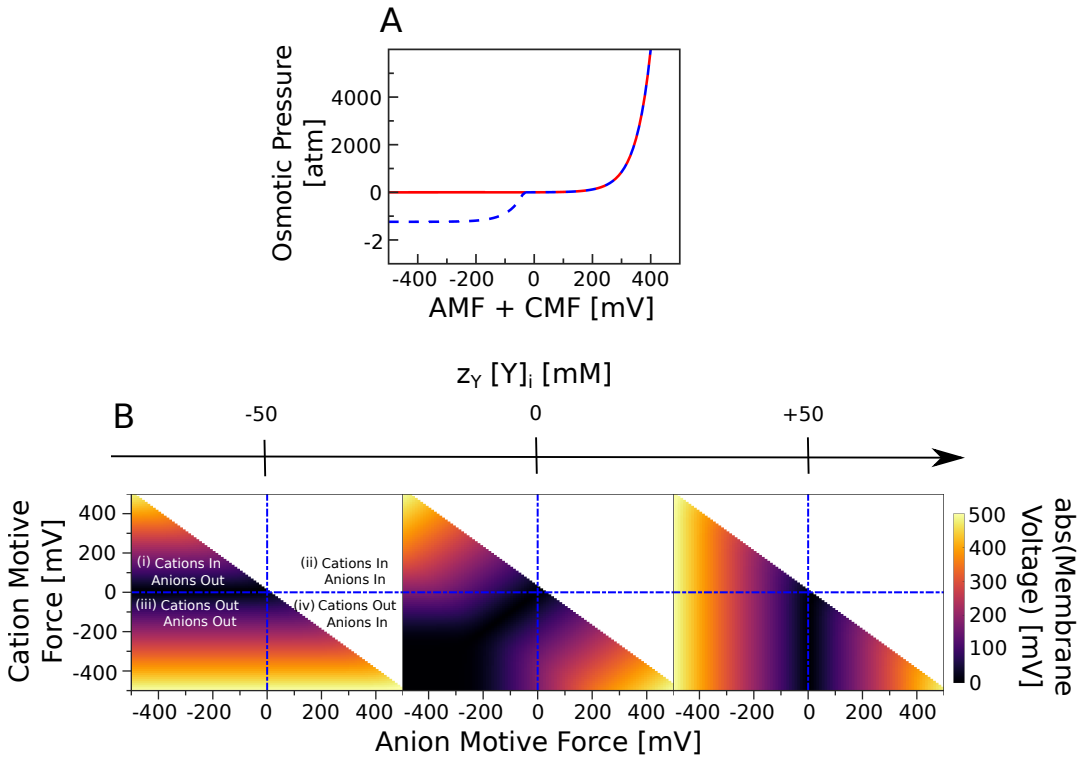


FIGURE 8: Membrane voltage and osmotic pressure generated when both small cations and anions are pumped ($\Delta G_{C^+} \neq 0$, $\Delta G_{A^+} \neq 0$). As in Fig. SI5 to 7 we keep $[\mathrm{CA}]_0 = 50$ mM, $\mathrm{pH}_i = \mathrm{pH}_e = 7$. (A) Relationship between osmotic pressure and AMF + CMF. Red and blue are for $z_Y[Y]_i$ respectively 0 and ± 50 mM. Keeping the osmotic pressure in check translates to $\Delta G_{A^-} + \Delta G_{C^+} \leq \approx 0$. The osmotic pressure is only a function of $z_Y[Y]_i$ and the sum of the ionic motive forces, irrespective of their relative values. (B) Absolute value of $\Delta\psi$ (colour map) is plotted for different CMF and AMF values; it is positive north-west and negative south-east. Only simulations resulting in $\Delta\Pi < 3$ atm are shown. Voltage is not sensitive to the AMF when there are negative captive charges of $z_Y[Y]_i = -50$ mM. Similarly, voltage is insensitive to the CMF when there are positive captive charges of $z_Y[Y]_i = +50$ mM.

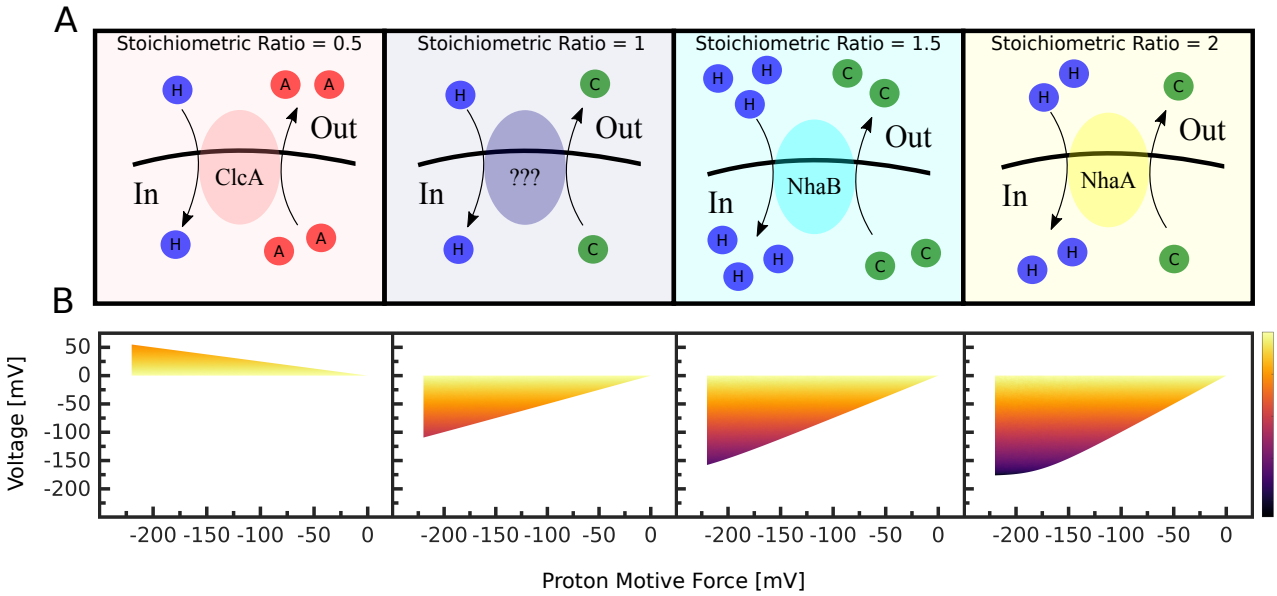


FIGURE 9: Voltage range that each proton:ion antiporter can maintain as a function of the PMF. Proton:anion antiporters enable maintenance of positive membrane voltage, while proton:cation antiporters enable maintenance of negative membrane voltage. The electroneutral proton:cation antiporter is able to maintain negative membrane voltage.

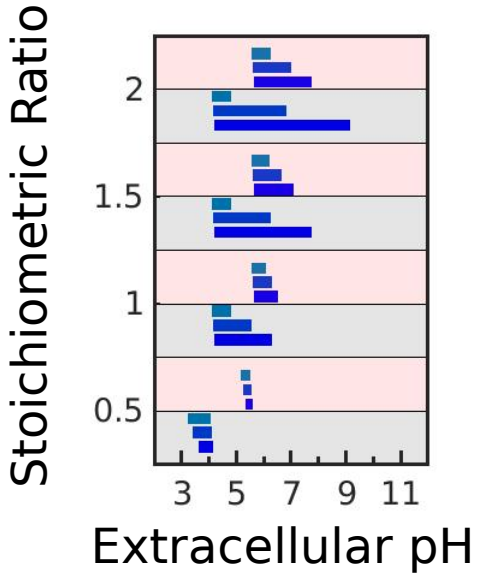


FIGURE 10: pH_e range within which *E. coli* maintains pH_i homeostasis (pH_i=7) for two values of PMF, −170 mV (representative of the aerobic regime, gray shaded areas) and −85 mV (representative of the anaerobic regime, red shaded areas). Each of the four antiporters displayed in the main text Fig. 1C is shown (indicated on the left) for different $z_Y \cdot [Y]_i$ values: -10,0 and +10 mM (deep blue to light blue). The range was obtained like in the main text Fig. 1D, i.e. by solving Eq. 5 (main text) for allowed values of $\Delta\psi$. Changing $z_Y[Y]_i$ influences the range of external pH over which *E. coli* maintains internal pH at 7, and for the same value of $z_Y[Y]_i$ that range still depends on the PMF value.

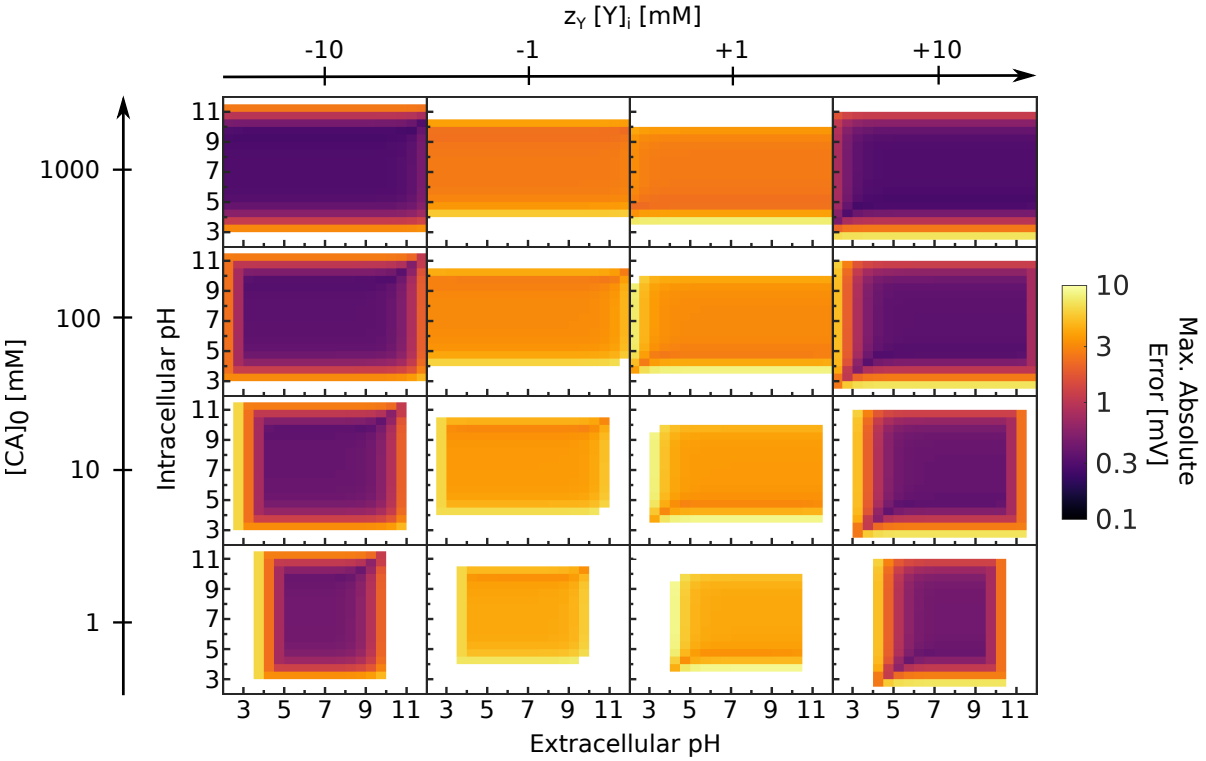


FIGURE 11: Values for $\Delta\psi$ in the main Fig. 1D were obtained by solving Eq. 5 in the main text for a fixed value of $[\mathrm{CA}]_0$ (specifically, 100 mM). Here we plot the maximal absolute error in membrane voltage value we obtain if we assume $[\mathrm{CA}]_0$ is large and pH_e=7, as opposed to any other value of these parameters. To compute the error we solve Eq. 5 in the main text and Eq. 23 in the *Supplementary text* with the above two mentioned assumption (see also 'Full equation derivation' section of the *Supplementary text*). We vary all 4 parameters: $z_Y[Y]_i$, $[\mathrm{CA}]_0$, pH_e and pH_i for an 11×11 grid of equally spaced ΔG_C and ΔG_A, values each in [-500,+500] mV range. The maximal error shown is for the pair $\{\Delta G_A, \Delta G_C\}$ that yields the maximal absolute error. Coordinates yielding absolute error greater than 10 mV are not displayed (and would correspond to the white regions in the figure). For $z_Y \cdot [Y]_i = 0$ (not shown), the approximated voltage Eq. 23 always yields the absolute error greater than 10 mV.

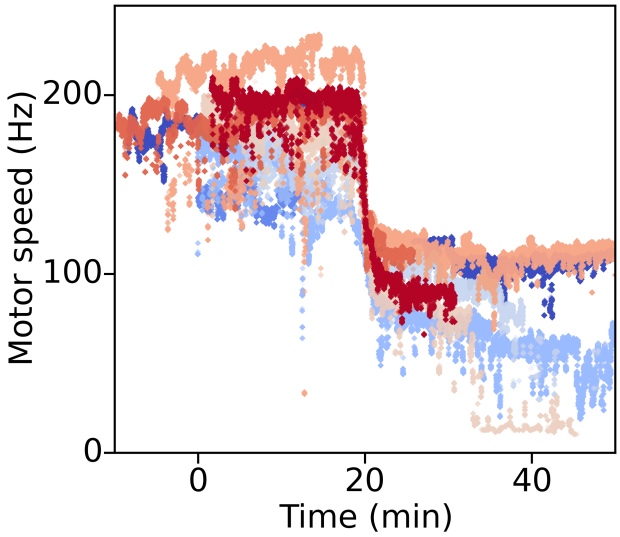


FIGURE 12: Single motor traces of *E. coli* cells (total of 8 each plotted with a different colour) in sealed tunnel-slides at pH_e=7.0 and in the presence of 20 mM glucose. The traces are aligned at the time of the speed drop, which is plotted at 20 min in the figure. In the experiment the time point of the drop varied between 20 and 30 min depending on the cell concentration and the period between sealing the tunnel-slide and the beginning of the recording.

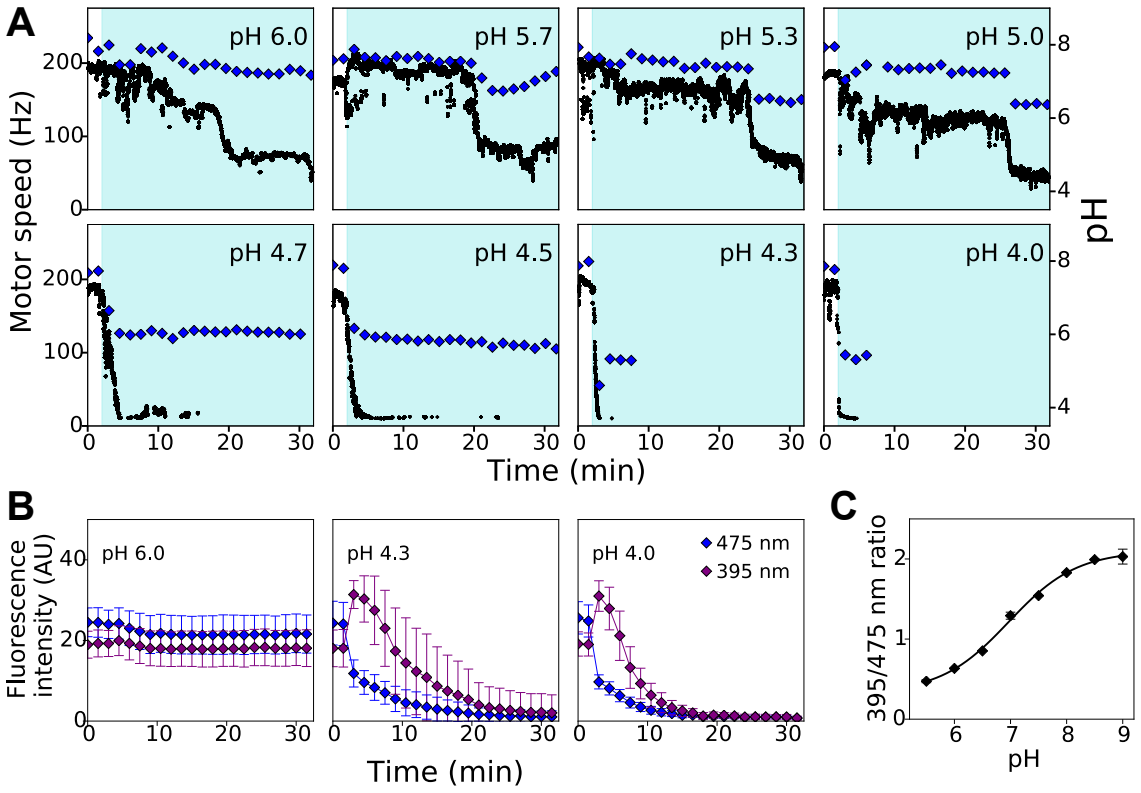


FIGURE 13: (A) Single cell examples of speed (black) and internal pH (blue) dynamics at different external pH values. Low pH buffers are introduced 2 min after the recording commences. Cyan shaded region shows the period spent at pH_e value indicated in each subplot. (B) and (C) demonstrate that at pH_e=4.3 and 4 pHluorin no longer serves as a good pH indicator. (B) Fluorescence is lost at low pH_e values at both relevant wavelengths (475 nm and 395 nm), which we plot in the figure as relative fluorescence intensity of ≈ 30 cells against time. Error bars represent standard deviation of the pixels intensities. (C) Linear range of pHluorin spans 6-8.5 pH range. The calibration curve is reproduced from [180], where the mean intensity ratio is plotted with standard deviation against pH and fitted with sigmoid function as described before [180]. Any value of pH_i lower than 5.5 can not be distinguished and will be detected as pH_i=5.5, where internal pH of the cells could be even lower.

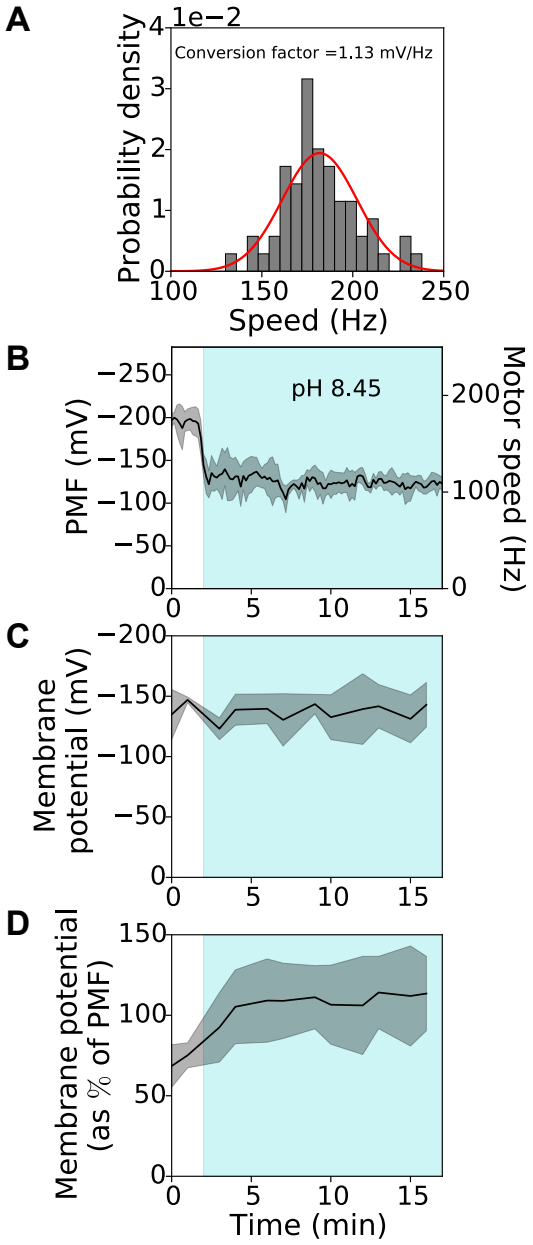


FIGURE 14: (A) We convert the motor speed to PMF by taking into account the predicted PMF range for cells respiring on glucose: $-170 \leq$ PMF ≤ -238 mV. We combine 60 single-cell (single-motor) traces collected at $pH_e = 7$ and compute the average motor speed for the first 90 s, i.e. prior to the pH_e shift. The histogram of the obtained motor speeds is plotted with the red line showing the fit to the Gaussian distribution. The median and the standard deviation thus obtained are 180.6 and 21.5 Hz. We calculate the conversion factor that maximizes the amount of traces within the predicted PMF range as $\frac{-170-238}{2} \cdot \frac{1}{180.6} \approx 1.13$ mV/Hz. (B) Mean PMF of the four cells experiencing an alkaline shift depicted with cyan shade (from pH 7 to 8.45) plotted against time. PMF is calculated from the speed trace using the conversion factor from (A). (C) Membrane potential in mV and (D) as % PMF for the same data set. Membrane potential is calculated according to the main text Eq. 1 for protons, where ΔG_{H^+} is the PMF taken from (B) and the logarithms of proton concentrations are obtained from measured internal pH_i and known external pH_e. pH_e is 7 for the first two minutes of the experiment and 8.45 for the rest of it (2-17 min). For plots (B)-(D) gray shading represents standard deviation.

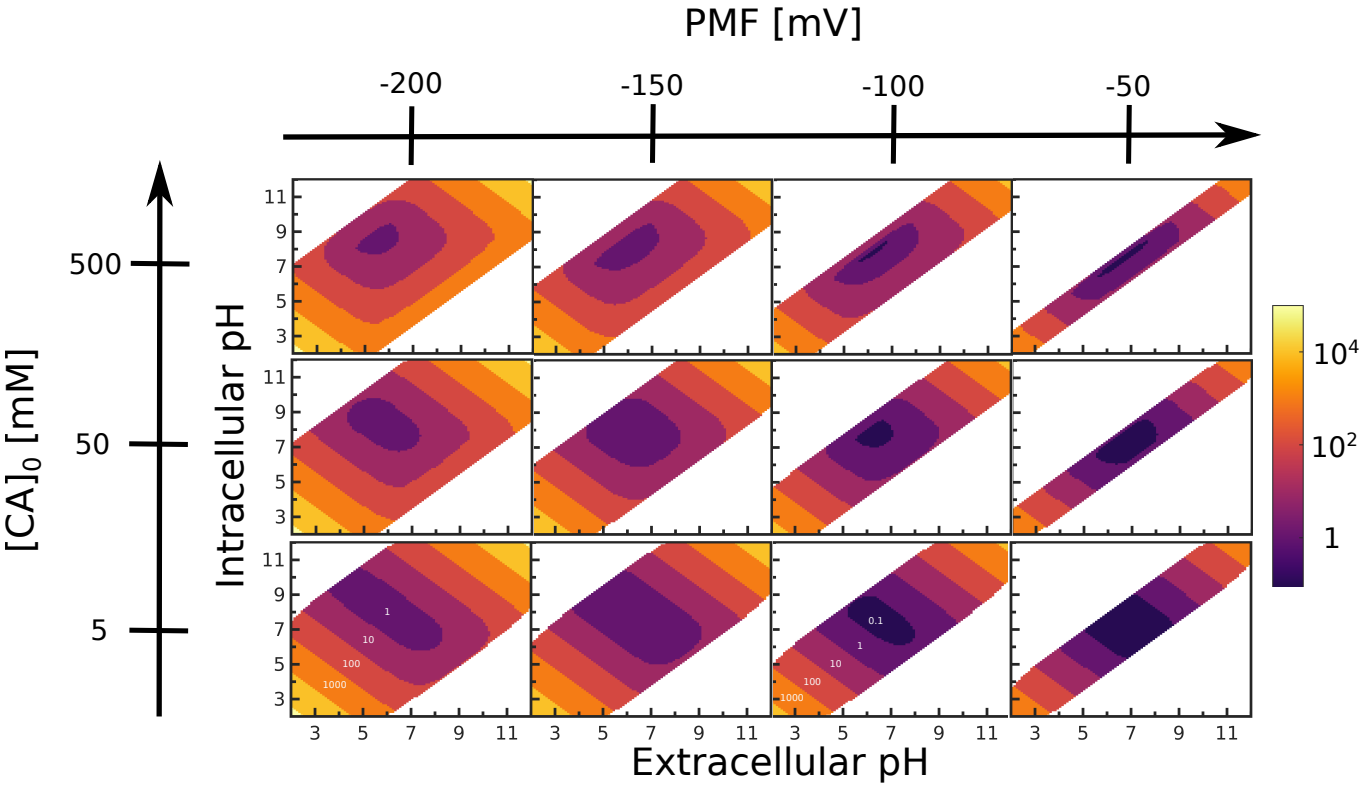


FIGURE 15: Minimal cost of maintaining time-invariant intracellular pH, PMF and osmotic pressure in a given environment defined by salinity $[\mathrm{CA}]_0$ and extracellular pH. Osmotic pressure maintained is set to 1 atmosphere. Permeabilities are set to $P_{\mathrm{H^+}} = P_{\mathrm{OH^-}} = 10^{-4}$ m/s, $P_{\mathrm{C^+}} = 5 \times 10^{-10}$ m/s and $P_{\mathrm{A^-}} = 1.5 \times 10^{-10}$. The rate of leakage is given by Erying's model. We first define the environment $\{[\mathrm{CA}]_0, \mathrm{pH}_e\}$ then for each $\{\mathrm{PMF}, \mathrm{pH}_i\}$ we sample for, we do the same as for main figure 4 (explained in last section of SI), to obtain the minimal cost of maintaining steady-state for electrophysiological homeostases in our model of *E.coli*. Sometimes the required $\{\mathrm{PMF}, \mathrm{pH}_i\}$ is simply not achievable by the model, regions which are depicted in white.

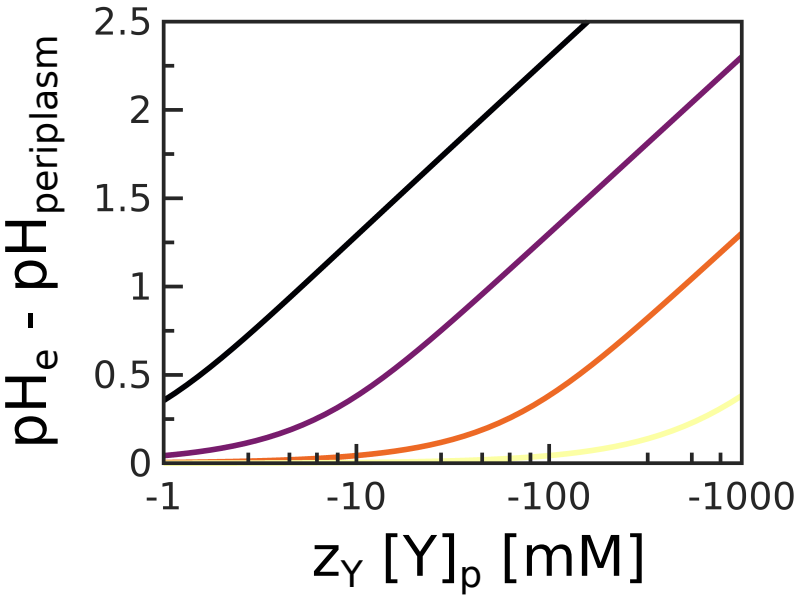


FIGURE 16: Difference between pH_e and the periplasmic pH is shown as a function of periplasmic captive charges ($z_Y[Y]_p$) and for different values of $[CA]_0$ (black to yellow show 1, 10, 100, 1000 mM respectively). We assume the periplasmic volume is 10% of the total cell volume (measured to be between 8 and 16% [230]). In addition, we set pH_e=7 and as discussed in the main text periplasm is at ionic equilibrium with the environment. At low salinity (e.g. yellow and orange lines), periplasmic captive charges may offset the pH_e as"observed" the inner membrane. The difference between pH_e at the inner membrane increases also with $[CA]_0$ even with no periplasmic captive charges.

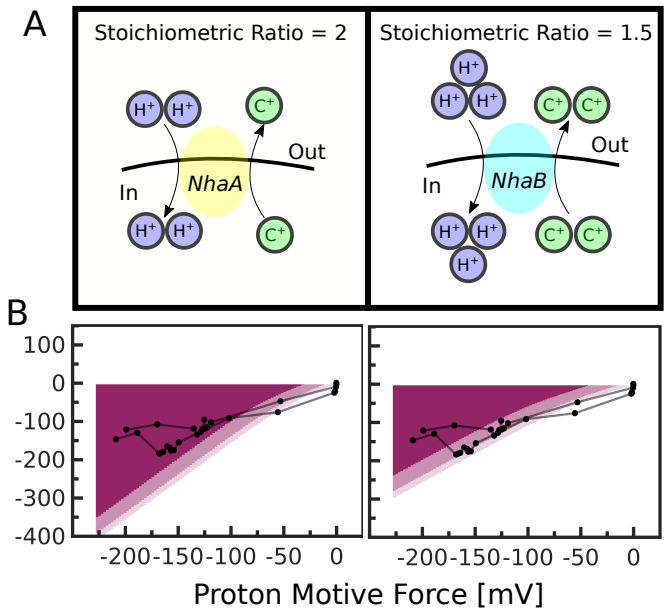


FIGURE 17: Catalytic Efficiency of *NhaA* and *NhaB* as a function of the PMF and membrane voltage maintained. Black dots are experimental points, identical to figure main 3. The three different regions correspond to different regime for catalytic efficiency, the deep purple area denotes catalytic efficiencies greater than 90%, the intermediate transparent area denotes catalytic efficiencies between 50 and 90% while the thin highly transparent area denotes catalytic efficiencies below 50%. the catalytic efficiency of a reaction n is defined as $1 - e^{\frac{F}{RT}\Delta G_n}$ (for $\Delta G_n < 0$). When ΔG_n is sufficiently negative then the catalytic efficiency goes to 1 (or 100%). When it gets closer to 0 it starts slowing down significantly the net rate, thus maintaining identical flux as ΔG_n goes closer to 0 would require increase in the forward flux by, *e.g.* increasing the number of transporters.

C. Definitions and Derivations

C.1. Cell shape

To calculate cells' surface area and volume we assume the cell is a spherocylinder with 3:1 length to width ratio (determined from our microscopy images [134] and consistent with [162]) and write:

$$S = \pi w \cdot l \tag{C.1}$$

$$V = \pi \left(\frac{w}{2}\right)^2 \left(l - \frac{w}{3}\right) \tag{C.2}$$

where l, w and V are cell length, width and volume.

C.2. Extracellular environment

NB: To keep derivations concise, we work in this subsection in molar units and in other subsections in mM units. Thus, any concentration introduced here needs to be multiplied by a factor 10^3 in other subsection.

We start with a solution of water with initial pH 7. To change pH_e we add either acid ($[\mathrm{AH}]_0$, mole of AH per mole of water) or base ($[\mathrm{COH}]_0$, mole of COH per mole of water). We add $[\mathrm{CA}]_0$ to change the external salt concentration. We assume that upon addition external environment equilibrates, which allows us to utilize the known dissociation and associations constants (pKa), the mass conservation and the charge neutrality of the solution to fully define the external environment.

By definition of pKa of water we have:

$$\mathrm{pKa}_w = -\log_{10}\left(\frac{[\mathrm{H_30^+}]_e[\mathrm{OH^-}]_e}{[\mathrm{H_2O}]_e^2}\right) \approx \mathrm{pH}_e + \mathrm{pOH}_e \tag{C.3}$$

where we treat the solvent water molecules as part of an ideal dilute solution, with an activity of 1 (valid in the range $\mathrm{pH}_e \in [2, 12]$).

Similarly,

$$\mathrm{pKa_{AH}} = -\log_{10}\left(\frac{[\mathrm{A^-}]_e \cdot [\mathrm{H_3O^+}]_e}{[\mathrm{AH}]_e}\right) \tag{C.4}$$

$$\mathrm{pKb_{COH}} = -\log_{10}\left(\frac{[\mathrm{C^+}]_e \cdot [\mathrm{OH^-}]_e}{[\mathrm{COH}]_e}\right) \tag{C.5}$$

and for salt, we assume it fully dissociates, $[\mathrm{AC}]_e \approx\!= 0$.

Next, we know that the total mass of A and C needs to be conserved:

$$[\mathrm{COH}]_e + [\mathrm{AC}]_e + [\mathrm{C^+}]_e = [\mathrm{COH}]_0 + [\mathrm{CA}]_0 \tag{C.6}$$

$$[\mathrm{AH}]_e + [\mathrm{AC}]_e + [\mathrm{A^-}]_e = [\mathrm{AH}]_0 + [\mathrm{CA}]_0 \tag{C.7}$$

as well as that the solutions remains charge neutral:

$$[\mathrm{H_3O^+}]_e - [\mathrm{OH^-}]_e + [\mathrm{C^+}]_e - [\mathrm{A^-}]_e = 0 \tag{C.8}$$

Using equations C.3 to C.8 we can now express $[\mathrm{OH^-}]_e$, $[\mathrm{C^+}]_e$ and $[\mathrm{A^-}]_e$ having set pH_e, $[\mathrm{AH}]_0$, $[\mathrm{COH}]_0$ and $[\mathrm{CA}]_0$:

$$[\mathrm{OH^-}]_e = 10^{\mathrm{pKa}_w - \mathrm{pH}_e} \tag{C.9}$$

$$[\mathrm{C^+}]_e \cdot \left(1 + 10^{\mathrm{pKb_{COH}} + \mathrm{pHe} - \mathrm{pKa}_w}\right) = [\mathrm{COH}]_0 + [\mathrm{CA}]_0 \tag{C.10}$$

$$[\mathrm{A^-}]_e \cdot \left(1 + 10^{\mathrm{pKa_{AH}} - \mathrm{pHe}}\right) = [\mathrm{AH}]_0 + [\mathrm{CA}]_0 \tag{C.11}$$

Note that to get there we first expressed $[\mathrm{C^+}]_e$ and $[\mathrm{A^-}]_e$ as a function of $[\mathrm{AH}]_e$ and $[\mathrm{COH}]_e$, and that we utilized the complete dissociation of the salt to simplify (C.6) and (C.7) to:

$$[\mathrm{COH}]_e + [\mathrm{C^+}]_e = [\mathrm{COH}]_0 + [\mathrm{CA}]_0 \tag{C.12}$$

$$[\mathrm{AH}]_e + [\mathrm{A^-}]_e = [\mathrm{AH}]_0 + [\mathrm{CA}]_0 \tag{C.13}$$

When pH_e is alkaline ($\mathrm{pH}_e > 7$) we assume $[\mathrm{AH}]_0 = 0$, and (C.11) becomes:

$$[\mathrm{A^-}]_e = [\mathrm{CA}]_0 \tag{C.14}$$

Using charge conservation ((C.8)) we also get:

$$[C^+]_e = [CA]_0 + 10^{pH_e - pKa_w} - 10^{-pH_e} \tag{C.15}$$

In acidic environments ($pH_e < 7$) we assume $[COH]_0 = 0$, and consequently (C.10) becomes:

$$[C^+]_e = [CA]_0 \tag{C.16}$$

Similarly as for the alkaline case, we use charge conservation ((C.8)) to get:

$$[A^-]_e = [CA]_0 - 10^{pH_e - pKa_w} + 10^{-pH_e} \tag{C.17}$$

We now notice that given inputs $\{[CA]_0, pHe\}$, (C.14) to (C.17) allow us to fully define the ionic composition of the environment.

External Environment	Model representation
Water	$[H_2O]_0 + [H_3O^+]_0 + [OH^-]_0 = 1$
Salt	$[CA]_0 \in [10^{-6}, 10^3]$ mol/m^3
Extracellular pH	$pHe \in [2, 12]$
Extracellular Reactions	Equilibrium constraints
$2H_2O \rightleftharpoons H_3O^+ + OH^-$	(C.3)
$CA \rightleftharpoons A^- + C^+$	Complete dissociation
$AH + H_2O \rightleftharpoons A^- + H_3O^+$	(C.4)
$COH \rightleftharpoons C^+ + OH^-$	(C.5)
Conservation Laws	Constraints
Cation mass conservation	(C.6)
Anion mass conservation	(C.7)
Charge neutrality	(C.8)

TABLE 1: Summary of the extracellular space as presented in the model. We change the extracellular space by adding salt, acid or a base (the later two to change pH). We assume that all extracellular reactions are in thermodynamic equilibrium and thus follow detailed balance. We also assume that cation and anion mass is conserved and keep charge neutrality of the external environment. As a result, fixing $\{pHe, [CA]_0\}$, and $[H_2O]_0 + [H_3O^+]_0 + [OH^-]_0 = 1$ is enough to obtain the extracellular space composition, which in our case consists of 7 species.

C.3. Full derivation of equations for $\Delta\psi$

To solve Eq. 2 in the main text we first rewrite it as follows:

$$\Delta\psi = \frac{F}{S \cdot C_m} V \left[z_Y \cdot [Y]_i + \sum_{x \in \text{small ion}} [x]_e \cdot e^{\frac{F}{RT}(\Delta G_x - z_x \Delta\psi)} \right] \tag{C.18}$$

where Y_i are the captive charges with valency z_Y. Next we split the sum of small ion to include only those we consider in the model and get:

$$\Delta\psi = \frac{F}{S \cdot C_m} V \left[z_Y \cdot [\mathrm{Y}]_i + [\mathrm{H}^+]_i - [\mathrm{OH}^-]_i + [\mathrm{C}^+]_i - [\mathrm{A}^-]_i \right] \tag{C.19}$$

We now use Eq. 1 in the main text to express $[\mathrm{C}^+]_i$ and $[\mathrm{A}^-]_i$ as a function of $[\mathrm{C}^+]_e$ and $[\mathrm{A}^+]_e$, and get:

$$\begin{aligned} \Delta\psi = \frac{F}{S \cdot C_m} V \Bigg(& z_Y \cdot [\mathrm{Y}]_i + [\mathrm{H}^+]_i - [\mathrm{OH}^-]_i + [\mathrm{C}^+]_e \cdot e^{\frac{F}{RT}(\Delta G_{C^+} - \Delta\psi)} \\ & - [\mathrm{A}^-]_e \cdot e^{\frac{F}{RT}(\Delta G_{A^-} + \Delta\psi)} \Bigg) \end{aligned} \tag{C.20}$$

Next, and as discussed in the main text, we disregard the contribution from $[\mathrm{H}^+]_i$ and $[\mathrm{OH}^-]_i$ and calculate $\frac{F}{S \cdot C_m} V \sim 3.5$ Vmol^{-1}m^{-3} to get Eq. 5 in the main text, and for the case of Donnan potential ($\Delta G_x = 0$), Eq. 4 in the main text. Because there are multiple variables in the model, we usually vary some while keeping others fixed. For example, in Fig. 1D in the main text we fix the total external ion concentration, the captive charges concentration as well as pH_i, while we change the PMF and pH_e to obtain allowed IMF values. We may wish to know, however, how will the selection of the values for variables we keep fixed, influence our conclusion. For the purposes it is convenient to express $[A^-]_e$ and $[C^+]_e$ as a total ion concentration, $[\mathrm{Ion}]_e$. If we do so, (C.20) becomes:

$$\begin{aligned} \Delta\psi = 3.5 \cdot \Bigg(& z_Y \cdot [\mathrm{Y}]_i + [\mathrm{Ion}]_e \cdot \\ & \left(\alpha_{C^+} \cdot e^{\frac{F}{RT}(\Delta G_{C^+} - \Delta\psi)} - \alpha_{A^-} \cdot e^{\frac{F}{RT}(\Delta G_{A^-} + \Delta\psi)} \right) \Bigg) \end{aligned} \tag{C.21}$$

where α_x is the fraction of either cation or anion in the environment, with $\sum_x \alpha_x = 1$. If we also introduce $\alpha_Y := (z_Y \cdot [\mathrm{Y}]_i)/[\mathrm{Ion}]_e$ we can rewrite (C.21) as:

$$\frac{1}{3.5} \cdot \frac{\Delta\psi}{[\mathrm{Ion}]_e} = \alpha_Y + \left(\alpha_{C^+} \cdot e^{\frac{F}{RT}(\Delta G_{C^+} - \Delta\psi)} - \alpha_{A^-} \cdot e^{\frac{F}{RT}(\Delta G_{A^-} + \Delta\psi)} \right) \tag{C.22}$$

or in a more compact form:

$$\frac{1}{3.5} \cdot \frac{\Delta\psi}{[\mathrm{Ion}]_e} = \alpha_Y + \sum_x z_x \alpha_x \cdot e^{\frac{F}{RT}(\Delta G_x - z_x \Delta\psi)} \tag{C.23}$$

When pH_e is alkaline ($\mathrm{pH}_e > 7$)

$$[\mathrm{Ion}]_e = 2 \cdot [\mathrm{CA}]_0 + 10^{\mathrm{pHe}-\mathrm{pKa}_w} - 10^{-\mathrm{pHe}} \tag{C.24a}$$

$$\alpha_{C^+} = \frac{[\mathrm{CA}]_0 + 10^{\mathrm{pHe}-\mathrm{pKa}_w} - 10^{-\mathrm{pHe}}}{2 \cdot [\mathrm{CA}]_0 + \mathrm{abs}\left(10^{\mathrm{pHe}-\mathrm{pKa}_w} - 10^{-\mathrm{pHe}}\right)} \tag{C.24b}$$

$$\alpha_{A^-} = \frac{1}{2 + \dfrac{\mathrm{abs}\left(10^{\mathrm{pHe}-\mathrm{pKa}_w} - 10^{-\mathrm{pHe}}\right)}{[\mathrm{CA}]_0}} \tag{C.24c}$$

and in acidic environments ($\mathrm{pH}_e < 7$)

$$[\mathrm{Ion}]_e = 2 \cdot [\mathrm{CA}]_0 - 10^{\mathrm{pHe}-\mathrm{pKa}_w} + 10^{-\mathrm{pHe}} \tag{C.25a}$$

$$\alpha_{C^+} = \frac{1}{2 + \dfrac{\mathrm{abs}\left(10^{\mathrm{pHe}-\mathrm{pKa}_w} - 10^{-\mathrm{pHe}}\right)}{[\mathrm{CA}]_0}} \tag{C.25b}$$

$$\alpha_{A^-} = \frac{[\mathrm{CA}]_0 - 10^{\mathrm{pHe}-\mathrm{pKa}_w} + 10^{-\mathrm{pHe}}}{2 \cdot [\mathrm{CA}]_0 + \mathrm{abs}\left(10^{\mathrm{pHe}-\mathrm{pKa}_w} - 10^{-\mathrm{pHe}}\right)} \tag{C.25c}$$

where $\mathrm{pKa}_w = 14$.

We now note that at $[\mathrm{CA}]_0$=100 mM, which we chose in Fig. 1 in the main text, left hand side of (C.23) is small.We also notice that for large $[\mathrm{CA}]_0$ and pH_e=7, $\alpha_{C^+} = \alpha_{A^-} = 1/2$. We can now ask what would be the error in calculating $\Delta\psi$ if we assume left hand side of the equation is zero ($[\mathrm{CA}]_0$ is large) and $\alpha_{C^+} = \alpha_{A^-} = 1/2$ (pH_e=7) as opposed to calculating the exact value of $\Delta\psi$. The results are given in Fig. SI 10, showing that the value of $\Delta\psi$ is quite robust in a relatively wide range of $[\mathrm{CA}]_0$, pH_e and $z_Y \cdot [Y]_i$ values and that a good approximation for membrane

potential is given by:

$$0 = \alpha_Y + \frac{1}{2}\left(e^{\frac{F}{RT}\cdot\left(\Delta G_{\mathrm{C}^+} - \Delta\psi\right)} - e^{\frac{F}{RT}\cdot\left(\Delta G_{\mathrm{A}^-} + \Delta\psi\right)} \right) \tag{C.26}$$

$$[\mathrm{Ion}]_e = 2 \cdot [\mathrm{CA}]_0 \tag{C.27}$$

Which is independent on both the intracellular and extracellular pHs.

C.4. Describing the movement of ions

To describe the movement of ions across a biological membrane we use Eq. (6) in the main text:

$$\frac{d[x]_i}{dt} = -\frac{d[x]_e}{dt} = j_x + \sum_n \sigma_{x,n} \cdot j_n \tag{C.28}$$

where j_x is the flux of ions due to leakage, j_n flux of ions due to a specific pumping reaction n (we use units of mol $\mathrm{m}^{-3}\mathrm{s}^{-1}$) and $\sigma_{x,n}$ the stoichiometric coefficient of that reaction.

Active Transport To describe the flux of ions due to pumping we assume all transport reactions n are reversible and can be decomposed into the rate of forward rate j_n^+, and the backward rate, j_n^- [200]:

$$j_n = j_n^+ - j_n^- = j_n^+ \cdot \left(1 - \frac{j_n^-}{j_n^+}\right) \tag{C.29}$$

The Gibbs free energy ΔG_n of a reaction n is a quantity that if negative entails that the reaction is spontaneous, *i.e.* $j_n > 0 \Leftrightarrow j_n^+ > j_n^-$ and the reaction goes forward. On the other hand, if ΔG_n is positive then the reaction goes spontaneously backward. Assuming for any reaction its forward and backward flux are strictly positive (every reaction has a non-null probability to occur in a time interval) means 0 net flux j_n is only achieved for $\Delta G_n = 0$. This restricts the forward and backward rates to functional dependencies on the state that follow:

$$\frac{j_n^-(\mathbf{x}|j_n = 0)}{j_n^+(\mathbf{x}|j_n = 0)} = \frac{F}{RT} \underbrace{\Delta G_n(\mathbf{x}|j_n = 0)}_{=0} + 1 \tag{C.30}$$

$$\frac{j_n^-(\mathbf{x}|j_n > 0)}{j_n^+(\mathbf{x}|j_n > 0)} < 1 \tag{C.31}$$

$$\frac{j_n^-(\mathbf{x}|j_n < 0)}{j_n^+(\mathbf{x}|j_n < 0)} > 1 \tag{C.32}$$

where we write $(\mathbf{x}|j_n = 0)$ for any state of the system (characterized by a vector or matrix $\mathbf{x}$) such that $j_n = 0$. There are now several possible functional dependencies of the rates on the state that are compatible with the constraints above. As such,

one can sometimes see kinetics described by:

$$j_n(\mathbf{x}) = -j_n^+(\mathbf{x}) \cdot \frac{F}{RT}\Delta G_n(\mathbf{x}) \tag{C.33}$$

$$\frac{j_n^-(\mathbf{x})}{j_n^+(x)} = \frac{F}{RT}\Delta G(\mathbf{x}) + 1 \tag{C.34}$$

which follows constraints Eqs. (C.30) to (C.32). We can see however than if n is an elementary reaction, then Eq. (C.34) must violate either the definition of ΔG_n, which we know scales with the logarithm of the product of concentrations or mass-action kinetics for fluxes, which we know scales linearly with the product of concentrations. In fact, for elementary reactions, the only way for constraints Eqs. (C.30) to (C.32) as well as the linearity of rate with the products of concentrations and the logarithmic scaling of ΔG_n with the products of concentrations is to write:

$$j_n = j_n^+ \cdot \left(1 - e^{\frac{F}{RT}\Delta G_n}\right) \tag{C.35}$$

$$\Delta G_n \equiv \frac{RT}{F} \ln\left(\frac{j_n^-}{j_n^+}\right) \tag{C.36}$$

as in [231, 200]. At steady-state, the dependency Eq. (C.35) of the net rate of a reaction on its Gibbs free energy, can be generalized to any reaction scheme composed of elementary reactions, where j_n^+ is the function that describes the specifics of the transport mechanism and will depend on the reaction scheme and the specifics parameters of each step.

To define the Gibbs free energy of a reaction we first need to introduce the electrochemical potential of species x in compartment m as:

$$\overline{\mu_x^{(m)}} = \mu_x^{(0),m} + z_x \cdot F \cdot \psi_m + RT \cdot \ln([x]_m/[x]_0) \tag{C.37}$$

where $[x]_0$ is the concentration of reference and ψ_m is the voltage in compartment m and $\mu_x^{(0),m}$ is the standard chemical potential. The electrochemical potential is here effectively the amount of potential and kinetic energies that are added (if positive) or removed (if negative) to the compartment m by addition of one mole of x. While the $\ln([x])$ term accounts for the entropic contribution to energy change, the term with ψ_m accounts for electrostatic potential energy. The Gibbs free energy of any reaction n at constant temperature and pressure can now be

expressed from above as:

$$F \cdot \Delta G_n = \sum_m \left(\sum_{x \in \text{Products}} \sigma_{x_m,n} \cdot \overline{\mu_x^{(0),m}} - \sum_{x \in \text{Reactants}} \sigma_{x_m,n} \cdot \overline{\mu_x^{(0),m}} \right) \tag{C.38}$$

Where the F in the left hand term is to express ΔG_n in volts rather than in joules per mole. For instance for the leakage of protons $r_{\text{H}^+} := \text{H}_e^+ \rightleftharpoons \text{H}_i^+$ we recover:

$$\Delta G_{\text{H}^+} = z_x \cdot \Delta\psi + \frac{RT}{F} \cdot \ln\left(\frac{[\text{H}^+]_i}{[\text{H}^+]_e}\right) \tag{C.39}$$

where the membrane potential $\Delta\psi = \psi_i - \psi_e$ is the voltage difference between the intracellular and extracellular compartments and where the standard potential $\mu_{\text{H}^+}^{(0)}$ is equal in both compartments[19]. Another example, for ATP hydrolysis $r_{\text{ATP}} := \text{ATP} \rightleftharpoons \text{ADP} + \text{Pi}$:

$$\Delta G_{\text{ATP}} = \Delta G_{\text{ATP}}^{(0)} + \frac{RT}{F} \cdot \ln\left(\frac{[\text{ADP}] \cdot [\text{Pi}]}{[\text{ATP}]}\right) \tag{C.40}$$

where $\Delta G_{\text{ATP}}^{(0)}$ is given by the concentrations of the molecules involved in the reaction at equilibrium:

$$\Delta G_{\text{ATP}}(j_{\text{ATP}} = 0) = 0 \Leftrightarrow \Delta G_{\text{ATP}}^{(0)} = \frac{RT}{F} \cdot \ln\left(\frac{[\text{ATP}]_{eq}}{[\text{ADP}]_{eq} \cdot [\text{Pi}]_{eq}}\right) \tag{C.41}$$

where we used the notation, *e.g.* $[\text{ATP}]_{eq} \equiv [\text{ATP}](j_{\text{ATP}} = 0)$, or equilibrium concentration for ATP is equivalent to ATP concentration in a state where there is 0 net flux for ATP hydrolysis.

Finally, we note that we can compute the Gibbs free energy of complex reactions by:

$$\Delta G_n = \sum_{r \in \text{simplex}} \sigma_{r,n} \cdot \Delta G_r \tag{C.42}$$

where the sum is over all simplex reactions, *i.e.* all reactions that have only one substrate or one product. For instance leakage reactions are simplex reactions, ATP hydrolysis $\text{ATP} \rightleftharpoons \text{ADP} + \text{Pi}$ is a simplex reaction, however an antiporter reaction or F1F_o are not simplex reactions but however can be built from simplex

[19] This can be derived assuming that at null membrane potential, there is not net passive diffusion of protons across the membrane if and only if proton concentrations are equal in both compartments.

reactions:

$$r_{\mathrm{F1F}_o} := -1 \cdot r_{\mathrm{ATP}} + 3.3 \cdot r_{\mathrm{H^+}} \equiv \mathrm{ADP} + \mathrm{Pi} + 3.3 \cdot \mathrm{H}_e^+ \rightleftharpoons \mathrm{ATP} + 3.3 \cdot \mathrm{H}_i^+ \tag{C.43}$$

$$r_{\mathrm{NhaB}} := -2 \cdot r_{\mathrm{C^+}} + 3 \cdot r_{\mathrm{H^+}} \equiv 3 \cdot \mathrm{H}_e^+ + 2 \cdot \mathrm{C}_i^+ \rightleftharpoons 3 \cdot \mathrm{H}_i^+ + 2 \cdot \mathrm{C}_e^+ \tag{C.44}$$

where $\sigma_{r,n}$ in Eq. (C.42) denotes the number of simplex reactions r needed to build the more complex reaction n. In the two examples above: $\sigma_{\mathrm{ATP,F1F}_o} = -1$, $\sigma_{\mathrm{H^+,F1F}_o} = 3.3$, $\sigma_{\mathrm{H^+,NhaB}} = 3$, $\sigma_{\mathrm{C^+,NhaB}} = 2$.

Passive Transport To describe the flux of ions due to leakage we use a common form for j_x based on the "trapezoidal energy barrier" model [42]:

$$j_x = \frac{S}{V} \cdot P_x \cdot b \cdot \frac{F}{RT} \cdot z_x \cdot \Delta\psi \cdot \frac{[x]_e \cdot e^{-\frac{F}{RT} z_x \Delta\psi/2} - [x]_i \cdot e^{+\frac{F}{RT} z_x \Delta\psi/2}}{e^{-b\frac{F}{RT} z_x \Delta\psi/2} - e^{+b\frac{F}{RT} z_x \Delta\psi/2}} \tag{C.45}$$

where $0 \leq b \leq 1$ is is so-called "fractional width of the trapezoid" and P_x the permeability of the membrane for ion x both of which depend on the membrane's properties.

We notice that (C.45) can be rewritten as:

$$j_x = P_x \cdot [x]_e \cdot b \cdot \frac{F}{RT} \cdot z_x \cdot \Delta\psi \cdot \frac{e^{-\frac{F}{RT} z_x \Delta\psi/2}}{e^{-b\frac{F}{RT} z_x \Delta\psi/2} - e^{+b\frac{F}{RT} z_x \Delta\psi/2}} \left(1 - e^{\frac{F}{RT} \Delta G_x}\right) \tag{C.46}$$

where ΔG_x is the electrochemical potential defined in the main text. Thus, the flux of ions due to leakage has the same functional form as the flux of ions due to pumping given in (C.35):

$$j_x = j_x^+ \cdot \left(1 - e^{\frac{F}{RT} \Delta G_x}\right) \tag{C.47}$$

where

$$j_x^+ = \frac{S}{V} \cdot P_x \cdot [x]_e \cdot f_b(z_x \cdot \Delta\psi) \tag{C.48}$$

$$f_b(z_x \cdot \Delta\psi) = +b \cdot z_x \cdot \Delta\psi \cdot \frac{e^{-\frac{F}{RT} z_x \Delta\psi/2}}{e^{-b\frac{F}{RT} z_x \Delta\psi/2} - e^{+b\frac{F}{RT} z_x \Delta\psi/2}} \tag{C.49}$$

In its limits for b ($b = 0$ and $b = 1$), the forward flux become:

$$f_0(\Delta\psi) = e^{-z_x \frac{F}{RT} \Delta\psi/2} \tag{C.50}$$

$$f_1(\Delta\psi) = \frac{F}{RT} \cdot \frac{z_x \cdot \Delta\psi}{e^{z_x \frac{F}{RT} \Delta\psi} - 1} \tag{C.51}$$

Where we recognize that when $b = 1$, $f_b(\Delta\psi)$ reduces to Goldman–Hodgkin–Katz flux equation and when $b = 0$ to Erying's single barrier model [42].

Cost of maintaining an electrophysiological Steady-State. To take into account the cost of maintaining a given electrophysiological steady-state we consider the number of protons a cell needs to pump outwards to compensate for the ion leakage (j_x), the action of proton:ion antiporter (j_n) as well as protons released by intracellular self-ionization of water:

$$\text{Cost} = j_{\text{H}^+} + j_w + \sum_n \sigma_{H^+,n} \cdot j_n$$

where j_w is the rate of the reaction $2\text{H}_2\text{O} \rightleftharpoons \text{H}_3\text{O}^+ + \text{OH}^-$. Assuming hydroxide ions are not actively transported: $\frac{d[\text{OH}^-]_i}{dt} = 0 = j_{\text{OH}^-} + j_w$, the equation above becomes:

$$\text{Cost} = j_{\text{H}^+} - j_{\text{OH}^-} + \sum_n \sigma_{H^+,n} \cdot j_n \tag{C.52}$$

This formula holds in general for any model possessing an arbitrary number of chemically driven proton pumps and proton driven ionic transport systems (proton:ion antiporters or symporters) and the cost is effectively the total rate of protons (in mM per second) exchanged by a unit volume of cell with its environment *via* passive diffusion, self ionization of water and activity of proton:ion exchangers.

C.5. Energy budget of *E. coli*

To calculate the reference energy budget of *E. coli* (main Fig. 4D) we use the following references. [232] reports that *E. coli* growing at 0.89 h^{-1} on glucose consumes 19.8 $mM{\cdot}h^{-1}$ of oxygen per gram of dry weight, and when growing at 1 h^{-1} the dry weight of *E. coli* is $258{\cdot}10^{-15}$ g (dry weight) per cell [233]. Assuming oxygen consumption and mass per cell are comparable between the two experiments this gives: $19.8 \cdot 10^{-3} \cdot N_A \cdot 258 \cdot 10^{-15} = 3.08 \cdot 10^9$ O_2 per cell per hour. Given a stoichiometry of the respiratory chain ($\sigma_{H,R} = 10$ per $1/2O_2$ [234]) this corresponds to a "budget" of 61.6×10^9 protons per cell per hour. We will assume this budget for our conditions of reference defined by the geometrical parameter of *E. coli* on MM9+glucose [162], the oxygen consumption rate from [232] and the dry weight per cell of [233] and express the cost of maintaining cellular homeostases as a fraction of the total proton budget for that reference condition. For instance, if we compute that the cost of maintaining the electrophysiological steady state is 30.8 billions protons per cell per hour, we will express that quantity as 50% percent of the budget of reference, that we computed here is 61.6 billions protons per cell per hour.

C.6. Periplasm

In (C.18) $\Delta\psi$ was expressed as a function of external concentration $[\mathrm{x}]_e$, which in the presence of periplasmic space becomes the periplasmic concentration $[\mathrm{x}]_p$

$$\Delta\psi = \frac{F}{S \cdot C_m} V \left[z_Y \cdot [Y]_i + \sum_x [x]_p \cdot e^{\frac{F}{RT}(\Delta G_x - z_x \Delta\psi)} \right] \tag{C.53}$$

where $[\mathrm{x}]_p$ is given as in the main text

$$[x]_e = [x]_p \cdot e^{-\frac{F z_x}{RT} \cdot \Delta\psi_p} \tag{C.54}$$

(C.53) now becomes

$$\Delta\psi = \frac{F}{S \cdot C_m} V \left[z_Y \cdot [Y]_i + \sum_{x \in \text{small ion}} [x]_e \cdot e^{\frac{F}{RT}(\Delta G_x - z_x(\Delta\psi + \Delta\psi_p))} \right] \tag{C.55}$$

The rest of the derivation to arrive to Eq. (20) in the main text follows the derivation given in SI C.18 to C.21.

D. Model of E.coli Electrophysiology

D.1. Model Reactions and Parameters

The full model of *E.coli* electrophysiology, we study in Main Figure (4), has access to the reactions from table 2. Other model's parameters are shown in table 3. In particular the reactions of ATP hydrolysis and NADH reduction are chemostated (*i.e.* take fixed values). We obtained the value for ΔG_{NADH} from "eQuilibrator" [184], which gives Gibbs free energy of two half-reactions ($\mathrm{NADH(aq)} \rightleftharpoons \mathrm{NAD^+(aq)} + 2e^-$ and $\mathrm{O_2(aq)} + 4e^- \rightleftharpoons 2\mathrm{H_2O}$) at neutral pH and 100 mM ionic strength as -64.1 kJ/mol and -314.5 kJ/mol, respectively. Given that we know

$$\frac{1}{2}\mathrm{O_2} + \mathrm{NADH} + \mathrm{H^+} \rightleftharpoons \mathrm{H_2O} + \mathrm{NAD^+} \tag{D.1}$$

$\Delta G_{\mathrm{NADH}} = -64.1 - 314.5/2 = 221.3$ kJ/mole, which we then convert to Volts to obtain the value in Table 3. Similarly, for ATP hydrolysis we use standard Gibbs free energy of $\Delta G^{\circ}_{\mathrm{ATP}} = -37.6$ kJ/mol [235], and assume that in *E. coli* [ATP] = 10 mM, [ADP] = 0.6 mM, [Pi] = 20 mM [182]. Thus, $\Delta G_{\mathrm{ATP}} = \Delta G^{\circ}_{\mathrm{ATP}} + RT \ln \frac{[\mathrm{ATP}]}{[\mathrm{ADP}][\mathrm{Pi}]} = -37600 + 8.31 \times 298 \times \ln \frac{0.01}{0.02 \times 0.0006} \approx -54$ kJ/mol, which we then convert to Volts to obtain the value in Table 3.

Note that the models in figure Main (1) and (3) are defined similarly but have only access to one active pump for either cations or anions. The pump these simpler models have access to are defined in the corresponding figures' schemes.

Flux j_n	Reaction	Free Energy Change
$j_{\mathrm{H^+}}$	$\mathrm{H^+_e} \rightleftharpoons \mathrm{H^+_i}$	$\Delta G_{\mathrm{H^+}}$
$j_{\mathrm{OH^-}}$	$\mathrm{OH^-_e} \rightleftharpoons \mathrm{OH^-_i}$	$\Delta G_{\mathrm{OH^-}}$
$j_{\mathrm{C^+}}$	$\mathrm{C^+_e} \rightleftharpoons \mathrm{C^+_i}$	$\Delta G_{\mathrm{C^+}}$
$j_{\mathrm{A^-}}$	$\mathrm{A^-_e} \rightleftharpoons \mathrm{A^-_i}$	$\Delta G_{\mathrm{A^-}}$
j_{R}	$\mathrm{R^\star} + 10\cdot\ \mathrm{H^+_i} \rightleftharpoons \mathrm{R} + 10\cdot\ \mathrm{H^+_e}$	$\Delta G_{\mathrm{R}} = \Delta G_{\mathrm{NADH}} - 10 \cdot \Delta G_{\mathrm{H^+}}$
$j_{\mathrm{F1F_o}}$	$\mathrm{ATP} + 3.3\cdot\ \mathrm{H^+_e} \rightleftharpoons \mathrm{ADP} + 3.3\cdot\ \mathrm{H^+_i}$	$\Delta G_{\mathrm{F1F_o}} = \Delta G_{\mathrm{ATP}} + 3.3 \cdot \Delta G_{\mathrm{H^+}}$
j_{NhaB}	$3\cdot\ \mathrm{H^+_e} + 2\cdot \mathrm{C^+_i} \rightleftharpoons 3\cdot\ \mathrm{H^+_i} + 2\cdot\ \mathrm{C^+_e}$	$\Delta G_{\mathrm{NhaB}} = 3 \cdot \Delta G_{\mathrm{H^+}} - 2 \cdot \Delta G_{\mathrm{C^+}}$
j_{NhaA}	$2\cdot\ \mathrm{H^+_e} + \mathrm{C^+_i} \rightleftharpoons 2\cdot\ \mathrm{H^+_i} + \mathrm{C^+_e}$	$\Delta G_{\mathrm{NhaA}} = 2 \cdot \Delta G_{\mathrm{H^+}} - \Delta G_{\mathrm{C^+}}$
j_{ClcA}	$\mathrm{H^+_e} + 2\cdot \mathrm{A^-_i} \rightleftharpoons \mathrm{H^+_i} + 2\cdot\ \mathrm{A^-_e}$	$\Delta G_{\mathrm{ClcA}} = \Delta G_{\mathrm{H^+}} - 2 \cdot \Delta G_{\mathrm{A^-}}$

Table 2: Summary of all the reactions we considered in the model. Stoichiometric coefficients are based on previous literature.

Name	Symbol	Units	Value	Ref.
Faraday Constant	F	C/mole	96485	
Gas Constant	R	J/mole/K	8.31	
Temperature	T	K	298	
Dissociation Constant HCl	$\mathrm{pKa}_{\mathrm{AH}}$	Dimensionless	-6.3	
Dissociation Constant NaOH	$\mathrm{pKb}_{\mathrm{COH}}$	Dimensionless	-0.56	
Dissociation Constant H_2O	pKa_w	Dimensionless	14	
Membrane Capacitance	C_m	$\mathrm{C/m^2}$	6.5×10^{-3}	[41]
Cell width	w	m	1.07×10^{-6}	[162, 29]
Cell length	l	m	2.95×10^{-6}	[162, 29]
Cell Surface	S	$\mathrm{m^2}$	??	[162, 29]
Cell Volume	V	$\mathrm{m^3}$	??	[162, 29]
Gibbs free energy of NADH reduction	ΔG_{NADH}	V	-2.290	[184]
Gibbs free energy of ATP hydrolysis	ΔG_{ATP}	V	-0.560	[184]
Fractional Width Trapezoid	b	Dimensionless	1	Arbitrary
Proton Permeability	$P_{\mathrm{H^+}}$	m/s	10−4	[42][20]
Hydroxide ion Permeability	$P_{\mathrm{OH^-}}$	m/s	10−4	Arbitrary
Sodium Permeability	$P_{\mathrm{C^+}}$	m/s	5×10^{-10}	[163]
Chloride Permeability	$P_{\mathrm{A^-}}$	m/s	2×10^{-10}	[163]

TABLE 3: List of constants in our model and their values.

D.2. Steady-State Characterization

We further note that we are considering only steady-state solutions, so from (C.28) and the reactions from table 2 we have at steady-state for intracellular protons and hydroxide ions:

$$\begin{aligned}\frac{d[\mathrm{H^+}]_i}{dt} = 0 = j_{\mathrm{H_2O}} + j_{\mathrm{H^+}} \\ + \sigma_{\mathrm{H^+,R}} \cdot j_{\mathrm{R}} + \sigma_{\mathrm{H^+,F1F_o}} \cdot j_{\mathrm{F1F_o}} \\ + \sigma_{\mathrm{H^+,NhaB}} \cdot j_{\mathrm{NhaB}} + \sigma_{\mathrm{H^+,NhaA}} \cdot j_{\mathrm{NhaA}} + \sigma_{\mathrm{H^+,ClcA}} \cdot j_{\mathrm{ClcA}}\end{aligned} \tag{D.2}$$

$$\frac{d[\mathrm{OH^-}]_i}{dt} = 0 = j_{\mathrm{OH^-}} + j_{\mathrm{H_2O}} \tag{D.3}$$

Similarly, steady-state for small cations $\mathrm{C^+}$ and anions $\mathrm{A^-}$ is characterized by:

$$\frac{d[\mathrm{C^+}]_i}{dt} = 0 = j_{\mathrm{C^+}} + \sigma_{\mathrm{C^+,NhaB}} \cdot j_{\mathrm{NhaB}} + \sigma_{\mathrm{C^+,NhaA}} \cdot j_{\mathrm{NhaA}} \tag{D.4}$$

$$\frac{d[\mathrm{A^-}]_i}{dt} = 0 = j_{\mathrm{A^-}} + \sigma_{\mathrm{A^-,ClcA}} \cdot j_{\mathrm{ClcA}} \tag{D.5}$$

Thus, taking into account ClcA stoichiometric coefficient and (C.35), j_{ClcA} can we written as:

$$j^{+}_{\mathrm{ClcA}} = \frac{1}{2} \cdot \frac{j_{\mathrm{A}^-}}{1 - e^{\frac{F}{RT} \cdot \Delta G_{\mathrm{ClcA}}}} \tag{D.6}$$

whereas j_{NhaA} and j_{NhaB} are constrained by:

$$\begin{aligned} -\frac{S}{V} \cdot P_{\mathrm{C}^+} \cdot [\mathrm{C}^+]_e \cdot f_b(+\Delta\psi) \cdot \left(1 - e^{\frac{F}{RT} \Delta G_{\mathrm{C}^+}}\right) = \\ j^{+}_{\mathrm{NhaB}} \cdot \left(1 - e^{\frac{F}{RT} \cdot \Delta G_{\mathrm{NhaB}}}\right) + j^{+}_{\mathrm{NhaA}} \cdot \left(1 - e^{\frac{F}{RT} \cdot \Delta G_{\mathrm{NhaA}}}\right) \end{aligned} \tag{D.7}$$

The general cost Eq. (C.52) can be expressed for our model of *E.coli* as:

$$\mathrm{Cost} = j_{\mathrm{H}^+} - j_{\mathrm{OH}^-} + \sigma_{\mathrm{H}^+,\mathrm{NhaB}} \cdot j_{\mathrm{NhaB}} + \sigma_{\mathrm{H}^+,\mathrm{NhaA}} \cdot j_{\mathrm{NhaA}} + \sigma_{\mathrm{H}^+,\mathrm{ClcA}} \cdot j_{\mathrm{ClcA}} \tag{D.8}$$

The leakage fluxes $\forall x \in \{\mathrm{H}^+, \mathrm{OH}^-, \mathrm{C}^+, \mathrm{A}^-\} : j_x$ are given in (C.45). We now have a set of equations that allow us to: *(i)* Enumerate all the achievable steady state, which we do in subsection D.3 and *(ii)* calculate the cost of maintaining a certain allowed combination of IMFs in a given external environment, as well as to determine which combination of IMFs and antiporters' activities gives minimal cost which we do in subsection D.4.

D.3. Boundaries on Electrochemical potentials

In this section, we derive the range of ionic motive forces that can be maintained at steady-state for the model of *E.coli* in table 2. Given fixed potential of ATP hydrolysis and NADH reduction, extracellular concentrations of ions as well as intracellular concentration and average valency of captive molecules, this enumerates all the states that the model can possibly maintain. Any IMF not in the range defined below will violate either the steady-state condition for the ion, or the second principle of thermodynamics here defined as the direction of a reaction in relation to its Gibbs free energy.

Boundaries on $\Delta G_{\mathbf{A}^-}$

Result We show that for our model of *E.coli*, the range of electrochemical potential of A^- compatible with time-invariant intracellular concentration of small anions $[A^-]$ is:

$$\frac{1}{2} \cdot \Delta G_{H^+} \leq \Delta G_{A^-} \leq 0 \tag{D.9}$$

Proof We rewrite the steady state condition for small anions:

$$\frac{d[A^-]_i}{dt} = 0 = j_{A^-} + \underbrace{\sigma_{A^-,ClcA}}_{-2} \cdot j_{ClcA} \tag{D.10}$$

In words, the proof consists in identifying forbidden pairs of electrochemical potentials $\{\Delta G_{A^-}, \Delta + H^+\}$ at steady-state, meaning such pairs that result in flux j_{A^-} and $\sigma_{A^-,ClcA} \cdot j_{ClcA}$ in Eq. (D.10) of identical signs. Indeed, if these two terms are of identical signs, then $\frac{d[A^-]_i}{dt}$ is strictly negative or strictly positive and therefore the system is not in steady-state. The mathematical derivation is then as follows.

We wish to study steady-state behaviours and thus it forbids from Eq. (D.5):

$$\frac{d[A^-]_i}{dt} > 0 \Leftarrow \begin{cases} & j_{A^-} > 0 \\ \sigma_{A^-,ClcA} \cdot j_{ClcA} > 0 \Leftrightarrow & j_{ClcA} < 0 \end{cases} \tag{D.11}$$

$$\frac{d[A^-]_i}{dt} < 0 \Leftarrow \begin{cases} & j_{A^-} < 0 \\ \sigma_{A^-,ClcA} \cdot j_{ClcA} < 0 \Leftrightarrow & j_{ClcA} > 0 \end{cases} \tag{D.12}$$

Which by Eq. (C.35), substituting the free energy of *ClcA* by its definition in table 2, is equivalent to:

$$\frac{d[A^-]_i}{dt} > 0 \Leftarrow \begin{cases} \Delta G_{A^-} & < 0 \\ \Delta G_{A^-} & < \frac{1}{2} \cdot \Delta G_{H^+} \end{cases} \tag{D.13}$$

$$\frac{d[A^-]_i}{dt} < 0 \Leftarrow \begin{cases} \Delta G_{A^-} & > 0 \\ \Delta G_{A^-} & > \frac{1}{2} \cdot \Delta G_{H^+} \end{cases} \tag{D.14}$$

We assume that $\Delta G_{H^+} \leq 0$ (which we will show later) and consequently if $\Delta G_{A^-} > 0$ we are in the forbidden regime (D.14). In addition, since $\Delta G_{H^+} \leq 0$, to prevent the second forbidden regime (D.13) entails $\Delta G_{A^-} > 1/2 \cdot \Delta G_{H^+}$. From

those two inequalities we obtain the thermodynamically viable range of ΔG_{A^-} at steady state inequality (D.10).

Boundaries on $\Delta G_{\mathbf{C}^+}$

Results We show that for our model of *E.coli*, the range of electrochemical potential of C^- compatible with steady-state of chemiosmotic processes is:

$$2 \cdot \Delta G_{\mathrm{H}^+} \leq \Delta G_{\mathrm{C}^+} \leq 0 \tag{D.15}$$

We further notice that in our model NhaB can work as an efflux or influx pump for C^+ conditionally on the chemiosmotic state that is maintained:

$$\text{NhaB influx pump} \Leftrightarrow 2 \cdot \Delta G_{\mathrm{H}^+} \leq \Delta G_{\mathrm{C}^+} < \frac{3}{2} \cdot \Delta G_{\mathrm{H}^+} \tag{D.16}$$

$$\text{NhaB efflux pump} \Leftrightarrow \frac{3}{2} \cdot \Delta G_{\mathrm{H}^+} < \Delta G_{\mathrm{C}^+} \leq 0 \tag{D.17}$$

The denomination *"influx"* or *"efflux"* pumps thus do not in general hold but are rather conditional on the chemiosmotic state.

Proof The proof is similar to the previous one. In words, we are proving that electrochemical potentials not fulfilling Eq. (D.15) will result in strictly positive or negative $\frac{d[\mathrm{C}]_i}{dt}$, therefore forbidding the system to be in steady-state. The mathematical derivation then is as follows. We rewrite the steady-state condition for small cations Eq. (D.4):

$$\frac{d[\mathrm{C}]_i}{dt} = 0 = j_{\mathrm{C}^+} + \underbrace{\sigma_{\mathrm{C}^+,\mathrm{NhaB}}}_{-2} \cdot j_{\mathrm{NhaB}} + \underbrace{\sigma_{\mathrm{C}^+,\mathrm{NhaA}}}_{-1} \cdot j_{\mathrm{NhaA}} \tag{D.18}$$

We seek to study steady-state behaviours, therefore from Eq.(D.4) it forbids:

$$\frac{d[\mathrm{C}^+]_i}{dt} > 0 \Leftarrow \begin{cases} & j_{\mathrm{C}^+} > 0 \\ \sigma_{\mathrm{C}^+,\mathrm{NhaB}} \cdot j_{\mathrm{NhaB}} > 0 \Leftrightarrow & j_{\mathrm{NhaB}} < 0 \\ \sigma_{\mathrm{C}^+,\mathrm{NhaA}} \cdot j_{\mathrm{NhaA}} > 0 \Leftrightarrow & j_{\mathrm{NhaA}} < 0 \end{cases} \tag{D.19}$$

$$\frac{d[\mathrm{C}^+]_i}{dt} < 0 \Leftarrow \begin{cases} & j_{\mathrm{C}^+} < 0 \\ \sigma_{\mathrm{C}^+,\mathrm{NhaB}} \cdot j_{\mathrm{NhaB}} < 0 \Leftrightarrow & j_{\mathrm{NhaB}} > 0 \\ \sigma_{\mathrm{C}^+,\mathrm{NhaA}} \cdot j_{\mathrm{NhaA}} < 0 \Leftrightarrow & j_{\mathrm{NhaA}} > 0 \end{cases} \tag{D.20}$$

Which is equivalent by Eq. (C.35), substituting by definitions of reactions' Gibbs free energy table 2 to:

$$\frac{d[\mathrm{C}^+]_i}{dt} > 0 \Leftarrow \begin{cases} \Delta G_{\mathrm{C}^+} & < 0 \\ \Delta G_{\mathrm{C}^+} & < \frac{3}{2} \cdot \Delta G_{\mathrm{H}^+} \\ \Delta G_{\mathrm{C}^+} & < 2 \cdot \Delta G_{\mathrm{H}^+} \end{cases} \tag{D.21}$$

$$\frac{d[\mathrm{C}^+]_i}{dt} < 0 \Leftarrow \begin{cases} \Delta G_{\mathrm{C}^+} & > 0 \\ \Delta G_{\mathrm{C}^+} & > \frac{3}{2} \cdot \Delta G_{\mathrm{H}^+} \\ \Delta G_{\mathrm{C}^+} & > 2 \cdot \Delta G_{\mathrm{H}^+} \end{cases} \tag{D.22}$$

We assume that $\Delta G_{\mathrm{H}^+} \leq 0$ (which we will show later), thus $\Delta G_{\mathrm{C}^+} > 0$ necessarily implies we are in the forbidden regime (D.21). In addition, since $\Delta G_{\mathrm{H}^+} \leq 0$, to prevent the second forbidden regime (D.22) entails $\Delta G_{\mathrm{C}^+} > 2 \cdot \Delta G_{\mathrm{H}^+}$. From those two inequalities we obtain the thermodynamically viable range of ΔG_{C^+} at steady state inequality (D.15).

We can furthermore distinguish two regimes compatible with the steady-state condition for C^+:

1. Indeed, both NhaB and NhaA working as efflux pump for C^+ is equivalent to $\{\Delta G_{\mathrm{NhaA}} < 0, \Delta G_{\mathrm{NhaB}} < 0\}$ which substituting by Gibbs free energy definition table 2 is equivalent to inequality (D.17).

2. In the other viable regime, NhaA still works as an efflux pump for C^+ whereas NhaB works as an influx pump. This is equivalent to $\{\Delta G_{\mathrm{NhaA}} <$

$0, \Delta G_{\text{NhaB}} > 0\}$. Substituting by the definitions of reactions' Gibbs free energies table 2 is equivalent to inequality (D.16).

Boundaries on $\Delta G_{\mathbf{H}^+}$

Result We show that: *(i)* at steady state, *(*ii) given reactions in table 2, *(iii)* spontaneously occurring NADH reduction and ATP hydrolysis: $\Delta G_{\text{NADH}} < 0$, $\Delta G_{\text{ATP}} < 0$, then PMF must be in the interval:

$$\min\left(\frac{1}{10}\cdot\Delta G_{\text{NADH}}, \frac{1}{3.3}\cdot\Delta G_{\text{ATP}}\right) \leq \Delta G_{\text{H}^+} \leq 0 \tag{D.23}$$

where $\min(a, b)$ is a function that returns a if $a < b$ and b if $b < a$.

We further show that in order for energy transduction to occur, *i.e.* the process of converting the free energy under NADH form to ATP *via* F1F$_o$ requires:

$$\frac{1}{10} \leq \Delta G_{\text{H}^+} \leq \Delta G_{\text{H}^+} \leq \frac{1}{3.3}\cdot\Delta G_{\text{ATP}} \tag{D.24}$$

Setting $\Delta G_{\text{NADH}} = -2290$ mV, $\Delta G_{\text{ATP}} = -560$ mV as in table 3, Eqs. (D.23) and (D.24) becomes:

$$\text{if Energy Transduction:} \quad -238\text{mV} \leq \Delta G_{\text{H}^+} < -170 \text{ mV} \tag{D.25}$$

$$\text{No Energy Transduction:} \quad -170\text{mV} \leq \Delta G_{\text{H}^+} \leq 0 \tag{D.26}$$

When the respiratory chain does not work, *e.g.* in anaerobic conditions, then the PMF must be in regime defined by (D.26) and ATP is hydrolyzed to maintain the PMF.

Proof The reasoning is similar to the previous proof and seek to identify the values of ΔG_{H^+} that forbids the system to be in steady-state, *i.e.* that result in strictly positive or negative $\frac{d[\text{H}^+]_i}{dt}$. The mathematical derivation is then as follows. We rewrite the steady state condition for protons Eq. (D.2) substituting

j_{H_2O} using Eq. (D.3):

$$\begin{aligned}\frac{d[\mathrm{H}^+]_i}{dt} = 0 = & j_{\mathrm{H}^+} - j_{\mathrm{OH}^-} \\ & + \underbrace{\sigma_{\mathrm{H}^+,\mathrm{R}} \cdot j_{\mathrm{R}}}_{-10} + \underbrace{\sigma_{\mathrm{H}^+,\mathrm{F1F}_o} \cdot j_{\mathrm{F1F}_o}}_{-3.3} \\ & + \underbrace{\sigma_{\mathrm{H}^+,\mathrm{ClcA}}}_{1} \cdot j_{\mathrm{ClcA}} + \underbrace{\sigma_{\mathrm{H}^+,\mathrm{NhaB}}}_{3} \cdot j_{\mathrm{NhaB}} + \underbrace{\sigma_{\mathrm{H}^+,\mathrm{NhaA}}}_{2} \cdot j_{\mathrm{NhaA}}\end{aligned} \tag{D.27}$$

The steady-state condition forbids the following regimes (where we ignore j_{OH^-} since it is necessarily of opposite sign to j_{H^+}):

$$\frac{d[\mathrm{H}^+]_i}{dt} > 0 \Leftarrow \begin{cases} & j_{\mathrm{H}^+} > 0 \\ \sigma_{\mathrm{H}^+,\mathrm{R}} \cdot j_{\mathrm{R}} > 0 \Leftrightarrow & j_{\mathrm{R}} < 0 \\ \sigma_{\mathrm{H}^+,\mathrm{F1F}_o} \cdot j_{\mathrm{F1F}_o} > 0 \Leftrightarrow & j_{\mathrm{F1F}_o} < 0 \\ \sigma_{\mathrm{H}^+,\mathrm{ClcA}} \cdot j_{\mathrm{ClcA}} > 0 \Leftrightarrow & j_{\mathrm{ClcA}} > 0 \\ \sigma_{\mathrm{H}^+,\mathrm{NhaB}} \cdot j_{\mathrm{NhaB}} > 0 \Leftrightarrow & j_{\mathrm{NhaB}} > 0 \\ \sigma_{\mathrm{H}^+,\mathrm{NhaA}} \cdot j_{\mathrm{NhaA}} > 0 \Leftrightarrow & j_{\mathrm{NhaA}} > 0 \end{cases} \tag{D.28}$$

$$\frac{d[\mathrm{H}^+]_i}{dt} < 0 \Leftarrow \begin{cases} & j_{\mathrm{H}^+} < 0 \\ \sigma_{\mathrm{H}^+,\mathrm{R}} \cdot j_{\mathrm{R}} < 0 \Leftrightarrow & j_{\mathrm{R}} > 0 \\ \sigma_{\mathrm{H}^+,\mathrm{F1F}_o} \cdot j_{\mathrm{F1F}_o} < 0 \Leftrightarrow & j_{\mathrm{F1F}_o} > 0 \\ \sigma_{\mathrm{H}^+,\mathrm{ClcA}} \cdot j_{\mathrm{ClcA}} < 0 \Leftrightarrow & j_{\mathrm{ClcA}} < 0 \\ \sigma_{\mathrm{H}^+,\mathrm{NhaB}} \cdot j_{\mathrm{NhaB}} < 0 \Leftrightarrow & j_{\mathrm{NhaB}} < 0 \\ \sigma_{\mathrm{H}^+,\mathrm{NhaA}} \cdot j_{\mathrm{NhaA}} < 0 \Leftrightarrow & j_{\mathrm{NhaA}} < 0 \end{cases} \tag{D.29}$$

Which is equivalent by Eq. (C.35) and definitions of Gibbs free energies in table 2 to:

$$\frac{d[\mathrm{H}^+]_i}{dt} > 0 \Leftarrow \begin{cases} \Delta G_{\mathrm{H}^+} & < 0 \\ \Delta G_{\mathrm{H}^+} & < 1/10 \cdot \Delta G_{\mathrm{NADH}} \\ \Delta G_{\mathrm{H}^+} & < 1/3.3 \cdot \Delta G_{\mathrm{ATP}} \\ \Delta G_{\mathrm{H}^+} & < 2 \cdot \Delta G_{\mathrm{A}^-} \\ \Delta G_{\mathrm{H}^+} & < 2/3 \cdot \Delta G_{\mathrm{C}^+} \\ \Delta G_{\mathrm{H}^+} & < 1/2 \cdot \Delta G_{\mathrm{C}^+} \end{cases} \tag{D.30}$$

$$\frac{d[\mathrm{H}^+]_i}{dt} < 0 \Leftarrow \begin{cases} \Delta G_{\mathrm{H}^+} & > 0 \\ \Delta G_{\mathrm{H}^+} & > 1/10 \cdot \Delta G_{\mathrm{NADH}} \\ \Delta G_{\mathrm{H}^+} & > 1/3.3 \cdot \Delta G_{\mathrm{ATP}} \\ \Delta G_{\mathrm{H}^+} & > 2 \cdot \Delta G_{\mathrm{A}^-} \\ \Delta G_{\mathrm{H}^+} & > 2/3 \cdot \Delta G_{\mathrm{C}^+} \\ \Delta G_{\mathrm{H}^+} & > 1/2 \cdot \Delta G_{\mathrm{C}^+} \end{cases} \tag{D.31}$$

We first seek to show that $\Delta G_{\mathrm{H}^+} \leq 0$. To demonstrate it is equivalent to show that if that it is not the case ($\Delta G_{\mathrm{H}^+} > 0$) then all other inequalities characterizating the forbidden regime (D.31) hold. We first notice that we assumed $\Delta G_{\mathrm{NADH}} < 0$ and $\Delta G_{\mathrm{ATP}} < 0$ so the second and third inequality characterizing the forbidden regime (D.31) must hold if $\Delta G_{\mathrm{H}^+} > 0$. We then turn ourselves to the fourth inequality and distinguish two cases:

1. if $\Delta G_{\mathrm{A}^-} > 0$, then to prevent the forbidden regime for anions second inequality of regime (D.14) we must have that $2 \cdot \Delta G_{\mathrm{A}^-} \leq \Delta G_{\mathrm{H}^+}$. Consequently the fourth inequality in the forbidden regime (D.31) must hold.

2. If $\Delta G_{\mathrm{A}^-} < 0$, then the fourth inequality in regime (D.31) must hold since we assumed $\Delta G_{\mathrm{H}^+} > 0$.

The same reasoning applies for the fifth and sixth inequality. Indeed if ΔG_{C^+} then for the forbidden regime (D.22) on $\frac{d[\mathrm{C}^+]_i}{dt}$ to be avoided means that fifth and sixth inequality of forbidden regime (D.31) must hold. Thus whenever $\Delta G_{\mathrm{H}^+} > 0$ the model is the forbidden regime (D.31) and thus in order for the model to maintain

a thermodynamically viable steady-state requires the PMF to be negative:

$$\Delta G_{H^+} \leq 0 \tag{D.32}$$

We next turn ourselves to establishing the lower limit on the PMF. We first notice that fourth, fifth and sixth inequalities of the forbidden regime (D.30) must hold from the boundaries on ΔG_{A^-} (D.9) and ΔG_{C^+} (D.15) we established before. We also showed that $\Delta G_{H^+} < 0$ and assumed that $\Delta G_{NADH} < 0$, $\Delta G_{ATP} < 0$, consequently to avoid forbidden regime (D.30) is equivalent to:

$$\Delta G_{H^+} > \min\left(\frac{1}{10} \cdot \Delta G_{NADH}, \frac{1}{3.3} \cdot \Delta G_{ATP}\right) \tag{D.33}$$

Combining inequalities (D.32) and (D.33) we obtain the range of viable PMF (D.23).

Requiring the PMF to allow for ATP synthesis requires $j_{F1F_o} > 0 \Leftrightarrow \Delta G_{F1F_o} < 0$. Substituting ΔG_{F1F_o} by its definition in table 2 we obtain the upper limit as in inequality (D.24).

This concludes the enumeration of all viable IMFs our model can maintain, given by inequalities (D.9), (D.15) and (D.23). Note that the range of ΔG_{OH^-} is given by applying Eq. (C.9) for both extracellular and intracellular concentration.

D.4. Optimal Strategies for Chemiosmotic maintenance

We now seek to derive what is the optimal strategy of the cell in order to maintain a given electrophysiological steady-state (osmotic pressure, PMF, pH_i). The results below will allow us to determine unambiguously: *(i)* the IMFs that need to be maintained, *(ii)* the intracellular concentration and average valency of captive molecules as well as *(iii)* the forward activity of each proton:ion antiporter. We summarize here what follows, *i.e.* the three behaviors that characterize the optimal strategy:

1. When $\Delta G_{C^+} > 3/2 \cdot \Delta G_{H^+}$ then the entirety of cation pumping must be performed by *NhaB*, otherwise by *NhaA*.

2. When the membrane potential is negative, the cell must not pump at all small anions, when it is positive the cell must not pump at all cations.

3. The cell needs to make the average valency of captive molecules as negative/positive as possible when the membrane potential is negative/positive. Restricted to a value for maintained osmotic pressure, this entails minimization of the intracellular concentration of captive charges.

Cost of chemiosmotic maintenance We first remind the cost of electrophysiological maintenance within our model Eq. (D.34):

$$\text{Cost} = j_{\text{H}^+} - j_{\text{OH}^-} + \sigma_{\text{H}^+,\text{NhaB}} \cdot j_{\text{NhaB}} + \sigma_{\text{H}^+,\text{NhaA}} \cdot j_{\text{NhaA}} + \sigma_{\text{H}^+,\text{ClcA}} \cdot j_{\text{ClcA}} \quad \text{(D.34)}$$

that depends among other things, on the permeability of the membrane to the considered ions (protons, hydroxide ions, anions and cations).

Optimal Coordination of Cation Antiporters

Result We fix the – relative to the extracellular environment– electrophysiological state, characterized by $\{\Delta G_{\text{H}^+}, \Delta G_{\text{C}^+}, \Delta G_{\text{A}^-}, z_{\text{Y}}, [\text{Y}]_i\}$ and the extracellular composition, *i.e.* $\{\text{pH}_e, [\text{CA}]_0\} \to \{[\text{H}^+]_e, [\text{OH}^-]_e, [\text{C}^+]_e, [\text{A}^-]_e\}$ such that all state variables (concentrations, membrane potential, osmotic pressure, electrochemical potentials, Gibbs free energy of every reactions) are known. We also fix the membrane properties: $\{b, \mathbf{P}, S/V\}$ where $\mathbf{P}$ is the vector collecting the permeability of the membrane to all small ionic species.

We then rewrite the steady-state for C^+ (D.7) as:

$$\begin{aligned} 0 = &+ \frac{S}{V} \cdot P_{\text{C}^+} \cdot [\text{C}^+]_e \cdot f_b(+\Delta\psi) \cdot \left(1 - e^{\frac{F}{RT}\Delta G_{\text{C}^+}}\right) \\ &+ j^+_{\text{NhaB}} \cdot \left(1 - e^{\frac{F}{RT}\cdot\Delta G_{\text{NhaB}}}\right) + j^+_{\text{NhaA}} \cdot \left(1 - e^{\frac{F}{RT}\cdot\Delta G_{\text{NhaA}}}\right) \end{aligned} \quad \text{(D.35)}$$

and notice that the the activity of proton:cation antiporters is under-determined by the state, *i.e.* the defined overall state is achievable with many distinct pairs of $\{j^+_{\text{NhaB}}, j^+_{\text{NhaB}}\}$.

Note that such is not the case for the forward activity of the sole anion:antiporter ClcA which was given by Eq. (D.6). It is indeed uniquely defined by the state variables. The leakage fluxes j_{H^+}, j_{OH^-} are also uniquely defined by the state variables *via* Eq. (C.45), such that given an electrophysiological state in a given

environment, the only degree of freedom to modulate the cost of chemiosmotic maintenance is, within the scope of this model, to modulate the activity of proton:cation antiporters.

We now seek to define the optimal pair of $\{j^+_{\mathrm{NhaB}}, j^+_{\mathrm{NhaB}}\}$ to maintain state-variables, a.k.a. the coordination of antiporters that minimizes the cost (D.34). We find that it only depends on the regime for ΔG_{C^+} and that it must follow:

$$\text{if } \frac{3}{2}\cdot\Delta G_{\mathrm{H}^+} < \Delta G_{\mathrm{C}^+} \leq 0 : \begin{cases} j_{\mathrm{NhaB}^+} & = \frac{1}{2}\cdot\dfrac{j_{\mathrm{C}^+}}{1-e^{\frac{F}{RT}\cdot\Delta G_{\mathrm{NhaB}}}} \\ j_{\mathrm{NhaA}^+} & = 0 \\ \mathrm{Cost} & = j_{\mathrm{H}^+} - j_{\mathrm{OH}^-} + \frac{3}{2}\cdot j_{\mathrm{C}^+} + \frac{1}{2}\cdot j_{\mathrm{A}^-} \end{cases} \tag{D.36}$$

$$\text{if } 2\cdot\Delta G_{\mathrm{H}^+} \leq \Delta G_{\mathrm{C}^+} \leq \frac{3}{2}\cdot\Delta G_{\mathrm{H}^+} : \begin{cases} j_{\mathrm{NhaB}^+} & = 0 \\ j_{\mathrm{NhaA}^+} & = \dfrac{j_{\mathrm{C}^+}}{1-e^{\frac{F}{RT}\cdot\Delta G_{\mathrm{NhaA}}}} \\ \mathrm{Cost} & = j_{\mathrm{H}^+} - j_{\mathrm{OH}^-} + 2\cdot j_{\mathrm{C}^+} + \frac{1}{2}\cdot j_{\mathrm{A}^-} \end{cases} \tag{D.37}$$

Interestingly, although the cost of chemiosmotic maintenance does not generally depend solely on state variables, the optimal cost does. The latter actually holds for models with arbitrary number of ions and proton:ion exchangers (antiporters or/and symporters) as shown in subsection D.4.

Proof We demonstrate the result above in three steps:

1. Preliminary rewriting of the cost. Rearranging the definition of the cost using the steady-state for C^+ and A^- Eqs.(D.4), (D.5) is useful for the next

steps. It can be done in either ways:

$$\begin{aligned}\text{Cost} = &+ j_{H^+} - j_{OH^-} \\ &+ \sigma_{H^+,\text{NhaB}} \cdot \left[-\frac{1}{\sigma_{C^+,\text{NhaB}}} \cdot j_{C^+} + j_{\text{NhaA}} \cdot \frac{\sigma_{C^+,\text{NhaA}}}{\sigma_{C^+,\text{NhaB}}} \left(\frac{\sigma_{H^+,\text{NhaA}}}{\sigma_{C^+,\text{NhaA}}} \cdot \frac{\sigma_{C^+,\text{NhaB}}}{\sigma_{H^+,\text{NhaB}}} - 1 \right) \right] \\ &- \frac{\sigma_{H^+,\text{ClcA}}}{\sigma_{A^-,\text{ClcA}}} \cdot j_{A^-}\end{aligned} \tag{D.38}$$

$$\begin{aligned}\text{Cost} = &+ j_{H^+} - j_{OH^-} \\ &+ \sigma_{H^+,\text{NhaA}} \cdot \left[-\frac{1}{\sigma_{C^+,\text{NhaA}}} \cdot j_{C^+} + j_{\text{NhaB}} \cdot \frac{\sigma_{C^+,\text{NhaB}}}{\sigma_{C^+,\text{NhaA}}} \left(\frac{\sigma_{H^+,\text{NhaB}}}{\sigma_{C^+,\text{NhaB}}} \cdot \frac{\sigma_{C^+,\text{NhaA}}}{\sigma_{H^+,\text{NhaA}}} - 1 \right) \right] \\ &- \frac{\sigma_{H^+,\text{ClcA}}}{\sigma_{A^-,\text{ClcA}}} \cdot j_{A^-}\end{aligned} \tag{D.39}$$

Substituting the stoichiometries by their values defined in table 2 Eqs. (**??**), (D.35) the equations above:

$$\text{Cost} = +j_{H^+} - j_{OH^-} + 3 \cdot \left[\frac{1}{2} \cdot j_{C^+} + \frac{1}{6} \cdot j_{\text{NhaA}} \right] + \frac{1}{2} \cdot j_{A^-} \tag{D.40}$$

$$\text{Cost} = +j_{H^+} - j_{OH^-} + 2 \cdot \left[j_{C^+} - \frac{1}{2} \cdot j_{\text{NhaB}} \right] + \frac{1}{2} \cdot j_{A^-} \tag{D.41}$$

2. Regime where *NhaB* works as a cation efflux pump. We first place ourselves in the regime (D.17) for ΔG_{C^+}:

$$\frac{3}{2} \cdot \Delta G_{H^+} < \Delta G_{C^+} \leq 0 \tag{D.42}$$

In that regime we have from the definitions of Gibbs free energy for NhaB, NhaA table 2 the following directional regimes of NhaB, NhaA:

$$\Delta G_{\text{NhaB}} < 0 \Leftrightarrow j_{\text{NhaB}} > 0 \tag{D.43}$$

$$\Delta G_{\text{NhaA}} < 0 \Leftrightarrow j_{\text{NhaA}} > 0 \tag{D.44}$$

i.e. in that regime both NhaB and NhaA work as efflux pumps for C^+.

We then look at the cost Eq. (D.40) and notice that in the range of cationic motive force (D.42) $j_{\text{NhaA}} > 0$ by Eq. (C.35), thus the cost is monotonically decreasing with j^+_{NhaA}. Its minimum is thus attained when $j^+_{\text{NhaA}} = 0 \Rightarrow$

$j_{\mathrm{NhaA}} = 0$ and follows:

$$\mathrm{Cost} = j_{\mathrm{H^+}} - j_{\mathrm{OH^-}} + \frac{3}{2} \cdot j_{\mathrm{C^+}} + \frac{1}{2} \cdot j_{\mathrm{A^-}} \tag{D.45}$$

Since $j_{\mathrm{NhaA}} = 0$, from the steady-state condition for $\mathrm{C^+}$, Eq. (D.4), and the relation between net and forward flux Eq. (C.35) we obtain the forward flux for NhaB required to maintain a given $\Delta G_{\mathrm{C^+}}$:

$$j^+_{\mathrm{NhaB}} = \frac{1}{2} \cdot \frac{j_{\mathrm{C^+}}}{1 - e^{\frac{F}{RT} \cdot (3 \cdot \Delta G_{\mathrm{H^+}} - 2 \cdot \Delta G_{\mathrm{C^+}})}} \tag{D.46}$$

where we substituted ΔG_{NhaB} by its definition in table 2 in the exponential term. Note that if $\Delta G_{\mathrm{C^+}} < 0$, the leakage flux is positive $j_{\mathrm{C^+}} > 0$. Also $j^+_{\mathrm{NhaB}} \geq 0$.

We further distinguish the particular case (which we will make use of later):

$$\text{if } \Delta G_{\mathrm{C^+}} = 0 : \begin{cases} j^+_{\mathrm{NhaB}} & = 0 \\ j^+_{\mathrm{NhaA}} & = 0 \\ \mathrm{Cost} & = j_{\mathrm{H^+}} - j_{\mathrm{OH^-}} + \frac{1}{2} \cdot j_{\mathrm{A^-}} \end{cases} \tag{D.47}$$

That is the optimal cost when $\Delta G_{\mathrm{C^+}} = 0$.

3. Regime *NhaB* works as a cation influx pump. We place ourselves in the regime (D.16) for $\Delta G_{\mathrm{C^+}}$:

$$2 \cdot \Delta G_{\mathrm{H^+}} \leq \Delta G_{\mathrm{C^+}} < \frac{3}{2} \cdot \Delta G_{\mathrm{H^+}} \tag{D.48}$$

In that regime, from the definition of the reactions' Gibbs free energies in table 2 we have:

$$\Delta G_{\mathrm{NhaB}} > 0 \Leftrightarrow j_{\mathrm{NhaB}} < 0 \tag{D.49}$$

$$\Delta G_{\mathrm{NhaA}} < 0 \Leftrightarrow j_{\mathrm{NhaA}} > 0 \tag{D.50}$$

i.e. in that regime NhaB/NhaA work respectively as an influx/efflux pump for $\mathrm{C^+}$.

We then look at the cost Eq. (D.41) and notice that since $j_{\mathrm{NhaB}} < 0$ it is monotonically decreasing with $j^+_{\mathrm{NhaB}} \geq 0$. Its minimum is thus attained

when $j_{\mathrm{NhaB}^+} = 0 \Rightarrow j_{\mathrm{NhaB}} = 0$ and is:

$$\mathrm{Cost} = j_{\mathrm{H}^+} - j_{\mathrm{OH}^-} + 2 \cdot j_{\mathrm{C}^+} + \frac{1}{2} \cdot j_{\mathrm{A}^-} \tag{D.51}$$

Since $j_{\mathrm{NhaB}} = 0$, from steady-state condition for C^+ Eq. (D.4) and the relation between forward and net flux Eq. (C.35) we get:

$$j^+_{\mathrm{NhaA}} = \frac{j_{\mathrm{C}^+}}{1 - e^{\frac{F}{RT} \cdot \Delta G_{\mathrm{NhaA}}}} \tag{D.52}$$

Optimal electrochemical potentials for chemiosmotic maintenance We now know by the previous paragraph how to set the activities of the various antiporters so that the electrophysiological maintenance cost is minimized, that is given a pair of $\{\Delta G_{\mathrm{A}^-}, \Delta G_{\mathrm{C}^-}\}$ that is sought to be maintain. We now derive the value such pair must take in order to minimize the cost of maintaining a given membrane potential.

Result We fix the extracellular composition:
$\{\mathrm{pH}_e, [\mathrm{CA}]_0\} \rightarrow \{[\mathrm{H}^+]_e, [\mathrm{OH}^-]_e, [\mathrm{C}^+]_e, [\mathrm{A}^-]_e, \}$ and values for electrophysiological homeostases sought to be maintained $\{\Delta G_{\mathrm{H}^+}, \mathrm{pH}_i, \Delta\Pi\}$ given a content in intracellular captive molecules $[\mathrm{Y}]_i$ such that the voltage is uniquely defined by rearranging the definition of the PMF

$$\Delta\psi = \Delta G_{\mathrm{H}^+} - \frac{RT}{F} \cdot \ln(10) \cdot (\mathrm{pH}_e - \mathrm{pH}_i) \tag{D.53}$$

The overall state is however under-determined as many distinct pairs $\{\Delta G_{\mathrm{C}^+}, \Delta G_{\mathrm{A}^-}\}$ of the electrochemical potential are compatible with maintenance of the membrane voltage, as is visible by Eq. (C.23).

We show here that in order to minimize the cost:

$$\text{if } \Delta\psi = 0 : \begin{cases} \Delta G_{\mathrm{C}^+} = \Delta G_{\mathrm{A}^-} & = 0 \\ \min(\text{Cost}) & = j_{\mathrm{H}^+} - j_{\mathrm{OH}^-} \end{cases} \tag{D.54}$$

$$\text{if } \Delta\psi < 0 : \begin{cases} \Delta G_{\mathrm{A}^-} & = 0 \\ \min(\text{Cost}) & = j_{\mathrm{H}^+} - j_{\mathrm{OH}^-} + \nu \cdot j_{\mathrm{C}^+} \end{cases} \tag{D.55}$$

$$\text{if } \Delta\psi > 0 : \begin{cases} \Delta G_{\mathrm{C}^+} & = 0 \\ \min(\text{Cost}) & = j_{\mathrm{H}^+} - j_{\mathrm{OH}^-} + \frac{1}{2} \cdot j_{\mathrm{A}^-} \end{cases} \tag{D.56}$$

Where $\nu \in \{2, 3/2\}$ in Eq. (D.55) depends on the ΔG_{C^+} regime as shown by Eqs. (D.36) and (D.37).

Proof We now show that if $\{\Delta G_{\mathrm{C}^+}, \Delta G_{\mathrm{A}^-}\}$ are not as indicated in Eqs. (D.54), (D.55), (D.56), then the cost of chemiosmotic maintenance must increase. We first notice that the cost is always monotonically increasing with either ΔG_{C^+} or ΔG_{A^-} becoming more negative and that they are both less or equal to 0 by inequalities (D.9) and (D.15), therefore:

1. if $\Delta\psi = 0$: Trivially any other pair $\{\Delta G_{\mathrm{C}^+} = 0, \Delta G_{\mathrm{A}^-} = 0\}$ will come at a higher maintenance cost.

2. if $\Delta\psi < 0$: By Eq. (C.23), the membrane potential is monotonically decreasing as ΔG_{C^+} becomes more negative and monotonically increasing as ΔG_{A^-} becomes more negative. Consequently, fixing the other degrees of freedom in the membrane potential: $\{z_{\mathrm{Y}}, [\mathrm{Y}]_i, \mathrm{pH}_i\}$ to maintain identical $\Delta\psi < 0$ as ΔG_{A^-} deviates from 0 (becomes more negative) means making ΔG_{C^+} more negative as well. Since the only solution when deviating from $\Delta G_{\mathrm{A}^-} = 0$ is to make ΔG_{C^+} more negative, since the cost is monotonically increasing with both ΔG_{C^+}, ΔG_{A^-} becoming more negative the minimal cost given $\{z_{\mathrm{Y}}, [\mathrm{Y}]_i, \mathrm{pH}_i\}$ is indeed for $\Delta G_{\mathrm{A}^-} = 0$.

3. if $\Delta\psi > 0$: the reasoning is identical as above but this time we have to notice that given $\{z_{\mathrm{Y}}, [\mathrm{Y}]_i, \mathrm{pH}_i\}$, ΔG_{C^+} deviating from 0 means that ΔG_{A^-} must become more negative in order to maintain a positive membrane potential invariant by the said variation in ΔG_{C^+}.

Optimal composition in captive molecules We look as before at three regimes for $\Delta\psi$:

1. if $\Delta\psi = 0$: We saw in the last paragraph that the optimal strategy imposes $\Delta G_{\mathrm{C}^+} = \Delta G_{\mathrm{A}^-} = 0$ and thus $[\mathrm{C}^+]_e = [\mathrm{C}^+]_i$, $[\mathrm{A}^-]_e = [\mathrm{A}^-]_i$. Rearranging the definition of osmotic pressure we therefore obtain the total intracellular concentration of captive molecules required to maintain the osmotic pressure:

$$[\mathrm{Y}]_i = \frac{\Delta\Pi}{RT} + [\mathrm{H}^+]_e + [\mathrm{OH}^-]_e - [\mathrm{H}^+]_i - [\mathrm{OH}^-]_i \tag{D.57}$$

Note that since $[\mathrm{Y}]_i$ is a concentration it must be greater than 0; consequently for equation above to hold for any intra/extracellular pH $\in [2, 12]$ requires $\frac{\Delta\Pi}{RT} > -\min\left([\mathrm{H}^+]_e + [\mathrm{OH}^-]_e - [\mathrm{H}^+]_i - [\mathrm{OH}^-]_i\right)$ which is given by:

$$\begin{aligned} &-\min\left([\mathrm{H}^+]_e + [\mathrm{OH}^-]_e - [\mathrm{H}^+]_i - [\mathrm{OH}^-]_i\right) \\ &= -10^3 \cdot \left(2 \cdot 10^{-7} - 10^{-2} - 10^{-12}\right) \approx 10\mathrm{mM} \end{aligned} \tag{D.58}$$

which corresponds to $10 \times R \times T / 10^5 \approx 0.25$ atmospheres. Further rearranging the membrane potential Eq. (C.19) we obtain the average valency of captive molecules required to maintain $\Delta\psi = \Delta G_{\mathrm{C}^+} = \Delta G_{\mathrm{A}^-} = 0$:

$$z_{\mathrm{Y}} = \frac{1}{[\mathrm{Y}]_i}([\mathrm{OH}^+]_i - [\mathrm{H}^+]_i) \tag{D.59}$$

Substituting $[\mathrm{Y}]_i$ above from Eq. (D.57) we obtain:

$$z_{\mathrm{Y}} = \frac{[\mathrm{OH}^+]_i - [\mathrm{H}^+]_i}{\frac{\Delta\Pi}{RT} + [\mathrm{H}^+]_e + [\mathrm{OH}^-]_e - [\mathrm{H}^+]_i - [\mathrm{OH}^-]_i} \tag{D.60}$$

We find computationally (not shown) that in order for $2 \leq z_{\mathrm{Y}} \leq +2$ to hold for all intra/extracellular pH $\in [2, 12]$ then the osmotic pressure needs to be $\Delta\Pi > 0.4$ atmospheres. We later set the desired osmotic pressure to 1 atmosphere, such that there is always a viable state given $\Delta\psi = 0$.

2. If $\Delta\psi < 0$: We set $\Delta G_{\mathrm{A}^-} = 0$ (see last paragraph) such that we see from the membrane potential Eq. (C.19) that to minimize the cost (*i.e.* getting ΔG_{C^+} closer to 0) while maintaining identical membrane potential one needs to make the contribution of captive molecules to membrane potential $z_{\mathrm{Y}} \cdot [\mathrm{Y}]_i$

Name	Symbol	Units	Range
Valency of x	z_x	Charge/Particle	Input ± 1
Extracellular pH	pH_e	Dimensionless	Input $\in [2, 12]$
Salinity	$[\mathrm{CA}]_0$	$\mathrm{M/m^3}$	Input $\in [1, 1000]$
Osmotic Pressure	$\Delta\Pi$	atmosphere	Input $= 1$
Intracellular pH	pH_i	Dimensionless	Input $\in [2, 12]$
Electrochemical Potential of x	ΔG_x	Volts	Output $\in [\min(\Delta G_x), \max(\Delta G_x)]$
PMF	ΔG_{H^+}	Volts	Input $\in [\min(\Delta G_{\mathrm{H}^+}), \max(\Delta G_{\mathrm{H}^+})]$
Intracellular concentration of x	$[x]_i$	$\mathrm{M/m^3}$	Output
Intracelular Captive Molecules Y	$[\mathrm{Y}]_i$	$\mathrm{M/m^3}$	Output
Average Valency of Y Molecules	z_{Y}	Average Charge/Particle	Output $\in [-2, +2]$
Optimal Forward Activity of antiporter r	j_r^+	reactions/cell/hour	Output $\in \mathbb{R}^+$
Minimal Cost	Cost	Protons/cell/hour	Output $\in \mathbb{R}^+$

TABLE 4: The variables we sample across in our computational experiments, as well as the ranges we sample across and whether the variable is an input or output of the model.

as negative as possible. Rearranging the osmotic pressure we can write the value of $[\mathrm{Y}]_i$ required to maintain osmotic pressure as:

$$[\mathrm{Y}]_i = \frac{\Delta\Pi}{RT} + [\mathrm{H}^+]_e + [\mathrm{OH}^-]_e - [\mathrm{H}^+]_i - [\mathrm{OH}^-]_i + [\mathrm{C}]_e \cdot \left(1 - e^{\frac{F}{RT}\cdot(\Delta G_{\mathrm{C}^+} - \Delta\psi)}\right) \tag{D.61}$$

Such that as we make the cost of maintaining the membrane potential smaller (ΔG_{C^+} closer to 0, $z_{\mathrm{Y}} \cdot [\mathrm{Y}]_i$ more negative), $[\mathrm{Y}]_i$ decreases by Eq. (D.61) and since we need to make at the same time make $z_{\mathrm{Y}} \cdot [\mathrm{Y}]_i$ more negative this implies minimizing z_{Y} (making it more negative).

3. If $\Delta\psi > 0$: the reasoning is identical as above but this time to make the cost of maintaining the membrane potential smaller means getting ΔG_{A^-} closer to 0, $[\mathrm{Y}]_i$ smaller and z_{Y} more positive.

D.5. Solving Model of *E.coli*'s Electrophysiology

We first summarize in table 4 the ranges of input we solve the model for.

We now devise the steps we follow to solve the model analytically:

1. For each extracellular pH and salinity we compute the full extracellular composition:

$$\{\mathrm{pH}_e, [\mathrm{CA}]_0\} \to \{[\mathrm{H}^+]_e, [\mathrm{OH}^-]_e, [\mathrm{C}^+]_e, [\mathrm{A}^-]_e, \}$$

2. For each PMF value we wish to maintain we obtain the allowed IMFs:

$$\{\sigma, \Delta G_{\mathrm{H^+}}\} \rightarrow \{\min(\Delta G_{\mathrm{C^+}}), \max(\Delta G_{\mathrm{C^+}}), \min(\Delta G_{\mathrm{A^-}}), \max(\Delta G_{\mathrm{A^-}})\}$$

3. For each intracellular pH and PMF we wish to maintain we compute the required membrane potential:

$$\{\mathrm{pH}_e, \mathrm{pH}_i, \Delta G_{\mathrm{H^+}}\} \rightarrow \Delta\psi$$

4. Using the values from Step 1 to 3 we compute the full intracellular composition: Given pH_i we obtain proton and hydroxide ion concentrations

$$\mathrm{pH}_i \rightarrow \{[\mathrm{H^+}]_i, [\mathrm{OH^-}]_i\}$$

To compute $[\mathrm{C^+}]_i, [\mathrm{A^-}]_i$ and $z_{\mathrm{Y}}, [\mathrm{Y}]_i$ we distinguish three scenarios based on the value of $\Delta\psi$:

(a) $\underline{\Delta\psi = 0}$ In this scenario we do not need to sample for $[\mathrm{Y}]_i$ and can directly obtain the value of which minimizes the cost while maintaining the chemiosmotic homeostases to the desired values. By Eqs. (D.54) setting $\Delta G_{\mathrm{C^+}} = \Delta G_{\mathrm{A^-}} = 0$ is the optimal solution when $\Delta\psi = 0$. Such that the the intracellular composition in $[\mathrm{C^+}]_i$, $[\mathrm{A^-}]_i$ is simply given as:

$$[\mathrm{C^+}]_i = [\mathrm{C^+}]_e \tag{D.62}$$
$$[\mathrm{A^-}]_i = [\mathrm{A^-}]_e \tag{D.63}$$

We then use Eq. (D.57) to obtain $[\mathrm{Y}]_i$ and Eq. (D.60) to obtain z_{Y}. Note that as explained before, this strategy for solving the model only holds for $\Delta\Pi > 0.4$ atmospheres.

(b) $\underline{\Delta\psi \neq 0}$:

i. $\underline{\text{if } \Delta\psi < 0}$: We know that minimizing the cost involves setting $\Delta G_{\mathrm{A^-}} = 0$. Accordingly we first compute $[\mathrm{A^-}]_i$ from Nernst equation:

$$[\mathrm{A^-}]_i = [\mathrm{A^-}]_e \cdot e^{\frac{F}{RT}\cdot\Delta\psi} \tag{D.64}$$

We then rearrange the osmotic pressure to get the intracellular concentration of C^+ required to maintain $\Delta\Pi$ given *(i)* $[A^-]_i$ (given by the membrane potential and $[A^-]_e$) and *(ii)* the total concentration of captive molecules $[Y]_i$):

$$[C^+]_i = \sum_x [x]_e + \frac{\Delta\Pi}{RT} - [H^+]_i - [OH^-]_i - [A^-]_i - [Y]_i \quad \text{(D.65)}$$

At this stage, we know from Eq. (D.61) that the optimal strategy is to minimize $[Y]_i$ and make z_Y as negative as possible. However $[Y]_i$ and z_Y cannot take any value and are bounded by lower and upper limits (arbitrarily set for z_Y, deriving from the boundaries on electrochemical potential and/or z_Y for $[Y]_i$ as we shall see just now).

Indeed, from inequality (D.15): $\Delta G_{C^+} \geq 2{\cdot}\Delta G_{H^+}$, thus rearranging the definition of ΔG_{C^+} we obtain a lower limit on $[C^+]_i$:

$$[C^+]_i \geq [C^+]_e \cdot e^{\frac{F}{RT}\cdot(2\cdot\Delta G_{H^+} - \Delta\psi)} \quad \text{(D.66)}$$

Substituting $[C^+]_i$ using Eq. (D.65) above thus gives a upper limit on the total concentration of captive molecules:

$$[Y]_i \leq \sum_x [x]_e + \frac{\Delta\Pi}{RT} - [H^+]_i - [OH^-]_i - [A^-]_i - [C^+]_e \cdot e^{\frac{F}{RT}\cdot(2\cdot\Delta G_{H^+} - \Delta\psi)} \quad \text{(D.67)}$$

Similarly, we know from inequality (D.15) that $\Delta G_{C^+} \leq 0$ which turns into an lower limit for $[Y]_i$:

$$[Y]_i \geq \underbrace{\sum_x [x]_e + \frac{\Delta\Pi}{RT} - [H^+]_i - [OH^-]_i - [A^-]_i - [C^+]_e \cdot e^{-\frac{F}{RT}\cdot\Delta\psi}}_{\min^{(1)}([Y]_i)} \quad \text{(D.68)}$$

which we label $\min^{(1)}([Y]_i)$ since we will see in couple of equations later that there are two concurrent lower limits.

We next rearrange the definition of the membrane potential Eq. (C.19) to express the average valency of captive molecules as a function

of intracellular concentrations and membrane potential:

$$z_{\mathrm{Y}} = \frac{1}{[\mathrm{Y}]_i} \cdot \left(\frac{S}{V} \cdot \frac{C_m}{F} \cdot \Delta\psi - [\mathrm{H}^+]_i + [\mathrm{OH}^-]_i - [\mathrm{C}^+]_i + [\mathrm{A}^-]_i \right) \tag{D.69}$$

and substitute $[\mathrm{C}^+]_i$ in the equation above by its expression given in Eq. (D.65) to obtain:

$$z_{\mathrm{Y}} = \frac{1}{[\mathrm{Y}]_i} \cdot \left(\frac{S}{V} \cdot \frac{C_m}{F} \cdot \Delta\psi - \frac{\Delta\Pi}{RT} + 2 \cdot [\mathrm{OH}^-]_i + 2 \cdot [\mathrm{A}^-]_i - \sum_x [x]_e \right) + 1 \tag{D.70}$$

The average valency of captive molecules z_{Y} has an lower limit $\min(z_{\mathrm{Y}})$ (here assumed to be -2), and consequently we may therefrom obtain an lower limit on $[\mathrm{Y}]_i$ from Eq. (D.69):

$$[\mathrm{Y}]_i \geq \underbrace{-\frac{1}{1 - \min(z_{\mathrm{Y}})} \cdot \left(\frac{S}{V} \cdot \frac{C_m}{F} \cdot \Delta\psi - \frac{\Delta\Pi}{RT} + 2 \cdot [\mathrm{OH}^-]_i + 2 \cdot [\mathrm{A}^-]_i - \sum_x [x]_e \right)}_{\min^{(2)}([\mathrm{Y}]_i)} \tag{D.71}$$

We also have a upper limit for the average valency of captive molecules $z_{\mathrm{Y}} \leq \max(z_{\mathrm{Y}})$ which is equivalent by Eq. (D.70) to:

$$[\mathrm{Y}]_i \geq \frac{1}{\max(z_{\mathrm{Y}}) - 1} \left(\frac{S}{V} \cdot \frac{C_m}{F} \cdot \Delta\psi - \frac{\Delta\Pi}{RT} + 2 \cdot [\mathrm{OH}^-]_i + 2 \cdot [\mathrm{A}^-]_i - \sum_x [x]_e \right) \tag{D.72}$$

We find computationally that when $\Delta\psi < 0$ the lower limit given by inequality (D.71) is always upper than that in the inequality above (D.72), such that we have no use of the latter.
Finally the lower limit on $[\mathrm{Y}]_i$ is given by selecting one of the two concurrent lower limits, respectively Eqs. (D.68) and (D.71), that is maximal:

$$[\mathrm{Y}]_i \geq \underbrace{\max \left[\min^{(1)}([\mathrm{Y}]_i), \min^{(2)}([\mathrm{Y}]_i) \right]}_{\min([\mathrm{Y}]_i)} \tag{D.73}$$

Finally, we know from Eq. (D.61) that the minimal cost is achieved by minimizing $[\mathrm{Y}]_i$. To solve for the optimal intracellular state, we thus *(i)* equate $[\mathrm{Y}]_i$ to its minimal value given in the right-hand side of inequality (D.73), *(ii)* compute $[\mathrm{C}^+]_i$ from Eq. (D.65) and *(iii)*

compute the average valency of captive charges with Eq. (D.70). If no viable value of $[\mathrm{Y}]_i$ exists, *i.e.* if $\min([\mathrm{Y}]_i) > \max([\mathrm{Y}]_i)$ (the lower limit is greater than the upper limit), then the current state is not achievable by our model of *E. coli*. Indeed it means that the current state will either have ΔG_{C^+} or z_{Y} out of its viable interval.

ii. if $\Delta\psi > 0$: We assume $\Delta G_{\mathrm{C}^+} = 0$. Accordingly we compute $[\mathrm{C}^+]_i$ from Nernst equation:

$$[\mathrm{C}^+]_i = [\mathrm{C}^+]_e \cdot e^{-\frac{F}{RT}\cdot\Delta\psi} \tag{D.74}$$

We then rearrange the osmotic pressure Eq. (**??**) to get the intracellular concentration of A^- required to maintain $\Delta\psi$ given *(i)* $[\mathrm{C}^+]_i$ (given by the membrane potential and $[\mathrm{C}^+]_e$) and *(ii)* the total concentration of captive molecules $[\mathrm{Y}]_i$:

$$[\mathrm{A}^-]_i = \sum_x [x]_e + \frac{\Delta\Pi}{RT} - [\mathrm{H}^+]_i - [\mathrm{OH}^-]_i - [\mathrm{C}^+]_i - [\mathrm{Y}]_i \tag{D.75}$$

We then proceed similarly as before and obtain the boundaries on $[\mathrm{Y}]_i$:

$$[\mathrm{Y}]_i \leq \underbrace{\sum_x [x]_e + \frac{\Delta\Pi}{RT} - [\mathrm{H}^+]_i - [\mathrm{OH}^-]_i - [\mathrm{C}^+]_i - [\mathrm{A}^+]_e \cdot e^{\frac{F}{RT}\cdot(1/2\cdot\Delta G_{\mathrm{H}^+} + \Delta\psi)}}_{\max([\mathrm{Y}]_i)} \tag{D.76}$$

$$[\mathrm{Y}]_i \geq \underbrace{\sum_x [x]_e + \frac{\Delta\Pi}{RT} - [\mathrm{H}^+]_i - [\mathrm{OH}^-]_i - [\mathrm{C}^+]_i - [\mathrm{A}^-]_e \cdot e^{+\frac{F}{RT}\cdot\Delta\psi}}_{\min^{(1)}([\mathrm{Y}]_i)} \tag{D.77}$$

$$[\mathrm{Y}]_i \geq \underbrace{\frac{1}{1+\max(z_\mathrm{Y})} \cdot \left(\frac{S}{V} \cdot \frac{C_m}{F} \cdot \Delta\psi + \frac{\Delta\Pi}{RT} - 2\cdot[\mathrm{H}^+]_i - 2\cdot[\mathrm{C}^+]_i + \sum_x [x]_e \right)}_{\min^{(2)}([\mathrm{Y}]_i)} \tag{D.78}$$

$$[\mathrm{Y}]_i \geq \underbrace{-\frac{1}{\min(z_\mathrm{Y})-1} \cdot \left(\frac{S}{V} \cdot \frac{C_m}{F} \cdot \Delta\psi + \frac{\Delta\Pi}{RT} - 2\cdot[\mathrm{H}^+]_i - 2\cdot[\mathrm{C}^+]_i + \sum_x [x]_e \right)}_{\min^{(3)}([\mathrm{Y}]_i)} \tag{D.79}$$

Similarly as before we find computationally that the lower limit given by inequality (D.79) is always greater than that given by inequality (D.78) when $\Delta\psi > 0$ such that we can forget about the lower limit $\min^{(3)}([\mathrm{Y}]_i)$. We then *(i)* equate $[\mathrm{Y}]_i$ to its maximal value as indicated in inequality (D.73), *(ii)* Compute $[\mathrm{A}^-]_i$ from Eq. (D.75) and *(iii)* the average valency of captive molecules with Eq. (D.70).

5. We now check whether all solutions obtained in the previous steps are indeed within the required boundaries, *i.e.* the intervals for state-variables $\{z_\mathrm{Y}, \Delta G_{\mathrm{C}^+}, \Delta G_{\mathrm{A}^-}\}$:

$$-2 \leq z_\mathrm{Y} \leq +2 \tag{D.80}$$

$$2\cdot\Delta G_{\mathrm{H}^+} \leq \Delta G_{\mathrm{C}^+} \leq 0 \tag{D.81}$$

$$\frac{1}{2}\cdot\Delta G_{\mathrm{H}^+} \leq \Delta G_{\mathrm{A}^-} \leq 0 \tag{D.82}$$

And indeed computationally all viables simulations follow the inequality above for any $\{\Delta G_{\mathrm{H}^+}, \mathrm{pH}_i, \mathrm{pH}_e, [\mathrm{CA}]_0\}$ within their sampling bounds (setting $\Delta\Pi = 1$ atmosphere).

6. We compute the leakage flux for each ion:

$$\forall x : \{b, P_x, [x]_e, \Delta\psi, \Delta G_x\} \rightarrow j_x \tag{D.83}$$

7. We then compute the Gibbs free energy change for all transport reactions: $\{\Delta G_{\mathrm{ClcA}}, \Delta G_{\mathrm{NhaB}}, \Delta G_{\mathrm{NhaA}}\}$ from the definitions in table 2 and compute the forward activity of each antiporter $\{j^+_{\mathrm{ClcA}}, j^+_{\mathrm{NhaB}}, j^+_{\mathrm{NhaA}}\}$ that minimizes the cost of maintaining electrochemical potentials $\{\Delta G_{\mathrm{C}^+}, \Delta G_{\mathrm{A}^-}$ as in Eqs. (D.36), (D.37).

8. Finally, we compute as in Eqs. (D.54), (D.55), (D.56) the minimal cost of maintaining cellular homeostases $\{\Delta\Pi, \mathrm{pH}_i, \Delta G_{\mathrm{H}^+}\}$ in the said extracellular environment $\{\mathrm{pH}_e, [\mathrm{CA}]_0\}$.

E. Generalization to other Models of Electrophysiology

In this appendix, we generalize some of the results we derived for the model of *E.coli*. In particular we generalize our heuristics for deriving thermodynamically viable steady-states for arbitrary electrophysiological models. Also we show that the optimal coordination of a model possessing an arbitrary number of antiporters is given in a similar way than the model of *E.coli*. Note that this section is not referred to in the main content of this chapter (at the beginning) and can be read as a standalone (a bit dry) section summarizing results that pertains to a large family of electrophysiological models the model we studied until now belongs to.

E.1. Thermodynamically Viable Steady-States for Arbitrary number and type of Transporters

Here we generalize how to obtain the allowed range of each IMF that is thermodynamically viable at steady state. We first consider a case where an ion x can be moved across the membrane by an arbitrary number of transporter, each of which is coupled to a spontaneously occurring reaction with arbitrary associated

Gibbs free energy. We then enrich the model with arbitrary influx pumps and show that the motive force of such an ion must be in the range:

$$\min_{1\leq i\leq n}\left(-\frac{1}{\sigma_{x,i}}\Delta G_{\mathrm{E}_i}\right)\leq \Delta G_x \leq \max_{1\leq k\leq m}\left(-\frac{1}{\sigma_{x,k}}\Delta G_{\mathrm{I}_k}\right) \tag{E.1}$$

where i selects a specific efflux pump, k a specific influx pump, and ΔG_{E_i}, $\Delta G_{I,k}$ are the driving force to which movement of ion x is coupled.

Case with n efflux pumps We may generalize the process of how we derived the allowed range of electrochemical potential for the model of *E.coli* to an arbitrary model where ion x has access to n efflux pumps:

$$\begin{aligned}
\mathrm{E}_1^\star + \sigma_{x,1}\cdot x_e &\rightleftharpoons \mathrm{E}_1 + \sigma_{x,1}\cdot x_i \\
\mathrm{E}_2^\star + \sigma_{x,2}\cdot x_e &\rightleftharpoons \mathrm{E}_2 + \sigma_{x,2}\cdot x_i \\
&\vdots \\
\mathrm{E}_n^\star + \sigma_{x,n}\cdot x_e &\rightleftharpoons \mathrm{E}_n + \sigma_{x,n}\cdot x_i
\end{aligned} \tag{E.2}$$

where $\forall i$ such that $1\leq i\leq n : \sigma_{x,i} < 0$ and the i^{th} efflux reaction has free energy change:

$$\Delta G_i = \Delta G_{E_i} + \sigma_{x,i}\cdot \Delta G_x \tag{E.3}$$

Where $\forall i : \Delta G_{E_i} < 0$. The reasoning we use is identical as for the model of *E.coli*, *i.e.* for a steady state to be achieved forbids:

$$\frac{d[x]_i}{dt} < 0 \Leftarrow \begin{cases} j_x & < 0 \\ \forall i \text{ such that } 1\leq i\leq n : \sigma_{x,i}\cdot j_i & < 0 \end{cases} \tag{E.4}$$

$$\frac{d[x]_i}{dt} > 0 \Leftarrow \begin{cases} j_x & > 0 \\ \forall i \text{ such that } 1\leq i\leq n : \sigma_{x,i}\cdot j_i & > 0 \end{cases} \tag{E.5}$$

Which is equivalent by Eq. (C.35) to:

$$\frac{d[x]_i}{dt} < 0 \Leftarrow \begin{cases} \Delta G_x & > 0 \\ \forall i \text{ such that } 1 \leq i \leq n : \Delta G_x & < -\dfrac{1}{\sigma_{x,i}} \cdot \Delta G_{E_i} \end{cases} \tag{E.6}$$

$$\frac{d[x]_i}{dt} > 0 \Leftarrow \begin{cases} \Delta G_x & < 0 \\ \forall i \text{ such that } 1 \leq i \leq n : \Delta G_x & > -\dfrac{1}{\sigma_{x,i}} \cdot \Delta G_{E_i} \end{cases} \tag{E.7}$$

Since we assumed $\Delta G_{E_i} < 0$ we obtain by Eq. (E.7) the upper limit on ΔG_x:

$$\Delta G_x \leq 0 \tag{E.8}$$

Since the upper limit Eq. (E.8) must hold we also obtain from Eq. (E.6) the lower limit:

$$\Delta G_x \geq \min_{1 \leq i \leq n} \left(-\frac{1}{\sigma_{x,i}} \cdot \Delta G_{E_i} \right) \tag{E.9}$$

and combining Eqs. (E.8),(E.9) the boundaries on ΔG_x are:

$$\min_{1 \leq i \leq n} \left(-\frac{1}{\sigma_{x,i}} \cdot \Delta G_{E_i} \right) \leq \Delta G_x \leq 0 \tag{E.10}$$

When all efflux pumps are proton:ion antiporters we have:

$$\Delta G_{E_i} = \sigma_{\mathrm{H}^+,i} \cdot \Delta G_{\mathrm{H}^+} \tag{E.11}$$

and Eq. (E.10) becomes:

$$\max_{1 \leq i \leq n} \left(-\frac{\sigma_{\mathrm{H}^+,i}}{\sigma_{x,i}} \right) \cdot \Delta G_{\mathrm{H}^+} \leq \Delta G_x \leq 0 \tag{E.12}$$

Accounting for influx pumps We now consider on top of the n efflux pumps (E.2), m influx pumps:

$$\begin{aligned} \mathrm{I}_1^\star + \sigma_{x,1} \cdot x_e &\rightleftharpoons \mathrm{I}_1 + \sigma_{x,1} \cdot x_i \\ \mathrm{I}_2^\star + \sigma_{x,2} \cdot x_e &\rightleftharpoons \mathrm{I}_2 + \sigma_{x,2} \cdot x_i \\ &\vdots \\ \mathrm{I}_m^\star + \sigma_{x,m} \cdot x_e &\rightleftharpoons \mathrm{I}_m + \sigma_{x,m} \cdot x_i \end{aligned} \tag{E.13}$$

Where $\forall 1 \leq k \leq m : \sigma_{x,k} > 0$ and the k^{th} has free energy change:

$$\Delta G_k = \Delta G_{\mathrm{I}_k} + \sigma_{x,k} \cdot \Delta G_x \tag{E.14}$$

where $\forall 1 \leq k \leq m : \Delta G_{\mathrm{I}_k} < 0$.

The reasoning we use is identical as for the case with n efflux pumps, *i.e.* for a steady state to be achieved forbids:

$$\frac{d[x]_i}{dt} < 0 \Leftarrow \begin{cases} & j_x < 0 \\ \forall i \text{ such that } 1 \leq i \leq n : & \sigma_{x,i} \cdot j_i < 0 \\ \forall k \text{ such that } 1 \leq k \leq m : & \sigma_{x,k} \cdot j_k < 0 \end{cases} \tag{E.15}$$

$$\frac{d[x]_i}{dt} > 0 \Leftarrow \begin{cases} & j_x > 0 \\ \forall i \text{ such that } 1 \leq i \leq n : & \sigma_{x,i} \cdot j_i > 0 \\ \forall k \text{ such that } 1 \leq k \leq m : & \sigma_{x,k} \cdot j_k < 0 \end{cases} \tag{E.16}$$

Which is equivalent by Eq. (C.35) to:

$$\frac{d[x]_i}{dt} < 0 \Leftarrow \begin{cases} \Delta G_x & > 0 \\ \forall i \text{ such that } 1 \leq i \leq n : \Delta G_x & < -\dfrac{1}{\sigma_{x,i}} \cdot \Delta G_{E_i} \\ \forall k \text{ such that } 1 \leq k \leq m : \Delta G_x & > -\dfrac{1}{\sigma_{x,k}} \cdot \Delta G_{\mathrm{I}_k} \end{cases} \tag{E.17}$$

$$\frac{d[x]_i}{dt} > 0 \Leftarrow \begin{cases} \Delta G_x & < 0 \\ \forall i \text{ such that } 1 \leq i \leq n : \Delta G_x & > -\dfrac{1}{\sigma_{x,i}} \cdot \Delta G_{E_i} \\ \forall k \text{ such that } 1 \leq k \leq n : \Delta G_x & > -\dfrac{1}{\sigma_{x,k}} \cdot \Delta G_{\mathrm{I}_k} \end{cases} \tag{E.18}$$

Since we assumed $\Delta G_{\mathrm{I}_k} < 0$, $\sigma_{x,k} > 0$ we obtain by Eq. (E.18) the upper limit on ΔG_x:

$$\Delta G_x \leq \max_{1 \leq k \leq m} \left(-\frac{1}{\sigma_{x,k}} \Delta G_{\mathrm{I}_k} \right) \tag{E.19}$$

The lower limit is obtained in the same way than for Eq. (E.9) and for a steady-state to exist impose the following interval for ΔG_x:

$$\min_{1 \leq i \leq n} \left(-\frac{1}{\sigma_{x,i}} \Delta G_{\mathrm{E}_i} \right) \leq \Delta G_x \leq \max_{1 \leq k \leq m} \left(-\frac{1}{\sigma_{x,k}} \Delta G_{\mathrm{I}_k} \right) \tag{E.20}$$

When all influx pumps are proton:ion symporters then:

$$\Delta G_{\mathrm{I}_k} = \sigma_{\mathrm{H}^+} \cdot \Delta G_{\mathrm{H}^+} \tag{E.21}$$

If all efflux pumps are proton:ion antiporters then we also have Eq. (E.11) and together with Eq. (E.21), Eq. (E.20) becomes:

$$\max_{1\leq i\leq n}\left(-\frac{\sigma_{\mathrm{H}^+,i}}{\sigma_{x,i}}\right)\cdot\Delta G_{\mathrm{H}^+} \leq \Delta G_x \leq -\max_{1\leq k\leq m}\left(\frac{\sigma_{\mathrm{H}^+,k}}{\sigma_{x,k}}\right)\cdot\Delta G_{\mathrm{H}^+} \tag{E.22}$$

E.2. Thermodynamically Viable Steady-States for the Coupling ion (here Proton)

We now wish to generalize our results before that PMF is bounded by:

$$\min\left(-\frac{1}{\sigma_{\mathrm{H}^+,\mathrm{F1F}_o}}\cdot\Delta G_{\mathrm{ATP}}, -\frac{1}{\sigma_{\mathrm{H}^+,\mathrm{R}}}\cdot\Delta G_{\mathrm{NADH}}\right) \leq \Delta G_{\mathrm{H}^+} \leq 0 \tag{E.23}$$

for a model possessing the oxidative respiratory chain, $\mathrm{F1F}_o$ and an arbitrary number of proton:ion antiporters (antiporters and symporters). We first consider the case where a single ion is pumped, before demonstrating the inequality above for an arbitrary number of ions proton transport is coupled to.

Case with one ion The four forbidden regimes are now defined as follows:

$$\frac{d[\mathrm{H}^+]_i}{dt} > 0 \Leftarrow \begin{cases} \Delta G_{\mathrm{H}^+} & < 0 \\ \Delta G_{\mathrm{H}^+} & < -\dfrac{1}{\sigma_{\mathrm{H}^+,\mathrm{F1F}_o}} \cdot \Delta G_{\mathrm{ATP}} \\ \Delta G_{\mathrm{H}^+} & < -\dfrac{1}{\sigma_{\mathrm{H}^+,\mathrm{R}}} \cdot \Delta G_{\mathrm{NADH}} \\ \Delta G_{\mathrm{H}^+} & < -\dfrac{\sigma_{x,1}}{\sigma_{\mathrm{H}^+,1}} \cdot \Delta G_x \\ & \vdots \\ \Delta G_{\mathrm{H}^+} & < -\dfrac{\sigma_{x,n}}{\sigma_{\mathrm{H}^+,n}} \cdot \Delta G_x \end{cases} \quad (+,\cdot)$$

$$\frac{d[\mathrm{H}^+]_i}{dt} < 0 \Leftarrow \begin{cases} \Delta G_{\mathrm{H}^+} & > 0 \\ \Delta G_{\mathrm{H}^+} & > -\dfrac{1}{\sigma_{\mathrm{H}^+,\mathrm{F1F}_o}} \cdot \Delta G_{\mathrm{ATP}} \\ \Delta G_{\mathrm{H}^+} & > -\dfrac{1}{\sigma_{\mathrm{H}^+,\mathrm{R}}} \cdot \Delta G_{\mathrm{NADH}} \\ \Delta G_{\mathrm{H}^+} & > -\dfrac{\sigma_{x,1}}{\sigma_{\mathrm{H}^+,1}} \cdot \Delta G_x \\ & \vdots \\ \Delta G_{\mathrm{H}^+} & > -\dfrac{\sigma_{x,n}}{\sigma_{\mathrm{H}^+,n}} \cdot \Delta G_x \end{cases} \quad (-,\cdot)$$

$$\frac{d[x]_i}{dt} > 0 \Leftarrow \begin{cases} \Delta G_x & < 0 \\ \Delta G_x & < -\dfrac{\sigma_{\mathrm{H}^+,1}}{\sigma_{x,1}} \cdot \Delta G_{\mathrm{H}^+} \\ & \vdots \\ \Delta G_x & < -\dfrac{\sigma_{\mathrm{H}^+,n}}{\sigma_{x,n}} \cdot \Delta G_{\mathrm{H}^+} \end{cases} \quad (\cdot,+)$$

$$\frac{d[x]_i}{dt} < 0 \Leftarrow \begin{cases} \Delta G_x & > 0 \\ \Delta G_x & > -\dfrac{\sigma_{\mathrm{H}^+,1}}{\sigma_{x,1}} \cdot \Delta G_{\mathrm{H}^+} \\ & \vdots \\ \Delta G_x & > -\dfrac{\sigma_{\mathrm{H}^+,n}}{\sigma_{x,n}} \cdot \Delta G_{\mathrm{H}^+} \end{cases} \quad (\cdot,-)$$

We then:

1. Obtain the upper limit on the PMF following an identical reasoning as for the model of *E.coli*:

$$\Delta G_{\mathrm{H}^+} \leq 0 \quad \text{(E.24)}$$

2. Obtain the upper limit on ΔG_x following an identical reasoning as for the model of *E.coli*:

$$\Delta G_x \leq 0 \tag{E.25}$$

3. Obtain the lower limit on ΔG_x so that we are not in the forbidden regime ($\cdot$,+) as in Eq. (E.12):

$$\Delta G_x \geq \max_{1\leq i\leq n}\left(-\frac{\sigma_{\mathrm{H}^+,i}}{\sigma_{x,i}}\right)\cdot\Delta G_{\mathrm{H}^+} \tag{E.26}$$

4. Obtain the lower limit on PMF as for the model of *E.coli*.

Thus we have the boundaries on both PMF and ΔG_x:

$$\min\left(-\frac{1}{\sigma_{\mathrm{H}^+,\mathrm{F1F}_o}}\cdot\Delta G_{\mathrm{ATP}}, -\frac{1}{\sigma_{\mathrm{H}^+,\mathrm{R}}}\cdot\Delta G_{\mathrm{NADH}}\right)\leq\Delta G_{\mathrm{H}^+}\leq 0 \tag{E.27}$$

$$\max_{1\leq i\leq n}\left(-\frac{\sigma_{\mathrm{H}^+,i}}{\sigma_{x,i}}\right)\cdot\Delta G_{\mathrm{H}^+}\leq\Delta G_x\leq 0 \tag{E.28}$$

Boundary on PMF with arbitrary number of proton:ion antiporters (several ions). The process of generalized demonstration can be described in a similar way as before:

- Obtain upper limit on PMF.
- for each secondary ionic species:
  1. Obtain upper limit.
  2. Obtain lower limit
- Obtain lower limit on PMF.

and we obtain one viable interval for each ionic species:

$$\min\left(-\frac{1}{\sigma_{\mathrm{H}^+,\mathrm{F1F}_o}}\cdot\Delta G_{\mathrm{ATP}}, -\frac{1}{\sigma_{\mathrm{H}^+,\mathrm{R}}}\cdot\Delta G_{\mathrm{NADH}}\right)\leq\Delta G_{\mathrm{H}^+}\leq 0 \tag{E.29}$$

$$\forall x:\max_{1\leq i\leq n}\left(-\frac{\sigma_{\mathrm{H}^+,i}}{\sigma_{x,i}}\right)\cdot\Delta G_{\mathrm{H}^+}\leq\Delta G_x\leq 0 \tag{E.30}$$

Case with influx pumps The reasoning is similar as before and we obtain the viable interval for each ionic species as:

$$\min\left(-\frac{1}{\sigma_{\mathrm{H^+,F1F_o}}}\cdot\Delta G_{\mathrm{ATP}}, -\frac{1}{\sigma_{\mathrm{H^+,R}}}\cdot\Delta G_{\mathrm{NADH}}\right)\leq\Delta G_{\mathrm{H^+}}\leq 0 \tag{E.31}$$

$$\forall x : \max_{1\leq i\leq n}\left(-\frac{\sigma_{\mathrm{H^+},i}}{\sigma_{x,i}}\right)\cdot\Delta G_{\mathrm{H^+}}\leq\Delta G_x\leq -\max_{1\leq k\leq m}\left(\frac{\sigma_{\mathrm{H^+},k}}{\sigma_{x,k}}\right)\cdot\Delta G_{\mathrm{H^+}} \tag{E.32}$$

Limitations of the current approach We restricted the case study as a single ion (protons) being both a source and a sink of driving force. It is not obvious what would happen if let us say another ion was both a source and a sink of driving force by for instance considering an ATP-driven efflux for potassium.

E.3. Generalizing the Optimal Coordination of Cotransporters

Summary We now turn ourselves to the problem a cell may be facing when maintaining a chemiosmotic state: *How to coordinate the activity of proton:ion pumps so that the energetic cost of doing so is minimized ?*

We first notice as stated in the last paragraph that fixing the PMF, pHi and other parameters (surface, volume, permeabilities) there is no room for cost optimization in the proton and hydroxide leakage contribution. Thus the problem of overall cost minimization can be reduced to how to minimize the cost of maintaining each electrochemical gradient x: Cost_x.

We eventually show that the strategy minimizing that cost contribution is to set for each secondary ion the forward flux of the pump k having the least negative ΔG to:

$$\forall x \in \text{ secondary ions } : j_k^+ = -\frac{j_x}{\sigma_{x,k}}$$

and all the other pumps i to null activity: $j_i^+ = 0$.

Assuming the cell optimally maintains a set of electrochemical gradients (in the sense of minimizing the cost of doing so) therefore simplifies the problem of coordinating the activity of multiple pumps considerably since we have the guarantee that there is only a single pump working for each secondary ion in any regime. The demonstration that the strategy above is indeed optimal is shown below.

Step 1: Cost of maintaining the electrochemical gradient of a single ion. We first look at the cost of maintaining the electrochemical gradient of a single ion x, *i.e.* the total flux of protons going through cotransporters that have non-null stoichiometry for x:

$$\text{Cost}_x(\Delta G_x, j_1^+, j_2^+, \ldots, j_n^+) = \sum_{n|\sigma_{x,n}\neq 0} \sigma_{\text{H}^+,n} \cdot j_n^+ \left(1 - e^{\frac{F}{RT}\Delta G_n}\right) \tag{E.33}$$

$$\Delta G_n = \sigma_{\text{H}^+,n} \cdot \Delta G_{\text{H}^+} + \sigma_{x,n} \cdot \Delta G_x \tag{E.34}$$

and the problem is to find for a given ΔG_{H^+} the set of forward fluxes $\{j_1^+, j_2^+, \ldots, j_n^+\}$ that minimize Cost_x while maintaining ΔG_x to some value.

We postulate the following optimal strategy:

$$\text{if } \max_{\forall i|\Delta G_i<0}(\Delta G_i) = \Delta G_k \text{ then: } \begin{cases} j_k^+ & = -\dfrac{j_x}{\sigma_{x,k}} \\ \forall 1 \leq i \leq n, i \neq k : j_i^+ & = 0 \end{cases} \tag{E.35}$$

Which can be read as: *"the optimal strategy*[21] *is to maximize the activity of the pump that has maximal ΔG_n from all pumps having negative ΔG_n and set to 0 the activity of all other pumps"*.

To demonstrate this, we first pick a pump k and rewrite Eq. (E.35) as:

$$j_k = -\frac{1}{\sigma_{x,k}} \cdot \left(j_x + \sum_{i\neq k} \sigma_{x,i} \cdot j_i\right) \tag{E.36}$$

So we can rearrange Eq. (E.33) as:

$$\text{Cost}_x = -\frac{\sigma_{\text{H}^+,k}}{\sigma_{x,k}} \cdot \left(j_x + \sum_{i\neq k} \sigma_{x,i} \cdot j_i\right) + \sum_{i\neq k} \sigma_{\text{H}^+,i} \cdot j_i \tag{E.37}$$

which can be factorized as:

$$\text{Cost}_x = \sigma_{\text{H}^+,k} \left(-\frac{1}{\sigma_{x,k}} \cdot j_x + \sum_{i\neq k} j_i \cdot \frac{\sigma_{x,i}}{\sigma_{x,k}} \cdot \left[\frac{\sigma_{\text{H}^+,i}}{\sigma_{x,i}} \cdot \frac{\sigma_{x,k}}{\sigma_{\text{H}^+,k}} - 1\right]\right) \tag{E.38}$$

[21] Here defined as the strategy minimizing the energetic cost of maintaining an IMF at steady-state; *e.g.* does not take into account the catalytic efficiency: the fact that different pumps may have different rates, thus a choice of pump that is energetically optimal may induce lower overall rate per pump, therefore different requirements in terms of number of pumps, consequently different requirements in terms of the amount of resources required to synthesize these pumps.

To show that the strategy minimizing the cost is to set $j_i^+ = 0$ is equivalent to show that:

$$\arg\min_{1\leq i\leq n}\left[\mathrm{Cost}_x(\Delta G_x, j_1^+, j_2^+, \ldots, j_n^+)\right] = -\frac{\sigma_{\mathrm{H}^+,k}}{\sigma_{x,k}}\cdot j_x \tag{E.39}$$

or equivalently:

$$\forall i \neq k : j_i \cdot \frac{\sigma_{x,i}}{\sigma_{x,k}} \cdot \left[\frac{\sigma_{\mathrm{H}^+,i}}{\sigma_{x,i}} \cdot \frac{\sigma_{x,k}}{\sigma_{\mathrm{H}^+,k}} - 1\right] \geq 0 \tag{E.40}$$

Such that every term in the sum of Eq. (E.38) is monotonically decreasing with j_i^+ which we know the minimum is $j_i^+ = 0$.

Step 2: Increasing activity of any pump else than k monotonically increases the cost of maintaing the electrochemical gradient for x. We then assume that we picked k as in Eq. (E.35) and show that inequality (E.40) always hold. We also assume all along $\Delta G_{\mathrm{H}^+} < 0$. We decompose the problem in 2×3 subproblems, where we distinguish between two regimes for ΔG_x:

1. Given $\Delta G_x > 0$ we distinguish between three distinct types of i pumps: *(a)* Those having $\Delta G_i > 0$ (which implies that i is a proton:ion symporter, *i.e.* $\sigma_{x,i} > 0$), *(b)* proton:ion antiporters (which implies that $\sigma_{x,i} < 0$) and *(c)* proton:ion symporters such that $\Delta G_i < 0$. We also assume that we picked k as in Eq. (E.35) such that for (b) and (c) we have $\Delta G_i < \Delta G_k$.

   (a) $\underline{\Delta G_i > 0.}$ We first notice that:

$$\Delta G_i > 0 \Leftrightarrow \sigma_{\mathrm{H}^+,i} \cdot \Delta G_{\mathrm{H}^+} + \sigma_{x,i} \cdot \Delta G_x > 0 \tag{E.41}$$

$$\Delta G_k < 0 \Leftrightarrow \sigma_{\mathrm{H}^+,k} \cdot \Delta G_{\mathrm{H}^+} + \sigma_{x,k} \cdot \Delta G_x < 0 \tag{E.42}$$

   Since $\Delta G_x > 0$, $\Delta G_i > 0$ is only achievable for proton:x symporters and consequently $\sigma_{x,i} > 0$. Also, k needs to be a proton:x symporter since $\Delta G_x > 0$ being achievable by a single pump requires this pump to be an influx pump, so $\sigma_{x,k} > 0$. We can now rearrange in two steps

the inequalities (E.41), (E.42) as:

$$\frac{\sigma_{\mathrm{H}^+,i}}{\sigma_{x,i}} \cdot \frac{\Delta G_{\mathrm{H}^+}}{\Delta G_x} + 1 > 0 \tag{E.43}$$

$$\frac{\sigma_{x,k}}{\sigma_{\mathrm{H}^+,k}} \cdot \frac{\Delta G_x}{\Delta G_{\mathrm{H}^+}} + 1 > 0 \tag{E.44}$$

And the direction in the inequality changes in Eq. (E.43) since $\sigma_{\mathrm{H}^+,k} \cdot \Delta G_{\mathrm{H}^+} < 0$. We then rearrange the above as:

$$\frac{\sigma_{\mathrm{H}^+,i}}{\sigma_{x,i}} < -\frac{\Delta G_x}{\Delta G_{\mathrm{H}^+}} \tag{E.45}$$

$$\frac{\sigma_{x,k}}{\sigma_{\mathrm{H}^+,k}} < -\frac{\Delta G_{\mathrm{H}^+}}{\Delta G_x} \tag{E.46}$$

where we used that $\Delta G_{\mathrm{H}^+}/\Delta G_x < 0$. Finally we combine both inequalities and obtain:

$$\frac{\sigma_{\mathrm{H}^+,i}}{\sigma_{x,i}} \cdot \frac{\sigma_{x,k}}{\sigma_{\mathrm{H}^+,k}} < 1 \tag{E.47}$$

By inequality (E.47), since $\sigma_{x,i} > 0$, $\sigma_{x,k} > 0$, because from Eq. (C.35): $\Delta G_i > 0 \Leftrightarrow j_i \leq 0$ Inequality (E.41) holds.

(b) $\Delta G_i < \Delta G_k$, $\sigma_{x,i} < 0$. Note that $\sigma_{x,i} < 0$ means that the pump i is an antiporter. Since $\sigma_{x,k} > 0$ and since from Eq. (C.35): $\Delta G_i < 0 \Leftrightarrow j_i \geq 0$ we have that inequality (E.40) holds.

(c) $\Delta G_i < \Delta G_k$, $\sigma_{x,i} > 0$. We have:

$$\Delta G_k \leq 0 \tag{E.48}$$

$$\Delta G_i < \Delta G_k \tag{E.49}$$

Substituting ΔG_k by its definition, inequality (E.49) is equivalent to:

$$-\frac{\sigma_{\mathrm{H}^+,k}}{\sigma_{x,k}} \cdot \Delta G_{\mathrm{H}^+} \geq \Delta G_x \tag{E.50}$$

We then substitute ΔG_i, ΔG_k by their definitions in inequality (E.50) to obtain:

$$\sigma_{\mathrm{H}^+,i} \cdot \Delta G_{\mathrm{H}^+} + \sigma_{x,i} \cdot \Delta G_x < \sigma_{\mathrm{H}^+,k} \cdot \Delta G_{\mathrm{H}^+} + \sigma_{x,k} \cdot \Delta G_x \tag{E.51}$$

Which we rearrange as:

$$\sigma_{\mathrm{H}^+,i} \cdot \Delta G_{\mathrm{H}^+} < \sigma_{\mathrm{H}^+,k} \cdot \Delta G_{\mathrm{H}^+} + (\sigma_{x,k} - \sigma_{x,i}) \cdot \Delta G_x \tag{E.52}$$

Substituting ΔG_x in the inequality above using inequality (E.50) implies that:

$$\sigma_{\mathrm{H}^+,i} \cdot \Delta G_{\mathrm{H}^+} < \sigma_{\mathrm{H}^+,k} \cdot \Delta G_{\mathrm{H}^+} - \frac{\sigma_{\mathrm{H}^+,k}}{\sigma_{x,k}} \cdot (\sigma_{x,k} - \sigma_{x,i}) \cdot \Delta G_{\mathrm{H}^+} \tag{E.53}$$

Which, subtracting $\sigma_{\mathrm{H}^+,i} \cdot \Delta G_{\mathrm{H}^+}$ on both sides becomes:

$$0 < \Delta G_{\mathrm{H}^+} \left(\sigma_{x,i} \cdot \frac{\sigma_{\mathrm{H}^+,k}}{\sigma_{x,k}} - \sigma_{\mathrm{H}^+,i} \right) \tag{E.54}$$

Since $\Delta G_{\mathrm{H}^+} < 0$ this is equivalent to:

$$0 > \sigma_{x,i} \cdot \frac{\sigma_{\mathrm{H}^+,k}}{\sigma_{x,k}} - \sigma_{\mathrm{H}^+,i} \tag{E.55}$$

And since $\sigma_{x,i} > 0$ we finally obtain:

$$\frac{\sigma_{\mathrm{H}^+,i}}{\sigma_{x,i}} > \frac{\sigma_{\mathrm{H}^+,k}}{\sigma_{x,k}} \Leftrightarrow \frac{\sigma_{\mathrm{H}^+,i}}{\sigma_{x,i}} \cdot \frac{\sigma_{x,k}}{\sigma_{\mathrm{H}^+,k}} > 1 \tag{E.56}$$

Because $\Delta G_i < 0 \Leftrightarrow j_i \geq 0$ by Eq. (C.35), since $\sigma_{x,i} > 0$, $\sigma_{x,k} > 0$ from inequality (E.56) we know that inequality (E.40) holds.

2. Given $\Delta G_x < 0$ we distinguish between three distinct types of i pumps: *(a)* Those having $\Delta G_i > 0$ (which implies that i is a proton:ion antiporters, *i.e.* $\sigma_{x,i} < 0$), *(b)* proton:ion symporters (which implies that $\sigma_{x,i} > 0$) and *(c)* proton:ion antiporters such that $\Delta G_i < 0$. We also assume that we picked k as in Eq. (E.35) such that for (b) and (c) we have $\Delta G_i < \Delta G_k$.

   (a) $\underline{\Delta G_i > 0.}$ Inequalities (E.41), (E.42) hold. Since $\Delta G_x < 0$, $\Delta G_i > 0$ is only achievable for proton:x antiporters and consequently $\sigma_{x,i} < 0$. Also k needs to be a proton:x antiporter since $\Delta G_x < 0$ being achievable by a single pump requires this pump to be an efflux pump, so $\sigma_{x,k} < 0$. We therefore have $\sigma_{x,i} \cdot \Delta G_x > 0$ and $\sigma_{x,k} \cdot \Delta G_x > 0$ such that we can rearrange Inequalities (E.41), (E.42) to give inequalities (E.43), (E.43). We assumed $\Delta G_x < 0$ such that $\Delta G_{\mathrm{H}^+}/\Delta G_x > 0$, consequently we

obtain from inequalities (E.42), (E.43):

$$\frac{\sigma_{\mathrm{H}^+,i}}{\sigma_{x,i}} > -\frac{\Delta G_x}{\Delta G_{\mathrm{H}^+}} \tag{E.57}$$

$$\frac{\sigma_{x,k}}{\sigma_{\mathrm{H}^+,k}} > -\frac{\Delta G_{\mathrm{H}^+}}{\Delta G_x} \tag{E.58}$$

Which we rewrite as:

$$-\frac{\sigma_{\mathrm{H}^+,i}}{\sigma_{x,i}} < \frac{\Delta G_x}{\Delta G_{\mathrm{H}^+}} \tag{E.59}$$

$$-\frac{\sigma_{x,k}}{\sigma_{\mathrm{H}^+,k}} < \frac{\Delta G_{\mathrm{H}^+}}{\Delta G_x} \tag{E.60}$$

where all terms are positive so we can combine the two inequalities above we obtain:

$$\frac{\sigma_{\mathrm{H}^+,i}}{\sigma_{x,i}} \cdot \frac{\sigma_{x,k}}{\sigma_{\mathrm{H}^+,k}} < 1 \tag{E.61}$$

Consequently, since $\sigma_{x,i} > 0$, $\sigma_{x,k} > 0$, $\Delta G_i > 0 \Leftrightarrow j_i \leq 0$ we have from inequality (E.62) that inequality (E.40) holds.

(b) $\underline{\Delta G_i < \Delta G_k,\ \sigma_{x,i} > 0.}$ Note that $\sigma_{x,i} > 0$ means that the pump i is a symporter. Since $\sigma_{x,k} < 0$ and because from Eq. (C.35): $\Delta G_i < 0 \Leftrightarrow j_i \geq 0$ we have that inequality (E.40) holds.

(c) $\underline{\Delta G_i < \Delta G_k,\ \sigma_{x,i} < 0.}$ The steps from inequality (E.48) to (E.55) remain unchanged. Since $\sigma_{x,i} < 0$, Inequality (E.55) becomes in that case:

$$\frac{\sigma_{\mathrm{H}^+,i}}{\sigma_{x,i}} < \frac{\sigma_{\mathrm{H}^+,k}}{\sigma_{x,k}} \tag{E.62}$$

and because $\sigma_{x,k} < 0$, $\sigma_{x,i} < 0$ the above is equivalent to:

$$\frac{\sigma_{\mathrm{H}^+,i}}{\sigma_{x,i}} \cdot \frac{\sigma_{x,k}}{\sigma_{\mathrm{H}^+,k}} > 1 \tag{E.63}$$

Since $\sigma_{x,i} < 0$, $\sigma_{x,k} < 0$ and $\Delta G_i < 0 \Leftrightarrow j_i \geq 0$ by Eq. (C.35), from inequality (E.63), inequality (E.40) holds.

Step 3: Generalization to maintenance of multiple secondary ions' electrochemical gradients. It is straightforward to generalize it to the optimal strategy to maintain multiple electrochemical gradients for secondary ions. Indeed,

$\Delta G_k < 0$	$\Delta G_x > 0$, $\sigma_{x,k} > 0$	$\Delta G_x < 0$, $\sigma_{x,k} < 0$
$\Delta G_i > 0$, $\sigma_{x,i} > 0$	1.(a)	Not viable
$\Delta G_i < \Delta G_k$, $\sigma_{x,i} < 0$	1.(b)	2.(c)
$\Delta G_i > 0$, $\sigma_{x,i} < 0$	Not Viable	2.(a)
$\Delta G_i < \Delta G_k$, $\sigma_{x,i} > 0$	1.(c)	2.(b)

TABLE 5: Summary of the different regimes we consider in the proof. They cover all possible cases since we assumed $\Delta G_{\mathrm{H}^+} < 0$ and: *(i)* $\Delta G_x > 0$ requires $\sigma_{x,k} > 0$ *i.e.* k to be a symporter, *(ii)* $\Delta G_x < 0$ requires $\sigma_{x,k} < 0$ *i.e.* k to be an antiporter.

we may rewrite Eq. (E.38) as:

$$\mathrm{Cost}_x\left(\Delta\mathbf{G}, j_1^+, \ldots, j_n^+\right) = \sum_{x\in\text{secondary ion}} f_x(\Delta G_x, j_1^+, \ldots, j_n^+) \tag{E.64}$$

$$f_x(\Delta G_x, j_1^+, \ldots, j_n^+) = \sigma_{\mathrm{H}^+,k(x)}\left(-\frac{1}{\sigma_{x,k(x)}}\cdot j_x + \sum_{i\neq k(x)} j_i \cdot \frac{\sigma_{x,i}}{\sigma_{x,k(x)}} \cdot \left[\frac{\sigma_{\mathrm{H}^+,i}}{\sigma_{x,i}}\cdot\frac{\sigma_{x,k(x)}}{\sigma_{\mathrm{H}^+,k(x)}} - 1\right]\right) \tag{E.65}$$

where $\Delta\mathbf{G}$ is a vector collecting all ΔG_x (of secondary ions) to maintain and $f_x()$ is the cost of maintaining the electrochemical gradient of x. Also, to account for the cost of maintaining all secondary ions' electrochemical gradients we made $k(x)$ function of the secondary ion to reflect that optimally maintaining ΔG_x requires expression of a different pump for each x.

Importantly, we shall assume that we have only proton:ion symporters/antiporters such that a pump can only be responsible for the influx/efflux of a single secondary ion. Consequently, the problem of minimizing the overall cost can be reformulated as independently minimizing the cost of maintaining every electrochemical gradient (each of which is defined in Eq. (E.65)). It is thus sufficient to apply the reasoning of **Step 2** to each secondary ion to find the overall cost minimizing strategy:

$$\forall x \in \text{secondary ions} : \begin{cases} j^+_{k(x)} & = -\dfrac{j_x}{\sigma_{x,k(x)}} \\ \forall i \neq k(x) : j_i^+ & = 0 \end{cases} \tag{E.66}$$

where $k(x)$ is picked as explained in Eq. (E.35). The minimal cost can thus be expressed as:

$$\arg\min_x\left(\mathrm{Cost}_x\right) = -\sum_x \frac{\sigma_{\mathrm{H}^+,k(x)}}{\sigma_{x,k(x)}}\cdot j_x \tag{E.67}$$

Mapping to stoichiometric ratio diagrams It is interesting at this stage to propose a more intuitive way on how to select the optimal pump given a certain pair of $\{\Delta G_x, \Delta G_{\mathrm{H}^+}\}$.

To do that we first consider a cell that has access to $n+m$ proton driven pumps for a ion x (n antiporters and m symporters). We then order them by their stoichiometric ratio $\sigma_{\mathrm{H}^+,i}/\sigma_{x,i}$ such that $i=1$ denotes the pump with the minimal stoichiometric ratio (an antiporter if the stoichiometric ratio is negative) and $i=n+m$ denotes the pump with the maximal stoichiometric ratio (positive if there is at least one proton:x symporter $m>0$).

We start of with the minimum ΔG_x attainable, from Eq. (E.32):

$$\min\left(\Delta G_x\right) = \frac{\sigma_{\mathrm{H}^+,1}}{\sigma_{x,1}} \cdot \Delta G_{\mathrm{H}^+} \tag{E.68}$$

In that case the optimality condition Eq. (E.35) is trivial since we have only the pump $i=1$ that has $\Delta G_1 \leq 0$ (in that case $\Delta G_1 = 0$). We then gradually increase ΔG_x and notice that as soon as ΔG_2 shifts (if $i=2$ is an antiporter, ΔG_x must remain negative) from positive to negative, then the optimality criterion Eq. (E.35) shifts from maximizing pump $i=1$ to pump $i=2$. We can repeat that reasoning for $i>2$ pumps and:

$$\text{if: } \frac{\sigma_{\mathrm{H}^+,1}}{\sigma_{x,1}} \leq -\frac{\Delta G_x}{\Delta G_{\mathrm{H}^+}} < \frac{\sigma_{\mathrm{H}^+,2}}{\sigma_{x,2}} \text{ then Optimal strategy is:}$$

$$\begin{cases} j_1 & = -\dfrac{j_x}{\sigma_{x,1}} \\ \forall i \neq 1 : j_i^+ & = 0 \end{cases} \tag{E.69}$$

$$\text{if: } \frac{\sigma_{\mathrm{H}^+,2}}{\sigma_{x,2}} \leq -\frac{\Delta G_x}{\Delta G_{\mathrm{H}^+}} < \frac{\sigma_{\mathrm{H}^+,3}}{\sigma_{x,3}} \text{ then Optimal strategy is:}$$

$$\begin{cases} j_1 & = -\dfrac{j_x}{\sigma_{x,2}} \\ \forall i \neq 2 : j_i^+ & = 0 \end{cases} \tag{E.70}$$

$$\vdots \tag{E.71}$$

$$\text{if: } \frac{\sigma_{\mathrm{H}^+,n-1}}{\sigma_{x,n-1}} \leq -\frac{\Delta G_x}{\Delta G_{\mathrm{H}^+}} < \frac{\sigma_{\mathrm{H}^+,n}}{\sigma_{x,n}} \text{ then Optimal strategy is:}$$

$$\begin{cases} j_n & = -\dfrac{j_x}{\sigma_{x,n}} \\ \forall i \neq n : j_i^+ & = 0 \end{cases} \tag{E.72}$$

And note that we have a "singularity[22]" when ΔG_x shifts from positive to negative. In which case, since we labelled n the antiporter with the maximal stoichiometric ratio (negative since antiporter) and $n+1$ the symporter with minimal stoichiometric ratio (positive since symporter):

$$\text{if: } \frac{\sigma_{\mathrm{H}^+,n}}{\sigma_{x,n}} \leq -\frac{\Delta G_x}{\Delta G_{\mathrm{H}^+}} < 0 \text{ then Optimal strategy is:}$$

$$\begin{cases} j_n & = -\dfrac{j_x}{\sigma_{x,n}} \\ \forall i \neq n : j_i^+ & = 0 \end{cases} \tag{E.73}$$

$$\text{if: } 0 < -\frac{\Delta G_x}{\Delta G_{\mathrm{H}^+}} < \frac{\sigma_{\mathrm{H}^+,n+1}}{\sigma_{x,n+1}} \text{ then Optimal strategy is:}$$

$$\begin{cases} j_{n+1} & = -\dfrac{j_x}{\sigma_{x,n+1}} \\ \forall i \neq n+1 : j_i^+ & = 0 \end{cases} \tag{E.74}$$

In the range $\Delta G_x > 0$ the same reasoning than in Eq. (E.75) can be applied but this time to the stoichiometric ratio of antiporters:

$$\text{if: } \frac{\sigma_{\mathrm{H}^+,n+1}}{\sigma_{x,n+1}} \leq -\frac{\Delta G_x}{\Delta G_{\mathrm{H}^+}} < \frac{\sigma_{\mathrm{H}^+,n+2}}{\sigma_{x,n+2}} \text{ then Optimal strategy is:}$$

$$\begin{cases} j_{n+2} & = -\dfrac{j_x}{\sigma_{x,n+2}} \\ \forall i \neq n+2 : j_i^+ & = 0 \end{cases} \tag{E.75}$$

$$\vdots \tag{E.76}$$

$$\text{if: } \frac{\sigma_{\mathrm{H}^+,n+m-1}}{\sigma_{x,n+m-1}} \leq -\frac{\Delta G_x}{\Delta G_{\mathrm{H}^+}} < \frac{\sigma_{\mathrm{H}^+,n+m}}{\sigma_{x,n+m}} \text{ then Optimal strategy is:}$$

$$\begin{cases} j_{n+m} & = -\dfrac{j_x}{\sigma_{x,n+m}} \\ \forall i \neq n+m : j_i^+ & = 0 \end{cases} \tag{E.77}$$

In this way we may decompose the state-space (for small ions) of electrochemical gradients in different optimality regions, reflecting how a cell may choose to "quantized" the state-space. Note that describing the state space of small ions in terms of electrochemical potentials is equivalent to the description of the state space in terms of intracellular concentrations *given* a membrane potential and the

[22]Here meant as the condition for verifying optimality changes, as can be seen comparing the optimality criterion in the following equations (E.73) and (E.74).

extracellular ionic composition.

E. Algorithms

Result: Main Figure 1 to 3
Set invariants $\{F, R, T, S, V, C_m\}$.;
Select antiporters to sample for: 1:2 proton:anion (ClcA), 1:1 proton:cation, 3:2 protom:cation (NhaB) and 2:1 proton:cation (NhaA).;
Set salinity $[\mathrm{CA}]_0 = 100$ mM.;
Set $\mathrm{pH}_i = 7$;
Compute minimal and maximal PMF attainable from stoichiometries of oxidative respiratory chain, $\mathrm{F1F}_o$ as well as the Gibbs free energy for NADH reduction and ATP hydrolysis.;
Set captive molecules to $\{-10, 0, +10\}$ mM.;
for *Each* ΔG_{H^+} **do**
  for *Each antiporter* **do**
    if *Antiporter is a proton:cation antiporter* **then**
      Compute boundaries $\min(\Delta G_{\mathrm{C}^+})$, $\max(\Delta G_{\mathrm{C}^+})$ on ΔG_{C^+}, given current ΔG_{H^+}.;
    else
      Compute boundaries $\min(\Delta G_{\mathrm{A}^-})$, $\max(\Delta G_{\mathrm{A}^-})$ on ΔG_{A^-}, given current ΔG_{H^+}.;
    end
  end
  for *Each* $pH_e \in [2, 12]$ **do**
    Compute extracellular composition $\{[\mathrm{H}^+]_e, [\mathrm{OH}^-]_e, [\mathrm{C}^+]_e, [\mathrm{A}^-]_e\}$ from $\{\mathrm{pH}_e, [\mathrm{CA}]_0\}$.;
    Compute membrane potential required to maintain neutral pH_i for the current ΔG_{H^+} and pH_e (rearranging definition of PMF).;
    for *Each* $z_Y \cdot [Y]_i \in \{-10, 0, +10\}$ **do**
      for *Each Antiporter* **do**
        if *Antiporter is a proton:cation antiporter* **then**
          Compute ΔG_{C^+} required to maintain that membrane potential (assuming $\Delta G_{\mathrm{A}^-} = 0$), given current $z_{\mathrm{Y}} \cdot [\mathrm{Y}]_i$ and $\{\mathrm{pH}_e, [\mathrm{CA}]_0\}$.;
          if $\min(\Delta G_{C^+}) \leq \Delta G_{C^+} \leq \max(\Delta G_{C^+})$ **then**
            Set current antiporter as able to maintain $\mathrm{pH}_i = 7$ in the current$\{\mathrm{pH}_e, \Delta G_{\mathrm{H}^+}\}$.;
          end
        else
          Compute ΔG_{A^-} required to maintain that membrane potential (assuming $\Delta G_{\mathrm{C}^+} = 0$), given current $z_{\mathrm{Y}} \cdot [\mathrm{Y}]_i$ and $\{\mathrm{pH}_e, [\mathrm{CA}]_0\}$.;
          if $\min(\Delta G_{A^-}) \leq \Delta G_{A^-} \leq \max(\Delta G_{A^-})$ **then**
            Set current antiporter as able to maintain $\mathrm{pH}_i = 7$ in the current$\{\mathrm{pH}_e, \Delta G_{\mathrm{H}^+}\}$.;
          end
        end
      end
    end
  end
end

Algorithm 1: Description of the algorithm used to generate main text figures 1.

Chapter 3

Interactions of Electrophysiological Maintenance with Growth Behaviors

I. Preamble

My Contributions to this Chapter. I am the sole contributor to the work in this chapter.

Articulation with previous chapters. Insofar, this thesis has been mostly concerned with studying the electrophysiology of microbes as an isolated component of their overall physiology, *i.e.* their ability to maintain cellular homeostaeses: PMF, intracellular pH, osmotic pressure across different extracellular pH depending on the transport machinery they have access to. Although we derived in chapter 3 the cost of maintaining cellular homeostaeses across different pH_e and salinity, we did not consider however how this modulation of energy requirements used for maintenance of cellular homeostaeses could impact global cellular behaviours such as growth-rate or growth-yield[1].

[1]We shall use growth-yield as equivalent to carbon yield: the amount carbon incorporated in dry mass relative to the amount of carbon from a sugar (for instance glucose) consumed by cellular metabolism.

II. Introduction

Microbial growth patterns at different pH_e/salinity. Indeed growth-rate of *E.coli* [216] and other bacterial strains[2] [236] is impacted by extracellular pH. As seen in Figure. 3.1, the extracellular pH at which growth is maximized as well as the range of extracellular pH wherein a cell can support non-null growth is strain-dependent (and also likely depends on the other components of the growth-medium). Likewise, growth-rate of *E.coli* was shown to decrease with increasing NaCl [237, 238][3]. The growth-yield was also shown to decrease with increasing NaCl in both *E. coli* [239] and *Saccharomyces cerevisiae* [240] as well as with pH_e deviating from neutrality in *Chlorella vulgaris* [241]. Detrimental effects to growth of high NaCl concentrations is not a phenomenon specific to *E.coli* alone but occurs as well in at least 44 different bacterial species [242]. The effects of varying extracellular pH on growth also occur in many (if not all) species (see Fig. 3.1). This calls for a species-wide common mechanism by which extracellular pH and salinity impact growth.

Motivations for understanding how growth behaviours and environmental pH/salinity are related. Motivations for understanding how environmental pH and salinity impact growth behaviours of microbes are numerous, non exhaustively:

- *From an ecological perspective:* It is one of the necessary steps required to anticipate how microbial communities will respond to ocean acidification [244] which is one of the main concern when it comes to predict the impact of climate change on biogeochemical cycling (*e.g.* the carbon cycle) by microorganisms [245]. Depending on how microbial communities respond to global acidification one could for instance expect a positive or negative feedback of climate change on the planet-wide ability of microorganism to contribute to CO_2 sequestration by soils and oceans.
- *From an industrial perspective:* many studies on how bacterial growth behaviours depend on extracellular pH are motivated by evaluating the efficiency of food preservatives (some of which are acidic compounds) [246, 216]. For similar reasons, the bacterial growth response to NaCl –one of

[2]Note that in this chapter I mean by strain not the usual meaning (a genetic variant among a given species), but rather a genetic variant. Thus two distinct strains rigorously refers to two cells being genetically distinct, and they could belong to the same species of to two different species.

[3]also shows shift to fermentative metabolism at high NaCl.

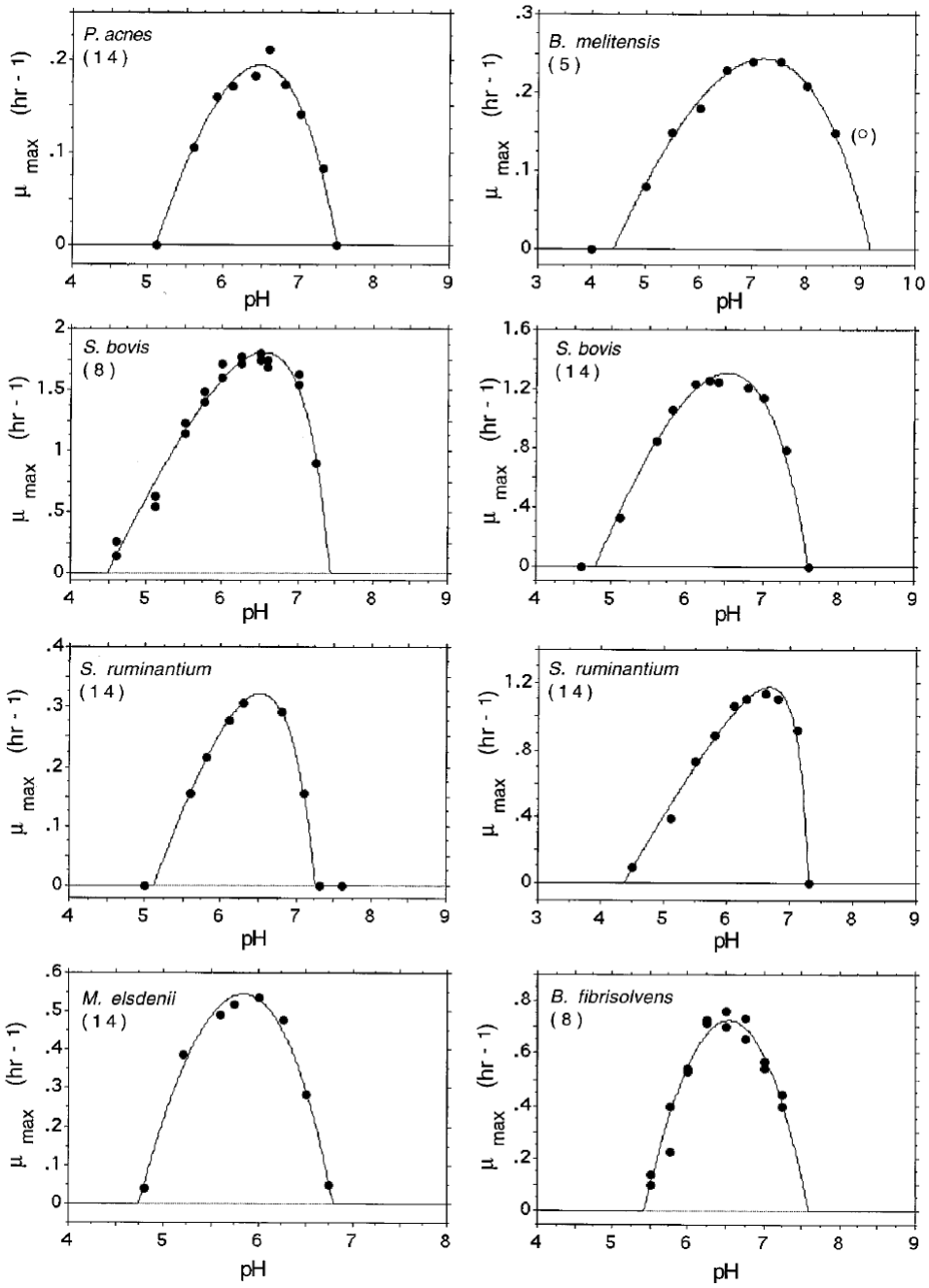


FIGURE 3.1: Figure taken from [243]. The growth-rate is shown as a function of the extracellular pH for different bacterial strains. Black dots are for experimentally obtained values. Black lines are for empirical equations fitted to the data.

the main food preservative since thousand of years– as well as the synergies between pH_e and NaCl are of industrial interests [4].

- *From a medical perspective:* The efficiency of some antibiotics depends on pH_e [247, 248] and the between pH_e and antibiotics on growth inhibition is strain dependent [249, 250]. In a *in vivo* setup (pathogenic bacteria within *e.g.* blood, bladder, *etc.*) the extracellular pH depends on the environment the infection takes place. Understanding how pH_e or NaCl impact the physiology of pathogenic bacteria may help in pinpointing what are the mechanisms underlying the environmental-dependent efficacy of some antibiotics, thus a step forward in rationalizing antibiotic treatments.

Many recent models of cellular growth [99, 92, 251], consisting of relatively simple auto-catalytic network of reactions –we will coin them auto-catalytic growth models–, have however largely ignored that a fraction of cellular energy had to be dedicated to non-growth related processes, for instance maintenance of the electrophysiological homeostases. Another stream of growth-models, rather empirical and not described as a set coarse-grained chemical reactions have included such non-growth related energetic expenditures for a long time. Indeed, as early as the 19$^{\text{th}}$ century, Duclaux [219] distinguished between two possible use of an amount of energy substrate ds taken up by the cell in an interval dt:

$$ds = \underbrace{A \cdot dx}_{\text{Energy required for growth}} + \underbrace{m \cdot x \cdot dt}_{\text{Energy required for maintenance}} \tag{II.1}$$

where dx is the amount of biomass formed in dt, A is the amount of biomass made per energy unit s, m is the rate of energy s utilization required to maintain a unit of biomass in a healthy state and x the amount of organism present. The distinction between these two contributions is of particular interest since while the first one scales with the amount of biomass produced, independently of the time it takes, the second depends on time, independently of the biomass produced. Building on Eq. (II.1), Pirt derived more than half a century later a fundamental growth law showing that the relationship between growth-rate and growth-yield was crucially determined by the so-called maintenance coefficient m [220]:

$$\frac{1}{Y} = \frac{m}{\mu} + \frac{1}{Y_G} \tag{II.2}$$

[4] See https://www.ncbi.nlm.nih.gov/books/NBK50952/.

where Y is the yield, μ the specific growth-rate and Y_G an empirical parameter sometimes referred to as maximal yield. The equation above has important implications in that it predicts that, should the maintenance rate be an invariant, the growth-yield is expected to decrease with decreasing growth-rate as shown in the left-end regime of figure. 3.2, a phenomenon which has been extensively observed, see review from [252]. Pirt already postulated in 1965 that the maintenance cost in Eq. (II.2) was not a constant characteristic of an organism but rather a function of the environmental conditions, *e.g.* extracellular pH. It is nowadays widely accepted that the maintenance cost indeed depends on many different processes [253, 254].

The approach to auto-catalytic growth models and the model briefly mentioned above are quite different. Indeed, auto-catalytic growth models use growth-rate and distribution of the mass into different types of catalysts as predictors for fitting kinetic parameters, *e.g.* the rate at which ribosome translate and how it depends on translational inhibitors in [99] or how transcription of different types of catalyst depend on the availability of precursors to translation in [92]. The yield/rate models, a simple example was introduced above, use the growth rate and the growth yield as predictors for fitting phenomenological variables, *e.g.* in this example the theoretically maximal growth yield achievable Y_G and the maintenance coefficient m. While the auto-catalytic approach has been ignoring the yield and non-growth related energy expenditures, the second phenomenological approach has not considered how the empirical parameters Y_G and m may depend on the underlying cellular physiology. The auto-catalytic approach has been quite successful in the previous decade. This likely seeds from its compelling ability to connect *(a)* what is the cell doing in terms of regulation, *i.e.* how it distributes its mass between different catalytic functions and *(b)* instantaneous growth-rate, arguably one (of many) factor underlying the evolutionary success of a species (a.k.a. fitness). The growth-yield is nevertheless another factor that contributes to fitness. Indeed, in environments where the quantity of resources is sometimes scarce[5], the efficiency –or yield– at which cells convert those resources to biomass will set the long term growth-rate of a monogenic population, thus will likely contribute to its fitness in a competitive environment. What is more is that as opposed to the simple model from Eq. (II.2), the yield does not always monotonically increases with the rate upon an environmental perturbation as

[5] *a priori* any environment.

highlighted in figure 3.1 which depicts what is thought to be a general phenomena: the decrease in yield at high growth-rate [252]. In addition, cells sometimes have to arbitrate between maximizing the yield and the rate as highlighted in [255] who show that the choice of catabolism may be governed by such a tradeoff. With that in mind, it calls for auto-catalytic models that are able to recover yield and the other phenomenological variables on which it depends: the maximal yield and the maintenance coefficient.

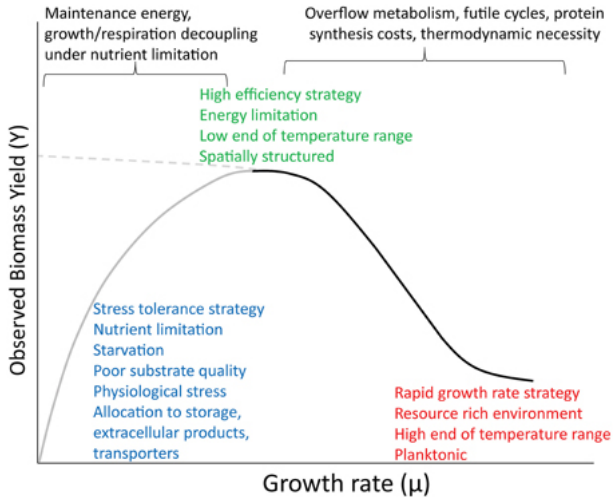


FIGURE 3.2: Figure taken from [252] depicting the growth rate/yield trade-off. There are two regimes: *(i)* at low growth-rate the yield increases with increasing growth-rates, which is well explained by the growth law from [220], showing that as the growth-rate decreases the fraction of energy used to fuel maintenance processes relative to that used for growth increases. The right-end regime, shows that at high growth-rate, the yield decreases with increasing growth-rate. This regime may be partially explained by overflow metabolism, *i.e.* the switch from high yield/low catalytic efficiency catabolic pathway (high amount of energy extracted per processed substrate, low rate of extraction per unit catalyst invested) to low yield/high catalytic efficiency catabolic pathways (Typically a shift from aerobic respiration to fermentation.) [255].

But how to mechanistically account for the maintenance coefficient in auto-catalytic models is not trivial. The maintenance coefficient from Eq. (II.2) indeed depends on many factors: "(1) shifts in metabolic pathways, (2) energy spilling reactions, (3) cell motility, (4) changes in stored polymeric carbon, (5) osmoregulation, (6) extracellular losses of compounds not involved in osmoregulation, (7) proofreading, synthesis and, turnover of macromolecular compounds such as enzymes and RNA, and (8) defense against O2 stress" [60]. As noted by the same author, all those factors are not strictly speaking part of maintenance. Indeed, whether the cell is using one metabolic pathway or another merely changes the

stoichiometries of energy production (for instance the number of ATP produced per metabolized sugar) and clearly should not be understood as a change in the energetic cost of maintaining the cell in a healthy state, although it will change the amount of substrate required to produce an identical amount of energy. Likewise, an increased intracellular pool of metabolites (a.k.a. higher storage) is not necessarily expected to cost additional energy to sustain, although it will impact growth kinetics [256]. What is the process dominating the maintenance coefficient is also subject to debate and includes maintenance of the electrochemical gradient of potassium across the membrane [257] and turnover of DNA, RNA, proteins [258] to the odd concept of energy-spilling reactions [259] [6].

Plan for this chapter. We shall postulate in this chapter that all maintenance expenditures seed from the maintenance of electrochemical gradients of ions across the membrane. This allows us to propose a generic mechanism for how pH_e and NaCl impact growth of microorganisms, *i.e. via* the modulation of maintenance expenditures. The strain-specific response to these challenges is shown to be specific to the permeability of their membrane for each ion, the values they seek to maintain pH_i, PMF and osmotic pressure as well as their choice of catabolic pathway. We propose a simple autocatalytic model (similar to that of [100]) which *(i)* recapitulates the growth-law from [220] and explicits how the phenomenological maximal yield and maintenance coefficient depends on other underlying factors; *(ii)* connects growth to electrophysiological behaviours and *(iii)* allows study of the interaction between challenges that increase the maintenance cost and inhibitors of biosynthetic (for instance chloramphenicol) or catabolic processes. We then propose an extension of the model with an additional catabolic pathway to show that existence of tradeoffs between growth-rate and growth-yield are dependent on the cost of physiological maintenance. Last, we propose that some of the variability of the growth-rate within a population may seed from uneven cell-to-cell surface to volume ratio.

[6] The idea that bacteria produce excess energy and consume it in futile cycles, or reactions that have no other functions but to consume the excess energy produced

III. Results

i. A Model for Studying Growth-Rate and Yield at Different Extracellular pH and Salinity.

Description of the Model's Reactions We consider a coarse-grained model of a cell made of five reactions:

- The cell is able to transport an extracellular glucose s_e inside:

$$s_e \xrightarrow{j_T} s_i$$

- Intracellular glucose can be used as a substrate by aerobic respiration (a common catabolic pathway among cells), and in the process generate an electrochemical gradient of protons:

$$s_i + 6 \cdot O_2 + \sigma_{H^+,C} \cdot H_i^+ \xrightarrow{j_C} 6 \cdot CO_2 + 6 \cdot H_2O + \sigma_{H^+,C} \cdot H_e^+$$

  where $\sigma_{H^+,C} = 12 \cdot \sigma_{H^+,R} = 120$ is the number of protons moved per catabolized glucose; $\sigma_{H^+,R}$ is the amount of protons moved per oxygen consumed and we set it to 10 as in chapter 3. We neglect in this chapter the contribution of glycolysis to glucose catabolism[7], which only produces 2 ATP whereas protons moved through the respiratory chain can generate up to 36 ATP.
- Protons can be used for two distinct set of processes:
  - *"True"* Maintenance:

$$H_e^+ \xrightarrow{j_M} H_i^+$$

    Which itself is a coarse grained reaction. Indeed the rate j_M is given by a submodel of how a cell maintains its cellular homeostases: PMF, pH_i and osmotic pressure. Correspondingly, this maintenance terms discounts the energy required for any maintenance process other than the maintenance of PMF, pH_i and osmotic pressure. We shall use the simplified model of *E. coli*'s electrophysiology introduced in chapter 3, such that when we study the behaviour of the model as a function of

[7] Only when glucose is respired, in which case the ATP yield coming from glycolysis is negligible. When we study non respiratory catabolism, we do not ignore glycolysis as it becomes an important contribution to the ATP yield of non respiratory catabolisms.

pH_e, salinity, PMF, pH_i and osmotic pressure that are maintained the maintenance rate is given by:

$$j_M = \underbrace{2 \cdot j_{\mathrm{ClcA}} + 3 \cdot j_{\mathrm{NhaB}} + 2 \cdot j_{\mathrm{NhaA}}}_{\text{Antiporters}} + \underbrace{j_{\mathrm{H^+}} - j_{\mathrm{OH^-}}}_{\text{Leakage}}$$

where the fluxes of the antiport reactions are chosen so that j_M is optimal (*i.e.* are picked so that j_M has the minimal possible value; that is given PMF, pH_i, osmotic pressure sought to be maintained and extracellular pH and salinity) as explained in chapter 3. Note that we refer to it as *"true"* maintenance because as opposed to the maintenance coefficient introduced in Eq. (II.2), j_M is rigorously a component of the physiological maintenance in the sense of [60]. In this model we shall ignore other possible contributions to maintenance cost, such as the turnover of RNA, DNA, proteins which we will assume are negligible[8]. It is by the way likely reasonable to neglect turnover of RNA, DNA and proteins during the exponential phase of growth as the amount of energy required for biosynthesis of one cell is enough to sustain maintenance expenditures during stationary phase for 20 days [261], which is orders of magnitude less than the maintenance rate we predict for electrophysiological maintenance, *i.e.* nearly 50% per hour of the energy required for doubling in exponentially growing *E.coli* on glucose, see appendix Eq. (F.84)[9]. Note that in addition to the values for PMF, pH_i and osmotic pressure that are maintained and the environmental composition j_M also depends on the set of ionic transporters that are available and on the permeability of the membranes for each of the ions.

– ATP synthesis *via* $F1F_o$:

$$\sigma_{\mathrm{H^+,F1F_o}} \cdot \mathrm{H_e^+} + \mathrm{ADP} \xrightarrow{j_{\mathrm{F1F_o}}} \sigma_{\mathrm{H^+,F1F_o}} \cdot \mathrm{H_i^+} + \mathrm{ATP}$$

[8]By turnover I mean here replacing proteins that are degraded. For high enough half life of macromolecules the energetic cost of relacing those that get degraded becomes negligible. For half-life of those macromolecules identical to the average half-life of proteins in *E.coli* (20 hours [260], it is equivalent to ignoring $1/(2 \times 20) \times$ biosynthetic cost $\approx 3.75 \times 10^8$ ATP per cell per hour (where we assume biosynthetic cost of 15 billions ATP per cell), which is quite small in comparison to the cost of electrophysiological maintenance as we shall see later.

[9]Note that since those predictions rely heavily on the permeability of the membrane to different ionic species (which has been measured with high level of uncertainty), our predictions are to be taken carefully.

and we will use $\sigma_{\mathrm{H}^+,\mathrm{F1F}_o} = 3.3$ as in chapter 3.

- Finally, the model includes a reaction for biosynthesis, which consumes ATP to turn intracellular sugar into a fraction $1/\sigma_{s,A}$ of a cell with mass m_0:

$$\sigma_{\mathrm{ATP},A} \cdot \mathrm{ATP} + s_i \xrightarrow{j_A} \frac{1}{\sigma_{s,A}} \cdot m_0$$

This abstraction for the "growth" reaction is worth discussing further. First, we pick mass per cell of reference $m_0 = 258 \times 10^{-15}$ grams; such that all the fluxes are expressed in units reaction per time per cell of mass m_0. Second, $6 \times \sigma_{s,A} = 6 \times 1.1 \times 10^9$ holds for the number of carbon atoms in a cell of mass m_0, assuming 50% of a cell's mass is made of carbon [262]. Note that we implicitly assume any other substrate than sugar and ATP for biosynthesis are always in excess and are incorporated in biomass according to the elemental composition of the cell. Third, $\sigma_{\mathrm{ATP},A} = 15.45$ is the ATP cost of turning 6 carbon atoms under glucose form to 6 carbon atoms into final biomass product form. It is evaluated assuming biosynthesis cost of the cell derived by [263] corrected for the cost of producing lipids, see Appendix Eq. (F.71). The ATP cost of making biomass $\sigma_{\mathrm{ATP},A}$ is not expected to be a true invariant of a cell. Indeed, one would for instance expect that this would decrease significantly as amino acids or ribonucleotides are readily provided in the medium thus cutting down the energetic cost of turning raw materials (sugar, nitrogen) into high-end valuable biosynthetic products (amino acids, ribonucleotides). Also, different amino acids do not have the same ATP cost per mass, thus tuning the amino acid composition of the proteome may be a way to modulate $\sigma_{\mathrm{ATP},A}$ as suggested by [264].

Steady-State Growth-Rate and Yield At balanced growth (invariant intracellular composition per unit of mass), assuming the intracellular quantities of intermediary molecules (s_i, H^+_i, ATP) are negligible, the growth-rate and growth-yield of the model follow (see Appendix sections. F.1 and F.3):

$$\mu = \max\left(\frac{1}{\sigma_{s,A}} \cdot \frac{\sigma_{\mathrm{H}^+,C} \cdot j_C - j_M}{\sigma_{\mathrm{H}^+,\mathrm{F1F}_o} \cdot \sigma_{\mathrm{ATP},A}}, 0\right) \geq 0 \tag{III.1}$$

$$Y = \frac{1}{1 + \dfrac{\sigma_{\mathrm{H}^+,\mathrm{F1F}_o} \cdot \sigma_{\mathrm{ATP},A}}{\sigma_{\mathrm{H}^+,C}} + \dfrac{j_M}{\sigma_{s,A} \cdot \sigma_{\mathrm{H}^+,C} \cdot \mu}} \tag{III.2}$$

Where the growth-rate is set to 0 if the maintenance expenditures j_M exceed the catabolic flux – in proton per hour per cell – $\sigma_{\mathrm{H}^+,C} \cdot j_C$. We use "growth-yield" in this chapter to talk in fact of the *carbon yield*, a.k.a. the fraction of internalized carbon that is incorporated into biomass or the ratio of the biosynthetic flux to the transport flux: j_A/j_T.

Finite Proteome Constraints We shall now take into account the tradeoff between allocation of biomass to catabolic enzymes or biosynthetic enzymes in the fashion of [99]. We shall however still consider that transport, maintenance and F1F$_o$ fluxes can be maintained with very little biomass allocated to their respective enzymes such that whatever transport, maintenance or F1F$_o$ flux that is required will be achieved without modulating the availability of biomass. We then assume that catabolic and biosynthetic enzymes account for a fixed fraction of the biomass ϕ_p[10]:

$$\phi_C + \phi_A = \phi_p \tag{III.3}$$

where ϕ_C, ϕ_A are the mass fraction made of catabolic, biosynthetic enzymes respectively and $1 - \phi_p$ is the fixed mass fraction allocated to other functions (lipids, metabolites, DNA, mRNA, other enzymes). The rates of catabolism and biosynthesis are assumed to be 1-order kinetic models:

$$j_C = \phi_C \cdot \varepsilon_C \tag{III.4}$$

$$j_A = \phi_A \cdot \varepsilon_A \tag{III.5}$$

where $\varepsilon_C = 4.4 \times 10^9$ sugar per hour per cell of mass m_0 corresponds to the catabolic rate if 100% of cellular mass is dedicated to catabolism. Likewise ε_A corresponds to the biosynthetic rate if 100% of the cell mass is dedicated to biosynthesis. We fit ε_A according to appendix Eq. (F.83), see fig. 13 to guarantee that, given values for ϕ_p, the ATP cost of biosynthesis $\sigma_{\mathrm{ATP},A} = 15.45$ and the number of carbon atoms $6 \times \sigma_{s,A} = 6 \times 1.1 \times 10^9$ per m_0, the doubling rate and catabolic flux j_C are identical to that measured by [232] for *E.coli* on glucose. We then set $\phi_p = 50\%$ as assumed by [92, 265, 99] and find the corresponding catalytic efficiency of biosynthesis $6 \times \varepsilon_A = 6 \times 1.8 \times 10^9$ carbons incorporated into biomass per hour for m_0 mass invested in biosynthetic enzymes.

[10]Equivalent assumption than in [99] if if biosynthetic enzymes are identified as ribosomes.

Finally, we can derive the solution that guarantees equal production and consumption of ATP, see appendix subsection F.3, as:

$$\boxed{\phi_A = \begin{cases} \dfrac{a \cdot [b \cdot \phi_p - j_M]}{1 + a \cdot b} & \text{if } j_M < b \cdot \phi_p \\ 0 & \text{if } j_M \geq b \cdot \phi_p \end{cases}} \tag{III.6}$$

where $\phi_C = \phi_p - \phi_A$ and we defined a and b to simplify the equation as:

$$a = \frac{1}{\varepsilon_A \cdot \sigma_{\mathrm{H^+},\mathrm{F1F_o}} \cdot \sigma_{\mathrm{ATP},A}} \tag{III.7}$$

$$b = \sigma_{\mathrm{H^+},C} \cdot \varepsilon_C \tag{III.8}$$

The growth-rate follows:

$$\mu = \frac{1}{\sigma_{s,A}} \cdot j_A = \frac{1}{\sigma_{s,A}} \cdot \phi_A \cdot \varepsilon_A \tag{III.9}$$

The growth yield is still computed according to Eq. (III.2). We are now set for discussing the behaviours of the model.

ii. Relation of our Model to Pirt's Growth Law

The first interesting result of this chapter is to reinterpret the empirical parameters from Eq. (II.2) within the scope of our model. Indeed, our model reproduces Pirt growth law Eq. (II.2) given the maintenance coefficient m and the maximal growth yield are:

$$m = \frac{j_M}{\sigma_{s,A} \cdot \sigma_{\mathrm{H^+},C}} \tag{III.10}$$

$$Y_G = Y(j_M = 0) = \frac{1}{1 + \dfrac{\sigma_{\mathrm{H^+},\mathrm{F1F_o}} \cdot \sigma_{\mathrm{ATP},A}}{\sigma_{\mathrm{H^+},C}}} \tag{III.11}$$

which we obtain by equating Eqs. (II.2) and (III.2). Eq. (III.10) solves the problem raised by [60] and in the introduction that the maintenance coefficient depends on the choice of catabolism and the amount of carbon storage. Indeed, here m is shown as a function of a "true" component of physiological maintenance j_M, depends on the choice of catabolism *via* $\sigma_{\mathrm{H^+},C}$ (a.k.a. catabolic yield) and the amount of carbon stored *via* $\sigma_{s,A}$ and $\sigma_{\mathrm{ATP},A}$. Indeed $\sigma_{s,A}$ is expected to change

as storage of carbon occurs as the molecular form under which carbon is stored will not necessarily have the same elemental composition than the rest of the biomass; likewise $\sigma_{\mathrm{ATP},A}$ should change in response to an accrued fraction of the biomass made of molecules under which carbon is stored, indeed there are no reasons whatsoever for the ATP cost of incorporating one sugar under carbon storage molecule to be identical to the ATP cost of incorporating 6 carbons from the sugar into other components of the biomass[11].

The maximal yield Eq. (III.11) is in the scope of the model, instead of usually being determined as an empirical parameter, expressed as variables that characterize the cell's behaviour in a given environment. Indeed, the maximal yield in the model is a function of the choice of catabolism *via* $\sigma_{\mathrm{H}^+,C}$ and on the energetic cost of biosynthesis $\sigma_{\mathrm{ATP},A}$. Shift to a less efficient catabolism (lower $\sigma_{\mathrm{H}^+,C}$) will typically result in lower maximal yield. On the opposite, lower energetic cost of biosynthesis which is typically expected if building blocks of macromolecules (*e.g.* amino acids, ribonucleotides) are readily available in the medium thus do not need to be anabolized by the cell[12]. For the chosen stoichiometries of the reaction of biosynthesis, the maximal yield is $\approx 70\%$ when glucose goes through aerobic respiration.

Note that the catabolic yield in ATP equivalent is given by $\sigma_{\mathrm{H}\cdot C}/\sigma_{\mathrm{H}^+,\mathrm{F1F}_o}$ (≈ 36 ATP per glucose for aerobic respiration) such that Eqs. (III.10) and (III.11) can be written as functions of the ATP catabolic yield rather than the proton catabolic yield.

iii. Dependence of Growth-Rate on Electrophysiological Variables

With the growth-model in hand, we now seek to evaluate how the growth-rate depends on the variables that composed the model of *E.coli* electrophysiology from chapter 2:

1. The Environmental Variables: extracellular pH and salinity.

[11] In other words, the ATP cost of turning 6 carbons atoms from glucose into *e.g.* 6 carbon atomes under glycogen form is not the same ATP cost than incorporating 6 carbon atoms from glucose into 6 carbon atoms under proteins, rRNA, DNA form, so varying the fraction of the mass of the cell that is glycogen should impact the ATP cost of replicating this cell.

[12] Note that we neglect in this case the ATP cost of importing high value substrates (for instance amino acid) into the cell, indeed the energetic cost of transport does not exceed 1 ATP equivalent (from *E.coli* transporters belonging to the ABC superfamily [266] taking ATP cost from the corresponding transporters in ecocyc).) while the ATP cost of making an amino acid from scratch is about 15 ATP.

2. The Homeostatic Variables: Intracellular pH and PMF.

3. The Cellular Properties: the permeability of the membrane for each ionic species.

Before we do that, we first briefly describe how the model responds to varying energy requirements imposed by the maintenance of electrophysiological homeostases.

Qualitative response of the model to increased maintenance cost. We first draw a scheme of the model described before figure 3.3 (A), where the cell can tune how the biomass is partitioned into biosynthetic and catabolic capabilities in response to varying maintenance cost, imposed by the model of *E.coli*'s electrophysiology. We show in fig. 3.3 (B) how the model qualitatively responds to increased maintenance cost with respect to how it partitions its mass between catabolic and biosynthetic enzymes and how it partitions its energy between maintenance and biosynthetic energy. As the maintenance energy requirement increases an accrued fraction of the model's biomass is dedicated to energy production at the detriment of biosynthetic enzymes. The pool of available energy increases but a higher fraction of it is dedicated to maintenance, while the absolute amount of biosynthetic energy decreases to match the decreased rate of biosynthesis due to less mass being invested in biosynthetic enzymes. This results in decreasing growth-rate and growth-yield upon increase in maintenance cost.

Growth-rate shows a catalytic-limiting regime and an energy-limiting regime. We then look in figure. 3.4 at how the doubling rate is expected to change as a function of extracellular pH when tuning different variables the cost of electrophysiological maintenance is a function of. The growth-rate is computed using Eq. (III.1), and its variations reflect the change of the maintenance cost j_M in different environments (pH_e, salinity), for different electrophysiological states sought to be maintained (PMF, pH_i), for different properties of the membrane (permeability to each ion) shown in chapter 3. We use Eqs. (III.6)–(III.9) to compute the growth-rate.

We first observe there are two regimes for how the growth-rate depends on extracellular pH: *(i)* a near-plateau around the pH_e at which growth-rate is maximized, around which the growth-rate has low sensitivity to pH_e variations

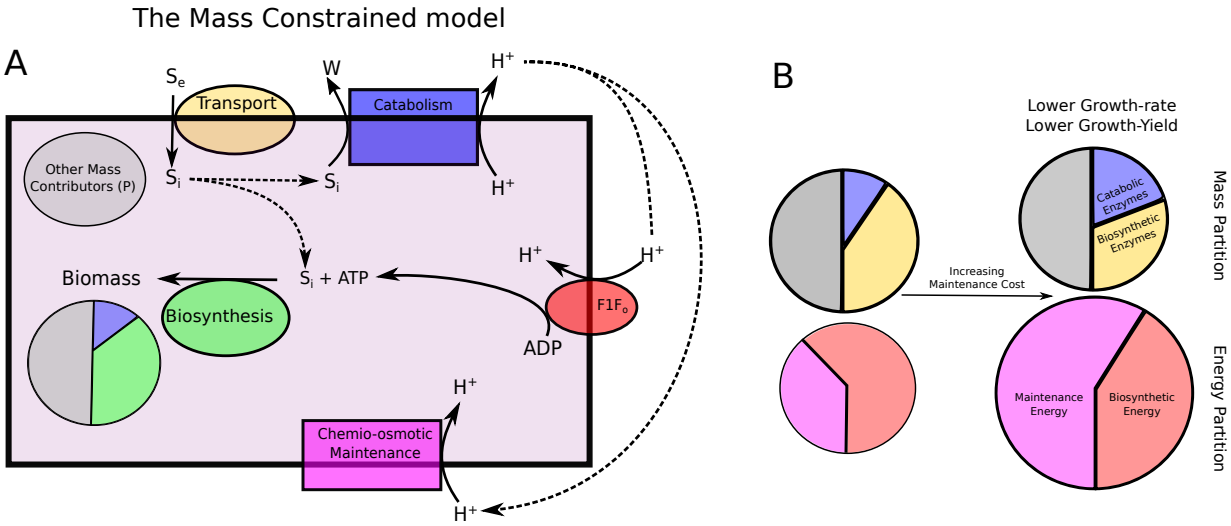


FIGURE 3.3: (A) The growth model, Consisting of reactions (F.1) to (F.5). Sugar is transported in the cell then is partitioned between energy generating processes (catabolism and F1F$_o$) and biosynthetic processes. Energy (at the Proton gradient layer) is partitioned between maintenance and biosynthetic processes. We assume contributions to the cell mass of transporters, F1F$_o$, maintenance enzymes are negligible. (B) The mass of the cell is distributed between catabolic enzymes with mass fraction ϕ_C, biosynthetic enzymes with mass fraction ϕ_A and other contributors to the mass which function is not described with fixed mass fraction $1 - \phi_p = 0.5$. (A) Adaptation (qualitative) of the mass constrained model to an increase in maintenance cost. As maintenance cost increase, the model increases its mass fraction allocated to catabolic enzymes, increasing in the process the total amount of energy available. It also consequently decreases the amount of mass available for biosynthetic processes thereby decreasing the growth-rate.

and subsequently to increased maintenance cost and *(ii)* a regime where growth drops abruptly in a similar fashion when pH_e deviates significantly from its optimal value (value at which growth is maximized). In the plateau regime, the growth-rate is limited by the availability of biosynthetic enzymes and large increase in energy production can be performed for a relatively small fraction of biosynthetic enzymes substituted by catabolic enzymes, *i.e.* it takes $\approx 25\%$ decrease in ϕ_A (and thus in μ) to make the double of the catabolic flux of reference $j_C = 5.1 \times 10^8$ protons per hour per cell which accommodates a $\approx 350\%$ increase from the maintenance cost of reference for which the doubling rate = 0.89 per hour. This translates in near growth-rate invariance on the maintenance cost in environments with near neutral pH_e and low enough salinity. This motivates an assumption that is sometimes made by some authors [100], that the maintenance cost is negligible. In fact, this assumption is relevant in environments where the maintenance cost is low enough, as expected by the growth-media they use (relatively low salinity and near neutral pH_e. As we see here, this assumption needs to be alleviated as soon as the cost of maintaining the electrophysiological state becomes high enough, as we predict is the case in environments bearing high salinity and far from neutrality pH_e.

Drop in PMF is Predicted to be an Adaptive Strategy to alkaline challenge but not to acidic challenges As we showed in chapter 2, making the PMF closer to 0 reduces the maintenance cost. Therefore at pH_e values importantly deviating from neutrality, decreasing the PMF (closer to 0) allows reduction of the maintenance cost and subsequent increase in the growth-rate as depicted in figure 3.4 (A). We however do not account here for the fact that the ability to respire is PMF-dependent: in this model, transduction of energy from NADH to ATP occurs independently of the PMF. We should come back to this topic at the end of the chapter. Be as it may, decrease in the PMF significantly increases the growth-rate at slightly alkaline pH_e (8.15 and 8.45). This could explain why we experimentally observed a drop in PMF subsequent to alkalinization of the medium in chapter 2. Notably, while reduction of the PMF allows rescue of growth-rate at slightly alkaline pH_e, such is not the case at slightly acidic pH_e. Per the results of figure 3.4 we indeed expect no significant increase in growth-rate due to a shift from -150 to -50 mV PMF in the acidic range. Thus we expect PMF reduction to be an adaptive strategy in alkaline range but not in acidic range. Consistent with our prediction low PMF values

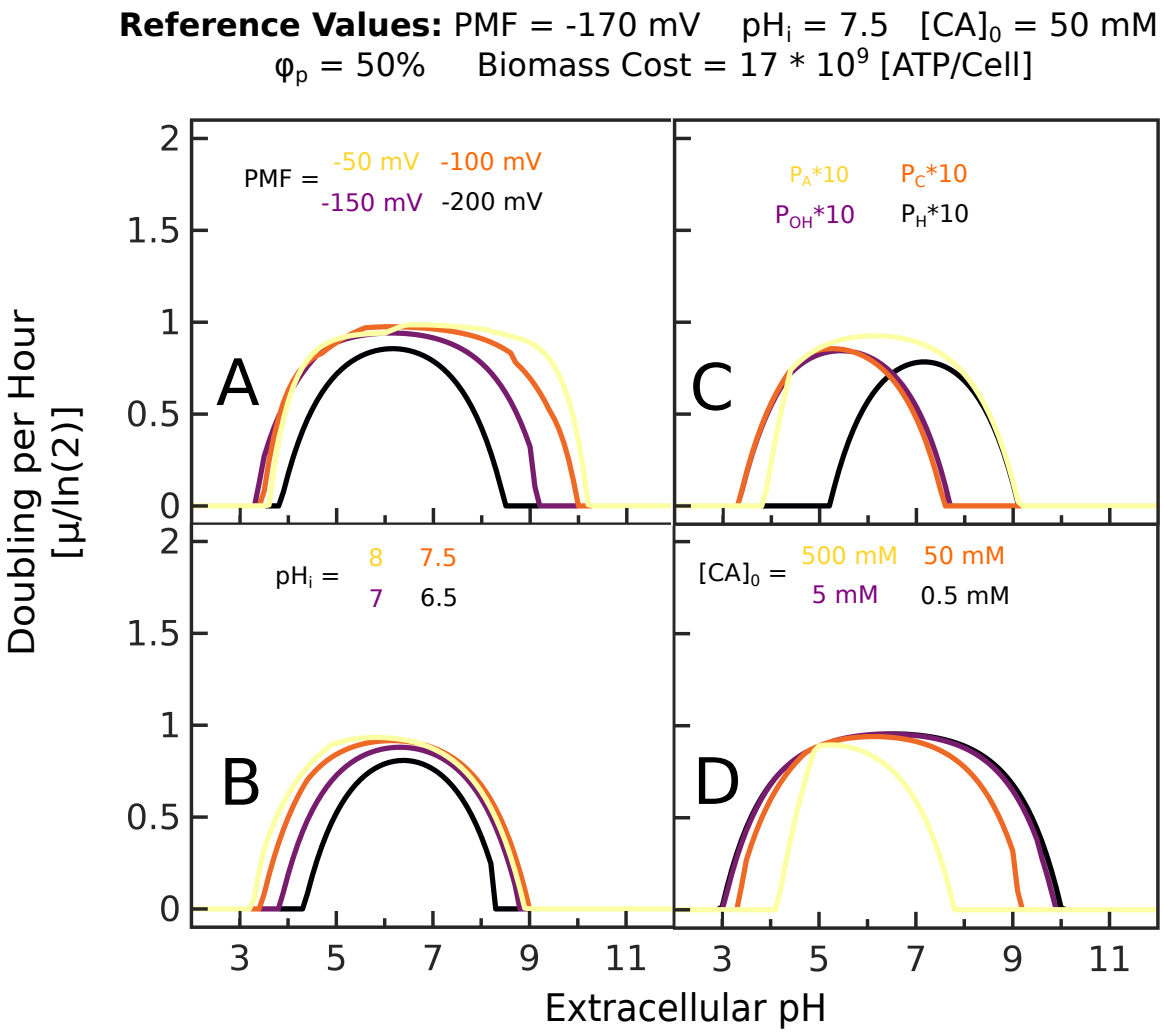


FIGURE 3.4: The catalytic efficiency of catabolic processes is $\varepsilon_C = 4.4 \times 10^9$ catabolized sugar per hour per m_0 mass invested in catabolism. The mass fraction allocated to non-catabolic, non-biosynthetic processes is $\phi_p = 0.5$, the corresponding catalytic efficiency of biosynthetic processes is $\varepsilon_A = 9.9 \times 10^8$ sugars (carbon atoms equivalent) incorporated into biomass per hour per m_0 mass invested in biosynthesis (guaranteeing the state of reference from [232]). The maintenance cost is computed as a function of extracellular pH, salinity, PMF/osmotic pressure/pH$_i$ maintained as in chapter 2 for permeabilities of reference $P_{H^+} = P_{OH^-} = 10^{-4}$ m/s, $P_{C^+} = 5 \times 10^{-10}$ m/s, $P_{A^-} = 1.5 \times 10^{-8}$ m/s and osmotic pressure of 1 atmosphere. At some pH$_e$, maintaining the chosen pH$_i$ may be too costly for the model, in such cases the model will maintain the closest pH$_i$ possible to the chosen value given its energetic capabilities. The different figures are doubling rates as a function of extracellular pH for (A) different PMF maintained, (B) different pH$_i$ maintained, (C) increase of each permeability by a factor 10 when compared to the permeabilities of reference, (D) different salinities.

are reported in alkalinophiles whereas acidophiles are able to maintain high PMF [4][13].

Slightly Alkaline Intracellular pH Maximizes the Growth-Rate We then look at figure 3.4 (B), and observe that the growth-rate is maximized for slightly alkaline pH_i values (with no visible difference between 7.5 and 8). This could explain why *E.coli* indeed maintains pH_i around 7.5 [11]. Note that we do not take into account here any other effect of pH_i than the cost of maintenance. Shall neutral pH_i be optimal for, *e.g.* functioning of biochemical processes, the effective pH_i a cell "decides" to set would be a compromise between optimizing biochemistry proper functioning and minimization of the maintenance cost.

Impact on Growth of Ionophores is Specific to their Affinity to Each Ions and the Extracellular pH The growth-rate is now evaluated as before at different pH_e, however for increase of the permeability to the different types of ions composing the model. While increasing permeability to small anions is only detrimental is a narrow very acidic pH_e range, increase in permeability of small cations impairs growth-rate in a large range of pH_e 5–9. This is because maintenance of PMF and pH_i above $pH_e \approx 5$ entails negative membrane voltage, thus maintenance of Cationic Motive Force (CMF) and only when the cell maintains CMF, the maintenance cost depends on permeability of the membrane for small cations. In that range, no Anionic Motive Force (AMF) is required to optimally maintain the electrophysiological state and thus modulating the permeability for anions has no impact on the maintenance cost thus the growth-rate.

Increase in permeability to hydroxide ions/protons specifically impairs growth-rate in the alkaline/acidic range respectively. This is due to higher concentrations of hydroxide ions/protons in the alkaline/acidic range and thus higher sensitivity of the absolute maintenance cost on increasing permeability for hydroxide ions/protons.

Should one have ionophores that are specific to different types of ions and aiming at using them to impair growth-rate, we give here a rule of thumbs for selection of the ionophore to use depending on the pH_e the bacteria is in.

[13] Certainly those behaviors could be due to other phenomenons than the one we are hypothesizing, though our hypothesis is consistent with these observations.

Acidifying pH is Predicted to Rescue Growth-Rate at High Salinity How the growth-rate varies with extracellular pH for different salinity of the medium is shown in figure 3.4 (D). Interestingly, while high salinity is detrimental to growth-rate for extracellular pH below 5 or above 6, in between these values, the growth-rate is approximately invariant by variations of the salinity. In fact, this corresponds to a range of pH_e for which simultaneous maintenance of $pH_i = 7.5$ and PMF $= -170$ mV entails near 0 membrane potential. Since increase in salinity specifically increases the cost of maintaining the CMF and AMF, since to achieve near 0 voltage the optimal behaviour is to maintain null CMF and AMF, in the pH_e range corresponding to near 0 voltage the maintenance cost has low sensitivity on salinity changes. Therefore in that pH_e range, it is predicted that salinity does not impair growth-rate. This predicts a counter-intuitive behavior, that is shifting pH_e from 7 to 5 would increase the growth-rate at high salinity.

Loss of Catabolic Regulation Predicts Increased sensitivity to pH challenges. Figure 14 is a twin plot of figure 3.4 but for a model with fixed catabolic flux, *i.e.* a model unable to shift the proteome allocation from biosynthesis to catabolism upon increased in maintenance requirements. Unsuprisingly, the model predicts much more narrow growth-permissive pH_e ranges. Perhaps suppressing fundamental components of the catabolite repression pathway in *E.coli* [267] could yield similar pH-dependency of growth in the Wild-Type *versus* the modified strain.

iv. Geometry-Dependent Cost of Maintenance Predicts Cell Cycle-Dependent Metabolic Oscillations and Environment-Dependent Distributions of Growth-Rates

We so far considered a cell with fixed surface to volume ratio when computing the maintenance cost of electrophysiological maintenance. It was shown however in chapter 2, that such a maintenance cost increases proportionally to the surface to volume ratio.

Spherical Shapes Decrease Maintenance Cost We show in figure. 3.5 (A) how the maintenance cost of maintaining an identical electrophysiological state depends on the cellular shape for different cellular volumes. The maintenance cost of reference is defined as the cost of performing electrophysiological maintenance

for a spherocylindric shaped cell with 3:1 length to width ratio of mass m_0 (corresponding to reference volume of $\approx 3.0\mu\text{m}^3$). We see that the "winner" shape when it comes to minimization of the maintenance cost for a given volume is the sphere whereas increasing length to width ratio spherocylinders have higher maintenance cost. Should a cell be able to modulate its shape, we expect that decreasing its surface to volume ratio, by for instance turning into a sphere, would be a viable strategy to mitigate the increased in maintenance costs seeding from *e.g.* high salinity, acidic or alkaline challenges[14].

Maintenance Cost is Dependent on the Position in the Cell Cycle We next consider that if a cell is shaped as a 3:1 length to width ratio spherocylinder (as is *E.coli* [29]) and conserves this shape all along its cell cycle, then its surface to volume ratio, thus its maintenance cost requirement, shall depend on its position in the cell cycle[15]. We show such a dependency between position in the cell cycle and maintenance requirement in figure. 3.6 (B), assuming the electrophysiological state maintained by the cell and therefore its maintenance cost per surface to volume ratio is invariant by the position in the cell cycle. As a cell grows and gets closer to division it is expected to have decreasing maintenance requirements. Perhaps this is a plausible explanation to why oscillations in NADH with a periodicity of the cell cycle length occurs in *E.coli* [269], with lower levels of NADH (potentially indicating accrued energy demand, *e.g.* from maintenance) early in the cell cycle, qualitatively consistent with a surface to volume ratio-dependent maintenance cost.

Variability of Cell Size is Predicted to Increase at High Maintenance Cost Last, we show in (C) a length distribution of *E.coli* cells as observed by [268] on glucose (average doubling time ≈ 75 minutes). We then extrapolate in (D) a distribution of maintenance cost across cells assuming all cells have identical shape 3:1 length to width ratio spherocylinders and that the electrophysiological state maintained is identical across all cells. We then use as an input this distribution to the growth-model Eqs. (III.6)–(III.9) to show the corresponding distribution on growth-rate for different population-average maintenance cost in figure (E). Notably, we predict that, should the shape and maintained electrophysiological

[14] I would for instance expect to see more coccoids than bacilli in saline conditions.

[15] Note that we assume that the 3:1 length to width ratio as well as the spherocylindric shape are invariant along a cell cycle.

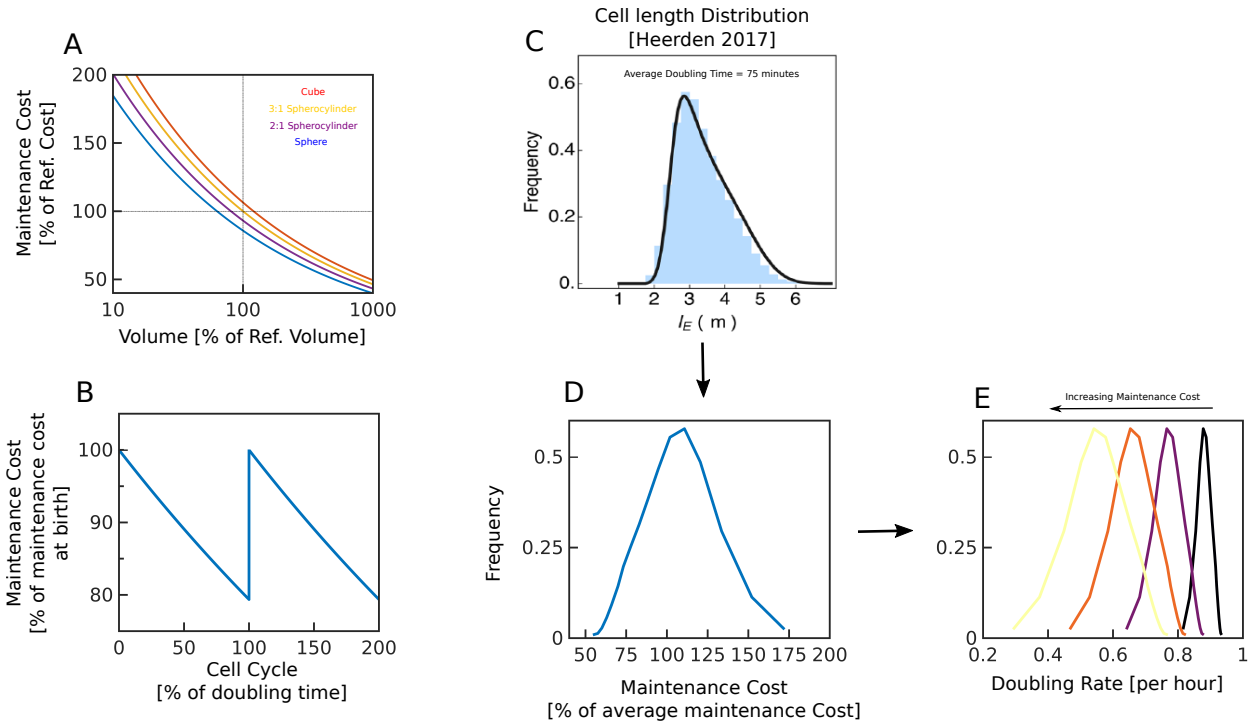


FIGURE 3.5: All the maintenance cost-dependent-variables are set (pH_i, pH_e, PMF, osmotic pressure, permeabilities) but the surface to volume ratio. The maintenance cost of reference is 27×10^9 protons per cell per hour, extrapolated from [232] and the ATP cost of biosynthesis. (A) Relative change of the maintenance cost (per volume unit) as a function of the cell volume for different cellular shapes. (B) Assuming the cell conserves a shape 3:1 length to width ratio spherocylinder all along the cell cycle, we show how the maintenance cost (relative to that of birth, per unit volume) varies as a function of the position in the cell cycle; we assume the division volume is twice the birth volume. (C) Distribution of cell length from [268] is taken then turned into a distribution for surface to volume ratio assuming invariant-by-length shape 3:1 length to width ratio spherocylinder. (D) The distribution of the maintenance cost (per unit volume) corresponds to the distribution of the surface to volume ratio because we assume all maintenance cost-dependent-variables are length-invariant but the surface and volume. (E) Assuming invariant cell size distribution by change in maintenance cost (we use the distribution from (C), thus the distribution of surface to volume ratio or on relative maintenance cost of (D)), the doubling rate distribution is computed for different maintenance cost (100%, 200%, 300%, 400% of the reference maintenance cost 27×10^9 protons per cell per hour) with the proteome constrained model.

state be invariants by change in average maintenance costs, the distribution of growth-rate shall be wider (higher coefficient of variation) in media requiring high maintenance costs.

Limitations of our Evaluation of Geometry-dependent Maintenance Cost This paragraph merely contains qualitative predictions based upon seemingly quite stringent predicates: *(a)* cell-to-cell shape (surface to ratio) invariance, *(b)* cell-to-cell electrophysiological state maintained invariance, *(c)* cell-cycle shape invariance *(d)* condition-to-condition shape (surface to ratio) invariance. It however points out to some interesting phenomena that one could observe (if the latter hypotheses are "true enough") with respect to relationship between maintenance (thus growth) and *(i)* shape maintained, *(ii)* cell cycle position, related to metabolic oscillations and *(iii)* growth-rate variability. Consistent (with these predictions) cellular adaptations could feature: transition to spherical shape when maintenance cost are high (cell at birth, acidic pH, high NaCl, *etc.*), loss of electrophysiological homeostases (to reduce maintenance cost) for small cells, *e.g.* at birth or at low growth-rate [270]. Also, in media requiring high maintenance cost, shape may become one of the dominant contributions to variability in growth-rate, a factor that could refine models seeking to predict growth-rate variability [265].

Transport/Maintenance Trade-Offs As postulated by [271], the content in membrane protein is expected to be capped so that the membrane cannot have more than 50% of its mass made of proteins. This has a potential to give a different spin to the discussion around surface to volume ratio. Indeed, one could make the postulate that increased surface to volume allows the cell to have an accrued amount of membrane proteins per mass unit, for instance transporters, enzymes involved in the respiratory chain, *etc.* Such that it is possible to imagine scenarios where the cell increases its surface to volume ratio to increase its catalytic capabilities for nutrient transport, respiratory catabolism, which leaves open the problem of whether the cell should minimize or maximize its surface to volume ratio. Indeed, should the cell minimize maintenance cost at the detriment of having *e.g.* less transporter/respiratory enzymes available ? Or perhaps should it maximize its transport and/or respiratory fluxes by increasing its surface to volume ratio at the cost of increasing its maintenance cost ? Be as it may, this choice likely depends on the cellular species and the environmental condition it is facing. We leave this topic open for further studies and won't discuss it further.

v. Growth-Rate and Yield Co-vary in a Stress-Specific Way

In this section, will directly modulate the maintenance cost j_M rather than computing it as a function of electrophysiological state of the cell, keeping in mind how j_M changes with pH_e, salinity, cellular homeostases maintained and permeabilities.

Increased Maintenance Cost Results in Higher Yield Loss than Rate when Compared to Substrate Restrictions We now characterize how the growth-rate and yield of co-vary in response to increased maintenance cost (along a line) in figures 3.7 and 3.8. While we look at how increase in maintenance cost synergizes with inhibitors of biosynthetic processes (for instance chloramphenicol) in 3.7 we look at how it synergizes with inhibitors of catabolism in figure 3.8. To that aim, we compute the growth-rate according to Eqs. (III.6)–(III.9) and the yield according to Eq. (III.2) for different pairs of catalytic efficiency of biosynthesis ε_A (figure 3.7) or catalytic efficiency of catabolism (figure 3.8) and maintenance cost j_M.

The first observation is that when subjected to increase in maintenance cost, the model predicts "faster" loss of yield than rate, in the sense that in the yield-/rate plan the lines are sublinears. This is a qualitatively different behavior than what usually observed when controlling the growth-rate *via* substrate restrictions as depicted in the left regime of figure 3.2.

We next look specifically how the two types of inhibitions (catabolic or biosynthesis) synergize with increase in maintenance cost.

At low Maintenance Cost Biosynthesis Inhibition is more Efficient at Impairing Growth-Rate than Catabolic Inhibition While decrease in the growth-rate is nearly linear with the degree of biosynthetic inhibition for any maintenance cost, see figures 3.7 (B), such is not the case with the degree of catabolic inhibition, see figures 3.8 (B). Indeed, at low maintenance cost, inhibiting catabolism has a small impact on growth-rate. This is because at low maintenance cost, a lower fraction of the proteome needs to be dedicated to catabolism than biosynthetic processes: $\approx 40\%$ for biosynthesis and $\approx 10\%$ for catabolism. Such that a 50% decrease in the efficiency of catabolism can be accommodated by

doubling the proteome fraction allocated to catabolism to make it 20%. That corresponds to a shift of proteome fraction allocated to biosynthesis from 40% to 30%, which in turns results in a $10/40 = 25\%$ decrease in growth-rate.

At High Maintenance Cost Catabolic Inhibition is more Efficient at Impairing Growth-Rate than Biosynthesis Inhibition As the maintenance cost increases, this pattern changes, and for sufficiently high maintenance cost, catabolic inhibition impairs more growth-rate than biosynthesis inhibition, as seen by comparing the high maintenance cost orange line in figures 3.7 (B) and 3.8 (B). Also, while large extent of biosynthetic inhibition are still permissive for small growth-rates, see figure 3.7 (D), such is not the case for catabolic inhibition. If it falls under a certain threshold, that is dependent on the maintenance cost, then no growth is allowed, see figure 3.8 (D). This is given by the degree of catabolic inhibition for which even for 50% of the proteome allocated to catabolism, the amount of energy produced is still insufficient to accommodate the given maintenance cost. In such scenarios, the cell would not have sufficient energy to maintain its electrophysiological homeostases, potentially leading to death.

Low/High Degree of Biosynthetic Inhibition Impairs more/less the Yield than Low/High Degree of Catabolic Inhibition A similar pattern is visible for the growth yield. Indeed, if the degree of inhibition of biosynthetic processes is low, then an equal extent of inhibition of catabolic processes decrease less the yield, as can be seen by comparing figures 3.7 (C, E) to figures 3.8 (C, E). As the degree of inhibition increases, this becomes the opposite and small increase in the inhibition of catabolism can have higher detrimental impact on the yield than equivalent inhibition of biosynthetic processes.

Perspective Offered by Characterization of Rate-Yield Covariation upon Environmental Challenges As shown in this simple model, rich interplay between different stresses can emerge. Accounting for both the growth-rate and the growth-yield allows better characterization (equivalently finer classification) of the impact of these challenges on cellular physiology. Shall one know precisely how yield and rate contribute to fitness, in an environment-dependent manner

(composition of the environment denoted by vector or matrix $[\mathbf{x}]_e$):

$$\text{fitness} = f(\text{Yield}, \text{Rate}, [\mathbf{x}]_e)$$

one would see quite different responses of the fitness function to the combinations of stresses we imposed. Perhaps, these challenges are even qualitatively different to one another, *e.g.* result in the fitness function having negative/positive sign, potentially enriching our understanding of the underlying physiological reasons to antibiotics being bactericidal or bacteriostatic.

vi. Existence of a Trade-Off between Rate and Yield Depends on the Maintenance Cost

Having two Catabolic Pathways Enable the Emergence of Trade-Offs between Growth-Rate and Growth-Yield [16]

We first notice with the model we introduced previously, that has access to only one catabolic pathway, maximizing growth-rate always resulted in maximizing growth-yield, see Eq. (III.2). We increment the model before by considering that the model has now access to two distinct catabolic pathways: the first one as before, accounting for oxidative respiration and the second as:

$$s_i + \sigma_{\mathrm{H}^+,F} \cdot \mathrm{H}_i^+ \xrightarrow{j_F = \phi_F \cdot \varepsilon_F} w + \sigma_{\mathrm{H}^+,F} \cdot \mathrm{H}_e^+ \tag{III.12}$$

where w denotes the byproducts of that catabolic pathway[17].

For a fraction γ of the catabolized sugar processed by pathway F (the alternative – to respiration – catabolic pathway), we can derive the steady-state fraction of the proteome allocated to biosynthesis as:

$$\phi_A = \frac{a \cdot (b \cdot \phi_p - j_M)}{1 + a \cdot b} \tag{III.13}$$

$$a = \frac{1}{\varepsilon_A \cdot \sigma_{\mathrm{H}^+,\mathrm{F1F}_o} \cdot \sigma_{\mathrm{ATP},A}} \tag{III.14}$$

$$b = \left(1 + \frac{\varepsilon_C}{\varepsilon_F} \cdot \frac{\gamma}{1-\gamma}\right)^{-1} \cdot \varepsilon_C \cdot \left(\sigma_{\mathrm{H}^+,C} + \sigma_{\mathrm{H}^+,F} \cdot \frac{\gamma}{1-\gamma}\right) \tag{III.15}$$

[16] This is not a novelty and is a standard expectation in the literature *e.g.* [255].

[17] For a fermentative catabolism the byproduct could be lactate, acetate, lactate, *etc.* depending on the specific pathway used by the cell.

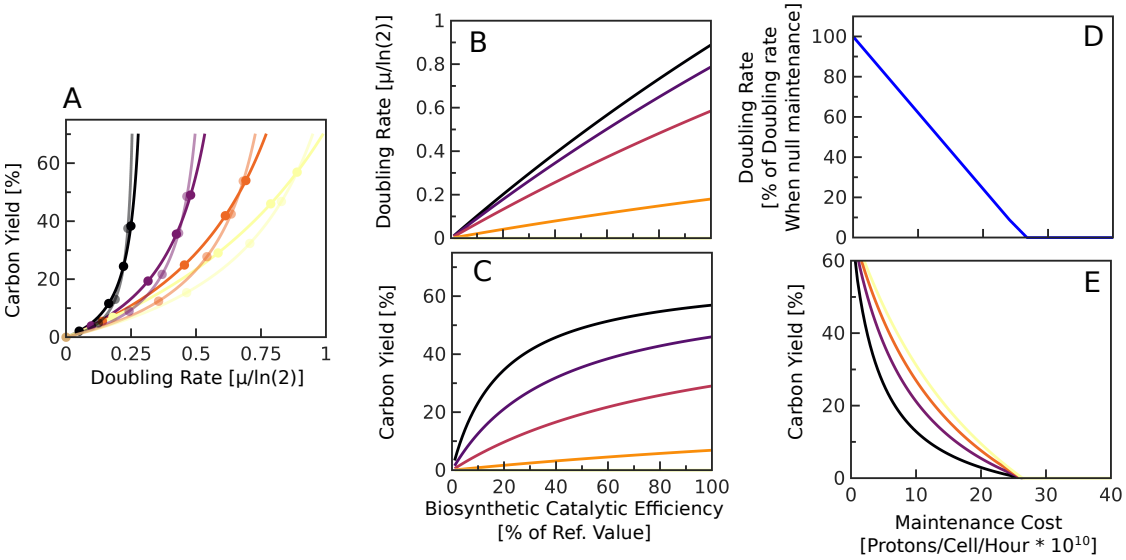


FIGURE 3.6: Interactions between biosynthesis inhibition and increased maintenance Cost. (A) Each line corresponds to a different degree of inhibition of ε_A, the catalytic efficiency of biosynthetic processes, Yellow to black 100%, 75%, 50%, 25% of the reference value $\varepsilon_A = 9.9 \times 10^8$ sugar per hour per cell. Along a line of a given color, ε_A is kept fixed and the maintenance cost increases. Different dots correspond to locations for specific maintenance cost: from right to left along a line 100%, 200%, 400%, 800% of the maintenance cost of reference 27×10^9 protons per cell per hour. The two different transparencies correspond to 2 different values of ϕ_p the mass fraction available for catabolic and biosynthetic processes. The slightly transparent lines are for $\phi_p = 0.8$, the other lines for $\phi_p = 0.5$. The catalytic efficiency of biosynthetic processes depends on ϕ_p and is 1.8×10^9 when $\phi_p = 0.5$ and 9.9×10^8 when $\phi_p = 0.8$ in units sugar incorporated per mass m_0 of biosynthetic enzymes. The chosen dependency of ε_A on ϕ_p guarantees that for any ϕ_p the doubling rate, catabolic rate and maintenance cost are identical to that of the reference behaviour from [232]. For the other figures we set $\phi_p = 0.5$. (B & C) the different lines correspond to different maintenance costs (from black to orange 100%, 200%, 400%, 800% of the reference maintenance cost 27×10^9 protons per cell per hour); (B) Doubling Rate and (C) Carbon yield as a function of the catalytic efficiency of biosynthetic processes (expressed as a % of its reference value). (D & E) As a function of the maintenance cost, for different inhibition in the catalytic efficiency of biosynthetic processes (yellow to black 100%, 75%, 50%, 25% of the reference value): (D) the doubling rate expressed for each catalytic efficiency as a fraction of the doubling rate when maintenance cost is null; with that rescaling all catalytic efficiency have the same dependency of their fractional doubling rate on the maintenance cost and (E) carbon yield.

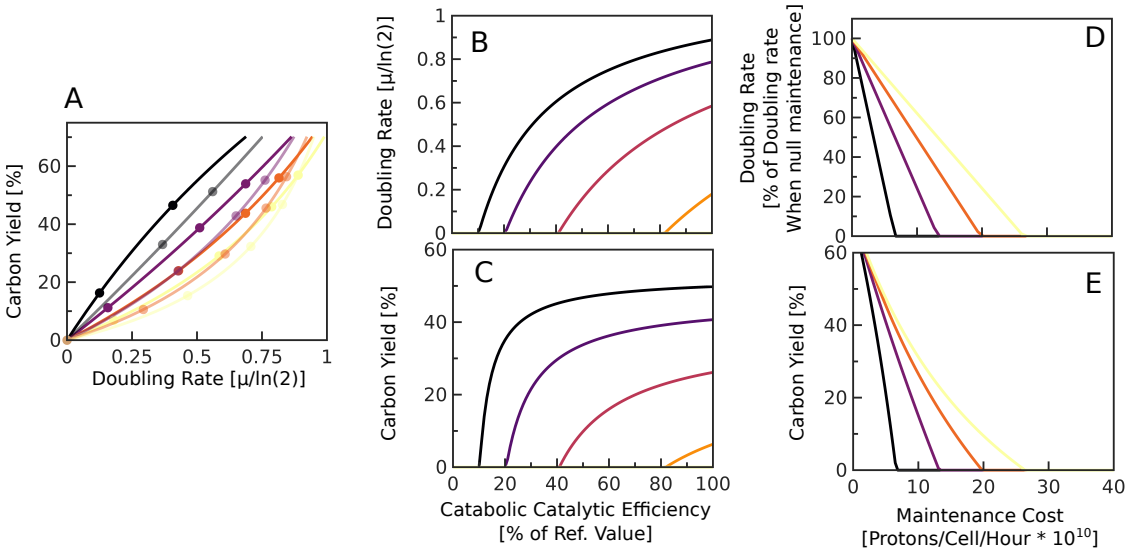


FIGURE 3.7: Interactions between catabolic inhibition and increased maintenance Cost. (A) Each line corresponds to a different degree of inhibition of ε_C, the catalytic efficiency of catabolic processes, Yellow to black 100%, 75%, 50%, 25% of the reference value: $\varepsilon_C = 4.4 \times 10^9$ sugar per hour per cell. Along a line of a given color, ε_C is kept fixed and the maintenance cost increases. Different dots correspond to locations for specific maintenance cost: from right to left along a line 100%, 200%, 400%, 800% of the maintenance cost of reference 27×10^9 protons per cell per hour. The two different transparencies correspond to 2 different values of ϕ_p the mass fraction available for catabolic and biosynthetic processes. The transparent lines are for $\phi_p = 0.8$, the other lines for $\phi_p = 0.5$. The catalytic efficiency of biosynthetic processes depends on ϕ_p and is $\varepsilon_A = 1.8 \times 10^9$ when $\phi_p = 0.5$ and 9.9×10^8 when $\phi_p = 0.8$ in units sugar incorporated per mass m_0 of biosynthetic enzymes. The chosen dependency of ε_A on ϕ_p guarantees that for any ϕ_p the doubling rate, catabolic rate and maintenance cost are identical to that of the reference behaviour from [232]. For the other figures we set $\phi_p = 0.5$. (B & C) the different lines correspond to different maintenance costs (from black to orange 100%, 200%, 400%, 800% of the reference maintenance cost 27×10^9 protons per cell per hour); (B) Doubling Rate and (C) Carbon yield as a function of the catalytic efficiency of biosynthetic processes (expressed as a % of its reference value). (D & E) As a function of the maintenance cost, for different inhibition in the catalytic efficiency of catabolic processes (yellow to black 100%, 75%, 50%, 25% of the reference value): (D) the doubling rate expressed for each catalytic efficiency as a fraction of the doubling rate when maintenance cost is null and (E) carbon yield.

see appendix F.4, where the growth yield is now defined as:

$$Y = \frac{1}{1 + \frac{j_C + j_F}{\sigma_{s,a} \cdot \mu}} \tag{III.16}$$

and the growth-rate as before by Eq. (III.9).

We then look in figure 3.8 (A,B) how various partitions of the sugar s_i between pathways C and F result in different co-variations of the rate and yield. We can see in those figures that depending on the partition of sugar between two pathways (along each line), the cell has now a choice of maximizing either rate and yield. For sufficiently low maintenance costs, a catabolism performed entirely with pathway F will maximize the rate at the detriment of the yield, while a catabolism performed entirely with pathway C will maximize the yield at the detriment of the rate.

Two conditions are required for rate/yield tradeoffs to occur: *(i)* the energetic yield of pathway F is less than that of pathway C, $\sigma_{\mathrm{H}^+,F}/\sigma_{\mathrm{H}^+,C} = \alpha < 1$ (pathway C produces more energy per catabolized sugar than pathway F) and *(ii)* In spite of the reduced energetic yield, pathway F produces energy faster than pathway C for an equivalent amount of mass fraction invested in both processes: $\varepsilon_F \cdot \alpha > \varepsilon_C$. Those two conditions have in fact previously been used to explain how a cell could maximize its growth-rate by shifting from aerobic respiration to fermentation [271, 100]. More recently, [255] showed that such a shift between respiration and fermentation could seed from a yield/rate tradeoff.

The Trade-Offs Between Yield and Rate are Maintenance Cost Dependent As visible in figures 3.8 (A, B), when the maintenance cost goes beyond a threshold value, the trade-off between rate and yield disappears and maximizing rate always results in yield maximization. We next extend our study to how shift from the pathway C (oxidative respiration) defined before to different pathways F impacts the growth-rate and growth-yield. A given pathway F is defined by its energetic yield relative to pathway C: $\alpha = \sigma_{\mathrm{H}^+,F}/\sigma_{\mathrm{H}^+,C}$ and all pathways F are assumed to have twice the catalytic efficiency for ATP production when compared to that of C: $\varepsilon_F = 2 \cdot \alpha \cdot \varepsilon_C$ which roughly corresponds to the values assumed in [100] for the difference in catalytic efficiency between fermentation and oxidative

respiration.

We then observe two phenomenons:

1. First in figures 3.8 (C, D) we see that, independently on α and the maintenance cost, shifting to pathway F always maximizes the growth-rate. The extent to which growth-rate increases by shifting to pathway F is greater at high maintenance cost.

2. Such is not the case however for the change in yield subsequent to a shift to pathway F. Indeed, as the yield decreases upon shift to pathway F, in a manner depending on the value of α at sufficiently low maintenance cost. Above a maintenance cost threshold, which depends on α, the yield is maximized by shifting to F. This counterintuitive phenomenon can be explained from [220] Eq. (II.2): the yield decreases with growth-rate, such that for low enough growth-rates, maximization of the growth-rate by shifting to pathway F offsets the expected yield reduction due to a shift to a lower yield catabolic pathway.

vii. Yield Maximization Predicts Shift to Fermentative Catabolism upon Salinity or/and pH Challenges

The Availability of some Catabolic Pathways and the Maintenance Cost Depend on the PMF We so far considered the choice of catabolic pathway and the cost of electrophysiological maintenance to be independent variables. However, as we discussed in chapter 3, the ability to respire is tied to the maintenance of high PMF values. As we saw further in chapter 2, the cost of electrophysiological maintenance decreases when maintaining lower PMF leading in fig. **??** (A) to higher growth-rates when lower PMF are maintained[18].

We now seek to apply the models developed in this thesis to their full capabilities, *i.e.* we now compare two types of cells: *(Cell A)* maintains high PMF = -200 mV, is solely performing respiratory catabolism, defined by its catalytic efficiency and energetic yield and *(Cell B)* maintains low PMF = -100 mV, is solely performing fermentative catabolism, defined by catalytic efficiency $\varepsilon_F = 12 \cdot 2 \cdot \varepsilon_C$

[18] given that both PMF allow maintenance of an identical intracellular pH.

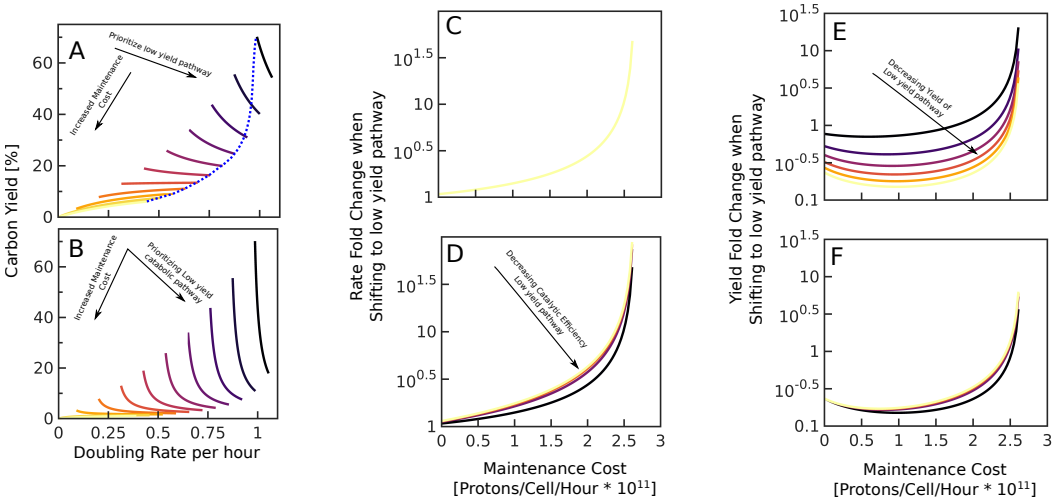


FIGURE 3.8: Two catabolic pathways. (A & B) Each line corresponds to a different maintenance cost from black 30×10^{10} to yellow 3×10^{10} protons per cell per hour with increment of 3×10^{10} when going from a line to another. Along Each line, different fraction of catabolized sugar go through catabolic pathway C or F (Right end of a line 100% of catabolism is performed by pathway F, Left end of a line 100% of catabolism is performed by pathway C). The blue line denotes an example transition from C to F and the resulting yield-rate line when increasing maintenance cost. Two catabolic pathways. (A) The second catabolic pathway F has yield $\sigma_{\mathrm{H}^+,F} = 60$ protons per sugar (or $60/3.3 \approx 18$ ATP equivalent) and catalytic efficiency $\varepsilon_F = 4 \cdot \varepsilon_C$ such that the rate of ATP equivalent production for the pathway F is twice higher than that of pathway C for equivalent amount of mass invested in each catabolic pathway. (B) The second catabolic pathways has yield $\sigma_{\mathrm{H}^+} = 10$ protons per sugar (or 3 ATP equivalent) and its catalytic efficiency is $\varepsilon_F = 24 \cdot \varepsilon_C$, such that the rate of ATP equivalent production for the pathway F is twice higher than that of pathway C for equivalent amount of mass invested in each catabolic pathway. (B & C) For different catabolic yield ratio between the two pathways $\alpha = \sigma_{\mathrm{H}^+,F}/\sigma_{\mathrm{H}^+,C} \in \{1/2, 1/4, 1/6, 1/8, 1/10, 1/12\}$ and fixed catalytic efficiency of the low yield pathway F relative to that of C (in ATP equivalent per mass invested per time): $\varepsilon_F = 2 \cdot \alpha \cdot \varepsilon_C$: (B) Fold change in growth rate when 100% of catabolism is performed by the low yield pathway relative to the rate when 100% of catabolism is performed by the high yield pathway as a function of the maintenance cost. Note that all different α yield an identical line; (C) Fold change in yield when 100% of catabolism is performed by the low yield pathway relative to the rate when 100% of catabolism is performed by the high yield pathway as a function of the maintenance cost. (D & E) For identical catabolic yield ratio between the two pathways $\alpha = \sigma_{\mathrm{H}^+,F}/\sigma_{\mathrm{H}^+,C} = 1/12$ and chaging catalytic efficiency of the low yield pathway relative to that of C: $\alpha \cdot \varepsilon_F/\varepsilon_C \in \{2, 4, 6, 8\}$ (2 black, 8 yellow). (D) Fold change in growth rate when 100% of catabolism is performed by the low yield pathway relative to the rate when 100% of catabolism is performed by the high yield pathway as a function of the maintenance cost. Note that all different α yield an identical line; (E) Fold change in yield when 100% of catabolism is performed by the low yield pathway relative to the rate when 100% of catabolism is performed by the high yield pathway as a function of the maintenance cost.

and its energetic yield $\sigma_{H^+,F} = \sigma_{H^+,C}/12$ (corresponding to fermentation). We then evaluate the electrophysiological maintenance cost of each of these cells for different pH_i maintained in a range of extracellular pH. The osmotic pressure is maintained as usual to 1 atmosphere. We then feed the maintenance cost to the growth-model Eqs. (III.6)–(III.9) to compute the doubling rate and use Eq. (III.2) to compute the yield.

Maximizing Yield but not Rate Predicts Shifts between Catabolic Pathways We then show in figure 3.9 (A,B,C,D) how these two types of cell perform for different pH_i maintained at different pH_e, fixing the salinity $[CA]_0 = 50$ mM. As discussed before, the respiratory cell has a lower rate than the fermentative cell, but has higher yield, that is in the $\{pH_i, pH_e\}$ regions it has access to. Indeed, the black regions denote the pH_i that are impossible to maintain at a given pH_e even investing all the biomass available to catabolic processes. The fermentative cell has thus access to excedent energy that allows it to grow (though a low yield) in both very acidic region ≈ 3 to ≈ 5 and alkaline region ≈ 8.5 to ≈ 9.5 although the pH_i maintained as a result deviate quite a lot from its usual homeostatic target 7.5. This may explain the PMF drop we experimentally observed in aerobic conditions that occur below pH_e 5, *i.e.* in these pH_e range the cell may chose to shift to fermentative catabolism to still sustain some growth and positive yield. The respiratory cell has however access to regions the fermentative cell has not access to, in particular to maintain slightly alkaline pH_i at acidic pH_e. This is due to the ability to generate higher voltage (and thus a wider ΔpH) at higher PMF, postulating cationic pumps are PMF-driven, as discussed in chapter 3. We further note that the growth-rate is always higher for fermentative catabolism. This is even more so than in the previous section because on top of the growth increase due to higher catabolic efficiency, the model has now also less maintenance requirements at the low PMF that is maintained in the fermentative regime. Therefore, if our model were to set its behavior in order to maximize growth-rate alone it would always perform fermentative catabolism.

Yield Maximization Predicts Shift to Fermentative Catabolism upon salinity or/and pH Challenges We then postulate the choice of catabolism to be made strictly in order to maximize yield and show in fig. 3.10 the regions in pH_e/pH_i plan for two different salinities in which the cell perform respiratory or

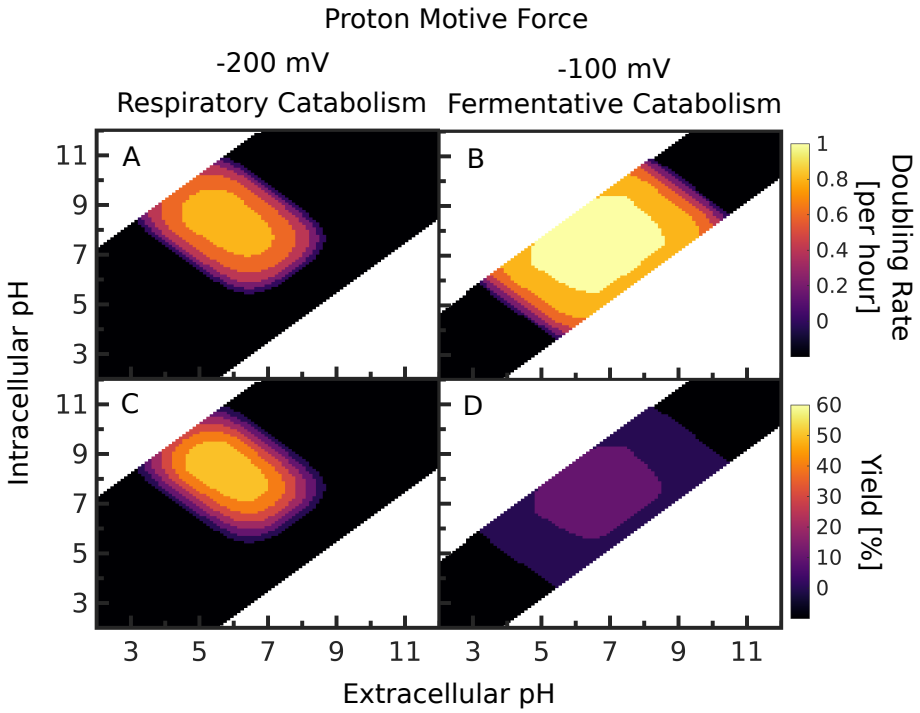


FIGURE 3.9: The cost of electrophysiological maintenance is computed for $[CA]_0 = 50$ mM, reference permeabilities, 1 atmosphere osmotic pressure and PMF, pH_e, pH_i values as indicated on the plots. The growth-rate and growth-yield are then evaluated from Eqs. (III.6)–(III.9) and Eq. (III.2). White areas correspond to regions the electrophysiological model is structurally not able to maintain (even with unlimited energy supply). Black areas correspond to area the model is not able to maintain due to the cost of maintenance exceeding the energy producing capabilities of the model.

fermentative catabolism. As discussed before, the cell should shift to fermentative catabolism at pH_e values that deviates significantly from neutrality, with a resulting pH_i quite far apart its homeostatic target. The point here is rather to compare the two different salinities [CA] = 50 mM *versus* 500 mM and to see that at high salinities, there is a wider area in which the cell should perform fermentative rather than respiratory catabolism. Should the cell indeed shift to fermentative catabolism as pH_e deviates sufficiently from neutrality, we predict that this shift should occur nearer neutral pH_e for higher salinities.

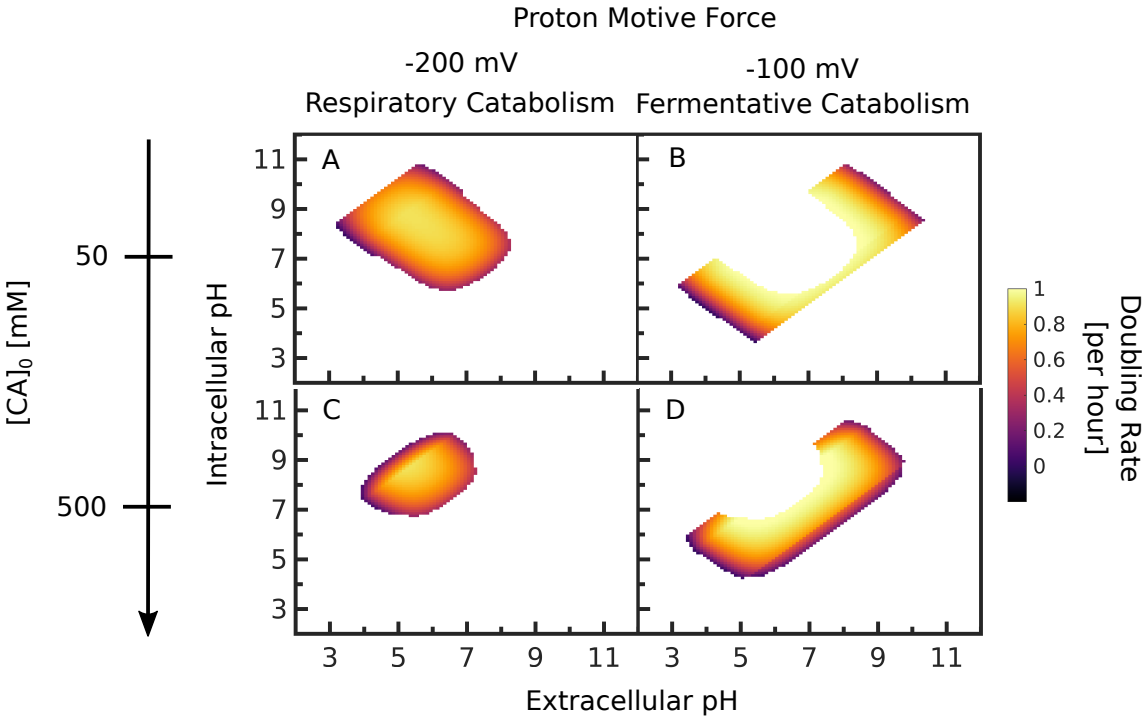


FIGURE 3.10: The cost of electrophysiological maintenance is computed for $[CA]_0 = 50$ mM (A & B) or 500 mM (C & D), reference permeabilities, 1 atmosphere osmotic pressure and PMF, pH_e, pH_i values as indicated on the plots. The growth-rate and growth-yield are then evaluated from Eqs. (III.6)–(III.9) and Eq. (III.2). We only show regions that the cell is able to maintain and wherein the choice of catabolism maximizes the yield (relative to the other catabolic pathway).

IV. DISCUSSION

In this chapter we developed an increasingly complex (although still relatively simple in its most complex form) model, see Fig. 3.11, eventually encompassing two mechanisms by which electrophysiology and growth are related, namely:

1. The energy the cell needs to spend to maintain time-invariant, electrophysiology-related cellular homeostases, namely osmotic pressure, PMF and intracellular pH[19].

2. The PMF-dependent ability to use a high yield catabolic pathway (a.k.a. respiration).

This is surely a simplification. Additional mechanisms by which growth and electrophysiology are related shall include: (1) pH_i-dependent cell ability to survive/grow; (2) dependence of the amount of oxidative damage on respiratory activity [272]; (3) PMF-dependent ability to internalize nutrients; (4) PMF-dependent ability to move (*via* flagella motors), thus to grow/survive in spatially structured environments; (5) PMF-dependent ability to use drug efflux pump, thus to survive/grow upon antibiotic challenge *etc.* all of which we completely ignore in this thesis. Crucially, we also entirely neglected –other than electrophysiological maintenance– any non-growth (as in not directly related to biosynthesis) associated function requiring energy to function, an example of which is powering flagella to move around.

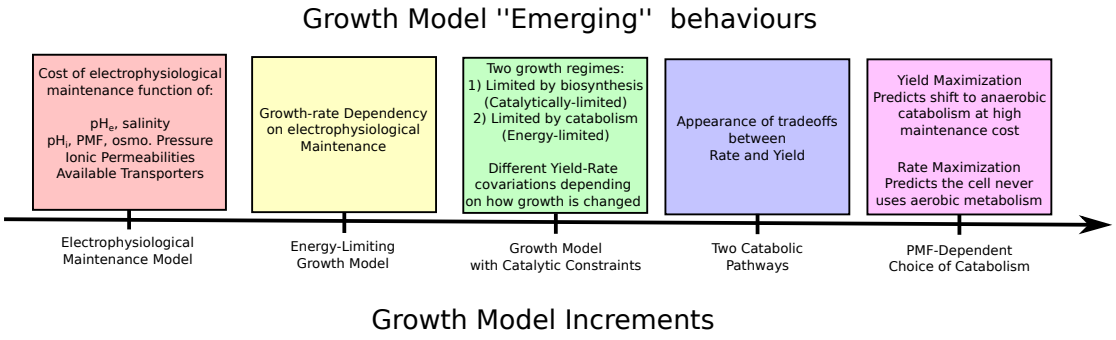


FIGURE 3.11: Summary of the model's development across this chapter and the corresponding emerging behaviours. The Energy-limiting growth model (Yellow) corresponds to the model without catabolic adaptation, behavior of which is shown in figure 2 in appendix F.

Comparison of our models with other growth-models. The distinction between growth-related (to power biosynthetic processes) and non-growth-related (a.k.a. maintenance) energy expenditures is not new and has seeded a body of literature

[19] As discussed extensively across this thesis, depending on the PMF and pH_i values the cell maintains, the ionic composition of the environment, the permeability of the membrane to various ions, and the types of transporters the cell has access to, the cost of electrophysiological maintenance changes. Evaluation of the electrophysiological cost of maintenance as a function of its dependent variables mentioned above was done of the purpose of chapter 3.

that, among other things, focuses on explaining how growth-rate and growth-yield of a cell population covary upon certain perturbation of the medium [220, 255]. This has been however largely ignored in the most recent developments of microbial physiology, which focus on a single tradeoff emerging from the finite quantity of biomass available for catalysis, that needs to be distributed for distinct necessary functions to grow [99, 273, 92, 251]. These models often assume a single intermediary between the growth substrate and the end-products of biosynthesis (proteins, RNA, DNA, lipids) which intrinsically makes any identification of this intermediary ambiguous. Indeed some authors refer to it as ATP [251, 92] (see Fig. **??** (A)) while other think of it as amino acids [99] (see Fig. **??** (B))[20]. These models are therefore unable to discuss the relationship between yield and rate as they cannot guarantee *both* mass and energy conservation, *i.e.* if the intermediary is identified as ATP, then the model is energy-balanced but not mass-balanced, if the intermediary is identified as an amino acid the model is mass-balanced but not energy-balanced. Guaranteeing both mass and energy balance when discussing the phenomena underlying growth-rate variations for a class of perturbations may not be necessary, as demonstrated by the success of the aforementioned theories. It becomes however crucial to constrain the relationship between the rate and the yield, as well as to explain the shift between fermentative and respiratory catabolism. Indeed, some other recent cell models are inclusive of both mass and energy balance (see Fig. **??** (C)). This has allowed them to explain how a shift to catabolism with low energetic efficiency (fermentative) could maximize growth-rate [271, 100] (so-called overflow metabolism), and how the choice of catabolic pathway may be governed by a tradeoff between growth-rate and growth yield [255].

At that point it seems important to acknowledge that the model developed in this chapter is very similar to that of [100]. It is only different in few respects which are interesting to discuss:

- In [100] the total mass fraction allocated to fermentative and respiratory catalysts is bounded by $\phi_C + \phi_F < \max(\phi_C + \phi_F) < \phi_p$, such that even at null growth-rate there remains some mass allocated to biosynthesis (although a consequence is that their catalytic efficiency goes to 0). Including such an upper bound in the model herein will lower the maximal rate of energy

[20]Note that in this chapter we ignored pathway that might be necessary to the cycling of other intermediary that are necessary for biosynthetic processes such as NADPH, and simply considered it as an energy currency that is interchangeable with ATP.

production the model is currently able to sustain. As a consequence, the extreme values of extracellular pH where it can maintain its electrophysiology and grow are expected to be closer to neutrality. This is consistent with their proteome data and the reduction of catalytic efficiency of ribosomes at low growth-rates [233].

- Their model always has the ability to convert NADH to ATP via oxidative respiration (thus assume aerobic conditions and high maintained PMF), whereas in ours it is PMF-dependent thus related to the maintenance cost. In particular, this highlights that shifting to fermentative catabolism may not solely a choice motivated by its higher catalytic efficiency than respiration but also by its reduced associated cost of electrochemical maintenance. As noted previously, this may explain the PMF drop observed in chapter 3, even in aerobic conditions, when pH_e is acidic enough. We did not however compared the two following setups: *(a)* high PMF, the NADH cycled by fermentation can be used to make proton gradient then ATP, *(b)* low PMF, the NADH cycled by fermentation does not produce ATP. We would expect that a shift to low PMF is indeed an adaptation strategy if the subsequent decreasing maintenance cost saves more energy than the energy that could be produced by turning 3 NADH from fermentation into ATP. In addition, the distribution of catabolism between two pathways is in their case explicitly a function of the growth-rate and is fitted to the data.
- The maintenance cost is in our case an explicit function of cellular electrophysiology, which is our main contribution relative to [100].
- The predicted ATP cost of making biomass 18×10^9 ATP per cell is quite closed to ours, although it is obtained in different ways: in their case it is an empirical parameter fitted to the data, in ours it is based on [263] *i.e.* the stoichiometries of biosynthetic pathways for ATP.
- Finally, they ignore the maintenance cost although they include a term akin to maintenance to model an "energy dissipation" perturbation. Including the same term and making it a function cellular electrophysiology is precisely what allows us to draw predicates on how the growth behaviours and electrophysiology are related.

In the light of [100, 255] neglecting explicitly maintenance expenditures, it might be worthwhile at this point to wonder: *how much does maintenance really cost ?* We evaluated in this chapter that it should be 27×10^9 protons per hour per cell (of reference mass m_0) based on oxygen consumption and growth-rate

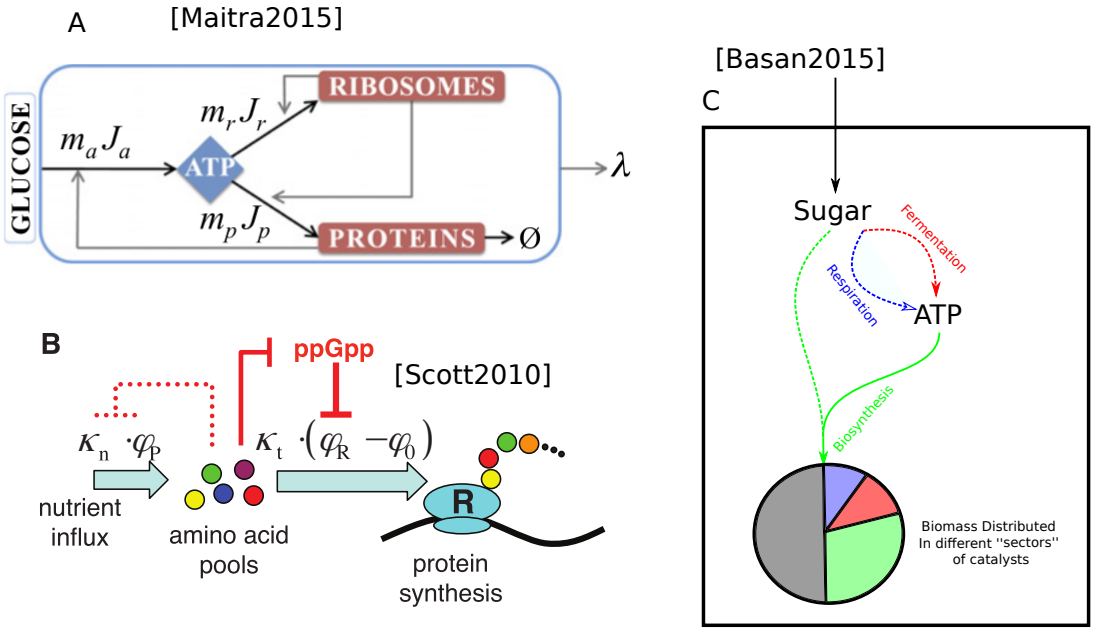


FIGURE 3.12: Comparison of three coarse-grained growth (auto-catalytic) models. The three models have in common that the biomass needs to be distributed in different catalytic functions several of which (at least 2) are required for growth. (A) Reproduced from [251], the intermediary substrate is identified as ATP *i.e.* the model is not mass-balanced (or carbon balanced) (B) Reproduced from [99], the intermediary substrate is identified as an amino acid *i.e.* the model is not energy-balanced (C) Scheme drawn based on the model from [100]. Two intermediary substrates, ATP and sugar, the model is thus energy and carbon-balanced assuming null maintenance cost.

measured by [232]. Other estimates are more conservative and give 4.1×10^9 protons per hour per cell [274][21], 4.8×10^9 protons per hour per cell for [275][22], whereas other estimations put that value closer to our estimate 24×10^9 protons per cell per hour for [276]. [277] gaves for growth on glucose a maintenance rate ranging from 3.6×10^9 protons/hour/cell at doubling rate of 0.0635 per hour to 15×10^9 protons/hour/cell at doubling rate of 0.5727 per hour[23], highlighting that the cost of maintenance is not growth-invariant and likely decreases for adaptation to both poor nutrient media and stationary phase of a growth culture. We expect that would result in a loss of electrophysiological homeostases: lower PMF, pH_i closer to pH_e. Our estimate of basal maintenance for the reference condition [232] is based on the stoichiometry of the respiratory chain (10 protons per oxygen) and $\mathrm{F1F}_o$ for protons (3.3 protons per ATP). Should the stoichiometry of the respiratory chain or/and the stoichiometry of $\mathrm{F1F}_o$ be higher this would lower our basal maintenance estimate from [232], *e.g.* assuming 8 protons per oxygen and 4 protons per ATP gives a maintenance cost closer to the lower estimates 7×10^9 protons per cell per hour. Be as it may, those estimates reflect the maintenance cost for the media with ionic compositions that usually maximizes the growth-rate and which therefore likely minimize maintenance expenditures. In such environments we showed that the maintenance cost has very little impact on growth-rate (though not necessarily on the yield) and it is therefore not surprising that, *e.g.* [100] is able to fit growth-rate data ignoring the contribution of maintenance expenditures.

This should not be the case however for media perturbations that increase sufficiently the cost of maintenance as we hypothesize may be the case when extracellular pH deviates from neutrality or/and when the salinity becomes high enough. Also, for our estimates of basal maintenance (evaluated from [232]), although neglecting it does not impact much the growth-rate, it significantly affects the yield (the yield would be 70% instead of 57% by neglecting maintenance expenditures).

We propose in this chapter that growth-yield, because (1) it is relatively easy to measure and (2) it is an important contribution to fitness[24], is an ideal

[21] Maintenance cost was converted from ATP assuming 3.3 protons is equivalent to 1 ATP

[22] We converted the maintenance cost in glucose units assuming 120 protons were extruded per glucose

[23] Conversion from ATP to protons is made assuming 3.3 protons per ATP

[24] Indeed, time series for the specific growth-rate complemented by time series of the carbon yield (when carbon is limiting) are necessary to compute the time-average growth-rate in a time-window that includes both exponential and stationary phase. Furthermore, as suggested

candidate variable to complement growth-rate when studying bacterial physiology. As motivating scenarios, we showed that four different types of challenges – reduced energy availability, increased maintenance cost, simultaneous increase in maintenance cost and biosynthesis inhibition, simultaneous increase in maintenance cost and catabolic inhibition– had very distinct signatures with respect to how rate and yield covary thus likely shaping the fitness landscape in different ways. We also showed, as it has been done before (for instance by [255]), that shift between two types of catabolisms has particular signatures in the yield/rate plan specific to the catalytic efficiency and the energetic yield of one relative to the other. The ability to understand how adaptation strategies to environmental challenges fare with respect not only to growth-rate but also to other emerging variables that impact fitness, such as the yield, is likely a first step towards predicting the evolutionary paths to antibiotic resistance. The aforementioned yield/rate signatures to different types of challenge actually do not require the electrophysiological component of the model and could have been performed with a model identical to that of [100].

Where our model "shines" is when it comes to bridge –*via* the maintenance cost– macroscopic behaviours such as rate and yield with electrophysiology. Indeed, given the "bottom-up" ability of our model to output the maintenance cost as a function of electrophysiological variables we were able to draw interesting predicates about how two variables would interact in impairing the growth-rate, *i.e.* are they synergistic, additive or antagonistic in the sense of [278]. Indeed, the model predicted several interesting interactions between extracellular pH and other electrophysiological maintenance dependent variables with respect to growth-rate:

1. Lowering the PMF is an adaptation strategy that is more effective at alkaline than acidic pH. This is perhaps one (of many) plausible explanation to why alkalinophile maintain low PMF, as opposed to acidophiles that maintain high PMF [4]. We also observed in chapter 3 that PMF starts decreasing in aerobic conditions for pH_e as low as 8.15 whereas it maintain in the acidic range until pH_e drops to ≈ 5.

2. That high salinity (*e.g.* increasing NaCl or/and KCl concentrations) and acidic challenge share a suppressive interaction. Meaning that under high

by the tradeoffs between yield and rate, the cell sometimes make the choice of lower rate for higher yield, which can only be explained if increasing yield increase fitness to a larger degree than the subsequent loss of growth-rate impacts fitness.

salinity, we predict that making the pH_e acid ≈ 5 rescues the growth-rate, acid challenge that would decrease growth-rate at not too high salinity. This has, to our knowledge, not been tested in the literature.

3. Perhaps most importantly with respect to antibiotic treatments, we showed that different ionophores would work best at inhibiting the growth-rate in different pH_e ranges. More specifically: *(i)* protonophores work best in acidic conditions, whereas *(ii)* cationophores work best in the alkaline range. In fact both these interactions have been observed experimentally. Indeed, Lactocin S, an antibiotic working as a protonophore [279], has higher killing efficiency in acidic environments for *P. acidilactici* [247]. As for cationophores, the antibiotics valinomycin and cereulide, that act as ionophores with high specificity for potassium, have been shown to work best on many gram-positive bacteria in alkaline environments [280], consistently with our predictions. These cationophores had however no effect on the growth of gram-negative bacteria, which would only be consistent with our model if the periplasmic wall prevents action of these antibiotics on the energized cytoplasmic membrane. Finally, in these two studies, the reduction in growth-rate were strongly correlated to important decrease in the maximal OD (a poor read-out of the growth yield), consistent with an effect of ionophores on growth-rate occurring *via* an increase in the maintenance cost.

The "bottom-up" cost estimates we made with the model of *E.coli* electrophysiology are however poised by poor reliability of the permeability coefficient to various ions which can differ by up to 4 orders of magnitude depending on the reports, *e.g.* [281] predicts 10^4 lower permeability of the membrane for sodium than [163]. In particular I could be accused in this chapter of cherry-picking permeabilities that yield sufficiently high cost of electrophysiological maintenance so that growth depends on it. For instance the reference permeability for protons was set to 10^{-4} m/s when several studies reported (see review [281]) proton permeability to be around 10^{-6} m/s, value for which our model of *E.coli* could still grow and perform electrophysiological maintenance at $pH_e = 2$. Some other studies however measured [282] a permeability ratio of potassium to protons in the range $\approx 10^{-8}$–10^{-7} and [42] of 10^6, which would mean a permeability for protons of 10^{-3}–10^{-2} m/s given permeability estimate for potassium made in [163]. Interestingly, the low permeability estimates [281, 282] come from experiments performed

on reconstituted lipid bilayers (with no membrane proteins) whereas the high permeability estimate [163] comes from a membrane that contains both the native proteins and lipids, which could explain the observed discrepancy. Indeed, as explained extensively in [42], the ionic permeabilities of bio-membranes are orders of magnitude more elevated than that of lipid bilayers, the hypothesized dominant leak pathway being through integral membrane proteins rather than through phospholipid groups. The reference permeabilities chosen should not therefore be thought as rigorous experimental measurements of the membrane properties of *E.coli* but rather consistent with *(i)* chloride and sodium permeabilities measured in [163] for oocytes of *xenopus laevis* and *(ii)* proton permeability set to be ≈ 6 orders of magnitudes greater than that of sodium [42] round down to 10^{-4}. Permeability for hydroxide ions was set arbitrarily to be the same as that of protons but is likely different [283]. Though the permeabilities are not exact, we expect that they are in the correct range based on *(a)* energetic estimates of membrane energization [276] in *E. coli*; *(b)* of the same order of magnitude than the expected proton leak in mitochondria, in the range 10–50% of protons spend for else-than-ATP-synthesis depending on the cell type an [284], *(c)* lower max. OD at pH_e deviating from neutrality [285], consistent[25] with an increased significant maintenance cost in such conditions, that is only predicted by the model for significantly higher permeability of the membrane to protons than that reported by [281] for lipid bilayers.

Permeability of the membrane to different ionic species is likely a degree of freedom for adaptation on evolutionary time scales. Acidophiles have a membrane that is for instance much less permeable to protons than that of *E.coli* [286], which is likely a necessary adaptation to be able to keep manageable maintenance cost in the pH_e range 2–3. Acidophiles, as does *E.coli* under extreme acid stress,furthermore maintain positive membrane voltage [4], that allows maintenance of near neutral pH_i even at $\mathrm{pH}_e = 2$. As discussed before, to achieve positive membrane voltage a cell needs to maintain an electrochemical gradient for small anions, *e.g.* chloride, and does not need to maintain electrochemical gradient for small cations (other than protons). A corollary is that cells maintaining positive membrane voltage, as acidophiles in their ecological niches, should be sensitive to ionophore specific to small anions and insensitive to cationophores. This has to our knowledge never

[25] Although consistent, not sufficient. A sufficient argument would require time series for the yield and specific growth-rate along the growth curve for which we have not found experimental data in the literature.

been tested. On the other end, alkalinophiles are expected to be more sensitive to any ionophore with, for example, high sodium /potassium specificity or ionophores increasing the permeability for hydroxide ions. Alkalinophile specific adaptation strategies are expected to feature low permeability for small cations (Na^+, K^+) and hydroxide ions, without much incentive for minimizing the permeability of the membrane to protons. Our predicted relative scale for the permeabilities to different type of ions in acidophiles, neutralophiles and alkalinophiles is shown in table 3.1, that is if each ionic permeability can be modulated independently other ionic permeabilities.

	Acidophiles	Neutralophiles	Alkalinophiles
P_{H^+}	Low	Medium	High
P_{OH^-}	High	Medium	Low
P_{C^+}	High	Medium	Low
P_{A^-}	Low	High	High

TABLE 3.1: Relative scale for expected permeabilities of acidophiles, neutralophiles and alkalinophiles to different types of small ions. Another way to interpret this table is that expected low permeabilities are under high selective pressure for minimization whereas high permeabilities are under low selective pressure for minimization. Importantly the table is not be compared row by row, *e.g.* low permeability for H^+ may correspond to high permeability for C^+.

This raises the question of whether there are tradeoffs in permeability of the membrane to different ions, for instance: does increasing the permeability for protons result in increased permeability for other ionic species ? This is to our knowledge unknown. If as discussed before the main leak pathway is through integral membrane proteins, such as glucose transporters, there may be additional tradeoffs the cell faces. Is a cell better off *(a)* increasing the density of transporters in its membrane thereby increasing its energetic production capabilities and maintenance cost (due to increased permeabilities) or *(b)* lowering it ? While choice *(a)* may increase growth at the detriment of the yield, choice *(b)* could have the opposite effect. Surely it would be sometimes beneficial to both rate and yield to increase or decrease the density of transporters. Be as it may, transporters being the dominant ionic leak pathways, could result in additional tradeoffs between rate and yield.

The discussion on the impact of ionic permeabilities to growth also pertains to changes in temperature, an environmental variable we have neglected so far, although it is present in every ionic transport equation in this thesis: everything

else remaining the same (including ionic permeabilities), the rate of any reaction increases with higher temperature. Temperature is one of the cardinal environmental factors on which the growth-rate of bacteria depends. Different species usually have different temperature range wherein they thrive [287]. The characteristic shape of growth as a function of temperature is a slow increase in rate as temperature increases followed by an abrupt drop in growth-rate once temperature has exceeded some strain-specific threshold [288]. Also, the maintenance cost was shown to increase with increasing temperatures in *E. coli* [275]. One plausible explanation is that the permeability of the membrane to protons and sodium exponentially increases with temperature for all strains studied in [289], although thermophiles have lower proton permeability than other bacteria at identical temperatures. Consistently with these observations, the model predicts higher maintenance cost for higher permeabilities. We think this is a plausible universal mechanism underlying the growth inhibition at high temperatures.

Finally, most of the model's behaviours seed from the fact that we impose to the model to spend as little energy as it can to preserve electrophysiological homeostases to the values we set. From a biological perspective this may make sense in some environmental scenarios. For instance, in the absence of cationophore, it is perhaps a better strategy (with respect to fitness[26]) to try to spend accrued amount of energy to maintain pH_i closed to neutrality upon alkaline challenge. Meaning it would be more detrimental for fitness to lose pH_i homeostasis and minimize the maintenance cost than to keep pH_i homeostasis and increase the maintenance cost. Such might not be the case however if the alkaline challenge is complemented with a cationophore, that would likely shape the tradeoff between maintaining pH_i and minimize energy expenditures differently. Indeed, in a limit scenario where we have sufficiently high amount of cationophore, a cell may decide to spend a lot of energy in an attempt to maintain pH_i and almost completely fail to do it, therefore spending energy for virtually no gain with respect to maintenance of a fitness-optimal pH_i. We imagine that a "smarter" cell could decide in such a setup (alkaline pH_e + cationophore) to simply stop spending energy in an impossible attempt to maintain pH_i. That "smart" cell would experience only the detrimental effect to fitness of losing pH_i homeostasis whereas the "less smart" cell

[26]We use in this paragraph the loose concept of fitness, that while depending on many other factors, we assume to be increasing with pH_i getting closer to its homeostatic target and decreasing with increasing maintenance cost.

would experience the detrimental effects to fitness of both losing pH_i homeostasis and having high maintenance costs. The ability to become "smart" or to evolve for having a regulation apparatus that distinguishes between the two scenarios: alkaline challenge *versus* alkaline challenge + cationophore, would require cells to experience frequent enough alkaline + cationophore challenges. If the alkaline challenge + cationophore only occurs at low frequency it may become a "regulatory blindspots", where the regulation performed by the cell works in a similar fashion than during alkaline challenge alone. In this case, alkaline regulation would be detrimental to cellular fitness during an alkaline + cationophore challenge. This is only one single example of such "regulatory blindspot". Another one could be, following a similar reasoning, acidic + protonophore challenge.

We may now connect the thought experiment we made in the previous paragraph to phenomena that pertains to the lower sensitivity of cells having low metabolic activity to antibiotic treatments.

First, Persister cells consist in a small fraction of a growing population and are characterized by low growth-rate, metabolic activity and high tolerance to antibiotic treatment [290]. One mechanism of dormancy induction is expression of the membrane channel *HokB*, that leaks intracellular ATP and disrupts membrane potential [291]. Perhaps dedicating a small fraction of the population to a dormant state (a.k.a. persister cells) is an adaptation strategy that allows, among other things, some cells to give up on electrophysiological maintenance, thereby minimizing their maintenance expenditures at the cost of sub-optimal values for electrophysiological homeostases. Should the population experience a regulatory blindspot, the fraction of the population that is dormant would have higher fitness than the other cells, because they only experience the detrimental effect of losing electrophysiological homeostases whereas other cells experience the detrimental effects of both losing electrophysiological homeostases and increased maintenance expenditures.

Second, the efficiency of bactericidal antibiotics is strongly related to bacterial metabolism and increases at high growth-rates [292]. With respect to catabolism it was shown that: (1) bactericidal antibiotics increase respiratory activity and (2) bacteria with higher respiration rates (*via* disruption of $F1F_o$) were more sensitive to bactericidal antibiotics [293]. Point (1) may indicate that the detrimental effects of bactericidal antibiotics on growth may be phenomenologically modeled

as increasing the maintenance energy requirements. How they increase maintenance cost shall be specific to the type of bactericidal antibiotic. For instance, beta-lactam antibiotics trigger cell wall degradation [294] thereby increasing maintenance expenditures *via* the accrued amount of energy continuously required to replace the degraded components of the cell wall. Daptomycin which permeabilizes the membrane [295] could increase maintenance cost *via* increase in energetic requirements for electrophysiological maintenance. Likewise for valinomycin and cereulide, two cationophores that display bactericidal activity [280]. Point (2) may suggest that the efficacy of antibiotics leading to increase in maintenance cost (a.k.a. bactericidal see point (1)) may in general be increased if applied in an environmental condition wherein cells have high basal cost of electrophysiological maintenance (*e.g.* high salinity). Because different cost-components of electrophysiological maintenance have different dependency on environmental conditions, the ability of a bactericidal antibiotic to synergize with for instance extracellular pH may depend on its specific mechanism of action, as we discussed before[27].

A different unifying mechanism for how bactericidal antibiotics act on bacteria was previously proposed: *via* the increased production of reactive oxygen species observed under bactericidal challenge [296], potential lethality of which is not considered in the maintenance cost. It is however debated as the efficacy of bactericidal antibiotics is identical in aerobic and anaerobic conditions [297][28]. This may suggest that reactive oxygen species are symptomatic of bactericidal challenge rather than the dominant mechanism leading to their efficacy. If *(a)* the quantity of reactive oxygen species increases with increased respiratory rates[29] and *(b)* if respiratory rates increase with higher maintenance requirements; the observation that many classes bactericidal antibiotics result in high production of reactive oxygen species could in fact be indicative that bactericidal challenges always involve higher maintenance requirement. Bacteriostatic antibiotics on the other hand have opposite effects than bactericidal antibiotics on cellular metabolism [298] and some of them have been shown to cause a decreased respiratory activity [293].

Although far-fetched, we hypothesize that while a bacteriostatic challenges

[27] For instance maintenance cost only increase significantly by addition of a cationophore when the cell maintains negative voltage, thus at alkaline enough pH_e.

[28] There are way less reactive oxygen species in the absence of oxygen, a.k.a. anaerobic conditions.

[29] After some comments from other scientists it seems to not be the case often, thus the reasoning herein is likely not valid.

can always be modeled as inhibiting the catalytic efficiency of a cellular process, bactericidal challenges can always be phenomenologically modeled as *(i)* an increase in the cost of electrophysiological maintenance or/and *(ii)* shorter half lives of costly cellular compounds (cell wall, proteins, *etc.*). If true, that would call for an appealing modular modeling framework, similar to what we have used in this thesis, *i.e.* one module is responsible for how growth-rate and yield depend on the nutrient composition of the medium and the phenomenological maintenance cost while the other module is responsible for evaluating the cost of maintenance as a function of the electrophysiological status of the cell and the ionic composition of the medium. Short half lives of end-products of biosynthesis could be phenomenologically modelled as a condition-dependent decay of the cellular mass (or negative growth-rate). Should such a modeling framework be able to recapitulate the different types of challenge aforementioned, we propose that an inclusive classification of environmental challenges should be based on how yield and rate co-vary for each different challenge.

Finally, another connection between the electrophysiological state and the sensitivity to antibiotics could be *via* the membrane potential-dependent accumulation of electrically charged antibiotics[30]. Aminoglycosides are, for instance, positively charged antibiotics [299]. A straightforward expectation is that more negative membrane potential promotes accumulation of such positively charged antibiotics[31], as it has been shown in multiple organisms under different environmental conditions (reviewed in [300]). There is however some ambiguity in the literature as to the underlying mechanism of aminoglycosides accumulation into the cell. This ambiguity likely seeds from *(i)* the observation that PMF disruption by, *e.g.* a protonophore CCCP, leads to inhibition of aminoglycoside entry [301] and *(ii)* that protonophores such as CCCP or DNP are understood as uncoupler of the PMF and membrane potential [300], *i.e.* they are postulated to collapse the PMF without affecting the membrane potential. This is however not the case, as we experimentally showed in chapter 2 that collapsing the PMF by CCCP led to a loss of membrane voltage, which is consistent with PMF driven voltage generation, as was discussed extensively. The simple accumulation mechanism we propose for aminoglycosides (essentially equilibration across the membrane of aminoglycosides

[30] that is not directly related to the growth model but rather on the relationships between PMF, membrane potential and pH_e we described in chapter 3

[31] Akin to Nernstian dyes.

depends on membrane potential and not PMF, akin to nernstian dye in chapter 1) is therefore consistent with observations that PMF is sometimes required for aminoglycoside accumulation. Interestingly, if our hypothetical mechanism is correct, it predicts that accumulation of aminoglycoside is inhibited as pH_e becomes acidic, where cells still maintain PMF but less negative membrane potential. It has in fact been known for a long time that the efficacy of aminoglycosides is impaired in acidic environments [302]. Following a similar reasoning, negatively charged antibiotics are expected to be more efficient at acidic pH_e, wherein the less negative membrane potential allows their entry. Indeed, penicillin is more effective as pH_e becomes more acid [303].

Appendices

F. Appendix

F.1. Description of the model

We postulate the following reactions:

$$s_e \xrightarrow{T} s_i \tag{F.1}$$

$$s_i + 6 \cdot \mathrm{O_2} + \sigma_{\mathrm{H^+},C} \cdot \mathrm{H_i^+} \xrightarrow{C} 6 \cdot \mathrm{CO_2} + \sigma_{\mathrm{H_2O},C} \cdot \mathrm{H_2O} + \sigma_{\mathrm{H^+},C} \cdot \mathrm{H_e^+} \tag{F.2}$$

$$\mathrm{H_e^+} \xrightarrow{M} \mathrm{H_i^+} \tag{F.3}$$

$$\sigma_{\mathrm{H^+,F1F_o}} \cdot \mathrm{H_e^+} + \mathrm{ADP} \xrightarrow{\mathrm{F1F_o}} \mathrm{ATP} + \sigma_{\mathrm{H^+,F1F_o}} \cdot \mathrm{H_i^+} \tag{F.4}$$

$$\sigma_{\mathrm{ATP},A} \cdot \mathrm{ATP} + \sigma_{s,A} \cdot s_i \xrightarrow{A} m_0 \tag{F.5}$$

the latter reaction can be rescaled as:

$$\sigma'_{\mathrm{ATP},A} \cdot \mathrm{ATP} + s_i \to \frac{1}{\sigma_{s,A}} \cdot m_0 \tag{F.6}$$

so j_A is expressed in the same units than j_T and j_C (number of sugar molecules processed per time); in which case $\sigma'_{\mathrm{ATP},A} = \dfrac{\sigma_{\mathrm{ATP},A}}{\sigma_{s,A}}$ denotes the ATP cost of incorporating 6 carbon atoms from sugar to biomass. We shall use the latter rescaled reaction instead of Rec. (F.5) and we will denote by $\sigma_{\mathrm{ATP},A}$ the definition of $\sigma'_{\mathrm{ATP},A}$ from now one.

Reaction (F.1) moves one molecule of extracellular sugar s_e into the intracellular compartment and the intracellular sugar is denoted s_i. Reaction (F.2) is the reaction for glucose combustion and turns one intracellular sugar into waste $\mathrm{CO_2}$ and in the process moves $\sigma_{H,C} = 12 \times \sigma_{\mathrm{H^+},R} = 120$ protons out of the cell (where we assumed $\sigma_{\mathrm{H^+},R} = 10$ protons moved per oxygen consumed). Reaction (F.3) is a reaction of internalization of protons, its flux j_M is the number of protons per unit of time that needs to be internalized in order to maintain chemio-osmotic variables (as described in previous chapters). Reaction (F.4) models an ATPase that in the process of moving $\sigma_{\mathrm{H,F1F_o}}$ protons inside makes one molecule of ATP. Reaction (F.5) describes the formation of a cell with mass m_0. $\sigma_{\mathrm{ATP},A}$ is the number of ATP required to a cell of mass m_0, whereas $6 \times \sigma_{s,A}$ is the number of carbon atoms in a cell of mass m_0 (where 6 is for the number of carbons in one sugar s_i).

In the energy limitation growth model, growth only requires ATP spending and no incorporation of carbons seeding from sugar into biomass such that in that

case (figures. 4.1 to 4.3) $\sigma_{s,A} = 0$.

Time derivative We then write the set of differential equations associated to the reactions previously written that describes the time-behaviour of the model.

$$\frac{ds_e(t)}{dt} = -j_T(M(t)) \tag{F.7}$$

$$\frac{ds_i(t)}{dt} = j_T(M(t)) - j_C(M(t)) - \sigma_{s,A} \cdot j_A(M(t)) \tag{F.8}$$

$$\frac{d\mathrm{H}_i^+(t)}{dt} = -\frac{d\mathrm{H}_e^+(t)}{dt} = j_M(M(t)) + \sigma_{\mathrm{H}^+,\mathrm{F1F}_o} \cdot j_{\mathrm{F1F}_o}(M(t)) - \sigma_{\mathrm{H}^+,C} \cdot j_C(M(t)) \tag{F.9}$$

$$\frac{d\mathrm{ATP}(t)}{dt} = j_{\mathrm{F1F}_o}(M(t)) - \sigma_{\mathrm{ATP},A} \cdot j_A(M(t)) \tag{F.10}$$

$$\frac{dN(t)}{dt} = \frac{1}{\sigma_{s,A}} \cdot j_A(M(t)) \tag{F.11}$$

where $\forall x \in \{s_e, s_i, \mathrm{H}_i^+, \mathrm{H}_e^+, \mathrm{ATP}, N\}$, $x(t)$ describes the number of species x at time t and $\forall r \in \{T, C, M, \mathrm{F1F}_o, A\}$, $j_r(M(t))$ is the flux of reaction r for a total cell mass $M(t)$.

growth-rate and Balanced growth The specific growth-rate is defined as:

$$\mu = \frac{1}{M(t)} \cdot \frac{dM(t)}{dt} \tag{F.12}$$

The number of a particule x per unit of mass follows:

$$\frac{d}{dt}\left(\frac{x(t)}{M(t)}\right) = \frac{1}{M(t)}\left(\frac{dx(t)}{dt} - x(t) \cdot \mu\right) \tag{F.13}$$

We will assume balanced growth, *i.e.* time-invariant intracellular compound counts relative to mass such that for an intracellular compound x:

$$\frac{d}{dt}\left(\frac{x(t)}{M(t)}\right) = 0 \Leftrightarrow \frac{dx(t)}{dt} = x(t) \cdot \mu \tag{F.14}$$

Rescaling the model for a reference mass m_0: We first postulate a time-invariant average mass per cell of reference m_0 such that the total cell mass $M(t)$

is 1-homogeneous with the number of cells $N(t)$:

$$M(t) = N(t) \cdot m_0 \tag{F.15}$$

We now wish to express the model fluxes in unit molecule/cell/time (or molecule per time per mass m_0 for a reference condition where the average mass per cell is m_0) instead of molecule per time over all the cells. To that aim, we assume the average cell has a mass m_0 and from now on we denote by *(*i) $j_r(m_0)$, $r \in \{T, C, M, A\}$ the flux of the reaction r per cell (for cell weighting m_0); *(ii)* denote by $x(m_0)$, $x \in \{s_i, \mathrm{H}_i^+, \mathrm{ATP}\}$ the number of x per cell (for a cell weighting m_0).

We do so for a system that follows balanced-growth (*i.e.* Eq. (F.14)) such that we substitute the left-hand terms of Eqs. (F.7) to (F.11) by Eq. (F.14) above and divide everything by the number of cells: $N(t) = M(t)/m_0$ to obtain

$$\frac{ds_e(t)}{dt} = -N(t) \cdot j_T(m_0) \tag{F.16}$$

$$\frac{d\mathrm{H}_e^+(t)}{dt} = N(t) \cdot \left[\sigma_{\mathrm{H}^+,C} \cdot j_C(m_0) - j_M(m_0) - \sigma_{\mathrm{H}^+,\mathrm{F1F}_o} \cdot j_{\mathrm{F1F}_o}(m_0)\right] \tag{F.17}$$

$$0 = j_T(m_0) - j_C(m_0) - j_A(m_0) - s_i(m_0) \cdot \mu \tag{F.18}$$

$$0 = j_M(m_0) + \sigma_{\mathrm{H}^+,\mathrm{F1F}_o} \cdot j_{\mathrm{F1F}_o}(m_0) - \sigma_{\mathrm{H}^+,C} \cdot j_C(m_0) - \mathrm{H}_i^+(m_0) \cdot \mu \tag{F.19}$$

$$0 = j_{\mathrm{F1F}_o}(m_0) - \sigma_{\mathrm{ATP},A} \cdot j_A(m_0) - \mathrm{ATP}(m_0) \cdot \mu \tag{F.20}$$

$$0 = \frac{1}{\sigma_{s,A}} \cdot j_A(m_0) - \mu \tag{F.21}$$

where we assumed that the flux of all reactions are 1-homogeneous with the mass:

$$\forall r : j_r(m_0) = \frac{m_0}{M(t)} \cdot j_r(M(t)) = \frac{1}{N(t)} \cdot j_r(M(t)) \tag{F.22}$$

We shall also assume that the intracellular quantities of all species are negligible, rigorously:

$$\forall x \in \{\mathrm{H}_i^+, s_i, \mathrm{ATP}\} : x(m_0) \cdot \mu = 0 \tag{F.23}$$

Consequently Eqs. (F.18) to (F.22) become:

$$0 = j_T - j_C - j_A \tag{F.24}$$

$$0 = j_M + \sigma_{\mathrm{H^+},\mathrm{F1F_o}} \cdot j_{\mathrm{F1F_o}} - \sigma_{\mathrm{H^+},C} \cdot j_C \tag{F.25}$$

$$0 = j_{\mathrm{F1F_o}} - \sigma_{\mathrm{ATP},A} \cdot j_A \tag{F.26}$$

$$\mu = \frac{1}{\sigma_{s,A}} \cdot j_A \tag{F.27}$$

where from now on we use the notation $j_r \equiv j_r(m_0)$ for any reaction r.

Reaction kinetics We assume for the kinetics simple models (michaelis-menten for transport, 1-order kinetic for other reactions)

$$j_T = \phi_T \cdot \varepsilon_T \cdot f(s_e) = \phi_T \cdot \varepsilon_T \cdot \frac{1}{1 + \dfrac{K_T}{s_e}} \tag{F.28}$$

$$j_C = \phi_C \cdot \varepsilon_C \tag{F.29}$$

$$j_A = \phi_A \cdot \varepsilon_A \tag{F.30}$$

$$j_M = \phi_M \cdot \varepsilon_M \tag{F.31}$$

$$j_{\mathrm{F1F_o}} = \phi_{\mathrm{F1F_o}} \cdot \varepsilon_{\mathrm{F1F_o}} \tag{F.32}$$

where $\forall r \in \{T, C, A, M, \mathrm{F1F_o}\}$, ϕ_r denote the fraction of the cellular mass that is allocated to catalysts playing a part in r and ε_r is the reaction rate per fraction of mass allocated to the reaction r in a cell of m_0 mass; in other words ε_r has units of molecules per time per cell per mass m_0 invested in catalysts performing r.

We denote by ϕ_p the fraction of the mass that is made of catalysts contributing to reactions T, C, A, M and $\mathrm{F1F_o}$ such that:

$$\phi_T + \phi_C + \phi_A + \phi_M + \phi_{\mathrm{F1F_o}} = \phi_p \tag{F.33}$$

We will in addition assume that ε_M is infinite such that any j_M can be achieved with $\phi_M = 0^+$ (infinitesimally close to 0) and likewise for transport and $\mathrm{F1F_o}$ such that:

$$\phi_C + \phi_A = \phi_p \tag{F.34}$$

F.2. Chemio-osmotic-dependent Maintenance cost

Computing maintenance cost as a function of extracellular ionic composition: To obtain figures. 4.1, 4.3 and **??** we compute the maintenance cost j_M (corresponding to the rate of reaction F.2) as a function of the extracellular pH and salinity as well as the cellular homeostases sought to be maintained: osmotic pressure, intracellular pH and PMF. To obtain j_M, we assume the simplified model of *E.coli*'s electrophysiology from Chapter 3, *i.e.* access to the three antiporters *ClcA*, *NhaB*, *NhaA* and ability to maintain average valency of captive molecules between -2 and $+2$ charge carried per molecule. j_M is then obtained as the optimal energetic cost of maintaining cellular homeostases in a given environment.

Maintenance cost dependency of cellular shape In figure **??** we look at how the cost of maintenance j_M (and subsequently the growth-rate) varies for different cellular shapes.

We now describe how to obtain the different panels of figure. **??**:

- In Figure. **??** (A) we take the reference volume V_{ref} to be that of *E.coli* with doubling time 60 minutes (3.3×10^{-18} m^3) and the reference maintenance cost to be that of a cell with volume V_{ref} and shaped as a 3:1 length to width ratio spherocylinder with corresponding surface of reference S_{ref}. The maintenance cost of a cell with surface S relative to the reference cost follows: S/S_{ref} (since all variables on which the cost, *i.e.* permeabilities, cellular homeostases, salinity extracellular pH, depends are assumed to be identical for differently shaped cells). The surface is then obtained as a function of the volume for differently shaped cell and Figure. **??** (A) is effectively S/S_{ref} plotted as a function of V/V_{ref} for differently shaped volumes.
- In figure. **??** (B) we assume a spherocylindrical cell with 3:1 length to width ratio, shape which is invariant by the position in the cell cycle. We then plot the surface relative to the surface at birth as a function of the position in the cell cycle assuming that the division volume is twice the birth volume.
- To obtain Figure. **??** (D) we first compute the mean surface and volume from the length distribution from (C) assuming 3:1 length to width ratio spherocylindrical cells and that all variables –but surface to volume ratio– on which the cost depends are identical for all cells. The maintenance cost relative to the mean maintenance cost is then given by dividing distribution of surface to volume ratio by the average surface to volume ratio: $S/V/(S_{\text{mean}}/V_{\text{mean}})$.

- To obtain Figure. **??** (E) we feed the distribution obtained in (D) to the mass constrained growth model for four different values of average maintenance cost.

F.3. Solving the model at balanced-growth

Unconstrained mass We first analyse the behaviour of the model playing with the fluxes alone (thus ignoring the constraints arising from limited total mass of catalysts available).

To that end, we first rewrite the balanced-growth Eq. (F.24) as:

$$j_T = j_C + j_A \tag{F.35}$$

i.e. the total flux of internalized carbon must equal its consumption by catabolism and biosynthetic processes.

We then combine Eqs. (F.25) and (F.26) to express the flux of carbon incorporated into biomass as a function of the maintenance cost and the flux of catabolized carbon:

$$j_A = \frac{\sigma_{\mathrm{H}^+,C} \cdot j_C - j_M}{\sigma_{\mathrm{H}^+,\mathrm{F1F}_o} \cdot \sigma_{\mathrm{ATP},A}} \tag{F.36}$$

Such that the growth-rate Eq. (F.27) can now be shown as a function of the of the maintenance cost and the catabolic flux:

$$\boxed{\mu = \frac{1}{\sigma_{s,A}} \cdot \frac{\sigma_{\mathrm{H}^+,C} \cdot j_C - j_M}{\sigma_{\mathrm{H}^+,\mathrm{F1F}_o} \cdot \sigma_{\mathrm{ATP},A}}} \tag{F.37}$$

We next define the carbon yield as the fraction of the internalized carbon that is turned into biomass:

$$Y := \frac{j_A}{j_T} \tag{F.38}$$

We substitute j_T by Eq. (F.35) and write the yield as:

$$Y = \frac{1}{1 + \dfrac{j_C}{j_A}} \tag{F.39}$$

Introducing the growth-rate from Eq. (F.27) and obtain:

$$\boxed{Y = \frac{1}{1 + \dfrac{j_C}{\sigma_{s,A} \cdot \mu}}} \tag{F.40}$$

Further using Eq. (F.37) we may write the yield as a function of the maintenance cost rather than the catabolic flux:

$$Y = \frac{1}{1 + \dfrac{1}{\sigma_{s,A} \cdot \mu} \cdot \dfrac{1}{\sigma_{\mathrm{H}^+,C}} \left(\sigma_{s,A} \cdot \sigma_{\mathrm{H}^+,\mathrm{F1F}_o} \cdot \sigma_{\mathrm{ATP},A} \cdot \mu + j_M \right)} \tag{F.41}$$

which becomes after a few simplifications:

$$Y = \frac{1}{1 + \dfrac{\sigma_{\mathrm{H}^+,\mathrm{F1F}_o} \cdot \sigma_{\mathrm{ATP},A}}{\sigma_{\mathrm{H}^+,C}} + \dfrac{j_M}{\sigma_{s,A} \cdot \sigma_{\mathrm{H}^+,C} \cdot \mu}} \tag{F.42}$$

And the maximum yield is defined as the yield when maintenance cost is null, meaning:

$$\boxed{Y_{\max} = \frac{1}{1 + \dfrac{\sigma_{\mathrm{H}^+,\mathrm{F1F}_o} \cdot \sigma_{\mathrm{ATP},A}}{\sigma_{\mathrm{H}^+,C}}}} \tag{F.43}$$

We can recover from Eq. (F.42) the classical growth law from [220] that connects growth to yield Eq. (II.2) by defining:

$$m \equiv \frac{j_M}{\sigma_{s,A} \cdot \sigma_{\mathrm{H}^+,C}} \tag{F.44}$$

$$Y_G \equiv Y_{\max} \tag{F.45}$$

which clarifies how Y_G and m depends on underlying cellular variables (within the scope of our simple model). In particular, what is usually referred to as the maintenance coefficient m depends on the variables that does not seem directly related to maintenance processes: *(i)* $\sigma_{s,A}$ (a.k.a. the number of sugar required to build a cell, in carbon equivalent) and *(ii)* $\sigma_{\mathrm{H}^+,C}$ the catabolic yield. Also, the maximum yield crucially depends on $\sigma_{\mathrm{ATP},A}$ the energetic cost of making a cell and $\sigma_{\mathrm{H}^+,C}$ the catabolic yield.

Constrained mass We now seek to derive the underlying allocation between catabolic and biosynthetic enzymes. We first substitute j_C, j_A by their expressions in Eqs. (F.29), (F.30) into Eq. (F.36) to obtain:

$$\phi_A = \frac{1}{\varepsilon_A} \cdot \frac{1}{\sigma_{\mathrm{H^+},\mathrm{F1F_o}} \cdot \sigma_{\mathrm{ATP},A}} \cdot \left(\sigma_{\mathrm{H^+},C} \cdot \phi_C \cdot \varepsilon_C - j_M\right) \tag{F.46}$$

We then use the constraint that $\phi_A + \phi_C$ occupies a fixed fraction of the mass ϕ_p and write:

$$\phi_A = a \cdot [b \cdot (\phi_p - \phi_A) - j_M] \tag{F.47}$$

$$a = \frac{1}{\varepsilon_A \cdot \sigma_{\mathrm{H^+},\mathrm{F1F_o}} \cdot \sigma_{\mathrm{ATP},A}} \tag{F.48}$$

$$b = \sigma_{\mathrm{H^+},C} \cdot \varepsilon_C \tag{F.49}$$

where we defined a and b to simplify the equation.

$$\boxed{\phi_A = \begin{cases} \dfrac{a \cdot [b \cdot \phi_p - j_M]}{1 + a \cdot b} & \text{if } j_M < b \cdot \phi_p \\ 0 & \text{if } j_M \geq b \cdot \phi_p \end{cases}} \tag{F.50}$$

and $\phi_A = 0$ when $j_M \geq b \cdot \phi_p$ because negative mass fraction are not allowed.

F.4. Model with two catabolic pathways

We now postulate that the cell has access to a distinct catabolic reaction:

$$s_i + \sigma_{\mathrm{H^+},F} \cdot \mathrm{H_i^+} \xrightarrow{F} w + \sigma_{\mathrm{H^+},F} \cdot \mathrm{H_e^+} \tag{F.51}$$

which has a lower catabolic yield than the reaction of reference we introduced previously:

$$\sigma_{\mathrm{H^+},F} < \sigma_{\mathrm{H^+},R} \tag{F.52}$$

but has however an higher rate of proton extrusion per mass fraction invested in catabolic enzymes:

$$\sigma_{\mathrm{H^+},F} \cdot \varepsilon_F > \sigma_{\mathrm{H^+},R} \cdot \varepsilon_R \tag{F.53}$$

i.e. the rate of proton extrusion by catabolism will be higher if the pathway F is used instead of pathway R, that is for an identical mass fraction allocated to F and R.

The the rate of sugar consumption by pathway F follows:

$$j_F = \phi_F \cdot \varepsilon_F \tag{F.54}$$

With the new catabolic pathway F, the balance for protons at balanced growth now follows (updated from Eq. (F.25)):

$$j_M + \sigma_{\mathrm{H^+,F1F_o}} \cdot j_{\mathrm{F1F_o}} - \sigma_{\mathrm{H^+},C} \cdot j_C - \sigma_{\mathrm{H^+},F} \cdot j_F = 0 \tag{F.55}$$

The balance for ATP Eq. (F.26) remains unchanged and thus we can write:

$$j_A = \frac{\sigma_{\mathrm{H^+},C} \cdot j_C + \sigma_{\mathrm{H^+},F} \cdot j_F - j_M}{\sigma_{\mathrm{H^+,F1F_o}} \cdot \sigma_{\mathrm{ATP},A}} \tag{F.56}$$

We now introduce γ the fraction of catabolized sugar that is processed by pathway F that we will use as a control variable to mimic the cell's behaviour without need for explicit regulation:

$$\gamma = \frac{j_F}{j_F + j_C} \Leftrightarrow j_F = j_C \cdot \frac{\gamma}{1-\gamma} \tag{F.57}$$

Substituting j_F, j_C in Eq. (F.57) by their kinetics Eqs. (F.29) and (F.54), the mass fraction of enzymes required for pathway F can be expressed as:

$$\boxed{\phi_F = \phi_C \cdot \frac{\varepsilon_C}{\varepsilon_F} \cdot \frac{\gamma}{1-\gamma}} \tag{F.58}$$

We then substitute in Eq. (F.56) j_F by its expression in Eq. (F.57) to obtain:

$$j_A = \frac{j_C \cdot \left(\sigma_{\mathrm{H^+},C} + \sigma_{\mathrm{H^+},F} \cdot \dfrac{\gamma}{1-\gamma}\right) - j_M}{\sigma_{\mathrm{H^+,F1F_o}} \cdot \sigma_{\mathrm{ATP},A}} \tag{F.59}$$

Further substituting above j_C using Eq. (F.29) we obtain:

$$\phi_A = \frac{1}{\varepsilon_A} \frac{\phi_C \cdot \varepsilon_C \cdot \left(\sigma_{\mathrm{H^+},C} + \sigma_{\mathrm{H^+},F} \cdot \dfrac{\gamma}{1-\gamma}\right) - j_M}{\sigma_{\mathrm{H^+,F1F_o}} \cdot \sigma_{\mathrm{ATP},A}} \tag{F.60}$$

We now rewrite the constraint that enzymes belonging to pathways A, C and F occupy a fixed mass fraction of the cell ϕ_p:

$$\phi_C = \phi_p - \phi_A - \phi_F \tag{F.61}$$

Substituting ϕ_F by Eq. (F.58) this becomes:

$$\boxed{\phi_C = \left(1 + \frac{\varepsilon_C}{\varepsilon_F}\frac{\gamma}{1-\gamma}\right)^{-1}(\phi_p - \phi_A)} \tag{F.62}$$

We now substitute ϕ_C by its expression above in Eq. (F.60) and write:

$$\phi_A = \frac{1}{\varepsilon_A}\frac{\left(1 + \frac{\varepsilon_C}{\varepsilon_F}\cdot\frac{\gamma}{1-\gamma}\right)^{-1}\cdot(\phi_p - \phi_A)\cdot\varepsilon_C\cdot\left(\sigma_{\mathrm{H^+},C} + \sigma_{\mathrm{H^+},F}\cdot\frac{\gamma}{1-\gamma}\right) - j_M}{\sigma_{\mathrm{H^+,F1F_o}}\cdot\sigma_{\mathrm{ATP},A}} \tag{F.63}$$

Which can be written in a more compact form introducing a and b:

$$\phi_A = a\cdot(b\cdot(\phi_p - \phi_A) - j_M) \tag{F.64}$$

$$a = \frac{1}{\varepsilon_A\cdot\sigma_{\mathrm{H^+,F1F_o}}\cdot\sigma_{\mathrm{ATP},A}} \tag{F.65}$$

$$b = \left(1 + \frac{\varepsilon_C}{\varepsilon_F}\cdot\frac{\gamma}{1-\gamma}\right)^{-1}\cdot\varepsilon_C\cdot\left(\sigma_{\mathrm{H^+},C} + \sigma_{\mathrm{H^+},F}\cdot\frac{\gamma}{1-\gamma}\right) \tag{F.66}$$

We finally obtain ϕ_A as:

$$\boxed{\phi_A = \frac{a\cdot(b\cdot\phi_p - j_M)}{1 + a\cdot b}} \tag{F.67}$$

The growth-rate remains unchanged and is still given by Eq. (F.27) whereas the yield is updated to:

$$\boxed{Y = \frac{1}{1 + \frac{j_C + j_F}{\sigma_{s,a}\cdot\mu}}} \tag{F.68}$$

i.e. the flux of glucose not being incorporated into biomass is now the total amount of sugar being catabolized $j_C + j_F$.

Cellular behaviour Since we have now two catabolic pathways, given a maintenance rate, the catalytic efficiencies of A, C, F and the stoichiometries of

the model there are various pairs of $\{\mu, Y\}$ achievable that only depend on the distribution of the catabolic substrate into the two catabolic pathways, encoded by γ.

We decide to model the cell's behaviour as an optimization problem:

$$\gamma = \underset{\gamma}{\text{argmax}}(\mu + \beta \cdot Y) \tag{F.69}$$

i.e. the allocation between the two catabolic pathways is set in order to maximize $\mu+\beta\cdot Y$. When $\beta = 0$, then the cell will pick the γ that maximizes the growth-rate, independently of the resulting yield. If $\beta \to +\infty$, then the cell will pick the γ that maximizes the yield, independently of the resulting growth-rate.

F.5. Parameter evaluation

Symbol	Value	Units	Reference	Notes
m_0	258×10^{-15}	grams	[304]	60 minutes doubling time
ϕ_p	0.5	Mass fraction	[99, 92]	
ε_C	4.4×10^9	sugar/hour/m_0	Extrapolated from [100]	See Eq. (F.79)
ε_A	9.9×10^8	sugar/hour/m_0	Extrapolated from [232, 99]	See Eq. (F.83)
l	3.3×10^{-6}	meter	Extrapolated from [305]	See Eq. (F.73)
l/w	3	length:width ratio	[29]	
$\sigma_{\text{ATP},A}$	15.45	ATP cost biosynthesis	Extrapolated from [263, 306, 236]	See Eq. (F.72)
$\sigma_{s,A}$	1.1×10^9	sugar per m_0	Extrapolated from [262]	See Eq. (F.70)

TABLE 2: Parameter values used for solving the model.

Required number of incorporated sugars to make one cell To evaluate $\sigma_{s,a}$, we first postulate that 50% of the mass of the cell is made of carbons [262] (in fact 47% which we round up to 50%). This corresponds for a cell of 258×10^{-15} grams to 129×10^{-15} grams carbon per cell, thus for 1/12 mol per gram of carbon we have that a cell is made of $129/12 \times 10^{-15} \times N_A = 6.5 \times 10^9$ atoms of carbons. For a molecule of sugar s with 6 atoms of carbon we thus obtain:

$$\sigma_{s,a} \approx 1.1 \times 10^9 \text{ sugar per } m_0 \tag{F.70}$$

Evaluation of energetic cost of biomass synthesis We assume that for a cell with doubling time 60 minutes, $m_0 \approx 258 \times 10^{-15}$ grams [233]. Old evaluations put the ATP cost per cell at 5.9×10^9 [307] or 12.1×10^9 [308], the most recent one evaluates the ATP cost of a cell to 15.65×10^9 (for a cell weighting

280×10^{-15} grams in the three cases). We renormalize this value for a cell of 258×10^{-15} grams and obtain $15.65 \times 10^9 \cdot 258/280 = 14.4 \times 10^9$ ATP per cell.

This evaluation only considers macromolecules biosynthesis (DNA, RNA, proteins) and ignores the energetic cost of lipid biosynthesis. To evaluate the cost of lipid biosynthesis we first consider that all lipids are palmitic acids, accordingly to build one molecule of palmitic acid requires 7 ATP and 14 NADH [306]. We convert the NADH in ATP equivalent, *i.e.* assuming 10 protons are transported per NADH and 1 ATP is formed per 3.3 protons this gives an ATP equivalent cost of building one palmitic acid of ≈ 49 ATP per molecule. A palmitic acid has molar mass of 256 gram per mol which corresponds to $256/N_A \approx 4.3 \times 10^{-22}$ gram per molecule of palmitic acid. We then consider that 9% of *E. coli* biomass is made of lipids [236], such that if all lipids are palmitic acid this corresponds (for a cell of weight 258×10^{-15} grams) to $258 \times 10^{-15} \cdot 0.09/(4.3 \times 10^{-22}) \approx 5.4 \times 10^7$ molecules of palmitic acids per cell. That corresponds to $49 \times 5.4 \times 10^7 \approx 2.6 \times 10^9$ ATP required to make all lipids in a cell of 258×10^{-15} grams.

Thus the total ATP cost of making a cell is evaluated to:

$$\text{ATP Cost per Cell with reference mass } \approx (2.6 + 14.4) \times 10^9 = 17 \times 10^9 \quad \text{(F.71)}$$

To obtain $\sigma_{\text{ATP},A}$ in reaction (F.5) we divide the number of incorporated sugar needed to make one m_0 biomass by the number of ATP needed to make m_0 biomass and obtain:

$$\sigma_{\text{ATP},A} = \frac{17 \times 10^9}{1.1 \times 10^9} = 15.45 \text{ ATP per incorporated sugar} \quad \text{(F.72)}$$

Shape properties We first evaluate the average volume per cell (with doubling time 60 minutes) according to the empirical relationship [305] between volume and specific growth-rate:

$$\text{Volume} = -0.53 \cdot \mu^2 + 2.41 \cdot \mu + 1.62 \quad \text{(F.73)}$$

where μ is the specific growth rate per hour and the volume is in μm^3. a doubling time of 60 minutes corresponds to $\mu = \ln(2)$ and by the empirical relationship above to a volume of $\approx 3.0\mu\text{m}^3$.

We then know that for a spherocylinder, the surface and volume follow:

$$S = \pi \cdot w \cdot l \tag{F.74}$$
$$V = \pi \cdot (w/2)^2 \cdot (l - w/3) \tag{F.75}$$

(see chapter 2). Assuming a length to width ratio of 3, the length and width required to obtain $V = 3.0 \times 10^{-18}$ m^3 are:

$$w = 1.1 \times 10^{-6} \text{ meter} \tag{F.76}$$
$$l = 3.3 \times 10^{-6} \text{ meter} \tag{F.77}$$

and the corresponding surface is:

$$S = 1.14 \times 10^{-11} \text{meter}^2 \tag{F.78}$$

Catabolic catalytic efficiency [100] experimentally shows that the flux of ATP production by respiration is $\phi_C \times 390$ mM of ATP per absorbance A_{600nm} per hour where ϕ_C is the proteome fraction of the cell ($0 \leq \phi_r \leq 1$) occupied by respiratory enzymes (in our case catabolic enzymes). The cell dry mass for one unit of A_{600nm} is 0.39 gram/L [309]. Which gives for our reference cell of $m_0 = 258 \times 10^{-15}$ gram a maximal ATP production of $390/0.39 \cdot 258 \times 10^{-15} \cdot N_A \times 10^3 = 1.6 \times 10^{11}$ (where we assumed null maintenance cost and $\phi_C = 1$). This gives a catabolic efficiency of:

$$\varepsilon_C = 4.4 \times 10^9 \text{catabolized glucose per hour per } m_0 \text{ mass of catabolic enzymes} \tag{F.79}$$

Fitting the reference state We first assume Doubling time 0.89 per hour(corresponding to $\mu = 0.89 \cdot \ln(2)$) [232]. In our model all catabolized sugar go through respiration, and from [232] we have an oxygen consumption rate of 3.08×10^9 O_2 per cell per hour which corresponds to:

$$j_C = 3.08 \times 10^9/6 \approx 5.1 \times 10^8 \text{ catabolized glucose per cell per hour} \tag{F.80}$$

where we assume 6 O_2 were consumed per catabolized glucose. This corresponds by Eq. (F.40) to a growth yield of $\approx 57\%$ which is quite close to other referenced values **REf**.

We then compute the associated mass fraction of catalysts:

$$\phi_C = j_C/\varepsilon_C \approx 11.6\% \tag{F.81}$$

which is consistent with the experimentally obtained proteome fraction at similar doubling time in [100].

The corresponding mass fraction of biosynthetic enzymes follows:

$$\phi_A = \phi_p - \phi_C \tag{F.82}$$

and depends on the mass fraction ϕ_p available for catabolic/biosynthetic processes.

We can then derive the catalytic efficiency of the mass contributing to biosynthetic processes:

$$\boxed{\varepsilon_A = j_A/\phi_A = \sigma_{s,A} \cdot \frac{\mu}{\phi_p - \phi_C}} \tag{F.83}$$

which for $\phi_p = 0.5$ is $\approx 1.8\times^9$ glucose incorporated into the biomass per cell per hour.

This correspond in addition to a maintenance cost of:

$$j_M = \sigma_{\mathrm{H}^+,C} \cdot j_C - \sigma_{\mathrm{H}^+,\mathrm{F1F}_o} \cdot \sigma_{\mathrm{ATP},A} \cdot \sigma_{s,A} \cdot \mu \approx 27 \times 10^9 \text{ Protons per cell per hour} \tag{F.84}$$

Assuming $\sigma_{\mathrm{H}^+,C} = 120$, $\sigma_{\mathrm{H}^+,\mathrm{F1F}_o} = 3.3$. Assuming some change in the parameters would predict an different maintenance cost:

- a lower proton extruded per consumed oxygen, *e.g.* $\sigma_{\mathrm{H}^+C,C} = 8 \cdot 12 = 96$, then $j_M = 14 \times 10^9$.
- An higher number of protons consumed per ATP $\sigma_{\mathrm{H}^+,\mathrm{F1F}_o} = 4$, yields $j_M = 19 \times 10^9$.
- Change of both protons extruded per oxygen consumed and higher protons consumed per ATP synthesized as above: $j_M = 7 \times 10^9$.

For parametrization equivalent to Eq. (F.84) we obtain a P/O ratio of:

$$\text{P/O Ratio} = \sigma_{\mathrm{H}^+,\mathrm{F1F}_o} \cdot \left(1 - \frac{j_M}{\sigma_{\mathrm{H}^+,C} \cdot j_C}\right) \approx 1.85 \tag{F.85}$$

The corresponding proton to ATP conversion efficiency is:

$$1 - \frac{j_M}{\sigma_{\mathrm{H}^+,C} \cdot j_C} \approx 56\% \tag{F.86}$$

i.e. 70% of the protons extruded by respiration are used to make ATP.

Biosynthesis catalytic efficiency The biosynthesis catalytic efficiency is evaluated by Eq. (F.83) and crucially depends on the amount of mass fraction ϕ_p that is available for catabolic and biosynthetic enzymes as shown in fig. 13.

G. Supplementary Figures

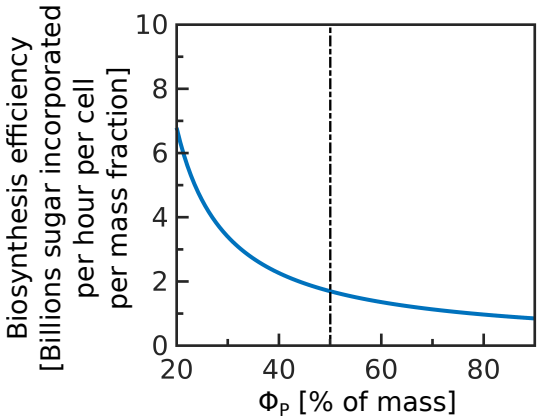


Figure 13: Fit of the biosynthetic catalytic efficiency using Eq. (F.83). The specific growth-rate $\mu = 0.89 \cdot \ln(2)$ and the mass fraction of catabolic enzymes $\phi_C = 11.6\%$ was set according to the reference state.

Reference Values: PMF = -170 mV pH_i = 7.5 $[CA]_0$ = 50 mM
Proton Budget = 61.6 * 10^9 [Proton/Cell/hour] Biomass Cost = 17 * 10^9 [ATP/Cell]

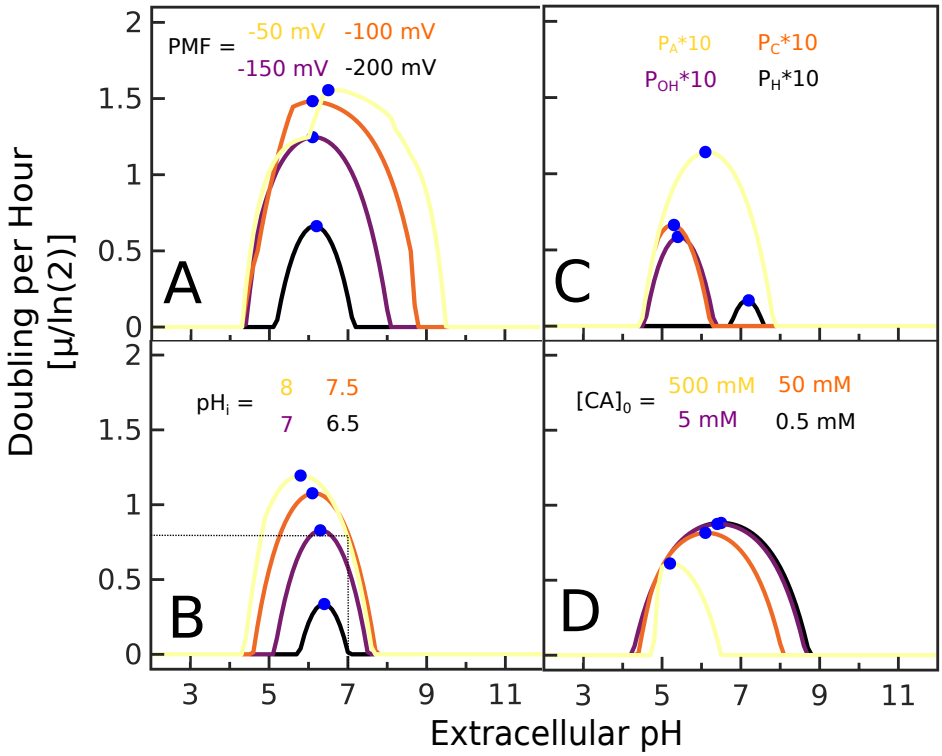


FIGURE 14: We now assume that the model lost its ability to up/down-regulate catabolism in response to varying energy demand of the electrophysiological component of the model. Consequently, the catabolic flux is invariant by changing maintenance cost and is set to 61.6×10^9 protons per cell per hour. The maintenance cost is evaluated as before by the model of *E.coli*'s electrophysiology. The growth-rate is then evaluated by Eq. (3) in the main text. (A, B, C, D) The doubling rate is shown as a function of extracellular pH for different sets of parameters. The maintenance rate as a function of pH_e, $[CA]_0$, PMF, pH_i and osmotic pressure is computed as in chapter 2. Osmotic pressure is set to 1 atm, permeabilities to $P_{H^+} = P_{OH^-} = 10^{-4}$ m/s; $P_{C^+} = 5 \times 10^{-10}$ m/s; $P_{A^-} = 1.5 \times 10^{-10}$ m/s. Reference values for maintenance cost-dependent variables are $pH_i = 7.5$, PMF $= -150$ mV, $[CA]_0 = 50$ mM. The total catabolic flux is set according to the oxygen consumption rate on MM9+glucose [232] and corresponds to 61.6×10^9 protons per cell per hour (assuming 10 protons are moved per oxygen consumed). The biomass cost is set to 26×10^9 ATP/Cell assuming that the ATP cost per unit biomass is identical for the cell than it is for amino acids. The shape properties are computed as in chapter 2 assuming length and width from [162] on MM9+glucose (corresponding to doubling time $\approx 60 minutes$ and a 3:1 length to width ratio spherocylindrical cell. The mass of a cell is set to 258×10^{-15} grams [233] for *E.coli* with doubling time 60 minutes. We then for each figure vary: (A) PMF maintained, (B) pH_i maintained, the dotted line shows that doubling rate ≈ 0.82 per hour is achieved for reference values (C) Each permeability multiplied by a factor 10 and (D) salinity.

Chapter 4

Discussion

I. Preamble

It is now the last chapter of this thesis. We already discussed extensively, at the end of each chapter, the biological implications of the models I have developed during the course of my Ph.D. Consequently, I will first proceed in this discussion with a brief summary of the previous chapters. To avoid redundancy, I shall discuss in particular the limitations of electrophysiological measurements in bacteria as well as discuss more thoroughly the limitations of our modeling assumptions and how to alleviate them. I will also discuss a few additional biological topics I wish I had the time to study as well as some preliminary studies in relation with the models herein. I will then elaborate on the modeling methodology that was succintly outlayed in chapter 2, which will conclude this thesis, and may almost be seen as an additional chapter fulfilling a educative function. Indeed, in chapter 2 we focused on the biological implications of simple models of ionic transports in *E. coli* and made experiments to support their predictions. In the second part of this discussion I will attempt to push a thermodynamic approach to the steady-state analysis of electrochemical coupling across membranes. I think this approach, if not directly outstanding from the point of view of the biological predicates it makes, gives nevertheless simple heuristics to visualize how models of electrochemically coupled ionic transports behave. That is, without making any stringent assumptions on how the kinetics are defined.

II. Summary of Previous Chapters

This thesis approached in each chapter a different aspect of microbial electrophysiology. I chose to first discuss the methods underlying the experimental measurements of electrophysiological behaviours of *E.coli* that contains this thesis. I shall then briefly recapitulate the biological implications of this thesis and take the opportunity to discuss on one hand the limitations of the models we used and the other hand three relevant biological topics we did not talk about before *(a)* heavy metal toxicity, *(b)* intracellular cation balance (between sodium and potassium) and *(c)* ionic environmental control by microbes. Finally, I will attempt to conceptually capture the modeling workflow of this thesis which may prove useful for approaching cellular electrophysiology.

III. Relevance to Additional Biological Topics

i. Limitations of Electrophysiological Measurements in Bacteria

The first chapter is essentially a cautionary tale for microbial electrophysiologist: measuring membrane voltage using ThT, a Nerstian dye, gives non physiological readouts of membrane voltage. This may extend to other Nerstian dyes, the model suggesting that part of the toxicity may be due to the addition in the growth medium of charged particles that the cell does not know how to pump, thereby impairing the membrane voltage, simply by the charged dye equilibrating across the membrane. Chapter 1 therefore outlays a way to design control experiments for the use of Nerstian dyes that could *a priori* test whether the specific dye at use is toxic for the cell or/and impair membrane voltage. The proposed controlled workflow for measuring membrane voltage with Nernstian dyes is, in spite of necessary, tedious as many controls must be repeated for each different environmental condition wherein one wishes to measure membrane voltage using Nernstian dyes. This calls, in my opinion, for the developments of other methods that would allow membrane voltage measurements.

In fact, we use in chapter 2 a new method for measuring membrane voltage, although it is an indirect one. Indeed, voltage, pH_i, pH_e and PMF being linked by the definition of the PMF, it is enough to measure three of the four variables to evaluate the last one. In the light of the results of chapter 1, and the lack

of alternatives for measuring membrane voltage[1], we proceeded with an indirect measurement of voltage, *i.e.* inferring it *via* simultaneous measurement of PMF and pH_i in an environment with controlled pH_e. This technique has its own limitations though. Indeed, though the rotational speed of the BFM (Bacterial Flagella Motor) was shown to scale linearly with the PMF, calibration of the BFM and the PMF is not trivial, *i.e.* setting the coefficient a in PMF $= a\times$ Motor Speed. We based our evaluation of a on the principle that in our reference condition MM9+glucose, a is chosen so that the number of cells maintaining PMF between -229 mV and -170 mV is maximized. Given that the motor speed in MM9+glucose is normally normally distributed, a is such that $a = \dfrac{(-229-170)/2}{\text{Mean Measured Motor Speed}} \approx -1.1$ mV/Hz, and for that a, approximatively 90% of the cell maintain PMF between -229 and -170 mV in MM9+glucose. Normally distributed motor speed is supported directly by experimental measurements Ekaterina Krasnopeeva made of PMF in various conditions [129, 179]. The choice of the bounds for PMF allowing respiration and ATP synthesis by F1Fo: between -229 and -170 mV relies on many underlying assumptions: the values for the physiological Gibbs free energy associated to NADH reduction and ATP synthesis as well as the coupling stoichiometries of protons to NADH for the respiratory chain and proton to ATP for $F1F_o$. Although I could not find evidence that the Gibbs free energy of NADH reduction or ATP hydrolysis vary significantly depending on the physiological state of the cell, it is nevertheless a possibility that in our environmental conditions, those values deviate significantly from the previously measured values we assumed[2].

On the other hand, while the coupling stoichiometry of the respiratory chain seems not subjected to debate [234], such is not the case for $F1F_o$. Without digging too much in details, this coupling stoichiometry is usually evaluated by dividing the number of c-subunits by 3. The number of c-subunits varies among organisms and has been measured to be 10 in *E.coli*, therefore the $10/3 \approx 3.3$ protons per ATP we assumed. Some authors [311] have argued that the number of protons travelling through F1Fo per synthesized ATP was not necessarily a

[1] with the exception I found of [310], that seems to be an interesting way of measuring the average resting membrane potential over a population of cell.

[2] Note that the bounds on PMF scale logarithmically with the concentration ratio of NADH reduction/ATP hydrolysis, such that they are quite robust to variations in the concentration ratios $[NADH]/[NAD^+]$ and [ATP/[ADP]. Indeed, multiplying (or dividing) $[NADH]/[NAD^+]$ by 10 would modify the lower bound from -229 mV to ≈ -235 mV (or -223 mV). Similarly, multiplying (or dividing) [ATP/[ADP] by 10 would modify the upper bound from -170 mV to ≈ -176 mV (or -164 mV). Multiplying these concentration ratios by 100 instead would modify the bounds by ± 12 mV, for a multiplication by 1000 the bounds are modified by ± 18 mV, *etc.*

constant for a given strain, indeed different laboratories reported different coupling stoichiometry H:ATP for F1Fo. This point of view has however been challenged [**?**] on the basis that the number of c-ring subunits per F1Fo is genetically encoded, thus the coupling stoichiometry H:ATP of F1Fo for a given strain shall not depend on the environmental condition. Be as it may, if the coupling stoichiometry H:ATP of F1Fo can vary (*i.e.* with different environmental conditions, among different individual belonging to the same genetic population) this would impact our experimental evaluation of a, thus of the PMF and subsequently that of membrane voltage.

Another limitation of this technique is due to the difficulty of measuring the motor speed of the BFM. Indeed, performing this experiment requires a significant amount of training, dedicated microscopes with optical trapping capability and is long to perform (of the order of 1 hour of experimental time per cell Ekaterina Krasnopeeva measured the PMF in chapter 2). This method for measuring voltage is thus insofar not very amenable to multi-dimensional screening of the environment, which as we mentioned earlier, would certainly be interesting to characterize the models further. For instance, simultaneous measurement of the electrophysiological homeostases (PMF, pH_i, membrane voltage) for a 2-D screening of the environment for pH_e and salinity could offer insight on how salt and pH challenges synergize to affect microbial physiology. In particular, it could validate our predictions that the extent to which salinity impairs cellular functioning is related to the membrane voltage this cell maintains in an environment with a given pH_e. Be as it may, some people in Pilizota's lab in collaboration with [312] are currently working on how to automatize the Motor speed measurement, which if functional, would solve that issue and allow high throughput screening of the PMF. Another potential limitation of the experimental measurement of the PMF we did not mention earlier, is that the coefficient a (and perhaps even the linearity of the relationship between motor speed and PMF) could in principle depend on the environmental conditions. Indeed, if previous controls have identified that this relationship was linear, one could argue that no controls were performed in *e.g.* very acidic conditions.

ii. Extending the Model for more Ions

I ignored in this thesis most of the diversity of small ions compounding growth media. For instance, we considered only one monovalent cation (on top of protons

or the dye) in the three chapters, ignoring that growth media contain several small monovalent ions: ammonium, potassium, sodium, *etc.*, divalent ions: magnesium, calcium, *etc.*, and essential plurivalent cations such as iron. We also ignored the diversity of small anions, for instance dihydrogen phosphate $H_2PO_4^-$. Before talking about the biological questions one could ask with respect to this diversity of small ions, we first introduce a compact rewriting of the membrane voltage definition that would be useful for studying models wherein more inorganic ions are considered (interest of which we will exemplify later in this subsection):

$$\frac{S}{V}\cdot\frac{C_m}{F}\cdot\frac{\Delta\psi}{[X]_e}=\phi_{y,i}+\sum_{z=-4}^{z=+4}z\cdot e^{-z\cdot\frac{F}{RT}\cdot\Delta\psi}\sum_{x|z_x=z}\phi_{x,e}\cdot e^{\frac{F}{RT}\cdot\Delta G_x} \tag{III.1}$$

which can easily be derived from the general definition of membrane voltage we introduced in the introduction, where $[X]_e := \sum_x [x]_e$ is the total extracellular concentration in small ions, $\phi_{y,i} := \sum_y z_y \cdot [y]_i/[X]_e = z_Y \cdot [Y]_i/[X]_e$ is the intracellular charge carried by captive molecules relative to $[X]_e$ and $\phi_{x,e} := [x]_e/[X]_e$ is the fractional composition of the medium in small ion x. Importantly, $\sum_{x|z_x=z}$ is a sum over small ions that have valency equal to z, while $\sum_{z=-4}^{z=+4}$ sums over all possible valencies small ions can have. Also when $[X]_e$ is high enough, the left hand term becomes negligible and the relationship between membrane voltage and other state variables is given by:

$$0=\phi_{y,i}+\sum_{z=-4}^{z=+4}z\cdot e^{-z\cdot\frac{F}{RT}\cdot\Delta\psi}\sum_{x|z_x=z}\phi_{x,e}\cdot e^{\frac{F}{RT}\cdot\Delta G_x} \tag{III.2}$$

Although we do not evaluate the validity range of that approximation in general, we evaluated its validity in the specific case where we considered only one monovalent cation C^+ and one monovalent anion A^- (on top of H^+ and OH^-) in chapter 2. From a computational point of view, the equation above has relatively low dimensionality. For n small ions considered, we have $n+2$ underdetermined variables in Eq. (III.1) and $n+1$ in Eq. (III.2) (1 electrochemical potential for each ion, 1 additional variable for the left hand term in Eq. (III.1) and 1 additional variable for the charge carried by captive molecules). Where Eq. (III.1)

demonstrates its capabilities is by introducing the following rewriting:

$$\phi_e^{(z)} := \sum_{x|z_x=z} \phi_{x,e} \tag{III.3}$$

$$\Delta G^{(z)} := \ln\left(\frac{\sum_{x|z_x=z}\phi_{x,e}\cdot e^{\frac{F}{RT}\cdot\Delta G_x}}{\phi_e^{(z)}}\right) \tag{III.4}$$

$$\frac{S}{V}\cdot\frac{C_m}{F}\cdot\frac{\Delta\psi}{[X]_e} = \phi_{y,i} + \sum_{z=-4}^{z=+4} z\cdot\phi_e^{(z)}\cdot e^{\frac{F}{RT}\left[\Delta G^{(z)}-z\cdot\Delta\psi\right]} \tag{III.5}$$

Bluntly, Eq. (III.5) allows mapping of models that consider different number of ions between one another, allowing a computational study that only gradually increases the dimensionality of the problem and can "attribute" some of the models' behaviours to certain dimensionalities. For instance, some behaviours of interest may require at least some dimensionality threshold to emerge and this is something we can talk about by incrementally increasing the dimensionality. I realize that what I wrote above may seem completely cryptic for now so let us take an example that will allow us a preliminary analysis of a model where we consider two monovalent cations: potassium K^+ and sodium Na^+ as opposed to the chapter 2 of this thesis where we considered only one monovalent cation C^+. If we consider a model with only monovalent ions then Eq. (III.5) reduces to:

$$\frac{S}{V}\cdot\frac{C_m}{F}\cdot\frac{\Delta\psi}{[X]_e} = \phi_{y,i} + \phi_e^{(z=+1)}\cdot e^{\frac{F}{RT}\left[\Delta G^{(z=+1)}-\Delta\psi\right]} - \phi_e^{(z=-1)}\cdot e^{\frac{F}{RT}\left[\Delta G^{(z=-1)}-\Delta\psi\right]} \tag{III.6}$$

In particular, assuming that $[H^+]_i = [OH^-]_i$ for simplicity (neutral pH_i), Eq. (III.6) is equivalent to the voltage equation in chapter 2 identifying $[C^+]_e \equiv \phi_e^{(z=+1)}\cdot[X]_e$, $\Delta G_{C^+} = \Delta G^{(z=+1)}$, $[A^-]_e \equiv \phi_e^{(z=-1)}\cdot[X]_e$ and $\Delta G_{A^-} = \Delta G^{(z=-1)}$. Now if we assume two monovalent cations (potassium and sodium) instead we will find that the voltage still can be written as Eq. (III.6) with the addition of two mapping

equations:

$$\phi_e^{(z=+1)} = \phi_{\mathrm{K}^+,e} + \phi_{\mathrm{Na}^+,e} \tag{III.7}$$

$$\frac{F}{RT} \cdot \Delta G^{(z=+1)} = \ln \left(\frac{\phi_{\mathrm{K}^+,e} \cdot e^{\frac{F}{RT} \cdot \Delta G_{\mathrm{K}^+}} + \phi_{\mathrm{Na}^+,e} \cdot e^{\frac{F}{RT} \cdot \Delta G_{\mathrm{Na}^+}}}{\phi_e^{(z=+1)}} \right) \tag{III.8}$$

that maps the model with two monovalent cations to the model with one monovalent cation. This means that the results of the analysis on how the voltage in the model with one monovalent cation covaries with its dependent variables (captive charge content, Anion Motive Force, Cation Motive Force) pertains as well to the analysis on how the voltage in the model with two monovalent cations covaries with its dependent variables. To see this, consider we found in the model with one monovalent cation, that at neutral pH_e (so $\phi_{\mathrm{C}^+,e} = \phi_{\mathrm{A}^-,e} = 1/2$ for $\phi_{y,i} = -0.1$ to maintain voltage $\Delta\psi = -140$ mV in the absence of anionic pumping (so $\Delta G_{\mathrm{A}^-} = 0$) the cell needs to maintain $\Delta G_{\mathrm{C}^+} = -180$ mV. Since reaching this result is computationally expensive, it is useful to solve a model with two monovalent cations by the inexpensive analytical solving of Eqs. (III.7) and (III.8). For instance, say we now wish the model that considers both potassium and sodium to maintain voltage -140 mV, with $\phi_{y,i} = -0.1$, neutral pH_i (so $\phi_{\mathrm{K}^+,e} + \phi_{\mathrm{Na}^+,e} = \phi_{\mathrm{A}^-} = 1/2$) and no anionic pumping (so $\Delta G_{\mathrm{A}^-} = 0$) in an environment where a fraction $\phi_{\mathrm{K}^+,e} = 0.05$ of the ions are potassium and the cell maintains a Potassium Motive Force $\Delta G_{\mathrm{K}^+} = -140$ mV, then using the two equations above and the result for $\Delta G_{\mathrm{C}^+} \equiv \Delta G^{(z=+1)} = -180$ mV from the model where we considered one monovalent ion we rearrange Eqs. (III.7), (III.8) as:

$$\phi_{\mathrm{Na}^+,e} = \phi_e^{(z=+1)} - \phi_{\mathrm{K}^+,e} \tag{III.9}$$

$$\Delta G_{\mathrm{Na}^+} = \frac{RT}{F} \cdot \ln \left(\frac{\phi_e^{(z=+1)} \cdot e^{\frac{F}{RT} \cdot \Delta G^{(z=+1)}} - \phi_{\mathrm{K}^+,e} \cdot e^{\frac{F}{RT} \cdot \Delta G_{\mathrm{K}^+}}}{\phi_{\mathrm{Na}^+,e}} \right) \tag{III.10}$$

and get that $\phi_{\mathrm{Na}^+,e} = 0.45$ and $\Delta G_{\mathrm{Na}^+} = -194$ mV. For some pairs $\{\phi_{\mathrm{K}^+,e}, \Delta G_{\mathrm{K}^+}\}$ the equation above may not have non-complex solutions, reflecting that the desired membrane voltage is not achievable given the extracellular composition in potassium and the set KMF.

Now why is the above relevant to some of the conclusions we drew in previous chapters ? For instance, the results in figure SI 4B of chapter 2 that we derived for a model with only one small monovalent cation extend in an identical way (the plot would be the same) for considering arbitrary number of monovalent cations restricted to the mapping defined by Eqs. (III.7), (III.8). Similarly the relationship between osmotic pressure and membrane voltage shown in chapter 2 figure SI 3A holds when considering arbitrary number of monovalent cations, restricted to the mapping defined above. What does it mean to be restricted to the mapping above ? I mean that the two models (one monovalent cations *versus* several monovalent cations) have identical: *(i)* membrane potential, *(ii)* electrochemical potential for anions, *(iii)* intracellular concentration and valency of captive molecules and *(iv)* membrane capacitance and cellular shape. In other words everything else but behaviours of monovalent cations (extracellular composition, cationic motive forces) remains the same[3]. This subsection highlights that some of the conclusions we made in this thesis for the model with one monovalent cation naturally extend to more complex models. This motivates the incremental complexification of such models.

Note that some conclusions of the simple model may not extrapolate to more complex models. For instance, we did not look at whether the allowed range at steady-state for electrochemical potentials would react to the aforementionned coarse-graining.

We will next discuss several biological topics I deem of interests that could have been part of this thesis (with more time or/and different choices of which questions to prioritize).

iii. Heavy Metal Homeostasis and Electrophysiological Maintenance

Heavy metals are a loosely defined group of atomic species that are toxic to all life forms [313]. Heavy metal toxicity however exemplifies the adage “Only the dose makes the poison” as many of them are essential trace elements and become

[3]Note that this does not include the analysis on the cost of maintaining a given electrophysiological steady-state. Indeed, the ΔG_{C^+} that is optimal for the maintenance of an electrophysiological steady-state in the model with only one monovalent cation (on top of protons) is not the $\Delta G^{(z=+1)}$ that would be optimal in a model with additional monovalent cations.

detrimental to survival only at sufficiently high concentrations [314][4]. Note that if addition of potassium and sodium at sufficiently high concentrations is also toxic for the cell, for *E. coli* cells, the concentrations at which potassium/sodium become toxic are orders of magnitude higher than that of heavy metals. A perfect example of this phenomenon is iron, an essential cofactor of many electron transport chains, which is hypothesized to have partaken in the metabolism of early life forms [315]. On the other hand, iron is at sufficiently high concentrations toxic for cells, notably because of the production of Reactive Oxygen Species (ROS) [5] *via* the Fenton reaction [316]. This duality is not restricted to iron as many heavy metals act as double edged swords for living cells: Copper, Zinc, Chromium, *etc.*[6], while some other toxic heavy metals do not fulfill any known beneficial functions: Mercury, Cadmium, *etc.* [314]. This duality of the impact of heavy metals on cells motivates the two following topics we shall discuss in relation with the maintenance of global electrophysiological homeostasis: intracellular pH, membrane voltage and PMF.

Potentiation of Heavy Metal accumulation by Membrane Voltage: Could it explain the universal "choice" of negative PMF ? Something that is important to notice for this aspect of the discussion is that the vast majority of heavy ions that are important for functioning of the cell (a.k.a. trace elements) are positively charged [314]. As indicated by the same author, bacteria use a variety of passive and active transport systems for heavy metals. In fact, a cell maintaining negative membrane voltage will passively accumulate heavy metals, *i.e.* assuming that they equilibrate across the membrane, rewriting Nernst equation yields:

$$[x]_i = [x]_e \cdot e^{-\frac{F}{RT} \cdot z_x \cdot \Delta\psi} \tag{III.11}$$

The valency plays an important part in the accumulation of such ion. For example, take an *E.coli* cell maintaining -140 mV membrane voltage (equivalent to PMF -170 mV, pH_i 7.5 at pH_e 7), a monovalent cation equilibrating across the membrane will have intracellular concentration $\approx$ 200 folds higher than its extracellular

[4] We will base a significant part of the discussion on this review.

[5] Briefly, when ROS are in excess, they damage biological macromolecules: lipids, proteins, DNA, *etc.*. Note that this mechanism mediating iron toxicity requires oxygen to be present, thus cannot explain potential toxicity of iron in oxygen deprived environments, such as these prior the "great oxygenation event".

[6] All of these are used as cofactors and are often necessary for CO2 fixation.

concentration. This figure ramps up to $\approx 5 \times 10^4$ for divalent cations (like most heavy metals: iron, zinc, copper) and 10^7 for trivalent cations (iron in an oxygenated environment, not too acid pH). Some authors claim that intracellular accumulation of, *e.g.* iron, 4–6 orders of magnitude greater than that of the environment requires active transport systems [317]. It is however compatible with passive transport alone depending on the membrane voltage the cell maintains and whether iron is present in its divalent or trivalent form. Interestingly, *E. coli* possesses both active and passive iron transporters, with expression of active transporters increasing in anaerobic conditions [318]. Perhaps the need for active transporters become more stringent in anaerobic conditions, wherein membrane potential is closer to 0, thus membrane voltage does not allow sufficient intracellular accumulation of iron *via* passive transport (equilibration across the membrane) alone[7]. Another immediate consequence of the intracellular accumulation of trace elements is that the assumption we made, that the environmental composition of ions was invariant on the cellular behaviour, is much less likely to hold for divalent heavy metals than for monovalent ions that the cell often accumulates. Together with the low extracellular concentrations of iron, this explains why iron is the limiting factor of growth of phytoplanktons in significant fractions of the oceans [317].

It is at this stage a good place to ask a seemingly naive question, which has (to my knowledge) never been asked: *Why do bacteria maintain negative PMF rather than positive PMF ? (or why do they pump protons outward rather than inward ?)*[8] Indeed, one could imagine cells maintaining positive PMF, orientating proton passive diffusion from the inner space to the outter space[9]: $H_i^+ \rightarrow H_e^+$ with other systems coupled to proton electrodiffusion being in the inverse direction. For instance in that virtual world where bacteria maintains positive PMF, ATP synthases would be oriented to power ATP synthesis *via* outward movement of protons[10], respiratory chain would power *via* redox reactions the inward movement of protons, membrane voltage would be generated *via* proton:cation symporters

[7] Alternatively, these transporters may be used to excrete irons, perharps because it is less necessary to fermentative metabolism, perhaps in an attempt to polarize the cell (generating more negative voltage).

[8] We mean here electrochemical gradient oriented inward rather than outward, equivalently spontaneous movement of protons directed inward and not outward.

[9] could be from the cytoplasm to the extracellular environment for a gram positive bacteria, from the cytoplasm to the intermembrane space for a gram negative, from the matrix to the intermembrane space for mitochondria, *etc.*

[10] Note that this does not necessarily mean that ATP synthesis would occur outside, but it may be that such ATPase have evolved the ability to couple proton movement to ATP synthesis

(negative membrane voltage) or proton:anion symporters (positive membrane voltage) while active sugar import would be powered by proton:sugar antiporters and not symporters.

One negative impact of generating positive PMF would be the accrued difficulty in accumulating necessary heavy ions (iron, sulfur, *etc.*). The majority of life thriving around neutral extracellular pH, maintaining positive PMF would entail positive membrane voltage to simultaneously keep PMF high enough to perform chemiosmotic coupling (oriented in the inverse direction) and near neutral intracellular pH. This positive membrane voltage would then work to drive passive accumulation of necessary heavy metals such as iron in the extracellular space, thereby requiring highly energized active iron transport systems to maintain high intracellular concentrations of iron relative to that of the extracellular space. It seems now natural for the reader to wonder *"what about acidophiles, for which negative PMF entails positive membrane voltage, detrimental to intracellular iron accumulation ? Surely, acidophiles must have developed sophisticated ways of accumulating iron"*. In answer to the question, in very acidic environments iron is more available than at other pH_e, in part dictated by higher solubility of iron ions at low pHs [319], such that the difficulty of accumulating iron when maintaining positive membrane voltage, is in part compensated by the higher extracellular availability of iron at pH_e where maintenance of negative PMF and near neutral pH_i entails maintenance of positive membrane voltage. What is more is that the higher solubility at low pHs is not restricted to iron but to most cationic metals [320]. One plausible reason underlying the evolutionary choice of maintaining positive rather than negative PMF is the fundamental asymmetry between heavy metal accumulation and membrane voltage. Of course, there are likely alternate reasons to this evolutionary choice we do not talk about there.

Toxicity of Heavy Metals. The reported mechanisms mediating the toxicity of heavy metals are diverse and in general specific to the heavy metal, *e.g.* iron or copper *via* the production of ROS, the interaction with phosphate metabolism for arsenic, *etc.* [314]. We hypothesize an additional mechanism which could mediate heavy metal toxicity that is analogous to the detrimental effect of ThT on membrane voltage in chapter 1. The presence of any positively charged particle in the medium the cell does extrude of the cell at a sufficient rate (the

in another way than known ATPase, *i.e.* in a way that ATP synthesis occurs inside and is powered by outward movement of protons.

extreme case being the cell has no efflux pump able to export the cation) is detrimental to the maintenance of negative membrane voltage. For the same reason following Eq. (III.11), the detrimental effect of non pumped cations on the maintenance of negative membrane voltage increases exponentially with the valency of the cation. This detrimental effect is also concentration dependent, as is the modeled effect of ThT in chapter 1. Although appealing, verifying if such a mechanism indeed mediates part of heavy metal toxicity seems difficult. One could for instance imagine that in acidic pH_e where the cell maintains near null membrane voltage (if still maintaining high PMF), addition of heavy metal would not be so detrimental to survival since voltage is already near zero. However, near 0 voltage would also mean less intracellular accumulation of heavy metals, thus mitigation of their detrimental effect on survival by other mechanisms too. For similar reasons, any evaluation of the detrimental effect of heavy metals in environment where cells maintain different membrane voltage would be ubiquitous to the mechanism we propose and other mechanisms hypothesized in the literature.

Finally, particularly relevant for metal ions, and phenomenon we have ignored during the course of this thesis is the possibility for some ions to form complexes with other molecules, thereby rendering them unavailable for their passive transport reaction, *i.e.* an ion A bonding with B in the intracellular space (where AB_i denotes bound A and B):

$$A_i + B_i \rightleftharpoons AB_i \tag{III.12}$$

would bias the passive transport reaction of A: $A_e \rightleftharpoons A_i$ in the forward direction as some "free" A_i is taken away by reaction (III.12) thus not contributing anymore in the electrochemical potential of A (the Gibbs free energy associated with the passive transport reaction). The effect is expected to depend on the equilibrium constant of the reaction (III.12), which is typically biased to the right-hand side for reactions involving strong bonding. An example of such a reaction is a heavy metal being chelated and as a result, its equilibrium intracellular concentration (*i.e.* its intracellular concentration if not actively pumped across the membrane) would depend on the presence and concentrations of compounds chelating it.

iv. Impact of Small Organic Ions on Membrane Voltage: Ammonium

An important organic small ion we did not consider in this thesis is ammonium NH_4^+. It is usually present at relatively high concentrations in the environment since it is an essential substrate for cellular growth. The nitrogen atom constitutes approximately 10% of *E.coli*'s mass [321]. The nitrogen source is most often ammonium which has a pKa of 9.25. At neutral and acidic pH it is mostly in ammonium form whereas for pH greater than 9.25 it is mostly in ammoniac form NH_3. For identical reasons that we mentioned in chapter 1 and in the previous subsection and since NH_4^+ is present at high concentrations in the environment, for the cell to be able to maintain negative enough membrane voltage requires generation of an electrochemical gradient for ammonium oriented inward (negative electrochemical potential). For other inorganic ions such as sodium and potassium, this can be performed by potassium/sodium efflux pumps. *E. coli* however does not seem to possess any efflux pump for ammonium[11]. Perhaps because there is no need for an efflux pump to generate negative electrochemical potential in the case of ammonium. Its intracellular concentration can be reduced by assimilation of nitrogen into the biomass by glutamate dehydrogenase, the dominant pathway of nitrogen assimilation in *E.coli* (along with the glutamine synthetase-glutamate synthase we will not mention further [322]). Assimilation of nitrogen *via* glutamate dehydrogenase follows:

$$\underbrace{C_5H_6O_5^{2-}}_{\text{2-oxoglutarate}} + NH_4^+ + \underbrace{C_{21}H_{30}N_7O_{17}P_3}_{\text{NADPH}} \rightleftharpoons \underbrace{C_5H_9NO_4^-}_{\text{glutamate}} + \underbrace{C_{21}H_{29}N_7O_{17}P_3}_{\text{NADP}^+} + H_2O \tag{III.13}$$

where we assumed that pH value results in negatively charged glutamate. It is now interesting to see whether the flux of NH_4^+ consumption by metabolism is of comparable order of magnitude to the efflux rate of potassium and sodium to check whether the rate of NH_4^+ assimilation is high enough to generate electrochemical gradient of ammonium comparable to that of sodium and potassium[12]. Consider a cell with doubling time of 60 minutes and corresponding biomass 258×10^{-15} grams (see previous chapters for references). Then, for 10% of this mass is made of

[11] I could not find any report of such pump in the literature, albeit it may exist and may have not been yet reported, or I might have missed it.

[12] Although that depends on permeability too, we shall assume for simplicity that permeability of the membrane to ammonium is comparable to that of sodium/potassium.

nitrogen we obtain 25.8×10^{-15} grams of nitrogen oer cell. The mass of a nitrogen atom is 2.33×10^{-23} grams, which gives roughly a flux of one billion ammonium assimilated per hour per cell. This is incidentally of a similar order of magnitude as the efflux rate of small inorganic cations required for maintaining membrane voltage of -140 mV when its extracellular concentration is 50 mM (using Eyring's model and permeability as in previous chapters: 5×10^{-10} meter/second). We therefore hypothesize that no ammonium pumps are needed to maintain membrane voltage specifically because ammonium is incorporated into the biomass, which consumes intracellular nitrogen thereby allowing generation of the negative electrochemical gradient for ammonium required to maintain physiological membrane voltage.

Our hypothesis has some interesting consequences. If the cell indeed possesses no efflux pump for ammonium, it means that the ability to generate a negative electrochemical gradient for ammonium, thus negative membrane voltage, relies on the assimilation of nitrogen by the cell. There are now two options: *(i)* the cell assimilates nitrogen independently of its growth-rate, which would imply accumulation of glutamate in the intracellular and/or extracellular space at low enough growth-rate or/and *(ii)* the cell assimilates nitrogen exclusively in a growth-dependent manner. Of course a mix of the two strategies is conceivable and even likely. Prevalence of strategy *(ii)* would provide a simple mechanism by which growth and membrane voltage are related:

$\downarrow$ Growth $\Rightarrow\downarrow$ Nitrogen Assimilation

$\Rightarrow$ Collapse of ammonium electrochemical gradient $\Rightarrow$ Voltage less negative

One could for instance imagine that this mediates membrane voltage collapse that was measured when transitioning from exponential to stationary phase in *E.coli* [310]. Prevalence of strategy *(i)* would require a decrease in growth due to factors different than carbon limitations. Indeed strategy *(i)* requires continuous supply of 2-oxoglutarate, a carbon rich intermediate[13]. In fact, major links between glutamate, nitrogen and bacterial electrophysiology have recently been reported in biofilms (briefly, spatially structured bacterial communities) [323]. While likely possible, it is unclear to me how would one adapt the electrophysiological models

[13]It is also a Krebs cycle intermediate, so its supply would be related to NADH supply, respiratory rates, hence to the maintenance of electrophysiology homeostaeses.

from this thesis for electrophysiological processes in biofilms. Likely the two-compartment view in this thesis is no longer suitable and may be substituted by reaction-electrodiffusion models where one explicitly defines how electrostatic potential and ionic concentrations depend on the specific location within the biofilm, making the problem quite challenging from a computational point of view.

In the light of the discussion above, I think that ammonium could be an important link that couples electrophysiological responses (related to maintenance of membrane voltage, pH_i, osmotic pressure, IMFs) to physiological responses (related to regulation of gene expression).

v. Intracellular sodium and potassium balance

We shall now consider a possible extension of the model with two monovalent cations, this time identified as sodium and potassium. What motivates this part of the discussion is the observation that in general, most cells maintain higher intracellular concentrations of potassium than sodium. Such is the case for *E.coli* [324], *S. cerevisiae* [325], some mammalian cells like neurons [17] or heart cells [326]. There are some exceptions, notably *E.coli* was shown to maintain higher intracellular sodium than potassium in stationary phase [327], demonstrating that the ratio of intracellular sodium to potassium may depend on the environment the cell inhabits or/and its physiological state. Several hypotheses coexist in the literature as to why cells maintain higher intracellular potassium than sodium, non-exhaustively: sodium is toxic thus cells need to pump it out [328], potassium is an important cofactor of universal biochemical processes such as translation [329] which may reflect the environments early life forms evolved in wherein potassium was more common than sodium [330]. It was however demonstrated that addition of potassium in the environment is just as toxic to the cell than increase in extracellular sodium for microbes living in soil [331], suggesting that toxicity of sodium is mediated by a mechanism that is common to both potassium and sodium ions, thus rendering the postulate that cells maintain higher intracellular potassium than sodium because sodium is toxic unlikely. On the other hand, efficient ribosomal activity indeed requires potassium in the range 60-150 mM [332], of the same order of magnitude than intracellular potassium concentrations often observed and orders of magnitude greater than observed intracellular sodium concentrations. In [330], it is proposed that early cells made

the choice of potassium rather than sodium as cofactors of crucial catalytic processes (such as ribosomes) because potassium was much more available in the extracellular space than sodium. This hypothesis however eludes the possibility than these *protocells* already possessed some electrophysiological abilities and that the availability of intracellular potassium relative to sodium may not only depend on the composition of the environment but also on *how* these protocells maintained a membrane potential (if any) across their membrane. Indeed, if the cell maintain negative membrane voltage by pumping out sodium, this drives accumulation of potassium inside the cell, as shown by [333].

We propose here that higher intracellular potassium than sodium may rather reflect an energetically efficient strategy for maintaining voltage. For the purpose of the demonstration we first need to introduce a new metric, which although interesting with respect to the analysis of energy transducing processes, has not been used before in this thesis:

$$E_x := -\Delta G_x \cdot j_x \tag{III.14}$$

E_x (always positive by construction) is the flow of energy dissipated by the passive diffusion of x across the membrane, where we remind that j_x is the flux of passive transport of x across the membrane and ΔG_x its electrochemical potential. E_x has units of Watt (joule per second). Another way of interpreting E_x, that we shall use next, is that it is the *minimal* flow of energy that the cell needs to spend to make ΔG_x time-invariant at steady-state. To see this, assume that the cell moves x against its electrochemical gradient *via* an active pump r with free energy $\Delta G_r = \Delta G_p - \Delta G_x$ (for simplicity we assumed stoichiometry of 1 x per reaction). We are at steady-state and consequently the intracellular concentration $[x]_i$ is time invariant:

$$\frac{d[x]_i}{dt} = j_x - j_r = 0 \tag{III.15}$$

Assume further that $j_x > 0$ (it is oriented inward, as expected for passive diffusion of cations in the presence of negative membrane potential) and consequently $\Delta G_x < 0$. In order to maintain steady state with the pump r, this entails that j_r needs to be positive, which is equivalent to $\Delta G_r < 0 \Leftrightarrow \Delta G_p < \Delta G_x$. Now consider the *effective* amount of power that the cell is spending for maintaining time-invariant $[x]_i$, it is given by $E_r = -\Delta G_p \cdot j_r$ with some energy being dissipated in the reaction r: $-\Delta G_r \cdot j_r$ and the remaining in the leak reaction: E_x, such that

the total flow of energy dissipation is $-\Delta G_r \cdot j_r + E_x = E_r$ and we have indeed energy conservation. Now the minimal amount of power the cell needs to provide to maintain time-invariant $[x]_i$ is by minimizing $-\Delta G_p$ (or equivalently makes ΔG_p closer to 0) restricted on $\Delta G_p < \Delta G_x$. The solution is given by bringing ΔG_p infinitely close to ΔG_x, *i.e.* to set $\Delta G_p^\star - \Delta G_x = 0^-$ where 0^- denotes infinitesimally close to 0 and $\Delta G_p^\star$ denotes the optimal ΔG_p, which is obviously a function of the ΔG_x that is maintained. Another way to put it, is that the pumping reaction works at nearly 100% energetic efficiency: nearly all the exergy provided to the reaction, *via* the energy providing half-reaction, is transferred to the electrochemical gradient of x.

After this modeling interlude, we can get back to biology. Although we derived the optimal $\Delta G_p^\star$ it may not be easy for the cell to achieve such a value. Indeed, specifying which reaction provides energy to the pumping r aforementioned, for instance a proton flowing along its electrochemical gradient, ΔG_p can be identified as the PMF ΔG_{H^+}. Such that maintaining optimal PMF $\Delta G_{\mathrm{H}^+}^\star$ as ΔG_x varies requires modulation of the PMF, which may not be an option if the cell is successfully trying to keep invariant PMF[14]. Another option to keep optimal $\Delta G_p^\star$ would have to shift in between proton:x antiporters with different coupling ratios. Successfully achieving the optimal $\Delta G_p^\star$ for any real value of ΔG_x would however require availability of a continuum of distinct coupling ratio (strictly requiring an infinite diversity of cotransporters) which does not seem to be a reasonable option either. Indeed, although bacteria have a diversity of coupling stoichiometries for antiporter reactions they usually only possess between 3 and 5 antiporters with redundant ionic exchange but distinct stoichiometries. For the following of the discussion we are therefore going to introduce a new *optimality criterion* that we are going to assume the cell is subjected to on evolutionarily timescales that is distinct from the energy minimization principle outlined in chapter 2. We shall assume that the cell is evolving *to minimize the minimal cost* of maintaining

[14] As we discussed earlier, maintaining invariant PMF may be motivated by keeping the ability to transduce energy from NADH to ATP.

electrophysiological variables or equivalently it is minimizing[15]:

$$E_{tot} := \sum_x E_x = -\sum_x \Delta G_x \cdot j_x \tag{III.16}$$

The amount of power required to maintain all IMFs time-invariant, assuming that all active transport reactions always work at near 100% energetic efficiency. In particular, we shall consider the case where the cell only maintains IMFs for sodium and potassium such that the minimal amount of power it needs to spend is given by:

$$E_{tot} = -\Delta G_{\mathrm{K}^+} \cdot j_{\mathrm{K}^+} - \Delta G_{\mathrm{Na}^+} \cdot j_{\mathrm{Na}^+} \tag{III.17}$$

which can be written without loss of generality (as in chapter 2) as:

$$\frac{E_{tot}}{f_b(\Delta\psi)} = -\Delta G_{\mathrm{K}^+} \cdot P_{\mathrm{K}^+} \cdot [\mathrm{K}^+]_e \cdot \left(1 - e^{\frac{F}{RT} \cdot \Delta G_{\mathrm{K}^+}}\right) - \Delta G_{\mathrm{Na}^+} \cdot P_{\mathrm{Na}^+} \cdot [\mathrm{Na}^+]_e \cdot \left(1 - e^{\frac{F}{RT} \cdot \Delta G_{\mathrm{Na}^+}}\right) \tag{III.18}$$

where $f_b(\Delta\psi)$ is a positive-valued function setting the specific kinetics properties of passive electrodiffusion across the membrane and depends on the membrane voltage that is maintained $\Delta\psi$ (as defined in previous chapters). It is already as this stage visible that minimizing E_{tot} of maintaining some value of membrane voltage in a given environment $\{[\mathrm{Na}^+]_e, [\mathrm{K}^+]_e\}$ is going to be given by a choice of $\{\Delta G_{\mathrm{K}^+}, \Delta G_{\mathrm{Na}^+}\}$ restricted to the other components of the electrophysiological state (membrane potential, captive charge properties, Anion Motive Force) and depend on the permeability of sodium relative to that of potassium. Such that, within this minimization framework, the intracellular balance in cations will depend on the permeabilities, their extracellular concentrations and the membrane voltage. Indeed, the intracellular ratio of sodium to potassium follows:

$$\frac{[\mathrm{Na}^+]_i}{[\mathrm{K}^+]_i} = \frac{[\mathrm{Na}^+]_e \cdot e^{\frac{F}{RT}(\Delta G_{\mathrm{Na}^+} - \Delta\psi)}}{[\mathrm{K}^+]_e \cdot e^{\frac{F}{RT}(\Delta G_{\mathrm{K}^+} - \Delta\psi)}} = \frac{[\mathrm{Na}^+]_e}{[\mathrm{K}^+]_e} \cdot e^{\frac{F}{RT}(\Delta G_{\mathrm{Na}^+} - \Delta G_{\mathrm{K}^+})} \tag{III.19}$$

[15] We are going to study how would stoichiometries evolve (on evolutionary time scales) if a cell is trying to minimize the equation below. Note that this does not mean the cell is doing so but we are studying some of the evolutionary implictations of the cell minimizing this equation. Notably, minimizing the equation below may give rise to other detrimental effects, which could impair the fitness, as we shall see later.

thus a choice of $\{\Delta G_{K^+}, \Delta G_{Na^+}\}$ minimizing the minimal cost of maintaining membrane voltage in a given environment $\{[Na^+]_e, [K^+]_e\}$ will have as a consequence the intracellular balance between sodium and potassium.

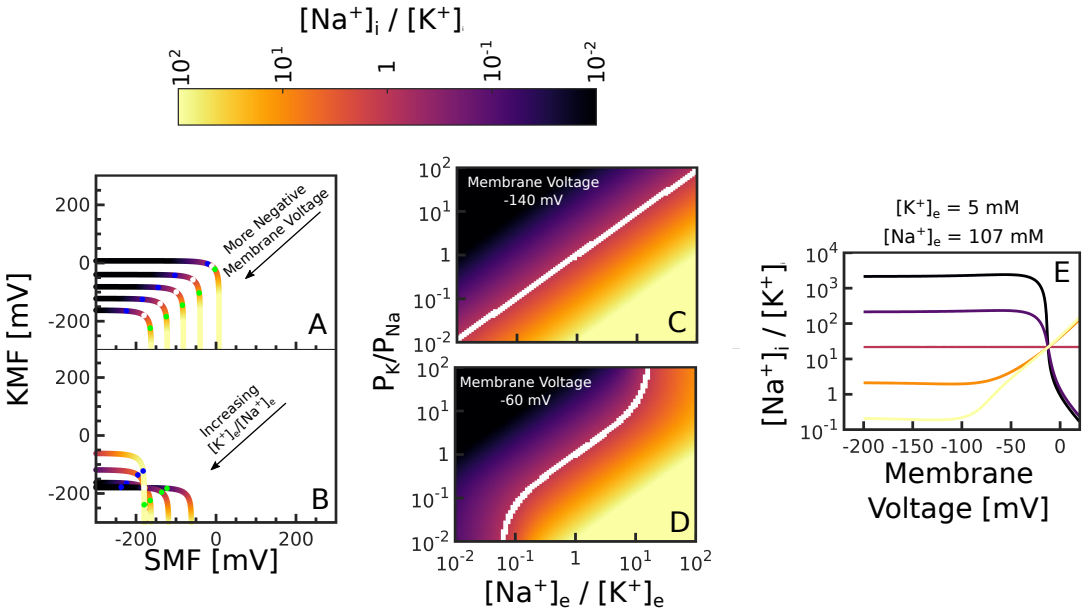


FIGURE 4.1: Intracellular balance of sodium and potassium reflects the strategy of membrane voltage generation that dissipates the least amount of energy. We set for all figures $\Delta G_{A^-} = 0$ (anions are not pumped) and captive charge content equal to $z_Y \cdot [Y]_i/[X]_e = -0.5$, where $[X]_e$ is the total extracellular concentration of small ions. We also assume that the contribution to voltage of hydroxide ions and protons is negligible (true when both pH_e and pH_i are close enough to neutrality, see chapter 2). (A & B & C & D) The color denotes the ratio between intracellular concentration of sodium and that of potassium. (A) We assume extracellular equi-partition between sodium and potassium: $[Na^+]_e = [K^+]_e = 50$ mM; each line is for a different membrane voltage ranging from -180 mV to -20 mV (with 40 mV increments). (B) We assume membrane voltage is -140 mV and each line denotes a different extracellular concentration ratio $[K^+]_e/[Na^+]_e$ of 0.01, 0.1, 1, 10 and 100. (A & B) Blue, white and green dots denote respectively the pair of electrochemical potential that minimizes energy dissipation for permeability ratio P_{K^+}/P_{Na^+} of 10, 1 and 0.1 respectively. (C & D) We show the intracellular composition resulting from the choice of electrochemical potentials that minimize energy dissipation for different extracellular compositions (x-axis) and different permeability ratio (y-axis). While (C) is for membrane voltage of -140 mV, (D) is for membrane voltage of -60 mV. (E) We set the extracellular composition as in [327] and plot the intracellular cation balance resulting from the choice of electrochemical potentials that minimize energy dissipation as a function of membrane voltage. Each line is for a different permeability ratio P_{K^+}/P_{Na^+} 0.01, 0.1, 1, 10, 100 (from yellow to black).

From these results we may provide an alternative hypothesis to that of [330]. The reasoning of this paper can be decomposed as follows: *(i)* Nowadays high intracellular potassium is required as it is a cofactor of important biochemical processes, *(ii)* potassium (rather than sodium) became a cofactor for biochemical processes because it was available at higher concentration in the medium. If

however, cells made the choice of potassium rather than sodium as a cofactor at a time where they already generated membrane voltage, then we clearly saw from the simple analysis in figure 4.1 that the fact that there is more intracellular potassium than sodium depends on the cellular strategy for maintaining membrane voltage. As such, one could imagine that some cells could have "chosen" a strategy resulting in intracellular enrichment in sodium rather than potassium which as we showed is possible if the KMF dominates over the SMF (the cell maintains more negative KMF than SMF), see figure 4.1 (A). However, as shown in figure 4.1 (B), the extracellular composition in cations restricts the sets of KMF and SMF available for maintaining a given voltage. In particular, when the extracellular environment has higher potassium than sodium, then most of the solutions involve KMF dominating the SMF. As we mentioned earlier, another ingredient setting the optimal strategy is the permeability of sodium and potassium. In fact, the extracellular composition and the permeability ratio potassium to sodium set the optimal intracellular cation balance as shown in figure 4.1. Perhaps unsurprisingly, cells evolving in environments enriched in potassium and/or with high permeability of potassium relative to sodium are expected to have higher intracellular potassium than sodium. In fact potassium has been measured to have higher permeability than sodium in *xenopus* [163]. Should that be generalizable to all biological membranes, perhaps owing to the smaller size of potassium than sodium ions, then we would expect cells to generate voltage with dominating SMF over KMF, resulting in higher potassium than sodium in the intracellular space. Thus we propose that the intracellular cation balance was set in early life forms to allow minimization of the cost of maintaining voltage, that would be the case if early membranes were more permeable to potassium than sodium and if those cells evolved in environments dominated by potassium. In which case, emergence of potassium as an important cofactor may have emerged later, made possible by high availability of *intracellular* (and not extracellular as in [330] potassium. Once potassium became an important cofactor then cells may have become "locked" into having sufficiently high potassium intracellular concentrations, requiring dominance of SMF over KMF when generating voltage. Of course, should have cells evolved crucial functions relying on the use of potassium as a cofactor before it even evolved the capability of sufficiently polarizing cells, then the hypothesis of [330] seems more relevant than ours. Interestingly, now assuming that cells have in general dominant SMF relative to KMF, resulting in low intracellular sodium relative to potassium, we can question the narrative that "cells maintain

low intracellular concentrations of sodium because it is toxic [328]". Indeed, in the light of the present discussion we can say that low intracellular sodium is just a reflection of how the cell is coordinating its ionic pumps to generate voltage. The mechanism by which sodium impairs growth/survival could be the higher cost of electrophysiological maintenance as we discussed in chapter 3, mechanism which has the advantage of explaining why both high extracellular of potassium and sodium are detrimental to cell survival as reported [331]. Finally, such a minimization heuristic predicts that the intracellular ratio of sodium to potassium is expected to increase as the cell depolarizes, see figure 4.1, as was observed by [327] when *E.coli* cells transition to stationary phase wherein cells maintain closer to 0 voltage [310].

vi. Choice of Coupling Stoichiometries and Energetic Efficiency of IMF Maintenance

Getting away from 100% energetic efficiency of IMF generation, the effective optimal cost of maintaining a given IMF (that is given a set of active transporter available for this ion x) is given at steady-state by:

$$E_r = -j_x \cdot \Delta G_p = -j_x \cdot \frac{\Delta G_x}{\epsilon_r} \tag{III.20}$$

where $\epsilon_r := \sigma_{r,x} \cdot \Delta G_x / \Delta G_p$ is the fraction of the free energy invested in reaction r that is converted to electrochemical gradient of x, a.k.a. the energetic efficiency of r and ΔG_p is the energy provided by the free-energy-providing (we assumed that r goes forward) half-reaction. We assume that the cell is minimizing the cost of maintaining the IMF for x, *i.e.* the equation above gives the minimal cost in the range of IMF where maximizing activity of the transporter r is optimal, see chapter 2. The energetic efficiency is I think a useful metric to analyze what drives the cell to evolve ionic transport systems with different coupling stoichiometries. Before diving into the question of what drives the cell to select specific active transporters, defined by their stoichiometry and the free energy providing half-reaction, it is I think useful to take an example to clarify what energetic efficiency pertains to.

Assume that the cell is generating -140 mV with equi-partition of extracellular sodium and potassium. Assume further that the permeability of potassium is 10

times that of sodium such that the optimal strategy is shown in figure 4.1 (A) as maintaining SMF≈ -195 mV and KMF ≈ -120 mV. Well, a quite unrealistic transport configuration allowing maximal energetic efficiency (close to 100%) could be maintaining a PMF of -1 mV, a proton:sodium antiporter with 195:1 coupling stoichiometry and a proton:potassium antiporter with 120:1 coupling stoichiometry. Should the cell now seek to maintain voltage of -100 mV in the same conditions as before, then the optimal strategy is to maintain SMF≈ -140 mV and KMF≈ -90 mV. To achieve maximal energetic efficiency could be achieved by maintaining PMF -1 mV, a proton:sodium antiporter with 140:1 coupling stoichiometry and a proton:potassium antiporter with 90:1 coupling stoichiometry. If the cell has only access to the 195:1 proton:sodium and 140:1 proton:potassium antiporters to maintain SMF≈ -140 mV and KMF≈ -90 mV, then the energetic efficiencies would be 140/190$\approx$ 73% for the proton:sodium antiporter and 90/140 $\approx$ 64% for the proton potassium antiporter. Now imagine a cell possessing 200 different proton:sodium antiporters with coupling stoichiometry $1:1, 1:2, \ldots, 1:200$; then keeping a PMF of -1 mV, it could always maintain above 99% energetic efficiency of sodium pumping for any SMF between -1 and -200 mV. It would however require a chimeric *E.coli* cell to dedicate $\approx$ 5% of its gene solely for proton:sodium antiporters. I think these dummy examples allow understanding of this simple tradeoff: the more diversity of coupling stoichiometries available a cell possesses, the more it can be energetically efficient across environmental or/and physiological states requiring maintenance of different IMFs. The latter comes however at the cost of having more genes.

More concretely, the reported diversity of proton:sodium and proton:potassium antiporters is about 10 genes for most bacteria [62]. Let us now say that we have 4 genes available for each of proton:sodium and proton:potassium antiporters and that the cell is trying to make a choice of coupling stoichiometry for each of those antiporters, how would it best do it ? We may outline three different factors upon which this choice shall rely on: *(i)* the PMF that is maintained as well as the coupling stoichiometries *that can possibly be evolved*[16], *(ii)* the range of SMF that the cell "wants" to have access to, that would set the an upper bound on the highest coupling stoichiometry required (along with the PMF), *(iii)* the frequency of each SMF sought to be maintained and the corresponding (to that frequency)

[16]Indeed it is likely that making an antiporter with for instance 1:195 coupling stoichiometry is simply not achievable by natural selection.

impact of the energy required to maintain that SMF on fitness. To simplify the problem and get first hints at what is expected to happen evolutionarily, we assume in figure 4.2 that the cell has 4 proton:sodium antiporters it needs to pick the coupling stoichiometry, always has fixed PMF = -100 mV and that the impact of the SMF maintenance cost on fitness is invariant by the SMF (which is obviously wrong). We then show in figure 4.2 two possible partitions of the SMF landscape with the 4 coupling stoichiometries at disposal. As derived in chapter 2, the arrows on top indicate the range of SMF for which each of the coupling stoichiometry needs to dominate in order to minimize the cost. The numbers on top denote the minimal energetic efficiencies for each of the antiporters demonstrating that the overall energetic efficiency of SMF maintenance is going to depend on the individual energetic efficiency (of each coupling stoichiometry, in the range they are optimal) and the SMF frequency. Also, one could expect that the energetic efficiency "resolution" of SMF generation depends on the frequency of the SMF that is maintained as examplified in figure 4.2 where the magenta antiporter works in a wider range right than left, due to the lower frequency of very negative SMF on the right compared to left. Of course, one shall in principle consider that the cost (which the energetic efficiency scales) is a function of the SMF. In particular for near 0 SMF, the SMF maintenance cost is very low, thus it is expected that cells do not need to have "high resolution" of coupling stoichiometries in the low SMF range. Therefore we expect that an antiporter with lowest coupling ratio (that takes care of the low-end SMF) operates most often in a wider SMF range than its higher coupling ratio counterparts. Also, because more negative SMF tend to depolarize the cell, more negative SMF will come at a higher maintenance cost. We may at this stage provide two rules of thumbs on how a cell should evolve its coupling stoichiometries:

1. Higher resolution in the most negative end of SMF.

2. Higher resolution in the most frequent range of SMF.

where we mean by resolution the density of distinct coupling stoichiometries being optimal in at least one location in a given SMF range. For instance, the density of coupling stoichiometry in figure 4.2 (right) in the range SMF$\in [-200 - 125]$ mV is one and that in figure 4.2 (left) in the same range is 3. Finally, we postulated coupling stoichiometries in figure 4.2 that have not been reported (to my knowledge) *i.e.* 7:4, 5:4, 3:4. Perhaps these coupling stoichiometries are simply too hard to evolve and may not be at disposal for cells. If true, this constrains

even more the choice of available antiport systems and emphasizes one of their important characteristic: that when working near maximal energetic efficiency they can only quantize SMF relative to the PMF, entailing that a choice of SMF (for a fixed PMF) necessarily provokes variations in the energetic efficiency of the SMF maintenance process. This bounces to the idea[17] that a crucial feature of the PMF (and the gain of having PMF driven processes) is that it provides cells with a lower energy quantum than ATP does, thereby allowing powering of processes requiring relatively low driving force to be performed at higher energetic efficiency.

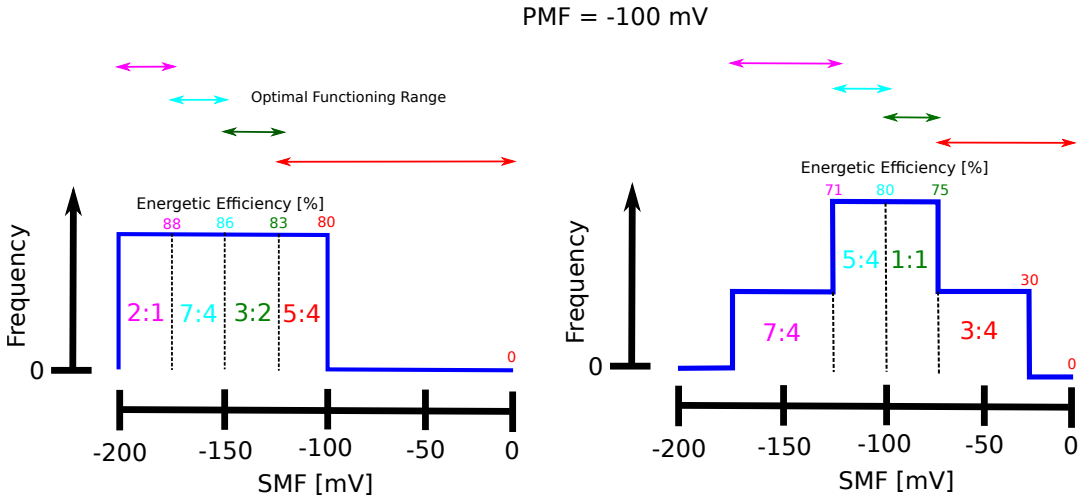


FIGURE 4.2: Examples of choice of coupling stoichiometries for SMF generating proton:sodium antiporters for PMF = -100 mV in two ecological niches (left and right) entailing different frequencies of physiologically maintained SMF. The coupling stoichiometries are defined by $\sigma_{H^+} : \sigma_{Na^+}$, the range in which each coupling stoichiometry must be maximized in order to minimize the cost of SMF maintenance is indicated by the same colored arrows on top. Of corresponding colors are depicted the energetic efficiencies each pump at the transitioning SMF (the SMF value for which the cell needs to shift prioritizing the activity of one pump to another).

vii. The Unreliability of the KO Experiment to Test Whether a pump Works as an Influx or Efflux Pump.

We will now talk about the relevance of some experiments aiming at the functional characterization of active transport systems for ions. Indeed, the most common way of experimentally assessing whether a pump p works as an efflux or as an influx pump for an ion x seems flawlessly straightforward: *(1)* Take a WT (Wild

[17] I think I remember having read this somewhere but I cannot find the reference anymore, the reader should therefore acknowledge that this idea is likely already present in the literature.

Type) cell, *(2)* Make a mutant by deleting from the WT the transporter p of interest (that we wish to study whether it is an efflux or influx pump for ion x), *(3)* measure intracellular concentration $[x]_i$ of x in WT and mutant, *(4)* conclude: if $[x]_i$ is higher in the mutant then p worked as an efflux pump, if $[x]_i$ is lower in the mutant then p worked as an influx pump. Although intuitive, this reasoning does not apply in general when studying ionic transport. It is quite straightforward to understand by writing couple of equations. First consider rearranging the electrochemical potential (as in chapter 2) to show how $[x]_i$ depends on its electrochemical potential and membrane voltage:

$$[x]_i = [x]_e \cdot e^{\frac{F}{RT}(\Delta G_x - z_x \cdot \Delta\psi)} \tag{III.21}$$

Now consider the membrane voltage and electrochemical potential in the mutant and the WT, we should write $\Delta G_x(WT)$, $\Delta\psi(WT)$ for the WT and $\Delta G_x(M)$, $\Delta\psi(M)$ for the mutant such that we explicitly write the efflux/influx condition according to the current literature, from Eq. (III.21):

$$[x]_i(WT) > [x]_i(M) \Leftrightarrow \Delta G_x(WT) - \Delta G_x(M) - z_x \cdot [\Delta\psi(WT) - \Delta\psi(M)] > 0 \tag{Influx (?)}$$

So the question is now: *can the above be positive in spite of being an efflux pump ?* To take a simple scenario, we shall assume that p is the sole pump responsible for maintenance of the IMF of x, such that after removal of it, x equilibrate across the membrane thus $\Delta G_x(WT) = 0$. Let us also assume for simplicity that $z_x = +1$ (*e.g.* $x \equiv \mathrm{K}^+$). Finally, let us assume that p is an efflux pump and check whether the Influx condition Eq. (Influx (?)) can still hold. If p is an efflux pump, then $\Delta G_x(WT) < 0$ such that dividing Eq. (Influx (?)) by $\Delta G_x(WT)$ yield:

$$\frac{\Delta\psi(WT) - \Delta\psi(M)}{\Delta G_x(WT)} > 1 \tag{III.22}$$

We also know that since we assumed p is an efflux pump of a monovalent cation x, its removal will result in cellular depolarization, thus the numerator of the above will be negative, and the left hand side positive. So now the question is: can the loss of $\Delta G_x(WT)$ units of motive force result in a more important loss in membrane voltage (in the same units).

We show in figure 4.3 that removal of a potassium efflux pump (such that

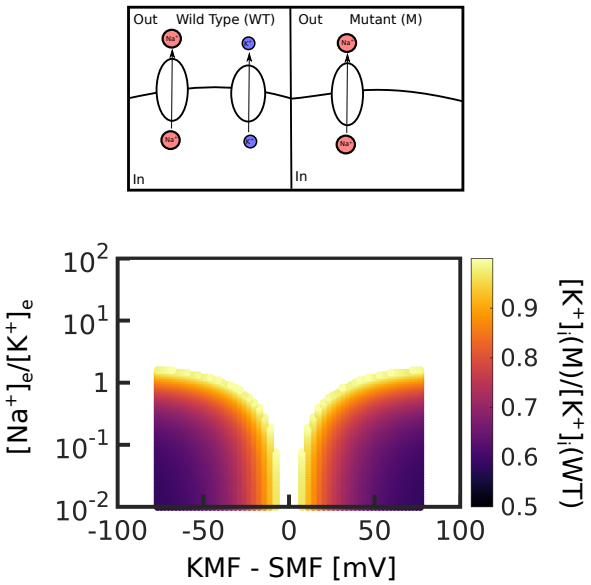


FIGURE 4.3: The total concentration of extracellular ion $[X]_e$ is set to 100 mM, captive charges are set to $z_Y \cdot [Y]_i/[X]_e = -0.5$ and $\Delta G_{\mathrm{A}^-} = 0$. For each extracellular ratio of sodium to potassium, we compute the KMF and SMF required to maintain membrane voltage -140 mV. We then plot the ratio of the intracellular potassium concentration for the WT (that maintains -140 mV membrane voltage) and the mutant for which KMF goes to 0. We only show the points that result in lower concentrations of potassium after removal of the potassium efflux pump.

the KMF goes from negative values to 0) can indeed decrease the intracellular concentration of potassium. In particular, this occurs at high extracellular potassium concentrations (relative to sodium), and when either the KMF or SMF dominates over the SMF or KMF (*i.e.* KMF - SMF away from 0). We made however two assumptions. First, we assumed that removal of the potassium efflux pump translates in equilibration of potassium across the membrane. While expected if the cell possesses only one potassium efflux pump, most bacteria seem to possess several efflux pumps for potassium, such that there is no guarantee that removal of any of them will indeed cause complete collapse of the KMF. Second, we assumed that the other voltage-dependent variables: captive charges, SMF, Chloride Motive Force remained invariant after removal of the potassium efflux pump. Such may not be the case if the cell adapts its electrophysiology to removal of a potassium efflux pump. Typically, any cellular adaptation that rescues the membrane voltage (*e.g.* SMF more negative subsequent to removal of potassium efflux pump) will tend to yield higher $[\mathrm{K}^+]_i$ in the mutant relative to the Wild type. On the other end, potassium equilibrating across the membrane may cause SMF going closer to 0 (even more depolarization than expected by potassium

equilibration alone), in which case even more lower $[K^+]_i$ in the mutant relative to WT is expected.

Be as it may, we just showed that in principle, measuring intracellular concentration of potassium after removal of an active potassium transporter, is not necessarily a reliable experiment to assess whether this transporter works as an efflux or influx pump. This, once again, emphasizes the need of studying the activity of ionic transports *in the electrophysiological context*. For instance, measuring in addition membrane voltage on top of the intracellular potassium concentration when performing one such experiment mentioned above is sufficient to determine with certainty if the active transporter indeed works as an influx of efflux.

viii. Relevance of Kinetic Asbtraction

I am now motivating why I think asbtracting the kinetics was a necessary component to the development of the electrophysiological component of this manuscript.

To refine what I mean, we should first abstract the classical approach of computational biology to *(i)* postulate a model defined by *(a)* the reactions available for the modeled biological process, *(b)* a kinetic model for each reaction. From *(a)* and *(b)* will naturally emerge a total number of parameters $\sum_r N(p, r)$, which denotes the sum over all reactions of the number of parameters per reaction. Some of these parameters $p \in K$ will be known from previous experimental assessments, *e.g.* the maximum translation rate per ribosome or the average mass of a catalyst [92], some other parameters $p \in E$ will be know by construction of the experiment (defining for instance the environmental composition), some other parameters $p \in U$ will be *underdetermined* by the existing body of biological knowledge. The function of a biological model will then roughly consist in its ability to regenerate values for a number of experimentally measured variables v for a number of environmental/physiological perturbations with a number of underdetermined parameters. The *quality* of this model will then be qualitatively evaluated as: high number of experimentally measured variables that are regenerated, high number of distinct environmental/physiological perturbations, low number of underdetermined parameters. The values of these underdetermined parameters will usually be set according to the process of fitting the data, *i.e.* find fixed $p \in U$, for a set of $v(p \in E, p \in U)$ upon fixing $p \in K$ and the model can be

seen as a set of function $M_v(p \in K, p \in E, p \in U)$ (or set of reaction with defined kinetic with each v having a specific functional dependency on the model's state) returning experimentally measured variables $v(p \in E)$:

$$v(p \in E) = M_v(p \in K, p \in E, p \in U) \tag{III.23}$$

Had we specified the kinetics of transporters, we would have had many additional underdetermined parameters and it would have had in my opinion weakened the main messages of chapter 2 and 3. For instance in chapter 2, the restricted number of underdetermined variables (the charge of captive molecules, the forward activity of 3 antiporters) strengthen the conclusions pertaining to which antiporters should be used to maintain a given electrophysiological state. Indeed, having similar functional form for each of the antiporter, they are only distinct by the free energy variation, the rectants/products and the stoichiometry of the reaction they catalyze. The model predicting qualitatively similar coordination of antiporters than what was observed, explained by how these variables (free energy, stoichiometries) play out in the maintenance of an electrophysiological state, we can say that these variables must be "chosen" (or evolved) carefully by the cell as these are crucial to the function of antiporters in electrophysiological maintenance. These crucial properties of antiporters have a determining impact of electrophysiology that must be chosen (or evolved) independently of the kinetics for each antiporter. For example, the following statement "a proton:cation antiporter with low stoichiometric ratio will never be able to maintain the voltage required for pH_i maintenance in alkaline environment" holds for any choice of kinetics of the said proton:cation antiporter. A high stoichiometric ratio is a necessary condition for a proton:cation antiporter to be able to maintain the cell in a highly polarized state (at physiological PMF); and as a necessary condition, it is independent of the choice of kinetics. Similarly, the conclusions relating to how lowering the PMF causes impairement of the ability of proton:ion antiporters to maintain voltage thus pHi rely on the stoichiometry ratio and not on the kinetics. Knowing the stoichiometric ratio of an antiporter is sufficient to determine that below some PMF, this antiporter won't be able to maintain a given voltage; as a sufficient condition, it holds for any choice of kinetics of the said antiporter. In other words, any choice of more complex kinetics will be constrained by some rules we can derive with our minimal kinetic models.

That does not mean that studying the kinetics of transporters is not interesting

for understanding electrophysiological processes. It rather means that the choice of a modeler of asbtracting or not the kinetics (or chosing how complex is the description or how many underdetermined variables the model include) influences the difficulty in finding the main components constraining a particular behavior. Say we had specified the kinetics of antiporters, such that we had 3 additional underdetermined parameters. To demonstrate "A high stoichiometric ratio is a necessary condition for a proton:cation antiporter to be able to maintain the cell in a highly polarized state", we would have had to evaluate whether this statement holds for any triplet of value of the newly introduced underdetermined parameters. Of particular interest to chapter 3, our model also allows derivation of the minimal cost of maintaining an electrophysiological state. This minimal cost holds for any choice of kinetics models, such that it sets a lower bound that needs to be verified for any other models wherein kinetics are specified. Specifying the kinetics would imply a different minimal cost, higher than the one we derive and depending on the choice of kinetics. This would however be much hard to derive, as the complexity of the minimization problem scales with the number of underdetermined parameters. In that regards, our approach allows screening of an absolute minimal cost (that a cell has an incentive to approach when choosing the kinetics for the antiporters) for maintenance of an electrophysiological state across several dimensions (salinity, pH_e, permeabilities, homeostatic values of PMF, pHi) that is computationally cheap. Such would not necessarily be the case for models specifying the kinetics, *i.e.* with additional underdetermined parameters on which the minimal cost of the model would depend.

Now what could be questions relating to electrophysiological maintenance that would require specifying the kinetics ? I can foresee three categories of questions in relation to the choice of kinetics:

1. Determining the maximal transport capacity for an ion. Indeed, there is a limited space in the membrane for hosting ionic transporters. Depending on the availability of substrate, the v_{max} of an ionic transport as well as the maximal density of ionic transporters of a certain type the membrane can support, one may derive an upper bound on the transport rate of an ion. That upper bound would depend on the composition of the environment and the electrophysiological state maintained by the cell, enlarging the spawn of constraints a cell has to manage and how to adapt to them, specifically by

evolving the kinetics of ionic transporters.

2. *How* the cell is implementing the coordination of antiporters in response to the environment and the physiological state it seeks to maintain. For instance, we derive in chapter 2 what must be the forward rate of each antiporter in order to maintain pH_i and PMF at a given pH_e. One could then wonder how to implement that coordination, e.g. what could be choices of kinetics that approximate well the solution that minimizes the cost. Is pH-gating of antiporters a necessary condition for energetically efficient maintenance of electrophysiological homeostases across different pH_e, salinity ? When does tuning gene expression of ionic transporters becomes necessary to adaptation to a new environment (as opposed to state-dependent activity of these ionic transporters) ? These are surely interesting questions that requires specification of the kinetics, and even sampling for different kinetic models.

3. Dynamic responses of the electrophysiological apparatus of the cell. Indeed, our approach is not very amenable to the study of dynamical responses of the cell to environmental/physiological changes. Because the forward rates are time-invariant, we most likely elude the possibility for our models to reproduce how a cell would dynamically respond to a change in the environment or of the physiological state it is maintaining. These questions also naturally requires the involvement of kinetics.

I then elaborate in the next section on what are the kind of observations the minimally complex kinetic models we used before in this thesis can relate to.

IV. Heuristics for Approaching Electrophysiological Processes

We shall now conclude this thesis giving examples of how the principle above can be applied to various models. Importantly, everything that follows is independent of the specific kinetics of the various enzymes. I imagine that the heuristics introduced could be useful to scientists willing to engineer electrophysiological protocells (membranes with only a few types of ionic transporters, without biochemistry, DNA, RNA, *etc.*) to have some prior expectations on the behaviours that such

protocells can achieve as a function of the types of ionic transporters it possesses and the Gibbs free energy of some chemostated reactions. First we introduce a standardized way for characterizing each active transporter. Second we look at how we can gain insight on a model possessing different active transporters from their standard characterization, that could for instance be used to determine the properties of existing electrophysiological models (*e.g.* [333]) that are independent of the choice of kinetics.

i. Characterization of Active Transport Systems

A Thought Experiment. For simplicity, we will consider a three dimensional state space consisting of three different IMFs (for instance PMF, cationic motive force, anionic motive force). It is at this stage worth to notice that describing the state space as a set of IMF is equivalent to the description in terms of intracellular concentrations given knowledge of the extracellular composition, capacitance, cellular geometry and contribution of captive charges. This is because membrane potential can be non ambiguously determined from the aforementioned variables. We shall now proceed with a three-step thought experiment that defines how an active transporter is characterized:

1. Step 1: The basis of the thought experiment is to first consider that the experimentalist has full control over the state space (which may be not feasible but this is not the point) of a protocell that does not possess any active transporter such that it can bring the protocell to any location in the 3-D euclidean space defined by three ionic motive forces in figure 4.4 (left).

2. Step 2: The second step consists in the experimentalist giving up control over 1 dimension, such that the achievable state-space becomes a plane that is a projection of the 3-D volume from step 1 onto the null coordinate of the IMF the experimentalist gave up control on as shown in figures 4.4 for dissipating each of the three IMFs.

3. Step 3: Add one active transporter that moves across the membrane the ionic species of which we gave up control on its IMF. The active transporter is then chacterized by the volume it can access in the 3-D IMF space and its attractors (locations it will bring the protocell in the state-space if its activity is very high).

We shall now introduce several examples to show how to characterize an active transporter in that framework. To that end, we will characterize active transport systems following the functional characterization outlined in the introduction, *i.e.* we will first characterize chemically driven ionic pumps (for one ion), then cotransporters for two ions, then chemically driven co transporters (two ions) and finally show an example of a cotransporter for three ions.

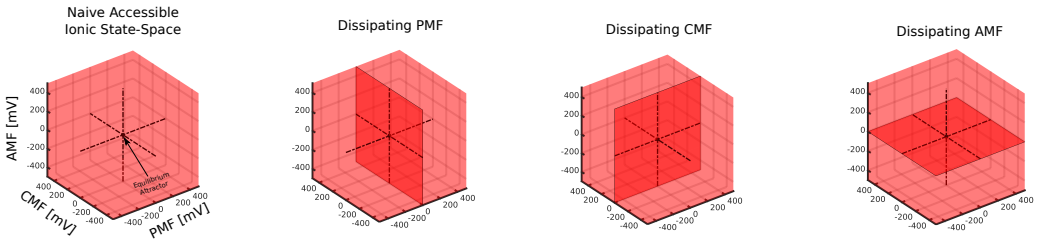


FIGURE 4.4: Visualization of the small ionic State-subspace when considering three small ions: small cations, small anions and protons. (Left) When the experimentalist has full control over the different IMFs, every coordinate is accessible (red cube). When the experimentalist is "giving up" control of one IMF and the protocell does not possess any active transport system for this ion, then the accessible state space becomes a 2-D plane intercepting 0 coordinate for the ion with null IMF. Null IMF can also be achieved by increasing indefinitely permeability of the membrane to that ion.

Characterization of Chemically Driven Ionic transporters. We first take the example of an ATP driven proton pump (*e.g.* F1F$_o$) in figure 4.5. We reason here in the 3-D space consisting of three IMFs (protons PMF, cations CMF, anions AMF) and show the locations in the state space a protocell containing only the schematized transporter can reach; that is with the experimentalist having full control over the AMF and CMF and none on the PMF (the PMF control is delegated to the ATP driven proton pump.) Such a pump allows access to a characteristically shaped volume in the 3-D IMF space that is a rectangular cuboid. The projection on either the CMF or AMF axis yields an identical rectangle and is independent on the values the CMF or AMF take. Another way to put it is that this chemically driven pump sets a range of allowed PMF, A range that is independent of both the CMF and AMF.

Of course, the shape of this volume depends on the Gibbs free energy of ATP hydrolysis, which was chemostated (a.k.a. fixed) in figure 4.5 to -560 mV per hydrolyzed ATP. Considering the Gibbs free energy of ATP hydrolysis ΔG_{ATP} as a fourth dimension the experimentalist is able to control, then the range of allowed PMF for an identical ATP driven proton pump depends on the value of

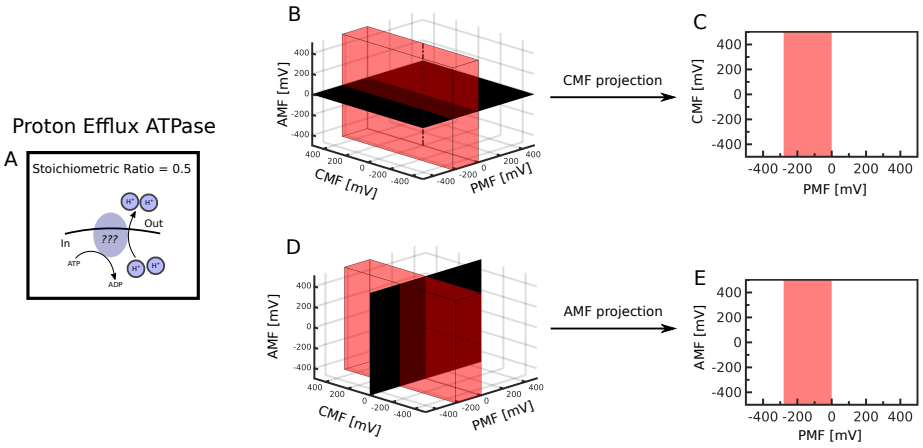


FIGURE 4.5: Characterization of the reachable state-space with a proton ATPase. The free energy of ATP hydrolysis was set to $\Delta G_{\text{ATP}} = -560$ mV. (A) Scheme of the pump. (B & D) the red rectangular cuboid denotes the fraction of the state space that is achievable when the experimentalist has full control over the AMF and CMF and has delegated PMF control to the pump described in (A). (C & E) Projection of the reachable state space on either the CMF or AMF axis results in an identically shaped rectangle, width of which is given by $\Delta G_{\text{ATP}} \times$ Stoichiometric Ratio $= -560 \cdot 0.5 = -230$ mV.

ΔG_{ATP} as shown in figure 4.6 (A). In particular, the maximum $|\Delta G_{\text{H}^+}|$ (|.| for absolute value) that is achievable scales linearly with $|\Delta G_{\text{ATP}}|$ with a slope equal to the stoichiometric ratio ATP:proton which in this example is equal to 1/2. As shown in figure 4.6, projection on the CMF or AMF as was done in figure 4.5 yield different rectangles depending on the value of ΔG_{ATP}. In particular, when ΔG_{ATP} is positive, then the pump works as an influx pump for protons and allows maintenance of positive PMF, when it is negative the pump works as an efflux pump for protons and allows maintenance of negative PMF, see figure 4.6 (B) and (C). Also, the width of the rectangles is proportional to the value of ΔG_{ATP}.

Now widening the analysis to different chemically driven ionic pumps figure 4.7, we see that they all have this characteristic rectangular shape in the IMF space, as for the ATP driven proton pump before. This rectangular shape in 2-D is in fact characteristic of any ionic species, IMF of which is shown on the y-axis, not partaking in the reaction catalyzed by the transport that is characterized. The range of accessible PMF figure 4.7 (B) shown for each chemically driven proton transport figure 4.7 (B) defines an accessible PMF range, lower bound of which is given by Stoichiometric ratio $\times$ the driving force which is either ATP hydrolysis (potential -560 mV), NADH reduction (potential -2230 mV), or nitrate reduction (potential -790 mV), where the stoichiometric ratio is the number of energy providing half-reaction (always one by convention) per the number of

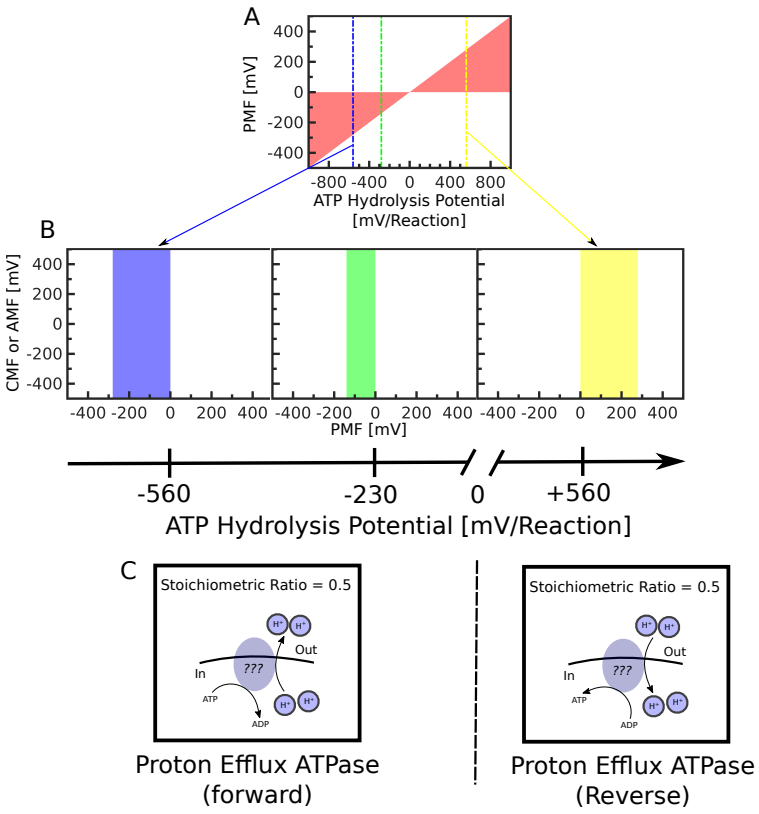


FIGURE 4.6: Characterization of the reachable state-space with a proton ATPase (efflux) for different ΔG_{ATP}. (A) The reachable PMF is independent of either the CMF or AMF and is thus solely a function of ΔG_{ATP}. This figure denotes a projection of the state space onto both CMF and AMF (for any pair $\{\Delta G_{\mathrm{C}^+}, \Delta G_{\mathrm{A}^-}\}$. (B) Projection on either the CMF or AMF axis for different values of ΔG_{ATP}. The width of the rectangle is equal to $\Delta G_{\mathrm{ATP}} \times$ Stoichiometric Ratio. The sign of the reachable PMF depends on the sign of ΔG_{ATP}. (C) In particular, when ATP synthesis is spontaneous (for sufficiently high $[\mathrm{ADP}] \cdot [\mathrm{Pi}]/[\mathrm{ATP}]$), the ATPase works as an influx pump.

protons moved across the membrane. All these pumps generate negative PMF as they couple a reaction which provides energy to efflux of protons. In figure 4.7 (C) we show the KdpFABC which couples ATP hydrolysis (energy providing) to *influx* of potassium, in which case the range of KMF 4.7 (D) (here shown as CMF) the pump is able to generate is positive.

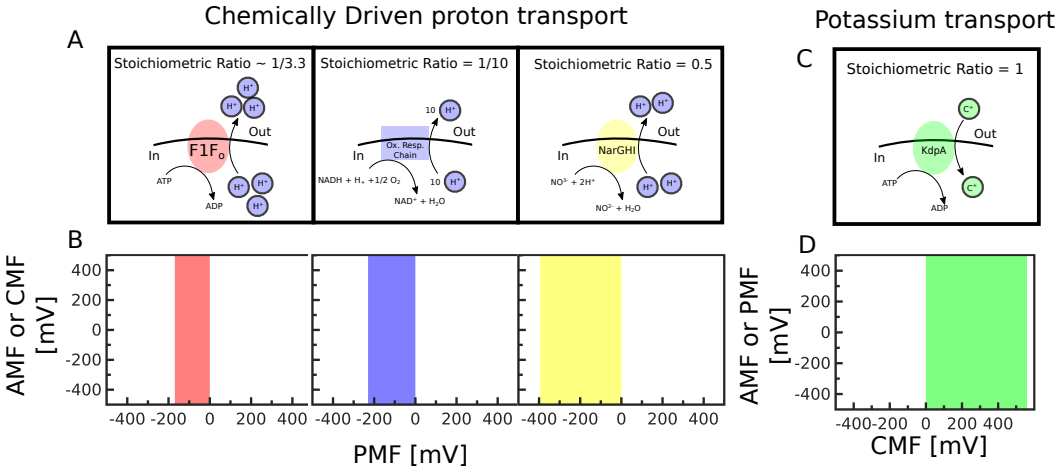


FIGURE 4.7: Characterization of the reachable state-space with different pumps. The free energy of ATP hydrolysis, NADH reduction and nitrate reduction are set to -560, -2230 and -790 mV respectively. (A) Schemes of different proton efflux pumps, driven by (left to right) ATP, NADH Reduction of nitrate reduction. (B) Projection on any IMF axis else than proton yields a rectangular shape, width of which is given by Free energy of energy providing half reaction × Stoichiometric Ratio. (C) Scheme of the ATP driven influx potassium pump KdpABC and (D) corresponding characterization of the reachable state space. Only positive CMF are achievable seeding from coupling of ATP hydrolysis (negative free energy) to inward movement of potassium.

To exemplify the dependency on the width of the rectangle on the coupling stoichiometry of the reaction we next compare in figure 4.8 the characteristic projection in the IMF space of ATP driven proton pumps with different amounts of protons moved per hydrolyzed ATP. When the stoichiometric ratio is negative (by convention hydrolyzed ATP is coupled to an influx of protons), then the PMF is in the positive range, when the stoichiometric ratio is positive (hydrolyzed ATP is coupled to an efflux of protons) then the PMF is in the negative range. The PMF further from 0 that can be generated with a given pump is always the stoichiometric ratio × the driving force (in this case ATP hydrolysis with potential -560 mV) as shown in figure 4.8 (A). This exemplifies the need to define a sign convention for each type of distinct driving force. We chose as a convention here to say that hydrolyzed ATP coupled to influx has negative stoichiometric ratio but could have picked otherwise, *e.g.* in figure 4.7(A) we chose opposite convention: hydrolyzed

ATP coupled to influx has positive stoichiometry. In fact, this convention needs to be consistent with the direction of reference that is picked for each reaction *simplex*[18]. For instance, we chose for the simplex reaction "passive transport of protons across the membrane" the reference direction $r_{\mathrm{H}^+} := \mathrm{H}_e^+ \rightarrow \mathrm{H}_i^+$, *i.e.* we say that proton leakage goes forward when there is net inward flow of protons due to its leakage reaction. For that convention on the simplex "proton leak", negative stoichiometric ratio for ATP hydrolysis coupled to proton efflux entails that the reference direction we pick for the simplex reaction "ATP hydrolysis/synthesis" needs to be: $r_{\mathrm{ATP}} := \mathrm{ATP} \rightarrow \mathrm{ADP} + \mathrm{Pi}$, *i.e.* it goes forward when it is hydrolyzed. Indeed for this choice of convention an ATP driven proton efflux pump will have a negative coupling ratio for instance:

$$r := \mathrm{ATP} + 3 \cdot \mathrm{H}_i^+ \rightleftharpoons \mathrm{ADP} + \mathrm{Pi} + 3 \cdot \mathrm{H}_e^+ := +1 \cdot r_{\mathrm{ATP}} - 3 \cdot r_{\mathrm{H}^+} \tag{IV.1}$$

and the coupling ratio $+1/-3$ is indeed negative. Note that the direction of reference the complex reaction (left hand term above) is defined with preserves the sign of the stoichiometric ratio, indeed defining the complex reaction above in the opposite way would yield coupling ratio $-1/+3$ which is still negative. It however does not preserve the formula for the Gibbs free energy. Indeed in the reaction above the Gibbs free energy of the reaction is $\Delta G_r = +1 \cdot \Delta G_{\mathrm{ATP}} - 3 \cdot \Delta G_{\mathrm{H}^+}$ which seeds from the constraint that negative ΔG_r entails (by convention) forward flow through the reaction r. If we had defined the complex reaction in the opposite reference direction:

$$r := \mathrm{ADP} + \mathrm{Pi} + 3 \cdot \mathrm{H}_e^+ \rightleftharpoons \mathrm{ATP} + 3 \cdot \mathrm{H}_i^+ := +1 \cdot r_{\mathrm{ATP}} + 3 \cdot r_{\mathrm{H}^+} \tag{IV.2}$$

then the gibbs free energy of the reaction becomes: $\Delta G_r = -1 \cdot \Delta G_{\mathrm{ATP}} + 3 \cdot \Delta G_{\mathrm{H}^+}$. In fact, the semantic we propose requires three layers of sign conventions:

1. Whether positive net flux of reaction r is associated to positive or negative ΔG_r (in this thesis we chose negative ΔG_r is equivalent to positive flux, as it is the case usually).

2. For each simplex reaction, define the forward direction (that associated with positive coupling stoichiometry), *e.g.* whether $\mathrm{H}_e^+ \rightarrow \mathrm{H}_i^+$ is defined as the forward or reverse direction of the proton leakage reaction (in this

[18] A reaction that cannot be constructed from distinct simplex reactions. Also, one must be able to construct all non-simplex reactions composing the model from simplex reactions.

thesis we always pick the convention that inward movement of ions is the forward direction). Note that consistency with convention 1. and definition of the IMF as the Gibbs free energy of the corresponding leak reaction will entail that this convention will determine whether negative IMF means spontaneous inward or outward flux. Indeed, say we chose the convention that the simplex "proton leak" goes in the forward direction when it is oriented inward, then positive net flux of proton leak entails negative PMF. On the other hand, say we chose the convention that the simplex "proton leak" goes in the forward direction when it is oriented outward, the positive net flux of protons leak entails negative PMF but this time defined as the Gibbs free energy of the outward movement of protons. This concurrent PMF definition has thus the opposite sign than the first PMF we defined.

3. For each complex reaction, defines the forward direction, that will determine whether this complex reaction is defined by positive or negative coupling for each of its reaction simplex it is composed of. Correspondingly, it will change how the Gibbs free energy of the complex reaction depends on the Gibbs free energy of the simplex reactions.

Although this convention interlude seems a bit tedious, I think it was necessary to convey the information that would be necessary to define a proper semantic for the heuristics we are drawing in this section.

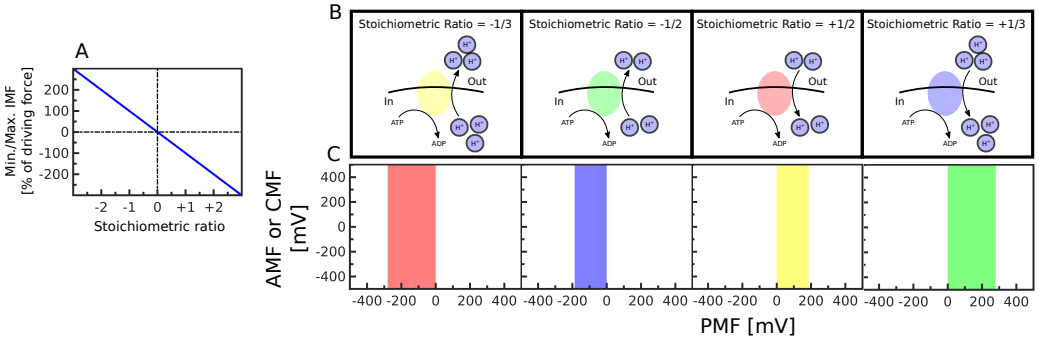


FIGURE 4.8: (A) The minimal (if negative) or maximal (if positive) IMF that can be generated by an ionic pump is shown as a function of the stoichiometric ratio. The driving force is always negative. (B) Reachability properties of proton:ATPase with different stoichiometric ratio.

Characterization of Cotransporters. We now turn ourselves to the characterization of cotransporters for two ions. Similarly as before, we assume the experimentalist has full control over the PMF and AMF and delegates the control

of the CMF to a 1:1 proton:cation antiporter in figure 4.9. The characteristic volume in the 3-D IMF space consists of 2 triangular prisms connected at 0 PMF with triangle rectangular base when projected on the AMF axis (or onto any axis consisting of the motive force of a simplex reaction not partaking in the cotransport). Projection on the axis defined by the motive force that drives the reaction (in this case the PMF) will yield a 2-D rectangle which width depends on the PMF value much like before the rectangle of a chemically driven ionic transport depended on the value of the driving force, *e.g.* that of ATP hydrolysis.

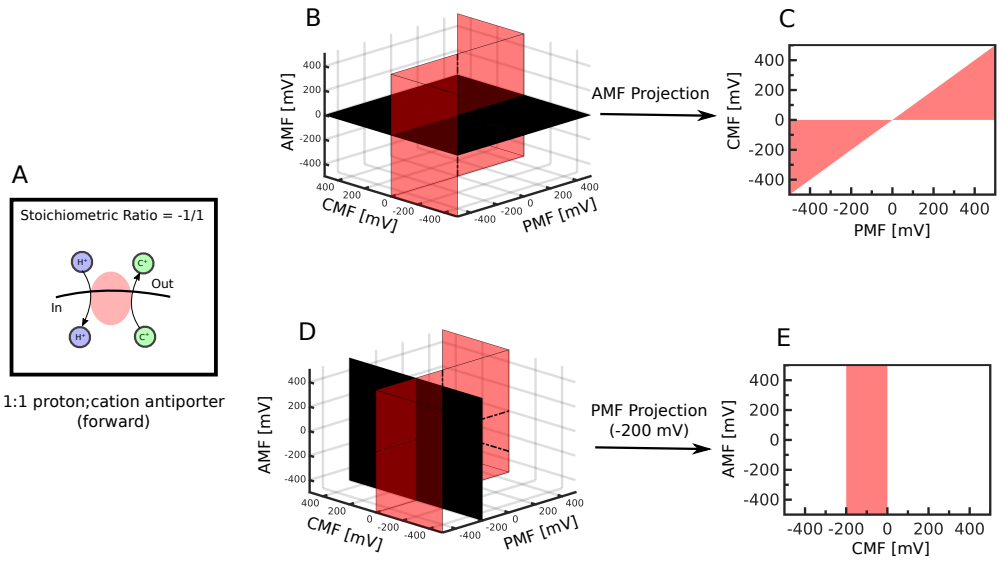


FIGURE 4.9: (A) Scheme of a proton:cation antiporter, the forward direction is by convention that for which protons flow in. (B & D) reachability properties of this antiporter (when it is PMF driven, generating CMF) in the 3-D space consisting of PMF, AMF and CMF. (C & E) Projection of the reachability space on the AMF and PMF axis respectively. When projected on the IMF that drives the antiporter, the reachability map is analogous to that of a chemically driven ionic transport.

Crucially, the shape of the 2-D triangles characteristic of a cotransporter (projection of the 3-D space onto the potential of a simplex not partaking in the reaction) depends on the coupling stoichiometry of the reaction. For a proton:cation antiporter, the further away from 0 ΔG_{C^+} achievable will be given by the coupling ratio $\times -\Delta G_{H^+}$ as shown in figure 4.10. This dependency of the allowed IMF range depending on the coupling stoichiometry is the cornerstone of the reasoning of chapter 2.

While antiporters (characterized by negative coupling stoichiometries) allow generation of an IMF of identical sign than the driving IMF, symporters as shown in figure 4.11 allow generation of an IMF of opposite sign than the driving IMF.

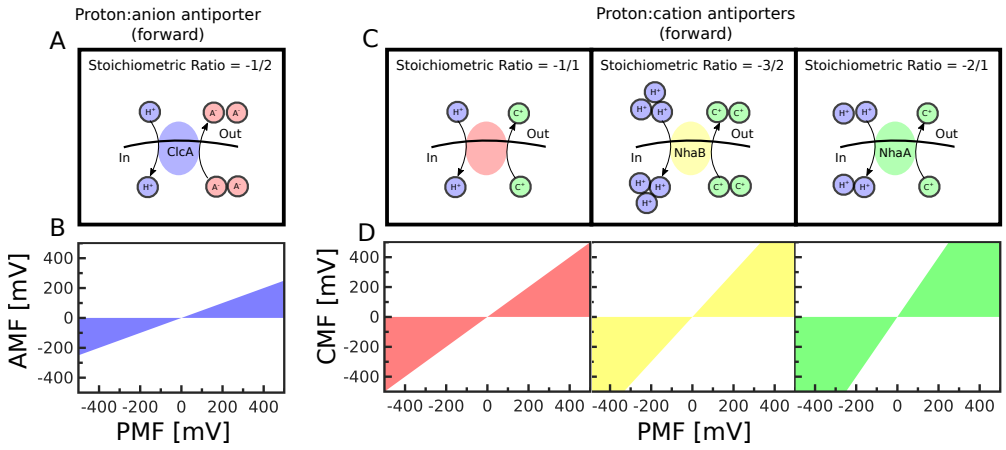


FIGURE 4.10: Reachability properties of (A) a proton:anion antiporter (PMF driven, generating AMF) and (B) of various proton:cation antiporters (PMF driven, generating CMF) with different coupling stoichiometries.

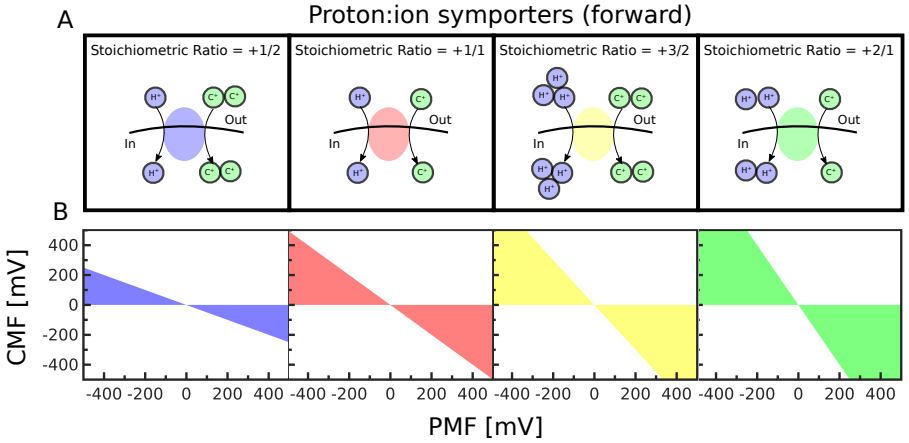


FIGURE 4.11: Reachability properties of various proton:cation symporters (PMF driven, generating CMF) with different coupling stoichiometries.

Importantly, we considered proton:ion antiporters which are proton driven. Structurally identical cotransporters may however generate a PMF and be ion driven. In which case the thought experiment we made before: "full control over PMF, AMF, delegate control of CMF to a proton:cation cotransporter" becomes: "full control over CMF, AMF, delegate control of PMF to a proton:cation cotransporters". The characteristic shape in the {PMF,CMF} plane of such a proton:cation cotransporter is given by complementing the squares the triangle characteristic of the experiments from figures 4.10, 4.11 belonged to, *i.e.* the coordinates which have identical signs for CMF and PMF for antiporters and opposite signs for symporters as shown by the green area in figure 4.12 (A) for a cation driven proton:cation antiporter and the red area in figure 4.12 for a cation driven proton:cation symporter. Note that the direction in which the cotransporter works depends on whether it is CMF or PMF driven. For the direction of reference chosen for the proton:cation antiporter in figure 4.12 (A), *i.e.* it goes forward if protons go in and cations out, the same antiporter driven by cations will work backward, meaning in the green area, the cotransporter works to move protons out, driven by cations flowing in. A symmetric reasoning applies to the symporter figure 4.12.

Attractor States of Ionic Pumps. We extensively characterized the *reachability properties* of chemically driven ionic pumps or cotransporters for two ions. It now seems like a good place to introduce another characteristic of such ionic pumps, that again does not depend on their specific kinetics, we call it the "Attractor States of an Ionic Pump". Rigorously, this is the set of locations in the state space that one will achieve by increasing indefinitely the forward activity of an active ionic pump. Consider for instance that the overall flux of an ion x is given by its simplex reaction (passive diffusion j_x) and the activity of multiples pumps, a particular pump p we will study and other pumps (sum over r):

$$\frac{d[x]_i}{dt} = 0 = j_x^+ \cdot \left(1 - e^{\frac{F}{RT}\Delta G_x}\right) + \sigma_{x,p} \cdot j_p^+ \cdot \left(1 - e^{\frac{F}{RT}\Delta G_p}\right) + \sum_{r \setminus p} \sigma_{x,r} \cdot j_r^+ \cdot \left(1 - e^{\frac{F}{RT}\Delta G_r}\right) \tag{IV.3}$$

This is at steady state. We now take the limit that $j_p^+ \to +\infty$ such that all other terms contributing to the movement of x become negligible and the steady-state is characterized by:

$$\Delta G_p(j_p^+ \to +\infty) = 0 \tag{IV.4}$$

An elegant way to approach it is to say that p is imposing its own equilibrium rule. Following a similar reasoning, increasing j_x^+ indefinitely, by for instance increasing the permeability of the membrane will lead to equilibration of x across the membrane $\Delta G_x = 0$. In fact, the effective ΔG_x achieved by a model consisting of multiple pumps can be seen as the result of several reactions competing to impose their own equilibrium rule, as is nicely stated by [200] in the case of biochemical reactions. The attractor state of a pump, as defined by Eq. (IV.4) is straightforward to visualize and is shown in figure 4.12 (A) and (B) by the black lines. It is first interesting to notice that these attractor states are identical whether the pump is working in the forward or reverse direction. Second, the attractor, defined as a two dimensional arrow departing from a prior state to the increase of j_p^+ will be oriented towards the 0 of the axis defining the IMF that is driving it and away from the 0 of the axis defining the IMF that is generated by the transporter. This is easily understandable considering that we have a proton:cation antiporter driven by protons. The antiporter consumes proton gradient thereby acting as a force that brings the PMF to 0, and generates cation gradient, acting as a force that brings it away from 0. Making the postulate that the driving force is *chemostated* (or fixed) will mean that the attractor departs vertically from the initial state (for 0 activity of the pump) to reach the attractor state given by the value to which the PMF was set (chemostated); that is when the antiporter is proton driven and assuming that the initial state was given in the absence of any pump for cations, *i.e.* $\Delta G_{C^+} = 0$. More simply, the attractor states of chemically driven pumps shown before can be visualized as the value of the IMF that is generated by the pump that is further away from 0, that is again assuming that the chemical driving force is chemostated.

Along with the characteristic reachable states, the attractor states define another intrinsic property of an ionic pump that is invariant of its specific kinetics.

Chemically Driven Cotransporters. To characterize chemically driven cotransporters we chemostat the simplex chemical reaction that drives the reaction (in the example shown $\Delta G_{ATP} = -560$ mV) and delegate control of the two IMFs of the ions partaking in the cotransport reaction to the chemically driven cotransporter. Chemically driven cotransporters are characterized by a triangular prism in a 3-D IMF space as seen in figure 4.13. As opposed to cotransporters, there is only one triangular prism, highlighting that each IMF of the two ions partaking in the reaction must be of a given sign. The projection on any axis consisting of the IMF

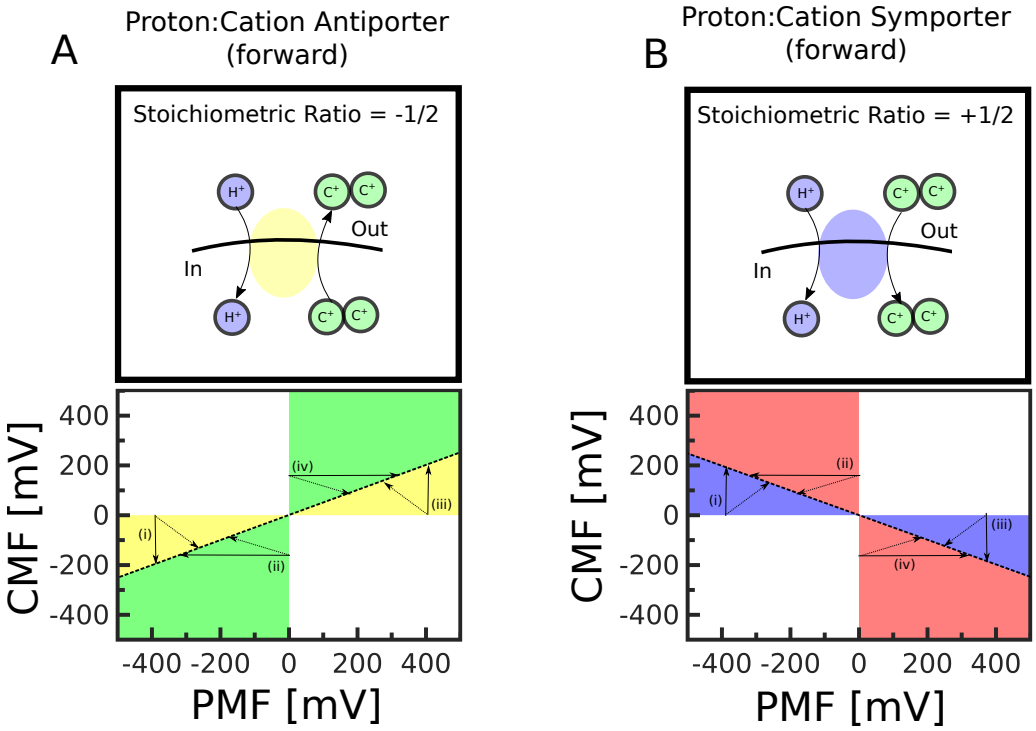


FIGURE 4.12: Reachability and attracting properties of cotransporters. (A) Reachability properties of a proton:cation antiporter. The yellow area denotes the region wherein the antiporter is PMF driven and generates CMF whereas the green area denotes the region wherein it is CMF driven and generates PMF. The black line separating the yellow and green areas deines the attracting state space: if the activity of the antiporter is increased indefinitely, the state will intercept with that line. When the antiporter is PMF driven, moving towards the attracting state (increasing activity of the pump) entails PMF going closer to 0 and CMF going away from 0. When it is CMF driven, moving towards the attracting state entails CMF moving closer to 0 and PMF moving away from 0. (B) Similar to (A) but this time for a proton:cation symporter.

on an ion not partaking in the reaction yields a rectangle triangle, rectangular angle being located at the $\{0, 0\}$ coordinate in the 2-D plane defined by the IMFs of the ions partaking in the reaction as shown in figure 4.13 (C) (which is distinct from the location of the rectangular angle in the case of cotransporters figures 4.10, 4.11).

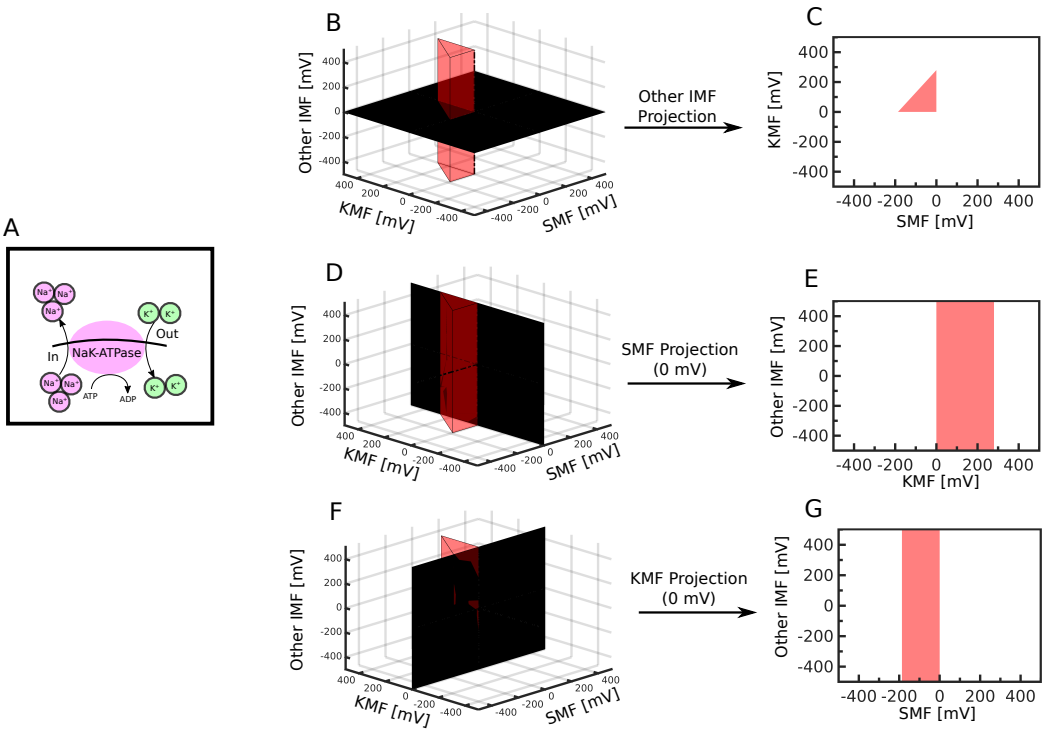


FIGURE 4.13: (A) Scheme of the NaK-ATPase, a chemically driven antiporter. (B & D & F) Reachability properties of the NaK-ATPase in the 3-D space consisting of SMF, KMF and another IMF. (C & E & G) Projection of the reachability space onto IMF, SMF or KMF.

As depicted in figure 4.14, depending on the direction in which each ion flows relative to ATP hydrolysis the sign of its achievable IMF will change. The attractor states are defined by the line delimiting the achievable states away from 0. The coupling stoichiometry for each ion will delimitate how far from 0 the IMF for this ion can reach as examplified in figure 4.14 (B) (Left) where the grey triangle denotes coupling stoichiometry of 3 for sodium while the blue triangle denotes a coupling stoichiometry of 2 for sodium. When the chemically driven cotransporter has identical coupling stoichiometries for the two ions then the triangle defining the reachable states is a right, isosceles triangle. Interestingly, the attractor state of such chemically driven cotransporters can be expressed as a function of the permeability ratio between the two ions taking part in the reaction.

Indeed consider the steady-state condition applied to both sodium and potassium:

$$0 = j_{\mathrm{Na}^+} + \sigma_{\mathrm{Na}^+,p} \cdot j_p \tag{IV.5}$$

$$0 = j_{\mathrm{K}^+} + \sigma_{\mathrm{K}^+,p} \cdot j_p \tag{IV.6}$$

where σs are the coupling stoichiometries of the pumps (negative if ATP hydrolysis coupled to efflux, positive if coupled to influx), j_x are leakage fluxes and j_p the rate of the pump (positive if associated to ATP hydrolysis). Combining both equations give:

$$j_{\mathrm{K}^+} - \frac{\sigma_{\mathrm{K}^+,p}}{\sigma_{\mathrm{Na}^+,p}} \cdot j_{\mathrm{Na}^+} = 0 \tag{IV.7}$$

substituting the leakage flux by the general trapezoidal energy barrier model introduced in chapter 1: $j_x = S/V \cdot P_x \cdot [x]_e \cdot f_b(z_x \cdot \Delta\psi) \cdot \left(1 - e^{\frac{F}{RT}}\right)$ and after few manipulations we obtain:

$$\begin{aligned} 0 = &- \frac{\sigma_{\mathrm{Na}^+,p}}{\sigma_{\mathrm{K}^+,p}} \cdot \frac{P_{\mathrm{Na}^+} \cdot [\mathrm{Na}^+]_e}{P_{\mathrm{K}^+} \cdot [\mathrm{K}^+]_e} \cdot \left(1 - e^{\frac{F}{RT} \cdot \Delta G_{\mathrm{Na}^+}}\right) \\ &+ \left(1 - e^{\frac{F}{RT} \frac{1}{\sigma_{\mathrm{K}^+,p}} \cdot (-\sigma_{\mathrm{Na}^+,p} \cdot \Delta G_{\mathrm{Na}^+} - \Delta G_{\mathrm{ATP}})}\right) \end{aligned} \tag{IV.8}$$

$$\Delta G_p = \Delta G_{\mathrm{ATP}} + \sigma_{\mathrm{K}^+,p} \cdot \Delta G_{\mathrm{K}^+} + \sigma_{\mathrm{Na}^+,p} \cdot \Delta G_{\mathrm{Na}^+} = 0 \tag{IV.9}$$

where the second equation defines the attractor states of the chemically driven cotransporter as in Eq. (IV.4) and the solving the first equation for the SMF gives the precise (unique) coordinate of the attractor state. Chemically driven cotransporters (moving simultaneously at least two distinct ionic species and coupled to a chemical reaction) have therefore what seems to be an unique feature when compared to chemically driven ionic transporters (moving only one ionic specie, coupled to a chemical reaction) or non chemically driven cotransporters (moving simultaneously at least two distinct ionic species and non coupled to a chemical reaction), indeed their attractor state can be tuned by the permeability of the two ions sodium and potassium. We shall come back to it later and revisit how the NaK ATPase has indeed unique properties (that other types of transporters have not) that allows action potential.

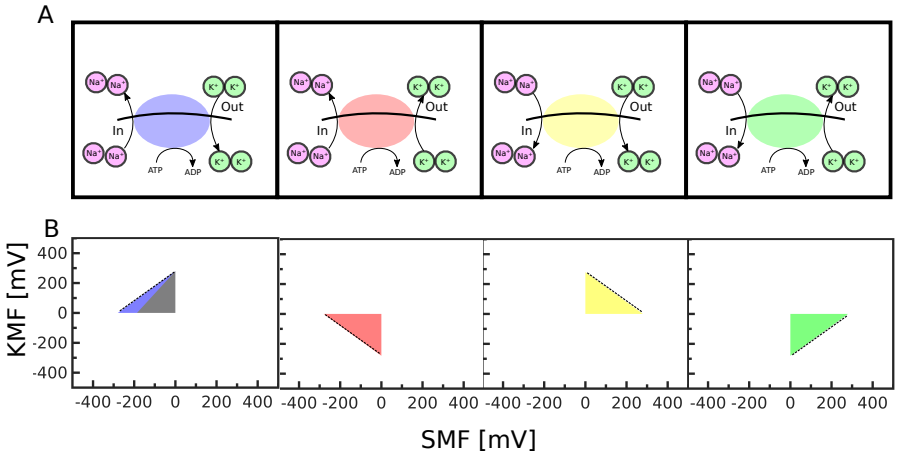


FIGURE 4.14: (A) Schemes of different chemically driven cotransporters coupling movement of ions with ATP hydrolysis in different directions. (B) Reachability properties for those pumps, fixing $\Delta G_{\text{ATP}} = -560$ mV. The black line denotes the attractor states. As outlined in the text, the precise attracting coordinate can be computed with knowledge of the permeabilities of the membrane to sodium and potassium as well as their extracellular concentrations.

Cotransporters for 3 Ions. Before we do that we briefly show the characteristic volume of cotransporters for 3 ions in the 3-D IMF space for the three ions partaking in the reaction in figure 4.15. To that end, we only show the regime wherein sodium drives the transport and accordingly assume that the experimentalist has full control over the SMF and delegates control of Chloride Motive Force and Potassium Motive Force to the NKCC cotransporter. The characteristic 3-D is once again unique (relative to the other functional families of ionic transporters) and consists of two triangular pyramids with rectangular triangle base oriented away from null SMF. Projection on the SMF axis (that which drives the reaction) yield characteristic achievable state spaces that look like chemically driven cotransporters with this time variable orientation of the triangle (depending on the sign of the SMF) and variable area of the triangle (depending on the amplitude of the SMF). In fact, drawing the achievable state space in the 3-D space consisting of $\{\Delta G_{\text{ATP}}, \text{SMF}, \text{KMF}\}$ for ATP driven cotransporters, not chemostating ΔG_{ATP} would give similar characteristic volumes than in 4.15 but this time substituting the SMF by the potential of the ATP hydrolysis simplex ΔG_{ATP}. The attractor states also behave in a similar fashion than those of chemically driven cotransporters, however if the SMF is not chemostated, the attactor of the NKCC cotransporter is characterized by a 3-D arrows with behaviours in the Chloride Motive Force and Potassium Motive Force dimensions alike SMF and KMF attractors in the case of chemically driven Sodium potassium cotransport,

with the difference that the arrow points in the third dimension (SMF) in the direction of null SMF. The latter seeds from SMF being not chemostated while ATP hydrolysis is.

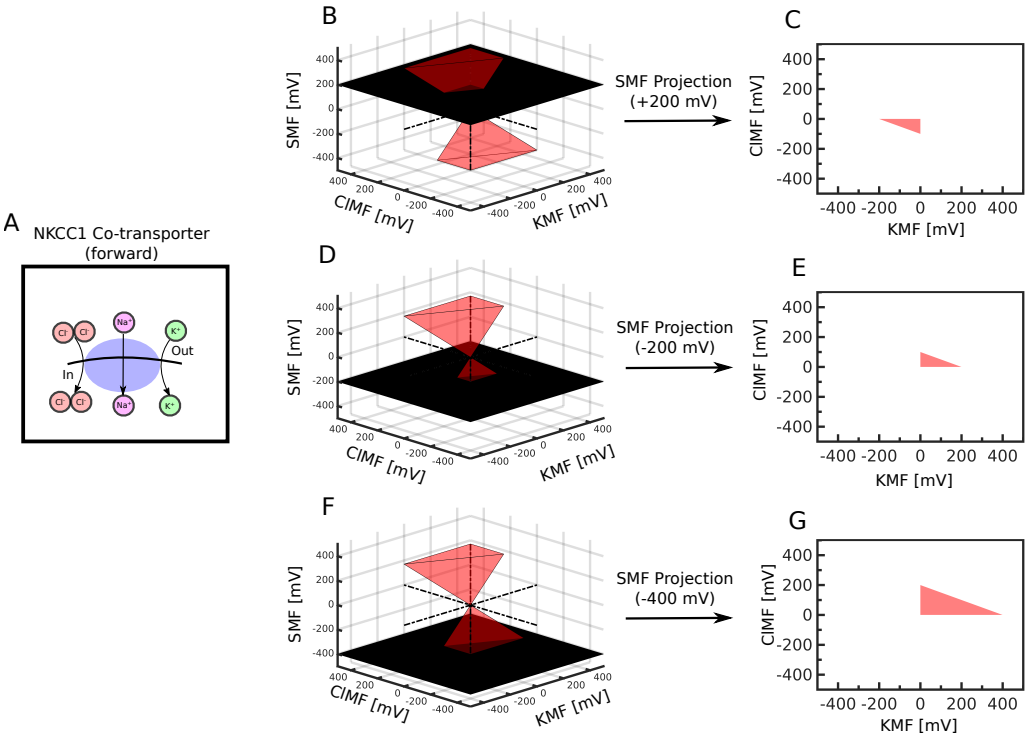


FIGURE 4.15: (A) Scheme of the NKCC cotransporter. (B & D & F) Reachabilities properties of the NKCC cotransporter (SMF driven, generating Chloride MF and KMF). (C & E % G) Projection for different SMF values.

ii. Composability of Active Ionic Transporters

After the extensive characterization of the different functional families of active ionic transport systems, we now get to the most interesting consequence of the characterization method we have employed for each transporter. Indeed, there is a simple heuristic on how to define the reachable state space of a model composed of an arbitrary number of transporters characterized as before, as well as the directional regimes and the limit behaviours (given by assuming that some transporters impose their own equilibrium rule).

The heuristic is as follows:

1. Step 1. Enumerate all transporters the model includes and characterize them individually as explained before.

2. Step 2. Group transporters by which ions they are generating gradient for. Superimpose reachability map of each such transporter (OR operator) which defines the reachable state space for a model consisting of different transporters generating a given IMF for which we have (still) control on all other potentials of simplex reactions and have delegated generation of that given IMF to multiple transporters. Depending on the coordinate within the reachable state-space, the direction in which these transporters work may change as we will exemplify thereafter.

3. Step 3. Merge the reachability maps for each IMF, only the coordinates which belong to all reachability maps are achievable. Notably, to achieve a coordinate other than the origin requires chemostating of at least one simplex reaction that is coupled to generation of other IMFs.

It is perhaps not obvious to understand as it is so let us take three different examples of models for which we shall define the reachable state space, the directional regimes and the attractors:

- The first example is the model of *E.coli*'s electrophysiology shown in chapter 2, consisting of the three antiporters with known stoichiometries *ClcA*, *NhaB*, *NhaA*, F1F$_o$ and the oxidative respiratory chain. Two potentials are chemostated: that of the simplexes "NADH reduction" to -2230 mV and "ATP hydrolysis" to -560 mV. In step 1 figure 4.16 we draw the reachability map of each of these 5 transporters. We then proceed with step 2 shown in figure 4.16 (Middle), and accordingly superimpose the maps of transporters contributing to the generation of each of the three axes (PMF, CMF, AMF). While the reachability of AMF remains unchanged from step 1 since there is only a single transporter for anions, the reachability for PMF and CMF is given by superimposing two reachability maps: for PMF that of the respiratory chain and F1Fo, that both drive proton movement, for CMF that of *NhaB* and *NhaA* that both drive cation movement. These define on each of the PMF and CMF axis two directional regimes, indeed depending on the specific PMF that is maintained within the allowed range, F1F$_o$ may either work in the forward or reverse direction, depending on the specific CMF that is maintained within the allowed range, *NhaB* may either work in the forward or reverse direction. Finally, step 3 consists in delegating full control of the diverse potentials (in this case IMFs) to the model (but that which are chemostated) and drawing the reachable state space of the model

figure 4.16 (left) in red, which correspond to all the coordinates that belong to each of the reachability map drawn in step 2. Interestingly, as shown in the 2-D projections, experimental assessment of any of the generated IMFs within the scope of model constrains the reachability state-space such that even an uncomplete experimental characterization of the state space is still informative in that it reduces the set of allowed IMFs in a way that is specific to the "vocabulary" of ionic transports the model possesses and the values to which were set the chemostated potentials. Another interesting observation is that the reachable state-space is decomposed into $2 \times 2 =$ four different regions, that correspond to different directional regimes (number of which is given by the product over each dimension of the dimension specific number of directional regimes). In principle this can be quite useful to an experimentalist. Indeed, measuring the direction in which an ionic transporter works is way easier than measuring the CMF. Then the experimentalist can use the prior information given in 4.16 (bottom) to map a measure of the direction in which *NhaB* works to the quite narrow green area in the reachable state space.

- The second example model, depicted in figure 4.17, is somehow simpler in that it consists of a model with only three active ionic pumps: the oxidative respiratory chain, an ATP driven potassium efflux pump (for instance KdpABC) and a 1:1 proton:potassium antiporter (for instance *ChaA*). The first step consists in, as in the previous example, characterizing the reachability properties of each of the 3 ionic pumps. There is one major difference however with the previous example: the proton:potassium antiporter needs now to be characterized for both scenarii whether it is KMF or PMF driven. This seeds from both potassium and proton having access to pumps whose driving force is chemostated (NADH reduction for protons, ATP hydrolysis for potassium). The step 2 then consists in merging (OR operator) the reachability maps along each IMF axis (PMF and KMF). The PMF reachability is obtained by superimposing the reachability maps of the oxidative respiratory chain and of *ChaA* (when it is KMF-driven), while the KMF reachability is obtained by superimposing the reachability maps of the KdpABC with that of *ChaA* (when it is PMF-driven). As in the previous example, the reachability map of the model (for chemostating NADH reduction and ATP hydrolysis) is obtained by merging (AND operator) the reachability maps for PMF and KMF obtained in Step

2. Three directional regimes are obtained: *Regime (i)* Oxidative respiratory chain works to move protons out (NADH driven, generating PMF), *ChaA* works to move potassium out (PMF driven, generating KMF); *Regime (ii)* Oxidative respiratory chain works to move protons out (NADH driven, generating PMF), *ChaA* works to move protons out (KMF driven, generating PMF); *Regime (iii)* oxidative respiratory chain works to regenerate NADH from NAD^+ (PMF driven) and *ChaA* works to move protons out (KMF driven, generating PMF). KdpABC always work in the same direction that moves potassium out (ATP driven, generating KMF). Interestingly, as *E.coli* possesses these three transporters, it has in principle the ability to transduce energy from ATP to NADH *via* the proton:potassium antiporter *ChaA* (*Regime (iii)*). *E.coli* could thus theoretically consumes ATP to make NADH from NAD^+, subsequently uses the Krebb's cycle to fixate carbon using energy from NADH reduction[19]. Now, the fact that *E.coli can* do this does not mean it physiologically *does* this. From our heuristics (of attracting regimes), we can say that transducing energy from ATP to NADH would require sufficiently high activity of KdpABC and *ChaA* so that the cell is in *regime (iii)*. Indeed, the attractor for KdpABC is the horizontal line that intercepts KMF = -560 mV and the attractor for *ChaA* is the diagonal dotted line in figure 4.17 (bottom step 3). Should one be able to freely tune the *in vivo* activity of KdpABC and *ChaA*, this could in principle raise the possibility of making *E. coli* fixing carbon *via* the Krebb's cycle.

- The final and most simple example is shown in figure 4.18 and consists of a model possessing only two ionic transporters: the NaK-ATPase and a 1:1 proton:sodium/potassium antiporters. In this model the step 2 can be bypassed since each of the IMFs (KMF, SMF, PMF) can only be generated by a single ionic pump (NaK-ATPase for SMF and KMF, NHE-1 for PMF). Here since only one energy source can drive movement of protons across the membrane (SMF *via* NHE-1), NHE-1 always works in the direction that moves protons out (SMF driven, generating PMF). In this example, as opposed to the model of pH regulation in *E.coli* figure 4.16 when the range of SMF achievable depends on the PMF, the ability to generate SMF (thus

[19]Reverse to the physiological direction which is assumed, *i.e.* Krebb's cycle degrade carbon chains to make NADH from NAD^+, which is in turn consumed by the respiratory chain to generate PMF

voltage[20]) is independent on the PMF. Therefore, and as opposed to the *E.coli* model, this simplified model of mammalian cells is able to decouple the ability to maintain membrane voltage and PMF. Although both this model and *E.coli*'s model can tune intracellular pH *via* activity of the proton:sodium antiporter, they do so *via* very different physiological mechanisms: while the *E.coli*'s model tune the activity of the proton:sodium antiporter to modulate voltage, thus tuning pH_i given a chemostated PMF and a pH_e, this model of mammalian cell tunes the activity of the proton:sodium antiporter to modulate PMF, thus tuning pH_i given a chemostated SMF (on which voltage depends) and a pH_e. Interestingly, as shown in figure 4.18 the range of PMF that can be maintained (thus the range of pH_e wherein the model can maintain fixed pH_i) depends on both the SMF and KMF, potentially being the source of a rich interplay between SMF/KMF maintenance (thus voltage) and pH_i homeostasis, albeit by a different mechanism than that of *E.coli*. To summarize how we understand the function of proton:cation antiporters in pH regulation in mammals *versus* *E.coli*:

- pH homeostasis in *E.coli*: Chemostated PMF, proton:cation antiporters are PMF driven, generate SMF/KMF, subsequently voltage. The activity of antiporters set the voltage maintained, thus the pH_i given the pH_e and the value to which PMF is chemostated.
- pH homeostasis in mammals: Chemostated SMF/KMF (thus voltage), proton:cation antiporters are SMF driven, generate PMF, therefore directly tune pH_i given pH_e and the chemostated SMF/KMF values (thus voltage).

The current paradigm for pH_i regulation that was described in the introduction of this thesis for bacteria and that we question in chapter 2 thus seems valid in the case of mammalian cells. This exemplifies that two cellular components having a similar mechanism of action (in this case a proton:sodium antiporter) can play a role in the same physiological function (pH homeostasis) *via* two different mechanisms in different classes of organisms (voltage modulation/Chemostated PMF in bacteria , PMF modulation/Chemostated voltage in mammals).

[20]We show in chapter 2 that contribution of protons and hydroxide ions to voltage generation is negligible.

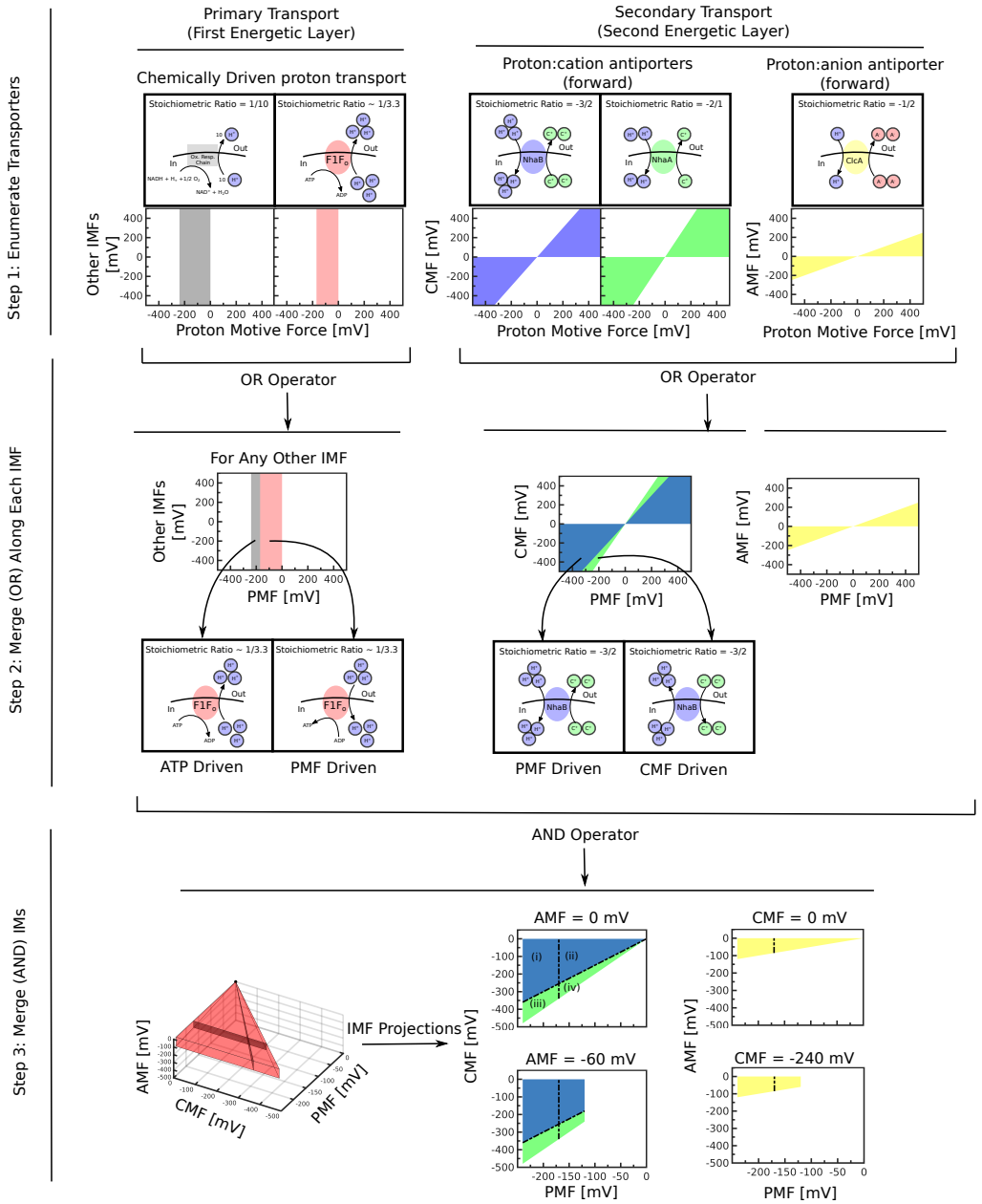


FIGURE 4.16: Characterization of the reachability properties of the model of *E.coli* Electrophysiology. (Top) Each transporter part of the model is characterized individually as explained before. (Middle) The reachability of each IMF is characterized. (Top) The reachability of the entire model is characterized. The reachable state space can be decomposed in four regimes as indicated by roman numbers, each of which corresponding to specific directions in which work the antiporter: *(i)* $F1F_o$ backward, *NhaB* forward, *(i)* $F1F_o$ forward, *NhaB* forward, *(iii)* $F1F_o$ backward, *NhaB* backward, *(iv)* $F1F_o$ forward, *NhaB* backward.

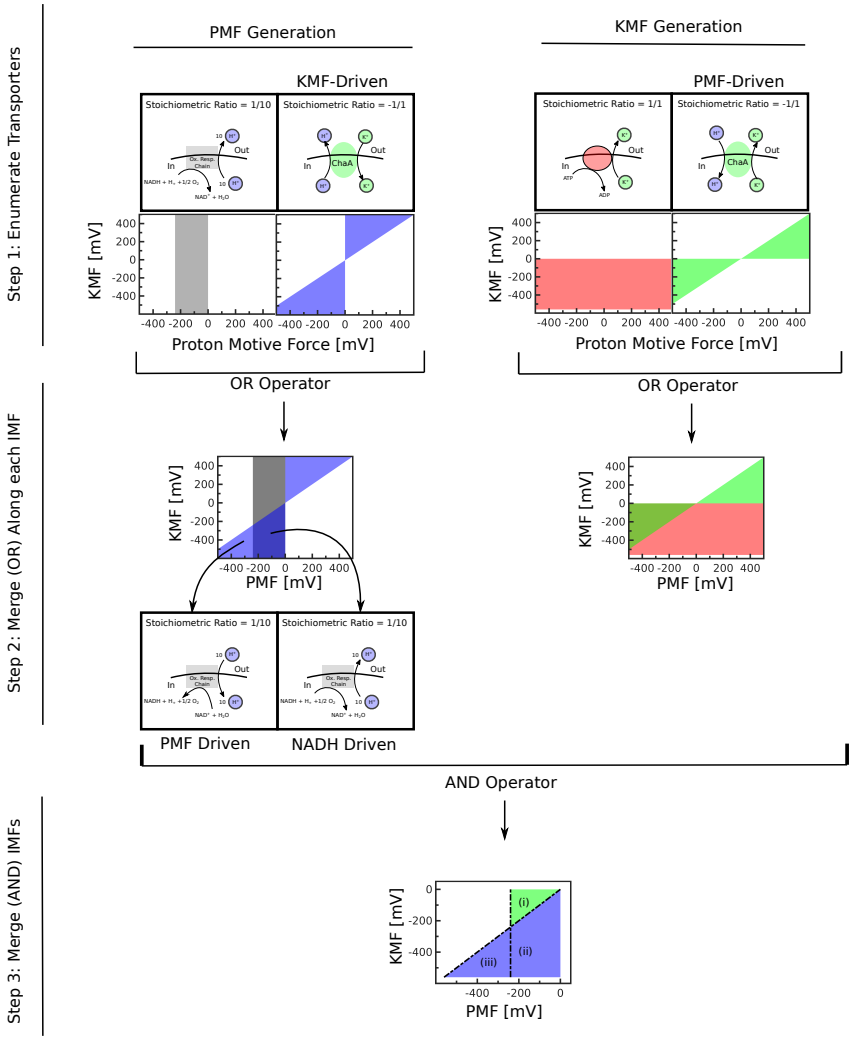


FIGURE 4.17: Reachability properties of a different model, including oxidative respiratory chain an ATP driven potassium efflux pump and a proton:potassium antiporter. (Top) Individual characterization of the reachability for each transporter. (Middle) Characterization of the reachability of each IMF. Importantly, the proton:potassium antiporter can be either PMF driven, generating KMF or KMF driven, generating PMF, such that it partakes to the characterization of the reachable state space of both IMFs. (Bottom) Characterization of the reachable state space for the entire model.

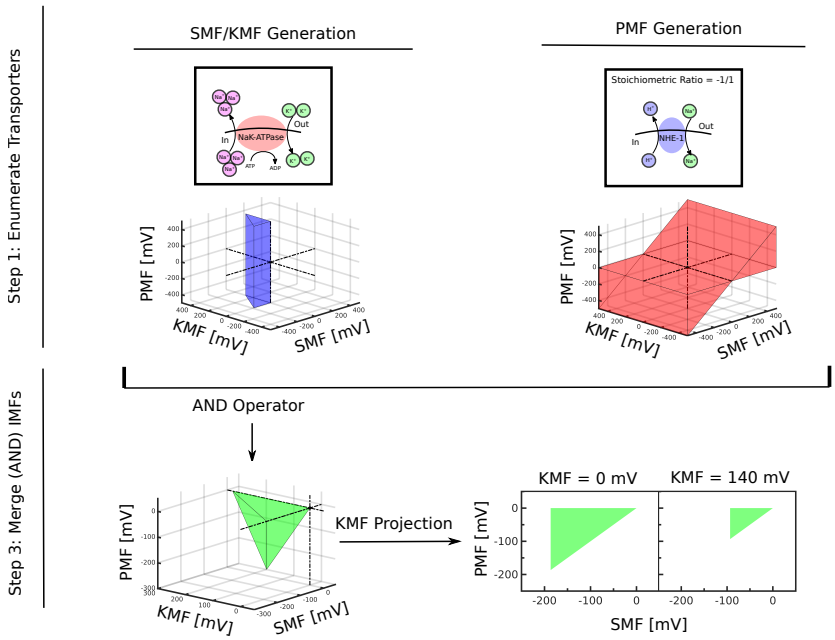


FIGURE 4.18: Model of pH regulation in mammalian cells. (Top) Characterization of the reachable state space for each of the two pumps. (Bottom) Reachable state space for the entire model. The PMF range that can be maintained is up to the value of the SMF maintained, thus the extent to which pH_i can be tuned depends on the SMF (and indirectly on the KMF, that constraints the range of SMF that can be maintained *via* the NaK-ATPase).

iii. Specificities of the NaK-ATPase

We shall now use our heuristics in order to study what makes the NaK-ATPase so specifics with respect to its ability to generate membrane voltage. To that aim, we are now comparing its reachability and attracting properties to other models with different transporters for potassium and sodium. In order to this, we next introduce the final component of our heuristic to analyze electrophysiological behaviours: we use that voltage depends on the IMFs to map how the reachability properties of ionic transporters set the range of membrane voltage that can be achieved (essentially combining visualizations in figure 4.1 and that of figures 4.4 to 4.18). In what follows we will consider for simplicity three ionic species (chloride, potassium, sodium), assume that chloride equilibrates across the membrane so that $\Delta G_{\mathrm{A}^-} = 0$, that $\mathrm{pH}_i = 7$ and that the contribution of captive molecules is $\phi_Y = z_Y \cdot [Y]_i/[X]_e = -0.5$ where $[X]_e = [\mathrm{Cl}^-]_e + [\mathrm{K}^+]_e + [\mathrm{Na}^+]_e = 300$ mM denotes the total extracellular concentration in small ions (else than protons/hydroxide ions).

Ability of Chemically Driven Antiporters to Maintain Negative Membrane Voltage Depends on the Extracellular Ionic Composition. We first compare in figure 4.19 the ability of two different chemically driven cotransporters to generate -70 mV membrane potential in environments with different concentrations of sodium relative to that of potassium. Interestingly, we notice that the imaginary ATP driven sodium:potassium symporter is more versatile than the NaK-ATPase (ATP driven sodium:potassium antiporter) in that it possesses the ability to generate -70 mV membrane potential for any extracellular balance between potassium and sodium. Indeed, the NaK-ATPase is only able to generate such membrane potential in environments with low concentrations of potassium relative to that of sodium. Accordingly, the ionic composition of body fluids in which mammalian cells are have higher sodium than potassium concentration that allow generation of -70 mV membrane voltage with the NaK-ATPase.

Chemically Driven Antiporters Allow "Continuous" Control of Membrane Potential by Permeabilities. In the face of ATP driven symporters being more versatile one could wonder why mammalian cells made the "choice" of generating voltage with the NaK-ATPase, that can only generate physiological membrane potentials for low extracellular potassium to sodium concentration ratios. To that end, we set $[K^+]_e = 5$ mM, $[Na^+]_e = 145$ mM (corresponding to blood plasma) and we compare in figure 4.20 the membrane potential generated in the attracting regimes of various ATP driven symporters (A, B, C, D) to the membrane potential generated in the attracting regimes of various ATP driven antiporters (E, F, G, H). In figures 4.20 (B) we show by the different dotted lines, the attractor regimes of ATP driven symporters with various stoichiometries for potassium and sodium. We next control the state by tuning the ratio $\frac{P_{Na^+} \cdot [Na_e^+}{P_{K^+} \cdot [K^+]_e}$ that sets the attracting state as seen by Eq. (IV.8) and Eq. (IV.9) and see that although SMF can be monotonically controlled by the permeability ratio see figure 4.20 (C), such is not the case for the membrane potential as shown in figure 4.20 (D). On top of that, when the membrane potential is maintained by ATP driven symporters, it is very sensitive to the permeability ratio and essentially can shift between two values in a threshold-like manner with highly depolarized intermediary state achieved when the permeability of the membrane for potassium and sodium is approximately identical. As opposed to ATP driven symporters and as seen in figure 4.20 (H), generation of membrane potential by ATP driven antiporters allows smooth and monotonic transition between different membrane potentials by control of the

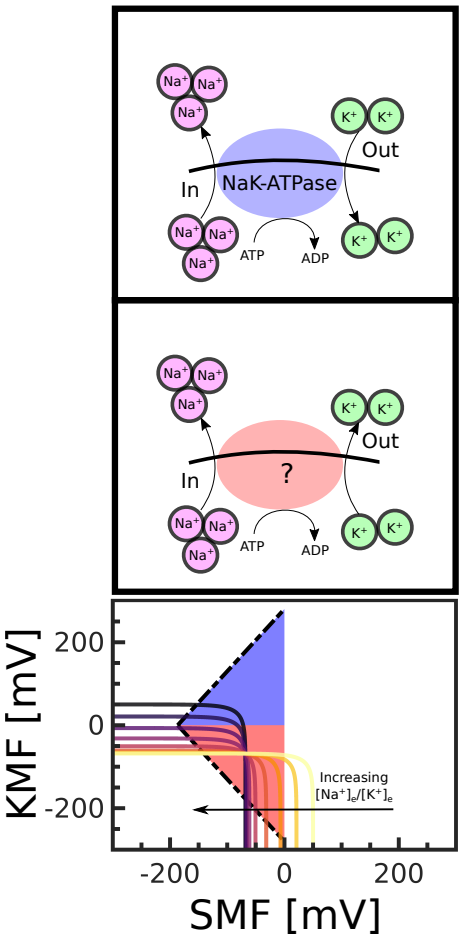


FIGURE 4.19: Membrane potential is set to -70 mV, $\phi_{y,i} = -0.5$, $\Delta G_{\mathrm{A}^-} = 0$ (null AMF) and $\Delta G_{\mathrm{ATP}} = -560$ mV. Top are two ATP driven cotransporters. Their corresponding reachability state space is indicted in the bottom plot by the two shaded regions with different colors. (Bottom) Lines indicate the pairs of KMF, SMF that are required for achieving -70 mV membrane potential for different extracellular composition in potassium and sodium: from black to yellow, $[\mathrm{Na}^+]_e/[\mathrm{K}^+]_e$ is set to 10^{-2}, $10^{-1.5}$, ..., 10^2. NaK-ATPase is only able to maintain -70 mV membrane potential for low enough extracellular potassium relative to sodium.

permeabilities. Therefrom we can highlight two features by which ATP driven antiporters are intrinsically "better at" than ATP driven symporters:

1. The signal "permeability ratio" is non-ambiguous with respect to membrane potential, in the sense that the cell "knows" that increasing the permeability ratio sodium to potassium is going to make membrane potential more positive. Such is not the case for ATP driven symporters, where membrane potential may become more negative or more positive depending on the precise value the permeability ratio initially takes.

2. The second advantage of ATP driven antiporters is that the transition between extreme membrane potentials is way less sensitive to the permeability ratio than for ATP driven symporters. This, I expect, would facilitate fine tuning of the membrane potential by modulations of the permeability ratio. The underlying assumption being that the cell has some control resolutions on the permeability ratios. Say for instance it can set the $\log_{10}$ permeability ratio with a precision ± 1, then if membrane potential is generated with ATP driven symporters, the cell will not be able to precisely set any intermediary values (between the two extrema) for the membrane potentials as seen in figure 4.20 (D). With identical precision, the cell would still be able however to have some continuous control over the membrane potential if it is generated by ATP driven antiporters as seen in figure 4.20 (H). Indeed, *both* membrane potential extrema achieved by setting $\log_{10}$ of the permeability ratio with a precision ± 1 are significantly different when the permeability ratio is moved between the range $[10, 10^3]$ in figure 4.20 (H); such is not the case for ATP driven symporters 4.20 (D).

Finally, we also note that the membrane potential resulting from the attracting state of the NaK-ATPase for previously reported permeability values of the membrane to potassium and sodium [163] is closed to -70 mV (close to the value most mammalian cells maintain), as shown by the black dot

NaK-ATPase Allows Fast-Paced Control of Membrane Voltage via Sodium and Potassium Permeabilities. Finally, we demonstrate once more how our heuristics allow straightforward characterization of electrophysiological models by comparing how two different models fare in controlling the membrane potential by tuning permeability of the membrane to sodium or potassium. The starting point being a quite (I find) natural question to ask, that is: *"Why do mammalian cells chose to generate membrane potential with an ATP driven antiporters rather than two*

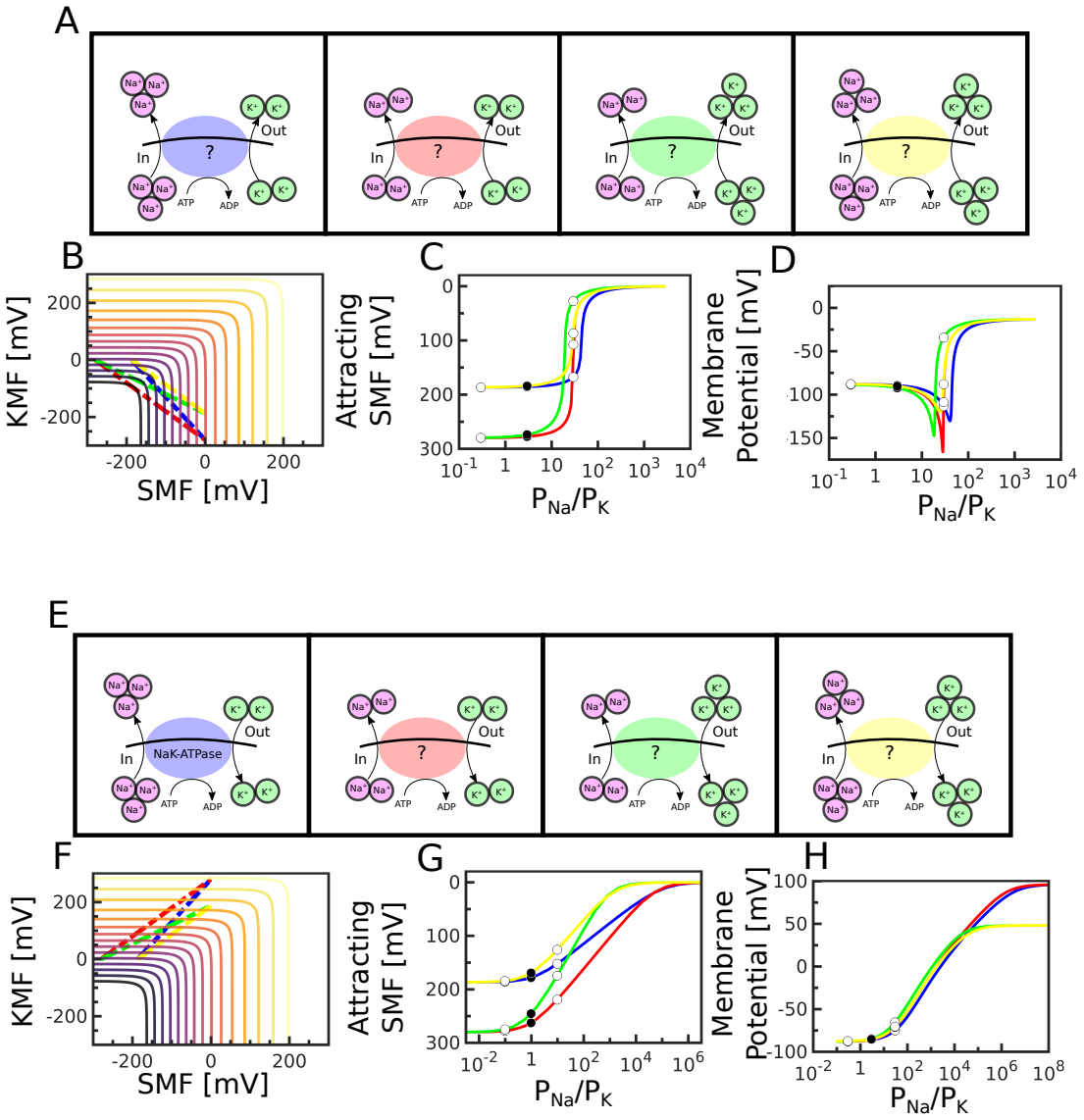


FIGURE 4.20: Controllability of membrane voltage by modulating permeability of the membrane to potassium and sodium.(A) Schemes of ATP driven potassium:sodium symporters. (B) Lines denote different membrane potentials ranging from -200 mV (black) to +80 mV (yellow) with +20 mV increments. The dotted lines of different colors correspond to the attracting states of the different ATP driven symporters. (C) Precise attracting x-coordinate (attracting SMF) on the lines in (B) is given as a function of the permeability ratio. (D) membrane potential resulting from the attracting SMF for the various transporters is shown as a function of the permeability ratio. (E) Schemes of ATP driven potassium:sodium antiporters with dotted lines in (F) denoting the attracting states, (G) showing the attracting SMF and (H) the resulting membrane potential as a function of the permeability ratio. (C & D & G & H) The black dot represent the state that is achieved for the reference permeability values $P_{K^+} = 5 \times 10^{-10}$ m/s and $P_{Na^+} = 1.7 \times 10^{-10}$ m/s [163] at the given extracellular composition $[[K^+]_e = 5$ mM and $[Na^+]_e = 145$ mM. The white dots denote the states achieved by multiplying/dividing by 10 the reference permeability ratio.

chemically driven pumps, one for potassium and one for sodium". Indeed, having two pumps rather than one is expected *a priori* to enable perhaps finer control on both SMF and KMF and thus on membrane potential. Indeed, as seen on figure 4.21 (Left), having two ATP driven pump (1:2 ATP:potassium ratio influx potassium pump and a 1:3 ATP:sodium ratio efflux sodium pump) allows a wider reachability space than the NaK-ATPase. However, departing from any initial states, characterized by $P_{\mathrm{K}^+} = 5 \times 10^{-10}$ m/s, $P_{\mathrm{Na}^+} = 1.5 \times 10^{-10}$ m/s, membrane potential -40 mV indicated by the black dotted line, only the NaK-ATPase allows control of membrane potential by *either* tuning the permeability of the membrane to potassium or/and sodium, as shown in figure 4.21 (Right) for the particular departing state denoted by the red dot in figure (Left) specified by the forward activities of the pumps [21]. Note that for this experiment we assume some first order kinetic model for the pumps as follows:

$$j_1 = k_1 \cdot [\mathrm{Na}^+]_i^3 \cdot e^{\frac{3}{2} \cdot \frac{F}{RT} \cdot \Delta\psi} \cdot \left(1 - e^{\frac{F}{RT}(\Delta G_{\mathrm{ATP}} - 3 \cdot \Delta G_{\mathrm{Na}^+})}\right) \tag{IV.10}$$

$$j_2 = k_2 \cdot [\mathrm{K}^+]_e^2 \cdot e^{-\frac{F}{RT} \cdot \Delta\psi} \cdot \left(1 - e^{\frac{F}{RT}(\Delta G_{\mathrm{ATP}} + 2 \cdot \Delta G_{\mathrm{K}^+})}\right) \tag{IV.11}$$

$$j_3 = k_3 \cdot [\mathrm{Na}^+]_i^3 \cdot [\mathrm{K}^+]_e^2 \cdot e^{\frac{1}{2} \cdot \frac{F}{RT} \cdot \Delta\psi} \cdot \left(1 - e^{\frac{F}{RT}(\Delta G_{\mathrm{ATP}} - 3 \cdot \Delta G_{\mathrm{Na}^+} + 2 \cdot \Delta G_{\mathrm{K}^+})}\right) \tag{IV.12}$$

where j_1, j_2, j_3 are respectively for the flux of the ATP driven sodium efflux pump, ATP driven potassium influx pump and the NaK-ATPase. The variables k_1, k_2, k_3 are the control variables we use to tune the forward activities. We also impose time-oscillating permeabilities with period equal to $10^{-3} \times V/S/P_{\mathrm{Na}^+} \approx 100$ milliseconds (for *E.coli*'s geometry), demonstrating fast paced ability to control of membrane voltage.

A Step Forward: Visualizing Kinetics in the IMF State-Space

Something I did not have the time to develop but that I think could be interesting to complement the framework presented herein would be the kinetic characterization

[21] This inability of the model with two pumps to have access to control of membrane potential by either of the permeabilities holds for any departing state on the dotted black line (Not shown).

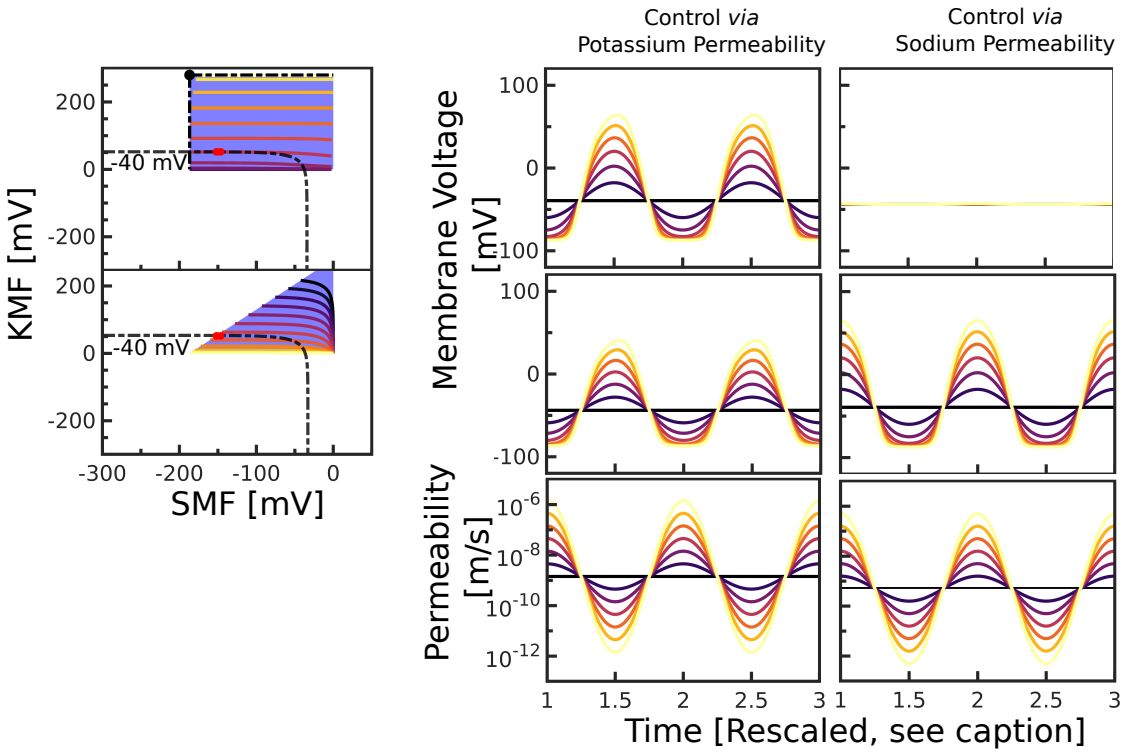


FIGURE 4.21: We set $\phi_{y,i} = -0.5$, $\Delta G_{\mathrm{A}^-} = 0$ (null AMF) and $\Delta G_{\mathrm{ATP}} = -560$ mV, $[\mathrm{K}^+]_e = 5$ mM, $[\mathrm{Na}^+]_e = 145$ mM. (Left) Reachability space of (Top) a model with one ATP driven efflux pump for sodium (3 sodium per ATP) and one ATP driven influx pump for sodium (2 potassium per ATP) and (Bottom) a model with the NaK-ATPase. The dotted line denotes the pairs of KMF, SMF yielding -40 mV membrane potential. For the model (Top) the forward rate of the ATP driven sodium efflux pump is increased along each colored line (as they go away from 0 SMF) and each different line corresponds to a different forward activity of the ATP driven potassium influx pump. For the model (Bottom) different lines correspond to different permeability ratios between sodium and potassium and along each line the forward activity of the NaK-ATPase is increased (as IMFs go away from 0). (Middle and Right Panels) we impose time oscillating permeability for either potassium (middle) or sodium (right) and plot the corresponding time-dependent membrane potential for each of the two models when departing from a model parametrization that yields the red dot coordinate in the left panel.

of an ionic transporter in the IMFs state-space. A simple visualization would be that shown in figure 4.22 where one would draw the line characterizing the kinetics of the transporter in a given context[22] as:

$$\frac{\partial \mathrm{SMF}}{\partial N_p} = f_{\mathrm{SMF}}([\vec{x}]_e, [\vec{x}]_i, \Delta\psi, \vec{k}) \tag{IV.13}$$

$$\frac{\partial \mathrm{KMF}}{\partial N_p} = f_{\mathrm{KMF}}([\vec{x}]_e, [\vec{x}]_i, \Delta\psi, \vec{k}) \tag{IV.14}$$

where N_p is the number of pumps and all the dependent variables of the functions above are uniquely defined for a coordinate in the plane (assuming a system with only sodium, potassium, chloride, null chloride motive force and invariant contribution of captive charges $\phi_{y,i}$). Indeed the plane is defined given an extracellular composition and subsequently intracellular potassium, sodium concentrations as well as membrane potential are all characterized by a pair of KMF, SMF. Experimentally assessing these quiver plots for protocells only possessing the transport that is sought to be characterized seems an ideal way to an inverse characterization of the kinetics of the transporter. Indeed, rather than the usual reasoning: *"This kinetic function can be fitted onto the data"*, the knowledge of the functions f_{SMF} and f_{KMF} might in principle allow procedural generations of all kinetic functions that are compatible with the experimental measurements.

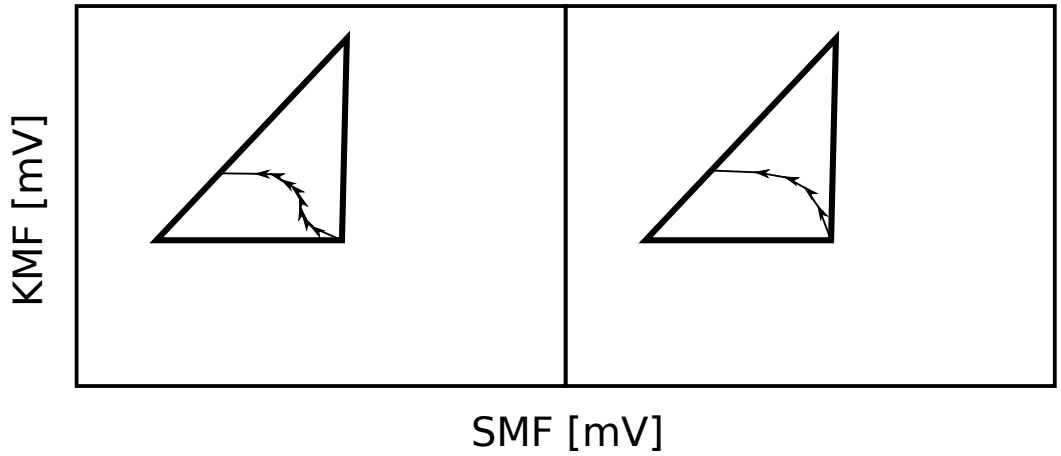


FIGURE 4.22: Stylized representation of two NaK-ATPase (Left and right) with different kinetic functions. While they have identical reachability and attracting properties, the trajectory in the plane resulting from gradually increasing the number of NaK-ATPase is not identical, and is characterized by *1)* the kinetic function of each NaK-ATPase and *2)* how other ionic pumps have their activity depending on the pair SMF, KMF.

[22] i.e. in the presence of other transport systems with defined kinetics

iv. Conclusion

The heuristics presented herein in fact were used as preliminary tools to the models developed in chapter 2 and in fact led to one of the main contribution of this thesis, *i.e.* the supported hypothesis that the ability to modulate voltage (thus pH_i) is *(i)* PMF dependent and *(ii)* dependent on the coupling stoichiometry. Accordingly, chronologically, figure 4.16 preceded the content of chapter 2. I choose the conclude this thesis by what may look like an additional chapter. I deemed however the various conclusions of this section not connected within a single narrative, but rather as a miscellaneous of small stories that are relatively straightforward to unfold based on what I think are a few basic principles, that *(i)* do not require much previous knowledge about electrophysiology and *(ii)* do not rely on any other assumptions than the definitions of membrane voltage and electrochemical potential we used along this manuscript as well as the second principle of thermodynamics. The choice of variables we made for defining the state-space (where axes are defined by Gibbs free energy of simplex reactions, *e.g.* IMFs) is crucial in the exercise we proceeded above and similar analysis is not possible by characterizing the state space as a set of so-called equilibrium potential, defined for an ion x as $E_x := RT/(z_x F)\ln([x]_e/[x]_i)$. This seeds from two reasons:

1. In the state-space where axes are defined as Gibbs free energy, the shape characterizing reachability properties of transporters are invariant (by choice of membrane potential and extracellular composition).

2. In the state-space where axes are defined as Gibbs free energy, the attractors are also invariant (by choice of membrane potential and extracellular composition).

This would not be the case by *e.g.* characterizing the state space by defining axis as equilibrium potentials for different species as examplified in figure 4.3 where we showed that decrease of the activity of an influx pump for potassium could lead to either increase or decrease in intracellular potassium, therefrom the attracting coordinates the equilibrium potential state-space are not invariant by the choice of *e.g.* membrane potential or extracellular concentrations. This, along with the apparent facility with which we can manipulate models of electrophysiological processes within the framework introduced in this discussion, may call for an alternative way of introducing electrophysiology in undergraduate textbooks.

Indeed, equilibrium potential is often used as the main introductory concept for discussing electrophysiological processes. In my opinion, this concept should not be used for any other purpose than introducing that two forces contribute to the electrochemical gradient: the concentration component, effectively the equilibrium potential, and the electric component a.k.a. membrane potential. In fact, learning fundamentals of electrophysiological heavily relies on the use of equilibrium potentials as control variables and it has been identified to be quite challenging for university students to apprehend [334, 335]. Some journals are even partly dedicated to this matter, for instance *Advances in Physiology Education*. Some have proposed analogy with springs' behaviors to approach resting membrane potential [336]. While the latter definitely does not look like a simpler modeling concept for students not familiar with basic physics, our approach rather uses similar concepts that are introduced in biochemistry and as such naturally complement some other courses usually part of a biologist training. What is more is that most teaching approaches to resting membrane potential are utterly specific to some transport configurations, *i.e.* they describe the "master equation" for membrane potential as the GHK voltage equation [337]. As discussed in the introduction, this equation has several underlying assumptions and as such: *(a)* does not hold in general and *(b)* is complex to rigorously apprehend as it requires additional knowledge of the assumptions that have been used and ideally the complete derivation from the definition of membrane voltage we use in this manuscript. Also, seeding from the use of the ionic permeabilites as control variables, I think it may lead to the misconception that membrane potential can be *generated* (rather than modulated) by tuning the permeabilities. Indeed the generic teaching model aims at explaining the action potential, wherein permeability can indeed be tuned to either polarize or depolarize the cell. This property is as we saw in figure 4.21 however highly specific to the characteristic of the NaK-ATpase and does not hold in general (*e.g.* for *E.coli*). For the latter to be clarified requires other concept than the use of equilibrium potentials and permeabilities as control variables for setting membrane potential *via* GHK voltage equation. Indeed, this choice of control variables invisibilizes how active transporters are necessary for membrane voltage maintenance. Accordingly, the concept of active transporters is sometimes only introduced in more advanced classes [337].

While I am surely biased towards thinking the approach to electrophysiology

we developed just before is more intuitive than what is currently proposed[23] it is perhaps worth a try for teaching purposes.

Accordingly, perhaps the reader can use the second part of this discussion for teaching purposes as well as preliminary tools for *(i)* comparing *in silico* what are the specific features of various transporters within a wider electrophysiological context and *(ii)* experimental designs of protocells with desired electrophysiological functions, perhaps a small contribution towards engineering bio-inspired electrochemical circuits.

Finally, I would like to thanks the reader for going through parts/all of this thesis. I am well aware that the subject of this thesis being quite broad and touching to quite thematically distant topics, some of which I may have not the best expertise in, it may contain flaws as well as unreferenced related work I am genuinely no aware of. I am happy to discuss whatever critics or/and corrections one would like to make about the content of this manuscript as well as related topics and research.

[23]Since I spent years reasoning along these lines.

Bibliography

[1] Fernando Baquero and Bruce R. Levin. Proximate and ultimate causes of the bactericidal action of antibiotics. *Nature Reviews Microbiology*, Oct 2020.

[2] A. K. Covington, R. G. Bates, and R. A. Durst. Definition of pH scales, standard reference values, measurement of pH and related terminology (Recommendations 1984). *Pure and Applied Chemistry*, 57(3):531 – 542, 01 Jan. 1985.

[3] Peter R. Wills, David J. Scott, and Donald J. Winzor. *Thermodynamics and Thermodynamic Nonideality*, pages 2583–2589. Springer Berlin Heidelberg, Berlin, Heidelberg, 2013.

[4] T. *et al.* Krulwich. Molecular aspects of bacterial pH sensing and homeostasis. *Nature Reviews*, 2011.

[5] Andrei V. Bandura and Serguei N. Lvov. The ionization constant of water over wide ranges of temperature and density. *Journal of Physical and Chemical Reference Data*, 35(1):15–30, 2006.

[6] Craig Baker-Austin and Mark Dopson. Life in acid: pH homeostasis in acidophiles. *Trends in Microbiology*, 15(4):165 – 171, 2007.

[7] J. *et al.* Slonczewski. Cytoplasmic pH Measurement and Homeostasis in Bacteria and Archaea. *Advances in Microbial Physiology*, 2009.

[8] T J Rink, R Y Tsien, and T Pozzan. Cytoplasmic pH and free Mg2+ in lymphocytes. *Journal of Cell Biology*, 95(1):189–196, 10 1982.

[9] W H Moolenaar, L G Tertoolen, and S W de Laat. The regulation of cytoplasmic pH in human fibroblasts. *Journal of Biological Chemistry*, 259(12):7563–9, 1984.

[10] Marie A. Schroeder, Pawel Swietach, Helen J. Atherton, Ferdia A. Gallagher, Phillip Lee, George K. Radda, Kieran Clarke, and Damian J. Tyler. Measuring intracellular pH in the heart using hyperpolarized carbon dioxide and bicarbonate: a 13C and 31P magnetic resonance spectroscopy study. *Cardiovascular Research*, 86(1):82–91, 12 2009.

[11] Joan L. Slonczewski, Barry P. Rosen, Jeffry R. Alger, and Robert M. Macnab. pH Homeostasis in *Escherichia coli*: Measurement by 31P Nuclear Magnetic Resonance of Methylphosphonate and Phosphate. *Proceedings of the National Academy of Sciences of the United States of America*, 78(10):6271–6275, 1981.

[12] Minoska Valli, Michael Sauer, Paola Branduardi, Nicole Borth, Danilo Porro, and Diethard Mattanovich. Intracellular pH Distribution in *Saccharomyces cerevisiae* Cell Populations, Analyzed by Flow Cytometry. *Applied and Environmental Microbiology*, 71(3):1515–1521, 2005.

[13] Vernon Ruffin, Ahlam Salameh, Walter Boron, and Mark Parker. Intracellular pH regulation by acid-base transporters in mammalian neurons. *Frontiers in Physiology*, 5:43, 2014.

[14] Hisae Tateishi-Karimata and Naoki Sugimoto. Structure, stability and behaviour of nucleic acids in ionic liquids. *Nucleic Acids Research*, 42(14):8831–8844, 07 2014.

[15] Kemper Talley and Emil Alexov. On the pH-optimum of activity and stability of proteins. *Proteins: Structure, Function, and Bioinformatics*, 78(12):2699–2706, 2010.

[16] Lars Konermann. *Protein Unfolding and Denaturants*. American Cancer Society, 2012.

[17] J. Keener and J. Sneyd. *Mathematical Physiology*. 2009.

[18] David W. Maughan and Robert E. Godt. Protein osmotic pressure and the state of water in frog myoplasm. *Biophysical Journal*, 80(1):435–442, 2001.

[19] Sopan K. Kushare, Vasim R. Shaikh, Santosh S. Terdale, Dilip H. Dagade, Rahul R. Kolhapurkar, and Kesharsingh J. Patil. Thermodynamics of aqueous polyethylene-glycol (peg) solutions at 298.15k: Activity, activity

coefficients and application of molecular theories. *Journal of Molecular Liquids*, 187:129–136, 2013.

[20] H. Frank Gibbard, George Scatchard, Raymond A. Rousseau, and Jefferson L. Creek. Liquid-vapor equilibrium of aqueous sodium chloride, from 298 to 373.deg.k and from 1 to 6 mol kg-1, and related properties. *Journal of Chemical & Engineering Data*, 19(3):281–288, Jul 1974.

[21] R. N. Robertson. *The lively membranes / R.N.Robertson.* Cambridge University Press, Cambridge, 1983.

[22] Alan R. Kay. How cells can control their size by pumping ions. *Frontiers in Cell and Developmental Biology*, 5:41, 2017.

[23] Marcelo D. Serpe and Mark A. Matthews. Growth, Pressure, and Wall Stress in Epidermal Cells of *Begonia argenteo-guttata L.* Leaves during Development. *International Journal of Plant Sciences*, 155(3):291–301, 1994.

[24] Yi Deng, Mingzhai Sun, and Joshua W. Shaevitz. Direct measurement of cell wall stress stiffening and turgor pressure in live bacterial cells. *Phys. Rev. Lett.*, 107:158101, Oct 2011.

[25] D. Scott Cayley, Harry J. Guttman, and M. Thomas Record. Biophysical Characterization of Changes in Amounts and Activity of *Escherichia coli* Cell and Compartment Water and Turgor Pressure in Response to Osmotic Stress. *Biophysical Journal*, 78(4):1748 – 1764, 2000.

[26] Arthur L. Koch and Ronald J. Doyle. The growth strategy of the Gram-positive rod. *FEMS Microbiology Reviews*, 1(3-4):247–254, 04 1986.

[27] Jörg Schaber, Miquel Àngel Adrover, Emma Eriksson, Serge Pelet, Elzbieta Petelenz-Kurdziel, Dagmara Klein, Francesc Posas, Mattias Goksör, Mathias Peter, Stefan Hohmann, and Edda Klipp. Biophysical properties of *Saccharomyces cerevisiae* and their relationship with HOG pathway activation. *European Biophysics Journal*, 39(11):1547–1556, Oct 2010.

[28] Janet M. Wood. Bacterial responses to osmotic challenges. *Journal of General Physiology*, 145(5):381–388, 04 2015.

[29] Renata Buda, Yunxiao Liu, Jin Yang, Smitha Hegde, Keiran Stevenson, Fan Bai, and Teuta Pilizota. Dynamics of escherichia coli's passive response to a sudden decrease in external osmolarity. *Proceedings of the National Academy of Sciences*, 113(40):E5838–E5846, 2016.

[30] Shaobao Liu, Ru Tao, Ming Wang, Jin Tian, Guy M. Genin, Tian Jian Lu, and Feng Xu. Regulation of cell behavior by hydrostatic pressure. *Applied Mechanics Reviews*, 71(4), Jul 2019. 040803.

[31] S.L. Rybak, F. Lanni, and R.F. Murphy. Theoretical considerations on the role of membrane potential in the regulation of endosomal pH. *Biophysical Journal*, 73(2):674 – 687, 1997.

[32] Michael Grabe and George Oster. Regulation of organelle acidity. *The Journal of General Physiology*, 117(4):329–344, 2001.

[33] Matthias Kahm, Clara Navarrete, Vicent Llopis-Torregrosa, Rito Herrera, Lina Barreto, Lynne Yenush, Joaquin Ariño, Jose Ramos, and Maik Kschischo. Potassium starvation in yeast: Mechanisms of homeostasis revealed by mathematical modeling. *PLOS Computational Biology*, 8(6):1–11, 06 2012.

[34] L Mancini and T Pilizota. Environmental conditions define the energetics of bacterial dormancy and its antibiotic susceptibility. preprint, Microbiology, June 2020.

[35] Clay M. Armstrong. The Na/K pump, Cl ion, and osmotic stabilization of cells. *Proceedings of the National Academy of Sciences*, 100(10):6257–6262, 2003.

[36] G. Bard Ermentrout and David H. Terman. *The Hodgkin–Huxley Equations*, pages 1–28. Springer New York, New York, NY, 2010.

[37] David E. Goldman. Potential, Impedance, and Rectification in Membranes. *Journal of General Physiology*, 27(1):37–60, 09 1943.

[38] Osvaldo Alvarez and Ramon Latorre. The enduring legacy of the "constant-field equation" in membrane ion transport. *Journal of General Physiology*, 149(10):911–920, 09 2017.

[39] D. Johnston and S.M.S. Wu. *Foundations of Cellular Neurophysiology*. A Bradford Book. MIT Press, 1994.

[40] A. Bradley. *Animal Physiology and Biochemistry*. EDTECH, 2018.

[41] Wei Bai, K.S. Zhao, and K. Asami. Dielectric properties of *E. coli* cell as simulated by the three-shell spheroidal model. *Biophysical Chemistry*, 122(2):136 – 142, 2006.

[42] Keith D. Garlid, Andrew D. Beavis, and Signe K. Ratkje. On the nature of ion leaks in energy-transducing membranes. *Biochimica et Biophysica Acta (BBA) - Bioenergetics*, 976(2):109 – 120, 1989.

[43] Dominique Debanne, Emilie Campanac, Andrzej Bialowas, Edmond Carlier, and Gisèle Alcaraz. Axon physiology. *Physiological Reviews*, 91(2):555–602, 2011. PMID: 21527732.

[44] A. L. Hodgkin and A. F. Huxley. A quantitative description of membrane current and its application to conduction and excitation in nerve. *The Journal of physiology*, 117(4):500–544, Aug 1952. 12991237[pmid].

[45] Lina Abdul Kadir, Michael Stacey, and Richard Barrett-Jolley. Emerging roles of the membrane potential: Action beyond the action potential. *Frontiers in Physiology*, 9:1661, 2018.

[46] Stephen M. Schuetze. The discovery of the action potential. *Trends in Neurosciences*, 6:164 – 168, 1983.

[47] Alexei Verkhratsky and Vladimir Parpura. *History of Electrophysiology and the Patch Clamp*, pages 1–19. Springer New York, New York, NY, 2014.

[48] Peter Mitchell. Coupling of Phosphorylation to Electron and Hydrogen Transfer by a Chemiosmotic type of Mechanism. *Nature*, 191:144, 1961.

[49] B. Griniuvienė, V. Chmieliauskaitė, and L. Grinius. Energy-linked transport of permeant ions in *Escherichia coli* cells: Evidence for membrane potential generation by proton-pump. *Biochemical and Biophysical Research Communications*, 56(1):206 – 213, 1974.

[50] Arthur Prindle, Jintao Liu, Munehiro Asally, San Ly, Jordi Garcia-Ojalvo, and Gürol M. Süel. Ion channels enable electrical communication in bacterial communities. *Nature*, 527(7576):59–63, Nov 2015.

[51] E. C. SLATER. Mechanism of phosphorylation in the respiratory chain. *Nature*, 172(4387):975–978, Nov 1953.

[52] Michel Morange. What history tells us xi. the complex history of the chemiosmotic theory. *Journal of Biosciences*, 32(3):1245–1250, Dec 2007.

[53] John N. Prebble. Contrasting approaches to a biological problem: Paul boyer, peter mitchell and the mechanism of the atp synthase, 1961–1985. *Journal of the History of Biology*, 46(4):699–737, Nov 2013.

[54] Jonatan M. Benarroch and Munehiro Asally. The microbiologist's guide to membrane potential dynamics. *Trends in Microbiology*, 28(4):304 – 314, 2020.

[55] Anne Rupprecht, Elena A. Sokolenko, Valeri Beck, Olaf Ninnemann, Martin Jaburek, Thorsten Trimbuch, Sergey S. Klishin, Petr Jezek, Vladimir P. Skulachev, and Elena E. Pohl. Role of the transmembrane potential in the membrane proton leak. *Biophysical Journal*, 98(8):1503 – 1511, 2010.

[56] Daniel A. Beard and Hong Qian. *Concepts from physical chemistry*, page 7–23. Cambridge Texts in Biomedical Engineering. Cambridge University Press, 2008.

[57] Kashket, E. R. The Proton Motive Force in Bacteria: A Critical Assessment of Methods. *Annual Review of Microbiology*, 39(1):219–242, 1985.

[58] Armen Y. Mulkidjanian, Pavel Dibrov, and Michael Y. Galperin. The past and present of sodium energetics: May the sodium-motive force be with you. *Biochimica et Biophysica Acta (BBA) - Bioenergetics*, 1777(7):985 – 992, 2008. 15th European Bioenergetics Conference 2008.

[59] Kunihiro Kasamo. Effect of Abscisic Acid on the K+ Efflux and Membrane Potential of *Nicotiana tabacum L.* Leaf Cells. *Plant and Cell Physiology*, 22(7):1257–1267, 11 1981.

[60] Peter van Bodegom. Microbial maintenance: A critical review on its quantification. *Microbial Ecology*, 53(4):513–523, 2007.

[61] Peter C. Maloney, E. R. Kashket, and T. Hastings Wilson. A protonmotive force drives atp synthesis in bacteria. *Proceedings of the National Academy of Sciences*, 71(10):3896–3900, 1974.

[62] Terry A. Krulwich, David B. Hicks, and Masahiro Ito. Cation/proton antiporter complements of bacteria: why so large and diverse? *Molecular Microbiology*, 74(2):257–260, 2009.

[63] John M. Russell. Sodium-potassium-chloride cotransport. *Physiological Reviews*, 80(1):211–276, 2000. PMID: 10617769.

[64] John F. Allen. Photosynthesis of ATP; Electrons, Proton Pumps, Rotors, and Poise. *Cell*, 110(3):273–276, Aug 2002.

[65] Ivan Gushchin, Pavel Chervakov, Pavel Kuzmichev, Alexander N. Popov, Ekaterina Round, Valentin Borshchevskiy, Andrii Ishchenko, Lada Petrovskaya, Vladimir Chupin, Dmitry A. Dolgikh, Alexander S. Arseniev, Mikhail Kirpichnikov, and Valentin Gordeliy. Structural insights into the proton pumping by unusual proteorhodopsin from nonmarine bacteria. *Proceedings of the National Academy of Sciences*, 110(31):12631–12636, 2013.

[66] Michael V. Clausen, Florian Hilbers, and Hanne Poulsen. The Structure and Function of the NaK-ATPase Isoforms in Health and Disease. *Frontiers in Physiology*, 8:371, 2017.

[67] Stefan Steigmiller, Paola Turina, and Peter Gräber. The thermodynamic H+/ATP ratios of the H+-ATPsynthases from chloroplasts and *Escherichia coli*. *Proceedings of the National Academy of Sciences*, 105(10):3745–3750, 2008.

[68] P.R. Rich. The molecular machinery of Keilin's respiratory chain. *Biochemical Society Transactions*, 31(6):1095–1105, 12 2003.

[69] W Epstein, V Whitelaw, and J Hesse. A K+ transport ATPase in *Escherichia coli*. *Journal of Biological Chemistry*, 253(19):6666–8, 1978.

[70] P. G. Vallés, V. Bocanegra, A. Gil Lorenzo, and V. V. Costantino. Physiological Functions and Regulation of the Na+/H+ Exchanger [NHE1] in Renal Tubule Epithelial Cells. *Kidney and Blood Pressure Research*, 40(5):452–466, 2015.

[71] Martha V. Radchenko, Kimihiro Tanaka, Rungaroon Waditee, Sawako Oshimi, Yasutomo Matsuzaki, Masahiro Fukuhara, Hiroshi Kobayashi, Teruhiro Takabe, and Tatsunosuke Nakamura. Potassium/Proton Antiport System

of *Escherichia coli*. *Journal of Biological Chemistry*, 281(29):19822–19829, 2006.

[72] E. Pinner, E. Padan, and S. Schuldiner. Kinetic properties of NhaB, a Na+/H+ antiporter from *Escherichia coli*. *Journal of Biological Chemistry*, 269(42):26274–26279, 1994.

[73] D Taglicht, E Padan, and S Schuldiner. Proton-sodium stoichiometry of NhaA, an electrogenic antiporter from *Escherichia coli*. *Journal of Biological Chemistry*, 268(8):5382–7, 1993.

[74] Alessio Accardi and Christopher Miller. Secondary active transport mediated by a prokaryotic homologue of ClC Cl- channels. *Nature*, 427(6977):803–807, Feb 2004.

[75] David L. Foster, Maria Luisa Garcia, Michael J. Newman, Lekha Patel, and H. Ronald Kaback. Lactose-proton symport by purified lac carrier protein. *Biochemistry*, 21(22):5634–5638, Oct 1982.

[76] Cristina V. Iancu, Jamillah Zamoon, Sang Bum Woo, Alexander Aleshin, and Jun-yong Choe. Crystal structure of a glucose/H+ symporter and its mechanism of action. *Proceedings of the National Academy of Sciences*, 110(44):17862–17867, 2013.

[77] Ichiro Yamato and Yasuhiro Anraku. Mechanism of Na+/proline symport in *Escherichia coli*: Reappraisal of the effect of cation binding to the Na+/proline symport carrier. *The Journal of Membrane Biology*, 114(2):143–151, Mar 1990.

[78] Lorena Rojas-Vega and Gerardo Gamba. Mini-review: regulation of the renal nacl cotransporter by hormones. *American Journal of Physiology-Renal Physiology*, 310(1):F10–F14, 2016.

[79] A. P. Garneau, A. A. Marcoux, S. Slimani, L. E. Tremblay, R. Frenette-Cotton, F. Mac-Way, and P. Isenring. Physiological roles and molecular mechanisms of K+-Cl- cotransport in the mammalian kidney and cardiovascular system: where are we? *The Journal of Physiology*, 597(6):1451–1465, 2019.

[80] Thomas Friedrich, Sven Geibel, Rolf Kalmbach, Igor Chizhov, Kenichi Ataka, Joachim Heberle, Martin Engelhard, and Ernst Bamberg. Proteorhodopsin is a light-driven proton pump with variable vectoriality. *Journal of Molecular Biology*, 321(5):821 – 838, 2002.

[81] Gal Masrati, Manish Dwivedi, Abraham Rimon, Yael Gluck-Margolin, Amit Kessel, Haim Ashkenazy, Itay Mayrose, Etana Padan, and Nir Ben-Tal. Broad phylogenetic analysis of cation/proton antiporters reveals transport determinants. *Nature Communications*, 9(1):4205, Oct 2018.

[82] Jr Saier, Milton H., Vamsee S. Reddy, Dorjee G. Tamang, and Åke Västermark. The Transporter Classification Database. *Nucleic Acids Research*, 42(D1):D251–D258, 11 2013.

[83] Nick Lane, John F. Allen, and William Martin. How did LUCA make a living? Chemiosmosis in the origin of life. *BioEssays*, 32(4):271–280, 2010.

[84] Shraddha Prakash, Garret Cooper, Soumya Singhi, and Milton H Saier. The ion transporter superfamily. *Biochimica et Biophysica Acta (BBA) - Biomembranes*, 1618(1):79–92, 2003.

[85] Christopher L. Brett, Mark Donowitz, and Rajini Rao. Evolutionary origins of eukaryotic sodium/proton exchangers. *American Journal of Physiology-Cell Physiology*, 288(2):C223–C239, 2005. PMID: 15643048.

[86] Laszlo N. Csonka and Andrew D. Hanson. Prokaryotic osmoregulation: Genetics and physiology. *Annual Review of Microbiology*, 45(1):569–606, 1991. PMID: 1741624.

[87] Janet M. Wood. Bacterial osmoregulation: A paradigm for the study of cellular homeostasis. *Annual Review of Microbiology*, 65(1):215–238, 2011. PMID: 21663439.

[88] Erhard Bremer and Reinhard Krämer. Responses of microorganisms to osmotic stress. *Annual Review of Microbiology*, 73(1):313–334, 2019. PMID: 31180805.

[89] Etana Padan, Eitan Bibi, Masahiro Ito, and Terry A. Krulwich. Alkaline pH homeostasis in bacteria: New insights. *Biochimica et Biophysica Acta (BBA) - Biomembranes*, 1717(2):67 – 88, 2005.

[90] U. *et al.* Kanjee. Mechanisms of acid resistance in *Escherichia coli*. *Annual Review of Microbiology*, 2013.

[91] J. Preben Morth, Bjørn P. Pedersen, Morten J. Buch-Pedersen, Jens Peter Andersen, Bente Vilsen, Michael G. Palmgren, and Poul Nissen. A structural overview of the plasma membrane Na+,K+-ATPase and H+-ATPase ion pumps. *Nature Reviews Molecular Cell Biology*, 12(1):60–70, Jan 2011.

[92] Andrea Y. Weiße, Diego A. Oyarzún, Vincent Danos, and Peter S. Swain. Mechanistic links between cellular trade-offs, gene expression, and growth. *Proceedings of the National Academy of Sciences*, 112(9):E1038–E1047, 2015.

[93] Boris Martinac, Yoshiro Saimi, and Ching Kung. Ion channels in microbes. *Physiol Rev*, 88(4):1449–1490, Oct 2008.

[94] Yandong Huang, Wei Chen, David L. Dotson, Oliver Beckstein, and Jana Shen. Mechanism of pH-dependent activation of the sodium-proton antiporter NhaA. *Nature Communications*, 7(1):12940, Oct 2016.

[95] Octavian Călinescu, Cristina Paulino, Werner Kühlbrandt, and Klaus Fendler. Keeping It Simple, Transport Mechanism and pH Regulation in Na+/H+ Exchangers. *Journal of Biological Chemistry*, 289(19):13168–13176, 2014.

[96] Thomas Mager, Abraham Rimon, Etana Padan, and Klaus Fendler. Transport Mechanism and pH Regulation of the Na+/H+ Antiporter NhaA from *Escherichia coli*: An Electrophysiological Study. *Journal of Biological Chemistry*, 286(26):23570–23581, 2011.

[97] H. Nikaido. Molecular basis of bacterial outer membrane permeability revisited. *Microbiology and Molecular Biology Reviews*, 2003.

[98] Qusheng Jin and Bethke M. Craig. The thermodynamics and kinetics of microbial metabolism. *American Journal of Science*, 307(4):643–677, 2007.

[99] Matthew Scott, Carl W. Gunderson, Eduard M. Mateescu, Zhongge Zhang, and Terence Hwa. Interdependence of cell growth and gene expression: Origins and consequences. *Science*, 330(6007):1099–1102, 2010.

[100] Markus Basan, Sheng Hui, Hiroyuki Okano, Zhongge Zhang, Yang Shen, James R. Williamson, and Terence Hwa. Overflow metabolism in *Escherichia*

coli results from efficient proteome allocation. *Nature*, 528(7580):99–104, Dec 2015. Article.

[101] J. Del Castillo and B. Katz. Quantal components of the end-plate potential. *J Physiol*, 124(3):560–573, 1954.

[102] Sofia Ramos and H. Ronald Kaback. The electrochemical proton gradient in escherichia coli membrane vesicles. *Biochemistry*, 16(5):848–854, 1977. PMID: 14664.

[103] C Bradbeer. The proton motive force drives the outer membrane transport of cobalamin in escherichia coli. *Journal of Bacteriology*, 175(10):3146–3150, 1993.

[104] Knut Jahreis, Elisângela F. Pimentel-Schmitt, Reinhold Brückner, and Fritz Titgemeyer. Ins and outs of glucose transport systems in eubacteria. *FEMS Microbiology Reviews*, 32(6):891–907, 2008.

[105] Janet M. Wood. Bacterial responses to osmotic challenges. *The Journal of General Physiology*, 145(5):381–388, 2015.

[106] Yoshiyuki Sowa and Richard Berry. Bacterial flagellar motor. *Q. Rev. Biophys.*, 41(2):103–132, 2008.

[107] Henrik Strahl and Leendert W. Hamoen. Membrane potential is important for bacterial cell division. *Proceedings of the National Academy of Sciences*, 107(27):12281–12286, 2010.

[108] J. Bernstein. Ueber den zeitlichen verlauf der negativen schwankung des nervenstroms. *Archiv für die gesamte Physiologie des Menschen und der Tiere*, 1(1):173–207, 1868.

[109] A L Hodgkin and A F Huxley. Action Potentials Recorded from Inside a Nerve Fibre. *Nature*, 144:710, 1939.

[110] Erwin Neher and Bert Sakmann. Single-channel currents recorded from membrane of denervated frog muscle fibres. *Nature*, 260:799, 1976.

[111] B Sakmann and E Neher. Patch clamp techniques for studying ionic channels in excitable membranes. *Annual Review of Physiology*, 46(1):455–472, 1984.

[112] G. Ling and R. W. Gerard. The normal membrane potential of frog sartorius fibers. *Journal of Cellular and Comparative Physiology*, 34(3):383–396, 1949.

[113] B Martinac, M Buechner, A H Delcour, J Adler, and C Kung. Pressure-sensitive ion channel in escherichia coli. *Proceedings of the National Academy of Sciences*, 84(8):2297–2301, 1987.

[114] Boris Martinac, Paul R. Rohde, Charles G. Cranfield, and Takeshi Nomura. *Patch Clamp Electrophysiology for the Study of Bacterial Ion Channels in Giant Spheroplasts of E. coli*, pages 367–380. Humana Press, Totowa, NJ, 2013.

[115] H. Felle, J. S. Porter, C. L. Slayman, and H. R. Kaback. Quantitative measurements of membrane potential in escherichia coli. *Biochemistry*, 19(15):3585–3590, 1980.

[116] Hidekazu Tsutsui, Satoshi Karasawa, Yasushi Okamura, and Atsushi Miyawaki. Improving membrane voltage measurements using FRET with new fluorescent proteins. *Nature Methods*, 5(8):683–685, 2008.

[117] Eric Fluhler, Valerie G. Burnham, and Leslie M. Loew. Spectra, membrane binding, and potentiometric responses of new charge shift probes. *Biochemistry*, 24(21):5749–5755, 1985.

[118] Joel M. Kralj, Daniel R. Hochbaum, Adam D. Douglass, and Adam E. Cohen. Electrical spiking in escherichia coli probed with a fluorescent voltage-indicating protein. *Science*, 333(6040):345–348, 2011.

[119] Peter J. Sims, Alan S. Waggoner, Chao-Huei Wang, and Joseph F. Hoffman. Mechanism by which cyanine dyes measure membrane potential in red blood cells and phosphatidylcholine vesicles. *Biochemistry*, 13(16):3315–3330, 1974.

[120] Chien-Jung Lo, Mark C. Leake, Teuta Pilizota, and Richard M. Berry. Nonequivalence of membrane voltage and ion-gradient as driving forces for the bacterial flagellar motor at low load. *Biophysical Journal*, 93(1):294 – 302, 2007.

[121] B. Ehrenberg, V. Montana, M. D. Wei, J. P. Wuskell, and L. M. Loew. Membrane potential can be determined in individual cells from the nernstian distribution of cationic dyes. *Biophysical journal*, 53(5):785–794, 1988.

[122] J. Derk te Winkel, Declan A. Gray, Kenneth H. Seistrup, Leendert W. Hamoen, and Henrik Strahl. Analysis of antimicrobial-triggered membrane depolarization using voltage sensitive dyes. *Frontiers in Cell and Developmental Biology*, 4:29, 2016.

[123] Ekaterina Krasnopeeva, Chien-Jung Lo, and Teuta Pilizota. Single-cell bacterial electrophysiology reveals mechanisms of stress-induced damage. *Biophysical Journal*, 116(12):2390 – 2399, 2019.

[124] Tomoya Baba, Takeshi Ara, Miki Hasegawa, Yuki Takai, Yoshiko Okumura, Miki Baba, Kirill A Datsenko, Masaru Tomita, Barry L Wanner, and Hirotada Mori. Construction of escherichia coli k-12 in-frame, single-gene knockout mutants: the keio collection. *Molecular Systems Biology*, 2(1), 2006.

[125] Kirill A. Datsenko and Barry L. Wanner. One-step inactivation of chromosomal genes in escherichia coli k-12 using pcr products. *Proceedings of the National Academy of Sciences*, 97(12):6640–6645, 2000.

[126] Teuta Pilizota and Joshua W. Shaevitz. Fast, multiphase volume adaptation to hyperosmotic shock by escherichia coli. *PLOS ONE*, 7(4):1–10, 2012.

[127] Jerko Rosko, Vincent A. Martinez, Wilson C. K. Poon, and Teuta Pilizota. Osmotaxis in escherichia coli through changes in motor speed. *Proceedings of the National Academy of Sciences*, 2017.

[128] Jerko Rosko. *Osmotaxis in Escherichia coli*. PhD thesis, University of Edinburgh, 2017.

[129] Ekaterina Krasnopeeva. *Single cell measurements of bacterial physiology traits during exposure to an external stress*. PhD thesis, School of Biological Sciences, 2009.

[130] Anna I. Sulatskaya, Andrey V. Lavysh, Alexander A. Maskevich, Irina M. Kuznetsova, and Konstantin K. Turoverov. Thioflavin T fluoresces as excimer in highly concentrated aqueous solutions and as monomer being incorporated in amyloid fibrils. *Scientific Reports*, 7(1):1–11, 2017.

[131] Alexander A. Maskevich, Vitali I. Stsiapura, Valeriy A. Kuzmitsky, Irina M. Kuznetsova, Olga I. Povarova, Vladimir N. Uversky, and Konstantin K.

Turoverov. Spectral properties of thioflavin t in solvents with different dielectric properties and in a fibril-incorporated form. *Journal of Proteome Research*, 6(4):1392–1401, 2007.

[132] A. A. Maskevich, A. V. Lavysh, I. M. Kuznetsova, A. I. Sulatskaya, and K. K. Turoverov. Spectral manifestations of thioflavin t aggregation. *Journal of Applied Spectroscopy*, 82(1):33–39, 2015.

[133] Natasha Vermeulen, Werden Keeler, Nandakumar Kanavillil, and Kam Leung. The bactericidal effect of ultraviolet and visible light onescherichia coli. 99:550–6, 2008.

[134] Renata Buda, Yunxiao Liu, Jin Yang, Smitha Hegde, Keiran Stevenson, Fan Bai, and Teuta Pilizota. Dynamics of escherichia coli's passive response to a sudden decrease in external osmolarity. *Proceedings of the National Academy of Sciences*, 113(40):E5838–E5846, 2016.

[135] Yao-Kuan Wang, Ekaterina Krasnopeeva, Ssu-Yuan Lin, Fan Bai, Teuta Pilizota, and Chien-Jung Lo. Comparison of escherichia coli surface attachment methods for single-cell, in vivo microscopy. *bioRxiv*, 2019.

[136] N. Otsu. A threshold selection method from gray-level histograms. *IEEE Transactions on Systems, Man, and Cybernetics*, 9(1):62–66, 1979.

[137] Peter S Swain, Keiran Stevenson, Allen Leary, Luis F Montano-Gutierrez, Ivan B N Clark, Jackie Vogel, and Teuta Pilizota. Inferring time derivatives including cell growth rates using Gaussian processes. *Nature Communications*, 7:13766, 2016.

[138] P. Nelson. *Biological Physics (Updated Edition)*. 2003.

[139] Keith D Garlid and Petr Paucek. Mitochondrial potassium transport: the k+ cycle. *Biochimica et Biophysica Acta (BBA) - Bioenergetics*, 1606(1):23 – 41, 2003.

[140] Wataru Shinoda. Permeability across lipid membranes. *Biochimica et Biophysica Acta (BBA) - Biomembranes*, 1858(10):2254 – 2265, 2016.

[141] Carolina Alvarez-Ortega, Jorge Olivares, and José L. Martínez. Rnd multidrug efflux pumps: what are they good for? *Front Microbiol*, 4:7–7, 2013.

[142] Jacek Lubelski, Wil N. Konings, and Arnold J. M. Driessen. Distribution and physiology of abc-type transporters contributing to multidrug resistance in bacteria. *Microbiol Mol Biol Rev*, 71(3):463–476, 2007.

[143] Hiroshi Nikaido and Yumiko Takatsuka. Mechanisms of rnd multidrug efflux pumps. *Biochim Biophys Acta*, 1794(5):769–781, 2009.

[144] Teruo Kuroda and Tomofusa Tsuchiya. Multidrug efflux transporters in the mate family. *Biochimica et Biophysica Acta (BBA) - Proteins and Proteomics*, 1794(5):763 – 768, 2009.

[145] Denice C. Bay, Kenton L. Rommens, and Raymond J. Turner. Small multidrug resistance proteins: A multidrug transporter family that continues to grow. *Biochimica et Biophysica Acta (BBA) - Biomembranes*, 1778(9):1814 – 1838, 2008.

[146] João Anes, Matthew P. McCusker, Séamus Fanning, and Marta Martins. The ins and outs of rnd efflux pumps in escherichia coli. *Front Microbiol*, 6:587–587, 2015.

[147] Girija Dhamdhere and Helen I. Zgurskaya. Metabolic shutdown in escherichia coli cells lacking the outer membrane channel tolc. *Molecular microbiology*, 77(3):743–754, 2010.

[148] Michael D. Manson, P.M. Tedesco, and Howard C. Berg. Energetics of flagellar rotation in bacteria. *Journal of Molecular Biology*, 138(3):541 – 561, 1980.

[149] Shusuke Matsuura, Jun ichi Shioi, and Yasuo Imae. Motility in bacillus subtilis driven by an artificial protonmotive force. *FEBS Letters*, 82(2):187 – 190, 1977.

[150] M. Meister and H. C. Berg. The stall torque of the bacterial flagellar motor. *Biophys J*, 52(3):413–419, 1987.

[151] David C. Fung and Howard C. Berg. Powering the flagellar motor of escherichia coli with an external voltage source, 1995.

[152] Christopher V. Gabel and Howard C. Berg. The speed of the flagellar rotary motor of *Escherichia coli* varies linearly with protonmotive force. *Proceedings of the National Academy of Sciences*, 100(15):8748–8751, 2003.

[153] Karel Svoboda, Christoph F. Schmidt, Bruce J. Schnapp, and Steven M. Block. Direct observation of kinesin stepping by optical trapping interferometry. *Nature*, 365:721 EP, 1993.

[154] William S. Ryu, Richard M. Berry, and Howard C. Berg. Torque-generating units of the flagellar motor of escherichia coli have a high duty ratio. *Nature*, 403:444, 2000.

[155] Fan Bai, Richard W. Branch, Dan V. Nicolau, Teuta Pilizota, Bradley C. Steel, Philip K. Maini, and Richard M. Berry. Conformational spread as a mechanism for cooperativity in the bacterial flagellar switch. *Science*, 327(5966):685–689, 2010.

[156] R. Lopez-Amoros, J. Comas, and J. Vives-Rego. Flow cytometric assessment of *Escherichia coli* and *Salmonella typhimurium* starvation-survival in seawater using rhodamine 123, propidium iodide, and oxonol. *Applied and Environmental Microbiology*, 61(7):2521–2526, 1995.

[157] Christina E. M. Krämer, Wolfgang Wiechert, and Dietrich Kohlheyer. Time-resolved, single-cell analysis of induced and programmed cell death via non-invasive propidium iodide and counterstain perfusion. *Scientific Reports*, 6:32104, 2016.

[158] Nathan Lord. *Fluctuation timescales in bacterial gene expression*. PhD thesis, Harvard University, 2014.

[159] M. Vaara. Agents that increase the permeability of the outer membrane. *Microbiological reviews*, 56(3):395–411, 1992.

[160] Virapong Prachayasittikul, Chartchalerm Isarankura-Na-Ayudhya, Tanawut Tantimongcolwat, Chanin Nantasenamat, and Hans-Joachim Galla. EDTA-induced Membrane Fluidization and Destabilization: Biophysical Studies on Artificial Lipid Membranes. *Acta Biochimica et Biophysica Sinica*, 39(11):901–913, 2007.

[161] YK Wang, E Krasnopeeva, SY Lin, F Bai, T Pilizota, and CJ Lo. Comparison of escherichia coli surface attachment methods for single-cell, in vivo microscopy. *In preparation*, 2019.

[162] Basan, Markus and Zhu, Manlu and Dai, Xiongfeng and Warren, Mya and Sévin, Daniel and Wang, Yi-Ping and Hwa, Terence. Inflating bacterial cells by increased protein synthesis. *Molecular Systems Biology*, 11(10), 2015.

[163] P F Costa, M G Emilio, P L Fernandes, H G Ferreira, and K G Ferreira. Determination of ionic permeability coefficients of the plasma membrane of *Xenopus laevis* oocytes under voltage clamp. *The Journal of Physiology*, 413(1):199–211, 1989.

[164] Keith A. Martinez, Ryan D. Kitko, J. Patrick Mershon, Haley E. Adcox, Kotiba A. Malek, Melanie B. Berkmen, and Joan L. Slonczewski. Cytoplasmic pH Response to Acid Stress in Individual Cells of *Escherichia coli* and *Bacillus subtilis* Observed by Fluorescence Ratio Imaging Microscopy. *Applied and Environmental Microbiology*, 78(10):3706–3714, 2012.

[165] James E. Hall, C. A. Mead, and Gabor Szabo. A barrier model for current flow in lipid bilayer membranes. *The Journal of Membrane Biology*, 11(1):75–97, Dec 1973.

[166] W.E. Morf. *The Principles of Ion-selective Electrodes and of Membrane Transport*. Studies in analytical chemistry. New York, 1981.

[167] H.J. Butt, M.K.H.J.B. Karlheinz Graf, H.J.B. Butt, K. Graf, and M. Kappl. *Physics and Chemistry of Interfaces*. Physics textbook. Wiley, 2003.

[168] Isaiah T. Arkin, Huafeng Xu, Morten Ø. Jensen, Eyal Arbely, Estelle R. Bennett, Kevin J. Bowers, Edmond Chow, Ron O. Dror, Michael P. Eastwood, Ravenna Flitman-Tene, Brent A. Gregersen, John L. Klepeis, István Kolossváry, Yibing Shan, and David E. Shaw. Mechanism of na+/h+ antiporting. *Science*, 317(5839):799–803, 2007.

[169] Malvina Papanastasiou, Georgia Orfanoudaki, Marina Koukaki, Nikos Kountourakis, Marios Frantzeskos Sardis, Michalis Aivaliotis, Spyridoula Karamanou, and Anastassios Economou. The escherichia coli peripheral inner membrane proteome. *Molecular & Cellular Proteomics*, 12(3):599–610, 2013.

[170] J B Stock, B Rauch, and S Roseman. Periplasmic space in salmonella typhimurium and escherichia coli. *Journal of Biological Chemistry*, 252(21):7850–61, 1977.

[171] An-Suei Yang and Barry Honig. On the ph dependence of protein stability. *Journal of Molecular Biology*, 231(2):459 – 474, 1993.

[172] Wataru Aoi and Yoshinori Marunaka. Importance of ph homeostasis in metabolic health and diseases: crucial role of membrane proton transport. *BioMed research international*, 2014:598986–598986, 2014. 25302301[pmid].

[173] Joan L. Slonczewski, Robert M. Macnab, Jeffry R. Alger, and Anna M. Castle. Effects of ph and repellent tactic stimuli on protein methylation levels in escherichia coli. *Journal of Bacteriology*, 152(1):384–399, 1982.

[174] Jessica C. Wilks and Joan L. Slonczewski. pH of the Cytoplasm and Periplasm of *Escherichia coli*: Rapid Measurement by Green Fluorescent Protein Fluorimetry. *Journal of Bacteriology*, 189(15):5601–5607, 2007.

[175] Keith A. Martinez, Ryan D. Kitko, J. Patrick Mershon, Haley E. Adcox, Kotiba A. Malek, Melanie B. Berkmen, and Joan L. Slonczewski. Cytoplasmic ph response to acid stress in individual cells of escherichia coli and bacillus subtilis observed by fluorescence ratio imaging microscopy. *Applied and Environmental Microbiology*, 78(10):3706–3714, 2012.

[176] Smarajit Chakraborty, Ricksen S. Winardhi, Leslie K. Morgan, Jie Yan, and Linda J. Kenney. Non-canonical activation of ompr drives acid and osmotic stress responses in single bacterial cells. *Nature Communications*, 8(1):1587, 2017.

[177] Smarajit Chakraborty and Linda J. Kenney. A new role of ompr in acid and osmotic stress in salmonella and e. coli. *Frontiers in Microbiology*, 9:2656, 2018.

[178] Andrew Tze Fui Liew, Yong Hwee Foo, Yunfeng Gao, Parisa Zangoui, Moirangthem Kiran Singh, Ranjit Gulvady, and Linda J Kenney. Single cell, super-resolution imaging reveals an acid pH-dependent conformational switch in SsrB regulates SPI-2. *eLife*, 8:e45311, April 2019.

[179] Ekaterina Krasnopeeva, Chien-Jung Lo, and Teuta Pilizota. Single-cell bacterial electrophysiology reveals mechanisms of stress-induced damage. *Biophysical Journal*, 116(12):2390 – 2399, 2019.

[180] Yao Kuan Wang, Ekaterina Krasnopeeva, Ssu-Yuan Lin, Fan Bai, Teuta Pilizota, and Chien-Jung Lo. Comparison of Escherichia coli surface attachment methods for single-cell microscopy. *Scientific Reports*, 9(December):2019, dec 2019.

[181] Chien-Jung Lo, Mark C. Leake, Teuta Pilizota, and Richard M. Berry. Nonequivalence of membrane voltage and ion-gradient as driving forces for the bacterial flagellar motor at low load. *Biophysical Journal*, 93(1):294–302, Jul 2007.

[182] Bryson D. Bennett, Elizabeth H. Kimball, Melissa Gao, Robin Osterhout, Stephen J. Van Dien, and Joshua D. Rabinowitz. Absolute metabolite concentrations and implied enzyme active site occupancy in *Escherichia coli*. *Nat. Chem. Biol.*, 5(8):593–599, 2009.

[183] D. Scott Cayley, Harry J. Guttman, and M. Thomas Record. Biophysical Characterization of Changes in Amounts and Activity of Escherichia coli Cell and Compartment Water and Turgor Pressure in Response to Osmotic Stress. *Biophysical Journal*, 78(4):1748–1764, April 2000.

[184] Avi Flamholz, Elad Noor, Arren Bar-Even, and Ron Milo. eQuilibrator—the biochemical thermodynamics calculator. *Nucleic Acids Research*, 40(D1):D770–D775, 11 2011.

[185] Gerardo Gamba. Molecular physiology and pathophysiology of electroneutral cation-chloride cotransporters. *Physiological Reviews*, 85(2):423–493, 2005. PMID: 15788703.

[186] Christopher Miller and Wang Nguitragool. A provisional transport mechanism for a chloride channel-type Cl-/H+ exchanger. *Philosophical Transactions of the Royal Society B: Biological Sciences*, 364(1514):175–180, 2009.

[187] Leonardo Mancini, Guillaume Terradot, Tian Tian, Ying Ying Pu, Yingxing Li, Chien Jung Lo, Fan Bai, and Teuta Pilizota. A General Workflow for Characterization of Nernstian Dyes and Their Effects on Bacterial Physiology. *Biophysical Journal*, 2019.

[188] G Kuwajima. Construction of a minimum-size functional flagellin of Escherichia coli. *J. Bacteriol.*, 170(7):3305–3309, jul 1988.

[189] Jerko Rosko, Vincent Martinez, Wilson Poon, and Teuta Pilizota. Osmotaxis in Escherichia coli through changes in motor speed. *Proc. Natl. Acad. Sci. U. S. A.*, 114(38):E7969–E7976, 2017.

[190] Ekaterina Krasnopeeva, Uriel E. Barboza-Perez, Jerko Rosko, Teuta Pilizota, and Chien-Jung Lo. Bacterial flagellar motor as a multimodal biosensor. *Methods*, 2020.

[191] Winfried Denk and Watt W. Webb. Optical measurement of picometer displacements of transparent microscopic objects. *Appl. Opt.*, 29(16):2382–2391, jun 1990.

[192] Jana Schwarz-Linek, Jochen Arlt, Alys Jepson, Angela Dawson, Teun Vissers, Dario Miroli, Teuta Pilizota, Vincent A. Martinez, and Wilson C.K. Poon. *Escherichia coli* as a model active colloid: A practical introduction. *Colloids and Surfaces B: Biointerfaces*, 137:2–16, jan 2016.

[193] Tomoya Honda, Jonas Cremer, Leonardo Mancini, Zhongge Zhang, Teuta Pilizota, and Terence Hwa.

[194] Jonas Cremer, Tomoya Honda, Ying Tang, Jerome Wong-Ng, Massimo Vergassola, and Terence Hwa. Chemotaxis as a navigation strategy to boost range expansion. *Nature*, 575(7784):658–663, nov 2019.

[195] Ben Z. Cavari and Y. Avi-Dor. Effect of carbonyl cyanide m-chlorophenylhydrazone on respiration and respiration-dependent phosphorylation in *Escherichia coli*. *The Biochemical Journal*, 103(2):601–608, 1967.

[196] Jack H. Kaplan. Biochemistry of na,k-atpase. *Annual Review of Biochemistry*, 71(1):511–535, 2002. PMID: 12045105.

[197] Robert I. Macey, Joseph S. Adorante, and Frank W. Orme. Erythrocyte membrane potentials determined by hydrogen ion distribution. *Biochimica et Biophysica Acta (BBA) - Biomembranes*, 512(2):284 – 295, 1978.

[198] Poul Bennekou and Palle Christophersen. Flux ratio of valinomycin-mediated k+ fluxes across the human red cell membrane in the presence of the protonophore cccp. *The Journal of Membrane Biology*, 93(3):221–227, Oct 1986.

[199] D Zilberstein, V Agmon, S Schuldiner, and E Padan. Escherichia coli intracellular ph, membrane potential, and cell growth. *Journal of Bacteriology*, 158(1):246–252, 1984.

[200] Matteo Polettini and Massimiliano Esposito. Irreversible thermodynamics of open chemical networks. I. Emergent cycles and broken conservation laws. *The Journal of Chemical Physics*, 141(2):024117, 2014.

[201] Etana Padan. The enlightening encounter between structure and function in the NhaA Na+–H+ antiporter. *Trends in Biochemical Sciences*, 33(9):435 – 443, 2008.

[202] D Taglicht, E Padan, and S Schuldiner. Overproduction and purification of a functional na+/h+ antiporter coded by nhaa (ant) from escherichia coli. *Journal of Biological Chemistry*, 266(17):11289–11294, 1991.

[203] Ramkumar Iyer, Tina M. Iverson, Alessio Accardi, and Christopher Miller. A biological role for prokaryotic clc chloride channels. *Nature*, 419(6908):715–718, 2002.

[204] Eugenia Pennacchietti, Fabio Giovannercole, and Daniela De Biase. Acid Survival Mechanisms in Neutralophilic Bacteria. In *Stress and Environmental Regulation of Gene Expression and Adaptation in Bacteria*, pages 911–926. John Wiley & Sons, Ltd, 2016.

[205] J. Lin, M. P. Smith, K. C. Chapin, H. S. Baik, G. N. Bennett, and J. W. Foster. Mechanisms of acid resistance in enterohemorrhagic *Escherichia coli*. *Applied and Environmental Microbiology*, 62(9):3094–3100, September 1996.

[206] Terry J. Beveridge. Structures of gram-negative cell walls and their derived membrane vesicles. *Journal of Bacteriology*, 181(16):4725–4733, 1999.

[207] Heiko Erhardt, Felix Dempwolff, Moritz Pfreundschuh, Marc Riehle, Caspar Schäfer, Thomas Pohl, Peter Graumann, and Thorsten Friedrich. Organization of the *Escherichia coli* aerobic enzyme complexes of oxidative phosphorylation in dynamic domains within the cytoplasmic membrane. *MicrobiologyOpen*, 3(3):316–326, 2014.

[208] Daniel O. Daley, Mikaela Rapp, Erik Granseth, Karin Melén, David Drew, and Gunnar von Heijne. Global Topology Analysis of the *Escherichia coli* Inner Membrane Proteome. *Science*, 308(5726):1321–1323, 2005.

[209] The UniProt Consortium. UniProt: a worldwide hub of protein knowledge. *Nucleic Acids Research*, 47(D1):D506–D515, 11 2018.

[210] Wonpil Im and Benoit Roux. Ion permeation and selectivity of ompf porin: A theoretical study based on molecular dynamics, brownian dynamics, and continuum electrodiffusion theory. *Journal of Molecular Biology*, 322(4):851 – 869, 2002.

[211] Hope Richard and John W. Foster. *Escherichia coli* Glutamate- and Arginine-Dependent Acid Resistance Systems Increase Internal pH and Reverse Transmembrane Potential. *Journal of Bacteriology*, 186(18):6032–6041, 2004.

[212] Daniel G. Fuster and R. Todd Alexander. Traditional and emerging roles for the SLC9 Na+/H+ exchangers. *Pflügers Archiv - European Journal of Physiology*, 466(1):61–76, 2014.

[213] M. Schwede, K. Garbett, K. Mirnics, D. H. Geschwind, and E. M. Morrow. Genes for endosomal nhe6 and nhe9 are misregulated in autism brains. *Molecular Psychiatry*, 19(3):277–279, 2014.

[214] Maya Schushan, Minghui Xiang, Pavel Bogomiakov, Etana Padan, Rajini Rao, and Nir Ben-Tal. Model-guided mutagenesis drives functional studies of human nha2, implicated in hypertension. *Journal of Molecular Biology*, 396(5):1181 – 1196, 2010.

[215] Yoichi Ishida, Smita Nayak, Joseph A Mindell, and Michael Grabe. A model of lysosomal ph regulation. *The Journal of general physiology*, 141(6):705—720, June 2013.

[216] K A Presser, D A Ratkowsky, and T Ross. Modelling the growth rate of escherichia coli as a function of ph and lactic acid concentration. *Applied and Environmental Microbiology*, 63(6):2355–60, 1997.

[217] Bowers. Influence of ph and temperature on growth characteristics of leading foodborne pathogens in a laboratory medium and select food beverages. 2018.

[218] Hugh G. Lawford and Joyce D. Rousseau. Effects of pH and acetic acid on glucose and xylose metabolism by a genetically engineered ethanologenic

Escherichia coli. *Applied Biochemistry and Biotechnology*, 39(1):301–322, Sep 1993.

[219] Emile Duclaux. *Traité de microbiologie*, volume 1. Paris,Masson,, 1898. http://www.biodiversitylibrary.org/bibliography/1842 — t. 1. Microbiologie générale. 1898. – t. 2. Diastases, toxines et veins. 1899. – t. 3. Fermentation alcoolique. 1900. – t. 4. Fermentations variées des diverses substances ternaires. 1901.

[220] S. J. Pirt. The maintenance energy of bacteria in growing cultures. *Proceedings of the Royal Society of London. Series B, Biological Sciences*, 163(991):224–231, 1965.

[221] R.L Buchanan and L.A. Klawitter. The effect of incubation temperature, initial pH, and sodium chloride on the growth kinetics of *Escherichia coli* O157:H7. *Food Microbiology*, 9(3):185 – 196, 1992.

[222] Xianghao Wu, Ronni Altman, Mark A. Eiteman, and Elliot Altman. Adaptation of escherichia coli to elevated sodium concentrations increases cation tolerance and enables greater lactic acid production. *Applied and Environmental Microbiology*, 80(9):2880–2888, 2014.

[223] Koki Horikoshi. Production of alkaline enzymes by alkalophilic microorganisms. *Agricultural and Biological Chemistry*, 35(9):1407–1414, 1971.

[224] Terry Ann Krulwich, Jun Liu, Masato Morino, Makoto Fujisawa, Masahiro Ito, and David B. Hicks. *Adaptive Mechanisms of Extreme Alkaliphiles*, pages 119–139. Springer Japan, Tokyo, 2011.

[225] Wil N. Konings, Sonja-Verena Albers, Sonja Koning, and Arnold J. M. Driessen. The cell membrane plays a crucial role in survival of bacteria and archaea in extreme environments. *Antonie van Leeuwenhoek*, 81(1):61–72, 2002.

[226] D McLaggan, M Keyhan, and A Matin. Chloride transport pathways and their bioenergetic implications in the obligate acidophile *Bacillus coagulans*. *Journal of Bacteriology*, 172(3):1485–1490, 1990.

[227] Yusuke V. Morimoto, Seiji Kojima, Keiichi Namba, and Tohru Minamino. M153R mutation in a pH-sensitive green fluorescent protein stabilizes its fusion proteins. *PLoS ONE*, 6(5):e19598, 2011.

[228] Gero Miesenböck, Dino A. De Angelis, and James E. Rothman. Visualizing secretion and synaptic transmission with pH-sensitive green fluorescent proteins. *Nature*, 394(6689):192–195, 1998.

[229] D. Scott Cayley, Harry J. Guttman, and M. Thomas Record. Biophysical Characterization of Changes in Amounts and Activity of *Escherichia coli* Cell and Compartment Water and Turgor Pressure in Response to Osmotic Stress. *Biophysical Journal*, 78(4):1748 – 1764, 2000.

[230] Neidhardt F. C., *et al. Escherichia coli and Salmonella: Cellular and Molecular Biology.* ASM Press, 1996.

[231] Daniel A. Beard and Hong Qian. *Chemical Biophysics: Quantitative Analysis of Cellular Systems.* Cambridge Texts in Biomedical Engineering. Cambridge University Press, 2008.

[232] K B Andersen and K von Meyenburg. Are growth rates of *Escherichia coli* in batch cultures limited by respiration? *Journal of Bacteriology*, 144(1):114–123, 1980.

[233] Dennis P Bremer H. Modulation of Chemical Composition and Other Parameters of the Cell at Different Exponential Growth Rates. *EcoSal Plus*, 2008.

[234] Guadalupe Guerra, Federico Martinez, and Juan Pablo Pardo. On the H+/2e- stoichiometry of the respiratory chain. *Biochemistry and Molecular Biology Education*, 30(6):363–367.

[235] Robert J. Silbey, Robert A. Alberty, and Moungi G. Bawendi. *Physical Chemistry, (3rd Edition).* 2003.

[236] A. Bock and Gary Sawers. Escherichia coli and salmonella: Cellular and molecular biology, 2nd edition. *Fermentation*, pages 262–282, 01 1996.

[237] A. Metris, S. M. George, F. Mulholland, A. T. Carter, and J. Baranyi. Metabolic Shift of *Escherichia coli* under Salt Stress in the Presence of Glycine Betaine. *Applied and Environmental Microbiology*, 80(15):4745–4756, 2014.

[238] Pushkar Malakar, Vivek K. Singh, Richa Karmakar, and Kareenhalli V. Venkatesh. Effect on β-galactosidase synthesis and burden on growth of osmotic stress in *Escherichia coli*. *SpringerPlus*, 3(1):748, Dec 2014.

[239] Shinichi Nagata, Hideaki Sasaki, Akinobu Oshima, Shirou Takeda, Yuki Hashimoto, and Akio Ishida. Effect of Proline and K+ on the Stimulation of Cellular Activities in *Escherichia coli* K-12 under High Salinity. *Bioscience, Biotechnology, and Biochemistry*, 69(4):740–746, 2005. PMID: 15849412.

[240] T. G. Watson. Effects of sodium chloride on steady-state growth and metabolism of saccharomyces cerevisiae. *Microbiology*, 64(1):91–99, 1970.

[241] Aloice W. Mayo and Tatsuya Noike. Effects of temperature and ph on the growth of heterotrophic bacteria in waste stabilization ponds. *Water Research*, 30(2):447 – 455, 1996.

[242] Markus Roeßler, Xaver Sewald, and Volker Müller. Chloride dependence of growth in bacteria. *FEMS Microbiology Letters*, 225(1):161–165, 08 2003.

[243] L Rosso, J R Lobry, S Bajard, and J P Flandrois. Convenient model to describe the combined effects of temperature and ph on microbial growth. *Applied and Environmental Microbiology*, 61(2):610–616, 1995.

[244] Ulf Riebesell and Jean-Pierre Gattuso. Lessons learned from ocean acidification research. *Nature Climate Change*, 5(1):12–14, Jan 2015.

[245] Ricardo Cavicchioli, William J. Ripple, Kenneth N. Timmis, Farooq Azam, Lars R. Bakken, Matthew Baylis, Michael J. Behrenfeld, Antje Boetius, Philip W. Boyd, Aimée T. Classen, Thomas W. Crowther, Roberto Danovaro, Christine M. Foreman, Jef Huisman, David A. Hutchins, Janet K. Jansson, David M. Karl, Britt Koskella, David B. Mark Welch, Jennifer B. H. Martiny, Mary Ann Moran, Victoria J. Orphan, David S. Reay, Justin V. Remais, Virginia I. Rich, Brajesh K. Singh, Lisa Y. Stein, Frank J. Stewart, Matthew B. Sullivan, Madeleine J. H. van Oppen, Scott C. Weaver, Eric A. Webb, and Nicole S. Webster. Scientists' warning to humanity: microorganisms and climate change. *Nature Reviews Microbiology*, 17(9):569–586, Sep 2019.

[246] T. M. Ng and D. W. Schaffner. Mathematical Models for the Effects of pH, Temperature, and Sodium Chloride on the Growth of *Bacillus*

stearothermophilus in Salty Carrots. *Applied and environmental microbiology*, 63(4):1237–1243, Apr 1997. 16535566[pmid].

[247] C I Mortvedt-Abildgaa, J Nissen-Meyer, B Jelle, B Grenov, M Skaugen, and I F Nes. Production and pH-Dependent Bactericidal Activity of Lactocin S, a Lantibiotic from *Lactobacillus sake* L45. *Applied and Environmental Microbiology*, 61(1):175–179, 1995.

[248] I. L. Bartek, M. J. Reichlen, R. W. Honaker, R. L. Leistikow, E. T. Clambey, M. S. Scobey, A. B. Hinds, S. E. Born, C. R. Covey, M. J. Schurr, A. J. Lenaerts, and M. I. Voskuil. Antibiotic Bactericidal Activity Is Countered by Maintaining pH Homeostasis in *Mycobacterium smegmatis*. *mSphere*, 1(4), 2016.

[249] John Thomas, Sara Linton, Linda Corum, Will Slone, Tyler Okel, and Steven L Percival. The affect of ph and bacterial phenotypic state on antibiotic efficacy. *International Wound Journal*, 9(4):428–435, 2012.

[250] C. Wiegand, M. Abel, P. Ruth, P. Elsner, and U.-C. Hipler. ph influence on antibacterial efficacy of common antiseptic substances. *Skin Pharmacology and Physiology*, 28(3):147–158, 2015.

[251] Arijit Maitra and Ken A. Dill. Bacterial growth laws reflect the evolutionary importance of energy efficiency. *Proceedings of the National Academy of Sciences*, 112(2):406–411, 2015.

[252] D. A. Lipson. The complex relationship between microbial growth rate and yield and its implications for ecosystem processes. *Frontiers in Microbiology*, 6:615, 2015.

[253] Thomas Ferenci. 'growth of bacterial cultures' 50 years on: towards an uncertainty principle instead of constants in bacterial growth kinetics. *Research in Microbiology*, 150(7):431 – 438, 1999.

[254] Gangsheng Wang and Wilfred M. Post. A theoretical reassessment of microbial maintenance and implications for microbial ecology modeling. *FEMS Microbiology Ecology*, 81(3):610–617, 09 2012.

[255] Matteo Mori, Enzo Marinari, and Andrea De Martino. A yield-cost tradeoff governs escherichia coli's decision between fermentation and respiration in

carbon-limited growth. *npj Systems Biology and Applications*, 5(1):16, May 2019.

[256] Guillaume Terradot, Andreea Beica, Andrea Weiße, and Vincent Danos. Survival of the fattest: Evolutionary trade-offs in cellular resource storage. *Electronic Notes in Theoretical Computer Science*, 335:91 – 112, 2018. 7th International Workshop on Static Analysis and Systems Biology (SASB 2016).

[257] David W. Tempest and Oense M. Neijssel. The status of yatp and maintenance energy as biologically interpretable phenomena. *Annual Review of Microbiology*, 38(1):459–513, 1984. PMID: 6388498.

[258] William Chesbro. The domains of slow bacterial growth. *Canadian Journal of Microbiology*, 34(4):427–435, 1988. PMID: 3052753.

[259] J B Russell and G M Cook. Energetics of bacterial growth: balance of anabolic and catabolic reactions. *Microbiology and Molecular Biology Reviews*, 59(1):48–62, 1995.

[260] A. L. KOCH and H. R. LEVY. Protein turnover in growing cultures of Escherichia coli. *J Biol Chem*, 217(2):947–957, Dec 1955.

[261] Severin J. Schink, Elena Biselli, Constantin Ammar, and Ulrich Gerland. Death Rate of *E. coli* during Starvation Is Set by Maintenance Cost and Biomass Recycling. *Cell Systems*, 9(1):64 – 73.e3, 2019.

[262] M Heldal, S Norland, and O Tumyr. X-ray microanalytic method for measurement of dry matter and elemental content of individual bacteria. *Applied and Environmental Microbiology*, 50(5):1251–1257, 1985.

[263] M. *et al.* Lynch. The bioenergetic costs of a gene. *PNAS*, 2015.

[264] Hiroshi Akashi and Takashi Gojobori. Metabolic efficiency and amino acid composition in the proteomes of *Escherichia coli* and *Bacillus subtilis*. *Proceedings of the National Academy of Sciences*, 99(6):3695–3700, 2002.

[265] P. Thomas, G. P. Terradot, V. Danos, and A. Weiße. Stochasticity of cellular growth: sources, propagation and consequences. Submitted, 2017.

[266] Arthur H.F Hosie and Philip S Poole. Bacterial abc transporters of amino acids. *Research in Microbiology*, 152(3):259–270, 2001.

[267] Boris Görke and Jörg Stülke. Carbon catabolite repression in bacteria: many ways to make the most out of nutrients. *Nature Reviews Microbiology*, 6(8):613–624, Aug 2008.

[268] Johan H. van Heerden, Hermannus Kempe, Anne Doerr, Timo Maarleveld, Niclas Nordholt, and Frank J. Bruggeman. Statistics and simulation of growth of single bacterial cells: illustrations with *B. subtilis* and *E. coli*. *Scientific Reports*, 7(1):16094, Nov 2017.

[269] Zheng Zhang, Andreas Milias-Argeitis, and Matthias Heinemann. Dynamic single-cell NAD(P)H measurement reveals oscillatory metabolism throughout the *E. coli* cell division cycle. *Scientific Reports*, 8(1):2162, Feb 2018.

[270] W. Donachie. Relationship between Cell Size and Time of Initiation of DNA Replication. *Nature*, 1968.

[271] D. *et al.* Molenaar. Shifts in growth strategies reflect tradeoffs in cellular economics. *Molecular Systems Biology*, 2009.

[272] Sergei Korshunov and James A. Imlay. Detection and quantification of superoxide formed within the periplasm of escherichia coli. *Journal of Bacteriology*, 188(17):6326–6334, 2006.

[273] Conghui You, Hiroyuki Okano, Sheng Hui, Zhongge Zhang, Minsu Kim, Carl W. Gunderson, Yi-Ping Wang, Peter Lenz, Dalai Yan, and Terence Hwa. Coordination of bacterial proteome with metabolism by cyclic AMP signalling. *Nature*, 500(7462):301–306, Aug 2013.

[274] Matteo Mori, Terence Hwa, Olivier C. Martin, Andrea De Martino, and Enzo Marinari. Constrained allocation flux balance analysis. *PLOS Computational Biology*, 12(6):1–24, 06 2016.

[275] R. John Wallace and W. Harry Holms. Maintenance coefficients and rates of turnover of cell material in *Escherichia coli* ML308 at different growth temperatures. *FEMS Microbiology Letters*, 37(3):317–320, 12 1986.

[276] A. H. Stouthamer and Corry W. Bettenhaussen. A continuous culture study of an ATPase-negative mutant of *Escherichia coli*. *Archives of Microbiology*, 113(3):185–189, 1977.

[277] Anke Kayser, Jan Weber, Volker Hecht, and Ursula Rinas. Metabolic flux analysis of *Escherichia coli* in glucose-limited continuous culture. I. Growth-rate-dependent metabolic efficiency at steady state. *Microbiology*, 151(3):693–706, 2005.

[278] Pamela J. Yeh, Matthew J. Hegreness, Aviva Presser Aiden, and Roy Kishony. Drug interactions and the evolution of antibiotic resistance. *Nature Reviews Microbiology*, 7(6):460–466, Jun 2009.

[279] Olivia McAuliffe, R. Paul Ross, and Colin Hill. Lantibiotics: structure, biosynthesis and mode of action. *FEMS Microbiology Reviews*, 25(3):285–308, 05 2001.

[280] Marcel H. Tempelaars, Susana Rodrigues, and Tjakko Abee. Comparative Analysis of Antimicrobial Activities of Valinomycin and Cereulide, the *Bacillus cereus* Emetic Toxin. *Applied and Environmental Microbiology*, 77(8):2755–2762, 2011.

[281] D. W. Deamer. Proton permeation of lipid bilayers. *Journal of Bioenergetics and Biomembranes*, 19(5):457–479, Oct 1987.

[282] S. Paula, A.G. Volkov, A.N. Van Hoek, T.H. Haines, and D.W. Deamer. Permeation of protons, potassium ions, and small polar molecules through phospholipid bilayers as a function of membrane thickness. *Biophysical Journal*, 70(1):339 – 348, 1996.

[283] J Gutknecht. Proton/hydroxide conductance and permeability through phospholipid bilayer membranes. *Proceedings of the National Academy of Sciences*, 84(18):6443–6446, 1987.

[284] Guy C. Brown, Michael P. Murphy, Martin Jastroch, Ajit S. Divakaruni, Shona Mookerjee, Jason R. Treberg, and Martin D. Brand. Mitochondrial proton and electron leaks. *Essays in Biochemistry*, 47:53–67, 06 2010.

[285] P. Reinikainen, J. Olkku, P. Markkanen, and A. Holmberg. Determination of pH and Temperature Profiles for the Growth of *Escherichia Coli*. *IFAC*

Proceedings Volumes, 18(17):219 – 224, 1985. 1st IFAC Symposium on Modelling and Control of Biotechnological Processes, Noordwijkerhout, The Netherlands, 11-13 December 1985.

[286] Marieke G.L. Elferink, Janny G. de Wit, Arnold J.M. Driessen, and Wil N. Konings. Stability and proton-permeability of liposomes composed of archaeal tetraether lipids. *Biochimica et Biophysica Acta (BBA) - Biomembranes*, 1193(2):247 – 254, 1994.

[287] D A Ratkowsky, J Olley, T A McMeekin, and A Ball. Relationship between temperature and growth rate of bacterial cultures. *Journal of Bacteriology*, 149(1):1–5, 1982.

[288] M H Zwietering, J T de Koos, B E Hasenack, J C de Witt, and K van't Riet. Modeling of bacterial growth as a function of temperature. *Applied and Environmental Microbiology*, 57(4):1094–1101, 1991.

[289] Arnold J.M. Driessen, Jack L.C.M. van de Vossenberg, and Wil N. Konings. Membrane composition and ion-permeability in extremophiles. *FEMS Microbiology Reviews*, 18(2):139 – 148, 1996. Papers presented at the First International Congress on Extremophiles.

[290] Kim Lewis. Persister cells, dormancy and infectious disease. *Nature Reviews Microbiology*, 5(1):48–56, Jan 2007.

[291] Dorien Wilmaerts, Mariam Bayoumi, Liselot Dewachter, Wouter Knapen, Jacek T. Mika, Johan Hofkens, Peter Dedecker, Giovanni Maglia, Natalie Verstraeten, and Jan Michiels. The Persistence-Inducing Toxin HokB Forms Dynamic Pores That Cause ATP Leakage. *mBio*, 9(4), 2018.

[292] Jonathan M. Stokes, Allison J. Lopatkin, Michael A. Lobritz, and James J. Collins. Bacterial metabolism and antibiotic efficacy. *Cell Metabolism*, 30(2):251 – 259, 2019.

[293] Michael A. Lobritz, Peter Belenky, Caroline B. M. Porter, Arnaud Gutierrez, Jason H. Yang, Eric G. Schwarz, Daniel J. Dwyer, Ahmad S. Khalil, and James J. Collins. Antibiotic efficacy is linked to bacterial cellular respiration. *Proceedings of the National Academy of Sciences*, 112(27):8173–8180, 2015.

[294] Hongbaek Cho, Tsuyoshi Uehara, and Thomas G. Bernhardt. Beta-lactam antibiotics induce a lethal malfunctioning of the bacterial cell wall synthesis machinery. *Cell*, 159(6):1300 – 1311, 2014.

[295] Scott D. Taylor and Michael Palmer. The action mechanism of daptomycin. *Bioorganic & Medicinal Chemistry*, 24(24):6253 – 6268, 2016. Discovery of Novel Antibacterials.

[296] Michael A. Kohanski, Daniel J. Dwyer, Boris Hayete, Carolyn A. Lawrence, and James J. Collins. A common mechanism of cellular death induced by bactericidal antibiotics. *Cell*, 130(5):797 – 810, 2007.

[297] Iris Keren, Yanxia Wu, Julio Inocencio, Lawrence R. Mulcahy, and Kim Lewis. Killing by bactericidal antibiotics does not depend on reactive oxygen species. *Science*, 339(6124):1213–1216, 2013.

[298] Xiangmin Lin, Liqun Kang, Hui Li, and Xuanxian Peng. Fluctuation of multiple metabolic pathways is required for *Escherichia coli* in response to chlortetracycline stress. *Mol. BioSyst.*, 10:901–908, 2014.

[299] Maciej Długosz, Jan M. Antosiewicz, and Joanna Trylska. Association of aminoglycosidic antibiotics with the ribosomal a-site studied with brownian dynamics. *Journal of Chemical Theory and Computation*, 4(4):549–559, Apr 2008.

[300] H W Taber, J P Mueller, P F Miller, and A S Arrow. Bacterial uptake of aminoglycoside antibiotics. *Microbiology and Molecular Biology Reviews*, 51(4):439–457, 1987.

[301] Kyle R. Allison, Mark P. Brynildsen, and James J. Collins. Metabolite-enabled eradication of bacterial persisters by aminoglycosides. *Nature*, 473(7346):216–220, May 2011.

[302] E.P. Abraham and E.S. Duthie. Effect of ph of the medium on activity of streptomycin and penicillin and other chemotherapeutic substances. *The Lancet*, 247(6396):455 – 459, 1946. Originally published as Volume 1, Issue 6396.

[303] H. Eagle, Mina Levy, and R. Fleischman. The effect of the <i xmlns=.

[304] H. *et al.* Bremer. Control of cyclic chromosome replication in escherichia coli. *Microbiological Reviews*, 1991.

[305] B. *et al.* Volkmer. Condition-Dependent Cell Volume and Concentration of *Escherichia coli* to Facilitate Data Conversion for Systems Biology Modeling. *Plos One*, 2011.

[306] David L Nelson and Michael M Cox. *Lehninger Principles of Biochemistry, Fourth Edition.* Fourth edition edition, 2004.

[307] A. Stouthamer. A theoretical study on the amount of ATP required for synthesis of microbial celt material. *Antonie van Leeuwenhoek*, 1973.

[308] Ian S. Farmer and Colin W. Jones. The Energetics of *Escherichia coli* during Aerobic Growth in Continuous Culture. *European Journal of Biochemistry*, 67(1):115–122.

[309] Julia Glazyrina, Eva-Maria Materne, Thomas Dreher, Dirk Storm, Stefan Junne, Thorsten Adams, Gerhard Greller, and Peter Neubauer. High cell density cultivation and recombinant protein production with *Escherichia coli* in a rocking-motion-type bioreactor. *Microbial Cell Factories*, 9(1):42, May 2010.

[310] Corina Teodora Bot and Camelia Prodan. Quantifying the membrane potential during *E. coli* growth stages. *Biophysical Chemistry*, 146(2):133 – 137, 2010.

[311] John J. Tomashek and William S. A. Brusilow. Stoichiometry of energy coupling by proton-translocating atpases: A history of variability. *Journal of Bioenergetics and Biomembranes*, 32(5):493–500, Oct 2000.

[312] Tom Zajdel. *Electronic Interfaces for Bacteria-Based Biosensing.* PhD thesis, EECS Department, University of California, Berkeley, Aug 2018.

[313] R.M. Sterritt and J.N. Lester. Interactions of heavy metals with bacteria. *Science of The Total Environment*, 14(1):5 – 17, 1980.

[314] D. H. Nies. Microbial heavy-metal resistance. *Applied Microbiology and Biotechnology*, 51(6):730–750, Jun 1999.

[315] Eloi Camprubi, Sean F. Jordan, Rafaela Vasiliadou, and Nick Lane. Iron catalysis at the origin of life. *IUBMB Life*, 69(6):373–381, 2017.

[316] Elaine R. Frawley and Ferric C. Fang. The ins and outs of bacterial iron metabolism. *Molecular Microbiology*, 93(4):609–616, 2014.

[317] Hanan Schoffman, Hagar Lis, Yeala Shaked, and Nir Keren. Iron–nutrient interactions within phytoplankton. *Frontiers in Plant Science*, 7:1223, 2016.

[318] Cheryl K. Y. Lau, Karla D. Krewulak, and Hans J. Vogel. Bacterial ferrous iron transport: the Feo system. *FEMS Microbiology Reviews*, 40(2):273–298, 2015.

[319] D. Barrie Johnson, Tadayoshi Kanao, and Sabrina Hedrich. Redox transformations of iron at extremely low ph: Fundamental and applied aspects. *Frontiers in Microbiology*, 3:96, 2012.

[320] D. Barrie Johnson and Kevin B. Hallberg. Carbon, iron and sulfur metabolism in acidophilic micro-organisms. volume 54 of *Advances in Microbial Physiology*, pages 201 – 255. Academic Press, 2008.

[321] James Patrick Folsom and Ross P. Carlson. Physiological, biomass elemental composition and proteomic analyses of *Escherichia coli* ammonium-limited chemostat growth, and comparison with iron- and glucose-limited chemostat growth. *Microbiology*, 161(8):1659–1670, 2015.

[322] Wally C. van Heeswijk, Hans V. Westerhoff, and Fred C. Boogerd. Nitrogen Assimilation in *Escherichia coli*: Putting Molecular Data into a Systems Perspective. *Microbiology and Molecular Biology Reviews*, 77(4):628–695, 2013.

[323] Rosa Martinez-Corral, Jintao Liu, Arthur Prindle, Gürol M. Süel, and Jordi Garcia-Ojalvo. Metabolic basis of brain-like electrical signalling in bacterial communities. *Philosophical Transactions of the Royal Society B: Biological Sciences*, 374(1774):20180382, 2019.

[324] M. *et al.* Maguire. Magnesium chemistry and biochemistry. *BioMetals*, 2002.

[325] Karen van Eunen, Jildau Bouwman, Pascale Daran-Lapujade, Jarne Postmus, André B. Canelas, Femke I. C. Mensonides, Rick Orij, Isil Tuzun, Joost van den Brink, Gertien J. Smits, Walter M. van Gulik, Stanley Brul,

Joseph J. Heijnen, Johannes H. de Winde, M. Joost Teixeira de Mattos, Carsten Kettner, Jens Nielsen, Hans V. Westerhoff, and Barbara M. Bakker. Measuring enzyme activities under standardized in vivo-like conditions for systems biology. *The FEBS Journal*, 277(3):749–760, Feb 2010.

[326] Joanne S. Ingwall and James A. Balshi. Energetics of the Na+ Pump in the Heart. *Journal of Cardiovascular Electrophysiology*, 17(s1):S127–S133, 2006.

[327] Stanley G. Schultz and A. K. Solomon. Cation transport in escherichia coli. *The Journal of General Physiology*, 45(2):355–369, 1961.

[328] Claudia C. Häse, Natalie D. Fedorova, Michael Y. Galperin, and Pavel A. Dibrov. Sodium ion cycle in bacterial pathogens: Evidence from cross-genome comparisons. *Microbiology and Molecular Biology Reviews*, 65(3):353–370, 2001.

[329] Thomas W. Conway. On the role of ammonium or potassium ion in amino acid polymerization. *Proceedings of the National Academy of Sciences*, 51(6):1216–1220, 1964.

[330] Armen Y. Mulkidjanian, Andrew Yu. Bychkov, Daria V. Dibrova, Michael Y. Galperin, and Eugene V. Koonin. Origin of first cells at terrestrial, anoxic geothermal fields. *Proceedings of the National Academy of Sciences*, 2012.

[331] Kristin M. Rath, Arpita Maheshwari, Per Bengtson, and Johannes Rousk. Comparative toxicities of salts on microbial processes in soil. *Applied and Environmental Microbiology*, 82(7):2012–2020, 2016.

[332] Knud H. Nierhaus. Mg2+, k+, and the ribosome. *Journal of Bacteriology*, 196(22):3817–3819, 2014.

[333] Víctor Sojo, Andrew Pomiankowski, and Nick Lane. A bioenergetic basis for membrane divergence in archaea and bacteria. *PLOS Biology*, 12(8):1–12, 08 2014.

[334] Jemima E. R. Sawyer, James E. Hennebry, Alexander Revill, and Angus M. Brown. The critical role of logarithmic transformation in nernstian equilibrium potential calculations. *Advances in Physiology Education*, 41(2):231–238, 2017. PMID: 28377437.

[335] Dee U. Silverthorn. Uncovering misconceptions about the resting membrane potential. *Advances in Physiology Education*, 26(2):69–71, 2002. PMID: 12031939.

[336] David L. Cardozo. A model for understanding membrane potential using springs. *Advances in Physiology Education*, 29(4):204–207, 2005. PMID: 16298957.

[337] Stephen H. Wright. Generation of resting membrane potential. *Advances in Physiology Education*, 28(4):139–142, 2004. PMID: 15545342.